THE JOURNAL
OF
CHEMICAL PHYSICS

VOLUME 21, NUMBER 4 APRIL, 1953

The Effect of Pressure on Diffusion in CS_2 Organic Mixtures*

R. C. KOELLER AND H. G. DRICKAMER
Department of Chemistry, University of Illinois, Urbana, Illinois

(Received August 26, 1952)

Diffusion coefficients are presented as a function of pressure to 10 000 atmospheres for the following systems:

50 mol percent *n*-heptane—50 percent CS_2 0°–20°–40°;
50 mol percent 2,4 dimethylpentane—50 percent CS_2 20°–40°;
50 mol percent toluene—50 percent CS_2 20°–40°;
50 mol percent methylcyclohexane—50 percent CS_2 0°–20°–40°;
50 mol percent *n*-octane—50 percent CS_2 20°C;
50 percent chlorobenzene—50 percent CS_2 20°–40°;
80 percent chlorobenzene—20 percent CS_2 40°;
50 percent *n*-butanol—50 percent CS_2 20°–40°;
50 percent iso-butanol—50 percent CS_2 20°–40°;

using S^{35} tagged CS_2.

The results are interpreted in terms of the activation volume, enthalpy, and entropy, and conclusions are drawn concerning the effect of pressure on the structure of the liquids.

IN a previous paper[1] a method was described for measuring diffusion coefficients under pressure to 10 000 atmospheres, and results were presented and discussed for self-diffusion in carbon disulfide. The method has been applied to five carbon disulfide-hydrocarbon mixtures: CS_2-*n*-heptane at 0°, 20°, and 40°C; CS_2-2,4 dimethylpentane at 20° and 40°C; CS_2-toluene at 20°C.

Results are also presented for the system CS_2-chlorobenzene in two concentrations, CS_2-*n*-butanol, and CS_2-iso-butanol.

In each case S^{35} tagged CS_2 was used, and the mole fraction CS_2 in both radioactive and nonradioactive cells was 0.50, except for one isotherm in the system chlorobenzene-CS_2.

The S^{35} tagged CS_2 was obtained from Tracerlab. The *n*-heptane, *n*-octane, 2,4 dimethylpentane, and methylcyclohexane were Phillips pure grade. The toluene, chlorobenzene, and alcohols were Eastman Kodak pure grade, and the cp carbon disulfide was obtained from J. T. Baker Chemical Company.

The method of measuring the concentration and of calculating the diffusion coefficient is described in detail in the previous work[1–3] and will not be discussed here.

The method of operation and for calculation of the diffusion coefficient from the experimental data is discussed in reference 1. The kinetic theory of liquids, the possible pressure effects on the structure of liquids in general, and the mechanism for calculation of the activation volume ($\Delta V^{\ddagger}$), the activation enthalpy ($\Delta H^{\ddagger}$), and the entropy of activation ($\Delta S^{\ddagger}$) above that at atmospheric pressure ($\Delta S_0^{\ddagger}$) are outlined completely in reference 1.

The results of the present study will be discussed in terms of these concepts.

RESULTS

The diffusion coefficients are shown in Tables I–IX. Each system is discussed in detail below, but it is desirable first to outline the premises upon which the discussion is based.

An understanding of, and cohesion among, the wide variety of results obtained in this study depends upon

* This work was supported in part by the U. S. Atomic Energy Commission.

[1] R. C. Koeller and H. G. Drickamer, J. Chem. Phys. **21**, 267 (1953).

[2] K. D. Timmerhaus and H. G. Drickamer, J. Chem. Phys. **19**, 1242 (1951).

[3] W. L. Robb and H. G. Drickamer, J. Chem. Phys. **19**, 1504 (1951).

TABLE I. Measured diffusion coefficients for 50 percent (mole) CS_2 in n-C_7H_{16}.[a]

Temp. °K	Pressure atmos	Effective cell length cm	Observed $D \times 10^5$ cm²/sec
293	150	0.504	2.88
293	5000	0.611	0.515
293	7000	0.611	0.375
273	100	0.504	2.00
273	1200	0.504	1.46
273	3050	0.557	0.455
293	600	0.504	2.75
293	1200	0.504	2.53
293	2800	0.557	1.18
313	100	0.504	4.36
313	1200	0.504	4.17
313	3500	0.557	1.92
313	5200	0.611	1.01
313	7000	0.611	0.526
313	10 000	0.665	0.43

[a] Maximum deviation in reproducibility 10 percent. Average deviation 5 percent.

having a satisfactory molecular picture of a liquid which consists of nonspherically symmetrical molecules. The various systems investigated will be discussed with the picture in mind that motion in a liquid, (or the residence time of a molecule) depends largely upon the free volume between molecules (or the intensity and shape of the force field around a given molecule).

The variation of the diffusion coefficient with pressure should depend upon the free volume change in the following manner: (1) The change in the diffusion coefficient for a given change in pressure will depend upon the amount by which the free volume has been decreased. That is, the rate of change of the intensity of the force field around a molecule (and also the rate of change of the diffusion coefficient) will depend upon the rate of change of the free volume. In general, as the free volume is decreased the diffusion coefficient will also decrease. (2) It is clear that the shape of the molecules involved will be of importance in determining the effect of free volume on D. That is, depending upon the shape of the molecules, it is conceivable that a given orientation will have a higher probability for motion than some other orientation. As pressure is increased and the force fields surrounding each molecule are intensified, the probability of the preferred orientation for motion may be decreased. Thus, we see that the residence time may be increased by decreasing the free volume if the molecular shape is such that the probability of motion is a function of orientation. This consideration is probably unimportant for spherically symmetrical molecules or for small molecules surrounded by larger ones. Carbon disulfide in organic solutions, as studied in this investigation, would probably fall into the second classification. (3) This third point is of importance only for nonspherically symmetrical molecules; however, this is the only type we are concerned with in the present study. We may speak of the "shape" of a force field since it is probably true that nonspherically symmetrical force fields are associated with nonspherically symmetrical molecules. In fact, this is precisely what we mean when we speak of a nonspherically symmetrical molecule (since physical measurements of molecular properties are actually measures of the properties of their associated force fields). When free volume is decreased, i.e., the force fields intensified, it is not necessarily true that the "shape" of the force field remains the same. It may be the case that the force field is

TABLE II. Measured diffusion coefficients for 50 percent (mole) CS_2 in n-C_8H_{18}.[a]

Temp. °K	Pressure atmos	Effective cell length cm	Observed $D \times 10^5$ cm²/sec
293	200	0.504	2.82
293	600	0.504	2.59
293	1200	0.504	2.62
293	2000	0.557	1.45
293	4000	0.611	0.628
293	6100	0.611	0.282

[a] Maximum deviation in reproducibility 10 percent. Average deviation 5 percent.

TABLE III. Measured diffusion coefficients for 50 percent (mole) CS_2 in 2,4 dimethylpentane.[a]

Temp. °K	Pressure atmos	Effective cell length cm	Observed $D \times 10^5$ cm²/sec
293	200	0.504	3.15
293	1200	0.504	1.78
293	3500	0.557	1.22
293	6700	0.611	0.479
313	200	0.504	4.46
313	900	0.504	3.52
313	2000	0.557	2.37
313	3500	0.557	1.80
313	4900	0.611	1.26
313	7000	0.611	0.842
313	7000	0.611	0.763
313	10 200	0.665	0.657

[a] Maximum deviation in reproducibility 10 percent. Average deviation 5 percent.

TABLE IV. Measured diffusion coefficients for 50 percent (mole) CS_2 in toluene.[a]

Temp. °K	Pressure atmos	Effective cell length cm	Observed $D \times 10^5$ cm²/sec
293	1	0.504	1.93
293	50	0.504	1.93
293	300	0.504	1.49
293	900	0.504	0.742
293	3300	0.557	0.575
293	7150	0.611	0.530
313	200	0.504	4.03
313	900	0.504	1.97
313	1500	0.665	1.49
313	3500	0.557	0.850
313	5750	0.611	0.710
313	9100	0.665	0.669

[a] Maximum deviation in reproducibility 10 percent. Average deviation 5 percent.

deformed in spite of the fact that sufficient energy is not applied to deform the molecule with which it is associated. In other words, we change the degree of "steric hindrance" on an intermolecular scale. The net effect could be to increase the necessity of there being a favorable orientation for migration with a corresponding increase in the residence time.

In the discussions to follow an occasional reference is made to a "lattice" or "packing" in the liquid. We do not wish to imply the existence of any structure which would be macroscopically observable. Rather, we mean that the free volume is such that the probability of the most favored orientation for motion of the organic molecules has decreased to a point where their residence time is long as compared with that of the CS_2 molecules. The residence time in normal liquids composed of single, free moving molecules, is of the order of 10^{-13} second. If this were reduced, by say a factor of 10, for the organic molecules through suitable intensification of force fields as described above, the motion would still be highly rapid and chaotic on a macroscopic scale. However, the organic molecules would present a relatively long-lived "lattice" to inhibit CS_2 migration. When we speak of a "stable lattice," "packing" or "structure," we mean that the most probable configuration does not change greatly with pressure.

The discussion above concerning the relation between free volume and motion in liquids is meant to apply to solutions not subject to hydrogen bonding, solvation, or any other phenomena which tend to bond molecules together.

TABLE V. Measured diffusion coefficients for 50 percent (mole) CS_2 in methylcyclohexane.[a]

Temp. °K	Pressure atmos	Effective cell length cm	Observed $D\times10^5$ cm²/sec
273	50	0.504	2.37
273	1200	0.504	0.621
273	3000	0.557	0.236
293	50	0.504	2.65
293	900	0.504	1.83
293	3000	0.557	0.585
293	7000	0.611	0.192
313	200	0.504	3.00
313	900	0.504	1.97
313	2000	0.557	1.34
313	4000	0.557	0.965
313	5000	0.611	0.690
313	6300	0.611	0.540
313	7750	0.665	0.485
313	10 000	0.665	0.351

[a] Maximum deviation in reproducibility 10 percent. Average deviation 5 percent.

TABLE VI. Measured diffusion coefficients for 50 percent (mole) CS_2 in chlorobenzene.[a]

Temp. °K	Pressure atmos	Effective cell length cm	$D\times10^5$ cm²/sec
293	218	0.504	2.60
293	1530	0.504	0.943
293	3500	0.557	0.870
293	7000	0.611	0.330
313	200	0.504	4.63
313	900	0.504	2.59
313	2000	0.504	1.84
313	2000	0.504	2.02
313	3000	0.557	2.18
313	3500	0.557	1.66
313	4850	0.557	1.05
313	8200	0.665	0.422
313	10 000	0.665	0.254

[a] Maximum deviation in reproducibility 10 percent. Average deviation 5 percent.

TABLE VII. Measured diffusion coefficients for 20 percent (mole) CS_2 in chlorobenzene.[a]

Temp. °K	Pressure atmos	Effective cell length cm	$D\times10^5$ cm²/sec
313	200	0.504	3.52
313	900	0.504	2.42
313	900	0.504	1.78
313	2000	0.504	1.29
313	2800	0.557	1.30
313	4400	0.557	0.912
313	7000	0.611	0.565

[a] Maximum deviation in reproducibility 10 percent. Average deviation 5 percent.

CARBON DISULFIDE IN NORMAL HEPTANE AND IN NORMAL OCTANE

The data are shown in Fig. 1 plotted as $\ln D$ as a function of pressure for the three isotherms 0°, 20°, and 40°C.

From the general shape of the isotherms in Fig. 1 it appears that in the low pressure range (up to about 2000 atmos at 40°) the heptane structure is quite loose and does not inhibit the movement of CS_2 molecules so that we have essentially self-diffusion in CS_2. As pressure is further increased the presence of the heptane becomes important and the structure begins to rapidly "close in" as shown by the rapid decline of D with pressure in the range 2000 to 7000 atmos at 40°C. Beyond 7000 atmos, however, the isotherm flattens out indicating a fairly stable heptane packing, and CS_2 moves through the interstices. The diffusion coefficient in the 7000 to

TABLE VIII. Measured diffusion coefficients for 50 percent (mole) CS_2 in *n*-butanol.[a]

Temp. °K	Pressure atmos	Effective cell length cm	$D\times10^5$ cm²/sec
293	200	0.504	3.06
293	1500	0.504	1.21
293	3500	0.557	0.714
293	7000	0.611	0.192
313	210	0.504	4.29
313	950	0.504	2.10
313	2000	0.504	1.42
313	3500	0.557	1.21
313	5450	0.665	0.963
313	7000	0.611	0.534
313	9000	0.665	0.315

[a] Maximum deviation in reproducibility 10 percent. Average deviation 5 percent.

TABLE IX. Measured diffusion coefficients for 50 percent (mole) CS_2 in *i*-butanol.[a]

Temp. °K	Pressure atmos	Effective cell length cm	$D \times 10^5$ cm²/sec
293	200	0.504	2.10
293	2000	0.504	1.03
293	3500	0.557	0.876
293	5000	0.557	0.454
293	5650	0.611	0.235
313	200	0.504	2.95
313	1500	0.504	2.34
313	2500	0.557	1.84
313	3500	0.557	0.494
313	3500	0.557	0.565
313	5000	0.557	0.368
313	5700	0.611	0.333
313	8000	0.611	0.232

[a] Maximum deviation in reproducibility 10 percent. Average deviation 5 percent.

10 000 atmos range at 40° for CS_2 in n-C_7 is about a factor of 5 less than that for pure CS_2 at the same temperature and pressure. This then is the factor by which the heptane structure inhibits the migration of CS_2 molecules in the high pressure range.

Diffusion coefficients were also determined for a 50 mole percent solution of carbon disulfide in normal octane along a 20° isotherm and are plotted in Fig. 1 with the isotherms for *n*-heptane. Comparing the two 20° isotherms it is seen that they are both identical in shape, with that for n-C_8 being slightly lower and tending to diverge further below the n-C_7 curve as pressure is increased. This observation fits in quite well with the analysis of the n-C_7 isotherms as given above. The addition of an extra -CH_2- to the *n*-heptane chain is seen merely to emphasize the effect of pressure on D. Thus, the octane structure becomes important in limiting the CS_2 diffusion at a slightly lower pressure than does the heptane structure and likewise, the octane reaches the "stable" configuration at a somewhat lower pressure.

In speaking of the heptane or octane structure it is not meant to imply that there exists a rigid static structure through which the CS_2 molecules must find their way.

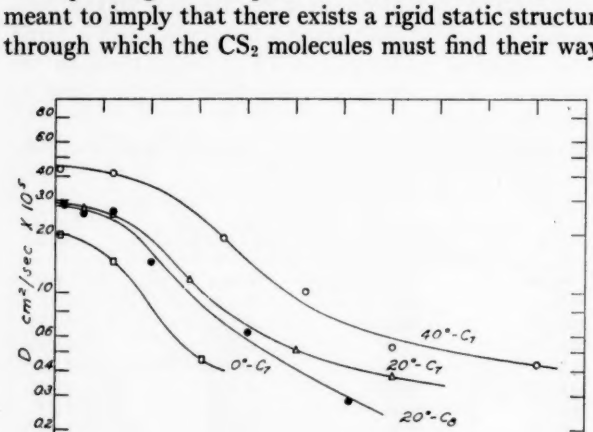

FIG. 1. Diffusion coefficient *versus* pressure. Systems: CS_2-*n* heptane, CS_2-*n* octane.

However, for purposes of discussion it is convenient to think of the long-chain molecules as being static relative to the movement of CS_2 molecules for an infinitesimal time; keeping in mind that the long chains are always in a state of random motion characteristic of liquid molecules. Thus, with this sort of a picture in mind one might, as an extreme case, think of a type of diffusion analogous to interstitial diffusion in crystalline solids. The analysis of the shape of the n-C_7-CS_2 isotherms given above provides evidence that a type of "interstitial" mechanism does exist in the high pressure range (beyond 7000 atmos at 40°).

A consideration of the change in activation entropy from that at atmospheric pressure further substantiates the existence of an interstitial type mechanism in the high pressure range. Values of $\Delta S_P^{\ddagger} - \Delta S_0^{\ddagger}$ are plotted as a function of pressure along a 20° isotherm in Fig. 2. The activation entropy increases rapidly beyond a pressure of 1000 atmos to a maximum of 9 cal/°K/mole,

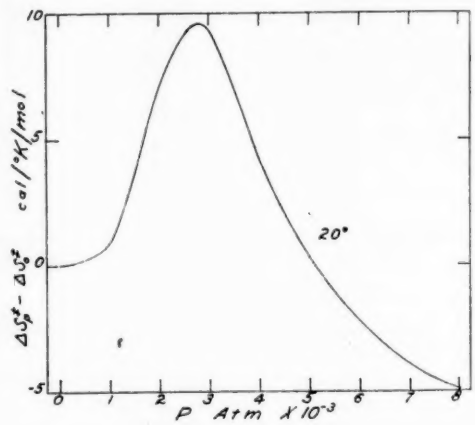

FIG. 2. Entropy of activation *versus* pressure. System: CS_2-*n* heptane.

above that at atmospheric pressure, at 2800 atmos. The difference then decreases and becomes negative so that at 8000 atmos the activation entropy is 5 eu below that at 1 atmos. The curve is leveling in such a manner that it would probably be asymptotic to about −6 eu at higher pressure. We shall assume that Eyring's[4] estimate that the activation entropy is essentially zero for atmospheric pressure diffusion is valid for this solution of n-C_7 in CS_2.

As pressure is increased from atmospheric, the heptane structure is at first loose enough so as to not greatly inhibit the diffusion of CS_2 and we find the activation entropy increasing slowly due to increasing order in the initial state. As the pressure is increased beyond 1000 atmos the presence of the heptane becomes of more importance and the liquid attains a higher degree of order and lower entropy level in the normal state. Therefore, the entropy change associated with a

[4] Eyring, Laidler, and Glasstone, *The Theory of Rate Processes* (McGraw-Hill Book Company, Inc., New York, 1941).

molecule entering the activated state is increasing. When that pressure is approached where the maximum value of $\Delta S_P^{\ddagger} - \Delta S_0^{\ddagger}$ occurs, the limitations imposed by the heptane become of increasingly greater consequence. Finally, at the maximum, the increased order of the normal state is offset by the compactness of the heptane structure which requires that the probability of a CS_2 molecule entering the activated state depends upon its orientation. Thus, the relative entropy of the activated state is decreased. This effect becomes more and more pronounced as pressure is increased until finally the activation entropy becomes negative (since we have assumed $\Delta S_0^{\ddagger}=0$). This picture might be more clearly seen by recalling that for the self-diffusion in CS_2[1] we accounted for high entropies of activation by pointing out that for a molecule to enter the activated state it must break loose from an ordered configuration, thus increasing its degrees of freedom. In this case, however, a diffusing molecule must pass through a hole in the heptane "lattice" and the possible directions it may take are limited compared to those available in pure CS_2. Thus, we see that the limitations imposed by the heptane structure are so stringent that a molecule in the activated state for diffusion has fewer degrees of freedom than one in the initial state and thus the entropy of activation is negative.

TABLE X. $\Delta F^{\ddagger} - \Delta F_0^{\ddagger}$ for n-C_7-CS_2 at 20°C.

P (atmos)	$\Delta F^{\ddagger} - \Delta F_0^{\ddagger}$ (cal/mol)
1000	31
2000	205
3000	526
4000	775
6000	1070
8000	1150

The curves of activation enthalpy *versus* pressure show the same maximum as does the entropy curve. Activation enthalpies are plotted in Fig. 3 for 282, 293, and 302°K. The dashed curve for 293° was estimated in order that the entropy data could be calculated using values of D at 293°K. The similarity of the curves of $\Delta H^{\ddagger}$ *vs* P and of $\Delta S_P^{\ddagger} - \Delta S_0^{\ddagger}$ *vs* P is consistent with Levi's observation[5] that a high heat of activation is associated with a high entropy of activation and vice versa; again, we would expect $\Delta F^{\ddagger}$ to remain substantially constant. $\Delta F_P^{\ddagger} - \Delta F_0^{\ddagger}$ for the 20° isotherm was calculated from the relation $\Delta F = \Delta H - T\Delta S$ and is tabulated in Table X.

It was assumed above that $\Delta S_0^{\ddagger} \cong 0$; therefore, $\Delta F_0^{\ddagger} = \Delta H_0^{\ddagger} = 3840$ cal/mole. On this basis then, the free energy of activation increases by only 30 percent in the 8000 atmosphere ranges. It is interesting to note that $\Delta F^{\ddagger}$ increases continuously with pressure and does not go through a maximum as do both $\Delta S^{\ddagger}$ and $\Delta H^{\ddagger}$.

[5] D. L. Levi, Trans. Faraday Soc. **42a**, 152 (1946).

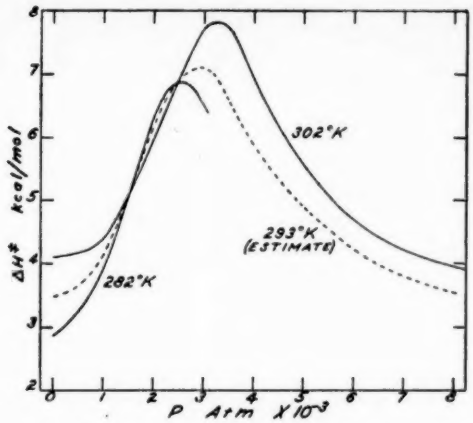

FIG. 3. Enthalpy of activation *versus* pressure. System: CS_2-n heptane.

The ratios of the activation volume to the molal volume for the three heptane isotherms and for the octane isotherm are plotted as a function of density in Fig. 4. In making these calculations the necessary compressibility and density data were estimated by assuming the solutions to be ideal and adding the properties of the pure components in proportion to their volume percent in solution.

In the very low density region of Fig. 4 it is seen that the activation volume is slightly negative. The truth of the matter is probably that the activation volume is zero and the negative value arises purely as a consequence of the difficulty in accurately determining the slope $\partial \ln D/\partial p$ at atmospheric pressure. $\Delta V^{\ddagger}/V$ rises slowly at first and then more rapidly to reach a maximum, at 40°C, of 18.5 percent of the molal volume at a density of about 1.02 g/cc; the ratio then decreases and levels out to a value of 3 percent at a density of 1.12 ($P=8500$ atmos). This same trend is also shown by the remaining isotherms. The maximum at 0° is 19 percent for $\rho \cong 0.99$, that at 20° is 15.5 for $\rho \cong 0.99$, and for the normal octane the maximum activation volume is 18.5 percent of the molal volume at $\rho \cong 0.97$.

The looseness of the heptane structure in the low pressure range is again apparent from a consideration of the activation volume. The slow initial rise of $\Delta V^{\ddagger}/\bar{V}$ with increasing density is analogous to that found for

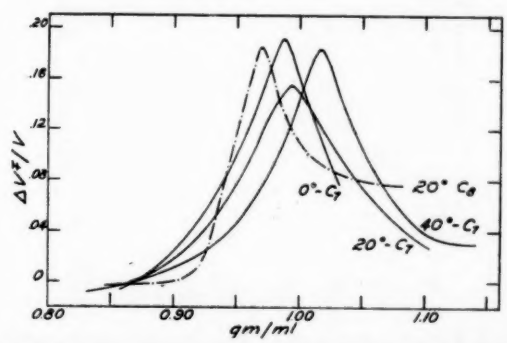

FIG. 4. Activation volume *versus* density. System: CS_2-n heptane.

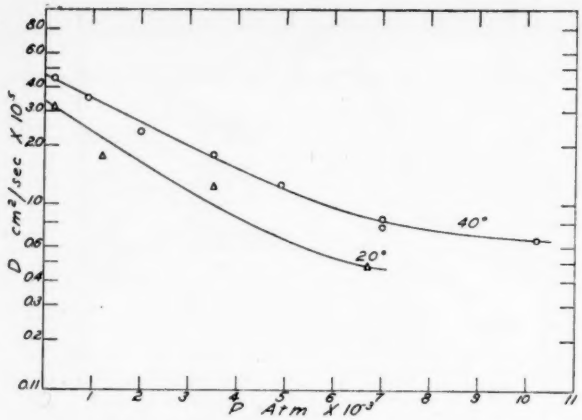

FIG. 5. Diffusion coefficient *versus* pressure. System: CS_2-2,4 dimethylpentane.

CS_2 and indicates the existence of a sufficient number of holes for diffusion to occur with only a slight local expansion. As density is increased the heptane molecules begin to impede the CS_2 to a greater extent and must be pushed back to permit diffusion. Therefore, we find the activation volume increasing. Where the activation volume begins to decrease and the diffusion coefficient drops off rapidly, the structure becomes "stable" and the CS_2 molecules tend to diffuse through existing holes. At this point the activation volume settles down to some constant fraction of the molal volume. The final, asymptotic value of $\Delta V^{\ddagger}/\bar{V}$ is greater at the higher temperature, being 3 percent at 40° and about 2 percent at 20° for n-C_7. The value for n-C_8 at 20° is much higher, about 7 percent.

CARBON DISULFIDE IN 2,4 DIMETHYLPENTANE

Diffusion coefficients were determined as a function of pressure along two isotherms in a 50 mole percent solution of carbon disulfide and 2,4-dimethylpentane, (i-C_7). This system was studied in order that a comparison could be made with the data for n-heptane in an effort to ascertain the effects of chain branching on the structure in isomeric liquid paraffins. The data obtained are shown graphically as ln$D$ plotted as a function of P in Fig. 5.

The atmospheric pressure diffusion coefficient at 40° is the same in both the iso and normal C_7, 4.6×10^{-5} cm²/sec. Thus, at atmospheric pressure both structures present the same impediment to CS_2 migration. As pressure is increased, however, the iso structure immediately begins to close in as evidenced by the steady decline of ln$D$ from atmospheric pressure. With further increase of pressure the relatively stable configuration of the iso-heptane packing takes form steadily and the slope of the curve decreases.

Compressibility data were not available for 2,4-dimethylpentane so that it was necessary to use n-heptane compressibilities. Bridgman[6] has shown that the compressibility varies only slightly among isomeric six-carbon paraffins.

The change in activation entropy with pressure is plotted as a function of pressure along a 20°C isotherm in Fig. 6. It is seen that as pressure is increased the activation entropy increases, almost linearly, and reaches a maximum of 6 cal/°K/mole, greater than that at 1 atmos, at 5000 atmos; it then drops off until at 7000 atmos it is only 4.4 eu greater than at atmospheric pressure. The shape of this curve indicates that as pressure is increased from atmospheric the iso-heptane structure is of immediate importance, contrary to the case for the normal isomer, and the liquid becomes more ordered, lowering the entropy level of the normal state. Thus, we find that the entropy change for a molecule to enter the activated state is increasing. At the pressure where the maximum value of $\Delta S_P^{\ddagger}-\Delta S_0^{\ddagger}$ is observed, (5000 atmos), the iso-heptane "lattice" has formed to such an extent that the degrees of freedom of a molecule activated for diffusion are restricted to a point where further increase in pressure decreases the activation entropy. When the pressure is increased beyond 5000 atmos the limitations on the possible orientations of an activated CS_2 molecule imposed by the packing increase at a greater rate than does the order in the normal state and the activation entropy decreases. From an analogy with the normal heptane data it is anticipated that if the pressure were increased beyond 7000 atmos, the i-C_7

TABLE XI. $\Delta F_P^{\ddagger}-\Delta F_0^{\ddagger}$ for CS_2 in i-C_7 at 20°C.

P (atmos)	$\Delta F_P^{\ddagger}-\Delta F_0^{\ddagger}$ (cal/mole)
1000	181
2000	366
3000	544
5000	879
7000	1065

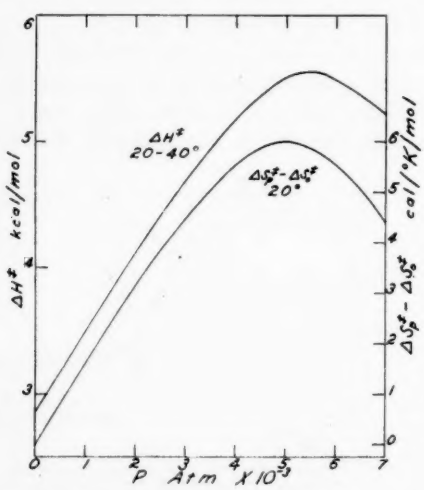

FIG. 6. Enthalpy and entropy of activation *versus* pressure. System: CS_2-2,4 dimethylpentane.

[6] P. W. Bridgman, *The Physics of High Pressure* (Macmillan Company, New York, 1931).

structure would become "stable" and the activation entropy would then be asymptotic to some low value.

The activation enthalpy varies in a similar manner with pressure as does the activation entropy. $\Delta H^{\ddagger}$ is plotted as a function of pressure in Fig. 6.

We shall again assume $\Delta S_0^{\ddagger} \cong 0$ so that $\Delta F_0^{\ddagger} = \Delta H_0^{\ddagger} = 2860$ cal/mole. It is seen from Table XI below that the free energy of activation increases continuously with pressure so that its value at 7000 atmos is 37 percent greater than that at 1 atmos. $\Delta F_P^{\ddagger} - \Delta F_0^{\ddagger}$ was calculated from the relationship $\Delta F = \Delta H - T\Delta S$.

The activation volume is shown in Fig. 7. From the initial slope of the curve of $\ln D$ *vs* P (Fig. 8) we know that the iso-heptane impedes the migration of CS_2 even in the very low pressure range. The structure remains flexible enough, however, so that it may be deformed to permit diffusion and we observe a relatively high activation volume. At the pressure where the maximum $\Delta V^{\ddagger}/\bar{V}$ occurs (2500 atmos) a point is reached where

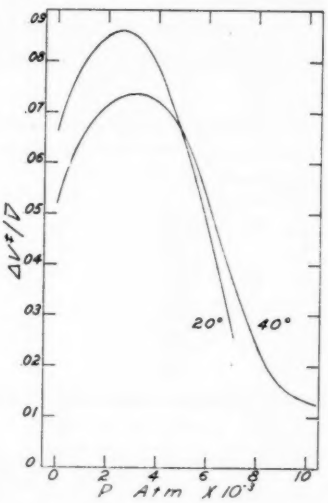

FIG. 7. Activation volume *versus* pressure. System: CS_2-2,4 dimethylpentane.

further compression strengthens the structure to such an extent that it will not yield easily and the activation volume begins to decrease as the diffusion takes place more and more through existing holes. The "stable" (stable in the sense that the most probable configuration does not vary greatly with pressure) structure of the i-C_7 is formed much more slowly with pressure than is that of the normal isomer. Thus, the limitations imposed upon the degrees of freedom of an activated molecule by the i-C_7 structure do not increase as rapidly with pressure as does the degree of order in the normal state until a much higher pressure is reached (5000 atmos). This is why the activation entropy continues to increase with pressure in the range 2500 to 5000 atmos even though diffusion is taking place more and more through existing holes and the activation volume is decreasing.

CARBON DISULFIDE IN TOLUENE

The logarithm of the diffusion coefficient for carbon disulfide in toluene is plotted as a function of pressure

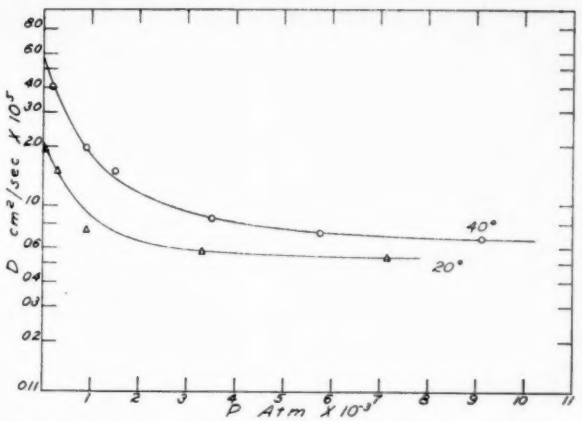

FIG. 8. Diffusion coefficient *versus* pressure. System: CS_2-toluene.

along 20 and 40°C isotherms in Fig. 8. The atmospheric pressure D at 40° is relatively high, 5.6×10^{-5} cm²/sec as compared with 4.6×10^{-5} for the three systems previously discussed (pure CS_2,[1] n-C_7-CS_2, i-C_7-CS_2) but drops off very rapidly with increasing pressure. At 3500 atmos the value is 0.85×10^{-5}, and with further compression it levels to become asymptotic to about 0.65×10^{-5}. With the initial application of pressure the toluene molecules, which are known to exist in the solid as flat plates, immediately begin to orient and impede diffusion of CS_2. As the solution is further compressed the orientation of the toluene structure increases until finally a configuration is reached wherein further compression does not alter the rate of CS_2 migration through holes in the toluene "lattice." The packing in the toluene is probably made up of flat molecular plates oriented parallel to each other. Once this configuration has been achieved, further compression will not appreciably alter it except that the distance between layers of plates may be decreased.

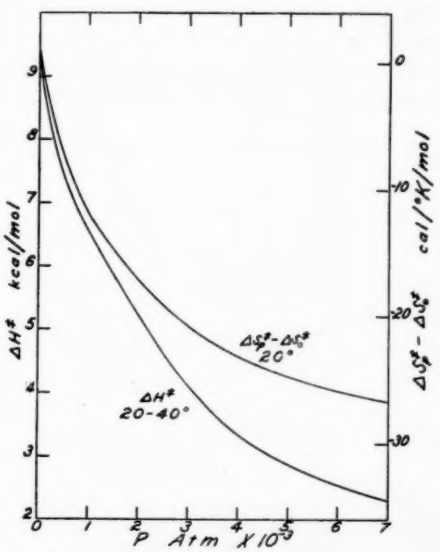

FIG. 9. Enthalpy and entropy of activation *versus* pressure. System: CS_2-toluene.

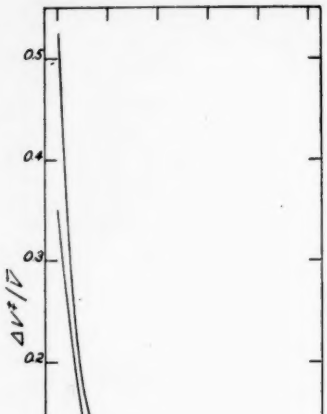

FIG. 10. Activation volume *versus* pressure. System: CS_2-toluene.

Compressibility data were not available for toluene. It was assumed that the compressibility of toluene would vary with pressure similarly to that for chlorobenzene, and also that its value at atmospheric pressure would be the same as the value for benzene. Since data are available for benzene and chlorobenzene,[6] the toluene compressibility was estimated on the basis of these two assumptions.

The change in activation entropy with pressure is plotted as a function of pressure in Fig. 9. The activation entropy decreases rapidly at first and then more slowly as pressure is increased. At 7000 atmos it is 26.7 cal/°K/mole less than the value at atmospheric pressure. The continual decrease of $\Delta S^{\ddagger}$ indicates that the restrictions imposed by the toluene on the most favorable orientation of an activated molecule are increasing at a rate greater than the rate at which the degrees of freedom of a molecule in the normal state are decreasing. The leveling of the curve of $\Delta S_P^{\ddagger} - \Delta S_0^{\ddagger}$ in the high pressure range indicates that the toluene lattice (i.e., the most probable configuration at any time) is virtually stabilized and further compression does not appreciably alter the relative entropy levels of a molecule of CS_2 in the initial and activated states.

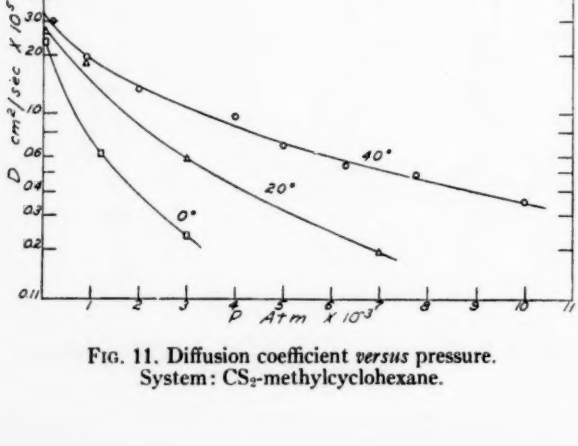

FIG. 11. Diffusion coefficient *versus* pressure. System: CS_2-methylcyclohexane.

$\Delta H^{\ddagger}$ is shown graphically as a function of pressure in Fig. 9. Similarly to the entropy of activation, it decreases rapidly with increasing pressure at first and then slowly begins to level off. At 7000 atmos $\Delta H^{\ddagger}$ is 2.3 kcal/mole. The high value of the heat of activation at atmospheric pressure indicates that the process of activation involves a considerable distortion of the structure in the low pressure area. Since this is the case, then it must also follow that the entropy of the activated state must be greater than that of the normal state; that is, an activated molecule has gained degrees of freedom over one in the initial state. Therefore, the assumption of an essentially zero entropy of activation at atmospheric pressure is probably not applicable to this system.

An inspection of the curve of $\Delta V^{\ddagger}/\bar{V}$ plotted as a function of pressure in Fig. 10 substantiates the deduction that activation at atmospheric pressure involves a considerable distortion of the liquid structure. The activation volume is 50 percent of the molal volume at 40°C and 1 atmos. It decreases at an extremely high rate with pressure to 18 percent at 1000 atmos and only 5 percent of the molal volume at 3500 atmos. Beyond 6000 atmos at 40° and 4500 atmos at 20°, the activation volume is constant at less than one percent of the molal volume. Allowing for errors in the calculations, the truth is probably that both isotherms level to a value of zero. Thus, it is seen that over the pressure range studied, the process of activation changes from being predominately one of structure deformation and hole formation to being mostly a matter of selecting favorably oriented molecules to diffuse through existing holes.

TABLE XII. $\Delta F^{\ddagger} - \Delta F_0^{\ddagger}$ for CS_2 in toluene at 20°C.

P (atmos)	$\Delta F^{\ddagger} - \Delta F_0^{\ddagger}$ (cal/mole)
500	293
1000	484
2000	633
3000	689
4000	712
5000	719
6000	721
7000	721

The change in the free energy of activation with pressure is quite small and $\Delta F^{\ddagger}$ becomes constant beyond 3000 atmos at 20°C. Values of $\Delta F^{\ddagger} - \Delta F_0^{\ddagger}$ are given in Table XII.

It was pointed out above that the assumption of a zero value for the entropy of activation at atmospheric pressure is probably not valid for this system. Thus, it is

impossible to estimate $\Delta F_0^{\ddagger}$. However, the constant value of $\Delta F^{\ddagger} - \Delta F_0^{\ddagger}$ is only 7.7 percent of $\Delta H_0^{\ddagger}$. ($\Delta H_0^{\ddagger} = 9400$ cal/mol.)

CARBON DISULFIDE IN METHYLCYCLOHEXANE

Three isotherms, 0°, 20° and 40°C, of D as a function of P are shown in Fig. 11.

In the previous discussion we assumed toluene molecules to exist in solution as flat plates. Cyclohexane is commonly throught to exist in one or the other of the familiar "chair" or "boat" forms. For this discussion, however, we shall assume only that the MCH molecule is a puckered type ring with one methyl group attached.

The atmospheric pressure diffusion coefficient for CS_2 in MCH at 40° is only 3.3×10^{-5} cm²/sec as compared with 5.6×10^{-5} in toluene. Thus, it is apparent that the puckered MCH ring inhibits migration of CS_2 at atmospheric pressure to a greater extent than does the flat toluene ring. The changes in diffusion mechanisms and structure which take place with increasing pressure can best be described for this system by considering the changes in activation enthalpy, entropy, and volume simultaneously. These variables have been calculated and are plotted as a function of pressure in Figs. 12 and 13.

TABLE XIII. $\Delta F_P^{\ddagger} - \Delta F_0^{\ddagger}$ for CS_2 in methylcyclohexane at 20°C.

P (atmos)	$\Delta F_P^{\ddagger} - \Delta F_0^{\ddagger}$ (cal/mole)
1000	360
2000	645
3000	865
5000	1210
7000	1475

The high value of the activation volume at atmospheric pressure, 20 percent of the molal volume at 40°C, indicates that there is a high degree of distortion and local expansion during activation for diffusion. As pressure is increased above atmospheric the activation volume decreases rapidly while $\Delta H^{\ddagger}$ and $\Delta S^{\ddagger}$ both increase at a high rate. The MCH molecules must tend to restrict or "trap" CS_2 molecules so that their entropy in the normal state becomes very low. Thus, we find that as the force fields are intensified (pressure increased) diffusion takes place more and more through existing holes, so that $\Delta V^{\ddagger}/\bar{V}$ decreases while the activation entropy increases because of the increasing order of the normal state. It must be assumed that in the lower pressure range (where $\Delta S^{\ddagger}$ is increasing rapidly) there are a sufficient number of holes available so that the probability of a molecule entering the activated state does not depend greatly upon its orientation. This mechanism becomes continually more prominent with pressure and gradually the number and size of holes is decreased so that certain orientations of the CS_2 molecule have a higher probability of migration than others. Thus, the entropy of the activated state begins to decrease and we find $\Delta S^{\ddagger} - \Delta S_0^{\ddagger}$ beginning to level. Beyond 4000 to 5000 atmos the ratio of the activation volume to the molal volume levels to become virtually constant at 0.07 at 20° and 0.04 at 40°. $\Delta S^{\ddagger}$ and $\Delta H^{\ddagger}$ also begin to level beyond this range and increase only slowly up to 7000 atmos. By comparison with the previous systems discussed it is anticipated that at some pressure beyond the range of our calculations $\Delta S_P^{\ddagger} - \Delta S_0^{\ddagger}$ would go through a maximum and then become asymptotic to some lower value.

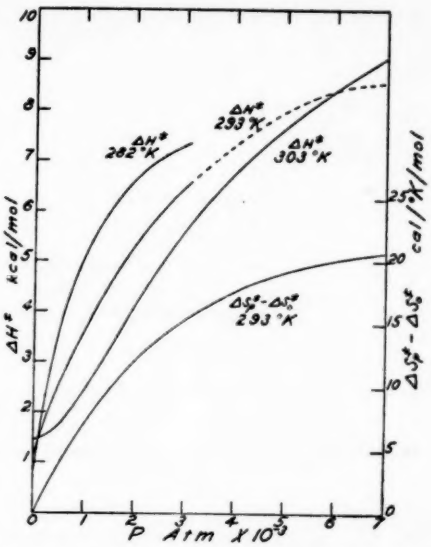

FIG. 12. Enthalpy and entropy of activation *versus* pressure. System: CS_2-methylcyclohexane.

We have consistently interpreted a decreasing activation entropy to mean that the packing of the organic molecules is ordered to such an extent that the probability of a CS_2 molecule becoming activated depends, with increasing pressure, more and more upon its

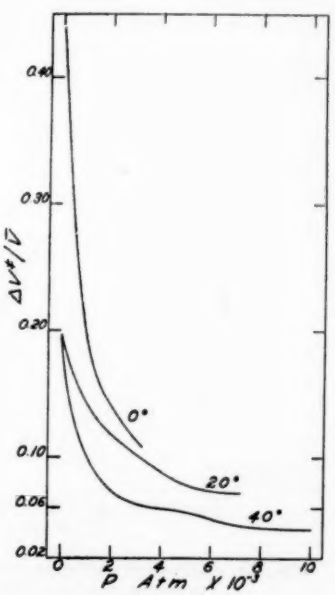

FIG. 13. Activation volume *versus* pressure. System: CS_2-methylcyclohexane.

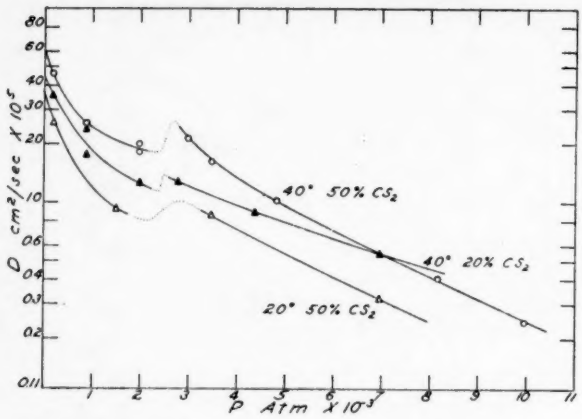

FIG. 14. Diffusion coefficients as a function of pressure. System: CS_2-chlorobenzene.

orientation. Or, in other words, that the hydrocarbon "lattice" has become a dominant factor. In toluene this situation was seen to exist over the entire pressure range. For CS_2 in n-C_7 it became prominent at 2800 atmos, while in i-C_7 the activation entropy did not begin to decrease until after 5000 atmos. For this system (MCH), although $\Delta S^\ddagger$ begins to level it is not seen to decrease in 7000 atmos. One might conclude then that for these four 7-carbon hydrocarbons, toluene molecules are the most easy to "align" with pressure, n-C_7 and i-C_7 are next in that order, with MCH being the most difficult.

The change in the free energy of activation from that at atmospheric pressure was calculated on the basis of the expression $\Delta F = \Delta H - T\Delta S$. From the values tabulated in Table XIII it is apparent that the free energy of activation is decidedly not constant with pressure, but

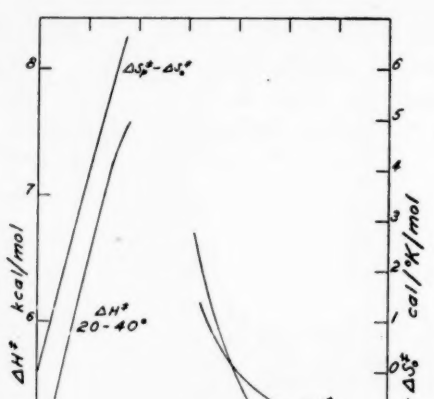

FIG. 15. Activation enthalpy and entropy as a function of pressure. System: CS_2-chlorobenzene.

rather, increases continuously. If it is valid to assume for this system that the entropy of activation is zero at 1 atmos, then $\Delta F_0^\ddagger = \Delta H_0^\ddagger = 1130$ cal/mole and the total increase in $\Delta F^\ddagger$ is 130 percent in 7000 atmos. However, in view of the high activation volume at 1 atmos it is probably not permissible to assume $\Delta S^\ddagger = 0$.

CARBON DISULFIDE IN CHLOROBENZENE

The diffusion coefficient was determined for carbon disulfide in two concentrations with chlorobenzene (PhCl). Two isotherms, 20 and 40°C, were obtained for a 50 mol percent solution and one 40°C isotherm was run for a solution of 20 mole percent CS_2 in PhCl. These data are plotted as a function of P in Fig. 14. The curves in this graph are immediately seen to be quite different from those previously discussed in that they show a discontinuity in the 2000 to 3000 atmos range. Below 2000 atmos and above 3000 atmos the isotherms appear to be quite normal. While the data were being obtained several attempts were made to determine D in the 2000 to 3000 atmos span, but reproducible results could not be obtained. It became apparent that some sort of structure transition takes place in this range which is extremely sensitive to pressure. Bridgman[7] observed anomalous behavior on the part of PhCl in making determinations of freezing parameters for the compound. He concluded that there exists a second solid form which replaces the ordinary form as the absolutely stable one at high temperatures (125°C and above). At lower temperatures the liquid shows a tendency to not freeze on passing the normal melting line but to freeze instead to the new form when the unstable melting line of the new form is reached. This new form is unstable with respect to the normal form and may or may not arbitrarily "flop" irreversibly to the ordinary stable form. Bridgman found the appearance of such "flopping" to be quite unpredictable. The unstable form appeared at temperatures as low as 25°C, at which temperature the equilibrium pressure is 5000 atmos. There is no reason to believe that the discontinuity we observe in the ln$D$ isotherms is due to any sort of freezing phenomenon; to the contrary, the diffusion coefficient on either side of the discontinuity is of the order of magnitude we expect in liquids.

Inspection of the curves of $\Delta S^\ddagger - \Delta S_0^\ddagger$, $\Delta H^\ddagger$, and $\Delta V^\ddagger/\bar{V}$, plotted as a function of pressure in Figs. 15 and 16, using the compressibility data of Bridgman[6] shows that, in the low pressure range before the discontinuity, they are similar to those for methylcyclohexane in the same pressure range. The activation volume drops rapidly from about 44 percent of the molal volume at atmospheric pressure to about 5 percent at 2000 atmos. Both the 20 and 40° isotherms show changes of the same order of magnitude. At the same time the average activation enthalpy increases, virtually linearly, from 4.8 to about 7.8 kcal/mole, while $\Delta S^\ddagger$ also increases

[7] P. W. Bridgman, Proc. Amer. Acad. Arts Sci. **74**, 1, 399 (1940).

linearly to 7 cal/°K/mole above its value at 1 atmos and 20°C. As in the case of MCH there is a high degree of structure distortion and local expansion at atmospheric pressure as shown by the large activation volume. The diffusion coefficient and $\Delta V^{\ddagger}/\bar{V}$, at 1 atmos are about twice as great in PhCl as they are in MCH and $\Delta H^{\ddagger}$ is a factor of 3.5 greater in the PhCl. The higher D and $\Delta V^{\ddagger}/\bar{V}$ indicate that the PhCl presents a structure at atmospheric pressure more susceptible to deformation than does the MCH.

As was the case with methylcyclohexane, the shape of the force fields associated with the chlorobenzene molecules must be such that decreasing the free volume leaves holes large enough for CS_2 diffusion. Thus, we find that as pressure is increased from one atmosphere, diffusion takes place more and more through these holes and the activation volume decreases. The holes must be of such number and shape that the probability of a CS_2 molecule becoming activated does not depend upon its orientation. This being the case, the entropy level of the activated state must not decrease as rapidly as does that of the initial state (which decreases due to the increasing order imposed by the decreasing free volume) for we find

TABLE XIV. $\Delta F^{\ddagger}-\Delta F_0^{\ddagger}$ for CS_2 in chlorobenzene at 20°C.

P (atmos)	$\Delta F^{\ddagger}-\Delta F_0^{\ddagger}$ cal/mol
500	410
1000	636
1750	812
3250	759
4000	893
5000	1050
7000	1340

the activation entropy increasing. This situation becomes increasingly predominant with pressure, at least as far as 2000 atmos.

There is undoubtedly some sort of radical structure transition which takes place in the 2000 to 3000 atmos range. We do not have sufficient data, however, to attempt an explanation.

Compressing beyond the transition range we find that the activation volume decreases rapidly to become constant at 9 percent of the molal volume at 20°C. The constant value of $\Delta V^{\ddagger}/\bar{V}$ at 40° is 10 percent. We also find $\Delta H^{\ddagger}$ and $\Delta S^{\ddagger}$ decreasing rapidly at first and then more slowly so that at 7000 atmos $\Delta H^{\ddagger}=5$ kcal/mole and $\Delta S^{\ddagger}-\Delta S_0^{\ddagger}=-3.8$ cal/°K/mole.

In conformance with arguments presented for the previously discussed systems, we conclude that these changes in $\Delta H^{\ddagger}$, $\Delta S^{\ddagger}$, and $\Delta V^{\ddagger}/\bar{V}$ indicate that the manner and amount by which the free volume has been decreased are such that a PhCl packing is forming with increasing pressure. As a consequence of this configuration, there is an increasing resistance to deformation and diffusion of CS_2 takes place more and more through existing holes. In addition, the number of available

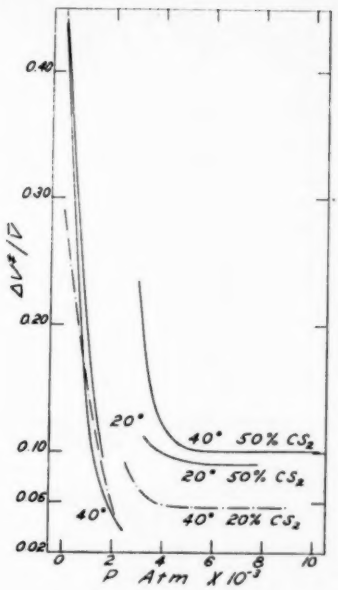

FIG. 16. Activation volume as a function of pressure. System: CS_2-chlorobenzene.

holes are limited so that the probability of a molecule entering the activated state is becoming more and more a function of its orientation. Thus, we see that $\Delta V^{\ddagger}/\bar{V}$ rapidly becomes constant and that the entropy of activation drops to a low level and appears to be approaching an asymptote.

The preceding discussion applies equally well to the diffusion of CS_2 in both 20 and 50 mole percent solutions of PhCl. The differences observed between the two concentrations are of degree rather than of kind. In the range below 2000 atmos the isotherms of $\Delta V^{\ddagger}/\bar{V}$ are the same for both concentrations within the accuracy of the data. The diffusion coefficient at 40°C in the 20 percent solution is lower than that in the 50 percent solution with its isotherm falling about half-way between the 20 and 40° isotherms for the more concentrated solution. Above 3000 atmos the ratio $\Delta V^{\ddagger}/\bar{V}$ becomes constant at a lower pressure in the dilute solution but at a lower value; 5.5 percent of the molal volume as compared to 10 percent in the 50 percent solution. The fact that the

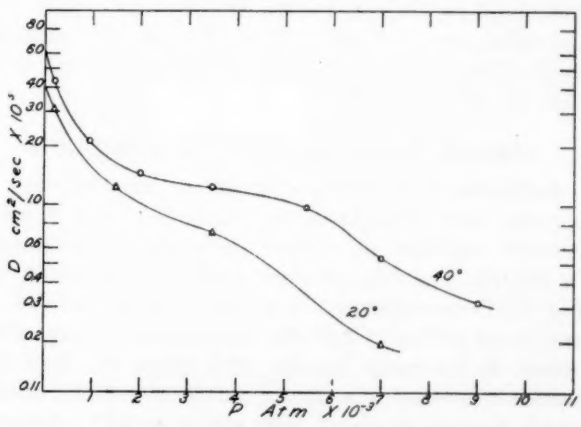

FIG. 17. Diffusion coefficients as a function of pressure. System: CS_2-n-butanol.

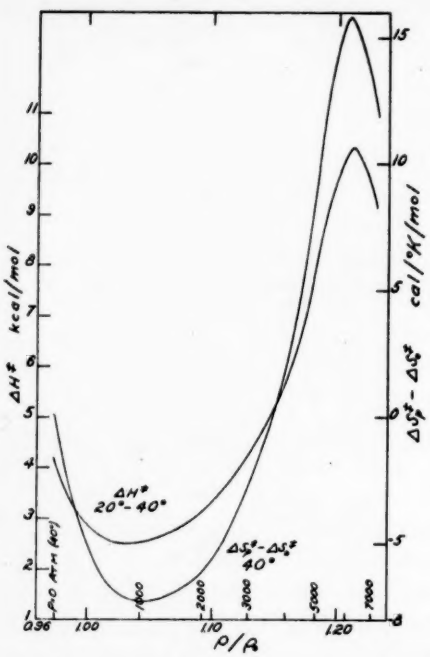

FIG. 18. Activation enthalpy and entropy as a function of reduced density. System: CS_2-*n*-butanol.

ratio $\Delta V^{\ddagger}/\bar{V}$ is constant at a lower pressure in the 20 percent solution indicates that the "stable" structure is more easily formed when there is less CS_2 present.

From the relationship

$$\Delta F = -T\Delta S + \Delta H$$
$$= -T\Delta S + \Delta H,$$

one might expect $\Delta F^{\ddagger}$ to be constant because of the close correspondence observed between changes in $\Delta H^{\ddagger}$ and in $\Delta S^{\ddagger}$. This is not the case, however, as can be seen from the values of $\Delta F^{\ddagger} - \Delta F_0^{\ddagger}$ tabulated in Table XIV below. In view of the high activation volume at one atmosphere it is probably not valid to assume $\Delta S_0^{\ddagger} \cong 0$ and set $\Delta F_0^{\ddagger} = \Delta H_0^{\ddagger}$. However, it is interesting to note that the maximum increase in the free energy of activation in 7000 atmos is only 28 percent of $\Delta H_0^{\ddagger}$ ($\Delta H_0^{\ddagger} = 4760$ cal/mole). Although $\Delta F_0^{\ddagger}$ rises over the entire pressure range, it does reflect the discontinuity in the 2000 to 3000 atmos span; but to a lesser extent than do $\Delta H^{\ddagger}$ and $\Delta S^{\ddagger}$.

CARBON DISULFIDE IN NORMAL BUTANOL

Isotherms of the diffusion coefficient as a function of pressure were determined at 20 and 40°C in a 50 mole percent solution of carbon disulfide in *n*-butanol (*n*-BuOH). The data obtained are shown graphically in Fig. 17. Both isotherms are similar in shape and show a very rapid decline of ln$D$ with pressure up to about 2000 atmos. In the range beyond 2000 atmos the slope decreases considerably so that a partial plateau is formed which extends to about 5500 atmos at 40°C. Beyond 5500 atmos ln$D$ drops off steadily with pressure. The 20° isotherm does not definitely show a plateau; however, the second derivative of ln$D$ with respect to P does pass through zero. From the shape of these isotherms it appears that the structure is being rapidly altered to cause a large decline in D in the region below 2000 atmos. The structure then becomes relatively unaffected by pressure and remains so until about 5500 atmos (at 40°). At this point the decreasing free volume again becomes important and D decreases with pressure. One might expect that the alcohol is associated, but no attempt will be made to consider this in the interpretation of the data since neither the degree nor the effects of association are known.

The change in activation entropy from that at atmospheric pressure is plotted as a function of the reduced density, ρ/ρ_0, in Fig. 18. The reduced density is the ratio of the density at any given pressure and temperature to that at 20°C and 1 atmos. Pressure is indicated along the abscissa to facilitate discussion of the curves. The activation enthalpy is plotted on the same graph for a similar reason. In this graph we can see both $\Delta H^{\ddagger}$ and $\Delta S^{\ddagger}$ dropping rapidly with the initial application of pressure. $\Delta S^{\ddagger} - \Delta S_0^{\ddagger}$ reaches a minimum of about 7 cal/°K/mol below that at 1 atmos (40°C) and at the same time $\Delta H^{\ddagger}$ falls from 4.1 to a minimum of 2.5 kcal/mol. Both minima are at about 1000 atmos. Compressing beyond 1000 atmos we find both entities increasing rapidly to a sharp maximum at 6000 atmos. At this point the activation enthalpy is 10.3 kcal/mole and the activation entropy has risen to 15.8 eu above its value at one atmos.

The ratio of the activation volume to the molal volume is shown plotted as a function of the reduced density in Fig. 19. At one atmos and 40° the activation volume is 55 percent of the molal volume, and 43 percent at 20°. Both isotherms drop rapidly to minima of 7

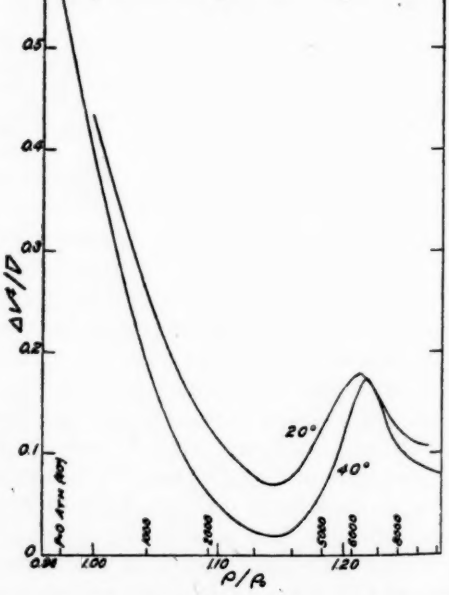

FIG. 19. Activation volume as a function of reduced density. System: CS_2-*n*-butanol.

percent at 20° and 3.5 percent at 40° at a pressure of about 3000 to 3500 atmos and then begin to increase again. A maximum of about 18 percent of the molal volume at 6000 atmos is shown at both temperatures.

Before carrying on with the discussion the reader is referred back to the curves of $\ln D$ *vs* P in Fig. 17. In drawing the curves it was reasonable that the 40° isotherm should be made a smooth curve through the experimental points and also, from observation of other systems, that the 20° isotherm should have a similar shape. However, the shapes of both curves could vary somewhat within the range of experimental error. $\Delta V^\ddagger/\bar{V}$, $\Delta H^\ddagger$, and $\Delta S^\ddagger - \Delta S_0^\ddagger$ vary critically with the slope of, and displacement between, the isotherms. Thus, it is felt that the maxima observed in these quantities at 6000 atmos may very well be a function of the manner in which the isotherms were drawn, within experimental error. No significance will be attached to these maxima without further proof of their existence. Similarly, the minima in $\Delta S^\ddagger - \Delta S_0^\ddagger$ and $\Delta H^\ddagger$ at 1000 atmos are open to doubt, and it is equally reasonable to assume that both of these variables rise continuously with pressure; the rise is very gradual in the low pressure range (up to about 2000 atmos).

TABLE XV. $\Delta F^\ddagger - \Delta F_0^\ddagger$ for CS_2 in *n*-BuOH at 40°C.

P (atmos)	$\Delta F^\ddagger - \Delta F_0^\ddagger$ (cal/mole)
500	449
1000	680
2000	831
3000	953
5000	1014
7000	1437

The high value of the activation volume at atmospheric pressure indicates that a high degree of distortion and local expansion accompany the activation process. The decline in $\Delta V^\ddagger/\bar{V}$ can be interpreted to mean that the entropy level of the activated state is decreasing; that is, its degree of order is increasing. If $\Delta S^\ddagger$ increases continually from one atmosphere, then we must conclude that the entropy of the initial state decreases faster than does that of the activated state.

The rapid decline of the diffusion coefficient in the low pressure range indicates that the free volume is rapidly being taken up. Finally, as the 3000- to 3500-atmos range is reached, the free volume has been decreased by a sufficient amount, and in such a manner that a minimum is observed in the activation volume. Beyond this point the local expansion necessary for activation begins to be felt throughout a greater portion of the fluid due to the compactness of the packing. As is anticipated, the entropy of the activated state begins to rise more rapidly as shown by the sharp increase of $\Delta S^\ddagger - \Delta S_0^\ddagger$ in this range.

If we accept the validity of the maxima observed in $\Delta H^\ddagger$, $\Delta S^\ddagger - \Delta S_0^\ddagger$, and $\Delta V^\ddagger/\bar{V}$ at 6000 atmos, they may be interpreted as follows: A *n*-BuOH "lattice" formation slowly takes place with increasing pressure. In the 6000-atmos range this packing is such that a CS_2 molecule has a higher probability of entering the activated state from certain orientations than from others. Thus, we find that beyond this range D begins to decrease more rapidly; the activation volume decreases because the structure resists deformation to a greater extent and diffusion takes place more and more through existing holes; and the activation entropy decreases because the entropy of the activated state decreases (certain orientations favored over others for activation).

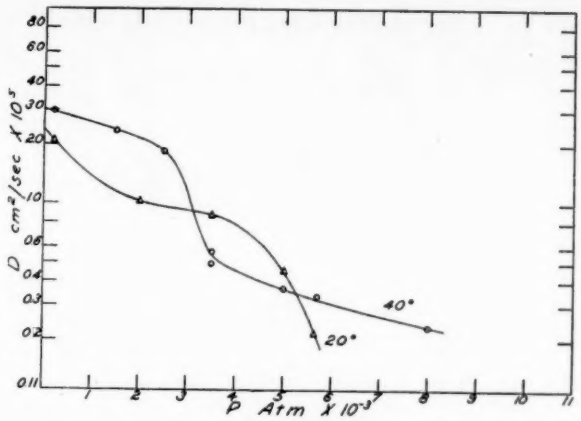

FIG. 20. Diffusion coefficients as a function of pressure. System: CS_2-*i*-butanol.

We have observed in the data for this system the usual correspondence between $\Delta H^\ddagger$ and $\Delta S^\ddagger$. The change in the free energy of activation at various pressures from that at one atmosphere is tabulated in Table XV. $\Delta F^\ddagger$ is seen to rise continuously with pressure; its value at 7000 atmos is 35 percent of $\Delta H_0^\ddagger$.

CARBON DISULFIDE IN ISO-BUTANOL

The isotherms of $\ln D$ as a function of P for a 50 mole percent solution of carbon disulfide in iso-butanol (*i*-BuOH) are shown in Fig. 20. The uniqueness of the data for this system as compared to that for the other systems is immediately obvious upon inspection of the

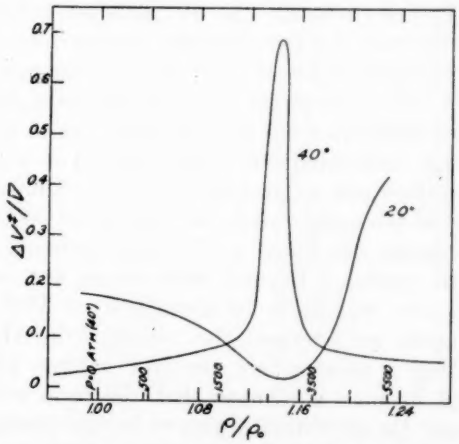

FIG. 21. Activation volume as a function of reduced density. System: CS_2-*i*-butanol.

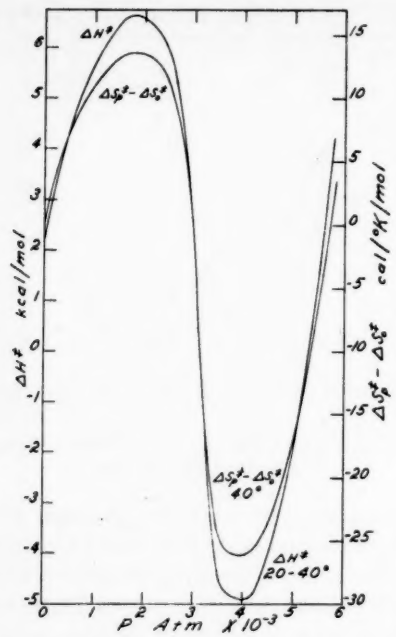

FIG. 22. Activation entropy and enthalpy as a function of reduced density. System: CS_2-*i*-butanol.

graph. The 20° isotherm is quite similar to the isotherms obtained for CS_2 in *n*-BuOH in that ln$D$ drops rapidly at first, settles to a partial plateau, and then continues to decline with pressure. The 40° isotherm, however, shows ln$D$ to decrease only slowly with pressure up to 2500 atmos. Between 2500 and 3500 atmos D drops radically by a factor of three and then settles to once again decline slowly with pressure. The two isotherms cross at 3100 and 5250 atmos so that in this range D is actually less at 40° than at 20°C. The experimental points are such that there can be no question but what this is the true situation. It might be the case that the alcohol is associated but no attempt will be made to consider this in the interpretation of the data since neither the degree nor effects of association are known.

The activation volume for both the 20 and 40° isotherms is plotted as $\Delta V^{\ddagger}/\bar{V}$ *versus* reduced density in Fig. 21. The curve for the 20° isotherm is similar in nature to those for the *n*-BuOH isotherms and can be analyzed in the same manner. That is, the moderately high $\Delta V^{\ddagger}/\bar{V}$ at one atmosphere (18 percent of the molal volume) indicates a fair amount of distortion and local expansion associated with activation. The activation volume decreases continuously until a minimum of 2 percent of the molal volume is observed at 3000 atmos. (A minimum was found at this same pressure for the *n*-BuOH system.) Beyond 3000 atmos the ratio increases very rapidly to be about 0.40 at 5500 atmos. Here again we interpret the minimum in $\Delta V^{\ddagger}/\bar{V}$ as indicating a point where the free volume has been reduced in such a manner that the local expansion necessary for activation begins to be felt throughout a greater portion of the fluid.

At 40° the atmospheric pressure activation volume is very low (2 percent of the molal volume). It increases very gradually with pressure to 9 percent at 2000 atmos, rises sharply to a peak of 69 percent at 3200 atmos, and then drops to 9 percent again at 4000 beyond where it decreases but gradually with pressure. The very low initial value of $\Delta V^{\ddagger}/\bar{V}$ indicates that, as in the case of *n*-C_7, the structure is initially very loose and permits activation with only a small amount of local expansion. Further, it must be the case that the molecular orientations and free volume are such that increasing pressure causes the local expansion for activation to be more generally felt throughout the liquid and the activation volume increases. It is certainly obvious that radical changes in structure must take place in order to cause the peak in $\Delta V^{\ddagger}/\bar{V}$ at 3200 atmos. With the limited data we have at this time, however, it would be pure conjecture to attempt to analyze the situation. In previous systems we have interpreted a decreasing activation volume in the high pressure range as indicating that an organic packing had been formed to such a degree that certain CS_2 orientations were preferred for activation and that migration took place more and more through existing holes. In conformance then, we must assume that the same situation prevails in this system after $\Delta V^{\ddagger}/\bar{V}$ passes through its peak and settles again to slowly decrease with pressure.

TABLE XVI. $\Delta F^{\ddagger}-\Delta F_0^{\ddagger}$ for CS_2 in *i*-BuOH at 40°C.

P (atmos)	$\Delta F^{\ddagger}-\Delta F_0^{\ddagger}$ (cal/mole)
1000	66
2000	178
3000	543
3500	973
4500	1170
5750	1310

The curves of activation enthalpy and the change in activation entropy are plotted as a function of pressure in Fig. 22. The activation enthalpy (the most important factor in determining $\Delta S^{\ddagger}-\Delta S_0^{\ddagger}$) was calculated as an average value between the 20 and 40° isotherms of ln$D$ *vs* P. Since these isotherms are so very dissimilar, it is doubtful whether information obtained from the curves of $\Delta H^{\ddagger}$ and $\Delta S^{\ddagger}-\Delta S_0^{\ddagger}$ is applicable to either isotherm. The only definite point to be observed is that the activation enthalpy is negative in the range 3100 to 5250 atmos. It is difficult to imagine what type of activation mechanism could have a negative activation enthalpy associated with it. It is apparent from the isotherms of ln$D$ *vs* P that different types of structures must exist at the two temperatures. No attempt will be made to analyze the situation at this time.

It is of interest to note, in Table XVI, that in spite of the radical variations observed in the other variables for this system, the free energy of activation rises continually with pressure as for other systems studied.

R. C. Koeller would like to acknowledge financial assistance from the Pan American Refining Corporation and from the U. S Atomic Energy Commission.

The Effect of Pressure on Diffusion in Water and in Sulfate Solutions

R. B. CUDDEBACK, R. C. KOELLER, AND H. G. DRICKAMER*
Department of Chemistry, University of Illinois, Urbana, Illinois
(Received September 26, 1952)

Diffusion coefficients are presented as a function of pressure to 10 000 atmospheres for the following systems:

THO—H_2O 0°–25°–50°;
0.1 N $H_2S^{35}O_4$ —0.1 N H_2SO_4 0°–5°–25°–50°;
0.1 N $Na_2S^{35}O_4$—0.1 N Na_2SO_4 0°–25°–50°;
1.0 N $Na_2S^{35}O_4$—1.0 N Na_2SO_4 0°–25°–50°;
0.1 N $K_2S^{35}O_4$ —0.1 N K_2SO_4 0°–25°–50°.

The results are interpreted in terms of the activation volume and the tetrahedrally coordinated structure of water. It is found that pressure tends to break down the structure, and in certain regions an increase in diffusion coefficient with pressure is noted.

In the salt solutions the water structure is controlling with some added effects due to solvation and ionic interaction.

IN previous papers[1,2] a method for measuring diffusion in liquids under pressures to 10 000 atmospheres was presented, along with results for some organic solutions. In this paper results are presented for diffusion of tritiated water into ordinary water, for diffusion of S^{35} tagged 0.1 N sulfuric acid into untagged 0.1 N sulfuric acid, and for diffusion in 0.1 N Na_2SO_4, 1.0 N Na_2SO_4, and 0.1 N K_2SO_4. The tritiated water was obtained from Tracerlab, the S^{35} tagged H_2SO_4 from Oak Ridge National Laboratory of the U. S. Atomic Energy Commission. The ordinary water was de-ionized, and degassed water was obtained from the Boiler Water Laboratory by courtesy of F. G. Straub. The salts were cp quality.

The method of operation and for calculation of the diffusion coefficients is completely discussed in reference 1. The kinetic theory of liquids and the method for calculating the enthalpy of activation ($\Delta H^\ddagger$), the entropy of activation ($\Delta S^\ddagger$) above the value at atmospheric pressure ($\Delta S_0^\ddagger$), the activation volume ($\Delta V^\ddagger$), and the free energy of activation ($\Delta F^\ddagger$) are discussed in references 1 and 2.

The results will be discussed in terms of these concepts. The data are shown in Tables I–V.

SELF-DIFFUSION IN WATER

In Fig. 1 the diffusion coefficients are plotted against density using Bridgman's[3] compressibility data. The excellent agreement with the data of Orr and Butler[4] at atmospheric pressure is to be noted. As a matter of fact, the fritted glass was calibrated using their data at 25°C. Since each isotherm has a unique shape, it is apparent that the molecular geometry and mechanisms of motion depend upon more than merely density. This system will be analyzed primarily on the basis of changes in the activation volume. The activation volume is purely a function of a single isotherm, whereas $\Delta H^\ddagger$ and $\Delta S^\ddagger$ depend upon the displacements between the three isotherms. The structure obviously varies radically with temperature and thus $\Delta H^\ddagger$ and $\Delta S^\ddagger$ calculated on the basis of the three isotherms probably do not apply to any of them.

TABLE I. Measured diffusion coefficients for THO in H_2O.[a]

Temp. °K	Pressure atmos	Effective cell length cm	Observed $D\times10^5$ cm²/sec
273	136	0.504	1.65
273	252	0.504	2.37
273	600	0.504	1.06
273	900	0.504	1.84
273	1240	0.504	1.45
273	2040	0.557	1.08
273	3500	0.557	0.787
273	5900	0.611	0.584
298	1	0.504	2.64
298	245	0.504	2.90
298	1300	0.504	3.24
298	2050	0.557	3.06
298	2500	0.557	3.04
298	3000	0.557	2.62
298	3000	0.557	2.36
298	3975	0.557	1.71
298	5000	0.557	1.15
298	7000	0.611	0.753
298	7000	0.611	0.843
298	9175	0.611	0.515
323	235	0.504	5.15
323	735	0.504	4.17
323	1300	0.504	3.48
323	2100	0.557	2.33
323	2500	0.557	1.86
323	2500	0.557	1.89
323	3500	0.557	1.82
323	4450	0.557	2.07
323	7000	0.611	2.25
323	10050	0.665	1.38

[a] Maximum deviation in reproducibility 10 percent. Average deviation 5 percent.

* This work was supported in part by the U. S. Atomic Energy Commission.

[1] R. C. Koeller and H. G. Drickamer, J. Chem. Phys. **21**, 267 (1953).

[2] R. C. Koeller and H. G. Drickamer, J. Chem. Phys. **21**, 575 (1953).

[3] P. W. Bridgman, *The Physics of High Pressure* (Macmillan Company, New York, 1931).

[4] W. J. C. Orr and J. A. V. Butler, J. Chem. Soc. (London) **1935**, 1273.

TABLE II. Measured diffusion coefficients for 0.1 N $H_2S^{35}O_4$ in 0.1 N H_2SO_4.[a]

Temp. °K	Pressure atmos	Effective cell length cm	Observed $D\times10^5$ cm²/sec
273	238	0.504	0.678
273	338	0.504	0.265
273	500	0.504	0.506
273	666	0.504	0.836
273	800	0.504	0.956
273	1340	0.504	0.764
273	1850	0.557	0.786
273	2500	0.557	0.656
273	4050	0.557	0.650
273	5500	0.611	0.415
278	100	0.504	1.05
278	250	0.504	0.940
278	303	0.504	0.741
278	355	0.504	0.956
278	515	0.504	1.38
278	1000	0.504	0.982
298	238	0.504	2.22
298	370	0.504	2.36
298	803	0.504	2.62
298	1000	0.504	2.47
298	3000	0.557	1.76
298	5000	0.557	1.13
298	6850	0.611	0.721
298	8500	0.611	0.502
323	524	0.504	3.20
323	1500	0.504	3.11
323	2050	0.611	2.67
323	3400	0.557	2.47
323	5100	0.611	1.66
323	6900	0.611	1.13
323	8900	0.665	0.806
323	10150	0.665	0.631

[a] Maximum deviation in reproducibility 10 percent. Average deviation 5 percent.

TABLE III. Diffusion coefficients, 0.1 N $Na_2S^{35}O_4-0.1$ N Na_2SO_4.[a]

Temp. °K	Pressure atmos	Effective cell length cm	Observed $D\times10^5$ cm²/sec
273	100	0.548	0.99
273	238	0.548	0.91
273	377	0.548	0.59
273	510	0.548	1.08
273	652	0.548	0.84
273	803	0.548	0.69
273	1304	0.548	0.72
273	1650	0.617	0.65
273	2050	0.617	0.54
273	4000	0.617	0.49
273	6000	0.676	0.47
298	1	0.676	1.41
298	252	0.548	1.58
298	640	0.548	1.92
298	1200	0.548	2.18
298	1900	0.617	2.89
298	2500	0.617	1.92
298	4550	0.617	1.16
298	6525	0.676	1.27
298	9000	0.676	0.96
323	120	0.548	4.32
323	510	0.548	2.90
323	1005	0.548	2.25
323	1950	0.617	1.44
323	2500	0.617	1.43
323	3500	0.617	2.93
323	4500	0.617	1.75
323	7000	0.724	1.52
323	10500	0.724	1.30

[a] Maximum deviation in reproducibility 15 percent. Average deviation 5 percent.

TABLE IV. Diffusion coefficients, 1 N $Na_2S^{35}O_4-1$ N Na_2SO_4.[a]

Temp. °K	Pressure atmos	Effective cell length cm	Observed $D\times10^5$ cm²/sec
273	20	0.548	0.28
273	210	0.548	0.33
273	400	0.548	0.29
273	600	0.548	0.39
273	1000	0.548	0.56
273	1800	0.548	0.91
273	3050	0.617	0.55
298	34	0.548	0.90
298	238	0.548	1.01
298	238	0.548	0.86
298	605	0.548	0.76
298	1000	0.548	1.07
298	2000	0.617	1.60
298	3225	0.617	0.78
298	4500	0.617	1.03
298	6050	0.676	0.80
323	20	0.548	4.86
323	265	0.548	1.24
323	640	0.548	1.14
323	1000	0.548	1.34
323	2200	0.617	1.88
323	3000	0.617	2.24
323	3000	0.617	2.27
323	4050	0.617	1.46
323	5100	0.617	1.26
323	6550	0.724	1.81
323	6950	0.676	1.54
323	10000	0.724	1.25

[a] Maximum deviation in reproducibility 15 percent. Average deviation 5 percent.

TABLE V. Diffusion coefficients, 0.1 N $K_2S^{35}O_4-0.1$ N K_2SO_4.[a]

Temp. °K	Pressure atmos	Effective cell length cm	Observed $D\times10^5$ cm²/sec
273	10	0.548	0.33
273	100	0.548	0.67
273	265	0.548	0.71
273	390	0.548	0.50
273	415	0.548	0.40
273	600	0.548	0.90
273	775	0.548	0.86
273	1060	0.548	0.83
273	1800	0.548	0.82
273	3075	0.617	0.66
298	100	0.548	1.40
298	252	0.548	0.98
298	258	0.548	1.04
298	610	0.548	1.30
298	610	0.548	1.44
298	1000	0.548	0.90
298	1210	0.548	0.84
298	1900	0.548	1.17
298	2850	0.617	1.59
298	3800	0.617	0.82
298	4650	0.617	0.87
323	100	0.548	3.92
323	230	0.548	2.48
323	1000	0.548	0.87
323	1500	0.548	0.75
323	1970	0.548	1.46
323	3000	0.617	2.06
323	4050	0.617	2.37
323	4950	0.617	1.44
323	6550	0.676	1.04
323	10250	0.724	0.58

[a] Maximum deviation in reproducibility 10 percent. Average deviation 5 percent.

From spectroscopic, dielectric, and x-ray diffraction studies, the modern view of water is that it retains the tetrahedrally coordinated structure of ice to a degree that decreases with increasing temperature. The molecules tend to arrange themselves in a tetrahedral manner in the solid because of the particular distribution of valence forces about the molecule. Upon melting, the regular structure is not completely destroyed, but persists over regions including tens or hundreds of molecules with the membership of the groups continually changing. The oxygen atoms tend to coordinate an extra hydrogen so that "hydrogen bonds" are formed between molecules. These bonds are stronger than ordinary intermolecular attractive forces.

The ratio of the activation volume to the molal volume is plotted for the three isotherms studied in Fig. 2. The compressibility data of Bridgman[3] was used. The 25° isotherm of ln$D$ in Fig. 1 shows the D increases with the initial increase of pressure above atmospheric.

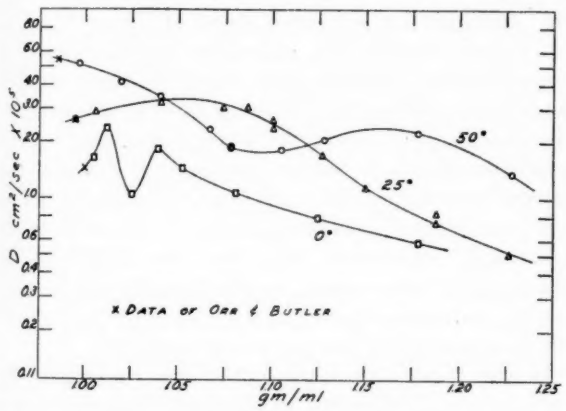

FIG. 1. Diffusion coefficients for the system THO–H_2O as a function of density.

This indicates that the tetrahedral structure in the water is broken down by pressure so that the average mobility of the molecules increases. The activation volume of 25° and 1 atmos is seen to be negative. From this we can conclude that the tetrahedral structure must be such that when a molecule migrates there is a localized collapse. As pressure is increased the percentage of molecules held in the characteristic tetrahedral structure apparently decreases and we find D slowly approaching a maximum while the activation volume approaches zero. Then, at the maximum in D (1500 atmos), $\Delta V^{\ddagger}/\bar{V}$ passes through zero. Further compression decreases D either because the tetrahedral structure is now completely destroyed, or because the effect of the increased compactness of the medium is greater than the influence of whatever remains of the structure. In any event, the activation volume increases because the local expansion necessary for activation is felt through a greater portion of the fluid as free volume is decreased. At 4000 atmos the slope of ln$D$ *vs* P begins to decrease rather than increase and $\Delta V^{\ddagger}/\bar{V}$ goes

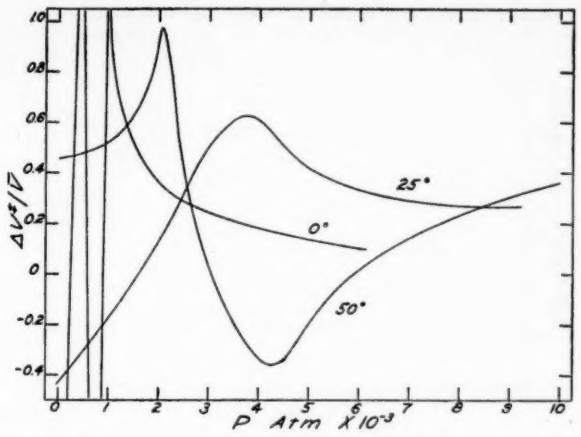

FIG. 2. Activation volume as a function of pressure. System: THO–H_2O.

through a maximum of 63 percent. The occurrence of this maximum and the relatively slow decrease of ln$D$ and $\Delta V^{\ddagger}/\bar{V}$ beyond it indicate that a stabilized structure is forming in the same sense that such structures were formed in the organic solutions.[1,2] That is, the configuration is becoming increasingly difficult to deform (either with increased pressure or during activation for diffusion), and diffusion takes place more and more through existing holes. Thus, we see that the activation volume settles down to approach an asymptote of about 25 percent of the molal volume.

Activation enthalpies are plotted *versus* pressure for 285, 298, and 310°K in Fig. 3. The change in activation entropy with pressure was calculated and is shown graphically in Fig. 4. The changes in $\Delta H^{\ddagger}$ and $\Delta S^{\ddagger}$ calculated for the 25° isotherm are probably reasonably correct since 25° is the median temperature. With the initial application of pressure the structure begins to be broken down to decrease the order and increase the entropy level of the normal state. Thus, we see that the activation entropy (the difference between entropy levels of the initial and activated states) decreases in this range to a minimum of 17 cal/°K/mole below that

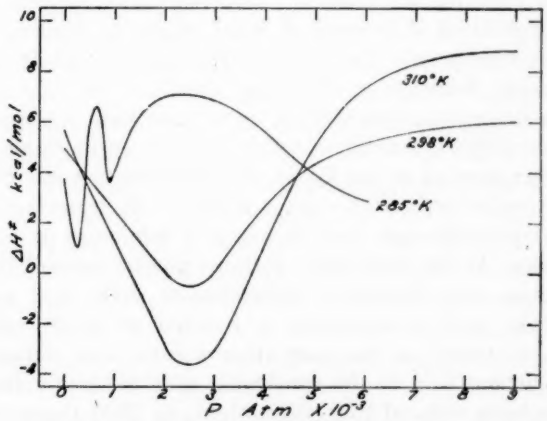

FIG. 3. Activation enthalpy as a function of pressure. System: THO–H_2O.

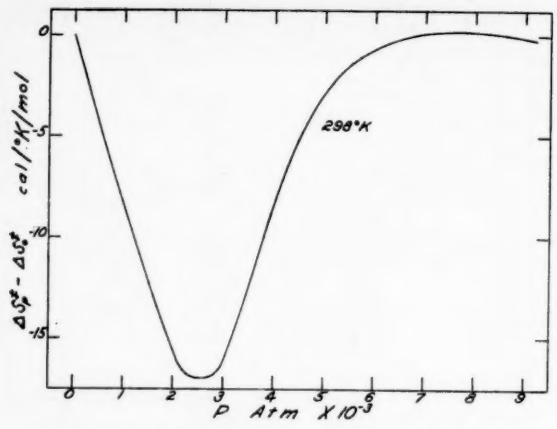

FIG. 4. Activation entropy as a function of pressure. System: THO–H_2O.

at 1 atmos. The minimum $\Delta S^{\ddagger}$ occurs in the same pressure region as does the zero activation volume. At this point the local expansion for activation becomes positive and the entropy of the activated state increases rapidly. The increase of $\Delta S^{\ddagger}$ continues (more gradually at higher pressure) until about 7000 atmos, where it levels to about the same value as at 1 atmos ($\Delta S_P^{\ddagger} - \Delta S_0^{\ddagger} \cong 0$). We saw above that the activation volume became virtually constant at this same pressure. The leveling of $\Delta S^{\ddagger}$ further substantiates the conclusion that a stabilized configuration has formed. Stabilized, that is, in the sense that the most probable configuration does not change greatly with pressure.

As a matter of general interest, $\Delta F_P^{\ddagger} - \Delta F_0^{\ddagger}$ was calculated at 25°. In Table VI below it is seen that the free energy of activation goes through a minimum at about 1500 atmos and then increases steadily. The total increase in 9000 atmos is 17 percent of $\Delta H_0^{\ddagger}$ ($\Delta H_0^{\ddagger} = 5000$ cal/mol).

From the isotherm of ln$D$ in Fig. 1 it is seen that at 50° the diffusion coefficient decreases with the initial application of pressure as is normally expected. Thus, it appears that the tetrahedral structure does not control molecular motion to any prominent extent in the low pressure range at 50°. The activation volume increases from 45 percent of molal volume at 1 atmos to a maximum of 99 percent at 2000 atmos, while D continually decreases in this range. From this we infer that the decreasing free volume causes the local expansion necessary for activation to be felt over an increasingly larger portion of the liquid. Compressing beyond 2000 atmos the activation volume is seen to decrease rapidly and pass through zero to reach a minimum at 4200 atmos. At the same time, D drops rapidly beyond 1800 atmos, goes through a minimum at 3000, and rises slowly until a maximum is reached at 5800 atmos. These trends in the activation volume and diffusion coefficient lead to the conclusion that the free volume has been reduced to a point where, at 2000 atmos, the same situation is beginning to prevail as existed at 25° and 1 atmos. Namely, the tetrahedrally coordinated structure controls the motion. D decreases more rapidly between 1800 and 2500 atmos because the average mobility of the molecules is decreasing as they become more and more tied up in the structure. Also, the activation volume decreases rapidly indicating that the activation process is beginning to involve collapse of the structure. Beyond 3000 atmos the structure begins to break down, the diffusion coefficient increases, and the major volume effect during activation becomes the localized collapsing of the structure so that $\Delta V^{\ddagger}$ becomes negative. $\Delta V^{\ddagger}/\bar{V}$ continues to decrease and goes through a minimum at 4200 atmos and then becomes zero again at 5800 where D is at a maximum. Above 5800 atmos the effect of whatever remains of the tetrahedral structure is no longer predominant, and the local expansion for diffusion becomes positive again. At 10 000 atmos $\Delta V^{\ddagger}/\bar{V}$ is 0.37 and appears to be leveling. It is anticipated that with further compression the activation volume would pass through a maximum and then settle to some constant lower value as the "stabilized" configuration is formed, as was the case at 25°.

It is to be noted in Fig. 3 that the enthalpy of activation is negative between 2300 and 2800 atmos at 298° and between 1400 and 3750 atmos at 310°. Even taking into consideration the tetrahedral structure and hydrogen bonding it is difficult to conceive of a situation wherein a molecule activated for diffusion would be at a lower energy level than it was in the initial state. It must be concluded then that the negative $\Delta H^{\ddagger}$ arises entirely as a result of the fact that at a given density the structure is radically different for the three widely separated isotherms we have studied.

At first glance one might feel that we have fixed the maximum and minimum in the low pressure range of the 0° isotherm with an insufficient amount of data (see Fig. 1). Although it is true that the position of these "critical" points may be shifted within the limits of experimental error, we are confident of their existence. The experimental runs were consistent within themselves, and also, other work on salt solutions (Figs. 7–9) has led us to expect such behavior in water and aqueous solutions. (See also the sulfuric acid data in Fig. 5.)

Since 0°C and 1 atmos is a triple point for water, it is to be expected that the liquid phase would contain large regions of the tetrahedrally coordinated structure in this pressure and temperature range. This accounts

TABLE VI. $\Delta F_P^{\ddagger} - \Delta F_0^{\ddagger}$ for self-diffusion in water at 25°C.

P (atmos)	$\Delta F_P^{\ddagger} - \Delta F_0^{\ddagger}$ (cal/mole)
500	−82
1000	−134
1500	−156
2000	−141
3000	−17
5000	416
7000	675
9000	843

for the fact that at 0° D rises from 1.45×10^{-5} at 1 atmos to a maximum of 2.35×10^{-5} in only 250 atmos (see Fig. 1). As rapidly as D rises to the maximum at 250 atmos, it falls again to a minimum of 1.06×10^{-5} at 600 atmos; ascends once more to a maximum of 1.85×10^{-5} at 900 beyond where it decreases gradually with pressure. The initial rise is explained by the same arguments used above concerning the breakdown of the structure and increase of mobility with pressure. The descent between 250 and 600 atmos must be caused by a secondary formation of the structure which ties up the molecules to decrease their mobility. Then once again this secondary structure suffers a breakdown with increasing pressure and D rises to its maximum at 900 atmos. The activation volume, plotted in Fig. 2, follows the same trends as would be expected on the basis of the arguments presented above for the 25° and 50° isotherms. At 1 atmos it is extremely negative, passes through zero at 250, becomes excessively large and positive, then descends to pass through zero at 600 atmos; between 600 and 900 atmos it goes extremely negative again and then ascends to some high positive value a little beyond 900 atmos. From this last positive maximum, $\Delta V^{\ddagger}/\bar{V}$ descends rapidly to 1.00 at 1000 and then more slowly to 0.36 at 2000 atmos. Beyond 2000 the descent is very gradual to 0.10 at 6000 atmos. It appears that with suitable compression, $\Delta V^{\ddagger}/\bar{V}$ would approach zero as an asymptote. From the gradual decline of D and of $\Delta V^{\ddagger}/\bar{V}$ beyond 2000 atmos it appears that the "stabilized" configuration is forming.

Bridgman[3] gives data for the viscosity of water as a function of pressure at 0, 10.3, 30, and 75°C. He observed anomalous behavior at temperatures below 30°C in that the viscosity decreases with the initial application of pressure. The effect diminishes with increasing temperature. At 0° the viscosity at 1000 atmos is 92 percent of that at 1 atmos and then increases rapidly with pressure; at 10° a minimum of 95 percent of the value at 1 atmos is found at about 1200 atmos; no decrease is observed at 30 or 75° but the initial increase is very slow. These trends in the viscosity could be the result of breakdown of the tetrahedral water structure with increasing pressure and temperature. The effect is of a lesser extent and smaller magnitude than that we have observed in the case of diffusion. For all the systems we have studied it has been true that diffusion is more sensitive to pressure than is viscosity. The Stokes-Einstein equation predicts that the product of diffusion coefficient times the viscosity should be a constant. That this does not hold for water is seen in Table VII below where the product of the relative viscosity times the diffusion coefficient is shown for 25 and 0°C. The product may be approaching a constant value at 0° in the high pressure range.

TABLE VII. The viscosity-diffusivity product for water.

Pressure atmos $\times10^{-3}$	$D\eta/\eta_0\times10^{-5}$ 0°	25°
0	1.46	1.40
1	1.60	1.78
2	1.05	1.87
3	0.876	1.62
4	0.810	1.17
5	0.792	0.91
6	0.794	0.77
7		0.69
8		0.62
9		0.57

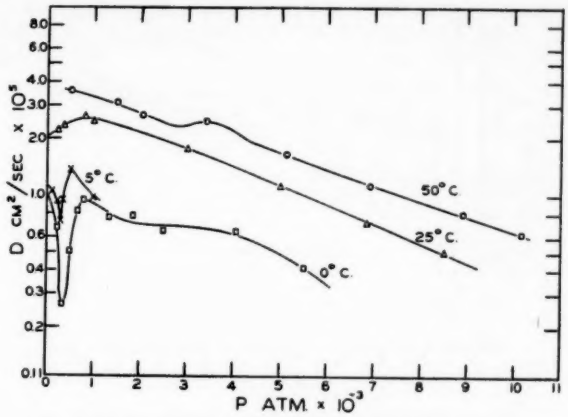

FIG. 5. Diffusion coefficients as a function of pressure. System: 0.1 N H_2SO_4–0.1 N $H_2S^{35}O_4$.

0.1 N $H_2S^{35}O_4$ IN 0.1 N H_2SO_4

Insofar as structure is concerned, the situation is probably much more complicated in sulfuric acid than in water. Along with having the tetrahedral water structure, the additional complication of solvation exists in the acid. The large size of the sulfate radical and its unbalanced valence forces probably cause further deviations from the water characteristics. It is impossible to give a unique interpretation to the diffusion data we have gathered. We shall not attempt to account for the effects of solvation or the sulfate radical but shall analyze the data giving consideration only to the characteristic tetrahedrally coordinated structure of water.

Isotherms of the diffusion coefficient are shown in a semilogarithmic plot against pressure in Fig. 5. Four temperatures were studied: 0, 5, 25, and 50°C. The ratio of the activation volume to the molal volume was calculated for the 0, 25, and 50° isotherms using compressibility data for water and is plotted in Fig. 6.

The isotherms in Fig. 5 show that D increases with the initial application of pressure at 25°C. Thus, it appears that the tetrahedral structure (modified by the acid) is a controlling factor for diffusion. Increasing pressure destroys the structure to increase the average sulfate mobility and D increases. The maximum value of D is found at about 900, and beyond this it decreases at a very steady rate with pressure. The activation volume (Fig. 6) is negative at one atmosphere and increases to pass through zero at about 900 atmos, where D was seen to be at a maximum. As in the case of water,

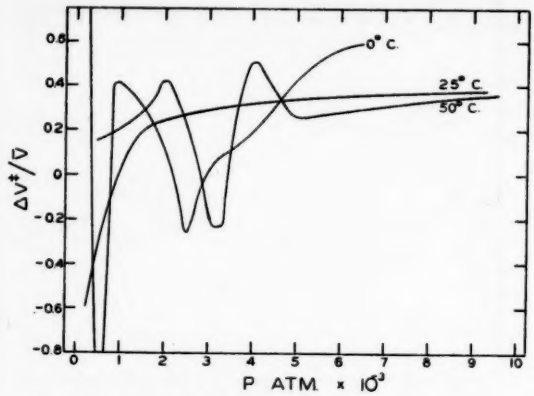

FIG. 6. Activation volumes as a function of pressure. System: 0.1 N H_2SO_4–0.1 N $H_2S^{35}O_4$.

the negative $\Delta V^{\ddagger}$ indicates that diffusion takes place almost entirely by localized collapse of the tetrahedral structure. Compressing beyond 900 atmos the activation volume increases indicating a positive local expansion in the activation process which is felt through an increasingly larger portion of the liquid as the free volume is decreased. At 3000 atmos $\Delta V^{\ddagger}$ has become virtually constant and increases only slightly with pressure to about 37 percent of the molal volume at 9000 atmos. The steady decrease of D and the very gradual increase of $\Delta V^{\ddagger}/\bar{V}$ beyond 3000 atmos indicate that the average configuration in the liquid must be stable with pressure.

At 50°C the situation is qualitatively similar to water at 50°. At first the diffusion coefficient decreases with pressure indicating a normal activation process relatively unaffected by the tetrahedral structure. At 3500 atmospheres the diffusion coefficient increases with pressure, passes through a maximum, and decreases in a normal manner.

The 0 and 5° isotherms of D are quite erratic and much like water at 0°. The influence of whatever structure may exist at atmospheric pressure is rapidly increased with the initial compression. This is shown by the rapid decline of D from about 1.0×10^{-5} at 1 atmos to about 0.27×10^{-5} at 335 atmos and 0°C. The subsequent ascent to a maximum of 0.95×10^{-5} at 840 atmos is equally rapid. Beyond 840 atmos D decreases and then settles to a plateau at 2000; at 3000 atmos it begins to decrease fairly rapidly again. In the range from 335 to 840 atmos the restricting configuration is apparently being broken down and D increases. At the 840 atmos maximum in D the tetrahedral structure no longer exists to a controlling extent, and we find the diffusion coefficient decreasing with pressure. The variation of the activation volume with pressure (Fig. 6) is consistent with our previous analysis.

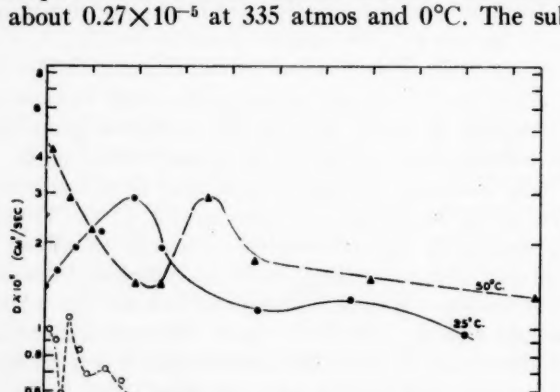

FIG. 7. Diffusion coefficients *versus* pressure 0.1 N Na_2SO_4.

It is seen in Fig. 5 that the 5° isotherm is similar to that for 0° as far as it was obtained (up to 1000 atmos).

The data for the three sulfate systems are shown in Tables III–V and Figs. 7–9. At first glance the results seem quite irregular, but the data were reproducible and very regular results were obtained for organic solutions on identical equipment. Extreme care was taken in nearly all cases to establish maximum and minimum points for the curves of diffusion coefficient *versus* pressure. This was accomplished either by making duplicate runs, or by making runs at small increments of pressure near what appeared tob e a peak or dip in the curve. These check runs were found to reproduce the data within a maximum deviation of 10 percent.

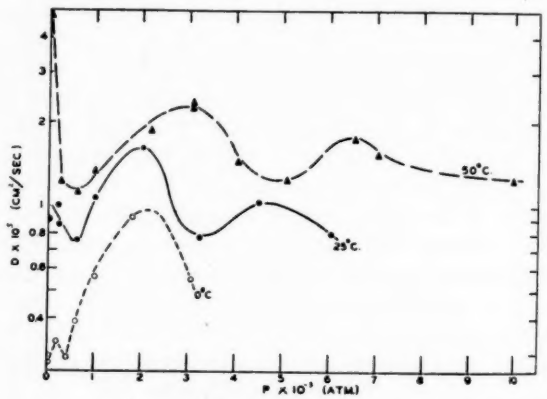

FIG. 8. Diffusion coefficients *versus* pressure in Na_2SO_4.

Closer inspection of the original data do show very definite regularities, and these can be compared best by plotting the data of several isotherms together (Figs. 10–17) and are discussed in detail below. From these curves definite general conclusions can be obtained which are briefly stated at the end of the following paper.

50°C ISOTHERMS

A plot of diffusion coefficient *versus* pressure for the sulfate solutions and the water and sulfuric acid data[5] at 50°C is shown in Fig. 10. The similarities to the water curve are evident. It appears that in all but a small pressure range (2250–4250 atmospheres) the process of diffusion in water is faster and that the motion of molecules is governed by effects which may be regarded

as superimposed on the factors that are influential in the case of water. Each of the three sulfate curves can logically be divided into three distinct sections, namely, from atmospheric pressure to the first minimum, from this point to the first maximum, and from this maximum onward to the highest pressure.

The minimum value for D occurs at 600 atmospheres for 1 N sodium sulfate, 1250 atmospheres for 0.1 N potassium sulfate and 2250 atmospheres for 0.1 N sodium sulfate. This decrease in D with initial application of pressure is normally expected, and molecular motion in this range involves, to a large extent, the pushing back of the surrounding medium as in normal liquids. It is evident from the slopes of the diffusion coefficient curves in this low pressure region that the ratio of activation volume to the molar volume of water,[5] $\Delta V^{\ddagger}/\bar{V}_w$, (see Fig. 11) for the aqueous sulfate solutions is greater than for water and is positive. Within the sulfate solutions the initial activation volume ratio is

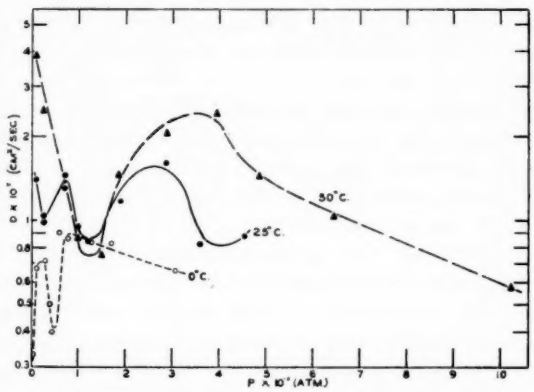

FIG. 9. Diffusion coefficients *versus* pressure 0.1 K_2SO_4.

largest for 1 N sodium sulfate followed by 0.1 N potassium sulfate and 0.1 N sodium sulfate, respectively.

As the pressure increases, the activation volume decreases and passes through a minimum, indicating that as the solution is compressed motion takes place preferentially by local collapse of the tetrahedral structure.

The activation volume ratio does not seem to be a function of the atomic volume of the cation, because the values for 0.1 N potassium sulfate lie between the values for 0.1 N and 1 N sodium sulfate, respectively. However, there is the possibility that a regular dependency of the activation volume ratio on the solvated volume exists which may be radically different from the corresponding atomic volumes of the cations.

In the second region, where D is increasing and the activation volume is negative, motion is apparently largely due to the local collapse of the structure.

In the pressure range beyond the last maximum value for D, the value of D decreases at a relatively slow rate while the activation volume ratio increases beyond zero for a short range, passes through a maximum, and

[5] Hereafter this will be referred to as the activation volume ratio.

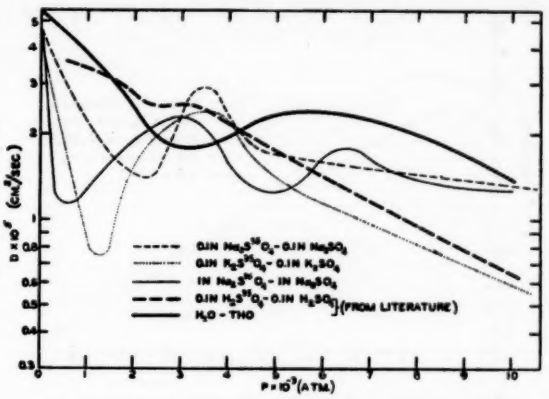
D x 10⁵ (cm²/sec)
P x 10⁻³ (ATM)
0.1N Na₂S³⁵O₃ - 0.1N Na₂SO₄
0.1N K₂S³⁵O₃ - 0.1N K₂SO₄
1N Na₂S³⁵O₃ - 1N Na₂SO₄
0.1N H₂S³⁵O₃ - 0.1N H₂SO₄
H₂O - THO
(FROM LITERATURE)

FIG. 10. Diffusion coefficients *versus* pressure sulfate solutions at 50°C.

then decreases at a decreasing rate which asymptotically approaches 0.08 for 1 N sodium sulfate, 0.10 for 0.1 N sodium sulfate, and 0.20 for 0.1 N potassium sulfate. These trends indicate that either the tetrahedral structure is completely destroyed, or the effect of the increased compactness of the medium is greater than the effect of whatever structure remains or any new structure which may have formed. Whichever the case may be, it is apparent that as the pressure is increased in this region a stabilized arrangement is forming and diffusion of the molecules is taking place more and more through the interstices which are not rapidly decreasing in size with pressure.

The irregularity in the 1 N Na_2SO_4 solution in the high pressure range may be due to ionic interaction at the higher concentration or to an additional desolvation effect not present at the lower concentrations.

25°C ISOTHERMS

The plots for the diffusion coefficient, activation volume ratio, activation enthalpy, and activation entropy[6] for the sulfate solutions and water and sulfuric acid are shown in Figs. 12, 13, 14, and 15, respectively. The activation volume ratio is obtained for each iso-

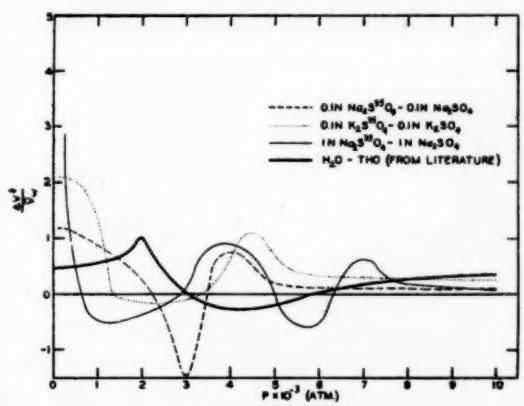

FIG. 11. Activation volume ratios for sulfate solutions at 50°C.

[6] This term will be used in place of $\Delta S_P^{\ddagger} - \Delta S_0^{\ddagger}$.

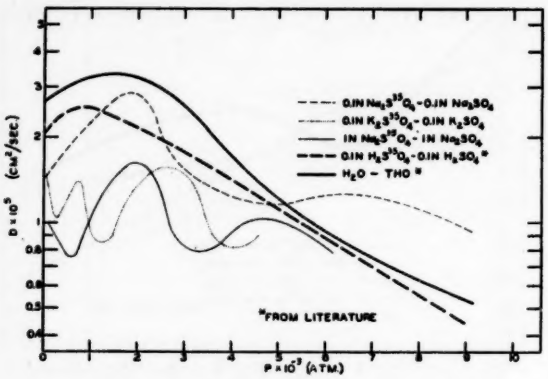

FIG. 12. Diffusion coefficients *versus* pressure sulfate solutions at 25°C.

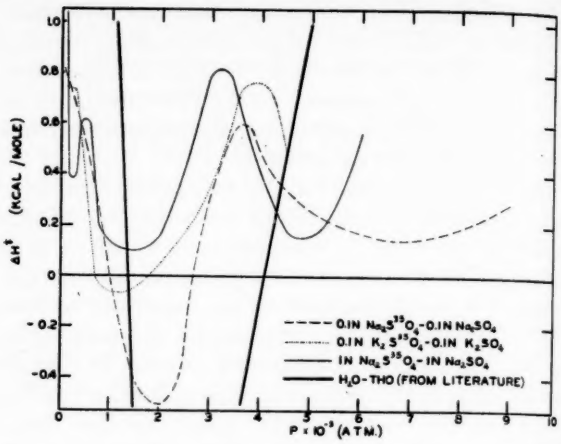

FIG. 14. Activation enthalpies for sulfate solutions at 37.5°C.

therm independently, while the activation enthalpy and entropy depend on the displacement between two or more isotherms. Inasmuch as the structure of the solution varies widely with temperature, the activation enthalpy and entropy calculated probably do not apply to any one isotherm.

The similarity between water, 0.1 *N* H_2SO_4 and 0.1 *N* Na_2SO_4 are evident from Figs. 12 and 13, but the 1*N* Na_2SO_4 and 0.1 *N* K_2SO_4 have additional maxima and minima which are not easily explainable but which are definitely present.

In the low pressure region the increase in *D* and the negative activation volume indicate that the tetrahedral structure collapses locally during molecular motion. At pressures beyond the point where the collapse of structure dominates the motion of molecules, the water and sulfuric acid display a high degree of regularity associated with normal liquids. However, in this region the sulfate curves show irregularities, i.e., additional maxima and minima, which probably could be explained on the basis of the pressure dependency of desolvation and ionic interaction.

In the high pressure region Figs. 11 and 13 show that the activation volume ratios for all the solutions asymptotically approach approximately the same relatively low value, indicating a similarly stable structure for all solutions at very high pressure at both 25° and 50°C.

0°C ISOTHERMS

Figures 16 and 17 are plots of diffusion coefficients and activation volume ratios, respectively, *versus* pressure for the sulfate solutions and water and sulfuric acid.

There is a definite similarity between these sulfate curves and the water curve, and the similarity is even clearer between the sulfuric acid and 0.1 *N* sodium sulfate and among the water, 0.1 *N* potassium sulfate, and 1 *N* sodium sulfate.

In the very low pressure range, it appears that molecular motion is influenced by the more rigid structure that exists at 0°C. With the exception of the increase of *D* with pressure for the 1 *N* sodium sulfate and 0.1 *N* potassium sulfate in the initial pressure range, the curves all show the value of *D* decreasing to a minimum, rising to a maximum and dropping off in the high pressure range.

Molecular motion in the region where *D* initially decreases is controlled by the decrease in free volume, and the rigid structure at 0°C remains so and does not undergo any pronounced rearrangement with the initial application of pressure. Beyond the pressure where *D* is maximum, there is a general decrease in the value of *D* and an asymptotic leveling of the activation volume

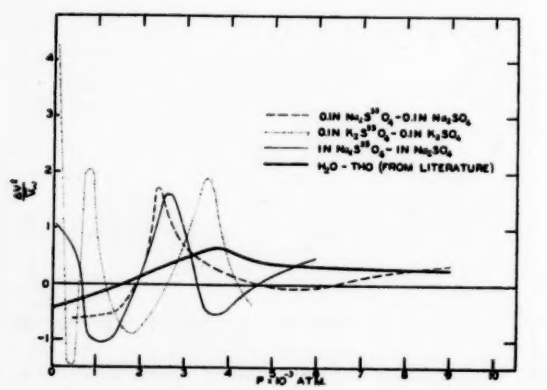

FIG. 13. Activation volume ratios for sulfate solutions at 25°C.

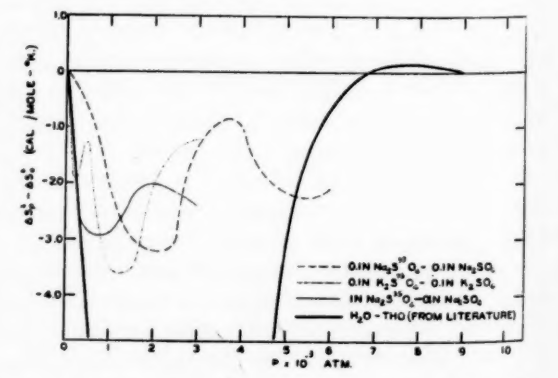

FIG. 15. Activation entropies for sulfate solutions at 25°C.

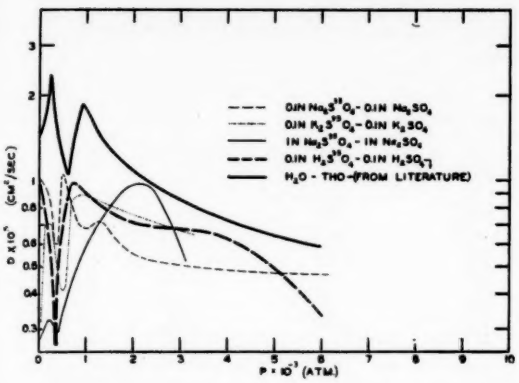
0.1N $Na_2S^{35}O_4$ - 0.1N Na_2SO_4
0.1N $K_2S^{35}O_4$ - 0.1N K_2SO_4
1N $Na_2S^{35}O_4$ - 1N Na_2SO_4
0.1N $H_2S^{35}O_4$ - 0.1N H_2SO_4
H_2O - THO (FROM LITERATURE)
D X 10^5 (CM^2/SEC)
P x 10^-3 (ATM.)

FIG. 16. Diffusion coefficients for sulfate solutions at 0°C.

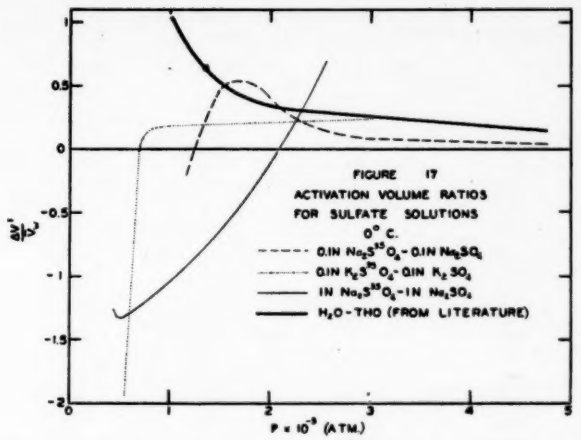

FIG. 17. Activation volume ratios for sulfate solutions at 0°C.

ratio to relatively small values (Fig. 17). Inasmuch as the activation volume ratios are extreme and their variations are compressed in the pressure range below 1000 atmospheres, only the high pressure values are plotted. It is this portion of the curves that indicate the formation of similarly stable structures for water and sulfate solutions.

The conductivity data of Zisman[7] on 0.01 N salt solutions (including Na_2SO_4) shows a maximum in the conductance at about 1000 atmospheres, followed by a linear decrease. The lack of detailed structure may be due to the decreased concentration or to the lack of sensitivity of conductance.

R. B. Cuddeback would like to acknowledge assistance from the Shell Fellowship Committee and from the U. S. Atomic Energy Commission.

R. C. Koeller would like to acknowledge assistance from the Pan American Refining Corporation and the U. S. Atomic Energy Commission.

[7] W. A. Zisman, Phys. Rev. **39**, 151 (1932).

THE JOURNAL OF CHEMICAL PHYSICS VOLUME 21, NUMBER 4 APRIL, 1953

The Effect of Pressure on Diffusion in Aqueous and Alcoholic Salt Solutions*

R. B. CUDDEBACK AND H. G. DRICKAMER
Department of Chemistry, University of Illinois, Urbana, Illinois

(Received August 26, 1952)

Diffusion coefficients have been measured as a function of pressure to 10 000 atmos for the following aqueous solutions:

0.1 N $Hg(NO_3)_2$ at 0°, 25°, 50°, 75°C,
0.1 N $CaCl_2$ at 25°, 50°C,
0.1 N $Ca(NO_3)_2$ at 25°C,
0.1 N $TlNO_3$ at 25°C,

and for 0.01 M $HgCl_2$ in n-butanol at 25° and 50°C. The results are interpreted in terms of the activation volume, and compared with previous data on water and sulfate solutions.

DIFFUSION coefficients have been measured as a function of pressure to 10 000 atmos in 0.1 N aqueous solutions of $Hg(NO_3)_2$ at 0°, 25°, 50°, and 75°C; $CaCl_2$ at 25° and 50°C; $Ca(NO_3)_2$ at 25°C; and $TlNO_3$ at 25°C. Measurements have also been made in a 0.01 M $HgCl_2$ in n-butanol solution.

In every case a radioactive tracer technique was used. The tracers (Hg^{203}, Ca^{45}, Tl^{204}) were obtained from Oak Ridge National Laboratory of the U. S. Atomic Energy Commission. The salts were of cp quality. The n-butanol was purchased from Eastman Kodak.

The experimental procedures, method of calculation of the diffusion coefficient, and the general theory have been previously discussed.[1,2,3]

The results are presented in Tables I–V and Figs. 1–5. These will be discussed under four headings; mercuric nitrate, comparison of nitrate isotherms, calcium chloride isotherms, and mercuric chloride-butanol isotherms.

* This work was supported in part by the U. S. Atomic Energy Commission.

[1] R. C. Koeller and H. G. Drickamer, J. Chem. Phys. **21**, 267 (1953).
[2] R. C. Koeller and H. G. Drickamer, J. Chem. Phys. **21**, 575 (1953).
[3] Cuddeback, Koeller, and Drickamer, J. Chem. Phys. **21**, 589 (1953)

TABLE I. Diffusion coefficients.
0.1 N $Hg^{203}(NO_3)_2$—0.1 N $Hg(NO_3)_2$ in 0.2 N HNO_3.[a]

Temp. °K	Pressure atmos	Effective cell length cm	Observed $D\times10^5$ cm²/sec
273	20	0.548	0.54
273	250	0.548	0.33
273	600	0.548	0.41
273	1200	0.548	0.48
273	2000	0.617	0.60
273	3000	0.617	0.75
273	4250	0.617	0.40
273	5000	0.676	0.57
298	20	0.548	0.86
298	50	0.548	1.24
298	250	0.548	2.05
298	600	0.548	1.26
298	1000	0.548	0.92
298	2000	0.617	1.02
298	3000	0.617	1.17
298	4000	0.617	0.70
298	5000	0.617	1.16
298	7000	0.676	1.45
298	9000	0.676	0.79
323	20	0.548	1.17
323	250	0.548	2.13
323	600	0.548	1.32
323	1200	0.548	1.17
323	2000	0.548	1.54
323	3000	0.617	1.87
323	4000	0.617	0.90
323	5500	0.617	1.85
323	7000	0.676	1.95
323	8500	0.724	1.29
348	20	0.548	2.56
348	250	0.548	3.28
348	600	0.548	5.17
348	1000	0.548	3.56
348	2000	0.617	3.87
348	3000	0.617	1.81
348	4000	0.617	2.34
348	5500	0.617	2.98
348	7000	0.676	2.54

[a] Maximum deviation in reproducibility 10 percent. Average deviation 5 percent.

TABLE II. Diffusion coefficients. 0.1 N $Ca^{45}Cl_2$—0.1 N $CaCl_2$.[a]

Temp. °K	Pressure atmos	Effective cell length cm	Observed $D\times10^5$ cm²/sec
298	100	0.583	1.08
298	250	0.583	0.83
298	600	0.583	0.82
298	1000	0.583	0.94
298	2000	0.646	0.84
298	3000	0.646	1.16
298	4250	0.646	0.49
298	5500	0.698	0.44
298	7000	0.698	0.33
298	9000	0.761	0.49
323	100	0.583	1.25
323	250	0.583	1.37
323	600	0.583	1.14
323	1000	0.583	1.22
323	2000	0.646	1.50
323	3000	0.646	1.41
323	4250	0.646	1.82
323	5500	0.646	1.48
323	7700	0.761	0.83

[a] Maximum deviation in reproducibility 10 percent. Average deviation 5 percent.

TABLE III. Diffusion coefficients.
0.1 N $Ca^{45}(NO_3)_2$—0.1 N $Ca(NO_3)_2$.[a]

Temp. °K	Pressure atmos	Effective cell length cm	Observed $D\times10^5$ cm²/sec
298	100	0.583	0.72
298	250	0.583	1.49
298	250	0.583	1.60
298	600	0.583	1.32
298	600	0.583	1.50
298	1000	0.583	1.43
298	2000	0.646	1.13
298	3000	0.646	1.17
298	4000	0.646	1.47
298	5000	0.698	0.75
298	7100	0.698	1.04
298	9000	0.698	1.24

[a] Maximum deviation in reproducibility 10 percent. Average deviation 5 percent.

MERCURIC NITRATE

The mercuric nitrate data are the best and most complete obtained in any one aqueous system because they include a larger temperature range and cover the entire pressure range used in this experimental work. The similarity among the curves is evident from Figs. 1 and 6. There is a minimum in each diffusion coefficient curve at approximately 4000 atmospheres, and this

TABLE IV. Diffusion coefficients. 0.1 N $Tl^{204}NO_3$—0.1 N $TlNO_3$.[a]

Temp. °K	Pressure atmos	Effective cell length cm	Observed $D\times10^5$ cm²/sec
298	20	0.583	2.07
298	250	0.583	1.35
298	600	0.583	1.80
298	600	0.583	1.69
298	1000	0.583	0.95
298	2000	0.646	2.00
298	3000	0.646	1.67
298	4000	0.646	1.03
298	5700	0.761	0.88
298	7000	0.698	1.48
298	9000	0.761	1.73

[a] Maximum deviation in reproducibility 10 percent. Average deviation 5 percent.

TABLE V. Diffusion coefficients.
0.01 M $Hg^{203}Cl_2$—0.01 M $HgCl_2$ in n-C_4HgOH.[a]

Temp. °K	Pressure atmos	Effective cell length cm	Observed $D\times10^5$ cm²/sec
298	200	0.548	1.61
298	1000	0.548	0.68
298	2000	0.548	0.40
298	3500	0.646	0.18
298	5000	0.646	0.084
298	7000	0.698	0.041
323	200	0.548	3.75
323	1000	0.548	2.29
323	2000	0.646	1.26
323	3500	0.646	0.70
323	5000	0.646	0.35
323	8500	0.761	0.088

[a] Maximum deviation in reproducibility 10 percent. Average deviation 5 percent.

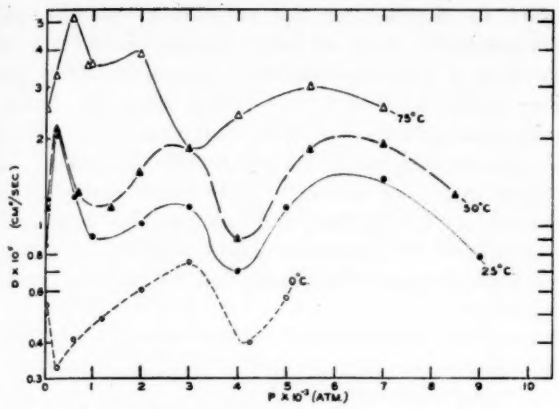

FIG. 1. Diffusion coefficients *versus* pressure, 0.1 N $Hg(NO_3)_2$.

minimum shifts toward lower pressure as the temperature increases. The curves also show a maximum in the pressure range 250–600 atmospheres which moves to

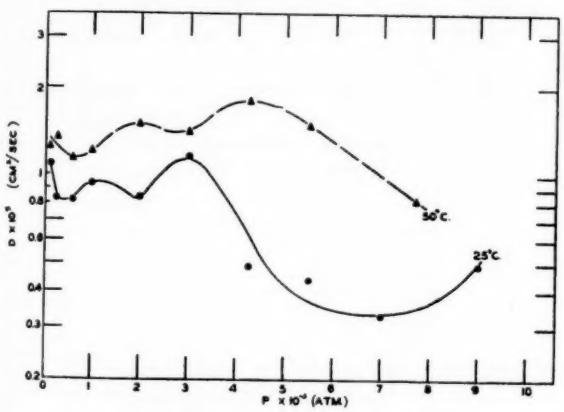

FIG. 2. Diffusion coefficients *versus* pressure, 0.1 N $CaCl_2$.

lower pressure as temperature decreases and disappears at 0°C.

Curves of activation enthalpy and the increase in

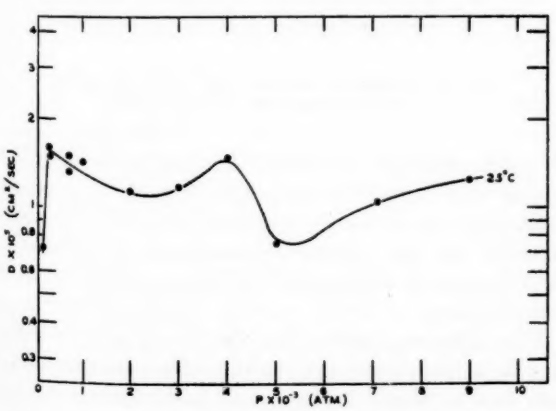

FIG. 3. Diffusion coefficients *versus* pressure, 0.1 N $Ca(NO_3)_2$.

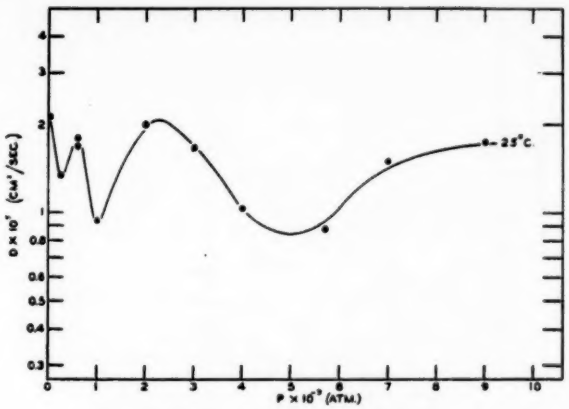

FIG. 4. Diffusion coefficients *versus* pressure, 0.1 N $TlNO_3$.

activation entropy from one atmosphere to P are shown in Figs. 7 and 8. Any interpretation of these curves

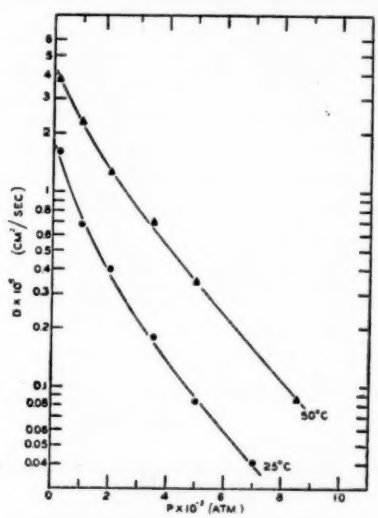

FIG. 5. Diffusion coefficients *versus* pressure, 0.01 M $HgCl_2$ in n-butanol.

would be dubious because the activation enthalpy and entropy depend on the displacement of two or more

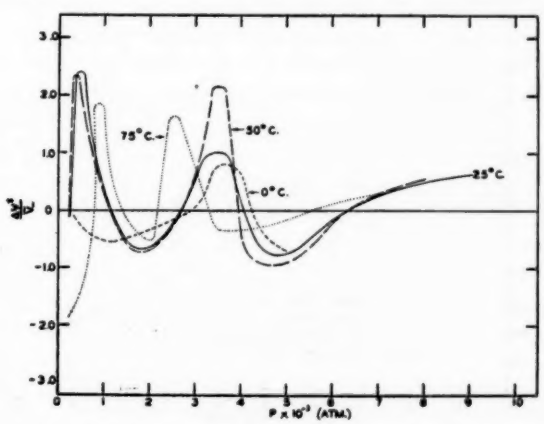

FIG. 6. Activation volume ratios *versus* pressure. 0.1 N $Hg(NO_3)_2$.

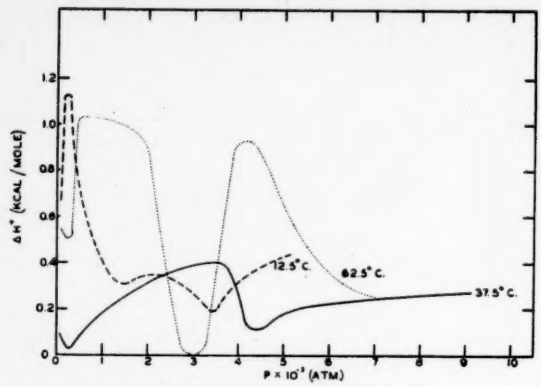

FIG. 7. Activation enthalpy *versus* pressure. 0.1 *N* $Hg(NO_3)_2$.

isotherms, and since the structure appears to vary radically with temperature, these values of activation enthalpy and entropy probably do not apply to any single isotherm.

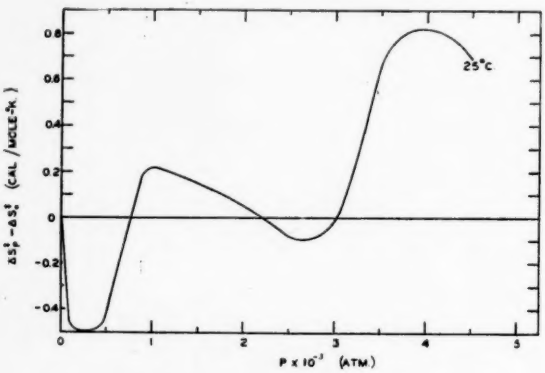

FIG. 8. Activation entropy *versus* pressure, 0.1 *N* $Hg(NO_3)_2$.

NITRATE SOLUTIONS AT 25°C

The curve for the diffusion coefficients and activation volume ratios *versus* pressure for the nitrate solutions at 25°C are shown in Figs. 9 and 10, respectively

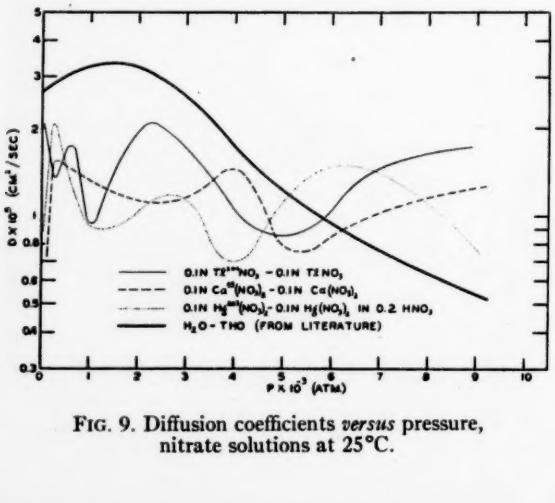

FIG. 9. Diffusion coefficients *versus* pressure, nitrate solutions at 25°C.

Figure 10 shows that the activation volume ratios asymptotically level at high pressure indicating the formation of a stable structure with motion in the interstices similar to that in the sulfate solutions. Further similarities between the nitrate solutions (Fig. 10) and the sulfate solutions (1) are readily apparent. The extreme values for the activation volume ratios are less for water indicating that molecular motion is generally more difficult in aqueous solutions, probably due to the large effective size of the ionic particles relative to those

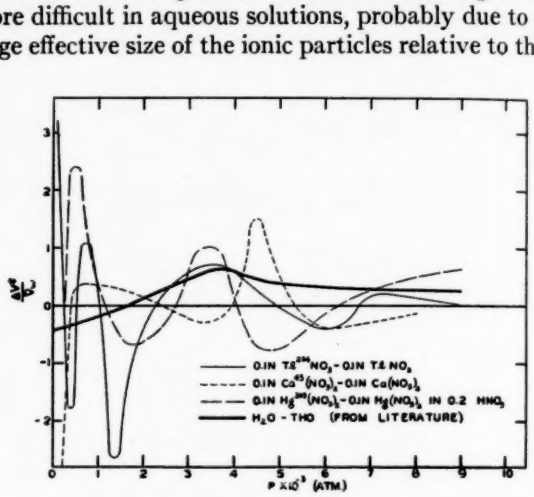

FIG. 10. Activation volume ratio *versus* pressure, nitrate solutions at 25°C.

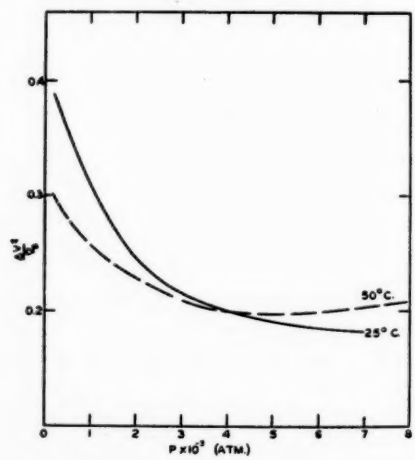

FIG. 11. Activation volume ratio *versus* pressure, 0.01 *M* $HgCl_2$ in *n*-butanol.

of water. Another noticeable feature is the relatively greater stability of the water structure toward pressure. A decrease in activation volume ratio occurs at lower pressure for the aqueous solution which indicates a local structural collapse at lower pressure than in the case of water.

The diffusional process in the nitrate solutions deviates more from water than in the sulfate solutions which indicates a larger influence of ionic interaction and degree of solvation on diffusion and a stronger pressure dependency on these two forces. At this time it is not

possible to say which forces (free volume, structural arrangement, degree of solvation, or ionic interaction) are responsible for the various maxima and minima in the diffusion coefficient curves. If the sudden initial decrease in D for 0.1 N thallous nitrate is discounted, then the nitrate curves display remarkable similarity. The diffusion coefficients pass through a maximum in the low pressure range (200–600 atmospheres), another in the intermediate pressure range (2000–4000 atmospheres) and rise to a final peak in the range 6000–10 000 atmospheres. There are, of course, corresponding minima for D and maxima and minima for the activation volume ratio. These effects are somewhat compressed for the 0.1 N mercuric nitrate solution.

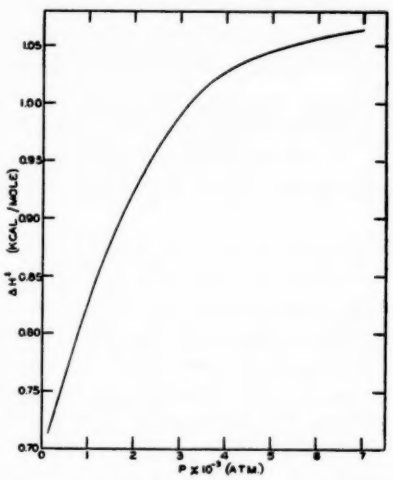

FIG. 12. Activation enthalpy *versus* pressure, 0.01 M $HgCl_2$ in n-butanol, 37.5°C.

CALCIUM CHLORIDE

The plot of diffusion coefficient *versus* pressure for 0.1 N $CaCl_2$ is shown in Fig. 2. The results show qualitatively the same variations exhibited by the other aqueous solutions. The rather low values at high pressure for this relatively small molecule indicate how little the diffusion rate depends on the ionic volume.

MERCURIC CHLORIDE IN n-BUTANOL

The diffusion coefficients are plotted *versus* pressure in Fig. 5. Figures 11, 12 and 13 are plots of activation volume ratio, activation enthalpy, and activation entropy, respectively, *versus* pressure. The pressure variation of D is very regular and the value of D, which is always higher at 50°C, decreases by a factor of 50 from atmospheric pressure to 8500 atmospheres at 50°C and 7000 atmospheres at 25°C. The relatively high value of the activation volume ratio at the initial pressure indicates that a high degree of distortion and local expansion accompany the activation process. The rapid decrease of activation volume ratio upon increased compression in the low pressure range indicates a more ordered arrangement of the n-butanol medium. The

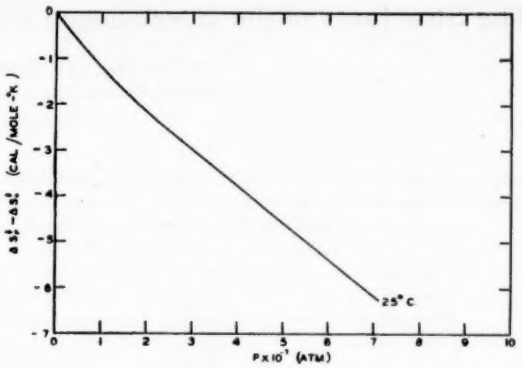

FIG. 13. Activation entropy *versus* pressure, 0.01 M $HgCl_2$ in n-butanol, 25°C.

decrease in activation entropy shows that a preferred orientation is developing in the n-butyl alcohol solution. In this same region the activation enthalpy increases.

At high pressure the activation volume asymptotically levels at values comparable to those for the aqueous solutions but at higher values than those for other organic solutions.[2,3] This trend in activation volume, the continual decrease in activation entropy, and the decreasing rate of increase of the activation enthalpy imply the formation of a more ordered and stable configuration through which molecular motion occurs.

It is evident that the butyl alcohol provides an essentially normal organic medium for motion even for an inorganic salt. $HgCl_2$ is probably almost entirely undissociated in the alcoholic solution.

From the work done on salt solutions it is possible to draw the following conclusions:

1. Molecular motion in aqueous solutions appears to be a combination of several effects: those which govern motion in water, the effects of pressure on the ionic interaction, and on the effects of solvation.
2. At high pressure a similarly stable structure develops for the water and aqueous solutions.
3. A definite similarity in the variation of diffusion coefficient with pressure exists among the curves in any set of comparative isotherms.
4. With the exception of a short range of pressure on a few isotherms, the diffusion coefficient for water is higher than for the salt solutions.
5. The structure of the aqueous salt solutions appears to be less stable towards pressure than water.
6. The extreme values of the activation volume ratio are smaller than those for aqueous salt solutions, indicating a smaller activation volume effect for water.
7. The diffusion of molecular salts in butyl alcohol is quite normal and gives no evidence of association or other unusual structure.

R. B. Cuddeback would like to acknowledge financial assistance from the Shell Fellowship Committee and from the U. S. Atomic Energy Commission.

The Structures of the Interhalogen Compounds.* I. Chlorine Trifluoride at −120°C

ROBINSON D. BURBANK AND FRANK N. BENSEY
K-25 Laboratories, Carbide and Carbon Chemicals Company, Oak Ridge, Tennessee

(Received September 30, 1952)

A technique has been developed for handling the extremely reactive interhalogen compounds which makes it possible to investigate their structures by x-ray diffraction at low temperatures. As the first step in a program of study of the interhalogen group the crystal structure of chlorine trifluoride has been determined at −120°C. The chlorine trifluoride molecule is planar with the point group symmetry mm. The Cl atom is bonded to one F atom at 1.621A and to two F atoms at 1.716A. The F−Cl−F bond angle is 86°59′. In the succeeding pages of this journal, a parallel investigation of the vapor phase by microwave spectroscopy is presented by Dr. D. F. Smith. The molecular configuration is identical in the two cases.

I. INTRODUCTION

THE difficulty of obtaining reliable structural information on the interhalogen compounds is well known. The extraordinary chemical reactivity of most members of the group has rendered many physical measurements either impractical or inaccurate. Experiments which depend on a trial and error approach to deduce a structure have frequently failed for lack of an initial guess which approximated to the truth. In principle the analysis of single crystal x-ray diffraction data should yield a direct answer for any of the interhalogens. Therefore, an experimental procedure has been developed which will provide the necessary data for such an analysis. Chlorine trifluoride was selected for the initial problem because it was apparent that if this compound could be handled successfully the other members of the series would follow in due course. Subsequent communications will deal with compounds such as bromine trifluoride, bromine pentafluoride, iodine pentafluoride, and iodine heptafluoride.

II. EXPERIMENTAL

A. General Considerations

The study by x-ray diffraction of single crystals of substances which are gases or liquids at room temperature has received great impetus from the recent work of Kaufman and Fankuchen;[1] Abrahams, Collin, Lipscomb, and Reed;[2] and Post, Schwartz, and Fankuchen.[3] In essence the method involves placing a sample in a small capillary on an x-ray camera and freezing the sample with a stream of cold gas. By controlled freezing and melting, a polycrystalline specimen is converted into a single crystal which is suitable for diffraction work.

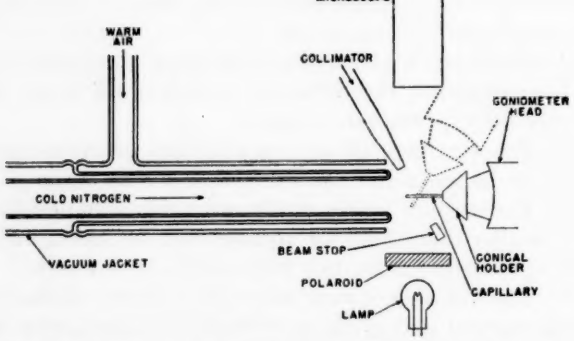

FIG. 1. Low temperature arrangements for precession camera.

The main problem in working with interhalogen compounds is to isolate and contain a sample in a capillary for the duration of an experiment. It has been found that fluorothene (trifluoromonochloropolyethylene) is a most satisfactory material of construction for any apparatus that will be used with interhalogen compounds. By rapidly stretching hot fluorothene tubing as it emerges from an extrusion die, it is possible to obtain capillary tubing less than 0.5 mm in diameter. The capillary tubing can be cut to any desired length with shears. It can be sealed by pinching with a pair of hot pliers. A sealed capillary can be mounted with fluorothene wax in a holder which is machined from solid fluorothene. The capillary holder can then be attached to the goniometer head of an x-ray camera.

Low temperature equipment identical in principle to that used by Post *et al.*[3] was adapted to a precession camera in the manner illustrated in Fig. 1. Cold gas flows through the central vacuum jacketed tube of the cooling nozzle and cools the capillary which is mounted in a simple conical holder. An auxiliary coaxial flow of warm gas around the cold gas stream serves to eliminate ice formation *provided that the outer tube is retracted slightly from the end of the inner tube.* The cooling nozzle is mounted horizontally and its axis makes an angle of 60° with the direction of the x-ray beam. When the camera is in motion with a precession angle of $\mu=30°$ the capillary oscillates over a 60° angle. At one end of the range it is parallel to the cooling nozzle and at the other end, indicated by the dotted portion of Fig. 1,

* This document is based on work performed for the U. S. Atomic Energy Commission by Carbide and Carbon Chemicals Company, a division of Union Carbide and Carbon Corporation, at Oak Ridge, Tennessee.

[1] H. S. Kaufman and I. Fankuchen, Rev. Sci. Instr. **20**, 733 (1949).
[2] Abrahams, Collin, Lipscomb, and Reed, Rev. Sci. Instr. **21**, 396 (1950).
[3] Post, Schwartz, and Fankuchen, Rev. Sci. Instr. **22**, 218 (1951).

it is inclined at 60° to the nozzle. For crystal-growing operations a polarizing microscope is mounted so that it will be normal to the axis of the capillary. To permit continuous operation over extended periods, the gas streams to the cooling nozzle are maintained as indicated in Fig. 2. The cold gas stream is obtained by boiling liquid nitrogen with an immersion heater. The boiler has a capacity of 100 liters which permits operating for several days before it is necessary to add liquid nitrogen through the feed funnel. The gas stream to the outer coaxial tube of the nozzle is obtained by passing the laboratory compressed air through a column of "Drierite." Two drying tubes are arranged in parallel and while one is in use the other can be removed, and the desiccant regenerated on a hot plate.

B. Precession Photography of Chlorine Trifluoride

Samples of chlorine trifluoride were prepared and sealed in fluorothene capillaries about 0.5 mm in diameter and about 1.5 cm long by Mr. A. V. Faloon and Mr. W. B. Kenna of this laboratory. The specimens were transported in a small Dewar of liquid nitrogen and placed on the low temperature apparatus with a minimum of delay.

Visual observations were of limited value in crystal growing because fluorothene capillaries give an intense pattern under the polarizing microscope. The precession camera is indispensable under these conditions. It is largely a matter of going through the melting and freezing cycle and then examining the sample by orientation photographs for evidence of a single crystal. All adjustments in crystal orientation were made by x-ray methods.

Grisard, Bernhardt, and Oliver[4] of this laboratory have shown that chlorine trifluoride has one crystalline phase which is stable only over a narrow 6° temperature interval from the freezing point of the liquid at −76.16°C down to a transition point of −82.50°C. Our specimens always seemed to supercool through this region. When a good crystal was obtained of the phase which is stable below −82.50°C it was preserved for over two months at a temperature of −120°C. All the x-ray data used in the structure analysis were recorded with this one crystal.

The system proved to be orthorhombic with the following cell constants:

$$a = 8.82_5 \pm 0.01\text{A};$$
$$b = 6.09 \pm 0.01\text{A};$$
$$c = 4.52 \pm 0.01\text{A};$$
$$\lambda \text{ for } Mok\alpha = 0.7107\text{A}.$$

With a precession angle of $\mu = 30°$ and the b axis of the crystal parallel to the dial axis of the camera, the following reflections were recorded:

$hk0$	$0kl$	h, k, h	$2h, \quad k, h$
$hk1$	$1kl$	$h, k, h\pm1$	$2h\pm1, k, h$
$hk2$	$2kl$	$h, k, h\pm2$	$2h\pm2, k, h$
	$3kl$		$2h\pm3, k, h$
	$4kl$		$2h\pm4, k, h.$

The degree of duplication of reflections on different levels is indicated in the following tabulation:

7 reflections are recorded on 6 different levels;
6 reflections are recorded on 5 different levels;
46 reflections are recorded on 4 different levels;
57 reflections are recorded on 3 different levels;
113 reflections are recorded on 2 different levels;
160 reflections are recorded on 1 level.

Of a total of 389 unique reflections which occur within a sphere of radius 1 reciprocal lattice unit, 324 were found

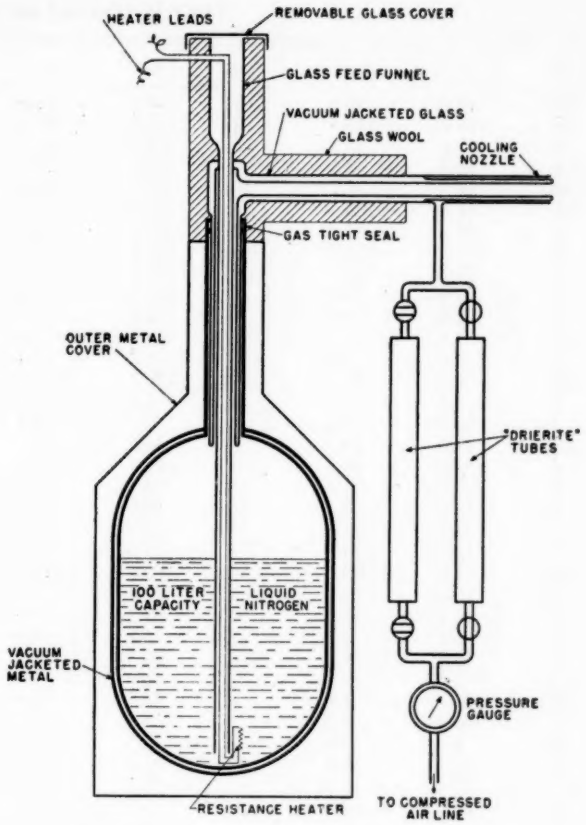

FIG. 2. Cooling system for continuous operation.

TABLE I. Final parameters including termination of series correction.

Atom	x	y	z
Cl	0.1582	1/4	0.3790
F_1	0.0422	1/4	0.1010
F_2	0.1517	0.5315	0.3634

[4] Grisard, Bernhardt, and Oliver, J. Am. Chem. Soc. **73**, 5725 (1951).

TABLE II. Observed and calculated structure factors.

hkl	F_0	F_c	hkl	F_0	F_c	hkl	F_0	F_c	hkl	F_0	F_c
020	48.7	− 50.6	011	79.9	− 86.5	561	5.3	+ 3.3	102	123.1	+122.8
4	113.7	+126.5	3	102.0	+ 98.4	7	33.4	+34.5	1	3.1	− 4.3
6	41.6	− 43.5	5	18.5	− 19.3	601	14.2	+17.4	2	<1.1	+ 2.3
8	32.3	+ 32.1	7	42.3	+ 41.9	1	30.9	−29.5	3	21.8	− 24.6
200	34.5	− 32.7	101	45.6	− 41.0	2	16.0	+17.2	4	63.7	+ 60.3
1	81.7	−100.9	1	41.6	+ 37.9	3	48.7	+42.9	5	4.2	− 7.2
2	34.9	− 34.4	2	37.2	− 34.8	4	7.8	+ 8.4	6	20.7	− 18.8
3	112.0	+118.3	3	59.4	− 55.3	5	10.7	− 9.7	7	20.7	− 16.9
4	10.2	− 12.5	4	19.1	− 16.0	6	<2.0	+ 2.1	8	19.8	+ 16.1
5	23.6	− 23.0	5	8.5	+ 7.9	7	25.2	+24.4	202	14.2	+ 12.4
6	<1.8	+ 0.1	6	<1.8	+ 0.5	701	61.0	−55.9	1	13.1	− 11.6
7	57.4	+ 51.8	7	29.4	− 27.0	1	6.0	+ 4.5	2	2.7	− 4.6
8	4.0	− 2.8	8	6.5	− 3.2	2	17.6	+ 9.4	3	<1.3	+ 3.6
400	87.5	− 97.3	201	120.2	−151.4	3	12.2	−10.9	4	5.1	+ 5.6
1	9.1	+ 11.2	1	3.1	− 5.0	4	31.6	−34.1	5	9.6	− 7.9
2	17.6	− 20.7	2	4.2	+ 6.2	5	5.3	+ 1.6	6	3.1	− 2.0
3	41.0	− 39.2	3	10.2	− 11.1	6	14.9	+12.5	7	<2.2	+ 0.7
4	53.6	− 45.8	4	72.6	− 65.1	801	53.2	−60.6	302	<1.1	+ 6.7
5	2.9	+ 1.3	5	3.1	− 3.5	1	6.7	+ 8.2	1	81.7	− 74.3
6	11.6	+ 10.3	6	20.0	+ 20.1	2	18.7	+14.7	2	26.5	+ 22.9
7	26.3	− 23.8	7	8.9	− 8.2	3	4.2	− 3.6	3	87.0	+ 94.0
8	12.9	− 14.8	8	15.6	− 16.4	4	32.7	−38.2	4	<2.2	+ 2.2
600	81.9	+100.2	301	160.7	+145.2	5	5.1	+ 6.9	5	25.4	− 25.3
1	10.7	− 13.0	1	20.9	− 18.5	6	18.3	+15.2	6	3.6	+ 4.4
2	13.4	− 15.2	2	29.2	− 29.5	901	25.4	+27.7	7	47.2	+ 46.7
3	6.7	− 7.4	3	3.8	+ 3.5	1	7.1	+ 2.1	402	<1.1	+ 8.4
4	59.2	+ 58.2	4	73.7	+ 71.7	2	8.9	− 5.7	1	4.0	− 4.2
5	6.2	− 12.3	5	6.9	− 9.5	3	10.9	−10.2	2	6.5	+ 3.0
6	26.7	− 21.9	6	27.8	− 26.9	4	16.0	+18.4	3	6.5	+ 5.5
7	10.2	− 7.8	7	4.2	− 1.3	5	<2.0	− 2.9	4	<1.6	+ 3.4
800	6.9	− 5.0	8	20.5	+ 19.8	10,0,1	7.1	+ 9.2	5	<1.8	− 0.2
1	49.2	− 50.8	401	63.2	+ 53.8	1	20.7	+20.4	6	<2.0	+ 0.3
2	17.1	+ 17.6	1	15.1	+ 13.2	2	7.1	− 5.5	7	3.8	+ 2.5
3	63.0	+ 63.4	2	8.5	+ 9.6	3	24.0	−27.6	502	121.5	−124.2
4	4.5	− 5.3	3	32.9	− 35.0	4	7.3	+ 6.6	1	7.1	+ 7.3
5	23.8	− 21.0	4	29.4	+ 27.7	11,0,1	<2.0	− 0.1	2	37.2	+ 29.5
6	8.0	+ 7.4	5	<1.8	− 0.6	1	18.7	−18.8	3	8.7	− 8.2
10,0,0	52.3	− 59.5	6	9.1	− 7.2	2	5.8	+10.0	4	68.3	− 73.4
1	12.9	+ 9.7	7	23.6	− 19.8	3	18.3	+22.8	5	5.3	+ 4.6
2	24.5	+ 16.2	8	7.8	+ 6.9	12,0,1	14.7	+18.6	6	28.3	+ 28.9
3	14.2	− 10.0	501	7.1	− 7.4	1	8.2	− 6.9	7	5.8	− 4.7
4	38.7	− 39.6	1	63.9	− 58.7	002	<1.1	+ 6.5	602	<1.3	− 1.8
5	7.8	+ 5.5	2	6.5	+ 3.2	2	24.7	−23.6	1	<1.6	− 4.9
12,0,0	18.9	+ 17.2	3	76.8	+ 69.0	4	4.0	+ 5.7	2	<1.6	− 6.5
1	14.7	+ 10.6	4	5.8	− 5.4	6	3.8	− 7.0	3	2.2	+ 5.5
2	8.9	− 4.4	5	24.3	− 22.3	8	4.5	+ 3.5	4	<1.8	+ 0.1

to have observable intensities. An intensity range of over 30 000 to 1 was measured by visual observation using a series of timed exposures which varied by a factor of 4 from one exposure to the next. A series of 6 exposures was sufficient for most levels. The intensities were corrected for the Lorentz and polarization factors by the method developed by Waser[5] for the zero levels while the upper levels were corrected by an analogous method which has been described by one of us.[6] With *Mokα* radiation the linear absorption coefficient is 14.2 cm^{-1} for chlorine trifluoride and 7.7 cm^{-1} for fluorothene. Thus, the effect of absorption on the intensities is not serious, and no corrections were made for it. For the reflections which were recorded on two or more levels an average was taken of the corrected intensities. Finally, a set of structure factors was obtained by taking the square root of the corrected intensities.

III. STRUCTURE ANALYSIS

Extrapolation of the density of liquid chlorine trifluoride to −120°C leads to 4 molecules per unit cell and an x-ray density of 2.53 g/cc. The systematic extinctions show that the space group symmetry is either *Pnma* or *Pn2a*. The statistical test devised by Howells, Phillips, and Rogers[7] for detecting centers of symmetry was applied to the 0*kl* reflections, and the centrosymmetric *Pnma* was indicated as the correct space group. From inspection of the *hk*0 reflections, it appeared that the Cl atom was on a mirror plane at $y=\frac{1}{4}$ in special position (c) of *Pnma* with $x_{Cl}\cong\frac{1}{8}$. This condition was sufficient to fix the signs of a few strong low order reflections. The Harker-Kasper inequalities[8] were ap-

[5] J. Waser, Rev. Sci. Instr. **22**, 567 (1951).
[6] R. D. Burbank, Rev. Sci. Instr. **23**, 321 (1952).
[7] Howells, Phillips, and Rogers, Acta Cryst. **3**, 210 (1950).
[8] D. Harker and J. S. Kasper, Acta Cryst. **1**, 70 (1948).

TABLE II—*Continued.*

hkl	F_o	F_c	hkl	F_o	F_c	hkl	F_o	F_c	hkl	F_o	F_c
652	<2.0	− 1.6	273	4.9	− 3.6	004	71.5	−92.5	834	36.5	− 35.5
6	<2.0	− 2.2	303	80.1	− 75.6	2	34.1	+26.3	904	<1.8	− 5.0
7	<2.2	+ 2.8	1	<1.3	+ 1.3	4	51.6	−58.3	1	<1.6	+ 0.2
702	23.4	+ 24.6	2	11.6	+ 5.2	6	23.6	+24.6	2	2.2	− 0.7
1	41.4	+ 31.3	3	5.1	+ 5.5	104	6.0	− 5.9	015	15.4	+ 15.2
2	4.7	− 1.0	4	43.4	− 44.3	1	3.8	− 6.1	3	23.8	− 26.5
3	47.4	− 45.8	5	<2.0	+ 3.4	2	5.8	− 7.9	5	2.1	+ 2.1
4	14.7	+ 16.3	6	17.6	+ 14.0	3	6.9	+ 8.1	105	8.7	+ 9.3
5	15.6	+ 10.0	7	5.1	+ 4.0	4	<1.8	− 2.0	1	19.6	− 17.8
6	9.1	− 5.5	403	19.8	+ 25.5	5	<1.8	− 1.3	2	3.6	+ 1.4
802	<1.6	− 3.2	1	17.1	+ 12.2	6	<1.8	− 2.4	3	20.0	+ 20.4
1	<1.8	− 6.8	2	2.9	+ 0.2	204	10.9	+16.7	4	7.3	+ 6.0
2	<1.8	+ 1.5	3	23.6	− 21.6	1	41.6	+39.4	5	13.4	− 8.6
3	<1.8	+ 3.4	4	16.2	+ 16.4	2	<1.6	+ 3.0	205	27.6	+ 36.2
4	<2.0	− 2.1	5	8.7	+ 3.5	3	52.5	−52.4	1	6.7	− 6.8
5	<2.0	− 5.6	6	5.6	− 5.6	4	9.6	+10.5	2	6.9	− 0.5
6	<2.2	+ 1.0	7	13.4	− 13.3	5	21.6	+15.1	3	8.7	+ 10.1
902	20.9	+ 24.6	503	5.6	+ 7.8	6	4.5	− 2.3	4	18.0	+ 23.0
1	21.4	− 18.9	1	33.4	+ 27.0	304	4.7	− 8.3	5	<2.0	− 1.8
2	<1.8	+ 7.1	2	3.8	− 4.3	1	7.1	−12.8	305	34.9	− 40.9
3	28.9	+ 25.3	3	49.4	− 41.3	2	2.4	+ 3.5	1	<1.8	+ 3.8
4	12.2	+ 14.6	4	4.2	+ 5.5	3	3.6	+ 5.8	2	22.5	+ 22.6
5	10.0	− 6.6	5	9.8	+ 7.4	4	3.1	− 5.1	3	<2.0	− 1.6
10,0,2	<1.8	− 1.4	6	4.0	− 3.1	5	8.2	−10.7	4	30.1	− 28.8
1	<2.0	− 0.7	603	4.5	+ 4.2	6	<2.0	+ 2.3	405	19.8	− 24.1
2	4.9	+ 5.8	1	27.6	− 27.0	404	33.2	+42.1	1	7.6	− 9.1
3	<2.0	+ 0.8	2	6.2	+ 11.5	1	17.6	−15.5	2	8.5	+ 3.0
4	<2.2	− 1.7	3	31.4	+ 32.5	2	7.3	− 1.2	3	11.4	+ 16.8
11,0,2	37.2	− 39.5	4	4.5	+ 1.8	3	22.5	+24.6	4	14.9	− 15.8
1	4.0	+ 7.0	5	14.2	− 12.8	4	25.2	+26.0	505	<1.6	+ 3.6
2	17.6	+ 12.8	703	32.9	+ 40.2	5	8.0	− 4.7	1	24.3	+ 27.8
3	<2.0	− 1.3	1	9.3	− 9.3	6	8.7	− 7.4	2	3.6	− 2.7
013	61.7	− 63.8	2	4.9	− 1.1	504	4.5	− 4.9	3	22.7	− 29.4
3	60.3	+ 67.8	3	13.4	+ 13.5	1	<1.8	− 0.9	605	5.6	− 12.7
5	27.6	− 27.9	4	20.5	+ 24.7	2	13.6	+16.4	1	15.1	+ 11.5
7	28.7	+ 34.0	5	4.7	− 3.3	3	<1.8	+ 0.9	2	<2.0	− 2.1
103	33.8	+ 39.1	803	52.5	− 46.3	4	5.1	− 5.1	3	18.3	− 18.2
1	23.4	− 21.8	1	8.9	+ 8.0	5	<2.0	− 0.3	705	22.0	+ 21.7
2	6.7	+ 8.3	2	26.9	+ 21.7	604	47.0	−49.6	1	5.3	− 3.7
3	40.3	+ 39.3	3	6.9	− 5.2	1	<1.8	+ 0.8	2	16.5	− 9.8
4	17.4	+ 21.1	4	37.2	− 31.9	2	22.9	+13.6	006	<1.3	− 4.5
5	5.8	− 4.0	5	5.1	+ 6.3	3	4.9	+ 6.8	2	8.9	+ 15.2
6	6.2	− 4.1	903	22.5	− 24.7	4	34.9	−33.3	106	21.6	− 29.9
7	23.8	+ 22.5	1	<1.8	− 4.1	5	<2.0	+ 4.9	1	8.5	− 6.8
203	74.1	− 78.0	2	10.9	+ 4.5	704	3.6	− 5.6	2	14.7	+ 7.3
1	3.3	− 5.1	3	9.1	+ 11.1	1	7.1	+ 5.1	206	<2.0	− 5.8
2	30.3	+ 25.7	4	19.6	− 16.5	2	<1.8	+ 1.7	1	4.9	+ 7.9
3	<1.6	− 2.8	10,0,3	7.9	+ 6.2	3	2.4	− 1.2	2	<2.0	+ 1.8
4	47.6	− 47.1	1	22.5	+ 20.8	804	3.1	+ 2.2	306	<2.0	− 4.3
5	<1.8	− 2.8	2	7.8	− 4.1	1	33.8	+28.2	1	23.4	+ 21.4
6	20.3	+ 21.1	3	21.8	− 23.9	2	6.7	− 8.8	2	<2.0	− 2.7
									406	<2.0	− 4.8

plied in the manner which one of us has described[9] and combined with the above information to yield sufficient signs for convergent Fourier syntheses of the *hk*0 and 0*kl* data. Because no structure factor computation was involved it was but a single day's work per projection to derive the signs and to perform the Fourier syntheses. The results of these first electron density projections, which are obtained directly from the x-ray diffraction data, indicate that quite roughly the chlorine trifluoride molecule is in the form of a "*T*." The structure analysis involves 7 parameters which define the positions of the Cl atom and one F atom (F_1) in special position (c) and one F atom (F_2) in general position (d) of *Pnma*. Resolution is limited on all three axial projections so that no accurate details of the structure were to be expected from 2-dimensional work.

IV. REFINEMENT

Accurate refinement of the structure was carried out by 3-dimensional Fourier syntheses. Lines and sections of electron density were computed in the early stages but for most of the analysis the method of peak location developed by Shoemaker, *et al.*[10] was used in which the 27 points in a 3 by 3 by 3 grid are fitted by least squares to a 10 parameter Gaussian function. The analysis

[9] R. D. Burbank, Acta Cryst. **4**, 140 (1951); **5**, 236 (1952).

[10] Shoemaker, Donohue, Schomaker, and Corey, J. Am. Chem. Soc. **72**, 2328 (1950).

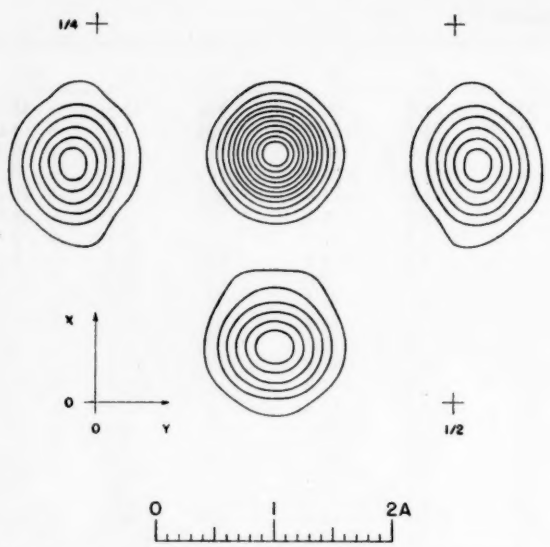

FIG. 3. Electron density in the plane $z=2x\times0.0397$. Lowest contours at $2e.A^{-3}$ on all peaks, then at intervals of $5e.A^{-3}$ on the chlorine peak and at intervals of $3e.A^{-3}$ on the fluorine peaks.

proceeded through six refinements in which the complete set of structure factors was calculated at each stage. At this point the signs of only a dozen small coefficients were uncertain. Several more refinements were made in which structure factor calculations were limited to these twelve coefficients and correction syntheses were added to the preceding syntheses. This process ended when the signs computed from the final synthesis agreed with the signs which were put into the synthesis. Termination of series corrections were applied in the usual manner[11] to the final parameters and were found to be quite small. The shift in radial position caused by these corrections amounted to 0.003A for the Cl and F_2 atoms and to 0.012A for the F_1 atom. The parameters after correction for termination of series effects are expressed as fractions of the cell constants in Table I.

Structure factor calculations were carried out with Hartree atomic scattering factors modified by an isotropic temperature correction of $B=1.68A^2$. The correlation function $F=\Sigma\big|\,|F_{obs}|-|F_{calc}|\,\big|/\Sigma|F_{obs}|$ has the value 0.157 if unobserved reflections are assumed to be zero, and the value 0.134 if unobserved reflections are omitted from the calculation. The final set of observed and calculated structure factors is presented in Table II.

The electron density data can be described most graphically by means of Fig. 3. Here for purposes of illustration we have evaluated the electron density in the plane $z=2x+0.0397$. The plane of the molecule is inclined to the plane of the electron density map by 5° with the result that the molecule is foreshortened along the x direction by 0.4 percent. All the atomic centers lie 0.07A above or below the plane of the map. At the atomic centers the peak densities are greater than in Fig. 3, being over $58e.^-/A^3$ for Cl and around $20e.^-/A^3$ for the F atoms.

V. DESCRIPTION OF STRUCTURE

The final parameters lead to a molecule which is exactly planar and which is illustrated in Fig. 4. The

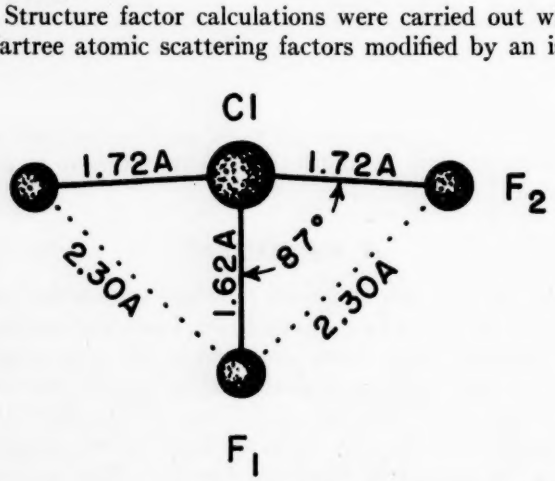

FIG. 4. Distances and angles in the chlorine trifluoride molecule.

[11] A. D. Booth, Proc. Roy. Soc. (London) **A188**, 77 (1946).

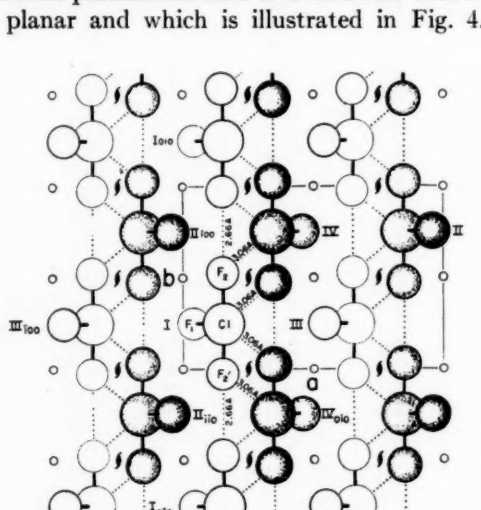

FIG. 5. Crystal structure of chlorine trifluoride. Positive direction of c axis points out of plane of figure.

molecule conforms to the point group symmetry mm. The Cl−F_1 bond distance is 1.621A while the Cl−F_2 bond distance is 1.716A. The F_1−Cl−F_2 bond angle is 86°59′. The F_1−F_2 distance is 2.298A.

The crystal structure is illustrated in projection along the c axis in Fig. 5. Each molecule makes contacts of less than 4A with fourteen neighboring molecules. The closest chlorine to fluorine contacts occur at a distance of 3.06A. These distances are related by screw axes so that they spiral through the structure parallel to the c axis. The closest fluorine to fluorine contacts occur at a distance of 2.66A. The net result is that the molecules are bound together in layers with the plane of a layer parallel to the (100) plane. The closest contacts within a layer are illustrated in Fig. 6. The plane of the figure

is parallel to the plane of a layer, and only molecules belonging to one layer are included in the drawing. All contacts between layers are longer than those illustrated. The F_1 atom is not involved in any of these close contacts. A summary of the intermolecular distances is presented in Table III. The numerals I, II, III, and IV designate molecules located at $x\frac{1}{4}z$; $\bar{x}\frac{3}{4}\bar{z}$; $\frac{1}{2}+x, \frac{1}{4}, \frac{1}{2}-z$ and $\frac{1}{2}-x, \frac{3}{4}, \frac{1}{2}+z$, respectively. Other molecules in adjacent unit cells are designated by the same numerals but a subscript is added to indicate the lattice translation involved in translating a molecule from the origin cell to an adjacent cell. To distinguish between F_2 atoms in the same molecule the convention has been used for all molecules that the atom with the larger y coordinate along the positive b axis direction is designated F_2, while the other atom is designated $F_{2'}$. The nomenclature is illustrated in Figs. 5 and 6.

TABLE III. Intermolecular distances.

From atom x on molecule I	To atom y	On molecule a	Equivalent contact[a] to molecule b	Distance in A
Cl	F_2	IV $0\bar{1}0$	IV $00\bar{1}$	3.06
	$F_{2'}$	IV	IV $0\bar{1}\bar{1}$	
Cl	F_2	IV $0\bar{1}\bar{1}$	IV	3.17
	$F_{2'}$	IV $00\bar{1}$	IV $0\bar{1}0$	
Cl	F_2	II $\bar{1}10$	II $\bar{1}00$	3.26
	$F_{2'}$	II $\bar{1}00$	II $\bar{1}10$	
Cl	F_1	III	III $\bar{1}00$	3.39
Cl	F_1	I 001	I $00\bar{1}$	3.42
F_2	$F_{2'}$	I 010	I $0\bar{1}0$	2.66
F_2	$F_{2'}$	IV	IV $0\bar{1}0$	2.87
	$F_{2'}$	IV $\bar{1}00$	IV $0\bar{1}\bar{1}$	
F_2	$F_{2'}$	II $\bar{1}00$	II $\bar{1}10$	2.97
F_1	F_2	II $\bar{1}\bar{1}\bar{1}$	II $\bar{1}0\bar{1}$	3.02
	$F_{2'}$	II $\bar{1}0\bar{1}$	II $\bar{1}\bar{1}\bar{1}$	
F_1	F_2	IV $0\bar{1}\bar{1}$	IV	3.20
	$F_{2'}$	IV $00\bar{1}$	IV $0\bar{1}0$	
F_1	F_2	II $\bar{1}10$	II $\bar{1}00$	3.25
	$F_{2'}$	II $\bar{1}00$	II $\bar{1}10$	
F_1	F_1	II $\bar{1}\bar{1}\bar{1}$		3.27
	F_1	II $\bar{1}0\bar{1}$		
F_1	F_2	III $\bar{1}00$	III	3.85
	$F_{2'}$	III $\bar{1}00$	III	
F_1	F_2	I $00\bar{1}$	I 001	3.87
	$F_{2'}$	I $00\bar{1}$	I 001	

[a] If the contact is from atom x on molecule I to atom y on molecule a, the equivalent contact is from atom y on molecule I to atom x on molecule b.

The pronounced layer-like characteristics of the structure lead one to ask whether there is any possibility of randomness in the way the layers stack together to form a crystal. The answer is that a randomness of this type does occur. With very strong exposures short streaks can be detected in the reciprocal lattice which are perpendicular to the reciprocal b axis. It is unlikely that the streaks are caused by thermal vibrations because they can still be observed on diffraction patterns recorded at $-180°$C.

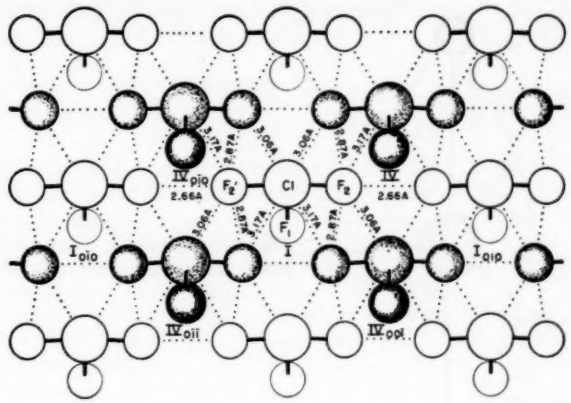

FIG. 6. Intermolecular contacts within a layer. Positive direction of a axis points out of plane of figure.

VI. STANDARD ERRORS

The standard errors in the parameters were calculated by the usual formula[12] involving the differences between F_{obs} and F_{calc} and the curvatures of the electron density at peak centers. The results are listed in Table IV. These lead to a standard error in the $Cl-F_1$ bond distance of 0.0058A, while the standard error in the $Cl-F_2$ bond distance is 0.0040A. The standard error in the F_1-Cl-F_2 bond angle is 0°15′, and the standard error in the F_1-F_2 distance is 0.0084A.

In the succeeding pages of this journal the structure of chlorine trifluoride in the vapor phase as determined by microwave spectroscopy is reported by Dr. D. F. Smith of this laboratory. In the vapor phase the $Cl-F_1$ distance is 1.598A, the $Cl-F_2$ distance is 1.698A, and the bond angle is 87°29′. The statistical procedure which we have used to estimate the standard errors in a crystal structure is not appropriate to the microwave case. However, let us make the conservative assumption that the microwave analysis involves standard errors of 0.005A in bond distances and 0°15′ in the bond angle. Following Cruickshank[12] we can then compute the probability that the difference in a bond distance or angle as determined by x-rays and by microwaves is not real and is caused by random errors. We obtain the following probabilities

$$\begin{aligned} Cl-F_1 \quad & P=0.00145, \\ Cl-F_2 \quad & P=0.00250, \\ \alpha \quad & P=0.07675. \end{aligned}$$

Using accepted levels of significance[12] we now state that the difference in bond distances is significant and real,

TABLE IV. Standard errors of parameters.

Atom	$\sigma(x)$	$\sigma(y)$	$\sigma(z)$
Cl	0.0016		0.0018A
F_1	0.0053		0.0057A
F_2	0.0062	0.0040	0.0080A

[12] D. W. J. Cruickshank, Acta Cryst. 2, 65 (1949).

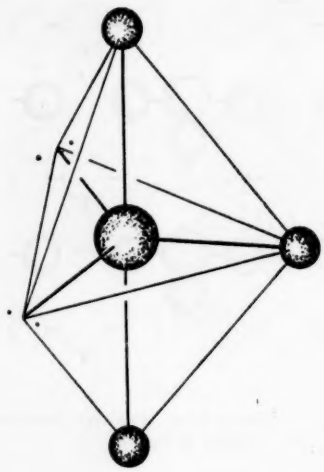

FIG. 7. Approximation of sp^3d orbitals to the chlorine trifluoride configuration.

while the difference in bond angle is not significant and may be attributed to random errors. Thus, the bond distances increase by 0.02A or 1.25 percent in going from the vapor phase to the crystalline phase, but the molecular configuration does not change. Finally, we should note that the probability that the difference between the observed bond angle of 87° and a 90° angle is caused by random errors is hardly worth considering, for it is of the order of 1×10^{-32}.

VII. DISCUSSION

The rather accurately known structure of chlorine trifluoride is difficult to explain in simple terms. As a first approximation we might consider hybridized sp^3d orbitals such as are illustrated in Fig. 7. In the ground state of chlorine there are two $3s$ and five $3p$ electrons. By promoting a $3s$ electron to a $3d$ orbidal one obtains hybrid sp^3d orbitals, in which three orbitals are available for bonding while two orbitals are filled with unshared electron pairs. The sp^3d orbitals are directed to the corners of a trigonal bipyramid and the configuration of chlorine trifluoride is approximated if one postulates that the two axial orbitals and one equatorial orbital are used for Cl—F bonds. However, this postulate does not seem very reasonable when we consider Fig. 8. Above, the chlorine trifluoride molecule has been drawn with the van der Waals radii shaded in. The F_1-F_2 distance is only 2.3A, and one would expect a great deal of repulsion between these atoms. Below, a hypothetical molecule has been drawn in which the fluorine atoms occupy the equatorial positions in sp^3d hybrid orbitals, and the Cl—F distance is assumed to be 1.62A, the distance found for the short bond in the real molecule. Now the F—F distances have increased by 0.5A to 2.8A and one would expect no repulsion between these atoms. However, chlorine trifluoride does not exist in this configuration, and it seems reasonable to ask whether there is some interaction other than van der Waals forces acting between the fluorine atoms.

The microwave analysis[13] of the vapor phase of chlorine monofluoride led to a Cl—F distance of 1.628A. This may be compared with the $Cl-F_1$ distance of 1.598A and the $Cl-F_2$ distance of 1.698A as determined by Smith for the vapor phase of chlorine trifluoride. If 1.628A represents the Cl—F single bond length, then the $Cl-F_1$ bond must be stronger, and the $Cl-F_2$ bond weaker, than a single bond. However, if the $Cl-F_1$ bond has some multiple bond character it raises an interesting question, because a fluorine atom has only one orbital available for bond formation. A way to make additional fluorine orbitals available is to transfer electrons from fluorine to the $3d$ orbitals of chlorine. This would imply a formal positive charge on the F_1 atom and a formal negative charge on the chlorine atom. The $Cl-F_1$ bond would no longer be cylindrical but would have some π character superimposed on a σ bond. The bonding electrons in the $Cl-F_2$ bonds might be expected to shift towards the F_2 atoms so that the $Cl-F_2$ bonds would become more ionic and less covalent in character. In effect there would be a transfer of negative charge from the F_1 atom to the F_2 atoms by way of the chlorine $3d$ orbitals. Then the electrostatic interaction between the fluorine atoms might lead to the 87° bond angle. It is a curious fact that the dipole moment of 0.554 D found for chlorine trifluoride[14] is less than the moment of 0.881 D found for chlorine monofluoride.[13] It is not clear whether this can be attributed to a fluorine to chlorine electron transfer or if it should be interpreted as a cancellation of the $Cl-F_1$ moment by chlorine lone pair hybrids.

FIG. 8. Above: Chlorine trifluoride molecule with van der Waals radii shaded in. Below: Hypothetical chlorine trifluoride molecule with van der Waals radii shaded in.

ACKNOWLEDGMENTS

Miss Virginia Feaster gave valuable assistance with the visual measurement of intensities. Many of the calculations were carried out on I.B.M. machines by Mr. E. C. Witt. We are indebted to Dr. S. C. Abrahams and Dr. E. Grison for helpful advice on low temperature techniques.

[13] Gilbert, Roberts, and Griswold, Phys. Rev. **76**, 1723 (1949).
[14] D. W. Magnuson, J. Chem. Phys. **20**, 229 (1952).

The Microwave Spectrum and Structure of Chlorine Trifluoride*

D. F. SMITH
K-25 Laboratories, Carbide and Carbon Chemicals Company, Oak Ridge, Tennessee
(Received September 30, 1952)

A microwave spectrometer designed for the study of the microwave spectra of corrosive fluorine compounds has been used to observe and measure a portion of the microwave spectrum of chlorine trifluoride. A number of transitions have been identified, and from these the moments of inertia and quadrupole coupling coefficients of both $Cl^{35}F_3$ and $Cl^{37}F_3$ obtained. An intensity alternation was observed showing that the ClF_3 molecule has a C_{2v} axis and is planar. The moments of inertia confirm this and further show that ClF_3 has a distorted "T" structure with one short (1.598A) and two long (1.698A) ClF bonds. The angle between the two different kinds of ClF bonds is 87°29′. The quadrupole coupling coefficients $\chi_{aa}(Cl^{35}F_3) = -81.2$ mc, $\chi_{bb}(Cl^{35}F_3) = -64.7$ mc, $\chi_{cc}(Cl^{35}F_3) = 146$ mc agree with the observed frequency, $f(Cl^{35}F_3) = 75.129_6$ mc, of the pure quadrupole spectrum of ClF_3, which corresponds to an eqQ of 150 mc.

INTRODUCTION

PRIOR to the present investigation and to the concurrent investigation of the x-ray diffraction of crystalline ClF_3 reported in the preceding paper, the structure of ClF_3 was known only to the extent that certain structures had been excluded. Thus, the planar symmetric structure had been ruled out by the observation of a dipole moment of 0.554 Debye units.[1] Further, the vibration spectrum[2] could not be interpreted on the basis of only four fundamentals required either for the planar symmetric structure, or for the symmetric pyramidal structure obtained from electron diffraction data.[3]

There was available further experimental evidence that ClF_3 is not a symmetric top molecule. The examination of the infrared spectrum at high resolution failed to show any resolvable rotation lines,[4] indicating rotational spacings of less than 0.4 cm^{-1}. An even closer spacing was at least suggested by the failure to obtain any appreciable increase in intensity of the strong infrared band near 14μ when this band was pressure broadened.[5] Such behavior could be expected for an asymmetric top structure which had appreciable asymmetry.

Somewhat earlier unreported studies of the microwave spectrum by Tidwell, Williams, and the author had failed to display any microwave lines that could be attributed to a symmetric top molecule, while weak lines that could be attributed to an asymmetric rotor were found. After unsuccessful attempts to demonstrate that these lines were due to an impurity, the work was interrupted for a considerable period, and resumed only shortly before the preliminary x-ray diffraction results were available.

EXPERIMENTAL DETAILS

The microwave spectrometer used for this work differs only slightly from the conventional Stark modulation spectrometer.[6] The few modifications in the usual design were made in order that reactive fluorine compounds could be studied, and hence relate only to the Stark absorption cell and the associated sample handling manifold. The problem of corrosion is a serious one, not in the ordinary sense, because of the destruction of the apparatus, which proceeds at a negligible rate at the low pressures (20–200 microns of mercury) required for resolved microwave spectra, but because this corrosion results in a destruction of the sample whose spectrum is desired. Absorption and adsorption on the cell walls are also of importance.

The Stark cell is an eight-foot length of 1-in. × ½-in. copper wave guide with a copper Stark electrode supported with Teflon spacers. The cell windows are of fluorothene polymer sheets. In order that these polymer sheets be reliably free of pin holes it is found necessary to use a thickness of 0.015 in. and to accept the resulting reflections. With this thickness it is possible to use a wax-free seal by turning groove and tongue circles on the wave guide flanges. This procedure is desirable since available fluorine resistant waxes are usable only over relatively narrow temperature ranges. The Stark electrode voltage lead-in wire has soldered to it a copper disk with a raised edge. The seal and insulation are then achieved with fluorothene gaskets, the seal being at the edge of the disk.

The sample manifold is of copper tubing either hard soldered or joined with brass flare fittings. Crane and Kerotest valves with fluorothene or nickel seats are used in this manifold.

With such a system spectral lines of such compounds as ClF, BrF, BrCl, COF_2, NO_2F, NOF, and ClF_3 have been observed. The reaction and absorptions on the surfaces, however, result in a dilution of the sample, with an observed decrease in line intensity. This has been studied in most detail for ClF. For the ClF lines, the intensities follow a decay curve $I = I_0 e^{-kt}$. The

* This document is based on work performed for the U. S. Atomic Energy Commission by Carbide and Carbon Chemicals Company a Division of Union Carbide and Carbon Corporation at Oak Ridge, Tennessee.

[1] D. W. Magnuson, J. Chem. Phys. **20**, 299 (1952).
[2] Jones, Parkinson, and Murray, J. Chem. Phys. **17**, 501 (1949).
[3] A. L. Wahrhaftig, quoted by P. W. Allen and L. E. Sutton, Acta Cryst. **3**, 46 (1950).
[4] Nielsen, Burke, and Jones, private communication.
[5] T. G. Burke, private conversation.
[6] McAfee, Hughes, and Wilson, Rev. Sci. Instr. **20**, 821 (1949).

constant k is strongly dependent on the past history of the absorption cell, especially the more immediate past history, while the decay curve can be extrapolated back to the time of filling with good reproducibility. The decay can be made more gradual by storing the sample in the system at a few inches pressure for a few hours before evacuating and admitting a fresh sample. Since it is difficult to reduce this decay rate to as small a value as desirable, the absorption cell has been fitted with an inlet port at the opposite end from the evacuation port. A needle valve in the inlet line is then used to regulate the flow from the sample reservoir where the sample is stored at several inches pressure. The pressure in the cell is then determined by the flow, and the spectrum observed is that of a relatively fresh sample at all times. For ClF the intensity corresponds closely to the extrapolated I_0 of a trapped sample.

The Stark modulation is achieved either with a zero based 93 kc/sec square wave generator[7] or with a 93 kc/sec sine wave generator with adjustable additional dc bias. The output signal is detected with a phase sensitive detector with a time constant of one second or less, and displayed on a meter. On occasion this output is also recorded with an L and N Speedomax recorder. Usually, pen records were made as the 2K33 klystron was slowly tuned by a motor drive on the klystron resonator tuning screw. When intensity measurements were made, the dc output of the spectrometer detector crystal was manually monitored by adjusting a variable microwave attenuator.

The frequency measurement system is similar to that of Untermeyer and Smith[8] but we used a 2C40 lighthouse triode tripler from 270 mc to 810 mc to replace the klystron multiplier used by them. In order to avoid the corrections arising from different time lags in the spectrometer and frequency measurement systems, the line frequencies were measured at what is essentially constant frequency. The klystron frequency is manually adjusted so that the spectrometer output meter indicates that this is the frequency of the line center, and the marker pip simultaneously tuned to measure the klystron frequency.

All of the studies of the spectrum of ClF_3 were made with most of the Stark cell packed in CO_2 snow in order to increase the line intensities. In the measurement of these intensities every effort was made to maintain a set of standard conditions, as regards sample pressure, spectrometer amplifier gain, sine modulation and bias, and detected crystal output. The microwave system was carefully tuned to obtain maximum spectrometer detector crystal output in the region of the lines to be measured. Even so the variations in standing waves can introduce relatively large errors, and an estimate of ± 25 percent precision on relative intensity measurements is considered optimistic, especially when the lines compared are remote in frequency.

Since it is difficult to purify ClF_3, and since it has proven impossible to store a sample of ClF_3 for an extended period without the sample becoming impure, commercial ClF_3, obtained from the Harshaw Chemical Company, was used for this work. High boiling components (as ClF) were occasionally removed by chilling the sample with CO_2 trichloroethylene slush and removing samples until the vapor pressure was less than 2 mm. Even with a sample, thus purified, the strongest ClF line (with an estimated concentration of less than 0.5 percent ClF present) was as intense as the strongest observed line of ClF_3, and it does not seem unlikely that some of the other lines observed are due to other impurities.

In addition to the microwave spectrum, Dr. Ralph Livingston of the Oak Ridge National Laboratory, cooperatively with the author, observed and measured the pure nuclear quadrupole spectrum of crystalline ClF_3. With the video method then used at ORNL, the lines were not observable with the sample at liquid nitrogen temperatures, and it was necessary to chill the sample with a liquid hydrogen bath. For this about twenty grams of ClF_3 were frozen in a small copper cell containing the oscillator coil. This copper cell was hard soldered to a ten inch length of nickel tubing which then formed the outer sheath of a coaxial line from the coil to the rest of the oscillator. The insulated seal was made at the end of the nickel tube in the same manner as the Stark spectrometer lead-in wire seal at the position where it was well out of the hydrogen bath and hence never cooled to such a low temperature that the gaskets shrank and the seal opened. The seal was tightened with the seal and gaskets cooled with liquid nitrogen before filling the cell through a side arm.

SPECTRUM OF ClF_3

Results and Interpretation

The regions from 19–21 kmc and from 23.5–25.5 kmc were searched in detail and approximately 70 weak lines were logged. Some of these could be identified as typical nuclear quadrupole coupling hyperfine structure lines for $\Delta J=0$, $\Delta F=0$ transitions.[9] The groups near 21 kmc could be unambiguously assigned as $\Delta J=0$, $J=5$ transitions. The groups in the region 25.22 kmc and 25.37 kmc were $\Delta J=0$, $J=8\pm1$ transitions, and the group in the region 24.325 kmc was a $\Delta J=0$, $J=5\pm1$ transition. These less certain assignments result on the one hand from the small spreads in frequency for the hyperfine groups, and on the other from the unusually large (±0.15 to ±0.05 mc) errors with which the frequencies of these weak lines were measured. In addition to these $\Delta J=0$ groups, there were two similar five line groups about 115 mc apart near 24.0 kmc. The relative intensities and spacings in these

[7] L. C. Hedrick, Rev. Sci. Instr. **20**, 781 (1949).
[8] R. R. Untermeyer and W. V. Smith, Rev. Sci. Instr. **19**, 580 (1948).
[9] Bragg, Madison, and Sharbaugh, Phys. Rev. **77**, 148 (1950).

FIG. 1. Tracing of chart records of microwave spectrum of ClF_3.

groups would appear to correspond to a very low J, $\Delta J=1$ transition. Pen records of some of these groups, given in Fig. 1 can be identified by reference to Table I. The low signal-to-noise ratio resulting from the low intensity should suggest some of the difficulties in working with this spectrum.

Of the assignments which were also consistent with these partial identifications, suggested by the preliminary x-ray diffraction results kindly supplied to the author by Dr. Burbank, one was found which yielded values of $(a-c)/2$ and κ which corresponds to the observed spectrum. In this fashion, four $\Delta J=0$ groups for $Cl^{35}F_3$, and the corresponding groups for $Cl^{37}F_3$ could be identified. The x-ray diffraction model also indicated the groups at 24.0 kmc were the $1_{0,1;-1}-2_{1,2;-1}$ transitions occurring at $a+3c$. In all then, some 38 lines could be identified.

The frequencies of these identified transitions are given in Table I. Included for comparison are the computed frequencies using the rotational parameters given in Table II, and the quadrupole coupling parameters of Table III.

The quadrupole coupling parameters were evaluated from the four resolved hyperfine components of the $1_{0,1;-1}-2_{1,2;-1}$ transitions. This choice was made since the evaluation can be made solely on the basis of proper identification of the components and their measured frequencies. The hyperfine structure of the $\Delta J=0$ transitions were then computed by the method of Bragg.[10] For this, values of $E_J{}^\tau(\kappa)$ and $dE_J{}^\tau(\kappa)/d\kappa$ are needed. The $E_J{}^\tau(\kappa)$ were computed by the continued fraction method of King, Hainer, and Cross,[11] and the values of $dE_J{}^\tau(\kappa)d\kappa$ were taken from calculated values of $E_J{}^\tau(\kappa)$ at intervals of κ of 0.0001, about the value of κ which give the best agreement between the observed and computed hypothetical unsplit frequencies of the $\Delta J=0$ transitions.

Since rigid rotor theory, without correction for centrifugal distortion was employed, since only an approximate first-order quadrupole coupling theory was used, and since the measured frequencies are subject to unusually large errors, the fit of the 38 lines to the 10 spectral parameters is adequate to verify the identification and the validity of the parameters derived. The similarities of the values of (ν obs$-\nu$ calc) for corresponding transitions of the two isotopic species indicate that the centrifugal distortion effects are similar in these two molecules, as would certainly be expected.

The experimental intensities given in Table I are in units of chart division pen deflection. The computed intensities were obtained by graphical interpolation in the line strength tables of Cross, Hainer, and King,[12] by reference to the conventional hyperfine intensity tables, and by using a 3:1 abundance ratio for $Cl^{35}:Cl^{37}$. Further, a 3:1 statistical weight factor for $a:s$ symmetry of the states involved in the transition has been included. This results if a C_{2v} axis with one pair of fluorine atoms (with nuclear spin, $I=\frac{1}{2}$) off the axis is assumed.[13] The relative intensities so obtained have been converted into pen deflections by a single experimental conversion factor, the ratio of the sums of the pen deflections for all the observed, identified, and resolved lines, to the sum of the relative intensities for these same lines. The agreement here is considered sufficiently good to verify the $a:s$ intensity alternation, if it is recognized that the precision of relative intensity measurements for lines remote in frequency (the $5_{0,5;-5}-5_{1,4;-3}$) is considerably poorer than for nearby lines and that with the Stark spectrometer unresolved

[10] J. K. Bragg, Phys. Rev. **75**, 735 (1949).
[11] King, Hainer, and Cross, J. Chem. Phys. **11**, 27 (1943).
[12] Cross, Hainer, and King, J. Chem. Phys. **12**, 210 (1944).
[13] G. Herzberg, *Infrared and Raman Spectra of Polyatomic Molecules* (D. Van Nostrand Company, Inc., New York, 1945), p. 53.

TABLE I. Identified and measured portion of microwave spectrum of ClF_3.

			$Cl^{35}F_3$						$Cl^{37}F_3$				
Designation	$(J_{K-1,K+1;\tau})''$ $-(J_{K-1,K+1;\tau})'$	F'' F'	Observed frequency in mc	Observed intensity in chart divisions	Calculated frequency in mc	Calculated intensity in chart divisions	Observed frequency minus calculated frequency in mc	Designation	Observed frequency in mc	Observed intensity in chart divisions	Calculated frequency in mc	Calculated intensity in chart divisions	Observed frequency minus calculated frequency in mc
A	$1_{0,1;-1}$	5/2- 5/2	24 063.80	7	24 063.78	9	−0.02	*a*	23 957.6_5	3	25 957.5_9	3	−0.06
B	$-2_{1,2;-1}$	1/2- 3/2	24 073.4_4	9	24 073.60	9	−0.26	*b*	23 965.2_3	3	25 965.3_2	3	−0.09
C		3/2- 5/2	24 084.0_0	21	24 084.09	21	+0.09	*c*	23 973.8_7	7	25 973.9_4	7	−0.07
D	(a)	5/2- 7/2	24 100.4_2	36	24 100.28	41	−0.14	*d*	23 986.7_5	11	25 986.7_2	13	−0.03
E		3/2- 3/2	24 110.3_2	21	24 110.16	12	−0.18	*e*	23 994.5_5	7	25 994.3_5	3	−0.20
		1/2- 1/2			24 110.10	11	−0.22				25 993.7_0	3	+0.15
F	$5_{0,5;-5}$	13/2-13/2	20 990.6_4	19	20 989.66	40	−0.98		[b]		20 989.95	13	−0.64
I	$-5_{1,4;-3}$	11/2-11/2	21 032.6_7	21	21 032.22	32	−0.46		20 023.9_5	8	21 023.40	11	−0.55
M		9/2- 9/2	21 021.1_1	20	21 020.21	26	−0.90	*m*	20 013.8_7	5	21 013.93	8	−0.94
N	(a)	7/2- 7/2	20 078.2_2	18	20 977.66	41	−0.56	*n*	20 981.3_6	6	20 980.59	7	−0.77
O	$5_{1,4;-3}$	13/2-13/2	24 309.1_2	[a]	24 309.56	69	+0.44	*o*	24 060.0_0	[a]	24 060.37	23	+0.37
P	$5_{2,3;-1}$	11/2-11/2	24 310.4_3	45	24 310.87	55	+0.44	*p*	24 062.0_9	6	24 061.23	18	+0.76
Q		9/2- 9/2	24 310.0_5	−50	24 310.48	44	+0.43			15	24 061.27	15	+0.82
R	(a)	7/2- 7/2	24 308.65		24 309.19	38	+0.54				24 060.19	13	+0.19
S	$6_{1,5;-4}$	15/2-15/2	24 321.86	32	24 322.65	28	+0.79		24 111.8_2	16	24 113.36	9	+0.54
T	$6_{2,4;-2}$	13/2-13/2	24 328.15	24	24 328.88	24	+0.73		24 118.2_0	6	24 118.62	8	+0.42
U	(s)	9/2- 9/2	24 326.60	23	24 327.41	20	+0.81	*u*	24 117.3_5	10	24 117.38	7	+0.03
V		7/2- 7/2	24 320.70	24	24 321.20	18	+0.83		[c]	—	24 112.12	—	—
W	$7_{1,6;-5}$	17/2-17/2	24 386.11	100	25 369.00	100	+0.99	*w*	25 215.40	21	25 216.36	33	+0.95
X	$7_{2,5;-3}$	15/2-15/2	25 379.38	68	25 380.35	85	+1.03	*x*	25 224.62	32	25 225.65	28	+1.03
Y		13/2-13/2	25 376.85	44	25 378.30	74	+1.44	*y*	25 222.97	27	25 223.76	24	+1.96
Z	(a)	11/2-11/2	25 365.84	51	25 361.72	66	+0.88	*z*	25 213.46	9	25 214.46	22	+1.00

[a] Hyperfine structure not completely resolved under standard conditions for intensity measurements.
[b] Obscured by 20 990.64 $Cl^{35}F_3$ line.
[c] Not resolved from 24 110.32 $Cl^{35}F_3$ line.

lines ($5_{1,4;-3}-5_{2,3;-1}$) can be displayed with intensities somewhat less than their anticipated sum because of phase cancellation. By modifying the observing conditions with some sacrifice of intensity, this $5_{1,4;-3}-5_{2,3;-1}$ transition can be resolved. This is shown in Fig. 2.

The intensity alternation is further substantiated by the low intensity of the $4_{1,3;-2}-4_{2,2;0}$ transition (of species *s*) which although observable was too weak to measure its frequency with adequate precision, and which occurred near another transition of comparable intensity.

The ratios of the $\chi_{aa}(Cl^{35}F_3):\chi_{aa}(Cl^{37}F_3)$ 1.24, and of $\chi_{bb}(Cl^{35}F_3):\chi_{bb}(Cl^{37}F_3)$ 1.26, agree as closely as can be expected to the accepted value of 1.268 for the ratio of the quadrupole moments of the chlorine isotopes.[14]

The frequencies of the pure nuclear quadrupole lines of crystalline ClF_3 are presented in Table IV together with the values of eqQ obtained using the α obtained with the χ_{aa}/χ_{bb} ratio pertaining in the microwave spectrum. This is to be compared with $X_{cc}[=-\chi_{aa}-\chi_{bb}]$ obtained in the microwave spectrum.

The agreement between the observed and fitted frequencies shows that the lines reported are all due to the same compound. The quadrupole structure shows that this compound contains only one chlorine atom. The intensity alternation shows that there is a C_2 or C_{2v} axis with atoms whose nuclei have spins $I>0$, and probably $I=\frac{1}{2}$ off this axis. The single chlorine atom must then lie on the C_{2v} axis. These required criteria together with success of establishing a structure for ClF_3 consistent with the spectrum are strong evidence that the reported spectrum is due to ClF_3, and not to an impurity in the ClF_3. The agreement on the one hand with the pure quadrupole spectrum of ClF_3 and on the other with the x-ray diffraction of ClF_3 establishes this more perfectly. Thus, even though impurity lines may have been observed and not identified as impurities, they have not entered into the interpretation presented.

The rotational constants obtained from the rotational parameters given in Table II are given in Table V. There is no isotope shift in the rotational constant *b*

TABLE II. Rotational parameters of ClF_3.

	$Cl^{35}F_3$	$Cl^{37}F_3$
$(a-c)/2$	5149.15 mc	5105.2 mc
κ	-0.7741_3	-0.7709_5
$a+3c$	24 110.3 mc	23 994.5 mc

TABLE III. Quadrupole coupling parameters of ClF_3.

	$Cl^{35}F_3$	$Cl^{37}F_3$
χ_{aa}	−81.25 mc	−65.41 mc
χ_{bb}	−64.67 mc	−51.11 mc

[14] R. Livingston, Phys. Rev. 82, 289 (1950).

TABLE IV. Pure nuclear quadrupole spectrum of ClF_3 at liquid hydrogen temperature.

	$Cl^{35}F_3$	$Cl^{37}F_3$
ν observed	75.1295 mc	59.2147 mc
2ν	150.2590 mc	118.4284 mc
$\lvert eqQ\rvert$	149.8 mc	118.1 mc
χ_{cc}	+146 mc	+116 mc

within the precision with which this is determined. From the rotational constants the moments of inertia given in Table VI are immediately obtained. The small value of the inertial defect $\Delta = I_c - (I_a + I_b)$ confirms the planar structures. Its finite value can be entirely attributed to zero-point vibration effects.

From I_b, these two fluorine atoms are each 1.697A from the C_{2v} axis. The positions of the Cl, F, and the projection of these two off axis fluorine atoms can be determined from the values of I_a^{35} and I_a^{37}. The resultant structure[15] is given in Fig. 3. The use of I_a^{35} and I_a^{37} in a quadratic equation has the usual two solutions. The solution not presented here is, however, clearly recognized as physically impossible since it involves a ClF bond distance much less than the normal chlorine covalent radius, so that no genuine ambiguity is present.

TABLE V. Rotational constants of ClF_3.

	$Cl^{35}F_3$	$Cl^{37}F_3$
a	13 747.7 mc	13 653.2 mc
b	4 611.7$_2$ mc	4 611.9$_0$ mc
c	3 448.7$_9$ mc	3 442.8$_1$ mc

The major uncertainties in this structure are not due to errors in frequency measurements, but rather the use of the rigid rotator theory. An examination of the calculated and observed frequencies further suggests that the zero-point vibration effects are much more serious than the centrifugal distortion effects. Present knowledge of the uncertainties introduced by zero-point vibration are inadequate to do more than place an upper limit on these uncertainties. The value of the inertial defect can be used as a clue to this uncertainty.

TABLE VI. Moments of inertia of ClF_3 in units of atomic mass units (angstroms)^2.

I_A	36.755	37.010
I_B	109.493	109.509
I_C	146.372	146.667
$I_A + I_B$	146.247	146.519
$\Delta = I_C - I_A - I_B$	0.125	0.148

[15] The author is indebted to Dr. J. Kraitchman of Columbia University who pointed out to the author that the "undistorted T" structure reported at the 1952 New York meeting of the American Physical Society had been incorrectly obtained from the moments of inertia. These incorrect results were due to a numerical mistake by the author.

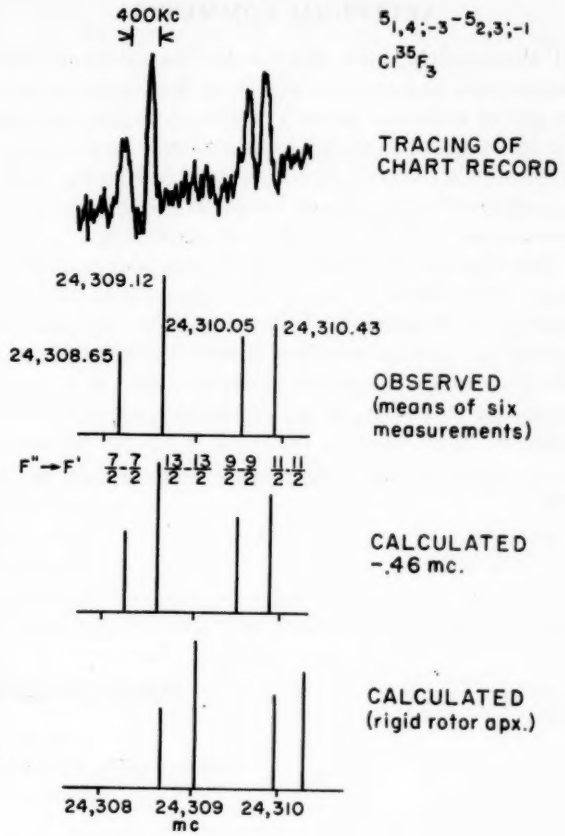

FIG. 2.

For an inertial defect of only ~0.01 percent, with no constituent atom lighter than fluorine, it seems unlikely that these values are incorrect by as much as 0.005A in any dimension, and perhaps no more than 0.002A.

The present results are in excellent agreement with the results of the x-ray diffraction study of crystalline ClF_3 reported in the preceding paper, while the small differences are believed to be real. The relationship between the observed structure and bonding theories has been discussed in the preceding paper. The interpretation of the unusual quadrupole coupling in terms of particular bond configurations is not yet in a satisfactory state, and work is in progress on this matter.

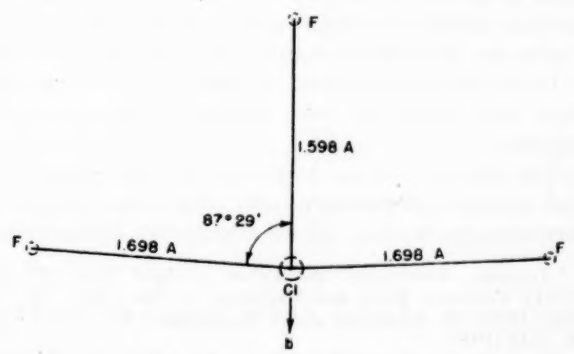

FIG. 3. Structure of ClF_3.

ADDITIONAL COMMENTS

Unfortunately, lines suitable for resolution of Stark components and the evaluation of the dipole moment are not of sufficient intensity to observe and measure. The low intensities of the lines, however, are in accord with a dipole moment as low as the 0.554 Debye units.[1] The observed structure of monomeric ClF_3 makes the existence of a dimer[1,16] somewhat perplexing.

The vibration spectrum of ClF_3 has been studied by Jones[2] and others at the K-25 Laboratories and more recently at Vanderbilt University. The experimental studies of such a reactive compound have been so difficult and the spectrum so unusual that it has been impossible to assign the six fundamental vibration frequencies. Since there is no third group of microwave lines showing spacings similar to the $Cl^{35}F_3$ $1_{0,1;-1}-2_{1,2;-1}$ observed within 500 mc of the ground state transition, it seems unlikely that any $1_{0,1;-1}-2_{1,2;-1}$ transition of molecules in an excited state vibration lines are strong enough to be observable at $-80°C$. This can be taken as evidence that there is unlikely to be a fundamental vibration as low as 200 cm^{-1}.

[16] H. Schmitz and H. J. Schumacher, Z. Naturforsch. **2a**, 363 (1947).

ACKNOWLEDGMENT

The author is indebted to Dr. R. D. Burbank for making available to him the preliminary x-ray diffraction results which greatly speeded the analysis of the spectrum; to Dr. Burbank and Dr. D. W. Magnuson for several helpful discussions; and to Mr. M. Tidwell and Mr. D. V. P. Williams, who had somewhat earlier established the optimum conditions for the observation of the ClF_3 microwave spectrum.

THE JOURNAL OF CHEMICAL PHYSICS VOLUME 21, NUMBER 4 APRIL, 1953

Stress Relaxation in Elastomers

A. M. BUECHE
General Electric Research Laboratory, Schenectady, New York
(Received November 18, 1952)

The process of chemical stress relaxation in elastomers is examined in some detail. It is predicted that in some cases it will be possible to determine the location of the chemical bond broken. The special cases of relaxation due to scission of cross links and random scission of the polymer are calculated. The shapes of the stress *vs* time curves are widely different.

THE measurement of tension as a function of time in elastomers held at constant elongation has been shown by Tobolsky to be a useful tool in investigating thermal and chemical degradation.[1] By varying the temperature and the time of the experiment the viscoelastic behavior also can be studied.[2] During the course of our work it was decided to investigate the possible types of stress relaxation data to be expected from thermal or chemical degradation on the basis of a few simple assumptions. In what follows it will be shown that for vulcanized elastomers it is possible in some cases to decide whether the stress relaxation is due to a random scission of polymer bonds or whether the bonds broken are of a special nature such as those introduced in the cross-linking process. In addition, of course, one may also determine rate constants and activation energies.

The tension τ in an elastomer network system (at high enough temperatures and long enough times of measurement so that viscous effects may be neglected) can be written as[3]

$$\tau = RT\nu\varphi(\alpha), \tag{1}$$

where R is the gas constant, T is the absolute temperature, ν is the number of moles of elastically active chains between cross links in a unit volume of polymer, and $\varphi(\alpha)$ is a function of the elongation which describes the shape of the stress-strain curve. Even though there is some doubt as to the accuracy with which this equation represents the data on elastomers, the approximation has been shown to be reasonably good provided it is applied at low elongations, and provided one lets ν include the number of chains formed because of accidental intertwining of one chain with another. It, at least, serves the purpose of pointing out that the tension is proportional to the number of chains introduced by chemical cross links and the effect of temperature.

In the following we will assume that Eq. (1) represents the facts. This implies that the experiments with which the results are to be compared are done in such a way as to eliminate viscous effects and that, if thermal or chemical bond scission were eliminated, τ would be constant with time provided that T and α

[1] Tobolsky, Prettyman, and Dillon, J. Appl. Phys. **15**, 380 (1944); Tobolsky, Metz, and Mesrobian, J. Am. Chem. Soc. **72**, 1942 (1950); M. Mochulsky and A. V. Tobolsky, Ind. Eng. Chem. **40**, 2155 (1948).

[2] Bischoff, Catsiff, and Tobolsky, J. Am. Chem. Soc. **74**, 3378 (1952).

[3] See, for example, P. J. Flory, Chem. Revs. **35**, 51 (1944).

are held constant. To investigate chemical relaxation then we must focus our attention on ν.

Two processes of stress relaxation will be of interest. In both cases we shall assume, as is generally found at low elongations, that the relative rate of relaxation is independent of the stress on the sample.[1] The first will be the one where the stress is relieved by the reaction of some chemical agent (held at a constant concentration) with the cross links.

We shall define a cross link by its action. It will be a structural unit which has the ability to join polymer molecules together in such a way as to require two cross links to form two polymer molecules into a closed ring. Such a ring will in general have branches, since in a random cross-linking process of a high polymer the probability of the ends being incorporated into the ring is very small. Thus, a cross link can be visualized as the reaction product between two trifunctional units each of which is incorporated in a polymer chain.

Flory[3] has pointed out that, if X_0 such cross links are added to a unit volume containing N_0 polymer molecules, the number of elastically active chains ν_0 is

$$\nu_0 = 2X_0 - 2N_0. \tag{2}$$

He has shown this relation to hold provided that X_0 is at least 1.5 N_0. If we let Z designate the degree of polymerization of the N_0 molecules, the average length Z_c of the polymer chains between cross links is

$$Z_c = N_0 Z / 2X_0. \tag{3}$$

Since the cross linking does not all occur at the ends of the initial polymer molecules there will be some dangling chain ends. These are not elastically active. The average length of the ends is Z_c. The fraction of the sample which is elastically active is then

$$\left(1 - \frac{2Z_c}{Z}\right). \tag{4}$$

Now if we assume that the cross links are broken according to the law

$$-\frac{1}{X}\frac{dX}{dt} = K, \tag{5}$$

where K is proportional to the rate constant given by the theory of absolute reaction rates, X becomes a function of time t, given by

$$X = X_0 \exp(-Kt). \tag{6}$$

The subscript refers to the value at $t=0$. This rate law has been chosen to demonstrate the principles involved. Analogous expressions could be developed for other rate laws. Combining Eqs. (1), (2), and (6) we find that

$$\tau = 2RT[X_0 \exp(-Kt) - N_0]\varphi(\alpha). \tag{7}$$

Thus, in general, a plot of log τ *vs* t will not give a straight line even though $T\varphi(\alpha)$ is held constant. If however, the number of cross links is large enough so that N_0 may be neglected with respect to X_0, the linear approximation will be good for small values of Kt. Theoretically, the deviation from linearity could be used to determine X_0/N_0. This would presumably require high precision measurements; the simple relationship given by Eq. (7) would not be expected to hold when X_0 and N_0 are of the same order of magnitude because of the approximation used in getting Eq. (2). For the same reason Eq. (7) would not be expected to hold for large values of Kt. In many practical cases, however, the contribution of N_0 will be small and one would expect, if the mechanism is the one postulated, to get a linear relationship between logτ and t.

So far we have limited the process causing the relaxation to a destruction of very special and highly localized bonds. There remains the possibility that any bond along the network chain could be destroyed. In a rubber cross linked by a random process one would expect a distribution of lengths of network chains. Since the reaction causing stress relaxation could occur at any bond along the chain, it seems probable that long chains will be destroyed at a higher rate than short ones. The observed rate of decrease of tension will then be due to the sum of the rates for the chains of different lengths.

Consider that at time $t=0$ we have ν_{i0} chains of length Z_i. Then by Eqs. (2) and (4)

$$\sum_i Z_i \nu_{i0} = N_0 Z(1 - 2Z_c/Z) = 2(X_0 - N_0)Z_c. \tag{8}$$

Now, if we make the reasonable assumption that the rate at which chains of length Z_i are broken is proportional to Z_i and that a rate law of the type used in Eq. (5) is correct, we can write

$$\nu = \sum_i \nu_{i0} \exp(-kZ_i t). \tag{9}$$

Before we can proceed we need to know the relationship between ν_{i0} and Z_i. For a process of random cross linking, we can estimate this relationship in the following way.

Consider the system of N_0 primary molecules of length Z joined by X_0 cross links. There would then be $N_0 Z$ chain elements. Referring to Eq. (4), we realize that the total number of these chain elements that are elastically active is

$$N_0 Z\left(1 - \frac{2Z_c}{Z}\right).$$

Of the latter, $2(X_0 - N_0)$ are trifunctional elements that are involved in cross links in excess of those needed to tie all the molecules together and thus contribute to the elastic properties. The fraction ρ of the elastically active elements that are trifunctional is

$$\rho = 2X_0/N_0 Z = 1/Z_c. \tag{10}$$

If we assume that these are distributed at random, it can

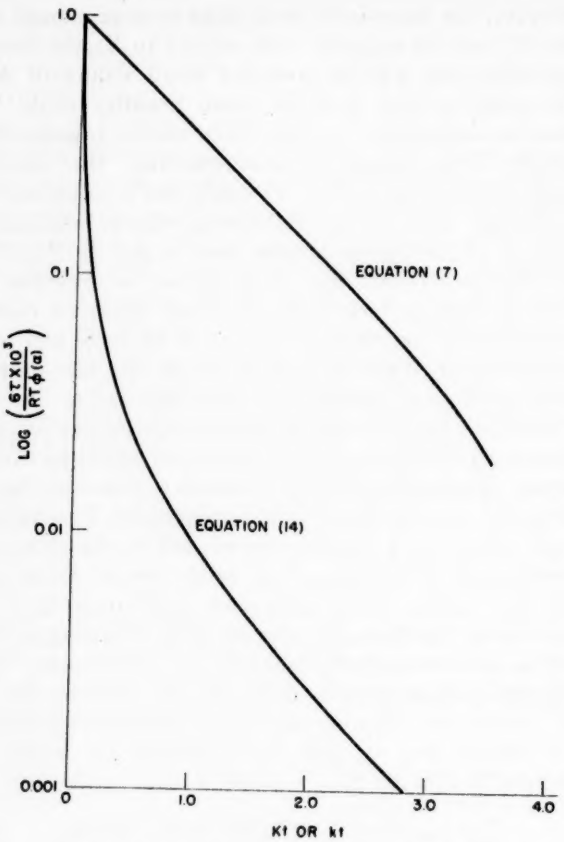

FIG. 1. Plot of $6\tau\times10^3/RT\varphi(\alpha)$ *vs* Kt or kt describing stress relaxation due to disruption of the cross links, Eq. (7), or due to random chain scission, Eq. (14).

be shown[4] that the number of chains of length Z_i is

$$\nu_{i0}=2(X_0-N_0)[\rho(1-\rho)^{Z_i-1}], \tag{11}$$

where a grouping having two trifunctional elements side by side is defined as a chain of $Z_i=1$. Substituting this into Eq. (9), we have

$$\nu=2(X_0-N_0)\rho\sum_{Z_i=1}^{\infty}[(1-\rho)^{Z_i-1}\exp(-kZ_it)]. \tag{12}$$

This sum can be evaluated to give

$$\nu=2(X_0-N_0)\rho[\exp(kt)-1+\rho]^{-1}, \tag{13}$$

and using Eq. (1)

$$\tau=2RT(X_0-N_0)\rho[\exp(kt)-1+\rho]^{-1}\varphi(\alpha). \tag{14}$$

For small values of kt the exponential term may be expanded giving

$$\tau=2RT(X_0-N_0)\rho\left[\rho+kt+\frac{(kt)^2}{2!}+\frac{(kt)^3}{3!}+\cdots\right]^{-1}\varphi(\alpha). \tag{15}$$

Thus from a plot of $1/\tau$ *vs* t it should be possible by inclusion of the term in $(kt)^2$ to get ρ and k. From these and the value of τ at $t=0$ the entire curve could be constructed. For large values of kt a plot of $\log\tau$ *vs* t should be linear with a slope of $-k$. In Fig. 1 are plotted the curves from Eqs. (14) and (7) assuming an original polymer of molecular weight 6×10^5, a density of unity, a degree of polymerization of 6×10^3, and 50 cross links per original molecule. As can be seen, the curves are quite different for the two mechanisms of stress relaxation.

We have assumed in obtaining Eq. (14) that all chains react with rates proportional to their lengths. This approximation may fail in the case of very short chains. For an example of an effect of this sort let us assume that chains of lengths up to and including $Z_i=j-1$ do not react at all and that chains with lengths $Z_i\geq j$ react with rates $(Z_i-j-1)k$. The expression corresponding to Eq. (12) becomes

$$\nu=2(X_0-N_0)\rho\left\{\sum_{Z_i=1}^{j-1}(1-\rho)^{Z_i-1}+\sum_{Z_i=j}^{\infty}(1-\rho)^{Z_i-1}\exp[-k(Z_i-j+1)t]\right\}. \tag{16}$$

Upon integration this will yield one term independent of time and another term that depends on time. A variety of stress relaxation curves can be obtained, depending on the value of j used. Thus the above expressions are sensitive to the relative chemical behavior of the short and long chains. There is also some doubt as to the effect very short chains exert on the elastic properties of the sample. In view of these unknowns it seems useless to generalize further at this time.

There is still another possibility for the analysis of stress relaxation data. Presumably, by the correct mathematical procedure, Eq. (9) could be inverted and the number of chains of length Z_i could be computed. The methods of handling such a problem are known.[5]

ACKNOWLEDGMENT

The author wishes to thank Dr. B. H. Zimm for his valuable suggestions in preparing this manuscript.

[4] The method is essentially the same as that used by P. J. Flory, J. Am. Chem. Soc. **58**, 1877 (1936).

[5] E. Blade and G. E. Kimball, J. Chem. Phys. **18**, 626 (1950).

The Shape and Thickness of Shock Fronts in Argon, Hydrogen, Nitrogen, and Oxygen*

E. F. GREENE AND D. F. HORNIG
Metcalf Chemical Laboratories, Brown University, Providence, Rhode Island

(Received September 30, 1952)

Measurements of shock front thicknesses in argon by the reflectivity method have been extended to Mach 2.09, and the shape of the front has been investigated by comparing the experimental results with the reflectivity expected on the basis of five simple models for the density change through the front. The thicknesses agree with Zoller's calculations but for the strongest shocks are considerably greater than those of other theoretical estimates. The magnitude and form of the reflectivity (as a function of $\lambda/L\cos\theta$) of shock fronts in three diatomic gases have been used to study the rate of equilibration of rotational with translational energy. Hydrogen requires more than one hundred and fifty collisions for this equilibration, while nitrogen and oxygen equilibrate much more rapidly. For the latter two gases there is evidence that at least two relaxation times are involved in the equilibration.

INTRODUCTION

EARLIER papers[1,2] have reported measurements on the thickness of shock fronts in argon and nitrogen with pressure ratios across the front ranging from 1.3 to 2.2 (Mach 1.12 to 1.40). It was concluded that the fronts were considerably thicker than predicted by Thomas[3] but that the results agreed with the theory of Wang Chang[4] when the shocks were weak; they appeared to approach the predictions of the Mott-Smith[5] theory as the shock strength increased.

In order to test these conclusions it seemed important to extend the measurements to more intense shock waves. Subsequently, Zoller[6] has published numerical calculations which predict that the thickness of shock fronts with pressure ratio 6.5 (Mach 2.3) is much greater than the Mott-Smith result. In addition to extending the range of thickness measurements it was desirable to test the sensitivity of the results to the density *vs* distance function chosen to represent the shock front.

The previous studies[2] also showed that whereas the energy in the rotational degrees of freedom in nitrogen remained substantially in equilibrium with the translational energy in a weak shock in which the molecules underwent fifty collisions during the compression, they were definitely not equilibrated after passing through a stronger shock front in which the compression took place in only twenty collisions. In the present investigation the degree of rotational equilibration was studied more extensively in hydrogen, oxygen, and nitrogen. In the case of hydrogen, both impact tube[7] and ultrasonic dispersion measurements[8] indicate that approximately three hundred collisions are required for rotational equilibration. Since the weakest shock fronts that could be studied included only fifty collisions, it was anticipated that hydrogen would behave substantially as a monatomic gas in that the excitation of rotational degrees of freedom would play no role in the shock front process. This was indeed found to be the case.

Equilibration in nitrogen is much more rapid but all of the methods face the common difficulty of separating the rotational and translational relaxation processes so that the results are much less accurate. Nevertheless, both of the other methods seemed to indicate a more rapid equilibration (7 collisions)[7,9] than did the study of the shock front (20 collisions).[2] Consequently, nitrogen was studied over a wide range of shock strengths in order to obtain a better understanding of the process of rotational equilibration.

Oxygen was of interest because it has been reported that the rotational equilibration is much slower than in nitrogen (30 *vs* 7 collisions).[10] Because of the similarity between these molecules this result was unexpected, and we undertook to compare the behavior of these molecules under circumstances where such a difference should have been plainly evident in the characteristics of the shock front.

EXPERIMENTAL METHOD

The index of refraction (and hence density) of a shock front as a function of distance along the direction of propagation was determined by measuring the optical reflectivity of the front as a function of wavelength of the light, angle of incidence, and initial pressure (with constant pressure ratio). This technique has been described in detail previously.[1,2]

The apparatus used in the present work was modified only in that a number of minor changes were made in an effort to increase the precision of the measurements. The carbon arc, which had previously been used as the light source, was replaced by a tungsten motion picture projection lamp (Westinghouse 1M/T12P 1000 w) operated at 118 v dc and approximately 6.5 amp. This

* The work reported here was supported by the U. S. Office of Naval Research under contract N7onr-358, task 3.

[1] G. R. Cowan and D. F. Hornig, J. Chem. Phys. **18**, 1008 (1950).
[2] Greene, Cowan, and Hornig, J. Chem. Phys. **19**, 427 (1951).
[3] L. H. Thomas, J. Chem. Phys. **12**, 449 (1944).
[4] C. S. Wang Chang, University of Michigan, Department of Engineering Research, Report UMH-3-F (APL/JHU CM-503) (1948).
[5] H. M. Mott-Smith, Phys. Rev. **82**, 885 (1951).
[6] K. Zoller, Z. Physik **130**, 1 (1951).
[7] W. Griffith, J. Appl. Phys. **21**, 1319 (1950).
[8] E. S. Stewart and J. L. Stewart, J. Acoust. Soc. Am. **24**, 194 (1952).
[9] A. J. Zmuda, J. Acoust. Soc. Am. **23**, 472 (1951).
[10] W. J. Thaler, J. Acoust. Soc. Am. **24**, 15 (1952).

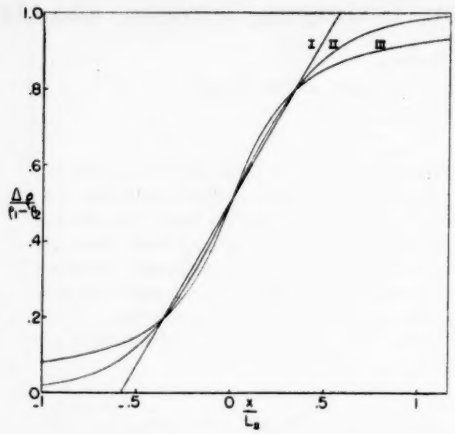

FIG. 1. Shock front models. Density profiles.

change made the heat absorbing glass which was used between the arc and condensing lenses unnecessary, so that the tungsten lamp had nearly the same useful intensity despite its lower temperature. The chief advantages of the tungsten lamp were its intensity stability and the increased ease with which the optical system could be aligned because of the large area of emitting surface. Its chief disadvantage was that small vibrations of the lamp caused by runs with strong shocks occasionally shorted the filament coils together and burned out the lamp. Nevertheless, a single lamp usually lasted for a large number of runs and when one lamp was substituted for another the change in light intensity did not exceed a few percent.

The best way to improve the measurements of shock front thickness is to extend the measurements to smaller values of the parameter $\lambda/L\cos\theta$ where λ is the wavelength, θ the angle of incidence, and L the thickness of shock front. Since this results in a decrease in the reflection intensity, it can only be accomplished by reducing the noise level of the system or by increasing the quantity of light which reaches the photomultiplier tube. With the latter end in mind the narrow band interference filters which were used previously were replaced by absorption filters (cobalt and yellow glass),

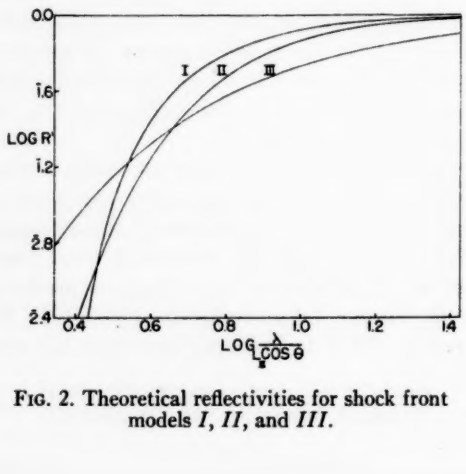

FIG. 2. Theoretical reflectivities for shock front models *I*, *II*, and *III*.

which, combined with the spectral sensitivity of the S-4 photocathode, resulted in pass bands of approximately 60 mμ half-width. The decrease in the accuracy with which the effective wavelength was known was not serious compared to the errors introduced from other sources.

In some of the most recent experiments described here the accuracy was improved by comparing the reflectivity of a single shock front at two wavelengths directly. This was accomplished by illuminating the shock front with unfiltered light, splitting the reflected beam with a half-silvered mirror and using a separate filter and photomultiplier tube in each beam. For the more favorable cases, this procedure yielded an average deviation from the mean reflectivity of individual runs of about five percent. This figure compares with eight percent obtained in the work reported earlier. For the strongest shocks used (Mach 2), however, the reproducibility was noticeably poorer.

TABLE I. Shock front models and associated reflectivity functions.

Model	$\frac{\Delta n(x)}{n_2-n_1}$	R'	
I	$\begin{matrix}0 & x\leqslant -L/2\\ (x+L/2)/L & -L/2\leqslant x\leqslant L/2\\ 1 & x\geqslant L/2\end{matrix}$	$\dfrac{\sin^2(2\pi L\cos\theta/\lambda)}{(2\pi L\cos\theta/\lambda)^2}$	(A)
II	$\dfrac{1}{1+\exp(-4x/L)}$	$\dfrac{(\pi^2 L\cos\theta/\lambda)^2}{\sinh^2(\pi^2 L\cos\theta/\lambda)}$	(B)
III	$\frac{1}{2}+[(\tan^{-1}\pi x/L)/\pi]$	$\exp(-8L\cos\theta/\lambda)$	(C)
IV	$\pi^{-\frac{1}{2}}\int_{-\infty}^{\pi^{\frac{1}{2}}x/L}\exp(-t^2)dt$	$\exp(-8\pi[L\cos\theta/\lambda]^2)$	(D)
V	$2\pi^{-1}\tan^{-1}\exp(\pi x/L)$	$\operatorname{sech}^2(2\pi L\cos\theta/\lambda)$	(E)

Despite the efforts described here and in the previous work to improve the precision of the measurements, it is not markedly better than in the early work. It now seems possible that a major part of the scatter is due to the shock fronts themselves, the most obvious source of error being small fluctuations in the angle between the shock front and the axis of the shock tube. For example, if this angle varied from 90° by only 0.5°, it would produce a decrease of approximately fifty percent in the apparent reflectivity in the optical system used here. From this point of view it is remarkable that the scatter is as small as it is, and we must conclude that the shock fronts are surprisingly stable.

THE SHAPE AND THICKNESS OF SHOCK

The density profile (shape) of a shock front is determined by comparing the experimental reflectivity with the curves derived from a set of models giving the density *vs* distance function along an axis perpendicular to the front. Five tractable analytical models which have been considered in this work, together with the

corresponding expressions for the reduced reflectivity, are given in Table I. This reduced reflectivity R' is related to the actual reflectivity R by

$$R'=4R/[(1+\tan^4\theta)(n_2-n_1)^2]. \quad (1)$$

The shock thickness L is defined in each case as

$$L=\frac{n_2-n_1}{(dn/dx)_{\max}}=\frac{\rho_2-\rho_1}{(d\rho/dx)_{\max}}. \quad (2)$$

The regions before and after the shock front are designated by the subscripts 1 and 2, respectively; n is the refractive index, ρ the density, and x the distance along the line of propagation of the shock.

If an attempt is made to represent a real shock front by one or the other of these models, the parameter L must be chosen so as to give some best average fit through the shock front. In general the value of L

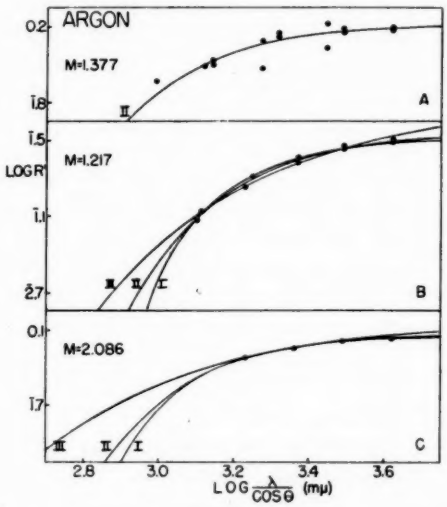

FIG. 3. Measured shock front reflectivities for argon. Solid lines are theoretical curves.

obtained from each model differs, even when the functions approximate each other closely. To illustrate this behavior, models *I–III* are plotted in Fig. 1 in such a way that they coincide at $\Delta\rho/(\rho_2-\rho_1)=0.2$ and 0.8. Models *IV* and *V* lie within two percent of model *II* at all points so they are omitted. Under these circumstances $L_I:L_{II}:L_{III}:L_{IV}:L_V=1.16:1.00:0.78:1.04:0.98$. The corresponding reflectivity curves are depicted in Fig. 2. L_{II} is taken as a standard because model *II* is that obtained theoretically in the Mott-Smith theory of the shock front, is the limiting expression for weak shocks in the Becker theory and is very close (within two percent at all points) to the expression obtained by Thomas throughout the range of shock fronts used in this work.

In comparing calculated reflectivities, R (as a function of $\lambda/L\cos\theta$) with experimental reflectivities, kR (as a function of $\lambda/\cos\theta$) there are two unknown scale

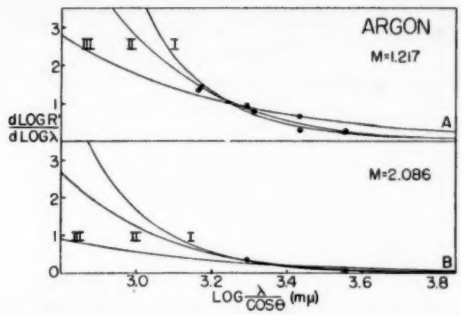

FIG. 4. Measured slopes of shock front reflectivities with wavelength for argon. Solid lines are theoretical curves.

factors—the sensitivity k of the apparatus and the shock thickness L. Because of this, it is convenient to compare instead plots of $\log R$ *vs* $\log\lambda/L\cos\theta$ with plots of $\log kR$ *vs* $\log\lambda/\cos\theta$. The relative vertical and horizontal adjustments required to match the two curves then determine k and L, respectively. For any model the vertical adjustment can be made most accurately from experiments at large $\lambda/L\cos\theta$, i.e., where the reflectivity varies the least with $\lambda/L\cos\theta$, while the horizontal matching is most accurate when points are available on the steepest part of the curve (or at small $\lambda/L\cos\theta$). For this reason it is important to have measurements over the largest possible range of $\lambda/L\cos\theta$. Points at intermediate values of $\lambda/L\cos\theta$ show the extent of agreement between the model and the experiments. Measurements accurate to ±5 percent in R' over a fourfold range of $\lambda/L\cos\theta$ and a range of approximately 0.5 in $\log R'$ (roughly the situation with some of the more consistent data reported here) are of just sufficient accuracy to begin to distinguish between models *I*, *II*, and *III*.

A large number of measurements (each point represents the average of three runs) on shock waves in argon at Mach 1.377 are fitted to a model *II* curve in Fig. 3(a). The scatter in the data, which was taken over a considerable time interval during which the apparatus was modified, is too great to permit any comparison in models.

In Figs. 3(b) and 3(c) (each point is the average of 4 and 5 points, respectively) are shown some more consistent measurements (Mach 1.217 and 2.086) which are compared with models *I*, *II*, and *III*. Because these results were obtained using the split beam technique described earlier and are really, therefore, measurements of the slope of the reflectivity curve, it is better to plot these slopes and compare them directly with the slopes for the three models. This is done in Fig. 4. Unfortunately, in the high Mach number runs (Fig. 3(c)) the experimental scatter was large—at each value of $\lambda/\cos\theta$ most of the runs gave reflectivities grouped together (as for the runs at other Mach numbers) but a few were much smaller (as low as thirty percent of this value). The results reported are the averages of the group of high reflectivity values because while many

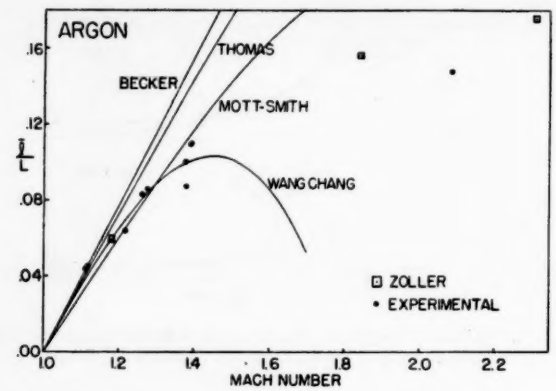

FIG. 5. Experimental shock front thicknesses in argon as a function of Mach number. Solid lines are theoretical curves.

factors can cause decreased reflectivity with strong shocks (e.g., instability or tilt of the front) nothing apparent can account for an unusually large reflectivity. In any case the averages of the slopes (Fig. 4(b)) were the same within experimental error (± 0.1) for the selected group as for the whole group.

It is seen that whereas in each case the differences between models are scarcely beyond the scatter in the experimental values, it appears that the best fit is obtained with model *II*. Cowan and Hornig arrived at the same conclusion in comparing models *I* and *II* for nitrogen shocks.

The thicknesses (on the basis of model *II*) obtained experimentally for shock fronts in argon in the present and previous paper[2] are compared with the available theories in Fig. 5. l is the mean free path ahead of the shock. The error in the experimental values is estimated at ± 15 percent, except for the point at Mach 2.09 where the fluctuations were larger, and the error may easily be ± 25 percent. Despite these uncertainties, it is clear that shocks of Mach number greater than 1.5 are much thicker than predicted by any theory except that of Zoller from which the deviation is within the experimental error.

The detailed properties of shock waves in argon and three diatomic gases are listed in Table II. P_3/P_1, ρ_2/ρ_1, ρ_3/ρ_1, and T_3 are values calculated from the measured Mach numbers. The subscripts 1, 2, and 3 refer to the regions before the shock, after the shock but before relaxation, and after complete relaxation, respectively. For argon regions 2 and 3 are identical. T_1 is 25°C, and the ratio of specific heats for argon, hydrogen, nitrogen, and oxygen are taken as 1.668, 1.410, 1.404, and 1.396, respectively. For the shock waves in diatomic gases two thicknesses are reported. The first is determined, as for argon, by the best fit of the experimental points to model *II*. This is the method used previously with nitrogen.[2] It gives, as is expected, a thickness larger than the correct one for complete relaxation. This increased L is ambiguous, however, because the fitting is accomplished by adjusting both k and L (the vertical and horizontal scaling factors) to a varying extent depending upon the region of the curve at which experimental points are available. For weak shocks where the experimental points extend nearly to the limiting value for large $\lambda/\cos\theta$, the adjustment from the correct curve for complete relaxation to the best fit to model *II* is almost entirely made by changing L while for stronger shocks the adjustment is partly accomplished by a change in k so that the derived L shows a correspondingly smaller increase over the correct value. The second thickness listed in Table II is for the completely relaxed case and is calculated from the thickness obtained in a suitable argon shock as described below. This latter thickness was the one used to calculate the number of collisions in the front (see reference 2).

THE EFFECT OF ROTATIONAL RELAXATION

At the present time no theoretical basis exists for setting up a density *vs* distance model for a gas exhibiting rotational relaxation, i.e., one in which rotational degrees of freedom are not in equilibrium with the translational motion. In the two limiting cases, (1) complete equilibration of rotation at all times and (2) very slow excitation of rotational degrees of freedom, the theory of Thomas predicts that the density profile is the same as in a monatomic gas. Furthermore, it has been pointed out before[2] that in these cases the conservation equations are sufficient to determine the total density change across the shock front, hence also the limiting reflectivity at large values of $\lambda/L\cos\theta$; consequently, the limiting cases can be distinguished by the absolute value of the limiting reflectivity as well as from the thickness of the front.

It has been shown previously that in very weak shocks nitrogen approximates the case of complete equilibration but that in stronger shocks there is definite evidence of rotational heat capacity lags. We shall postpone the further discussion of this case until after considering the case of very slow equilibration.

TABLE II. Shock waves in argon, hydrogen, nitrogen, and oxygen.

Gas	Mach No.	P_1 (atm)	P_3/P_1	ρ_2/ρ_1	ρ_3/ρ_1	T_3 (°C)	$L(P_1=1$ atm) (10^{-5} cm) [a]	[b]	Collisions through front[c]	Results plotted in Figs.
A	1.215	3.55	1.595	1.321	1.321	88	11.2	···	24	3b
A	1.217	4.70	1.603	1.324	1.324	88	11.2	···	24	3b
A	1.377	4.70	2.115	1.551	1.551	135	7.8	···	21	3a
A	2.086	2.73	5.190	2.369	2.369	381	4.6	···	15	3c
H_2	1.389	4.70	2.087	1.410	1.666	100	13.4	11.2	17	6
N_2	1.128	11.00	1.318	1.053	1.217	50	20.5	12.7	30	10a
N_2	1.131	11.01	1.326	1.057	1.222	51	20.5	12.7	30	10a
N_2	1.233	4.70	1.607	1.197	1.397	70	10.6	8.1	20	10b
N_2	1.287	5.19	1.767	1.268	1.491	80	8.5	7.0	19	10c
N_2	1.414	2.62	2.168	1.439	1.712	104	6.4	5.7	17	10d
N_2	1.417	6.76	2.178	1.443	1.717	105	6.4	5.7	17	10d
N_2	1.418	4.63	2.181	1.444	1.719	105	6.4	5.7	17	10d
N_2	2.061	2.73	4.793	2.177	2.748	247	4	4.1	18	10e
O_2	1.404	2.62	2.132	1.421	1.701	101	8.6	6.2	17	11
O_2	1.406	4.70	2.139	1.425	1.705	101	8.6	6.2	17	11

[a] Direct measurement using the best fit to model II.
[b] Calculated for the limit of complete relaxation by comparison with argon shock (see text).
[c] Using L calculated from argon shock.

(a) Negligible Equilibration, Hydrogen

According to the acoustic measurements the rotational equilibration process is so slow in hydrogen that we should expect it to behave like a monatomic gas in the shock front, i.e., it should be an example of the second limiting process. To check this conclusion we have compared its reflectivity (Mach 1.389) with that of argon. The relative value of the limiting reflectivity ($\lambda/L\cos\theta \gg 1$, $R' \to 1$) for any gas relative to argon is given by the expression (see Eq. (1))

$$\frac{R_x(\infty)}{R_A(\infty)} = \frac{[(\rho_L-\rho_1)(n_D-1)]_x^2}{[(\rho_L-\rho_1)(n_D-1)]_A^2}, \tag{3}$$

where n_D is the refractive index and ρ_L the limiting density. Since ρ_L was known for the completely equilibrated gas (i.e., ρ_3) from the measured shock velocity and could be calculated for the completely nonequilibrated gas (i.e., ρ_2),[11] the limiting reflectivity ratio was known for both cases without reference to shock front theories. Unfortunately, the measurements could not be carried to the limiting values so that the thickness of the shock front had to be taken into account also. This thickness for hydrogen was obtained by using the Wang Chang[4] expression to calculate the *ratio* of the thickness of shock fronts in hydrogen and argon for the two cases, together with the *empirical* value of the thickness in argon. Although this procedure is approximate, it should be somewhat more accurate than an absolute calculation.

The two limiting values and the model *II* reflectivity curves calculated for the two cases are shown in Fig. 6. The experimental points (each the average of 3 runs) are also shown. They were obtained by comparing the reflectivity of each shock wave with the reflectivity of an argon shock at the same $\lambda/\cos\theta$. It was assumed that the correct value for argon was that given by the model *II* reflectivity curve which best fitted the entire set of argon measurements. It is clear that under these circumstances there is essentially no energy transfer to the rotational levels in hydrogen.

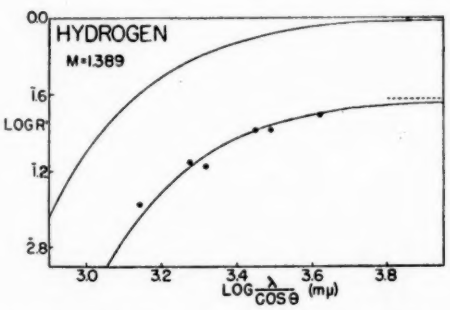

FIG. 6. Measured shock front reflectivities for hydrogen. Solid lines are theoretical curves.

[11] See reference 2, Eq. (10).

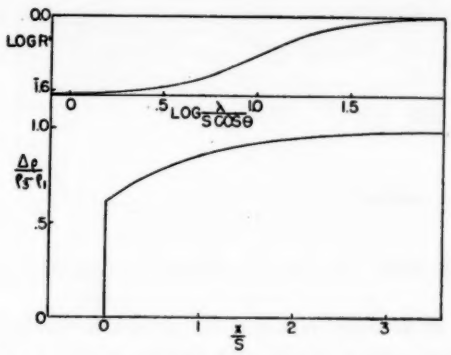

FIG. 7. Shock wave reflectivity and density profile. Very slow relaxation.

(b) Slow Equilibration

If the equilibration process is slow compared to the compression in the shock front, the over-all process can be thought of as occurring in two stages: (a) an initial compression in the shock front during which no internal degrees of freedom are excited, and (b) a subsequent slow relaxation during which the density changes from that characteristic of the unrelaxed state to that of the completely equilibrated state. If we are interested in the contribution of the second process to the reflectivity, a rough model of this situation might be an initial density discontinuity followed by an exponential relaxation to the final density, i.e., that

$$\begin{aligned} \rho(x) &= \rho_1 && x<0, \\ \rho(x) &= \rho_3-(\rho_3-\rho_2)\exp(-x/S) && x>0, \end{aligned} \tag{4}$$

where S is the distance required for the fraction $(1-1/e)$ of the relaxation to occur.

This model and the corresponding reflectivity curve are illustrated in Fig. 7, which is drawn using the values for the densities of the shock wave in hydrogen discussed in the previous section. The limiting reflectivity at small $\lambda/S\cos\theta$ is just the wavelength-independent reflectivity from the unrelaxed shock front, while that at large $\lambda/S\cos\theta$ corresponds to the equilibrated limit in Fig. 6. If the relaxation in hydrogen occurs in three hundred collisions, i.e., in a distance six times the thickness of the shock front, $S=3\times10^{-4}$ cm, and at the maximum $\lambda/\cos\theta$ used in the experiments the rise in $\log R'$ would have been 0.01, an undetectable amount. Since the experimental values of $\log R'$ are uncertain to approximately ±0.05, it can only be stated from our data that $S>1\times10^{-4}$, that the rotational relaxation requires more than one hundred and fifty collisions.

(c) Rapid Equilibration, Nitrogen and Oxygen

The preceding rough analysis is applicable when there is no appreciable overlap of the region of changing reflectivity resulting from the shock front and that arising from the relaxation process. When they do overlap this model must be refined further. In the absence of any quantitative theory of the over-all

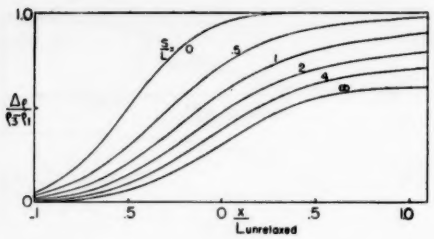

FIG. 8. Shock wave density profiles, including relaxation.

process it is only possible to invent a model which shows the correct qualitative behavior and which may be suitable for crude quantitative estimates.

We have done so by assuming that the shock front is described by model *IV* but that each infinitesimal compression is followed by a relaxation process similar to that of the preceding section. Model *IV* was chosen because it is essentially identical to model *II* except that the mathematics of superposition are more tractable. The resulting expression for the density ρ in the shock front is

$$\Delta\rho(x)=\rho-\rho_1=\frac{\rho_3-\rho_1}{\pi^{\frac{1}{2}}}\int_{-\infty}^{\pi^{\frac{1}{2}}x/L}\exp(-t^2)dt$$
$$-\frac{\rho_3-\rho_2}{\pi^{\frac{1}{2}}}\left[\exp\left(\frac{L^2}{4\pi S^2}-\frac{x}{S}\right)\right]$$
$$\times\int_{-\infty}^{\pi^{\frac{1}{2}}[x-(L^2/2\pi S)]/L}\exp(-t^2)dt. \quad (5)$$

The corresponding reflectivity expression is

$$R'=\left\{\left[\frac{\rho_2-\rho_1}{\rho_3-\rho_1}+\frac{(\rho_3-\rho_2/\rho_3-\rho_1)}{1+(16\pi^2S^2\cos^2\theta/\lambda^2)}\right]^2\right.$$
$$\left.+\frac{(\rho_3-\rho_2/\rho_3-\rho_1)16\pi^2S^2\cos^2\theta/\lambda^2}{[1+(16\pi^2S^2\cos^2\theta/\lambda^2)]^2}\right\}$$
$$\times\exp(-8\pi L^2\cos^2\theta/\lambda^2). \quad (6)$$

A further difficulty arises in that superposition can only be applied to linear phenomena whereas the shock front is nonlinear. This shows itself in that the preceding equations reduce to a simple model *IV* with the same L at both limits, $S/L\to 0$ and $S/L\to\infty$, while the true curves differ considerably in the value of L. This was taken into account by choosing L as a function of S/L which varied between the correct limits. At intermediate values of S/L it was chosen arbitrarily so that

$$L(S/L)=L(0)+([L(\infty)-L(0)][\Delta\rho(S/L)-\Delta\rho(0)]/[\Delta\rho(\infty)-\Delta\rho(0)]), \quad (7)$$

where $\Delta\rho(S/L)$ was calculated from (5) at $x/L=-0.25$. This value of x/L was chosen merely because it is on the toe of the density curve where the density change is more sensitive to the value of L than it is at higher values of $\Delta\rho$ where the value of S is especially important.

The resulting density and reflectivity functions are plotted for various values of S/L in Figs. 8 and 9. Here $(\rho_2-\rho_1)/(\rho_3-\rho_1)$ was chosen as 0.615, corresponding closely to a shock wave of Mach number 1.4 in nitrogen and oxygen. Although these reflectivity curves are undoubtedly based on oversimplified assumptions, they are, nevertheless, curves which show qualitatively what may be expected for a gas with a single relaxation time.

The results obtained in nitrogen are plotted in Fig. 10. For comparison, the model *II* curves corresponding to the two limits are also included. Clearly there is a more noticeable deviation from equilibrium for the stronger than for the weaker shocks. Thus at Mach 1.131 the two points available which are averages of ten runs each (see Fig. 10(a)) agree closely with the equilibrium curve although it is not possible to rule out a situation similar to that shown in Fig. 10(b) for Mach 1.233 (each point is the average of 4 runs) where there is appreciable deviation from the equilibrium curve at low values of $\lambda/\cos\theta$ but substantially complete agreement at higher values. This is just the behavior expected from our model for the case of relaxation rapid compared to the time required for the molecule to pass through the shock front (S/L small). Here the front is twenty collisions thick and a curve for $S/L=\frac{1}{4}$ would be a reasonable fit so we find that S corresponds to approximately five collisions. For the two points in Fig. 10(a), however, it is only possible to say (considering the estimated error in $\log R$ of ± 0.03) that the equilibration takes place in not more than ten collisions ($S/L<\frac{1}{2}$). Figure 10(c) shows a noticeable deviation from equilibrium for Mach 1.287 corresponding to $S/L=1$ or $S=19$ collisions (since there are nineteen collisions in the front) but, of course, a single point does not provide a test of the relaxation model.

Perhaps the most accurate experiments are those plotted in Fig. 10(d) for Mach 1.417 (each point is the average of 10 runs). Clearly for these points none of the curves of Fig. 9 for a single relaxation time provides a satisfactory fit. However, these points are qualitatively

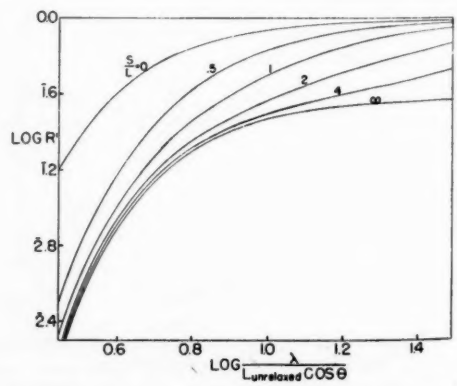

FIG. 9. Theoretical shock wave reflectivities, including relaxation.

consistent with a model including two (or more) relaxation times, one short and the other long compared to the time required for the molecules to flow through the shock front. This behavior is not surprising, because the equilibration involves transitions between energy levels which become further and further apart as the rotational quantum number increases.

Figure 10(e) shows some points for Mach 2.06. Two points are plotted for each value of $\lambda/\cos\theta$, one (circles) corresponding to an average of all the runs (six for the two points at low $\lambda/\cos\theta$ and nine for the two points at high $\lambda/\cos\theta$) and a second (squares) to the run giving the largest reflectivity. We believe the larger values of R are more reliable because, as with the high Mach number runs in argon, there was a tendency for several runs to be close to the maximum and then for a few others to show large decreases in amplitude occasionally even falling to ten percent or less of the maximum. We can conclude, therefore, in view of this larger experimental scatter only that there is perhaps somewhat less equilibration here than for the weaker shocks.

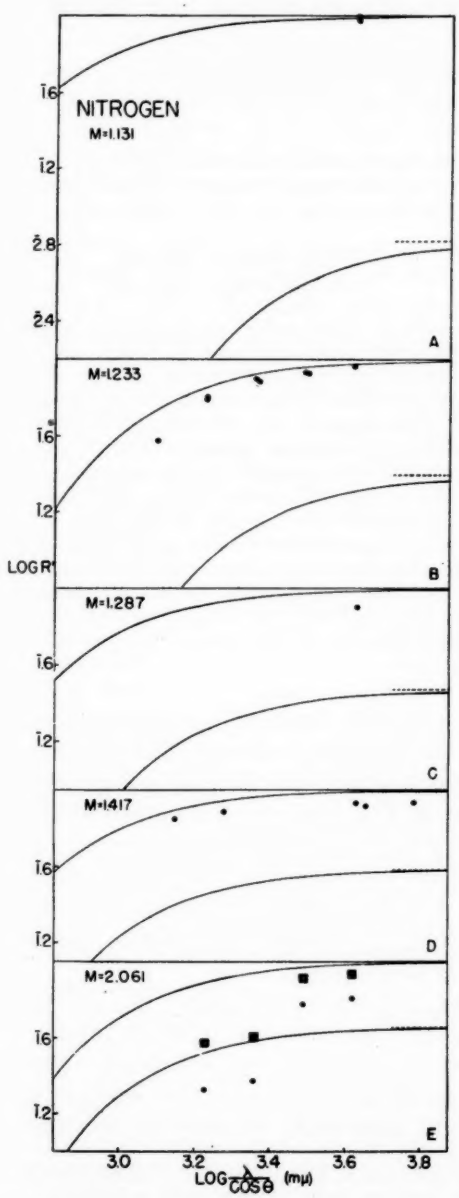

FIG. 10. Measured shock front reflectivities for nitrogen. Solid lines are theoretical curves.

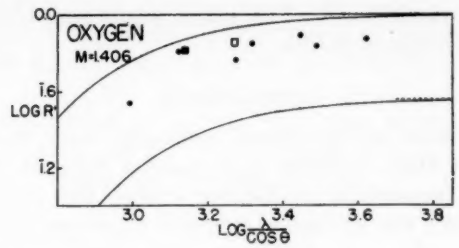

FIG. 11. Measured shock front reflectivities for oxygen. Solid lines are theoretical curves.

Table II shows that for the stronger shocks the number of collisions through the front is approximately constant. If in addition the relaxation always occurs in the same number of collisions, i.e., there is only one relaxation time, then there should be no decrease in the extent of equilibration as the shock strength increases; the presence of such a decrease thus provides evidence for slower equilibration at higher temperatures. This is consistent with reports of an extremely long rotational relaxation time (>10 000 collisions) for the OH radical in methane-air flames.[12]

Because of the similarity of oxygen and nitrogen- it is surprising that there should be such a large differ, ence in the relaxation times measured ultrasonically (oxygen 30 collisions, nitrogen 7 collisions). For this reason we investigated the relaxation behavior of oxygen in a shock wave approximately seventeen collisions thick which was expected to provide a clear test of the relative behavior of the two gases (Mach number 1.406). Figure 11 shows the results and again the two limiting model *II* curves are included. Each point is the average of three runs except for the two represented by squares which are the averages of ten runs and unlike the others were obtained from a shock of a lower P_1 (but the same Mach number) and placed on the curve with the scaling relation $P_1L=$ constant for a given P_2/P_1. There is more scatter here than for the corresponding nitrogen case (Fig. 10(d)) but even so the lack of complete equilibration is evident. On the whole, oxygen seems to be relaxing somewhat more slowly than nitrogen but not nearly as slowly as the ultrasonic results indicate. Again there is evidence for the presence of at least two different relaxation times, one short and the other long, so it is difficult to pick any single value for comparison with the ultrasonic work; however, relaxation in a time corresponding to thirty collisions would require a curve from the approximate super-

[12] H. P. Broida, J. Chem. Phys. **19**, 1383 (1951).

position model for $S \approx 1.8L$ which would pass below all the experimental points.

CONCLUSION

The results of the present work are: shock fronts in argon at Mach 2 appear to be thicker than any of the existing theoretical predictions except that of Zoller with which the agreement is within experimental error; hydrogen behaves in a shock of Mach 1.4 like a monatomic gas with negligible excitation of the rotational degrees of freedom; in nitrogen the rotational energy is rapidly equilibrated but there is evidence that at least two relaxation times are required to describe the process; oxygen behaves like nitrogen although perhaps with a slightly longer relaxation time and it also seems to require two relaxation times.

THE JOURNAL OF CHEMICAL PHYSICS VOLUME 21, NUMBER 4 APRIL, 1953

Adiabatic Correlation Rules for Reactions Involving Polyatomic Intermediate Complexes and their Application to the Formation of $OH(^2\Sigma^+)$ in the H_2-O_2 Flame

KURT E. SHULER
Applied Physics Laboratory, The Johns Hopkins University, Silver Spring, Maryland*
(Received March 17, 1952)

Adiabatic orbital and spin correlation rules applicable to a detailed study of elementary chemical reactions involving nonlinear polyatomic intermediate complexes have been formulated and are presented together with some pertinent correlation tables. These correlation rules and tables permit the determination of the adiabatically allowed term manifold of reaction products from the states of the separated reactants without reference to their detailed electronic configurations. The formulation presented here utilizes group theoretical arguments relating to the symmetry properties of the reactants, the intermediate reaction complex, and the products and is based principally upon the results obtained previously by Mulliken for the resolution of species into those of point groups of lower symmetry. The effects of the change of the (geometrical) configuration of the intermediate reaction complex during reaction and of the electronic-vibrational coupling on these correlations have been considered in detail. It is concluded that strict orbital *electronic* correlation rules are operative only for reactions where neither the reactants nor the products are polyatomic. For reactions involving polyatomic reactants and/or products, the vibrational-electronic coupling weakens the simple orbital electronic correlations so that detailed *vibronic* correlations will be necessary. The spin correlation rules, however, are not affected by these interactions and are identical with those given by Wigner and Witmer for atomic and diatomic systems.

These correlation rules are then applied to a study of the reactions

$$H+O_2 \rightarrow [HO_2] \rightarrow OH^*+O$$
$$O+H_2 \rightarrow [OH_2] \rightarrow OH^*+H$$

which may be of importance in the production of electronically excited $OH[OH(^2\Sigma^+)]$ in the hydrogen-oxygen flame. The mechanism of these reactions is investigated with special reference to the predissociating $OH(^2\Sigma^-)$ state discussed recently by Gaydon and Wolfhard. It is suggested that the interaction of and the consequent radiationless transition between HO_2 intermediate reaction complexes is primarily responsible for the formation of $OH(^2\Sigma^+)$ in its observed vibrational nonequilibrium distribution with the specific enhancement of the levels $v'=2$ and 3.

The adiabatic correlations for the special case of association (and dissociation) reactions involving linear polyatomic intermediate complexes and products are considered briefly in the Appendix. It is concluded that vibronic correlations are required for the determination of the product term manifold for these reactions.

I. INTRODUCTION

THE mechanisms of elementary reactions can best be studied in detail by constructing the relevant potential energy surfaces and investigating their properties and interactions.[1] To carry out such a program it is necessary to know the adiabatic correlations between the electronic states of reactants, intermediate reaction complexes, and products so that the resulting term manifold of the products can be determined from the states of the separated reactants. Such a knowledge is essential if the problems to be studied concern the formation of products in some specific electronic states from reactants in some specific electronic states. This is a topic which is of great importance in flame and photochemical reactions.

The correlation rules for the case atom+atom→diatomic molecule (via a diatomic intermediate complex) have been worked out by Wigner and Witmer[2] and discussed since in detail by several authors.[3,4] These correlation rules can readily be extended to the case of *linear* polyatomic molecules and *linear* intermediate complexes. A short discussion of these extended rules, together with the pertinent correlation tables, is presented in the Appendix.

In the main body of this paper (Sec. II) an attempt will be made to formulate adiabatic orbital and spin correlation rules for the more important case of nonlinear polyatomic molecules and reaction complexes in a form particularly suitable for the study of ele-

* Supported by the Bureau of Ordnance, U. S. Navy, under Contract NOrd 7386.

[1] K. J. Laidler and K. E. Shuler, Chem. Revs. 48, 153 (1951).

[2] E. Wigner and E. E. Witmer, Z. Physik **51**, 859 (1928).

[3] R. S. Mulliken, Revs. Modern Phys. **4**, 1 (1932).

[4] G. Herzberg, *Spectra of Diatomic Molecules* (D. Van Nostrand Company, Inc., New York, 1950), second edition, pp. 315–322.

mentary chemical reactions. In Sec. III, these correlation rules are then applied as a simple example of their utility to a discussion of the formation of $OH(^2\Sigma^+)$ in the hydrogen-oxygen flame.

II. CORRELATION RULES FOR NONLINEAR INTERMEDIATE REACTION COMPLEXES

A. General Formulation

The electronic states in which atoms and molecules may be produced in chemical reactions are determined by the adiabatic correlations which relate the states of reactants and products via those of the intermediate complex. In all reactions except those involving only two atoms the intermediate reaction complex will be polyatomic and most probably nonlinear, especially in reactions involving electrons in higher than *s* orbitals. In order for reactants and products to correlate, it will be necessary that the nonlinear intermediate complex (hereafter referred to as NLC) formed during the reaction have at least one electronic species in its term manifold which arises from the combination *both* of the reactants and of the products. In order to obtain the desired correlation rules, it is therefore necessary to relate adiabatically the states of the separated reactants with those of the products via the states of the NLC formed during the reaction.

The classification, designation, and correlation of the electronic states of nonlinear polyatomic molecules is based upon the symmetry properties of their electronic wave functions.[5,6,7] Making use of group theoretical methods, which are particularly suited to such systems, Mulliken[5,8] has worked out correlations between separated atomic and/or molecular components and nonlinear polyatomic molecules from a detailed consideration of the possible electron configurations of the various components. For application to chemical kinetics and for the study of reaction mechanisms it would, however, be more advantageous if these adiabatic correlations between reactants and products could be determined without any such detailed analysis of the electron configurations. Such a formulation, involving only a prior knowledge of the electronic states of the reactants can readily be carried through by utilizing the results obtained by Mulliken in the paper cited above.[5,9]

The spin correlation rules for linear and nonlinear polyatomic molecules are identical with those for diatomic molecules formed from separated atoms. This is due to the fact that the electron spin is not affected by the electric field arising from the interaction of the combining molecules.[10] The principal problem thus centers in the formulation of the orbital correlation rules.

These orbital correlation rules may be obtained in the following manner.[11] The reaction $A+BC\rightarrow AB+C$ may be written "configurationally" as

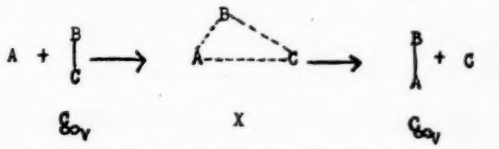

(1)

To correlate the states of the reactants A and BC and products AB and C via those of NLC (ABC) one sets up resolution tables which show the change of representations (species) in going from spherical symmetry (atoms) and linear symmetry (diatomic molecule) to the symmetry group X of the NLC. The allowed representations (i.e., electronic states) of the NLC (ABC) of symmetry group X are then obtained by forming the direct products of the representations found from the resolution tables $A\rightarrow X$ and $BC\rightarrow X$. This correlates the states of the reactants with those of the NLC. To obtain the correlation between the NLC and the products of the reaction, one forms the direct products of the representations of the resolutions $C\rightarrow X$ and $AB\rightarrow X$. Given states of reactants and products will then correlate if, and only if, the NLC has at least one species which arises *both* from the combination of these reactant and of these product states.

For a reaction between two diatomic molecules such as

$$\begin{matrix} AB+CD\rightarrow[ABCD]\rightarrow BC+AD \\ C_{\infty v}\ \ C_{\infty v}\quad\ Y\quad\ C_{\infty v}\ \ C_{\infty v} \end{matrix} \qquad (2)$$

which proceeds via a NLC belonging to symmetry group Y, one again follows the procedure outlined above except that one now needs resolution tables only for $C_{\infty v}\rightarrow Y$. The adiabatically allowed representations of the NLC are then obtained by forming the direct products of the representations of the $C_{\infty v}\rightarrow Y$ tables.

This procedure could readily be extended to reactions involving reactants, intermediate complexes, and products of higher and higher atomicity. However, as will be shown below, the orbital correlation rules impose only very weak restrictions (or none at all) on the adiabatically allowed product term manifold for reactions involving polyatomic reactants and products.

[5] R. S. Mulliken, Phys. Rev. **43**, 279 (1933).
[6] R. S. Mulliken, J. Phys. Chem. **41**, 159 (1937).
[7] H. Sponer and E. Teller, Revs. Modern Phys. **13**, 75 (1941).
[8] R. S. Mulliken, J. Chem. Phys. **3**, 517, 635 (1935); R. S. Mulliken and C. C. J. Roothaan, Chem. Revs. **41**, 219 (1947).
[9] Since that paper contains a very detailed account of the group theoretical arguments which underlie the discussion to follow, we shall content ourselves here in the main with the presentation of the method and the results rather than with their detailed derivation.

[10] These spin correlation rules are, just as for the case of diatomic molecules, strictly valid only for weak spin-orbit coupling in the polyatomic molecules, i.e., to the approximation that the spin part of the wave function can be separated from the orbital part. The spin correlation rules thus should not be used indiscriminately for molecules containing very heavy atoms.
[11] In the author's original formulation, the orbital correlations were established via linear intermediate complexes whose transformation to the actual NLC was analyzed by means of species resolution tables for linear to nonlinear point groups. The more elegant and direct method presented here was kindly pointed out to me by Professor R. S. Mulliken. I am very much indebted to Professor Mulliken for this and several other valuable contributions to this paper.

TABLE I. Resolution of atomic species into those of molecular symmetry groups.

Atom	C_{3v}	C_{2v}	C_s	C_1
S_g	A_1	A_1	A'	A
S_u	A_2	A_2	A''	A
P_g	A_2+E	$A_2+B_1+B_2$	$A'+2A''$	$3A$
P_u	A_1+E	$A_1+B_1+B_2$	$2A'+A''$	$3A$
D_g	A_1+2E	$2A_1+A_2+B_1+B_2$	$3A'+2A''$	$5A$
D_u	A_2+2E	$A_1+2A_2+B_1+B_2$	$2A'+3A''$	$5A$

The discussion and tables to follow will thus be limited in the main to reactions between diatomic molecules and between atoms and diatomic molecules proceeding via a tri- or tetratomic NLC.

Nonlinear complexes containing 3 or 4 atoms will usually belong to one of the symmetry groups C_1, C_s, C_{2v}, and C_{3v},[12] where molecules of point group C_1 have no symmetry elements at all. Resolution tables which show the change of atomic and diatomic species into those of the above (and other) point groups have been worked out by Mulliken.[5] For ready reference the pertinent tables are given below. The direct product of the species of Tables I and II which give the allowed species of the NLC can be obtained from the tables given by Sponer and Teller.[13]

Since the NLC will quite often be of symmetry C_s the complete correlation tables for that point group will be given here. These tables are obtained by combining Tables I and II and using the direct product rules for C_s, *viz.*, $A'\times A'=A'$, $A''\times A''=A'$, $A'\times A''=A''\times A'=A''$. The entries in Tables III and IV are the allowed states of the NLC of symmetry C_s arising from the combination of atomic and/or diatomic reactants in their various electronic states.

To give a concrete example which illustrates the above-described procedure, we shall consider briefly the reaction $CH+O_2\rightarrow CO+OH^*$ suggested by Gaydon[14] to account for the appearance of some of the electronically excited $OH^*(^2\Sigma^+)$ in hydrocarbon flames.[15] Writing

$$CH(X^2\Pi)+O_2(X^3\Sigma_u^-)\rightarrow O_2\cdot CH[C_s]\rightarrow CO(^1\Sigma^+)+OH(^2\Sigma^+) \quad (3)$$

where it is assumed, somewhat arbitrarily, that the intermediate complex $O_2\cdot CH$ is of symmetry C_s, i.e., planar, one finds from Table IV and the spin correlation rules that the reactants give rise to a NLC $[C_s]$ of species $^{2,4}A'$ and $^{2,4}A''$ and the products give rise to a NLC $[C_s]$ of species $^2A'$. Reactants and products thus correlate adiabatically via a surface of designation $^2A'$, so that reaction (3) as written above is an allowed one as regards both spin and orbital correlations. For $CH^*(A^2\Delta)$ and $CH^*(B^2\Sigma^-)$ reaction (3) also correlates with the above products via a $^2A'$ surface. For $CH^*(C^2\Sigma^+)$, however, reaction (3) cannot proceed via a NCL of symmetry C_s since the reactants now give rise to a NLC of species $^{2,4}A''$ whereas the NLC obtained from the products $CO(^1\Sigma^+)$ and $OH(^2\Sigma^+)$ is of species $^2A'$. The same analysis can also be undertaken for various other electronic states of O_2 with a fixed $CH(X^2\Pi)$ with the result that all the (stable) electronic states of O_2 correlate, both spin and orbital wise, with the products of reaction (3) via a NLC of symmetry C_s.

[12] In view of the discussion to follow, point group D_{3h} may be ruled out as being of no importance.

[13] See reference 7. The direct products for C_1, C_s, and C_{2v} can be obtained from Tables III and IV, those for C_{2v} from Tables VII and VIII of that paper.

[14] See, e.g., A. G. Gaydon, Quart. Revs. 4, 1 (1950).

[15] The superscript star here as in the equations to follow denotes the electronically excited species.

B. The Least Symmetrical Complex

In tracing the detailed configurational course of a chemical reaction, it will in general be an oversimplification to consider the NLC as being of the same symmetry throughout the reaction. A reaction such as $A+B_2\rightarrow AB+B$ may proceed configurationally by

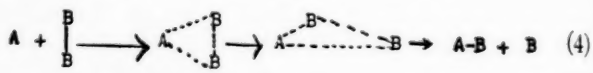

(4)

with a change of the NLC from symmetry group C_{2v} to C_s. In reactions involving intermediate complexes with more than three atoms, the NLC may change from a planar to a nonplanar configuration as the reaction proceeds toward the product side. A sequence of nonlinear complexes of different symmetry may thus be formed during the course of a chemical reaction.

TABLE II. Resolutions of diatomic species into those of other molecular symmetry groups.[a,b]

Diatomic molecules $D_{\infty h}$	Diatomic molecules $C_{\infty v}$	C_{3v}	C_{2v}	C_s $[\sigma_v]\rightarrow\sigma(xz, yz)$	C_1
Σ_g^+, Σ_u^+	Σ^+	A_1	A_1	A'	A
Σ_g^-, Σ_u^-	Σ^-	A_2	A_2	A''	A
Π_g, Π_u	Π	E	B_1+B_2	$A'+A''$	$2A$
Δ_g, Δ_u	Δ	E	A_1+A_2	$A'+A''$	$2A$

[a] Table II in the form given above holds only for resolutions in which the z axis of the diatomic molecule (i.e., the internuclear axis) coincides with the z axis (i.e., principal axis) of the other point groups (z axis for C_{2v} is in plane of molecule). Resolution tables for other axial (and planar) relationships may be obtained by the methods outlined in reference 5.

[b] Since the species B_i occurs as B_1+B_2 in point group C_{2v} for both atomic and diatomic resolutions, there will be no difficulty in correlating via a species B_i regardless of the choice of x and y axes for C_{2v}.

It can, however, readily be shown that the totality of adiabatically allowed correlations between reactants and products is obtained via the *least symmetrical complex* (LSC)[16] formed during the reaction and that it will not be necessary to consider explicitly the intermediate complexes of higher symmetry in arriving at the correlations. The least symmetrical complex, owing to its low symmetry, will impose the least number of symmetry conditions upon the orbital electronic wave functions of reactants and products which have to be met in order for correlations to be possible. The maxi-

[16] The "least symmetrical complex" is the NLC which belongs to the symmetry group with the smallest number of symmetry elements.

mum number of correlations between the states of the reactants and products for a given reaction is thus obtained via this complex of least symmetry. It can furthermore readily be verified from Tables I and II and from the resolution tables given by Mulliken[5] (and can also readily be shown by simple group theoretical arguments) that the species obtained for point groups of lower symmetry by resolution from point groups of higher symmetry are independent of the path of the resolution; the correlating species of the LSC obtained by the direct resolution of the separated reactants (or products) are thus identical with those that would be obtained by a gradual resolution via point groups of lower and lower symmetry. Since the correlations between the reactants (or the products) and the LSC are thus independent of the detailed mode of formation of this LSC during the reaction, the allowed correlations can be obtained via the LSC without any further consideration of the intervening complexes of higher symmetry.

As may be noted from Tables I and II and also from the discussion given above, the restrictions imposed on the allowed term manifold of the products of a chemical reaction by the necessity for adiabatic correlations between reactants and products become less important for LSC of lower symmetry groups. If, for instance, the LSC formed during a reaction is of symmetry group C_1 (which has no symmetry elements), there are no restrictions on the orbital correlations between reactants and products at all and the products may be formed in any and all orbital electronic states irrespective of the particular states of the reactants. Since the LSC for reactions involving nonlinear complexes will in general be of a rather low symmetry,[17] it is evident that the orbital electronic correlation rules do not play as important a role in reactions involving nonlinear intermediate complexes as they do for atomic association reactions and for the dissociation of diatomic molecules.[18]

TABLE III. Correlation table for reactants (or products) $A+BC$ and the NLC (ABC) of symmetry C_s.[a,b]

A \ BC	S_g	S_u	P_g	P_u	D_g	D_u
Σ^+	A'	A''	$A'+2A''$	$2A'+A''$	$3A'+2A''$	$2A'+3A''$
Σ^-	A''	A'	$2A'+A''$	$A'+2A''$	$2A'+3A''$	$3A'+2A''$
II, Δ, etc.	$A'+A''$	$A'+A''$	$3A'+3A''$	$3A'+3A''$	$5A'+5A''$	$5A'+5A''$

[a] Tables III and IV are also directly applicable to diatomic reactants (and products) of symmetry $D_{\infty h}$ as may be noted from the first two columns of Table II.

[b] The coefficients in front of the representation in Tables I to IV show the number of the resulting species of that designation.

TABLE IV. Correlation table for reactants (or products) $AB+CD$ and the NLC ($ABCD$) of symmetry C_s.

A–B \ C–D	Σ^+	Σ^-	II, Δ, etc.
Σ^+	A'	A''	$A'+A''$
Σ^-	A''	A'	$A'+A''$
II, Δ, etc.	$A'+A''$	$A'+A''$	$2A'+2A''$

For reactions of the type $ABCD+EFGH\rightarrow$products, where the reactants (or products) are n atomic molecules with $n\geq 3$ it seems unlikely that the LSC will have any symmetry elements at all. One would thus expect that the orbital correlation rules would impose no restrictions on the allowed product term manifold. If, however, one of the reactants has very high symmetry such as D_{6h}, the LSC formed during such reactions may, owing to the rather localized attack of the other reactant, not be distorted too much from the original symmetry of the highly symmetric reactant. In that case one may then have "weak" correlations rather than no correlation restrictions at all. This would be analogous to the "weak" selection rules for optical transitions of highly symmetrical polyatomic molecules which may have been distorted from their original symmetry by substituents or small side chains but which still retain a sufficient approximation to their former symmetry for the initially forbidden transitions to be weakly allowed in their new configuration. While there appears to be at present no experimental evidence bearing on this question of "weak" correlation rules, it would be of interest to see this point followed up in more detail.

C. The Influence of Vibrations

The discussion so far has been confined entirely to the electronic states of the reactants, intermediate complexes, and products and has neglected the influence of the molecular vibrations on the orbital correlations.[19,20] This is certainly valid for diatomic molecules where the vibrations cannot alter the molecular symmetry. For polyatomic molecules, however, where (nontotally symmetrical) vibrations can change the symmetry of the nuclear skeleton and thus alter the potential field in which the electrons move, this coupling of vibrational and electronic motion will have to be taken into account. This is particularly true for chemical reactions where a strong vibrational-electronic mixing is to be expected owing to the considerable vibrational excitation which accompanies the formation and breakup of the intermediate reaction complex.

[17] The most stable intermediate complex in a reaction is probably highly symmetric [see, e.g., J. L. Magee, J. Chem. Phys. 8, 677 (1940)] and it is thus likely on energetic grounds that a NLC of high symmetry is formed initially during a reaction. As the reaction proceeds this NLC will, however, be distorted as it begins to break up into the products (see e.g., reaction 4 above) and it is this distorted NLC which will in general be of a low symmetry.

[18] The spin correlation rules are of course still operative and applicable to within the degree of validity discussed in footnote 10.

[19] Within the approximation that the spin part of the wave function is separable from the orbital part, the vibration of the nuclear skeleton will not affect the spin correlations.

[20] This discussion will be limited to the interactions of the electronic and vibrational motions and will exclude the coupling with rotation. This may be permissible to a good approximation since the effects of the rotational coupling for polyatomic molecules, owing to their generally high moments of inertia and small angular velocities, are probably only second order compared to the vibrational-electronic ones.

To take account of the effect of the vibrational-electronic interaction on the reactant-product correlations, it will be necessary to investigate the correlations between the vibronic (vibrational-electronic) states of the reactants, the LSC and the products.[21] The requirement for an adiabatic vibronic correlation is, analogous to the electronic ones discussed above, that the LSC have a vibronic species which arises both from the combination of the vibronic states of the reactants and of the products. In carrying out such an analysis, it is found that (*a*) for reactions involving only atomic and/or diatomic reactants and products, vibronic and electronic correlations lead to identical results so that the vibrational-electronic interactions do not have to be taken into account explicitly; (*b*) for reactions involving polyatomic reactants or products the totality of the allowed adiabatic correlations between reactant and product states can be obtained only by making vibronic correlations so that in this case the vibrational-electronic interaction must be taken into account.

Case (a)

The "vibronic states" of atoms and diatomic molecules are identical with their electronic ones. The only polyatomic species involved in the reaction whose vibronic states must be determined is the LSC and the only mode of vibration of this LSC which must be taken into account in establishing the vibronic correlations is the vibration along the reaction coordinate[22] which brings about the breakup of the LSC into its separated constituents, i.e., the vibration which leads to reaction. None of the other modes of vibration of the LSC enter into this problem *since they do not lead to reaction.* The only difference between an electronic and a vibronic correlation is then that for the latter, one uses the vibronic states of the LSC obtained by forming the direct product of the electronic representations and the vibrational species which leads to reaction. To each electronic state of the LSC there corresponds then one, and only one, vibronic state which is pertinent to the reaction. It is readily evident that under these conditions, states of reactants and products which correlate electronically will also do so vibronically,[23] while, conversely, states which do not correlate electronically will not correlate vibronically either.[24]

Case (b)

In this case the vibrational-electronic interaction must be considered explicitly for both the LSC and the polyatomic reactants and/or products. The argument for the LSC follows along the lines given above in that only the vibrations along the reaction coordinate which lead to reaction need to be taken into account. For the polyatomic reactants and products, however, all modes of vibration must be taken into consideration since their vibrational motions are independent of those of the LSC owing to the rearrangement of the vibrational energy during the reaction. If one now tests the vibronic correlations between the various vibronic states of the reactants, the products, and that of the LSC, one finds that some of the states of reactants and products which did not correlate electronically will do so vibronically.[25] The vibrational-electronic coupling must therefore be taken into explicit account in establishing the correlations for these reactions.

For reactions involving polyatomic reactants, the LSC will in general be of a very low symmetry or have no symmetry properties at all so that there will be hardly any orbital electronic restrictions on the adiabatically allowed product term manifold. If to this one adds the additional product states allowed by the electronic-vibrational interaction, it becomes evident that the adiabatic orbital correlation rules impose very few, if any, restrictions on the allowed term manifold of the products of a chemical reaction.[26] One may thus state the quite general rule that, except for some exceptional cases, *there are no strong orbital restrictions on the adiabatically allowed electronic term manifold of the products formed in chemical reactions involving polyatomic reactants.*

III. THE FORMATION OF OH($^2\Sigma^+$) IN THE HYDROGEN-OXYGEN FLAME

The reactions

$$H+O_2 \rightarrow OH+O \tag{5}$$

and

$$O+H_2 \rightarrow OH+H \tag{6}$$

have been proposed by several authors[27] as chain

[21] The vibronic representations (states) are obtained by forming the direct product of the pertinent electronic and vibrational representations. For a detailed discussion, see reference 7. The vibrational species for various symmetry groups are discussed at length by G. Herzberg, *Infrared and Raman Spectra* (D. Van Nostrand Company, Inc., New York, 1945).

[22] For a discussion of the concept of "reaction coordinate" see Glasstone, Laidler, and Eyring, *The Theory of Rate Processes* (McGraw-Hill Book Company, Inc., New York, 1941), Ch. III.

[23] Thus, for example, reactants $A+B_2$ of species ^1S_g and $^1\Sigma_g^+$ will correlate electronically via a LSC (C_{2v}) of species $^1A_1$ with products $AB+B$ of species ^1P_u and $^1\Delta$. If the vibration along the reaction coordinate is of species B_2, then for a vibronic correlation one has: reactants $^{ev1}S_g+{}^{ev1}\Sigma \rightarrow \mathrm{LSC}(C_{2v})^{ev1}B_2$, products $^{ev1}P_u+{}^{ev1}\Delta \rightarrow \mathrm{LSC}(C_{2v})^{ev1}B_2$, $^{ev1}B_1$, $\cdots$, and various other vibronic species. Reactant and product states thus correlate vibronically via $^{ev1}B_2$ as they correlated electronically via $^1A_1$.

[24] An example of this case could readily be worked out by analogy with that presented in reference 23. The rule is based on the fact that ${}^eX\times{}^vY \neq {}^eZ\times{}^vY$ for $X\neq Z$ if X, Y, and Z are nondegenerate species. The above will also hold true, however, for degenerate species owing to the operation of the Jahn-Teller principle.

[25] For a simple example of vibronic correlations, see R. S. Mulliken, Phys. Rev. **60**, 506 (1941). Note, for instance, that while the $^1\Pi_g$ state of linear CO_2 does not correlate with the $^1A_2$ state of bent CO_2, certain corresponding vibronic states $^{ev1}\Sigma_u^-$ and $^{ev1}A_2$ will correlate vibronically.

[26] The adiabatic product term manifold for such a reaction is governed principally by the adiabatic spin correlations.

[27] B. Lewis and G. von Elbe, J. Chem. Phys. **10**, 366 (1942); C. N. Hinshelwood, Proc. Roy. Soc.(London) **A188**, 1 (1947).

branching steps in the H_2-O_2 reaction. The work of Gaydon and Wolfhard[28] and Broida and Shuler[29] on the specific enhancement of $OH(^2\Sigma^+)$ to the levels $v'=2$ and 3 seems to indicate that there is a large concentration of free atoms in the H_2-O_2 flame at atmospheric pressure. It is therefore reasonable to suppose that reactions (5) and (6) are of some importance in the hydrogen-oxygen flame at atmospheric pressure and will contribute to the formation of $OH(^2\Sigma^+)$ in these flames. It would be of particular interest to ascertain by what mechanism the electronically excited $OH(^2\Sigma^+)$ is produced preferentially in the levels $v'=2$ and 3. As will be shown below, the correlation rules developed in Sec. II will be of great help in arriving at a more detailed picture of these processes.

A. The Reaction $H+O_2\rightarrow OH^*+O$

The detailed features of the production of $OH(^2\Sigma^+)$ can best be brought out from a consideration of the relevant potential energy surfaces.[30] The only electronic states of the reactants which need be considered† are $H^2(S)$ and $O_2(^3\Sigma_g^-, {}^1\Delta_g, {}^1\Sigma_g^+, {}^3\Sigma_u^+, {}^3\Sigma_u^-)$. All other states of H and O_2, both homopolar or ionic, are energetically too high to be of importance. As far as the products are concerned, the electronic states which must be taken into account are $O(^3P_g, {}^1D_g)$ and $OH(^2\Pi, {}^2\Sigma^-, {}^2\Sigma^+)$ and the repulsive states of OH such as $^4\Sigma^-$ and $^4\Pi$. There is some question as to the nature of the $^2\Sigma^-$ state of OH. Gaydon and Wolfhard[28] have suggested a weakly attractive $OH(^2\Sigma^-)$ state on the basis of their spectroscopic findings, while a consideration of the electron configuration of $OH(^2\Sigma^-)[K(2s\sigma)^2(2p\sigma)^2(2p\pi)^2 \times(3s\sigma)]$ would seem to indicate that it may be a repulsive one. The weakly attractive $OH(^2\Sigma^-)$ state in the form suggested by Gaydon and Wolfhard has been chosen for the potential energy surfaces of Figs. 1 and 2. Since the role of the $^2\Sigma^-$ state of OH in reactions (5) and (6) is not affected by or dependent upon its stability, the arguments to follow will retain their validity even if further spectroscopic work should prove that the $OH(^2\Sigma^-)$ state is repulsive.

The LCS (HO_2) formed in reaction (5) is most probably of symmetry C_s so that the correlations between the reactants $H+O_2$ and the products $OH+O$ can be determined from Table III. Since reaction (5) involves only atomic and diatomic reactants and products, a purely electronic correlation will suffice to establish the adiabatic term manifold of the products (see case *a* above). The correlations pertinent to the formation of $OH(^2\Sigma^+)$ are shown in Fig. 1.[31] The potential curves for O_2 were taken from Herzberg,[4] the OH potential curves were calculated from Morse functions,[32] and that for $OH(^2\Sigma^-)$ is based on the work of Gaydon and Wolfhard.[28] It will be noted that the ground states of O_2 and OH, i.e., $O_2(^3\Sigma_g^-)$ and $OH(^2\Pi)$, correlate via $HO_2(^{2,4}A'')$; the excited states $O_2(^3\Sigma_u^-)$ and $OH(^2\Sigma^+)$ correlate via a different HO_2 surface of species $^{2,4}A''$. All of the states of O_2 which arise from $O(^3P)+O(^3P)$ correlate with $OH(^2\Sigma^-)$ via either $^eA'$ or $^eA''$ surfaces.

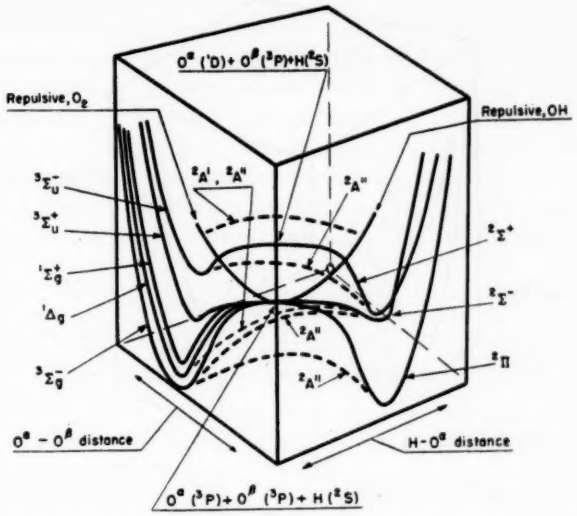

FIG. 1. Potential energy surfaces for $HO_2(C_s)$ relevant to the reaction $H+O_2\rightarrow OH+O$. The potential curves on the left and right-hand faces of the cube are for O_2 and OH, respectively.

The discussion of the behavior and properties of the potential surfaces in the interior of the cube will be limited to the ground state of O_2, in which most of the oxygen molecules will be found, and to the excited state $O_2(^3\Sigma_u^-)$ arising from $O(^3P)+O(^3P)$ which can correlate directly with $OH(^2\Sigma^+)$.[33] One of the ways in which $OH(^2\Sigma^+)$ can be formed utilizes excited $O_2(^3\Sigma_u^-)$ via the upper, excited $^2A''$ surface by

$$O_2(^3\Sigma_u^-)+H(^2S_g)\rightarrow HO_2(^2A'')\rightarrow OH(^2\Sigma^+)+O(^3P_g). \quad (7)$$

[28] A. G. Gaydon and H. G. Wolfhard, Proc. Roy. Soc. (London) A208, 63 (1951).

[29] H. P. Broida and K. E. Shuler, J. Chem. Phys. **20**, 168 (1952).

[30] For a comprehensive discussion on the use of potential energy surfaces in tracing the course of a chemical reaction and for details on the construction and properties of these surfaces, see reference 1.

† Dr. G. Herzberg has kindly informed the author that he has recently observed the $^3\Delta_u$ and $^1\Sigma_u^-$ states of O_2. These states, which are found to be close to the $^3\Sigma_u^+$ state, should be added to the above list of O_2 states. This addition will, however, not influence the arguments to follow since the main interest centers on the correlations involving $O_2(^3\Sigma_g^-)$ and $O_2(^3\Sigma_u^-)$.

[31] Figure 1 is based on certain simplifying assumptions which must be made in order for a graphical presentation of potential surfaces of polyatomic molecules to be feasible. Since only two spatial coordinates are available (the third coordinate giving the potential energy of the system), one must neglect the vibrations of the NLC and make the additional assumption that all bond angles remain constant during the reaction so that the two intermolecular distances H—O and O—O will be sufficient for a complete configurational (and thus energetic) specification of the reaction complex. Similar stratagems must be used for the construction of potential energy diagrams for all types of nonlinear polyatomic molecules. The use of this simplified model will, however, not affect the validity of the discussion to follow.

[32] K. E. Shuler, J. Chem. Phys. **18**, 1221 (1950).

[33] In writing down these correlations, only the lowest multiplicity of the intermediate reaction complex will be considered explicitly. In the absence of information to the contrary, it will be assumed that among surfaces of identical orbital species the one with the lowest multiplicity will be the lowest energetically and thus the one on which the reaction is most likely to proceed.

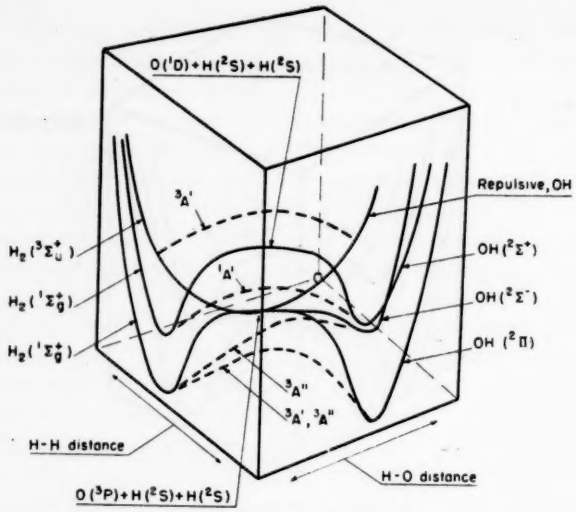

FIG. 2. Potential energy surfaces for $OH_2(C_s)$ relevant to the reaction $O+H_2 \rightarrow OH+H$. The potential curves on the left and right-hand faces of the cube are for H_2 and OH, respectively.

A path whereby $OH(^2\Sigma^+)$ can be formed from the ground state $O_2(^3\Sigma_g^-)$ is provided by the intersection in the interior of the cube[34] of the two $^2A''$ surfaces which correlate $O_2(^3\Sigma_g^-)$ with $OH(^2\Sigma^-)$ and $O_2(^3\Sigma_u^-)$ with $OH(^2\Sigma^+)$, respectively. This reaction can be written as

$$O_2(^3\Sigma_g^-)+H(^2S_g)\rightarrow HO_2(^2A'')\xrightarrow[\text{transition}]{\text{radiationless}}$$

$$HO_2(^2A'')\rightarrow OH(^2\Sigma^+)+O(^3P_g). \quad (8)$$

Since the two surfaces between which the radiationless transition of reaction (8) is supposed to take place are of the same orbital electronic species and multiplicity ($^2A''$), one would expect such a large repulsive interaction that this radiationless transition would seem to have only a very small probability of occurrence. It has, however, been shown by Teller[35] that potential surfaces of polyatomic molecules of the same electronic species may cross since now two or more parameters (internuclear distances, bond angles) are available whose variation will be sufficient in all cases to produce a degeneracy of such electronic states and thus allow a crossing of the surfaces. The probability of a radiationless transition of the reaction system at such a crossing *point* may be quite high, the transition probability being given by an equation analogous to that derived by Zener and Landau for diatomic molecules.[1] The radiationless transition shown in Eq. (8) may thus occur by this mechanism.

A radiationless transition between the two $^2A''$ surfaces of reaction (8) may also be brought about by the weak coupling of the two different charge distributions of the upper and lower $^2A''$ states. The upper $^2A''$ surface of HO_2 is formed from $O_2(^3\Sigma_u^-)$ and $H(^2S_g)$. It has been pointed out by Mulliken[36] that the $O_2(^3\Sigma_u^-)$ state is an ionic one (V state) resulting from O^+O^- and O^-O^+, and it may thus be assumed that the $HO_2(^2A'')$ resulting from it will have a certain amount of ionicity and may perhaps be written as $(HO)^+-O^-$ and $(HO^-)-O^+$. The $O_2(^3\Sigma_g^-)$ ground state is homopolar (N state) and the $HO_2(^2A'')$ formed from it is thus presumably homopolar. Since the interaction between these ionic and homopolar $^2A''$ states takes place at a rather large O—O internuclear distance (see Fig. 1), a radiationless transition between the two $^2A''$ surfaces may quite readily occur.[37] It is not possible to ascertain without a more detailed investigation which one of these two processes is more effective in reaction (8).

In order to account for the specific enhancement of the levels $v'=2$ and 3 of $OH(^2\Sigma^+)$ in the hydrogen-oxygen flame, Gaydon and Wolfhard[28] have suggested the "pre-association" reaction

$$O(^3P)+H(^2S)\rightarrow OH(^2\Sigma^-)\xrightarrow[\text{transition}]{\text{radiationless}}OH(^2\Sigma^+), \quad (9)$$

where it is postulated that the $OH(^2\Sigma^-)$ curve intersects the $OH(^2\Sigma^+)$ curve at about $v'=2$. The interaction of $OH(^2\Sigma^-)$ and $OH(^2\Sigma^+)$ is, however, very weak, being due to only a very small coupling between the electronic spin and the rotation of the internuclear axis. It is therefore doubtful whether the radiationless transition shown in reaction (9) is sufficiently strong to account for the observed vibrational nonequilibrium distribution of $OH(^2\Sigma^+)$. The radiationless transitions of polyatomic molecules are in general stronger than those brought about in diatomic molecules by the coupling of rotational and electronic motion. It is therefore suggested that reaction (8), with H atoms in excess of their thermal equilibrium concentration, is more efficient in producing $OH(^2\Sigma^+)$ in its specific vibrational nonequilibrium distribution than the two atom pre-association reaction put forth tentatively by Gaydon and Wolfhard.[38]

B. The Reaction $O+H_2 \rightarrow OH^*+H$

The LSC (OH_2) for this reaction is most probably of symmetry C_s so that Table III is to be used in establishing the correlation between reactants and products. The relevant electronic states which need to be con-

[34] This intersection could not readily be shown in Fig. 1. It is clear, however, that since $OH(^2\Sigma^+)$ and $OH(^2\Sigma^-)$ intersect, the surfaces which connect with these states must also intersect in the interior of the cube.

[35] E. Teller, J. Phys. Chem. **41**, 109 (1937).

[36] R. S. Mulliken, J. Chem. Phys. **7**, 20 (1939).

[37] The decisive factor here is the relative magnitude of the period of nuclear vibration and the time required for the electron to tunnel from one charge distribution to the other. This depends upon the internuclear distance at which the "crossing" takes place. For a more detailed discussion, see F. London, Z. Physik **74**, 143 (1932).

[38] Reaction (8) is also to be preferred for the production of $OH(^2\Sigma^+)$ over reaction (9) on the ground that the concentration of O_2 molecules in the hydrogen-oxygen flame is much larger than that of O atoms so that collisions between H and O_2 will be much more frequent than those between H and O atoms.

sidered on the basis of the available energy are $O(^3P_g)$ and $O(^1D_g)$, $OH(^2\Pi, {}^2\Sigma^-, {}^2\Sigma^+)$ and $H_2(^1\Sigma_g^+, {}^3\Sigma_u^+)$. All other states of H_2, both ionic and excited homopolar are energetically too high[39] to be of much importance in this reaction. The same holds true for $O(^1S_g)$ which is about 4.2 ev above $O(^3P_g)$. The pertinent correlations between the reactant and product states via the LSC (OH_2) of symmetry C_v are shown in Fig. 2.

It will be noted from Fig. 2 that if $OH(^2\Sigma^+)$ is to be produced from $O(^3P_g)$ and $H_2(^1\Sigma_g^+)$ there must be a radiationless transition between $OH_2(^1A')$ and $OH_2(^3A'')$. Owing to the difference in both spin and symmetry of the electronic wave functions, the interactions between these two states will be extremely weak. While the interaction of orbital electronic species may sometimes be enhanced sufficiently for radiationless transitions by the excitation of nontotally symmetric vibrations,[7] the interaction between triplet and singlet surfaces can be brought about only by spin-orbit coupling which for the light nuclei considered here would be extremely weak. The reaction

$$O(^3P_g)+H_2(^1\Sigma_g^+)\rightarrow OH_2(^3A'')\xrightarrow[\text{transition}]{\text{radiationless}}$$

$$OH_2(^1A')\rightarrow OH(^2\Sigma^+)+H(^2S_g) \quad (10)$$

would thus be much less effective than reaction (8) in producing $OH(^2\Sigma^+)$. Aside from possible energetic considerations, and by analogy with similar reactions which violate the spin correlation principle,[1] about 10^4 to 10^6 $OH(^2\Sigma^+)$ radicals will be produced by reaction (8) for every one formed by reaction (10).

The principal mechanism by which $OH(^2\Sigma^+)$ is formed directly from O plus H_2 in reaction (6) involves excited oxygen atoms and may be written as

$$O(^1D_g)+H_2(^1\Sigma_g^+)\rightarrow OH_2(^1A')\rightarrow OH(^2\Sigma^+)+H(^2S_g). \quad (11)$$

This reaction is the analog of reaction (7) involving H plus O_2 where both reactions proceed on excited complex surfaces. While reactions (7) and (11), like many other chemical reactions, may well give rise to products in some type of nonequilibrium distribution, they cannot account for the very specific enhancement of the levels $v'=2$ and 3 of $OH(^2\Sigma^+)$. If this observed nonequilibrium distribution is to be attributed to a specific chemical reaction, then the most likely one appears to be reaction (8) where the specific enhancement is brought about by the radiationless transition at the crossing point of the two $HO_2(^2A'')$ surfaces.

IV. ACKNOWLEDGMENTS

The authors wishes to acknowledge several helpful discussions with Dr. F. T. McClure and Professor K. J. Laidler in connection with this paper. He is very much indebted to Dr. G. Herzberg and Professor H. Sponer for their helpful suggestions and to Professor James Franck for an interesting discussion in regard to several points. He is particularly indebted to Professor R. S. Mulliken for his detailed comments and for the many valuable suggestions which he contributed to the formulation of the correlation rules presented in Sec. II of this paper. Many thanks are also due Miss A. Fogelgren for manifold assistance in the preparation of this manuscript.

[39] See, e.g., J. L. Magee and M. Burton, J. Am. Chem. Soc. 72, 1965 (1950).

APPENDIX

Correlation Rules for Reactions Involving Polyatomic Linear Complexes and Products

For simple association reactions where the only product is a linear polyatomic molecule, it seems quite likely that the intermediate complex will be of a linear equilibrium nuclear configuration throughout the course of the reaction. This type of reaction is exemplified by

$$O+CO\rightarrow O\cdots C\cdots +O-C-O$$
$$\qquad\quad C_{\infty v} \qquad\quad D_{\infty h}$$

and

$$N+NO\rightarrow N\cdots N\cdots O\rightarrow N-N-O,$$
$$\qquad\quad C_{\infty v} \qquad\quad C_{\infty v}$$

where the LSC is linear and of symmetry $C_{\infty v}$. The adiabatic correlation rules relating the states of these linear polyatomic products to those of the separated reactants are, owing to the presence of identical symmetry relations, very similar to those for the formation of diatomic molecules from separated atoms and can readily be obtained by a simple extension of the Wigner-Witmer rules.[3,4]

The electronic spin correlation rules are identical for the formation of both diatomic and linear polyatomic molecules. Depending upon the mode of formation of the linear polyatomic molecule (LPM) (atom +molecule or molecule+molecule), the orbital angular momentum quantum number Λ_P of the polyatomic molecule is given, in analogy with the diatomic case, by $\Lambda_P=|M_L+M_\Lambda|$ or $\Lambda_P=|M_\Lambda+M_{\Lambda'}|$ where M_L, M_Λ, and $M_{\Lambda'}$ are, respectively, the components of orbital angular momenta of the atoms and/or molecules which combine to form the linear polyatomic molecule. How-

TABLE V. Electronic states of linear polyatomic molecules ($C_{\infty v}$) arising from separated atoms and molecules.

States of separated groups	Resultant molecular states
$S_g+\Sigma^+$ or $S_u+\Sigma^-$	Σ^+
$S_g+\Sigma^-$ or $S_u+\Sigma^+$	Σ^-
$S_g+\Pi$ or $S_u+\Pi$	Π
$S_g+\Delta$ or $S_u+\Delta$	Δ
$P_g+\Sigma^+$ or $P_u+\Sigma^-$	Σ^-, Π
$P_g+\Sigma^-$ or $P_u+\Sigma^+$	Σ^+, Π
$P_g+\Pi$ or $P_u+\Pi$	Σ^+, Σ^-, Π, Δ
$P_g+\Delta$ or $P_u+\Delta$	Π, Δ, ϕ
$D_g+\Sigma^+$ or $D_u+\Sigma^-$	Σ^+, Π, Δ
$D_g+\Sigma^-$ or $D_u+\Sigma^+$	Σ^-, Π, Δ
$D_g+\Pi$ or $D_u+\Pi$	Σ^+, Σ^-, Π, Δ, ϕ
$D_g+\Delta$ or $D_u+\Delta$	Σ^+, Σ^-, Δ, ϕ, Γ

TABLE VI. Electronic states of linear polyatomic molecules ($C_{\infty v}$) arising from separated (different) molecules.

States of separated groups	Resultant molecular states
$\Sigma^+ + \Sigma^+$ or $\Sigma^- + \Sigma^-$	Σ^+
$\Sigma^+ + \Sigma^-$	Σ^-
$\Sigma^+ + \Pi$ or $\Sigma^- + \Pi$	Π
$\Sigma^+ + \Delta$ or $\Sigma^- + \Delta$	Δ
$\Pi + \Pi$	$\Sigma^+, \Sigma^-, \Delta$
$\Pi + \Delta$	Π, ϕ

ever, owing to the reduced symmetry of linear molecules as compared to atoms (cylindrical *vs* spherical), there will be less degeneracy in the molecular case and one has $M_\Lambda = \pm\Lambda$ in contrast to the $2L+1$ components M_L in the atomic case.

The adiabatic term manifolds of linear polayatomic molecules resulting from the combination of the various atomic and molecular states are collected in Tables V, VI, and VII.[40] For LPM of symmetry $D_{\infty h}$ all the allowed electronic states of Table V will appear as both *g* and *u*. The spin correlations have been included in Table VII since there the multiplicity of the species is dependent upon their parity.

The purely electronic orbital correlations given in Tables V to VII are greatly weakened when the vibrational-electronic interaction is taken into account. This arises from the fact that the modes of vibration of the LPM are independent of those of the LSC since the vibrational energy will be distributed among all the various available degrees of freedom during the course of the reaction.[41] It will then be necessary to take account of all the possible normal vibrations of the LPM and not just the one along the reaction coordinate as is the case for the LSC. The possibility of multiple excitation of vibrations and the possible degeneracy of some of the normal modes in such highly symmetrical systems will make for added complexity. It can probably be stated as a general rule that owing to the vibrational-electronic coupling, there are only weak orbital restrictions on the adiabatic term manifold of the LPM produced in simple association reactions for which Tables V to VII can serve as general guide posts. The adiabatic spin correlations which determine the multiplicity of the product states are not affected by the vibrational-electronic coupling.

TABLE VII. Electronic states of linear polyatomic molecules ($D_{\infty h}$) arising from separated (identical) molecules.

States of separated groups	Resultant molecular states
$^1\Sigma^+ + {}^1\Sigma^+$ or $^1\Sigma^- + {}^1\Sigma^-$	$^1\Sigma_g^+$
$^2\Sigma^+ + {}^2\Sigma^+$ or $^2\Sigma^- + {}^2\Sigma^-$	$^1\Sigma_g^+, {}^3\Sigma_u^+$
$^3\Sigma^+ + {}^3\Sigma^+$ or $^3\Sigma^- + {}^3\Sigma^-$	$^1\Sigma_g^+, {}^3\Sigma_u^+, {}^5\Sigma_g^+$
$^1\Pi + {}^1\Pi$	$^1\Sigma_g^+, {}^1\Sigma_u^-, {}^1\Delta_g$
$^2\Pi + {}^2\Pi$	$^1\Sigma_g^+, {}^1\Sigma_u^-, {}^1\Delta_g, {}^3\Sigma_u^+, {}^3\Sigma_g^-, {}^3\Delta_u$
$^3\Pi + {}^3\Pi$	$^1\Sigma_g^+, {}^1\Sigma_u^-, {}^1\Delta_g, {}^3\Sigma_u^+, {}^3\Sigma_g^-, {}^3\Delta_u, {}^5\Sigma_g^+, {}^5\Sigma_u^-, {}^5\Delta_g$
$^1\Delta + {}^1\Delta$	$^1\Sigma_g^+, {}^1\Sigma_u^-, {}^1\Gamma_g$
$^2\Delta + {}^2\Delta$	$^1\Sigma_g^+, {}^1\Sigma_u^-, {}^1\Gamma_g, {}^3\Sigma_u^+, {}^3\Sigma_g^-, {}^3\Gamma_u$
$^3\Delta + {}^3\Delta$	$^1\Sigma_g^+, {}^1\Sigma_u^-, {}^1\Gamma_g, {}^3\Sigma_u^+, {}^3\Sigma_g^-, {}^3\Gamma_u, {}^5\Sigma_g^+, {}^5\Sigma_u^-, {}^5\Gamma_g$

[40] These tables in the form given here were compiled by G. Herzberg. I am very much indebted to Dr. Herzberg for his kind permission to use them in this paper.

[41] For these types of dissociation (and association) reactions the large amplitude of the oscillations in conjunction with the anharmonicity of the potential energy will make for particularly effective interaction and coupling of the various normal modes of vibration.

Dielectric Relaxation and the Internal Field*

J. G. POWLES†
Frick Chemical Laboratory, Princeton University, Princeton, New Jersey‡
(Received July 28, 1952)

The paper discusses the relation of the relaxation time τ of a dielectric to the measured decay time of polarization T and proposes a new expression for the internal field in a dielectric subjected to an alternating field. It is found for this expression that $1<T/\tau<\frac{3}{2}$ and that in most instances no serious error is incurred in using T instead of τ. Application to the case of several distinct relaxation times shows that the new expression gives relations between the complex dielectric constant and frequency which are observed experimentally.

INTRODUCTION

THE concept of an effective internal field acting on a molecule within a dielectric subjected to a static electric field has received considerable attention because it enables one to relate the macroscopic dielectric constant to the molecular properties and interactions. In the first successful theory of the dielectric polarization produced by permanent dipoles, Debye[1(a)] used the Lorentz internal field[2] which is given by $F=E+(4\pi/3)P$, where E is the applied field and P is the polarization of the dielectric. This may be written $F=[(\epsilon_0+2)/3]E$, where ϵ_0 is the static dielectric constant. This expression was soon found to be inadequate for a dielectric with a high concentration of dipoles. Also, it leads to the prediction of ferroelectricity in many dielectrics at ordinary temperatures, which is not in fact observed. Onsager[3] proposed to use, as the internal field, the actual field in an empty macroscopic cavity about the molecule, which has the value $G=[3\epsilon_0/(2\epsilon_0+1)]E$. Expressions for the dielectric constant derived with the use of this field agree better with experiment except in certain cases.[4] More recent general theories of the static dielectric constant[5,6(a)] retain the Onsager internal field only in a modified sense and show that its use is justified only under certain special conditions.[6(b)] For gases and dilute solutions, in so far as one may speak of an internal field, the correct one is intermediate between those of Onsager and Lorentz.[7] In view of the difficulties of a rigorous theory, it seems at present desirable to retain the idea of an internal field as a useful approximation.

The present paper applies the concept of an internal field to *relaxing* dielectrics in an attempt to obtain an expression which corresponds in validity to the Onsager approximation in the static case.

The relaxation time τ is a quantity which is independent of the expression for the internal field. The significance of τ can be illustrated by reference to Debye's theory of the dielectric relaxation of a viscous liquid.[1(b)] τ is in this case related to the mean square angular deviation of a molecule in a given time and is of the order of magnitude of the time required for a given molecule, if fixed and then released, to revert to random orientation in the absence of resultant macroscopic polarization resulting from the surrounding molecules. τ can also be defined in other circumstances, as for instance for a molecule which changes position by jumps over an energy barrier,[8] τ is then one-half the average time a molecule waits before jumping. It is evident that the time τ is the quantity required for the interpretation of dielectric relaxation on a molecular scale. On the other hand, the measured quantity is the macroscopic dielectric constant ($\epsilon=\epsilon'-i\epsilon''$) and its variation with frequency, or less commonly, the decay of the macroscopic polarization of the dielectric with time. If the decay of polarization of the dielectric is exponential with time, it may be characterized by a decay function[9(a)]

$$\alpha(t)=(\epsilon_0-\epsilon_\infty)/\mathrm{T}\,\exp-t/\mathrm{T}, \tag{1}$$

where T is called the decay time.§ Using the relation

$$\epsilon-\epsilon_\infty=\int_0^\infty \alpha(t)\,\exp-i\omega t\cdot dt, \tag{2}$$

we find for ϵ

$$(\epsilon-\epsilon_\infty)/(\epsilon_0-\epsilon_\infty)=1/(1+i\omega\mathrm{T}). \tag{3}$$

The plot of ϵ'' *versus* ω obtained from (3) has a maximum when $\omega\mathrm{T}=1$, i.e., $\omega_c=1/\mathrm{T}$, where ω_c is defined as the

* This research has been supported in part by the U. S. Office of Naval Research. Reproduction, translation, publication, use or disposal in whole or in part by or for the United States Government is permitted.
† Supported by a Grant-in-Aid to the Chemistry Department, Princeton University, from E. I. du Pont de Nemours Company.
‡ Present address: Noyes Chemical Laboratory, University of Illinois, Urbana, Illinois.
[1] P. Debye, *Polar Molecules* (Dover Publications, New York, 1945). (a) p. 36, (b) p. 84, (c) p. 94, (d) p. 101.
[2] H. A. Lorentz, *Theory of Electrons* (Teubner, Leipzig, 1909), p. 303.
[3] L. Onsager, J. Am. Chem. Soc. **58**, 1486 (1936).
[4] C. F. J. Böttcher, Physica **6**, 59 (1939).
[5] J. G. Kirkwood, J. Chem. Phys. **7**, 911 (1939).
[6] H. Fröhlich, Trans. Faraday Soc. **44**, (a) p. 238, (b) p. 242 (1948).
[7] J. H. Van Vleck, J. Chem. Phys. **5**, 556 (1937), Ann. N. Y. Acad. Sci. **40**, 293 (1940).
[8] R. E. Powell and H. Eyring, *Advances in Colloid Science* (Interscience Publishers, Inc., New York, 1942), Vol. I, p. 214.
[9] H. Fröhlich, *Theory of Dielectrics* (Oxford University Press, London, 1949). (a) pp. 8 and 62, (b) p. 92, (c) p. 42.
§ T is the decay time for a condenser with constant voltage at the plates; for constant charge on the plates the decay time is $\epsilon_\infty/\epsilon_0\cdot\mathrm{T}$ [reference 9(c)].

critical angular frequency. T then is the experimentally measured quantity.‖

Experimental results are often not expressible in the form (3) but it is found that, in the absence of resonance absorption, any observed relation of ϵ to ω can be reproduced by writing a sum of terms with different T's on the right-hand side of (3). On the other hand, there are now known many materials for which (3) is very closely obeyed (e.g., ice,[10] water,[11] some liquid organic halides,[12] and dilute solutions of polar materials in a nonpolar solvent[13]). For these materials, therefore, the dielectric is characterized by a single decay time (we use the term decay time rather than relaxation time advisedly). The experimental evidence suggests therefore that (3) represents a very important limiting case in dielectric behavior and that it is of fundamental significance. We shall investigate the way in which (3) may arise and the relation between the quantities T and τ.

VARIOUS INTERNAL FIELDS

(a) Lorentz-Debye

In his theory of dielectric relaxation Debye used implicitly the internal field

$$F=[(\epsilon+2)/3]E, \tag{4}$$

where ϵ is now the complex dielectric constant and is, of course, frequency dependent. This leads to the well-known Debye equation[1(c)]

$$(\epsilon-\epsilon_\infty)/(\epsilon_0-\epsilon_\infty)=1\Big/\left[1+i\omega\left(\frac{\epsilon_0+2}{\epsilon_\infty+2}\right)\tau\right], \tag{5}$$

which has the same form as (3) with

$$\mathrm{T}=\frac{\epsilon_0+2}{\epsilon_\infty+2}\cdot\tau. \tag{6}$$

Equation (5) for a single relaxation time, therefore, corresponds to exponential relaxation of polarization with a decay time $\tau\cdot[(\epsilon_0+2)/(\epsilon_\infty+2)]$. The factor $[(\epsilon_0+2)/(\epsilon_\infty+2)]$ may be quite large, for water it is about 20. Equation (6) which expresses the tendency of the polarization to maintain itself on removal of a field, is connected with the prediction of ferroelectricity in the static case which has already been mentioned. It has long been suspected that this factor is excessively large, both because it is derived from an expression which is known to be invalid in the static case, and because the experimental value of τ obtained from (5), when taken together with Debye's expression relating τ to the molecular volume V[1(d)] gives values of V smaller than would be expected from other evidence.[14] Equations (8) and (13), which are discussed later, give better values of V. Most experimental results are now wisely expressed in terms of T or ω_c. The tendency of the polarization to maintain itself is always active to some extent so that T is always greater than τ.

(b) Onsager-Cole

Cole[14] has given a modified form of the Debye theory in which he puts for the internal field in the alternating current case,

$$G=3\epsilon E/(2\epsilon+1), \tag{7}$$

in analogy to the static case.[3] G is the field in an actual spherical cavity in the dielectric as is easily shown by considering the Rayleigh scattering of a plane wave by a spherical cavity in an infinite medium.[15] One obtains for ϵ using (7)

$$\frac{(\epsilon-\epsilon_\infty)(2\epsilon+\epsilon_\infty)}{\epsilon}=\frac{(\epsilon_0-\epsilon_\infty)(2\epsilon_0+\epsilon_\infty)}{\epsilon_0}\cdot\frac{1}{1+i\omega\tau}. \tag{8}$$

This expression has been frequently used as a starting point for other investigations.[16,17] Equation (8) cannot be put in the form (3) and therefore does not correspond to a single decay time or to exponential relaxation of polarization, although it is put forward for a dielectric characterized by a single relaxation time. It is, moreover, not possible to represent it by a spectrum of relaxation times in the usual manner since, on the Cole-Cole plot[18] (ϵ'' *versus* ϵ'), the curve for (8) always lies *outside* the semicircle for (3) with the same ϵ_0 and ϵ_∞, whereas it may be shown that the curve for Eq. (3), generalized to a spectrum of relaxation times, always falls *inside* this semicircle. If Eq. (8) is compared with Eq. (3) it is found that $\mathrm{T}\geqq\tau$ in contrast with the relation (6) for the Lorentz field (see Fig. 1).

Substituting for ϵ from (3) in (7) one finds

$$G/E=\frac{3\epsilon_\infty}{2\epsilon_\infty+1}+\left[\frac{3\epsilon_0}{2\epsilon_0+1}-\frac{3\epsilon_\infty}{2\epsilon_\infty+1}\right]\cdot\left[\frac{1}{1+i\omega\mathrm{T}\left(\frac{2\epsilon_\infty+1}{2\epsilon_0+1}\right)}\right]. \tag{9}$$

Thus the field in a real cavity in a medium characterized by a decay time T relaxes with a decay time $\mathrm{T}[(2\epsilon_\infty+1)/(2\epsilon_0+1)]$, i.e., more slowly than the polari-

‖ The distinction between τ and T is also clearly made by Böttcher (*Theory of Electric Polarisation*, Elsevier, New York, 1952), p. 356.

[10] R. P. Auty and R. H. Cole, J. Chem. Phys. **20**, 1309 (1952).

[11] Collie, Ritson, and Hasted, Proc. Phys. Soc. (London) **60**, 145 (1948).

[12] Hennelly, Heston, and Smyth, J. Am. Chem. Soc. **70**, 4102 (1948).

[13] W. Jackson and J. G. Powles, Trans. Faraday Soc. **42A**, 104 (1946).

[14] R. H. Cole, J. Chem. Phys. **6**, 385 (1938).

[15] J. A. Stratton, *Electromagnetic Theory* (McGraw-Hill Book Company, Inc., New York, 1941), p. 572.

[16] J. G. Kirkwood and R. M. Fuoss, J. Chem. Phys. **9**, 329 (1941).

[17] E. Fischer, Ann. Physik **6**, 117 (1949).

[18] K. S. Cole and R. H. Cole, J. Chem. Phys. **9**, 341 (1941).

zation in a continuous medium. This in part accounts for the complex relation (8).

In this connection it may be noted that in a recent article[19] a local field is used which corresponds to (9) but with τ in place of $T[(2\epsilon_\infty+1)/(2\epsilon_0+1)]$. It was assumed, therefore, that the local field relaxes exponentially with decay time τ, but there is no reason to suppose that this is in fact so. The final expression for ϵ there obtained does not correspond to exponential relaxation of the dielectric, since it is not of the form (3), hence the relaxation of the internal field is unlikely to be even exponential in character. In the analysis below the relaxation rate of the internal field is at first arbitrary and is then chosen so as to obtain exponential relaxation of the dielectric.

(c) A New Expression for the Internal Field

In view of the success of the Onsager internal field in the static case it seems desirable to retain an expression of the form (9) in the time dependent analysis. *Assume* therefore that the internal field H is given by

$$H/E=\frac{3\epsilon_\infty}{2\epsilon_\infty+1}+\left(\frac{3\epsilon_0}{2\epsilon_0+1}-\frac{3\epsilon_\infty}{2\epsilon_\infty+1}\right)\cdot\frac{1}{1+i\omega T^*}, \quad (10)$$

where T^* is as yet unknown. It is easily shown by appropriate modification of Mandel's[19] or Onsager and Cole's[3,14] analysis that the internal field H leads to the following expression for ϵ,

$$\frac{\epsilon-\epsilon_\infty}{\epsilon_0-\epsilon_\infty}=\frac{2\epsilon_0+\epsilon_\infty}{3\epsilon_0}\cdot\frac{1+\dfrac{\epsilon_0-\epsilon_\infty}{2\epsilon_0+\epsilon_\infty}\cdot\dfrac{1}{1+i\omega T^*}}{1+i\omega\tau}. \quad (11)$$

Equation (11) only reduces to the form (3) if

$$T^*=T=[3\epsilon_0/(2\epsilon_0+\epsilon_\infty)]\tau \quad (12)$$

and then becomes

$$\frac{\epsilon-\epsilon_\infty}{\epsilon_0-\epsilon_\infty}=1\Big/\left[1+i\omega\tau\left(\frac{3\epsilon_0}{2\epsilon_0+\epsilon_\infty}\right)\right]. \quad (13)$$

Hence the internal field (10) with (12) gives for a process with a single relaxation time a dielectric behavior characterized by a single decay time. The various relations between T and τ are compared in Fig. 1. For this internal field the tendency of the polarization to maintain itself is much less than for the Debye expression and the maximum error incurred in assuming T and τ identical is $33\frac{1}{3}$ percent which is likely to be of little significance in relating τ to molecular processes. If the rate equation is used for the analysis of the variation of τ with temperature[20] the use of T rather than τ, neglecting possible variation of ϵ_0 and ϵ_∞ with temperature, leads to a deduced value of the entropy of activation too small by 0.8 cal/°C/mole at the most.

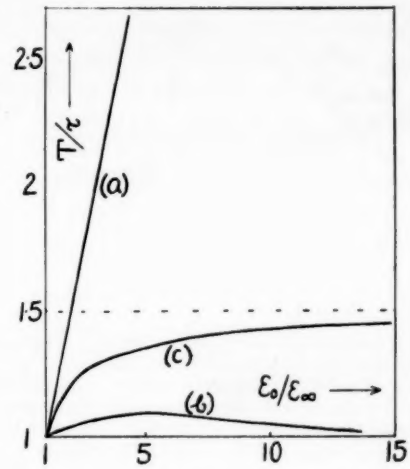

FIG. 1. Dependence of T/τ on the static dielectric constant assuming $\epsilon_\infty=2$, for various internal fields: (a) Lorentz-Debye, (b) Onsager-Cole, and (c) this paper.

There is at present no theoretical basis for asserting that a dielectric with single τ should indeed result in exponential decay of polarization, although this is an attractively simple result. The justification for the procedure given here must, therefore, rest largely on the experimental fact that, up to the present time, it has been possible to represent the behavior of all dielectrics by (3), as an important special case, or by its generalization to a spectrum of decay time.

DISTRIBUTION OF RELAXATION TIMES

(a) Two Relaxation Times

For a dielectric characterized by two decay times T_1 and T_2 we may write for the decay functions if the processes are independent

$$\alpha(t)=A_1\exp-t/T_1+A_2\exp-t/T_2. \quad (14)$$

The use of (2) then gives

$$\epsilon-\epsilon_\infty=A_1T_1/(1+i\omega T_1)+A_2T_2/(1+i\omega T_2). \quad (15)$$

For the case of two dispersion regions well separated in frequency, let ϵ_1 represent the intermediate dielectric constant. If the regions overlap, ϵ_1 is not observed but has the same significance. Equation (15) becomes

$$\epsilon-\epsilon_\infty=\frac{\epsilon_0-\epsilon_1}{1+i\omega T_1}+\frac{\epsilon_1-\epsilon_\infty}{1+i\omega T_2}, \quad (16)$$

which may be written

$$\epsilon-\epsilon_\infty=\epsilon_I+\epsilon_{II}. \quad (16)'$$

Equation (16) is certainly a reasonable generalization when T_1 and T_2 are very different, but there is some experimental evidence that, in some cases, it remains so

[19] M. Mandle, Bull. soc. chim. Belges **60**, 301 (1951); Physica **17**, 799 (1951).

[20] F. C. Frank, Trans. Faraday Soc. **32**, 1634 (1936); H. Eyring, J. Chem. Phys. **4**, 283 (1936); W. Kauzmann, Revs. Modern Phys. **14**, 12 (1942).

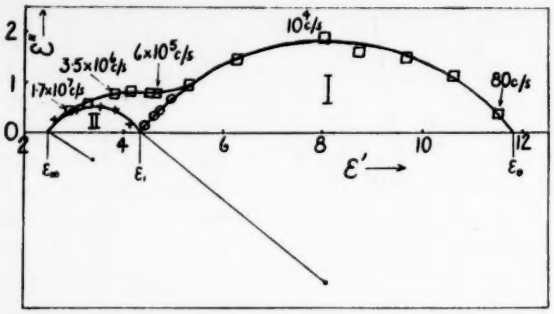

FIG. 2. An experimental curve for ϵ'' *versus* ϵ' which gives two dispersion regions with symmetrical distributions of decay times. Solid DBr at −193.7°C. □ Observed values; ○ calculated values for dispersion I alone, + calculated values for dispersion II alone. Critical frequency for dispersion I, $f_{cI}=10^4$ c/s. Critical frequency for dispersion II, $f_{cII}=5.5\times10^6$ c/s, $f_{cII}/f_{cI}=550$.

even when the regions overlap. It is convenient to consider again the plot of ϵ'' *versus* ϵ'.[18] Two well-separated regions of dispersion give for Eq. (16) two semicircular arcs on the plot, but if they overlap a more complex curve is obtained. HBr and DBr[21] have in the solid low temperature phase two dispersion regions which overlap appreciably at certain temperatures as shown in Fig. 2. It was proposed to separate the two regions[22,23] (in order to find T_1 and T_2) by empirically assuming a relation of the form (16) i.e., vector addition of ϵ_I and ϵ_{II} on the plot. The experimental curves could thus be accurately reproduced by suitable choice of T_1, T_2, and ϵ_1 and distributions about these most probable values of T. The two dispersion regions are shown in Fig. 2 as they would be if well separated in frequency and two normal arcs are obtained. More recent results on supercooled *n*-propanol¶ may be analyzed in the same way as shown in Fig. 3 which gives the high frequency end only of the Cole-Cole plot. The analysis separates the experimental curve into three relaxation regions each with a small distribution of decay times about the three most probable values. Equation (16) has, therefore, some experimental support.

It will be shown that of the three internal fields considered, only the new one gives for a dielectric with a line spectrum of relaxation times a macroscopic behavior defined by a line spectrum of decay times. Two relaxation times may be introduced by expressing the polarization in the form

$$P=[B_1/(1+i\omega\tau_1)+B_2/(1+i\omega\tau_2)]\times\text{internal field}. \quad (17)$$

The expression for ϵ as a function of frequency, derived by the use of (17) and the generalized Lorentz internal field (Eq. 4) or the Onsager field (Eq. 7) can in neither case be put in the form (16) when the two regions overlap. Neither corresponds therefore to the decay of polarization given by (14). If the internal field given by Eq. (10) for the case of two decay times T_1^* and T_2^* is used the following expression is obtained:

$$\epsilon-\epsilon_\infty=\frac{(\epsilon_0-\epsilon_1)(2\epsilon_0+\epsilon_1)}{3\epsilon_0}\cdot\frac{1+\dfrac{\epsilon_0-\epsilon_1}{2\epsilon_0+\epsilon_1}\cdot\dfrac{1}{1+i\omega T_1^*}}{1+i\omega\tau_1}$$
$$+\frac{(\epsilon_1-\epsilon_\infty)(2\epsilon_1+\epsilon_\infty)}{3\epsilon_1}\cdot\frac{1+\dfrac{\epsilon_1-\epsilon_\infty}{2\epsilon_1+\epsilon_\infty}\cdot\dfrac{1}{1+i\omega T_2^*}}{1+i\omega\tau_2}.$$

This can only be put in the form (16) if

$$T_1^*=T_1=\frac{3\epsilon_0}{2\epsilon_0+\epsilon_1}\tau_1 \quad\text{and}\quad T_2^*=T_2=\frac{3\epsilon_1}{2\epsilon_1+\epsilon_\infty}\tau_2 \quad (18)$$

in exact analogy with the single relaxation time case. This internal field is able, therefore, to give both the observed frequency dependence of ϵ in the cases quoted and the relation between T and τ. Again as in the treatment of Eq. (11) where the possibility of a single τ leading to a single T was discussed, there is no theoretical basis for supposing that Eq. (17) should imply Eq. (14). However there is some experimental support for such a supposition in the result of the analysis as shown in Figs. 2 and 3. It is unlikely that a satisfactory treatment of the spectrum of relaxation times in dielectric relaxation will emerge until the simplest case of exponential relaxation is better understood.

(b) Many Relaxation Times

The obvious generalization of (16), (17), and (18) to a number of relaxation times is

$$\epsilon-\epsilon_\infty=\sum_n\frac{\epsilon_n-\epsilon_{n+1}}{1+\dfrac{3\epsilon_n}{2\epsilon_n+\epsilon_{n+1}}\cdot i\omega\tau_{n+1}} \quad (19)$$

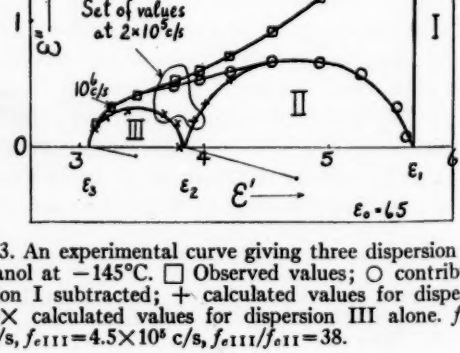

FIG. 3. An experimental curve giving three dispersion regions. *n*-Propanol at −145°C. □ Observed values; ○ contribution of dispersion I subtracted; + calculated values for dispersion II alone; ¶× calculated values for dispersion III alone. $f_{cII}=1.2\times10^4$ c/s, $f_{cIII}=4.5\times10^5$ c/s, $f_{cIII}/f_{cII}=38$.

[21] J. G. Powles, Compt. rend. **230**, 836 (1950); Nature **165**, 686 (1950).
[22] J. G. Powles, J. physique **13**, 121 (1952).
[23] R. Dalbert, thesis, Paris (1952).
¶ I am grateful to Professor R. H. Cole for allowing me to use his experimental results prior to publication.

and

$$T_{n+1}=\frac{3\epsilon_n}{2\epsilon_n+\epsilon_{n+1}}\cdot\tau_{n+1}.$$

The difference between T and τ is less the wider the distribution and, for a continuous distribution,

$$\epsilon-\epsilon_\infty=\int_0^\infty\frac{d(\epsilon)}{1+i\omega\tau}$$

in which $d(\epsilon)=KJ(\tau)d\tau$ determines the distribution of relaxation times $J(\tau)$. It may be shown that $T/\tau=1+x$ where x is a quantity derived from $J(\tau)$ which approaches zero for a broad continuous distribution of τ's and $[(\epsilon_0-\epsilon_\infty)/(2\epsilon_0+\epsilon_\infty)]$ for a single relaxation time, thus reproducing Eq. (12).

Asymmetric distributions of decay times have also been observed[24] which cannot be approximated by a line spectrum. It is possible that in such cases the different relaxation processes are less independent than is implied by use of Eqs. (14) and (17).

An expression similar to (19) is obtained, if it is assumed that the contributions of the groups of dipoles having different relaxation times superpose linearly.[9(b)] On the other hand, a different spectrum of relaxation times results from generalizing Eq. (8),[25] which illustrates the importance of the internal field for a relaxing dielectric. Not only the deduced value of τ but also its spectrum depend on the choice of the internal field.

[24] For example, R. H. Cole, J. Chem. Phys. **18**, 1417 (1950).
[25] R. M. Fuoss and J. G. Kirkwood, J. Am. Chem. Soc. **63**, 385 (1941).

THE JOURNAL OF CHEMICAL PHYSICS VOLUME 21, NUMBER 4 APRIL, 1953

Analysis of the Spectrum of the Nd^{+++} Ion in the Bromate Crystal*

ROBERT A. SATTEN†
Physics Department, University of California at Los Angeles, Los Angeles, California
(Received August 11, 1952)

The absorption spectrum of single crystals of $Nd(BrO_3)_3\cdot 9H_2O$ was photographed in the visible and near infrared and ultraviolet in σ and π polarizations. Empirical energy level diagrams are presented for some of the groups of lines, and in this way it is found that the $^4I_{9/2}$ ground state is split in the electric field into five levels at 0, 115, 184, 363, and 382 cm^{-1}. An analysis is made of the spectrum based on a Russell-Saunders coupling model and a knowledge of the expected splitting of the levels of the free Nd^{+++} ion in the electric field of the crystal. The electrostatic interaction energies of terms arising from f^3 electrons were computed by the Slater method and the results agree with those previously given by Racah. The Landé interval factors were also computed in order to predict the multiplet splitting. Trial values of the parameters were first found by extrapolation mainly from Pr^{+++}. Selection rules for transitions in an electric field of C_{3v} symmetry are presented, and the results applied to the neodymium bromate spectrum indicate that the transitions are not purely electric dipole, quadrupole, or magnetic dipole alone.

IT is generally agreed that the sharp line spectra of the triply ionized rare earths in crystals are due to transitions between states of the $4f^n$ configuration which is partially shielded by $5s^2$ and $5p^6$ electrons. It is also generally assumed that the mutual interaction of the electrons of a particular rare earth ion is greater than the interaction of these electrons with the field of the neighboring atoms and ions, which is taken to be predominantly electric. These assumptions lead to a spectrum having the general appearance of more or less widely separated groups of lines, each group corresponding to a transition between levels of the free ion, lines within a group resulting from the Stark-effect splitting of these free ion levels in the crystal field.

The simplest model likely to meet with some degree of success in accounting for the broader features of the visible, near infrared, and near ultraviolet spectrum is based on the assumption of Russell-Saunders coupling as a first approximation in the calculation of the energy levels of the free Nd^{+++} ion. Triply ionized neodymium has three electrons in the $4f$ shell. Applications of quantum-mechanical calculations to spectra involving two equivalent $4f$ electrons have been already made by Condon and Shortley (the $4f^2$ configuration of the La II spectrum), Lange (Pr^{+++}), and Spedding (Pr^{+++} spectrum analyzed in intermediate coupling approximation), which are referred to in more detail later. In this paper all terms are calculated for Russell-Saunders coupling and two are recalculated for intermediate coupling (the two terms with $J=1/2$). As far as the author knows there have been no previous attempts to apply the results of quantum mechanical calculations of *LSJ* energy levels to the identification and prediction of the spectra of rare earths having more than two equivalent f electrons (or more than two electrons missing

* This paper contains a part of the material to be found in a dissertation submitted in June, 1951, as part of the requirements for the degree Doctor of Philosophy at the University of California at Los Angeles.

† Present address: Physics Department, Massachusetts Institute of Technology, Cambridge, Massachusetts (on leave from University of California at Los Angeles).

TABLE I. Electrostatic interaction energies for terms of f^3 electrons.

$$
\begin{aligned}
&^4I = 3F_0 - 65F_2 - 141F_4 - 221F_6\\
&^4G = 3F_0 - 10F_2 - 75F_4 - 1222F_6\\
&^4F = 3F_0 - 30F_2 - 99F_4 - 858F_6\\
&^4D = 3F_0 + 25F_2 - 33F_4 - 1859F_6\\
&^4S = 3F_0 - 30F_2 - 99F_4 - 858F_6
\end{aligned}
$$

$$
\begin{aligned}
&^2L = 3F_2 - 63F_4 - 18F_6\\
&^2K = 3F_0 - 40F_2 + 1F_4 + 38F_6\\
&^2I = 3F_0 - 5F_2 - 6F_4 - 305F_6\\
&^2P = 3F_0 - 25F_2 - 44F_4 + 143F_6\\
&^2H = 3F_0 - 23F_2 - 46.5F_4 + 136F_6 \pm 1/2\Delta(^2H)\\
&^2G = 3F_0 + 7F_2 + 24.5F_4 - 620F_6 \pm 1/2\Delta(^2G)\\
&^2F = 3F_0 + 55F_2 + 55.5F_4 + 52F_6 \pm 1/2\Delta(^2F)\\
&^2D = 3F_0 - 7F_2 - 31.5F_4 - 130F_6 \pm 1/2\Delta(^2D)
\end{aligned}
$$

The Δ's are defined as follows:[a]

$$
\begin{aligned}
\Delta(^2H) &= 1/3[(128F_2 + 183F_4 - 2506F_6)^2 \\
&\quad + 29\,120(-F_2 + 3F_4 - 7F_6)^2]^{1/2},\\
\Delta(^2G) &= 1/31[(2306F_2 + 2903F_4 - 42\,784F_6)^2 \\
&\quad + 17\,160(20F_2 - 39F_4 + 14F_6)^2]^{1/2},\\
\Delta(^2F) &= [(-30F_2 + 153F_4 + 2184F_6)^2 + 352(5F_2 + 6F_4 - 91F_6)^2]^{1/2},\\
\Delta(^2D) &= 1/7[(-232F_2 + 2397F_4 - 11\,830F_6)^2 \\
&\quad + 2112(5F_2 + 6F_4 - 91F_6)^2]^{1/2}.
\end{aligned}
$$

[a] In general $\Delta = [(A-C)^2 + 4B^2]^{1/2}$ where A, B, C are matrix elements in the corresponding electrostatic interaction matrix of the form $\begin{pmatrix} A & B \\ B & C \end{pmatrix}$.

from a $4f$ shell which is more than half-filled). However, Mukherji[1] in 1937 made some quantum number assignments to transitions observed in neodymium salts by a misinterpretation of Hund's rule, applying the latter to deduce the relative order of *all* of the terms arising from f^3 electrons instead of using it for merely identifying the ground term.

The Russell-Saunders terms arising from f^3 electrons, first given by Gibbs, Wilber, and White,[2] are as follows: $^4(SDFGI)$ and $^2(P, 2D, 2F, 2G, 2H, I, K, L)$. Note that there are two each of the doublet terms D, F, G, and H. The energies of these terms arising from electrostatic interaction were first computed by Racah[3] using a method which he devised. We checked these results independently by the Slater[4] method and obtained complete agreement. The results in terms of the usual radial integrals F_k are given in Table I. In order to obtain the separate energies of the two ^2H, ^2G, ^2F, and ^2D terms the LSM_LM_S eigenfunctions were first found as linear combinations of products of single-electron eigenfunctions by the method of Gray and Wills.[5] The 2×2 matrices of electrostatic interaction in the LSM_LM_S basis could then be found for each of these four LS values and their respective second-degree secular equations solved for the required energies. These matrices are used to compute the eigenfunctions of the terms having the same LS value. The eigenfunctions in turn are used to obtain the contribution of spin-orbit interaction to the energy separations within a multiplet in the Russell-Saunders approximation.

As is well known, the calculation of spin-orbit interaction in Russell-Saunders coupling involves making the approximation of neglecting the off-diagonal elements of $H^1 = \sum \xi(r_i) L_i \cdot S_i$ in the $LSJM$ basis. The procedure for finding the Landé interval factors defined by

$$
\begin{aligned}
&(\gamma LSJM|H^1|\gamma LSJM)\\
&\quad = 1/2\zeta(\gamma LS)[J(J+L) - L(L+1) - S(S+1)] \quad (1)
\end{aligned}
$$

is given in Condon and Shortley.[6] The results obtained by using the diagonal sum method are given in Table II, whereas in Table III the ζ-factors for the individual LS values which occur twice are presented.

If $\psi(aLSM_LM_S)$ and $\psi(bLSM_LM_S)$ denote two orthogonal eigenfunctions having the same LSM_LM_S, the eigenfunctions which diagonalize the electrostatic interaction are linear combinations of these functions. The general expression for $\zeta(\gamma LS)$ in cases where a particular LS value occurs twice is given by

$$
\begin{aligned}
\zeta(\gamma LS) &= \zeta_{4f}/2M_LM_S\\
&\quad \times \left\{ u + w \mp \frac{(C-A)(u-w) - 4Bv}{[(A-C)^2 + 4B^2]^{1/2}} \right\}, \quad (2)
\end{aligned}
$$

where u, v, and w signify

$$
\begin{aligned}
u &= (aLSM_LM_S|H^1|aLSM_LM_S),\\
v &= (aLSM_LM_S|H^1|bLSM_LM_S),\\
w &= (bLSM_LM_S|H^1|bLSM_LM_S),
\end{aligned} \quad (3)
$$

and A, B, and C are the corresponding elements in electrostatic interaction matrices which are of the form

$$
\begin{pmatrix} A & B \\ B & C \end{pmatrix}. \quad (4)
$$

Although $\zeta(\gamma LS)$ is calculated for certain M_LM_S, it is independent of M_L and M_S. The minus sign in Eq. (2) holds when the plus sign is used in the energies of Table I. ζ_{4f} is the Landé interval factor for a single $4f$ electron. Since the exact potential in which such an electron finds itself is unknown, ζ_{4f} is regarded as a

TABLE II. Landé interval factors for terms of f^3 electrons.

From diagonal sum rule:

Quartet states: $\zeta = 1/3\zeta_{4f}$

$\zeta(^2L) = 1/4\zeta_{4f}$ $\quad$ $\zeta(^2K) = 9/28\zeta_{4f}$

$\zeta(^2I) = 2/21\zeta_{4f}$ $\quad$ $\zeta(^2P) = 0$

Average $\zeta(^2H) = 3/10\zeta_{4f}$

$\zeta(^2G) = 1/30\zeta_{4f}$

$\zeta(^2F) = 1/6\zeta_{4f}$

$\zeta(^2D) = 1/2\zeta_{4f}$

[1] P. C. Mukherji, Indian J. Phys. **11**, 123 (1937).
[2] Gibbs, Wilber, and White, Phys. Rev. **29**, 790 (1927).
[3] G. Racah, Phys. Rev. **62**, 438 (1942).
[4] E. U. Condon and G. H. Shortley, *The Theory of Atomic Spectra* (Cambridge University Press, Cambridge, 1935), p. 158.
[5] Reference 4, p. 226.
[6] Reference 4, pp. 193, 233.

parameter to be adjusted to the data, as are also the F_k's.

The energy in the Russell-Saunders approximation of a particular LSJ state of the free ion above the $^4I_{9/2}$ ground state can now be expressed as a function of four parameters: F_2, F_4, F_6, and ζ_{4f}. The center of gravity of an LS multiplet is given by the expressions in Table I and the separations within a multiplet are easily constructed by using the Landé interval rule. Also useful is the expression $S(L+1)\zeta(\gamma LS)$ for the energy separation of the center of gravity of a term above its lowest J value (for regular multiplets), and the expression $S(2L+1)\zeta(\gamma LS)$ for the total multiplet splitting.

Now, in order to correctly evaluate the four parameters, one must first be able to pick out groups of spectral absorption lines and correctly identify them, i.e., assign LSJ quantum numbers to the upper levels of the transition observed. The problem is to break through the vicious circle of needing to know the parameters in order to predict the location of the terms and of needing to know the location of the terms to compute the parameters. In fact it is just this situation which is the most important feature of the disagreement between Spedding's[7] and Lange's[8] interpretation of the Pr^{+++} spectrum, i.e., they identified certain groups of spectral lines differently. This is really independent of the fact that Spedding worked in intermediate coupling and Lange with Russell-Saunders coupling.

It will be seen that a way out of the difficulty is to bring together the above theoretical expressions involving the four parameters, experimental data, and results from other rare earths which can be related to this work. The basic idea is to extrapolate from other rare earths (chiefly Pr^{+++}) to get a first trial approximation to various desired quantities which enables some identifications to be made in the spectrum, and then to modify this approximation, if necessary after these identifications are made.

It must be pointed out that merely getting a good fit to the data at this stage of our knowledge without regard to much of what is already known about other rare earths and without sufficient assurance of the assignment of the quantum numbers is easy to do in more than one way and will not yield a result in which one can have much confidence.

EXPERIMENTAL DETAILS

The spectrum of $Nd(BrO_3)_3 \cdot 9H_2O$ was photographed[9] from 3500 to 11 000A using a Bausch and Lomb large Littrow spectrograph with interchangeable glass and quartz prisms. The glass prism was used primarily for the 6000 to 11 000A region with an average dispersion of about 65 cm^{-1}/mm. Photographs of the spectrum were taken on Eastman N and sensitized Z plates in the red and near infrared. The quartz prism was used in the region 6000 to 3500A with an average dispersion of about 45 cm^{-1}/mm. The spectra were photographed on Eastman 103-F3 and 33 plates in this region. From about 0.8 to 2.5μ the spectrum was recorded on a self-recording quartz spectrograph designed by Ellis.[10] The average dispersion was about 0.007μ/mm. When using the Bausch and Lomb spectrograph, the light source was an 18-amp, 6-volt ribbon filament microscope illuminator type bulb. The light from the source was focused on the crystal (optic axis perpendicular to light beam) by a 10-cm focal length quartz lens, and a similar lens on the other side focused the light that had come through the crystal onto a horizontal adjustable slit. Next came a Wollaston prism followed by a third lens which focused the final image on the slit of the spectrograph. The Wollaston resulted in the existence of two adjacent images of the horizontal slit, one polarized with electric vector parallel to the crystal optic axis, and the other polarized perpendicular to it. In this way both π- and σ-spectra were photographed simultaneously.

The spectrum was photographed at room and liquid nitrogen temperature, the cooling accomplished by surrounding the crystal with a cylindrical jacket containing liquid nitrogen. An iron arc was used as a comparison spectrum in the visible, whereas for the 8600A group, a sodium lab arc having mostly argon lines in this region was used. Wavelengths were assigned by linear interpolation between lines of the iron arc and measured visually on the viewing screen of an Applied Research comparitor-densitometer. Hartmann interpolation was used with the sodium and argon standards. The lines of the iron arc were identified with the aid of a very helpful set of photographs prepared at the Astrophysical Laboratory of the Vatican Observatory.[11] Table IV shows the results of the wavelength measurements, all of which unless otherwise stated were measured at liquid nitrogen temperature in order to take advantage of the increased sharpness at the low temperature.

TABLE III. Landé interval factors for terms of f^2 electrons whose L values occur twice.[a]

$$\zeta(^3H) = 3/10\zeta_{4f}\left[1 \mp \frac{1/3(128F_2+183F_4-2506F_6)}{\Delta(^3H)}\right]$$

$$\zeta(^3G) = 1/30\zeta_{4f}\left[1 \mp \frac{1066F_2-377F_4-9464F_6}{\Delta(^3G)}\right]$$

$$\zeta(^3F) = 1/6\zeta_{4f}\left[1 \mp \frac{(530F_2+69F_4-14\,560F_6)}{\Delta(^3F)}\right]$$

$$\zeta(^3D) = 1/2\zeta_{4f}\left[1 \mp \frac{1/3(-232F_2+2397F_4-11\,830F_6)}{\Delta(^3D)}\right]$$

[a] The Δ's are defined in Table I.

[7] F. Spedding, Phys. Rev. **58**, 255 (1940).
[8] H. Lange, Ann. Physik **31**, 609 (1938).
[9] The neodymium bromate was prepared from the oxide purchased as 99.9 percent pure (lot No. 222) from Research Chemical Company, Burbank, California.
[10] J. W. Ellis, J. Opt. Soc. Am. and Rev. Sci. Instr. **11**, 647 (1925).
[11] A. Gatterer and J. Junkes, *Arc Spectrum of Iron from 8388A to 2242A* (1947), second edition.

TERM ASSIGNMENTS AND PARAMETER VALUES

It can be seen from Table I that the following relations among the terms of maximum multiplicity hold regardless of the values assigned to the F_k integrals:

$$\begin{aligned} {}^4S &= {}^4F, \\ {}^4G - {}^4I &= 11/7({}^4F - {}^4I), \\ {}^4D - {}^4I &= 18/7({}^4F - {}^4I). \end{aligned} \tag{5}$$

Furthermore, if it is assumed that the F_k integrals vary approximately proportional to the effective nuclear charge $(Z-\sigma)$, where σ is the screening constant with a value in the vicinity of $\sigma=34$ and Z is the atomic number, then it is easy to show that simple relations exist among the terms of maximum multiplicity from one rare earth to another. For example, comparing ${}^3F-{}^3H$ for Pr^{+++} with ${}^4F-{}^4H$ for Nd^{+++} we obtain

$$({}^4F - {}^4I)_{Nd} = 7/3\, k({}^3F - {}^3H)_{Pr}, \tag{6}$$

TABLE IV. Absorption lines for $Nd(BrO_3)_3 \cdot 9H_2O$. Wavelengths and wave numbers are values in air. The error varies and may be of the order of 10 cm^{-1} for some broad, dim, or poorly resolved lines and is less than 1 cm^{-1} for some of the sharpest lines. Lines marked *T* are noticeably brighter at room temperature than at liquid nitrogen temperature. All lines are measured at liquid nitrogen temperature unless followed by the letter *R*. Intensities increase from 0–10. Comparisons are probably not valid from one spectral region to another. *vs* = very sharp; *B* = broad; *R* = measured at room temperature; *r* = barely resolved; *p* = resolved in polarized spectrum only; (2), (3) = probably double, triple, respectively.

λ A		ν cm⁻¹	Intensity σ	Intensity π
8937.1	*T*	11 189	1	3
8917.3	*T*	11 214	1	3
8901.6	*T*	11 234	0	1
8781.0		11 388	3	0
8762.3		11 413	3	1
8729.5		11 455	6	2
8710.6		11 480	5	3
8642.5		11 571	8	9
8622.6		11 597	9	8
8184	*T*	12 219	0	1
8175	*T*	12 232	1	0
8163	*T*	12 250	0	1
8067.0	*B*	12 396	0	3
8042.7		12 434	0	7
8032.3		12 450	3	0
8007		12 489	3	5
7998.5		12 502	9	0
7993.1		12 511	1	9
7935.4 }	*r* (3)	12 602	10	10
7923 }		12 621	10	10
7838.0		12 758	7	3
7805.5		12 811	5	1
7790.5		12 836	2	1
7595	*T*	13 167	1	0
7583	*T*	13 187	1	0
7546	*T B*	13 252	1	0
7524	*T*?	13 291	1	3
7508.7		13 318	5	7
7469.6		13 388	1	5
7444.7	*B*	13 432	10	0
7408	*B*	13 499	7	10
7380.7		13 549	7*vs*	10
7350.7 }	*r*	13 604	10	0
7343 }		13 618	10	0
7312.8 }	*r*	13 675	10	1
7308.9 }		13 682	10	1
6912.2	*T*	14 467	0	1
6906.2	*T B*	14 480	1	0
6899.5	*T*	14 494	0	1
6889.6	*T*	14 515	0	1
6827		14 648	0	5
6819.5		14 664	5	5
6796.3		14 714	7	0
6787.7		14 733	3	7
6765.5		14 781	1	5
6743.3		14 829	3	2
6735		14 849	3	1
6730.9		14 857	5	5
6713.0		14 897	5	1
6382	*T B*	15 669		
6374	*T*	15 688		
6325.9	*T*	15 808	1	3
6298.6	*B*	15 877	1	2
6276.9	*B*	15 931	3	0
6265.1	*B*	15 961	3	0
6252.8		15 993	0	5
6233.4		16 043	5	1
6229.8		16 052	5	1
6219.8		16 078	1	5
5920	*T*?	16 892		
5899.7	*T*	16 950	1	1
5883	*T B*	16 998	0	1
5872	*T B*	17 030	1	1
5851.8	*T*	17 089	1	3
5828.6		17 157	5	1
5815.7		17 195	5	5
5792	*B*	17 265	0	10
5776.3 }	*p*	17 312	5*vs*	10
5769.2 }		17 333	5*vs*	0
5754.1		17 379	10	7
5740.1		17 421	10	5
5724.5		17 469	7	10
5680	*B*	17 606	1	5
5647	*B*	17 709	1	1
5330.8	*T*	18 759		
5322.7	*T*	18 787		
5308.8	*T*	18 837		
5303	*T*	18 857		
5274.7		18 958	3	5
5255.2		19 029	3	0
5247.8		19 056	0	5
5232.7 }	*B r*	19 111	5	0
5230.5 }		19 119	5	5
5224.3	*vs*	19 141	5	0
5216.9	*vs*	19 169	10	5
5206.9 }	*r*	19 205	9	0?
5204.6 }		19 214	0	10
5202.0 }		19 223	0	10
5135.0 }	*r p*	19 474	?	5
5133.1 }		19 481	5	?
5129.3 }		19 496	3	3
5115.5		19 548	5	0
5109.3		19 572	5	0
5103.2		19 595	3	0
5097.8		19 616	3	0
5086.5		19 660	7	3
5069.5		19 726	0	3
5060.9		19 759	0	3
5053.1	*B*	19 790	5	0

TABLE IV.—*Continued.*

λ A		ν cm^{-1}	Intensity σ	Intensity π
4806.1	*T R*	20 807		
4765.0		20 986	5	5
4758.8		21 014	1	1
4751.3	*r*	21 047	7	7
4748.3		21 060	7	7
4743.6		21 081	5	0
4724.7		21 165	5	0
4722.7		21 174	7	1
4717.9	*vs*	21 196	5	1
4715.0		21 209	1	0
4690.7	(2)	21 319	7	7
4664.8		21 437		
4658		21 468		
4651.7		21 498		
4639.7		21 553	5	1
4633.4		21 582	5	3
4621	*B*	21 640		
4612.7		21 679	6	7
4603.5	*B*	21 723	6	7
4596.7	*B*	21 755	6	7
4344.3	*T*	23 019	0+	0+
4340.9	*T*	23 037	1	0+
4294.7		23 285	1	0
4273.7		23 398.9	7*vs*	9*vs*
4273.0*	*R*	23 402.8		
4217	*B*	23 714		
4200	*B*	23 807		
4188	*B*	23 877		
4179.3		23 927	5	3
4174.8		23 953	5	4
3812.7	*B*	26 228	0	3
3803.7	*vs*	26 290	5	5
3796.1		26 343	3	0
3583.6	*T*	27 905		
3561.7	*B*	28 077	3	0
3553.4		28 142	0	7
3552.4		28 150	5	0
3538.9		28 257	9	10
3537.6		28 268	9	10

*Same line as the one above but at room temperature.

where k equals approximately $(60-34)/(59-34)=1.04$.

On the other hand, the Landé interval factor ζ_{4f} should vary approximately according to $(Z-\sigma)^4$. Thus, a comparison of the ζ_{4f} for Nd^{+++} and Pr^{+++} yields

$$(\zeta_{4f})_{Nd}=k^4(\zeta_{4f})_{Pr}, \tag{7}$$

where k^4 equals approximately $(1.04)^4=1.17$. Comparing Nd^{+++} and Sm^{+++}, we obtain

$$(\zeta_{4f})_{Nd}=K^4(\zeta_{4f})_{Sm}, \tag{8}$$

where $K^4=0.73$ approximately.

Although Spedding and Lange identify many of the groups of lines of the Pr^{+++} spectrum differently, they do agree fairly well on the assignment of $^3F-{}^3H$. The two values are, respectively,

$$^3F-{}^3H=4120\ \text{cm}^{-1},\ \text{(Spedding)}; \tag{9}$$

and

$$^3F-{}^3H=4351\ \text{cm}^{-1},\ \text{(Lange)}. \tag{10}$$

Spedding's values for the Russell-Saunders term separations are a multiple of the values determined for the corresponding states of the $4f^2$ configuration of the La II spectrum, which was analyzed by Condon and Shortley from the term assignments made by Russell and Meggers from their data. In addition Spedding found that for the triplet terms of Pr^{+++} a value of $\zeta=400$ cm^{-1} was a good approximation, which implies a value of $\zeta_{4f}=800$ cm^{-1} for Pr^{+++}.

We thus obtain the trial values for neodymium: $^4F-{}^4I=10\times10^3$ cm^{-1}, and $\zeta_{4f}=936$ cm^{-1}. Thus, ζ (quartet terms) $=312$ cm^{-1}. The approximate position of all of the quartet terms can now be found and some identifications of groups of spectral lines made, which in turn can lead to a better value of ζ_{4f}, etc.

In order to make a more positive identification of the quartet levels, something must be known about the position of the doublet levels so that the danger of misidentification is minimized. One might again extrapolate from praseodymium and use a multiple of the F_k integrals together with the energy expressions in Table I. However, this is a very unsatisfactory procedure, for already two different sets of F_k's have been offered (i.e., Spedding's and Lange's). One can at least show that Lange's F_k values must be poor approximations.

The F_k integrals are defined as $F_2=F^2/225$, $F_4=F^4/1089$, and $F_6=F^6/7361.64$, where the F^k integrals can be easily seen from their definition[12] to be a decreasing function of the superscript k. Therefore, the F_k satisfy

$$\begin{aligned} F_4/F_2&<225/1089=0.206;\\ F_6/F_2&<225/7361.64=0.00306. \end{aligned} \tag{11}$$

Lange's F_k values must be rejected since they lead to the ratios $F_4/F_2=0.606$, which is three times too large, and $F_6/F_2=0.00446$, also too large.

Even the Condon and Shortley F_k ratios for La II used by Spedding are not too satisfactory, although this may be a consequence of the failure of Russell-Saunders coupling. The Condon and Shortley ratios are $F_4/F_2=0.231$, which is slightly too large, and $F_6/F_2=0.00281$, which is permitted.

Figure 1 is a plot of the height of Russell-Saunders term energies above the ^4I ground state *vs* the ratio F_4/F_2 with $F_6=0$. Only the region below 26×10^3 cm^{-1} is included. The plot has been extended to $F_4/F_2=0.6$, so that a comparison with the term order predicted by Lange's assignment can be made. Since F_6 is small, the effect of taking $F_6=0$ is not great enough to spoil the usefulness of the curves. The energies above the ^4I state

[12] Reference 4, p. 177.

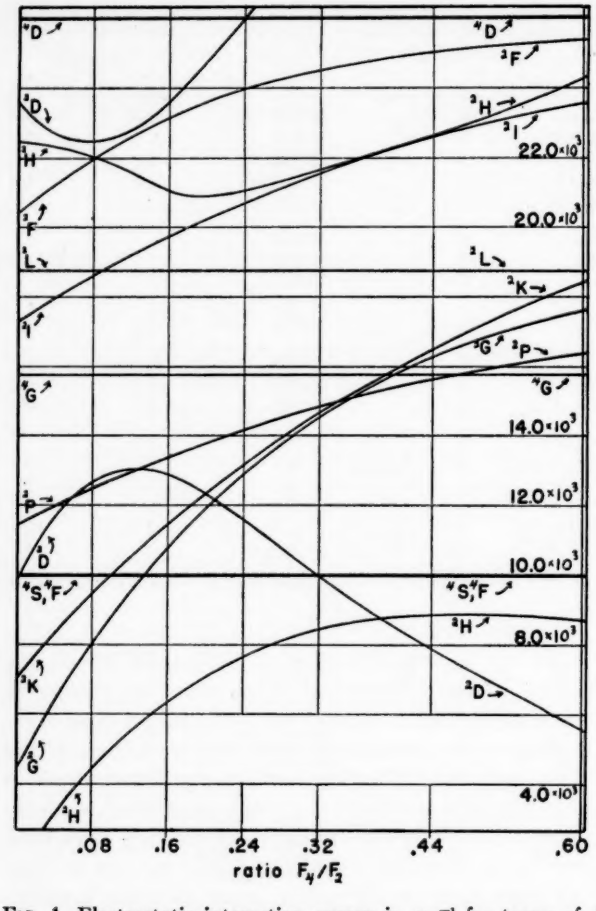

FIG. 1. Electrostatic interaction energy in cm^{-1} for terms of f^3 electrons *vs* ratio F_4/F_2 with $F_6=0$.

plotted in Fig. 1 were first calculated for a given F_4/F_2 ratio and then each multiplied by that constant which makes the $^4F-^4I$ energy equal to 10.02×10^3 cm^{-1}. This is the value which was finally decided upon as the best to use in the light of the advisory value previously discussed and some experimental results to be discussed below.

Between about 9000A and 1.6μ we find no evidence of electronic transitions in the neodymium bromate using crystals of a maximum thickness of about 4 mm. Furthermore, the entire group of lines in the vicinity of 8600A can be accounted for (see Fig. 2) within experimental error as transitions from a ground state which has been split into five levels at 0, 115, 184, 363, and 382 cm^{-1} to an upper state which is split into two levels by the crystal field. The Kramers degeneracy limits the splitting of a J level of the free ion in an electric field to a maximum of $J+1/2$ levels for an odd number of electrons, and a group theoretical analysis[13] shows that barring accidental degeneracy this maximum splitting will occur for the symmetry group at hand (C_{3v}).[14] Thus, five levels for the ground state splitting is consistent with a $^4I_{9/2}$ ground state. The two upper levels of Fig. 2 indicate the 8600A group of absorption lines is to be associated with transitions to a $J=3/2$ level. The only terms having $J=3/2$ are ^4F, ^4D, ^4S, ^2D, and ^2P. We believe that this group of lines should be identified as a transition to $^4F_{3/2}$ for the following reasons: When the energy separation $^4F_{3/2}-^4I_{9/2}$ is computed using the trial values of $^4F-^4I$ and of ζ_{4f}, one gets a good agreement with the observed separation. Furthermore, the next three major groups of lines towards decreasing wavelength are also consistent with transitions to $^4F_{5/2,\,7/2,\,9/2}$, respectively. As far as can be determined by observations at liquid nitrogen temperature, their term diagrams are compatible with the necessary $J+1/2$ levels and the energies are fairly close to the predicted positions. Actually the fit is better using a smaller ζ, and, therefore, the trial ζ for terms of maximum multiplicity is changed to $\zeta=300$ cm^{-1} implying $\zeta_{4f}=900$ cm^{-1}. With this value of ζ_{4f}, the total split of the ^4F multiplet is predicted quite accurately (see Table V) although the interval rule is not followed too well, which

TABLE V. Predicted energy levels of Nd^{+++} with some identified levels in comparison.

Term	Calculated[a] λ	Calculated[a] ν	Observed center ν	Observed center λ	Alternative identification
$^4I_{9/2}$		0			
$^4I_{11/2}$	5.38μ	1.86×10^3 cm^{-1}			
$^4I_{13/2}$	2.63	3.81			
$^4I_{15/2}$	1.65	6.06	5.880×10^3 cm^{-1}	1.705μ	
$^2H_{9/2}$	9800A	10.21			
$^4F_{3/2}$	8630	11.58	11.58	8630A	
$^4F_{5/2}$	8100	12.32	12.62	7920	
$^2H_{11/2}$	7630	13.09			
$^4F_{7/2}$	7480	13.37	13.59	7360	
$^4S_{3/2}$	7480	13.37			
$^2D_{3/2}$	6970	14.33			
$^4F_{9/2}$	6780	14.72	14.77	6770	
$^2K_{13/2}$	6300	15.87			
$^2G_{7/2}$	6270	15.94			
$^4G_{5/2}$	5920	16.85	16.00	6250	$^2G_{7/2}$
$^2G_{9/2}$	5730	17.11			
$^2D_{5/2}$	5770	17.32			
$^4G_{7/2}$	5580	17.90	17.39	5750	
$^2P_{1/2}$[b]	5560	17.95			
$^2K_{15/2}$	5540	18.03			
$^2P_{1/2}$	5500	18.16			
$^2P_{3/2}$	5500	18.16			
$^4G_{9/2}$	5190	19.25	19.18	5220	
$^4G_{11/2}$	4780	20.90	21.24	4710	
			21.65	4620	
$^2L_{15/2}$	4570	21.86			
$^2L_{17/2}$	4200	23.77			
$^2I_{11/2}$	4110	24.29			
$^2I_{13/2}$	4020	24.85			
$^2H_{9/2}$	3970	25.16			
$^2H_{11/2}$	3960	25.23			
$^2D_{5/2}$	3850	25.96			
$^2F_{5/2}$	3800	26.31			
$^2D_{3/2}$	3740	26.70	26.31	3800	
$^2F_{7/2}$	3630	27.48			
$^4D_{1/2}$	3600	27.77			
$^4D_{1/2}$[b]	3570	27.98	28.26	3540	$^4D_{3/2}$
$^4D_{3/2}$	3540	28.22			
$^4D_{5/2}$	3450	28.97			
$^4D_{7/2}$	3330	30.02			
$^2G_{9/2}$	2700	37.00			
$^2G_{7/2}$	2615	38.24			
$^2F_{7/2}$	1763	57.33			
$^2F_{5/2}$	1755	57.47			

[a] Calculations for the doublet states assume Condon and Shortley F_4 ratios and are therefore regarded as more uncertain than the quartet states. All calculated levels are increased by 210 cm^{-1} which is approximately the amount by which the lowest of the electrically split ground levels lies beneath the center of gravity of all five levels.

[b] Intermediate coupling values. Note these values differ from the corresponding Russell-Saunders coupling values by about 200 cm^{-1}.

[13] W. Opechowski, Physica **7**, 552 (1940).

[14] L. Helmholtz, J. Am. Chem. Soc. **61**, 1544 (1939).

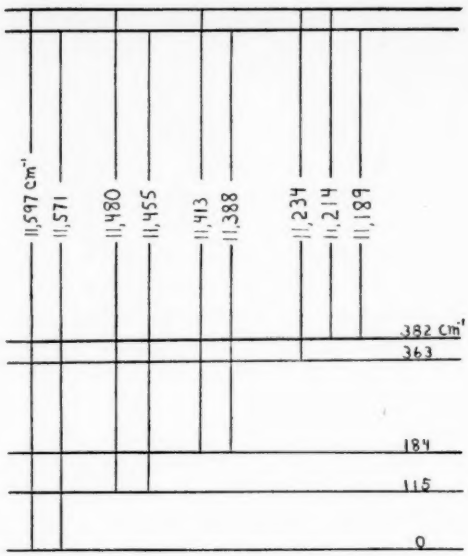

FIG. 2. Term diagram and observed transitions in the vicinity of 8600A for neodymium bromate crystals.

suggests the need to employ intermediate coupling calculations.

The other possible assignments for the 8600A group are rejected for the following reasons: No other explanation accounts so well for the pattern of the next four intense groups of lines which follow to shorter wavelength. Thus, $^4S_{3/2}$ is single, not a part of the pattern, and furthermore, is probably not as intense, involving as it does a much greater change in L. $^2P_{3/2}$ and one of the $^2D_{3/2}$ levels can be ruled out as definitely

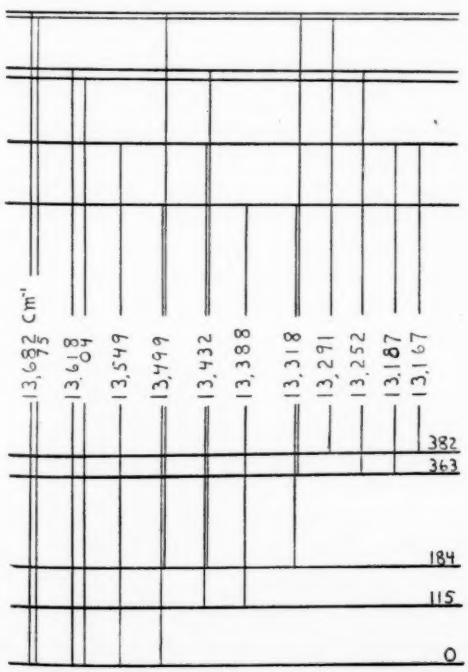

FIG. 3. Term diagram and observed transitions in the vicinity of 7400A.

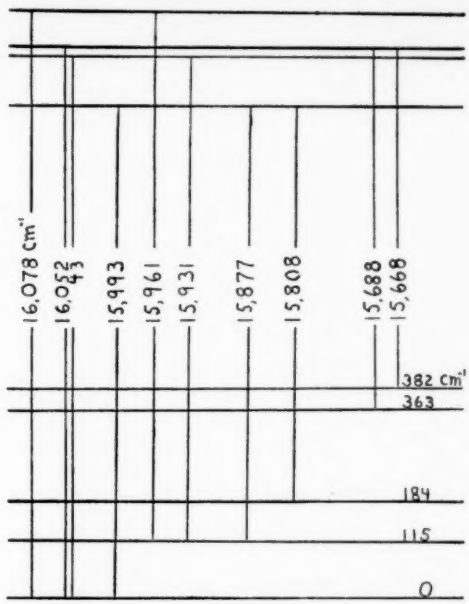

FIG. 4. Term diagram and observed transitions in the vicinity of 6200A.

out of range and the lower $^2D_{3/2}$ when calculated using Condon and Shortley La II F_k ratios is not very close to the observed group of lines. Even if the Condon and Shortley ratios are not used, the predicted values of the lower $^2D_{3/2}$ are still far from the observed position of the 8600A group as long as one uses ratios $0.04<F_4/F_2<0.24$. Furthermore, $^4F_{3/2}$ would ordinarily be more intense than $^2D_{3/2}$, involving as it does $\Delta S=0$ and a smaller ΔL. However, arguments concerning intensities of transitions in the relatively strong electric fields which obtain here are a bit shaky, and a study of the intensities in the Stark effect applicable to the rare

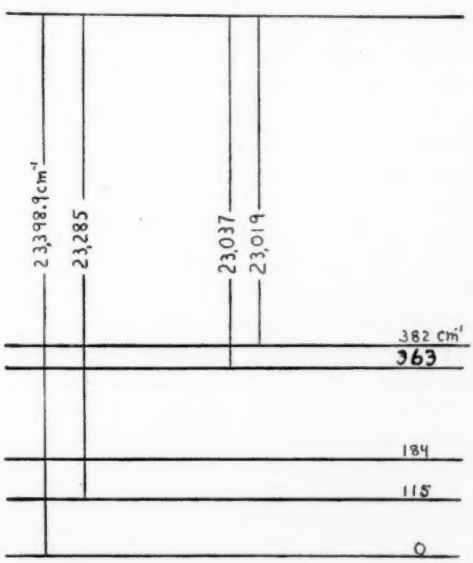

FIG. 5. Term diagram and observed transitions in the vicinity of 4300A.

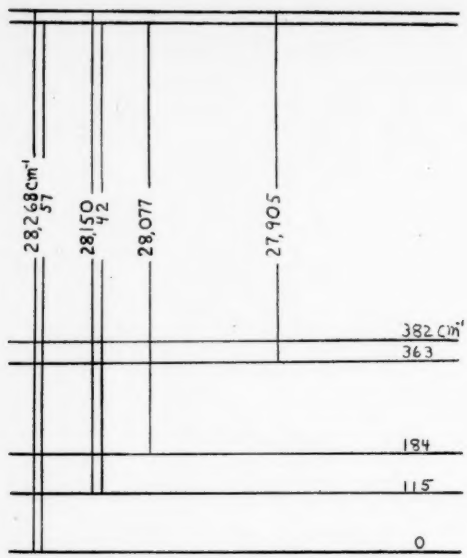

FIG. 6. Term diagram and observed transitions in the vicinity of 3500A.

earth crystals would be very helpful in identifying the spectral transitions.

Figures 2–6 are empirical energy level diagrams which have been constructed for some of the principal groups of lines in the region between 8900 and 3500A by searching for constant wave number differences and temperature dependent lines. Table VI shows the evidence for the splitting of the $^4I_{9/2}$ ground state into five levels. There remain ambiguities in some of the empirical term diagrams, as well as in the J level to be assigned, hence only five of the best groups are shown. Actually 13 energy level diagrams were drawn for 13 different groups, but all are not included pending further verification from a study at lower temperatures and of other compounds. Some of the ambiguities in the term diagrams can be removed by observation at liquid helium temperatures. The uncertainty of the J value assignment is often a result of the appearance of "extra levels" which may have more than one origin. Van Vleck[15] has pointed out that if there are any electric dipole transitions with distortion of the crystal field caused by vibration, then a selection rule on the vibrational quantum number $\Delta v = \pm 1$ holds for the most probable transitions. Then too it has been suggested that the neodymium ions are situated in two slightly different environments in the crystal. Whatever the cause or causes, it has been reported several times[16] that for liquid nitrogen temperatures and lower, the energy levels observed in rare earth crystal spectra seem to appear double.

It is interesting that of the transitions originating from excited levels of the $^4I_{9/2}$ state only those which come from 382 and 363 cm^{-1} levels appear noticeably brighter at room temperature than at liquid nitrogen temperature. This is characteristic of all spectral groups which have such transitions. Evidently, the sharpening of the lines at liquid nitrogen temperature compensates enough for the reduced population of the lower levels, so that they do not show this intensity change. Observations at liquid helium temperature should help to verify this conclusion.

In the following comments upon some of the individual groups of absorption lines and their empirical term diagrams, some of the difficulties and ambiguities in the interpretation will be mentioned. For a tabulation of all of the transitions tentatively identified along with the predicted positions of the remaining groups, see Table V.

1.7μ Group: The evidence that this is an electronic transition and not a vibration of H_2O is deduced from the fact that this group does not appear in the isomorphic crystals of samarium bromate or gadolinium bromate as do other water bands. In addition, a solution of neodymium bromate in D_2O showed the same group present (an H_2O solution is opaque in this region). The assignment of the value $\zeta_{4f} = 900$ cm^{-1} results in the identification of this group as the transition $^4I_{15/2} - {}^4I_{9/2}$, although the interval rule requires a slightly smaller value of ζ.

Our results are not in agreement with certain results reported by Gobrecht for the ground multiplet splitting.[17] In his article which surveys the multiplet splitting for the lowest lying multiplets of the various rare earths, he reports an absorption at 5200 cm^{-1} for Nd^{+++} in borax beads. Gobrecht assigns this to $^4I_{13/2} - {}^4I_{9/2}$, although he says the transition to $^4I_{15/2}$ predicted at 1.25μ on this basis was looked for in vain with a 4-cm path of concentrated neodymium nitrate solution. On the other hand, we found no absorption at 5200 cm^{-1} in the pure bromate crystal. Furthermore, such a transition if identified as to $^4I_{13/2}$ would imply $\zeta_{4f} = 1300$ cm^{-1}, which we believe to be much too large.

In the same paper Gobrecht also gives the results of his earlier work on the fluorescence of Sm^{+++} in which it is reported that the total multiplet separation $^6H_{15/2} - {}^6H_{5/2} = 6600$ cm^{-1}. This implies $\zeta_{4f} = 1200$ cm^{-1} for Sm^{+++} and is indeed in very good agreement with the value 1260 cm^{-1} obtained by extrapolation from Pr^{+++}. It also lends support to the value $\zeta_{4f} = 900$ cm^{-1} for Nd^{+++} rather than 1300 cm^{-1}, since by Eq. (8) extrapolation from samarium to neodymium implies $\zeta_{4f} = 876$ cm^{-1} for Nd^{+++}.

The only other explanation for this 1.7μ group, barring very large perturbations, would be a transition to $^2H_{9/2}$ if the F_4/F_2 ratio were considerably smaller than 0.24.

8600A Group: Discussed above.

7400A Group: We find here one of the clear cases of the appearance of "extra" levels. The two lines, 7312.8

[15] J. H. Van Vleck, J. Phys. Chem. **41**, 64 (1937).
[16] For example, see A. Hellwege and K. Hellwege, Z. Physik **127**, 334 (1950).
[17] H. Gobrecht, Ann. Physik **31**, 755 (1938).

TABLE VI. Evidence for the splitting of the $^4I_{9/2}$ ground state into five levels by the crystal field.

Level at 115 cm^{-1} above the ground state in the crystal		
11 597 cm^{-1}	−11 480 cm^{-1}	=117 cm^{-1}
11 571	−11 455	=116
12 621	−12 502	=119
12 602	−12 489	=113
13 549	−13 432	=117
13 499	−13 388	=111
14 897	−14 781	=116
14 849	−14 733	=116
14 829	−14 714	=115
14 781	−14 664	=117
16 078	−15 961	=117
16 043	−15 931	=112
15 993	−15 877	=116
17 379	−17 265	=114
17 312	−17 195	=117
19 223	−19 119	=114
19 169	−19 056	=113
19 141	−19 029	=112
19 660	−19 548	=112
19 595	−19 481	=114
21 196	−21 081	=115
21 174	−21 060	=114
21 165	−21 047	=118
21 755	−21 640	=115
21 582	−21 468	=114
21 553	−21 437	=116
23 399	−23 285	=114
26 343	−26 228	=115
28 268	−28 150	=118
28 257	−28 142	=115
Level at 184 cm^{-1}		
11 597 cm^{-1}	−11 413 cm^{-1}	=184 cm^{-1}
11 571	−11 388	=183
12 621	−12 434	=187
13 682	−13 499	=183
13 618	−13 432	=186
13 499	−13 318	=181
14 897	−14 714	=183
14 849	−14 664	=185
14 829	−14 648	=181
15 993	−15 808	=185
17 379	−17 195	=184
19 214	−19 029	=185
19 141	−18 958	=183
19 660	−19 474	=186
21 196	−21 014	=182
21 174	−20 986	=188
21 679	−21 498	=181
28 257	−28 077	=180
Level at 363 cm^{-1}		
11 597 cm^{-1}	−11 234 cm^{-1}	=363 cm^{-1}
12 758	−12 396	=362
13 682	−13 318	=364
13 618	−13 252	=366
13 549	−13 187	=362
14 857	−14 494	=363
14 829	−14 467	=362
16 052	−15 688	=364
17 312	−16 950	=362
19 223	−18 857	=366
21 174	−20 807[a]	=367
23 399	−23 037	=362
28 268	−27 905	=363
Level at 382 cm^{-1}		
11 597 cm^{-1}	−11 214 cm^{-1}	=383 cm^{-1}
11 571	−11 189	=382
12 621	−12 232	=389
12 602	−12 219	=383
13 675	−13 291	=384
13 549	−13 167	=382
14 897	−14 515	=382
14 857	−14 480	=377
14 849	−14 467	=382
16 052	−15 668	=384
17 469	−17 089	=380
17 421	−17 030	=391
17 379	−16 998	=381
17 333	−16 950	=383
19 223	−18 837	=386
19 169	−18 787	=382
19 141	−18 759	=382
23 399	−23 019	=380

[a] Measured at room temperature.

and 7308.9A, are barely resolved on our instrument using a glass prism, and even then one can discern that these lines are double only with very thin crystals at liquid nitrogen temperature. The 7350.7 and 7343A lines are also not well resolved. Counting each doubled level only once, we have a splitting due to the crystal field into four levels, hence $J=7/2$ identified as $^4F_{7/2}$.

6200A Group: This group is not as intense as the others assigned to the quartet states. The 6233.4 and 6229.8A lines are resolved only for thin crystals at liquid nitrogen temperature. Three levels are present (counting the double level once); hence $J=5/2$, probably $^4G_{5/2}$.

4300A Group: The single level that appears here is quite helpful in obtaining values for the splitting of the $^4I_{9/2}$ state. However, a single level implies $J=1/2$, and there is no such level predicted in the vicinity. Therefore, either a very large perturbation is involved, or there are simply electrically split levels to which transitions do not appear. If energy level diagrams can be drawn for other compounds than the bromate, it will be interesting to see whether this group continues to consist of transitions to a single level. The strong line at 4273A, which is sharp even at room temperature, shifted down 4 cm^{-1} in going from room to liquid nitrogen temperature.

3500A Group: This group is very intense and the doubling of the upper level becomes apparent only for very thin crystals and at liquid nitrogen temperature. Again, it is difficult to say for certain whether the doubling is due to the electric field splitting a $J=3/2$ state or whether $J=1/2$ and an extra level appears. The calculations for $^4D_{1/2}$ fit this group very well, but it would not be too great a discrepancy to call this a $^4D_{3/2}$ level since the ^4D multiplet splitting is small. Furthermore, we find in agreement with Giesekus (see discussion at end of paper) that the $^4D_{3/2}$ level of the free ion is also not split in a field of C_{3v} symmetry. However, in intermediate coupling there would probably be a slight splitting which may be responsible for the two closely spaced upper levels observed. The 3500A group is

followed very closely at the short wavelength end by other groups of lines, presumably the other ^4D transitions. Some of these lines, however, are not well resolved with our dispersion.

For the expressions for the energies of the two states having $J=1/2$ in intermediate coupling see the appendix to this article.

SELECTION RULES FOR C_{3v} SYMMETRY

As is well known, the matrix elements which must be examined in the case of electric dipole transitions are

$$X_{fi}=(\psi_f, X\psi_i), \tag{12}$$

$$Y_{fi}=(\psi_f, Y\psi_i), \tag{13}$$

and

$$Z_{fi}=(\psi_f, Z\psi_i), \tag{14}$$

where $X=x_1+x_2+\cdots+x_n$, etc. (x_i, y_i, z_i) are the coordinates of the ith electron, and for the neodymium ion we take $n=3$. The square of matrix elements (12), (13), and (14) are proportional to the transition probabilities involving incident light polarized in the x, y, and z directions, respectively. The z axis is assumed to lie along the threefold rotation axis of the crystal, i.e., the optic axis.

For an odd number of electrons, the eigenfunctions which are associated with a particular energy level in the crystal (ignoring Kramers' degeneracy for a moment) form a basis for one of three possible irreducible representations of the double group of C_{3v}. The double group is of course the group associated with C_{3v} through the homomorphism between the rotation and unitary unimodular groups. The six possible irreducible representations of the double group of C_{3v} are indicated in Table VII by their characters.[18] Each column in Table VII is headed by a typical member of a class of the double group. The first three representations are the single valued representations of C_{3v}, while the last three are the double-valued representations of C_{3v}.

Now X and Y together form a basis for the two dimensional representation of C_{3v}, and hence belong to $^2\Gamma_3$ of the double group. Since Z remains unchanged for all the operations of C_{3v}, it forms a basis for the identity representation $^1\Gamma_1$ of the double group. The ψ, on the other hand, belong[19] to either $^1\Gamma_4$, $^1\Gamma_5$, or $^2\Gamma_6$. All possible products of X and Y with the two ψ's belonging to $^2\Gamma_6$ are a basis for the direct product representation $^2\Gamma_3\times{}^2\Gamma_6$ of the double group. This is reducible, however:

$$^2\Gamma_3\times{}^2\Gamma_6={}^1\Gamma_4+{}^1\Gamma_5+{}^2\Gamma_6. \tag{15}$$

The remaining products needed for the determination of all of the selection rules are the following:

$$^1\Gamma_1\times\begin{cases}{}^1\Gamma_4={}^1\Gamma_4\\ {}^1\Gamma_5={}^1\Gamma_5,\\ {}^2\Gamma_6={}^2\Gamma_6\end{cases} \tag{16}$$

and

$$^2\Gamma_3\times\begin{cases}{}^1\Gamma_4={}^2\Gamma_6\\ {}^1\Gamma_5={}^2\Gamma_6.\end{cases} \tag{17}$$

We can now state the selection rules for electric dipole transitions with the incident light polarized with E vector along z (π polarization) and perpendicular to z (σ polarization). Owing to the fact that functions belonging to different representations are orthogonal, we can state that for π polarization

ψ_f's belonging to		ψ_i's belonging to
$^1\Gamma_4$	combine only with	$^1\Gamma_4$
$^1\Gamma_5$	combine only with	$^1\Gamma_5$
$^2\Gamma_6$	combine only with	$^2\Gamma_6$.

For σ polarization

ψ_f's belonging to		ψ_i's belonging to
$^1\Gamma_4$	combine only with	$^2\Gamma_6$
$^1\Gamma_5$	combine only with	$^2\Gamma_6$
$^2\Gamma_6$	combine only with	$^1\Gamma_4$, $^1\Gamma_5$, $^2\Gamma_6$.

It should be pointed out that when the stationary states ψ_i and ψ_f in the crystal are expressed approximately merely in terms of the degenerate ψ's of the free ion belonging to a certain J value of a term arising from the $4f^n$ configuration, then these approximate eigenfunctions do not have their proper symmetry. This is due to the fact that the free ion ψ's, and hence their linear combinations will still constitute a basis for the reflection group. Thus, terms from other configurations of opposite parity play an important role in the expansion of the eigenfunctions in the crystal in terms of the free ion eigenfunctions.

The selection rules for magnetic dipole transitions are obtained by considering the matrix elements of the x, y, and z components of the operator $\sum(L_i+2S_i)$ instead of X, Y, and Z. However, since these are also the components of a vector operator the same selection rules for the combination of states holds as for electric dipole transitions, but the polarization is just the opposite

TABLE VII. Characters of the irreducible representations of the double group of C_{3v}. Typical members of a class.[a]

Repr.	E	-1	(abc)	$-(abc)$	$i(ab)$	$-i(ab)$
$^1\Gamma_1$	1	1	1	1	1	1
$^1\Gamma_2$	1	1	1	1	-1	-1
$^2\Gamma_3$	2	2	-1	-1	0	0
$^1\Gamma_4$	1	-1	1	-1	i	$-i$
$^1\Gamma_5$	1	-1	1	-1	$-i$	i
$^2\Gamma_6$	2	-2	-1	1	0	0

[a] C_{3v} is isomorphic to the symmetric group of degree 3 and can be represented as the permutations of three things, say a, b, c. The double group can be regarded as generated by the elements $-(abc)$, $i(ab)$, and -1, where (ab) and (abc) are cyclic permutations and i has the multiplication properties of $\sqrt{-1}$, i.e., is order four. In this rather unconventional representation i and -1 commute with permutations of a, b, c.

[18] W. Opechowski, reference 13.

[19] It can be shown that $^1\Gamma_4$ and $^1\Gamma_5$ can be represented in a basis in which each is a linear combination of ψ's, having M quantum numbers which are multiples of $M=\pm 3/2$. For example, if $J=3/2$, $\psi(^1\Gamma_4)=\psi(M=3/2)+\psi(M=-3/2)$ and $\psi(^1\Gamma_5)=\psi(M=-3/2)-\psi(M=3/2)$. The other M values are associated with $^2\Gamma_6$ representations.

since the components of $\sum(L_i+2S_i)$ are associated with the magnetic field vector H instead of the electric field E. Since H is an axial vector, the major contribution to the transition probability is expected to come from the matrix elements between linear combinations of the degenerate states of the f^n configuration of the free ion, i.e., between terms of the same parity.

The electric quadrupole transitions in either σ or π polarization (E vector perpendicular or parallel to z) involve matrix elements of the operators $\sum y_iz_i$, $\sum x_iz_i$, $\sum x_iy_i$, $\sum(x_i^2-y_i^2)$ in various combinations. The first two functions form a basis for $^2\Gamma_3$ as also the second two. Hence, from Eqs. (16) and (17) we are led to the following selection rule for the σ and π polarizations in electric quadrupole transitions:

for both π and σ:

states belonging to		states belonging to
$^1\Gamma_4$	combine only with	$^2\Gamma_6$
$^1\Gamma_5$	combine only with	$^2\Gamma_6$
$^2\Gamma_6$	combine only with	$^1\Gamma_4$, $^1\Gamma_5$, $^2\Gamma_6$.

According to a theorem by Kramers, in an electric field the stationary states of an atomic system are always degenerate if the system contains an odd number of electrons, the degree of degeneracy being an even number. For this reason the energies associated with the representations $^1\Gamma_4$ and $^1\Gamma_5$ are degenerate in an electric field.[20] Table VIII summarizes the three types of transitions considered above, assuming that the $^1\Gamma_4$ and $^1\Gamma_5$ levels are degenerate.

The above selection rules become strictly the only rules for very strong fields of C_{3v} symmetry. However, for weaker fields it is to be expected that the selection rules on L and J will hold approximately. Van Vleck[21] points out that if fourth-degree terms in the expansion of the potential of the crystal field are the important ones, changes of L or J up to and including 5 units in electric dipole radiation are permitted. The electric quadrupole rules for the free ion are the customary restrictions on changes of L or J by more than 2 units, and similarly for magnetic dipole transition changes in L or J must not be more than one unit. These two rules are probably also broken down in the electric field of the crystal as shown in the discussion below.

Let us examine the 8600A group in the light of the selection rules. Since the transition is to $J=3/2$, we know that one of the upper levels is associated with $^2\Gamma_6$ and the other with $^1\Gamma_4$ and $^1\Gamma_5$ together. The two strongest lines 8622.6 and 8642.5A, coming from the ground state each to one of the two upper levels, appear strongly absorbed in both π and σ polarizations. From Table VIII we can conclude that neither electric dipole,

[20] The proof can be shown using a method of E. Wigner, Nachr. Akad. Wiss. Göttingen, Math.-Physik. Kl. 546, 1932. If $K\psi$ is the "Kramers' state" to ψ then $K\Psi$ belongs to the irreducible representation D^* if Ψ belongs to D. Also $K\Psi$ belongs to the same energy as Ψ. Table VII shows that $^1\Gamma_4$ and $^1\Gamma_5$ are complex conjugate representations; hence they are degenerate.

[21] J. H. Van Vleck, reference 15.

TABLE VIII. Allowed transitions in σ and π polarizations for an atom in an electric field of C_{3v} symmetry.

Electric dipole transitions

	Upper state: $^1\Gamma_4$ or $^1\Gamma_5$	Upper state: $^2\Gamma_6$
Lower state: $^1\Gamma_4$ or $^1\Gamma_5$	π	σ
Lower state: $^2\Gamma_6$	σ	π, σ

Magnetic dipole transitions

	Upper state: $^1\Gamma_4$ or $^1\Gamma_5$	Upper state: $^2\Gamma_6$
Lower state: $^1\Gamma_4$ or $^1\Gamma_5$	σ	π
Lower state: $^2\Gamma_6$	π	π, σ

Electric quadrupole transitions

	Upper state: $^1\Gamma_4$ or $^1\Gamma_5$	Upper state: $^2\Gamma_6$
Lower state: $^1\Gamma_4$ or $^1\Gamma_5$	—	π, σ
Lower state: $^2\Gamma_6$	π, σ	π, σ

quadrupole, nor magnetic dipole transitions can alone account for both of these absorption lines. The next two lines coming from the level 115 cm^{-1} above the lowest state are likewise found in both polarizations. The fact that the line at 8781A is present in the σ but not in the π polarization indicates that this is not an electric quadrupole transition. Thus, we cannot explain the entire group of lines as resulting from a single type of transition.

This together with the fact that we have a transition involving $\Delta J=3$ is a consequence of the fact that the eigenfunctions are not characterized by J in the crystal, but by representations of the crystal double group which, expressed approximately in terms of the free ion eigenfunctions, must involve a mixture of J as well as of M quantum numbers. Furthermore, as pointed out previously, if electric dipole transitions appear, the approximate eigenfunctions will involve also a mixture of free ion eigenfunctions of a different parity than $4f^3$ eigenfunctions, i.e., additional configurations would be important in the expansion. Of course, the selection rule on L is broken as well by sufficiently strong spin-orbit interaction since states in intermediate coupling are not characterized by L.

DISCUSSION

Looking over the large number of groups in Table V predicted rather close together, and considering the error that can be expected as a result of deviations from the coupling conditions of our simple model, it can be seen that we can justify our assignment of quantum numbers only by assuming that the intensity of quartets

is greater than the intensity of doublets. This leads us to interpret certain energy levels as "extra." Thus, we interpret the 7400A group as a transition to $^4F_{7/2}$ instead of $^2H_{11/2}$ and the 6200A group as $^4G_{5/2}$ instead of $^2G_{7/2}$. A study of the relative intensities to be expected in the crystal field would be of great value in making assignments. It will also be helpful to study in detail other compounds of neodymium than the bromate so that energy level diagrams can be drawn for the various groups and compared with those given (and others not presented) as a check on the J assignment by the number of levels found. Data at liquid helium temperatures should also be of help in removing some of the ambiguities in the term diagrams.

At present a study is being made to determine the crystal field which yields the observed splittings. If successful, such information could be of help in deciding upon doubtful assignments once a few states are well established.

A crystal field calculation has already been made by Giesekus[22] for the quartet states, assuming a distribution of point charges and dipoles at distances indicated by the x-ray crystal structure analysis for the location of the atoms surrounding a rare earth ion. However, the splitting of the $^4I_{9/2}$ ground state as calculated (0, 5.8, 18.6, 40.9, 77.7 cm^{-1}) does not agree with our observed splittings. We find a total splitting of about five times the value calculated by Giesekus, and what is perhaps worse, the relative positions of the crystal field split levels as calculated do not agree with that experimentally found. By making use of the Russell-Saunders eigenfunctions which we previously found in the process of computing the electrostatic and spin-orbit interaction energies for the twice occurring L values, it is possible to reduce the calculation of crystal field splittings to radial integrals over one-electron wave functions (as Giesekus did) for all the doublet as well as quartet LSJ states. This work is made considerably easier by the knowledge of the M dependence of the matrix elements involved given by Stevens.[23] The radial integrals must be regarded as parameters to be fit to the data at this stage of our knowledge. Preliminary results indicate that in order to obtain the observed splittings the fourth and sixth degree terms in the potential due to the crystal field have axial symmetry (terms yielding zero matrix elements between states for which $\Delta M \neq 0$) are very important, as are also terms in the potential which give rise to matrix elements between states of different M values. In the model used by Giesekus the latter terms are negligible and the former contribute very little. An investigation in the ultraviolet in the vicinity of 2600A is also to be carried out. If the groups of lines which are predicted in this region are found, their identification will be rather secure since they are the only groups expected there. Likewise, an investigation of the infrared to locate the transitions to $^4I_{11/2}$ and $^4I_{13/2}$ should be made.

[22] H. Giesekus, Ann. Physik 8, 350 (1951).
[23] K. W. H. Stevens, Proc. Phys. Soc. (London) 65A, 213 (1952).

APPENDIX

There are matrix elements of spin-orbit interaction H^1 (defined above) between states of different LS for a given JM. Thus, when the matrix of H^1 is computed in the $LSJM$ basis and the corresponding electrostatic interaction energies added to the diagonal elements of the H^1 matrix, the eigenvalues of the resulting matrix are the energies of the JM states in intermediate coupling. Even though each eigenfunction in intermediate coupling is a mixture of eigenfunctions corresponding to various L and S values, it is customary to keep the labels L and S to describe the eigenvalues if the spin-orbit interaction is not too large in comparison with the electrostatic interaction. It will be noted that there are only two states having $J=1/2$, viz. $^2P_{1/2}$ and $^4D_{1/2}$, so that it is not too difficult to solve the energies of these states in intermediate coupling. Now in Russell-Saunders coupling $^2P_{1/2}$ and $^2P_{3/2}$ turn out not to be separated; hence the off-diagonal terms are important in this case. However, as soon as one considers $J=3/2$, one is faced with a 6×6 secular determinant.

For $J=1/2$ the matrix whose secular determinant must be solved turns out to be

$$\begin{pmatrix} {}^2P & 1/2\ 10^{1/2}\zeta_{4f} \\ 1/2\ 10^{1/2}\zeta_{4f} & {}^4D-3/2\zeta_{4f} \end{pmatrix}, \tag{18}$$

where ^2P and ^4D are the electrostatic interaction energies of Table I. The contribution of H^1 to the diagonal terms are already noted, while the off-diagonal elements were found by forming the eigenfunctions of $^2P_{1/2}$ and $^4D_{1/2}$ for $M=1/2$ as linear combinations of the LSM_LM_S eigenfunctions previously found as mentioned above. The vector coupling formulas in Condon and Shortley[24] provided the coefficients $(M_SM_L|JM)$ in the expression $\psi(LSJM)=\sum(LSM_LM_S)(M_SM_L|JM)$. The off-diagonal matrix elements of (18) were found by first computing the matrix of H^1 in the nlm^lm_s basis which is easily done in terms of the single electron interaction parameter ζ_{4f} since H^1 is a quantity[25] of type F.

The resulting eigenvalues[26] in intermediate coupling were found to be

$$^2P_{1/2}=1/2(^2P+{}^4D-3/2\zeta_{4f}) -1/2[(^4D-{}^2P-3/2\zeta_{4f})^2+10\zeta_{4f}{}^2]^{1/2}, \tag{19}$$

$$^4D_{1/2}=1/2(^2P+{}^4D-3/2\zeta_{4f}) +1/2[(^4D-{}^2P-3/2\zeta_{4f})^2+10\zeta_{4f}{}^2]^{1/2}. \tag{20}$$

ACKNOWLEDGMENTS

It is a pleasure to acknowledge my gratitude to Professor E. Lee Kinsey who suggested this problem, Mr. Kenneth J. Harker who checked some of the calculations, and Mr. Clay Seaman who made runs on the self-recording infrared spectrograph.

[24] E. U. Condon and G. H. Shortley, reference 4, p. 76.
[25] See reference 4, pp. 169, 59.
[26] T. Ishidzu and S. Obi [J. Phys. Soc. Japan 5, 145 (1950)] have given the matrices of spin-orbit interatcion for all the J values of f^3 terms using Racah's method.

Infrared Intensity Measurements on Nitric Oxide, Hydrogen Chloride, and Hydrogen Bromide*†

S. S. PENNER‡ AND D. WEBER
Jet Propulsion Laboratory, California Institute of Technology, Pasadena, California
(Received October 28, 1952)

The results of absolute infrared intensity measurements are described for the fundamentals and first overtones of NO, HCl, and HBr. The new data are used to estimate the dependence of electric moment on internuclear distance.

I. INTRODUCTION

In previous publications infrared intensity measurements have been described for carbon monoxide.[1] By using experimental techniques similar to those employed for CO, absolute infrared intensities have been determined for NO, HCl, and HBr. Studies on these molecules are more difficult to carry out than for CO because (a) errors may be introduced by chemical reaction between the gas under study and the gaskets used in the absorption cells and (b) because, for strongly dipolar molecules, adsorption on the surface of metal walls may become a serious source of error. For weak absorption bands we have found our self-broadening technique most suitable, whereas for strong bands the Wilson-Wells extrapolation technique[2] utilizing infrared-inactive gases for broadening is to be preferred. The rotational spacing of HCl and HBr is so distant that pressures of 1500 psia or higher are probably required before adequate broadening of the rotational lines is obtained. Because of experimental errors resulting primarily from insufficient broadening of the rotational lines even at the highest pressures used (700 psia), the reliability of the intensity data for HCl and HBr is not as great as for CO. A summary of conservative estimates of "best values" derived from the work on NO, HCl, and HBr is given in Table I.

Details concerning the experimental results and the interpretation of available data are given for NO in Sec. II, for HCl in Sec. III, and for HBr in Sec. IV.

II. EXPERIMENTAL STUDIES ON NITRIC OXIDE

Using conventional notation[1,2] a quantity B is defined by the relation

$$B = pl\alpha' = 2.303 \int \log\left(\frac{T_{0\omega}}{T_\omega}\right) d\omega, \qquad (1)$$

where p is the partial pressure of absorbing gas, l equals the length of the optical path which is filled uniformly with absorbing molecules, α' represents the apparent integrated absorption for the vibration-rotation band under study, and $T_{0\omega}$ and T_ω are, respectively, the apparent incident and transmitted intensities of radiation observed when the instrument is set at the wave number ω. The correct value of the integrated absorption α is obtained by using either or both of the relations $\alpha' \to \alpha$ as $pl \to 0$ and $\alpha' \to \alpha$ as p_T is increased. Here p_T denotes the total pressure.

In the present applications some of the partial pressures of absorbing gas are so large that corrections must be introduced for gas imperfections. Since absorption of radiation is a colligative property, it is apparent that the important physical variable defining the optical density must be equal to the number of absorbing molecules in the light path. For this reason, the quantity pl has been replaced by $p^0 l$ throughout the following discussion, where p^0 represents the equivalent partial pressure of absorbing gas if the absorbing gas were an ideal gas. The quantity p^0 was obtained from p by using van der Waals' equation of state together with the known values of the van der Waals constants.[3] It should be noted that the ratio p^0/p was generally less than about 1.2. Hence, an error of 5 percent in the correction for gas imperfections would produce an error of 1 percent or less in the value of p^0, which represents adequate precision for the present purposes.

A. Intensity Measurements on the Fundamental

Measurements on the fundamental vibration-rotation band of NO were performed in uncoated metal cells

TABLE I. Summary of experimentally determined integrated intensities for NO, HCl, and HBr.

Molecule and vibration-rotation band	Integrated intensity (cm^{-2} $atmos^{-1}$ at $297 \pm 2°K$)
NO—fundamental	$\alpha_F = 63 \pm 5$
NO—first overtone	$\alpha_O = 2.1 \pm 0.5$
HCl—fundamental	$\alpha_F = 160 \pm 30$
HCl—first overtone	$\alpha_O = 3.68 \pm 0.30$
HBr—fundamental	$\alpha_F = 55 \pm 15$
HBr—first overtone	$\alpha_O = 0.70 \pm 0.30$

* This paper presents the results of one phase of research carried out at the Jet Propulsion Laboratory, California Institute of Technology, under Contract No. DA-04-495-ORD 18, sponsored by the U. S. Army Ordnance Department.

† Presented before the Symposium on Molecular Structure and Spectroscopy, Columbus, 1951.

‡ Present address: Guggenheim Jet Propulsion Center, California Institute of Technology.

[1] S. S. Penner and D. Weber, J. Chem. Phys. **19**, 807, 817, 974 (1951).

[2] E. B. Wilson, Jr., and A. J. Wells, J. Chem. Phys. **14**, 578 (1946).

[3] *Handbook of Chemistry and Physics* (Chemical Rubber Publishing Company, Cleveland, 1947), pp. 1810–1811.

TABLE II. Nominal composition of gases.

Gas	Purity
NO	98.7% or more of NO. The remaining gas consisted of N_2 and other oxides of nitrogen, chiefly N_2O.
HCl	99.5% HCl; 0.2% acetylene; 0.3% chlorinated hydrocarbon.
HBr	99.5% HBr; no free Br_2 or H_2O; main impurity N_2.

either by using a chemically inert and infrared-inactive gas (i.e., He in the present case) to obtain pressure-broadening, or else by utilizing a self-broadening method which was developed in connection with the experimental studies on CO.[1] Representative mass-spectrographic analyses§ of the contents of gas mixtures were used to verify concentrations calculated from the partial pressure of NO admitted to the absorption cell. The spectral resolution obtained for the studies on the fundamental of NO was about 1 cm^{-1}. The nominal compositions of NO, HCl, and HBr are given in Table II. Suitable corrections for the impurities were introduced in evaluating p^0 whenever gases were employed without purification.

The results of the experimental measurements on NO pressurized with He are shown in Fig. 1. Reference to Fig. 1 shows that the observed values of B are substantially independent of total pressure for $p_T \gtrsim 300$ psia. This observation is in accord with the results which were obtained previously on CO,[1] since the rotational spacing is similar for CO and NO and since the rotational half-widths also do not appear to differ greatly. The experimental results shown in Fig. 1 lead to the conclusion that $\alpha_F = 61.8$ cm^{-2} $atmos^{-1}$ at $297 \pm 2°K$.

At the highest total pressures, it is possible to obtain α_F directly. Thus, in Fig. 2 the spectral absorption coefficient P_ω is plotted as a function of ω for the experimental data obtained at $p_T = 700$ psia. The value of $\int P_\omega d_\omega$ is found to be 64.3 cm^{-2} $atmos^{-1}$, which is in good agreement with the value of α_F obtained by using the indirect Wilson-Wells extrapolation method.

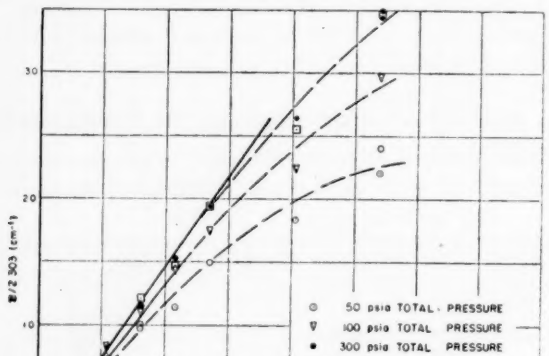

FIG. 1. Plot of $B/2.303$ as a function of p^0l for the fundamental of NO (pressure-broadened with He).

§ The analytical work was done at the Consolidated Engineering Corporation, Pasadena, California.

An independent experimental determination of α_F for NO was made by using our self-broadening technique.[1] Plots showing $B/2.303$ as a function of p^0l in cells of different lengths, in the absence of inert broadening agent, are presented in Fig. 3. Reference to Fig. 3 clearly shows that valid experimental results are not obtained unless the cell length is sufficiently small to yield adequate broadening at all of the pressures used for study. It should be noted that for $p^0l = 1$ cm atmos and $l = 0.0506$ cm, the pressure p^0 is in the neighborhood of 20 atm, which is sufficiently high to produce adequate broadening even when the broadening agent is He (compare Fig. 1) and would therefore also be expected to be sufficiently high for self-broadening. For p^0l somewhat less than unity, self-broadening is still adequate to yield significant data. Although the limiting

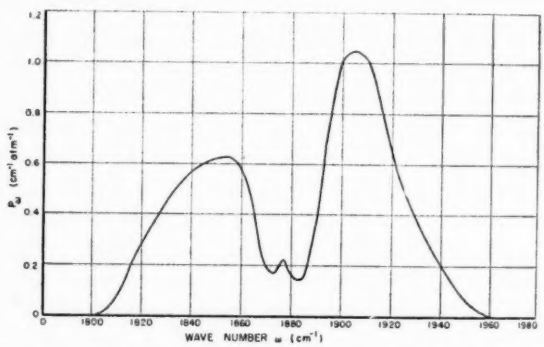

FIG. 2. Plot of P_ω *vs* ω for the fundamental of NO (pressure-broadened with He to 700 psia).

value $\alpha_F = 63.2$ cm^{-2} $atmos^{-1}$ at $297 \pm 2°K$ calculated from the results obtained in the cell of length 0.0506 cm is seen to be in excellent agreement with the numerical value derived from studies on gas mixtures, the data shown in Fig. 3 are not entirely sufficient to establish the correct value of α_F since it was not shown that the limiting slope remains constant as the cell length is decreased below 0.0506 cm. These additional experiments were not performed because the experimental problems arising in the use of gas cells with extremely short absorption paths are considerable.

On the basis of the available experimental results for NO it is concluded that $\alpha_F = 63 \pm 5$ cm^{-2} $atmos^{-1}$ at $297 \pm 2°K$.

B. Intensity Measurements on the First Overtone of NO‖

Representative experimental results obtained on the first overtone of NO (instrumental slit width $\simeq 9$ cm^{-1}),

‖ Experimental studies on the first overtone of NO were carried out with purified NO (total impurities less than 0.1 percent) supplied by Dr. H. Wise and Mr. M. Frech of the Jet Propulsion Laboratory.

using the method of self-broadening, are shown in Fig. 4 for cell lengths of 6.22 cm and 3.57 cm. The value of α_O obtained from the linear plot for the smaller absorption cell is 1.95 cm^{-2} $atmos^{-1}$ and is probably somewhat too low. A plot of α_O as a function of cell length, followed by extrapolation to zero cell length, yields a value of 2.24 cm^{-2} $atmos^{-1}$, which is probably somewhat too large. Hence, we adopt as the "best value" deduced from the available experimental data, the arithmetic mean of the preceding estimates, *viz.*, $\alpha_O = 2.1 \pm 0.5$ cm^{-2} $atmos^{-1}$ at $297 \pm 2°K$. The estimated limits of error are based on the assumption that line-broadening in NO proceeds, as a function of pressure, in a manner similar to that observed previously for CO.[4]

C. Comparison with the Results of Other Investigators

Absolute intensity estimates for the fundamental of NO have been reported by Havens[5] based on the results

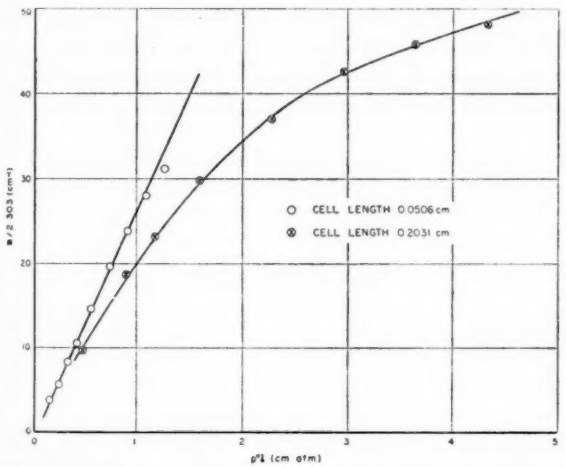

FIG. 3. Plot of $B/2.303$ as a function of p^0l for the fundamental of NO (self-broadened).

of infrared dispersion measurements, and by Dinsmore and Crawford[6] from indirect determinations of infrared intensities at total pressures not exceeding 2 atmos. Overtone intensities have also been obtained by Dinsmore and Crawford. The experimental results reported by different investigators are summarized in Table III. Reference to Table III shows satisfactory agreement for the value of α_O with the data of Dinsmore and Crawford.[6] On the other hand, the value of α_F obtained in the present studies is appreciably smaller than either of the previously reported values, the discrepancy being much larger than the probable errors of any of the measurements. In this connection, it should be noted that the value $\alpha_F = 63 \pm 5$ cm^{-2} $atmos^{-1}$ at $297 \pm 2°K$ is

[4] S. S. Penner and D. Weber, J. Chem. Phys. **19**, 1351, 1361 (1951).

[5] R. J. Havens, dissertation, University of Wisconsin, Madison (1938).

[6] H. L. Dinsmore and B. L. Crawford, Jr., Report NR-019-104, University of Minnesota (1949).

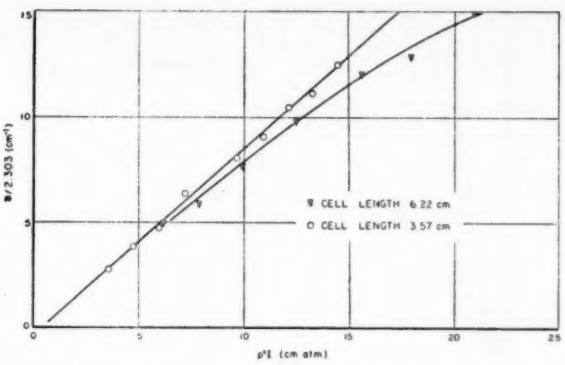

FIG. 4. Plot of $B/2.303$ as a function of p^0l for the first overtone of NO (self-broadened).

based on two completely independent experimental studies utilizing broadening by inert gases and self-broadening, respectively.¶

D. Electric Moment of NO as a Function of Internuclear Distance

The electric moment as a function of internuclear distance is obtained most conveniently from the analysis of Crawford and Dinsmore.[7] At room temperature the results of the theoretical analysis can be written, in adequate approximation, as

$$\alpha_F = (4\pi^3 N/3hcQ)\gamma^2(p_e')^2\omega_e(1-2x_e), \quad (2)$$

and

$$\alpha_O = (2\pi^3 N/3hcQ)\gamma^4(p_e')^2(\rho_e''+a_1)^2\omega_e(1-3x_e). \quad (3)$$

Here N represents the number of molecules per unit volume per unit pressure at the temperature used to perform the experiment, h is Planck's constant, c is the velocity of light, Q equals the complete partition function, $\gamma^2 = 2B_e/\omega_e$, $p_e' = \epsilon r_e$, where ϵ is the effective charge and r_e represents the equilibrium internuclear distance, a_1 = first mechanical anharmonicity constant, $\rho_e'' = p_e''/p_e'$, and ω_e, x_e, and B_e are the usual spectroscopic constants for the molecule under study. The quantities p_e' and p_e'' are calculated from the experimental data on the fundamental and first overtone by using Eqs. (2)

TABLE III. Infrared intensities for NO reported by different investigators.

	Havens (1938)	Dinsmore and Crawford (1949)	Present study
α_F (cm^{-2} $atmos^{-1}$)	110	133	63 ± 5
α_O (cm^{-2} $atmos^{-1}$)	...	2.35	2.1 ± 0.5

¶ We are unable to offer a satisfactory explanation for the discrepancy between our value for the integrated intensity of the fundamental of NO and the results of Havens (reference 5) and of Dinsmore and Crawford (reference 6). In the past, absolute intensities obtained from studies of infrared dispersion have been more accurate than data based on quantitative infrared intensity measurements.

[7] B. L. Crawford, Jr., and H. L. Dinsmore, J. Chem. Phys. **18**, 983, 1682 (1950).

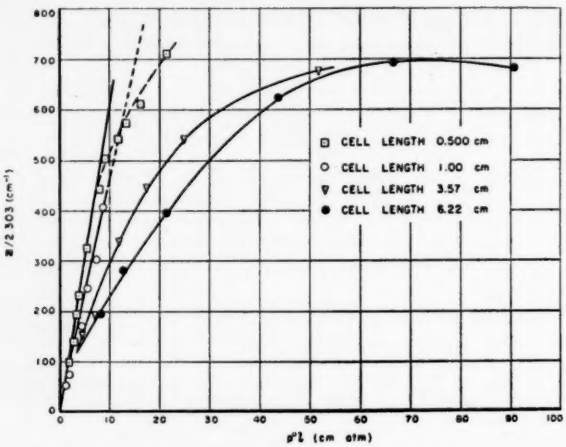

FIG. 5. Plot of $B/2.303$ as a function of p^0l for the fundamental of HCl (self-broadened).

and (3). They represent the coefficients of ξ and $\xi^2/2$, respectively, in the Taylor series expansion of the electric moment $p(\xi)$ about $\xi=0$ where $\xi=(r-r_e)/r_e$ denotes the reduced displacement of the interatomic distance from its equilibrium value.

From the experimentally determined values of α_F and α_Q for NO it is found that

$$p(\xi)=p_e{}^0\pm[1.94\times10^{-18}\xi + (7.67\times10^{-18}\xi^2 \text{ or } -2.70\times10^{-18}\xi^2)], \quad (4)$$

where $p_e{}^0$ is the permanent electric moment of NO.

III. EXPERIMENTAL STUDIES ON HYDROGEN CHLORIDE

Accurate intensity measurements on HCl are greatly complicated by adsorption problems, particularly for the fundamental where relatively low partial pressures of the infrared-active gas are involved. For this reason extensive use was made of self-broadening.

A. Intensity Measurements on the Fundamental

The results of self-broadening experiments on the fundamental of HCl, obtained in uncoated metal cells of varying lengths, are shown in Fig. 5. Reference to the plots of $B/2.303$ as a function of p^0l shows that the value of α_F observed in the smallest cell is 140 cm^{-2} $atmos^{-1}$, which therefore represents an approximate lower limit for the integrated intensity. In order to obtain a somewhat better estimate for α_F, the apparent values α_F' obtained from the data in Fig. 5 for the two smallest cell lengths were plotted as a function of cell length and extrapolated to zero cell length. In this manner a value of $\alpha_F=158$ cm^{-2} $atmos^{-1}$ was obtained.

Direct experimental determination of α_F as the integral over the spectral absorption coefficients requires the determination of P_ω as a function of ω. For studies utilizing the method of self-broadening it is advantageous to use experimental results only at pressures which are sufficiently high to give extensive self-broadening but which are not so large as to make the transmission insensitive to changes of p^0l. In the present studies P_ω was determined by plotting $\log(100T_\omega/T_{0\omega})$ *vs* p^0l and disregarding points for low total pressures (i.e., pressures below about 10 atmos) and for very large optical densities (corresponding to pressures above about 20 atmos). The results of calculations of this type lead to the conclusion that $\alpha_F=155$ cm^{-2} $atmos^{-1}$.

TABLE IV. Infrared intensities for HCl reported by different investigators.

	Bourgin (1928)	Dunham (1929)	Rollefson and Rollefson (1935)	Rollefson and Hammer (1948)	Present study
α_F (cm^{-2} $atmos^{-1}$)	156	...	173	158	160±30
α_O (cm^{-2} $atmos^{-1}$)	...	2.52	...	...	3.68±0.30

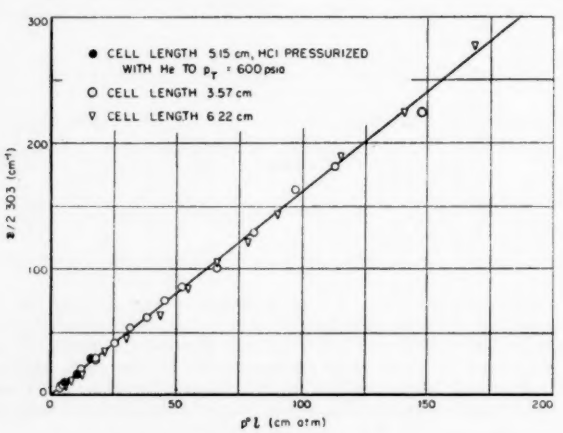

FIG. 6. Plot of $B/2.303$ as a function of p^0l for the first overtone of HCl (pressure-broadened and self-broadened).

Although the two independent methods for treating the set of experimental data on self-broadening of HCl have yielded concordant results, which are furthermore in excellent agreement with the best estimates of other investigators (see Sec. IIIC), the results cannot be considered to be reliable. Thus, the instrumental slit width employed was 4 to 6 cm^{-1}, which is not small compared to the apparent rotational half-width at the pressures used in the present investigations. A suggestion that the value of $\alpha_F=155$ cm^{-2} $atmos^{-1}$ is actually too low was obtained from self-broadening studies on HCl in very small stainless steel absorption cells fitted with stainless steel spacers and lithium fluoride windows. Since the estimated cell lengths may be in error by as much as ±10 percent, the result $\alpha_F=180$ cm^{-2} atm^{-1} may also be in error by perhaps ±36 cm^{-2} $atmos^{-1}$. However, even this value for α_F cannot be regarded as representing the true value of α_F. A reliable estimate for α_F of HCl could be obtained[8] by performing low resolution absorption studies on HCl with infrared-inactive broadening

[8] We are assuming here that the integrated absorption of HCl is independent of total pressure. For experimental studies showing a weak dependence of α on pressure see Welsh, Pashler, and Dunn, J. Chem. Phys. 19, 340 (1951).

agent utilizing a total pressure in the neighborhood of 1500 psia. Experiments of this sort are not easy to carry out since they require the use of lined absorption cells and of gas analyses for diminutive concentrations of HCl. In the absence of data of this type, it is concluded that $\alpha_F = 160 \pm 30$ cm^{-2} atmos^{-1} at 297 ± 2°K.

B. Intensity Measurements on the First Overtone

Experimental results obtained in studies on self-broadening of the first overtone of HCl are plotted in Fig. 6. Reference to Fig. 6 shows that excellent agreement has been obtained between self-broadening experiments and experiments in which the HCl was pressurized with He to a total pressure of 600 psia in a cell coated with silica. It should be noted that experimental measurements on weakly absorbing overtones are generally carried out with such large partial pressures of infrared-active gas that partial removal through selective adsorption on container walls does not play an

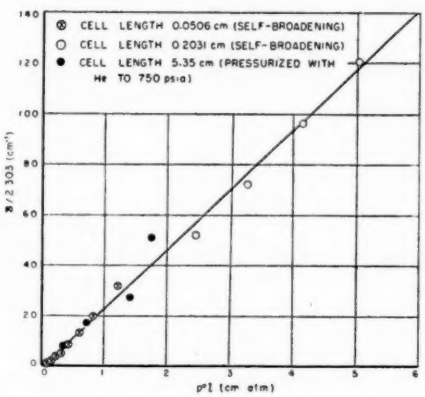
CELL LENGTH 0.0506 cm (SELF-BROADENING)
CELL LENGTH 0.203 cm (SELF-BROADENING)
CELL LENGTH 5.35 cm (PRESSURIZED WITH He TO 750 psia)
B/2.303 (cm⁻¹)
p⁰l (cm atm)

FIG. 7. Plot of $B/2.303$ as a function of p^0l for the fundamental of HBr (pressure-broadened and self-broadened).

important role. The instrumental slit width used for the data shown in Fig. 6 was about 16 cm^{-1}. The integrated intensity for the first overtone of HCl is found to be $\alpha_0 = 3.69$ cm^{-2} atmos^{-1}.

Alternate interpretation of experimental results involves the determination of P_ω as a function of ω, followed by integration over ω. Utilizing this method of calculation it was found that $\alpha_0 = 3.66$ cm^{-2} atmos^{-1}.

On the basis of the available data, the following estimate for the integrated absorption of the first overtone of HCl is obtained: $\alpha_0 = 3.68 \pm 0.30$ cm^{-2} atmos^{-1} at 297 ± 2°K.

C. Comparison with the Results of Other Investigators

Absolute intensity estimates for the fundamental of HCl have been reported by Bourgin[9,10] as the result of

[9] D. G. Bourgin, Phys. Rev. **29**, 794 (1927).
[10] D. G. Bourgin, Phys. Rev. **32**, 237 (1928).

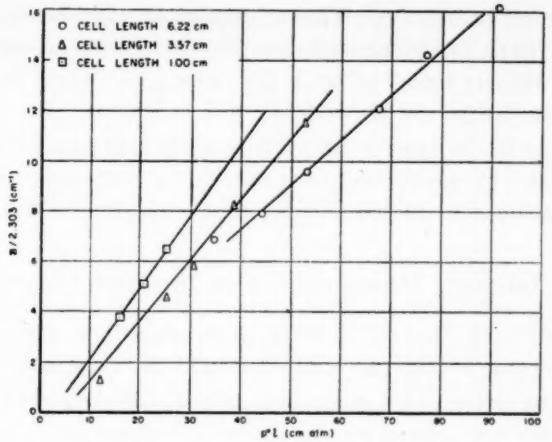

FIG. 8. Plot of $B/2.303$ as a function of p^0l for the first overtone of HBr (self-broadened).

direct intensity measurements with high resolution. Rollefson and Rollefson[11] have given estimates of α_F based on infrared dispersion measurements which have been revised recently by Hammer.[12] Direct measurements for the integrated intensity of the first overtone of HCl have been reported by Dunham.[13,14] These earlier estimates of infrared intensities are contrasted in Table IV with the results of the present studies.

D. Electric Moment of HCl as a Function of Internuclear Distance

Proceeding in the usual way (see Sec. IID) it is found that

$$p(\xi) = p_e^0 \pm [1.21 \times 10^{-18} \xi + (1.96 \times 10^{-18} \xi^2 \text{ or } -0.302 \times 10^{-18} \xi^2)]. \quad (5)$$

IV. EXPERIMENTAL STUDIES ON HYDROGEN BROMIDE

The experimental difficulties involved in accurate intensity measurements on HBr are similar to those encountered with HCl. Hydrogen bromide is more active chemically than HCl. However, it has a smaller value for the integrated absorption and closer spacing of the rotational lines, which is of advantage in performing quantitative intensity estimates.

A. Intensity Measurements on the Fundamental

The results of self-broadening experiments on the fundamental of HBr (slit width $\simeq 4$ cm^{-1}), as well as measurements in an absorption cell coated with fluorocarbon wax utilizing He to obtain broadening of the rotational lines, are summarized in Fig. 7. The experimental results obtained by using different cell lengths

[11] R. Rollefson and A. Rollefson, Phys. Rev. **48**, 779 (1935).
[12] C. F. Hammer, Jr., dissertation, University of Wisconsin (1948).
[13] J. L. Dunham, Phys. Rev. **34**, 438 (1929).
[14] J. L. Dunham, Phys. Rev. **35**, 1347 (1930).

for self-broadening are seen to agree well with the mixed gas data. The integrated absorption for the fundamental of HBr is found to have the value $\alpha_F = 55 \pm 15$ cm^{-2} atm^{-1} at 297 ± 2°K.

As in the case of the studies of HCl, it may be desirable to repeat these measurements at very large total pressures in absorption cells lined with glass or Teflon.

B. Intensity Measurements on the First Overtone

The results of self-broadening experiments on the first overtone of HBr (slit width $\simeq 9$ to 15 cm^{-1}) are summarized in Fig. 8 for absorption cells of different lengths. When the apparent value of the integrated absorption obtained for different values of l is extrapolated to $l=0$, it is found that $\alpha_0 = 0.70 \pm 0.30$ cm^{-2} atmos^{-1} at 297 ± 2°K.

C. Comparison with the Results of Other Investigators

Extensive measurements of integrated absorption have not been reported previously for HBr. Bartholomé[15] obtained a value for α_F of HBr which is less than one-half of the result calculated from the present experimental studies. This discrepancy is similar to the one observed for HCl and is probably the result of the fact that Bartholomé used very low spectral resolution.[16]

D. Electric Moment of HBr as a Function of Internuclear Distance

Proceeding in the usual way (see Sec. IID) it is found that

$$p(\xi) = p_e^0 \pm [0.820 \times 10^{-18} \xi + (1.83 \times 10^{-18} \xi^2 \text{ or } 0.169 \times 10^{-18} \xi^2)]. \quad (6)$$

[15] E. Bartholomé, Z. physik. Chem. **B23**, 131 (1933).
[16] E. C. Kemble, J. Chem. Phys. **3**, 316 (1935).

THE JOURNAL OF CHEMICAL PHYSICS VOLUME 21, NUMBER 4 APRIL, 1953

The Accommodation Coefficient Technique Applied to a Study of Molecular Oxygen Film on Tungsten*†

John L. Morrison and W. E. Grummitt‡
Department of Chemistry, University of Alberta, Edmonton, Alberta, Canada
(Received June 4, 1952)

The accommodation coefficient method of Roberts was used to measure the adsorption isotherms of the upper molecular oxygen film on tungsten at 25 and 100°C and at pressures from 9×10^{-9} to 1×10^{-4} mm Hg. The isotherms were found to fit Wang's theoretical isotherm for a mobile film with repulsive interaction. An entropy of adsorption was calculated from the surface pressure by Hill's method and found to be about four entropy units at low film concentrations. The large discrepancy between calculated and theoretical entropies suggests either or both irreversible effects and nonlinearity of the relation between accommodation coefficients and surface coverage. The minima which are exhibited during the growth with time of the adsorbed film at 100°C may be direct evidence for the presence of holes in the immobile first layer which are filled by activated diffusion from the upper layer.

INTRODUCTION

Roberts[1] has shown that the accommodation coefficient of neon with a tungsten surface can be used to detect the presence of adsorbed films. Morrison and Roberts[2] applied the method to a study of the kinetics of formation of the first, presumably atomic, oxygen film on tungsten and to a determination of the adsorption isotherm of the upper, presumably molecular, oxygen film. Also a new method was used to maintain very low measurable gas pressures.

The tungsten wire used by Morrison and Roberts had dimensions better designed for kinetic than for equilibrium studies. In the present paper, measurements were made with a wire more suited to equilibrium isotherm studies. The results are interpreted in the light of some recent statistical mechanical and thermodynamical theories of adsorption.[3–5]

EXPERIMENTAL

The apparatus and method are essentially the same as that used by Morrison and Roberts.[2] Oxygen contained in a large bulb at a known partial pressure flows first through a long fine capillary tube and then through wider tubes, in which the main resistance to flow arises from the presence of neon, to charcoal tubes immersed in liquid air, where it is removed. The wire (6.38×10^{-3} cm in diameter and 15.72 cm long) on which the adsorption takes place is situated in one of the wider tubes, and the pressure in its neighborhood can be calculated accurately from the kinetic theory of gases.

* Part of this work is from a thesis submitted by W. E. Grummitt in partial fulfillment of the requirements for the Master of Science degree at the University of Alberta.
† Presented to the Physical Chemistry Division, Annual Conference of the Chemical Institute of Canada, June 3, 1952.
‡ Present address: National Research Council, Chalk River, Ontario.
[1] J. K. Roberts, Proc. Roy. Soc. (London) **A152**, 445, 464, 477 (1935).
[2] J. L. Morrison and J. K. Roberts, Proc. Roy. Soc. (London) **A173**, 1, 13 (1939).
[3] J. S. Wang, Proc. Roy. Soc. (London) **A161**, 127 (1937).
[4] T. L. Hill, J. Chem. Phys. **17**, 520 (1949).
[5] C. Kemball, Proc. Roy. Soc. (London) **A187**, 73 (1946).

The accommodation coefficient of neon at a partial pressure of about 0.1-mm Hg was measured.

Adsorption isotherms were determined at bath temperatures of 24.8° and 100.5°C and corresponding average wire temperatures of 39.2° and 119.8°C, respectively. (These will be referred to hereinafter as the 25° and 100°C isotherms.)

RESULTS

The average values of the accommodation coefficient a for the clean wire at the beginning of an experiment were 0.043 at 25°C and 0.048 at 100°C. In each determination the accommodation coefficient increased to a fairly steady value about 120 minutes after admission of oxygen. The final values a_f at 120 minutes, determined for several oxygen pressures at 25° and 100°C are given in Tables I and II. The last two results at each temperature are only approximate as to pressures, because the gas flow cannot be calculated accurately

TABLE I. Adsorption isotherm at 25°C.

Pressure, dyne cm^{-2}	Accommodation coefficient at 120 min, a_f	θ
1.234×10^{-5}	0.1906	0.0419
3.167×10^{-5}	0.1988	0.0983
7.623×10^{-5}	0.2120	0.1890
7.718×10^{-5}	0.2102	0.1766
1.578×10^{-4}	0.2210	0.2508
2.514×10^{-4}	0.2272	0.2934
7.190×10^{-4}	0.2420	0.3952
3.157×10^{-3}	0.2640	0.5464
3.996×10^{-3}	0.2715	0.5980
9.486×10^{-3}	0.2845	0.6872
5.4×10^{-2}	0.3049	0.8274
9.4×10^{-2}	0.3177	0.9154

when the mean free path of the gas molecules becomes less than the diameter of the capillary tube.

An interesting phenomenon was observed in connection with the growth of the adsorbed layers. In Fig. 1, the change in the accommodation coefficient with time is shown for a number of experiments at various pressures at 100°C and for a single pressure at 25°C. The minimum in several of the curves is a feature common to all 100° experiments at lower pressures. The values of a at the minimum for seven experiments were 0.180, 0.183, 0.182, 0.174, 0.183, 0.182, and 0.182. The length of time that a remains at the minimum value before rising again increases as the pressure decreases. A similar relation holds for the time to reach the minimum value. The maximum value to which a rises before dropping to the minimum is also pressure dependent, the largest effect being obtained at about 7×10^{-5} dyne cm^{-2}. At pressures higher than 8×10^{-4} the effect is converted to a sharp change in slope. At still higher pressures the effect is completely masked, presumably by a too rapid adsorption of oxygen. At pressures lower than 1×10^{-5} the effect is reduced to a very slow change of a with time.

TABLE II. Adsorption isotherm at 100°C.

Pressure, dyne cm^{-2}	Accommodation coefficient at 120 min, a_f	θ
2.830×10^{-5}	0.2085	0.0484
5.884×10^{-5}	0.2152	0.0904
7.549×10^{-5}	0.2175	0.1050
1.155×10^{-4}	0.2213	0.1288
4.228×10^{-4}	0.2402	0.2476
1.081×10^{-3}	0.2580	0.3594
3.486×10^{-3}	0.2887	0.5522
7.735×10^{-3}	0.3110	0.6922
1.351×10^{-2}	0.3200	0.7488
8.0×10^{-2}	0.3350	0.8430
1.3×10^{-1}	0.3472	0.9196

The suggestion of a similar phenomenon at 25°C over a restricted pressure range about 3×10^{-5} is shown in Fig. 1 by a rapid change in slope without a minimum.

Following Van Cleave[6] and Morrison and Roberts,[2] the films were heated to various high temperatures in the presence of a small oxygen pressure. A minimum value of $a=0.146$ (100°C) occurs at about 1025°C. Above 1075°C there is no drift in a with time up to at least eight minutes after heating. The accommodation coefficients reached a maximum value of 0.173 (25°) and 0.183 (100°) when heated to 1425°C.

The observations of Morrison and Roberts[2] suggest that there are at least two films of oxygen on tungsten. The first film is shown to be composite[2,6] and is complete at all pressures. Most of it is stable up to 1400°C; this part is considered to be atomic oxygen. The remainder becomes unstable at from 600° to 800°C; this part is considered to be molecular oxygen adsorbed in the holes left in the atomic layer.[1,7] On top of the composite

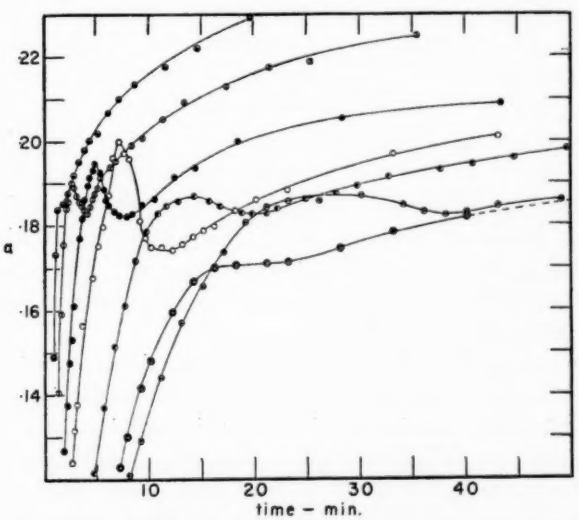

FIG. 1. Minima in the accommodation coefficient *versus* time curves. ⊖—2.83×10^{-5}, ◐—5.88×10^{-5}, ○—7.55×10^{-5}, ●—1.53×10^{-4}, ◑—2.94×10^{-4}, ◒—8.51×10^{-4} dyne cm^{-2} (all at 100°C); ⊙—3.17×10^{-5} dyne cm^{-2} (at 25°C).

[6] A. B. Van Cleave, Trans. Faraday Soc. **34**, 1174 (1938).
[7] J. K. Roberts and A. R. Miller, Proc. Cambridge Phil. Soc. **35**, 293 (1939).

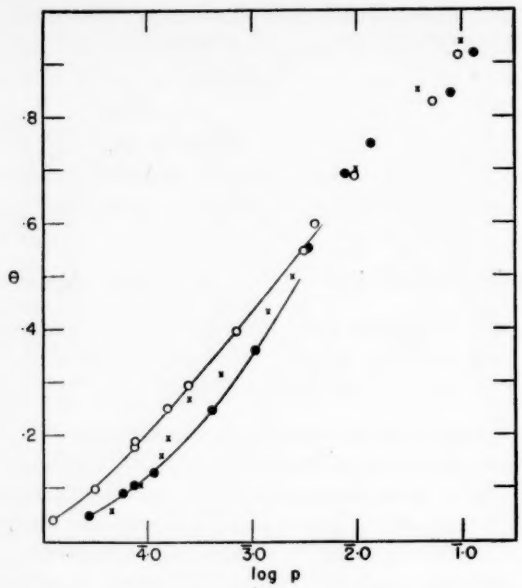

FIG. 2. Adsorption isotherms of molecular oxygen on tungsten. ○—25°C, ●—100°C, (×—25°C, from data of Morrison and Roberts, reference 2). Pressure in dyne cm^{-2}.

first film is adsorbed another film, presumably of molecular oxygen, the population of which depends on the gas pressure. It is the latter film as well as the minimum phenomenon which are the subjects of this paper.

It is considered that the extrapolation of a_f back to zero pressure marks the point at which the upper molecular oxygen film begins to build up. At high pressures a_f approaches a steady value which is also obtained by extrapolation. The best extrapolations for the 25° isotherm are $a_f=0.1845$ at zero pressure and $a_f=0.330$ at maximum pressure. Corresponding values for the 100° isotherm are 0.2008 and 0.360. An internal check on these extrapolations is shown when the ratios of the accommodation coefficient at the two temperatures (1) of the clean wire, (2) of the wire covered with the composite first film, and (3) of the wire covered with the upper molecular film are compared. These are 0.048/0.043=1.12, 0.2008/0.1845=1.09, and 0.360/0.330=1.09, respectively.

Letting θ be the fraction of *available* sites covered by molecular oxygen and assuming that a_f changes linearly with θ (the validity of this assumption will be discussed later), the initial and final extrapolated values of a_f then correspond to $\theta=0$ (no upper film) and $\theta=1$ (complete upper film), respectively. Thus, values of θ for each a_f are given in Tables I and II. In order to show the complete isotherms, θ is plotted against $\log p$ for both temperatures in Fig. 2. In addition, the values of θ for the lower temperature as obtained by Morrison and Roberts[2] are plotted as points for comparison.

DISCUSSION

Experimental and Theoretical Isotherms

The experimental isotherms, Fig. 2, were compared with the theoretical isotherms of Langmuir, Roberts,[8] Miller,[9] and Wang.[3] The most satisfactory fit was with Wang's, which is for a mobile[10] film with repulsive interaction. This is contrary to the earlier observations of Morrison and Roberts,[2] who found that their 25° isotherm fitted Roberts[8] equation for a mobile film without interaction. It is also contrary to calculations made by Miller[9] on the isotherm of Morrison and Roberts.

Wang's isotherm is expressed as follows:

$$\theta/1-\theta=\xi(1+\eta\epsilon/1+\epsilon)^z$$

and

$$\theta/1-\theta=\epsilon(1+\eta\epsilon/1+\epsilon),$$

where θ is the fraction of surface covered,

$$\eta=\exp(-V/kT),$$

V is the interaction energy, z is the number of neighboring sites to any given adsorption site, ϵ is determined by the second equation, and ξ is a function of the partition functions of the adsorbate in the gaseous and adsorbed states and is directly proportional to the pressure.

In the present case, z is taken as 4, and an estimate of the interaction energy was made from the apparent isosteric heats of adsorption. The latter are given in Table III and are calculated on the basis of the equation

$$q_{st}=RT^2(\partial \ln p/\partial T)_\theta$$

from Eq. (66) of Hill's paper.[4] Since the apparent isosteric heat of adsorption approaches zero at large θ, it is

TABLE III. Apparent isosteric heats of adsorption.

θ	q_{st} cal $mole^{-1}$
0.09	2520
0.15	3020
0.20	3050
0.25	2960
0.30	2770
0.40	2290
0.50	1720
0.60	1150
0.70	500

[8] J. K. Roberts, Proc. Cambridge Phil. Soc. **34**, 577 (1938).
[9] A. R. Miller, *The Adsorption of Gases on Solids* (Cambridge University Press, Cambridge, 1949), p. 98.
[10] "The idea of the distinction between immobile and mobile films adsorbed on fixed or localized sites was introduced by Roberts, Proc. Cambridge Phil. Soc. **34**, 399 (1938)." Quoted from A. R. Miller, Disc. Faraday Soc. **8**, 57 (1950). He further states, "Some authors appear to attempt to contrast 'localized' with 'mobile.' Since, however, for an array of localized sites, adsorbed films of the two types specified here (i.e., mobile and immobile) can be distinguished, it is preferable to use the word 'localized' to describe the array of sites and the contrasting words 'mobile' and 'immobile' to describe the types of film that can be adsorbed on an array of localized sites." (See reference 9.)

assumed that most of the adsorption energy is "used up" by the repulsive forces. This would make V about 750 cal mole^{-1}. Actually, by trial, it was found that $V=625$ cal gave the best fit for both isotherms. The constants of proportionality between ξ and p were chosen to make the theoretical isotherms pass through the experimental points A and B in Fig. 3.

Hill[4] gives a means of calculating the entropy of adsorption. Assuming that the isotherms are equilibrium isotherms, and using his Eq. (94),

$$\phi = KkT \int_0^p v d \ln p,$$

in the form

$$\phi = K'T \int_0^p \theta d \log p,$$

ϕ as a function of pressure was obtained from our data by graphical integration of each $\theta - \log p$ isotherm. As "it is not necessary to know the absolute value of ϕ" (reference 4, p. 531), the values given in Table IV are relative, but can be used to calculate the heats of adsorption at equal surface pressures, ϕ. Thus, by Hill's Eq. (85)

$$(\partial \ln p/\partial T)_\phi = [H_G - H_S]/RT^2$$

we obtain $H_G - H_S$. Since $H_G - H_S = T(S_G - S_S)$, we then obtain the difference in entropy between the adsorbed oxygen molecules and the oxygen molecules in the gas phase. The apparent values of this entropy change are also given in Table IV.

A fair "check" on the calculations in Table IV was obtained for the first part of the isotherms following Hill's suggestion,[4] using his Eq. (66).

The apparent entropies of adsorption were compared with theoretical calculations following Kemball[5] and Morrison and Drain.[11] Thus, assuming that on adsorption, one of the translational degrees of freedom is replaced by a vibration of about 8×10^{11} sec^{-1} perpendicular to the surface,[12] the entropy of adsorption was calculated theoretically at $\theta\sim0.1$ at which the pressure is about 5×10^{-11} atmos. This gave a difference of entropy of about 57 eu between the gas and adsorbed film. A large part of the difference, namely 47.1 eu, arises from the pressure term in the Sackur-Tetrode equation. Qualitatively, this means that there is a large entropy change in going from an extremely dilute gas to a relatively concentrated adsorbed film.

Obviously the present results are in disagreement with the theoretical model. It was suggested[11] that the two isotherms may not be reversible. This possibility was not tested experimentally. However, it is also possible that each isotherm may be reversible in itself, yet represent two different types of films with a transition occurring somewhere between 25 and 100°C. The discrepancy may also be explained in part by non-

[11] J. A. Morrison and L. E. Drain, private communication.
[12] T. L. Hill, J. Chem. Phys. **16**, 181 (1948).

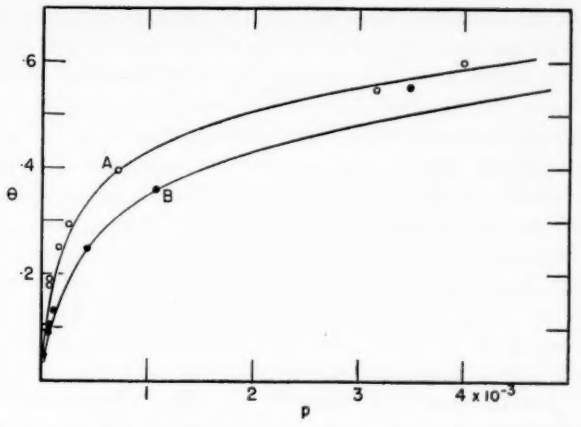

FIG. 3. Comparison of experimental data with theoretical isotherms of Wang (see reference 3). ○—25°C, ●—100°C. solid lines—theoretical isotherms at 25°C and 100°C.

linearity of a *versus* θ. This will be discussed in the last part.

An Explanation of the Occurrence of Minima

The minima probably represent a phenomenon occurring in the adsorbed film on the wire and not an experimental artifact. The fact that the minima occur only at 100° and not at 25° would seem to rule out either the evaporation of excessive adsorbed gas or thermal effects due to the high heat of adsorption of oxygen in the first layer. In the kinetic studies,[2] the system always showed steady-state conditions within two minutes after the admission of oxygen, and in the present case, for the pressure range over which the phenomenon occurs, a steady rate of increase in a was always established within one minute.

An alternative explanation is proposed: that the minima are caused by the activated diffusion of molecules from the second, molecular, layer into the holes in the first, atomic, layer.

Roberts[1] (see also references 7 and 9) has shown theoretically that immobile films may have holes or gaps in them. For example, if an oxygen molecule is to adsorb on a bare tungsten surface by dissociating into atoms that occupy neighboring sites, then a *pair* of neighboring

TABLE IV. Apparent heats of adsorption and entropies at equal surface pressures.

$\log p_{100}$	$\log p_{25}$	$k'\phi$	$H_G - H_S$ cal mole^{-1}	$S_G - S_S$ cal deg^{-1} mole^{-1}
$\bar{5}.850$	$\bar{5}.647$	10	1428	4.05
$\bar{4}.213$	$\bar{4}.007$	20	1449	4.12
$\bar{4}.463$	$\bar{4}.253$	30	1477	4.19
$\bar{4}.818$	$\bar{4}.628$	50	1336	3.79
$\bar{3}.094$	$\bar{4}.930$	70	1154	3.28
$\bar{3}.318$	$\bar{3}.182$	90	956	2.71
$\bar{3}.603$	$\bar{3}.512$	120	640	1.82
$\bar{3}.917$	$\bar{3}.892$	160	176	0.50

vacant sites must be available. It has been shown that at saturation at least 8 percent of the surface will contain single sites surrounded by four occupied sites. Similar deductions have been made for certain immobile molecular films.[8] The heating experiments[2,6] are considered indirect evidence for the existence of holes. Thus, in the present case, where a is measured at 100°C, the minimum of $a=0.146$ at 1025°C is interpreted to be the point of complete removal of molecules adsorbed in the holes, and the maximum of $a=0.183$ at 1425°C the point of complete mobility of the first, atomic, layer when separate holes become neighboring sites and the first layer becomes completely filled by atoms.

The minima occur between the time after the first, atomic, layer *with holes* is complete ($a=0.146$) and before the upper, molecular, layer is significantly started ($a=0.201$).

In order to give a detailed explanation, let us consider five distinct processes occurring while the oxygen film is being built up: (A) filling the first, atomic,[13] layer by collisions from the gas; (B) filling the first, atomic, layer by diffusion from the second, molecular, layer;[2] (C) filling the holes in the first layer by diffusion from the second layer; (D) filling the holes in the first layer by collisions from the gas; and (E) filling the second layer by collisions from the gas. In the relevant processes the second layer is assumed to be mobile and the first, composite, layer to be immobile.

The kinetics of processes (A), (B), (C), and (D) were studied by Morrison and Roberts[2] in the pressure range 2.5 to 5.3×10^{-6} dyne cm^{-2}, where the final values of a do not reach 0.201 (100°) at 120 minutes. The isotherms reported here were the end results of the process (E) and were measured in the pressure range 1×10^{-5} to 1×10^{-1}. The minima were observed over the pressure range 2×10^{-5} to 8×10^{-4} dyne cm^{-2}.

Considering the low pressure region first, it will be seen (Fig. 1) that the maximum reached, before the minimum occurs, is less than for higher pressures. It is suggested that in this pressure region the rates of (B) and (C) are not negligible compared with that of (A), so that many holes[14] will have already been filled by the time (A) and (B) are complete.[2] Process (D) is considered unimportant on steric grounds. The completion of the filling of holes by process (C) will then cause a drop in accommodation coefficient from a small maximum.

An explanation of a drop in a when molecules move from one part of the surface to another is required at this point. All first layer occupants are considered immobile, and second layer occupants mobile. It is suggested that a mobile molecule on a sparsely populated second layer will have a greater effect on a than when it is fixed in a hole in the first layer.

At higher pressures, the rate of (A) becomes very much more important. Process (B) would have a negligible role in filling the first layer. The condensation coefficient has been shown to be unity.[2] Moreover, the time to reach $a=0.18$ is 19 minutes for $p=2.83\times10^{-5}$ and only 80 seconds for $p=8.51\times10^{-4}$ dyne cm^{-2}. The effect of a preponderance of (A), a literal swamping of the bare surface, could be the sudden appearance of holes, which would then await filling by (C).

The number of holes is fixed, and eventually, with a still greater pressure, process (C) will become more effective again, because of its dependence on the population in the upper layer. Thus, the maxima will fall off, as is observed at pressures above 7.55×10^{-5}. With still greater pressures, the maximum disappears into a kink and then into a smooth curve, as the rate of process (E) becomes greater than (C).

The fact that minima are observed at 100° and not at 25° would be explained by the suggestion that process (C) has an appreciable energy of activation.

The Linearity of a *versus* θ

The assumption that a is linear with θ was made in the calculations of apparent heats and entropies of adsorption. For the first, immobile, layer it was shown[2] that shielding effects played an important role in the exchange of energy between neon gas and the tungsten wire. In general, the effect of shielding is to raise a_f above the "a_f *versus* θ" line.

In a mobile film, especially with repulsive interaction, mobility may also have an important effect on the accommodation coefficient. Mobility would also tend to raise a_f above the "a_f *versus* θ" line, and do so more effectively in dilute films.

On completion, the mobile film would be similar to a complete immobile film in its effect on a. Reasonable total changes in a are observed, 0.153 for the first complete layer and 0.159 for the second complete layer (at 100°). Similarly 0.142 and 0.145 are observed at 25°.

Shielding and mobility operate in the same direction to give higher measured values of a. If it were possible to correct for both effects, the correction of θ *versus* pressure would be in the direction of flattening the isotherms. If the flattening is proportional, it would not greatly alter the calculated heats and entropies. However, with an activated mobility the 100° isotherm would be more flattened than the 25° isotherm, resulting in higher calculated heats and entropies of adsorption. Such an effect may account for part of the discrepancy between theoretical and calculated values of the entropy of adsorption.

The suggestions of Dr. J. A. Morrison and Dr. L. E. Drain are gratefully acknowledged.

[13] Whether the first film is atomic or molecular does not affect the argument (see references 8 and 9).

[14] Holes must be carefully distinguished from pairs of neighboring vacant sites.

Photoelectric Observation of the Rate of Recombination of Iodine Atoms*†

ROYAL MARSHALL AND NORMAN DAVIDSON
Gates and Crellin Laboratories of Chemistry, California Institute of Technology, Pasadena, California
(Received October 7, 1952)

The rate of the homogeneous three-body recombination of iodine atoms, $I+I+M \rightarrow I_2+M$, $d[I_2]/dt = k[I]^2[M]$, is measured. A short intense pulse of light from a flash lamp dissociates 1–9 percent of the *ca* 10^{18} iodine molecules in a 200-cc cell, and the subsequent recombination of iodine atoms is followed by fast photoelectric techniques.

The measured values of k at room temperature are $4.2(\pm 0.4)\times 10^9$ liter^2 moles^{-2} sec^{-1} (argon), $58(\pm 4)\times 10^9$ (neopentane), $65(\pm 6)\times 10^9$ (pentane). The value for neopentane is the same at 200°C.

The large values of the recombination rate constants indicate that an important recombining process consists of a "sticky" collision between an I atom and an M molecule or atom, leading to the formation of a complex IM, which reacts with a second I atom. The lifetimes of the collision complexes are estimated.

The rates of the reverse process, the dissociation of I_2 by collision with M, are calculated; the pre-exponential factors are extraordinarily large.

The extinction coefficients of gaseous iodine have been remeasured.

A SHORT, intense pulse of light from a flash lamp can be used to produce an appreciable concentration of atoms, free radicals, or other photolysis products. If the flash time is comparable to or shorter than, the lifetime of these reactive species, it may be possible to detect them and to measure their rates of reaction by flash spectroscopy or photoelectric spectrophotometry. Norrish and Porter,[1] Ramsey and Herzberg,[2] and the authors[3] have independently introduced the use of flash lamps for the study of photochemical problems.

In the experiment described here, the pulse of light from the flash lamp, *FL* (Fig. 1), passes through the filter *G* and dissociates some (1–9 percent) of the *ca* 10^{18} iodine molecules in cell *C*. In the presence of an inert gas M, the iodine atoms thus formed subsequently recombine by the homogeneous three-body reaction

$$I+I+M \rightarrow I_2+M, \quad d[I_2]/dt = k[I]^2[M]. \qquad (1)$$

The iodine molecule concentration as a function of time is measured photoelectrically with the aid of the constant light beam *L* (wavelength selected by the filter *F*) and displayed as the vertical coordinate on the screen of an oscilloscope. A single sweep shows a large spike due to scattered light from the flash lamp. When this has decayed (point indicated by arrow), the photocurrent is greater than before the flash because of the decreased I_2 concentration. It returns to its steady value as reaction (1) occurs.

It should be recalled that the first reliable determinations of the rates of recombination of halogen atoms were made by observing spectrophotometrically the change in the steady-state concentration of halogen molecules when a system is illuminated by a constant light beam of large and known intensity.[4] This method is applicable when the quantum yield for photodissociation is known. An apparently less accurate determination of the recombination rate for bromine atoms is based on the comparison of the rates of thermal and photochemical bromination of hydrogen.[5]

EXPERIMENTAL

Chemistry

Linde argon, stated by the supplier to be better than 99.8 percent pure; Phillips Petroleum Company pure grade normal pentane, purity greater than 99 mole percent; a NBS standard sample of neopentane, 99.96 mole percent pure; and cp resublimed iodine were used. Iodine from the solid at 18–25° was vaporized into the cell through two stopcocks lubricated with Dow Corning silicone high vacuum grease. Iodine concentrations were of the order of $1-1.8\times 10^{-5}$ mole/liter. The other gas was then added to a measured pressure and, in the case of hydrocarbons, frozen down, and the cell sealed.

Electronics

The flash tube is of quartz, 4 mm i.d., 15 cm long, and filled with xenon at *ca* 12 cm pressure; it is similar to

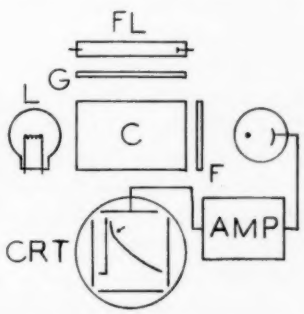

FIG. 1. Schematic diagram of the apparatus; *FL*, flash lamp; *C*, reaction cell; *L*, constant light source; *G* and *F*, filters; *CRT*, cathode-ray tube; *AMP*, amplifier.

* This research has been supported by the U. S. Office of Naval Research, under Contract Nonr-220 (01).
† Contribution No. 1741.

[1] R. G. W. Norrish and G. Porter, Nature **164**, 658 (1949); G. Porter, Proc. Roy. Soc. (London) **A200**, 284 (1950).

[2] G. Herzberg and D. A. Ramsey, Disc. Faraday Soc., No. 9, 80 (1950).

[3] Davidson, Marshall, Larsh, and Carrington, J. Chem. Phys. 19, 1311 (1951).

[4] E. Rabinowitch and H. L. Lehmann, Trans. Faraday Soc. **31**, 689 (1935); E. Rabinowitch and W. C. Wood, *ibid.* **32**, 907 (1936); J. Chem. Phys. 4, 497 (1936).

[5] K. Hilferding and W. Steiner, Z. physik. Chem. **B30**, 399 (1935).

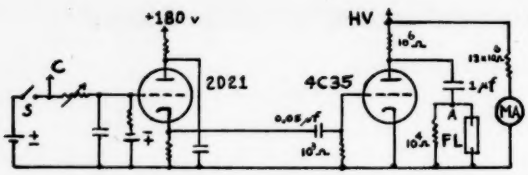

FIG. 2. Flash lamp firing circuit; *S*, firing switch; *C*, sweep trigger terminal on oscilloscope; *HV*, high voltage source; *FL*, flash lamp; *MA*, milliammeter.

the General Electric FT-127 tube. Fifty to seventy joules, stored at 10–12 kv in a 1 μf capacitor, can be discharged through the tube in about 10 μsec. Closing the switch *S* (Fig. 2) triggers a single sweep of the oscilloscope and also fires the 2D21 thyratron after a selected RC delay. The 90-v pulse across the cathode resistor of this tube fires the 4C35 hydrogen thyratron. This changes the potential at *A* from zero to minus 10–12 kv, and the flash lamp breaks down.

The lamp is mounted along the axis of an MgO coated parabolic reflector directed downwards toward a similar reflector in which the cell, a 10 cm long by 5 cm diameter Pyrex cylinder with Corex windows, rests. The beam from the constant light *L*, a 4-in. automobile spotlight run at 8 v from a storage battery, is limited by a circular aperture to a beam 2 cm in diameter through the center of the cell.

The photocurrent from a 929 vacuum phototube develops a voltage across a 10^6 ohm resistor. The resistance coupled ac amplifier with a gain of 100 consists of a cathode follower and a single stage of amplification, both using 6AK5 tubes. The amplified signal is fed into the amplifier of a Du Mont 304-H oscilloscope. The exponential rise and decay times of the amplifier-oscilloscope combination are 10 μsec and 0.12 sec. This system, of course, measures only the changes in the photocurrent and not its steady value.

The theoretical rms noise to signal ratio, due to statistical fluctuations of the photocurrent, is approximately $(e/it_r)^{\frac{1}{2}}$, i = dc photocurrent, e = electronic charge, t_r = rise time of amplifier. In a typical case, with $i = 2\times10^{-6}$ amp, this is 10^{-4}. The observed noise to signal ratio is just about equal to this. This is the order of magnitude of the minimum fractional change in photocurrent that can be detected. Amplifier noise is several times smaller than the photocell shot noise. Low frequency fluctuations (120 cycles or less) of *ca* 2×10^{-4} of the dc photocurrent are present and are presumably due to fluctuations in the light output of *L*. It is worthy of emphasis that in light modulation-spectrophotometric experiments of this nature, sensitivity is typically limited by the intensity and constancy of the light source.

Blocking of the amplifiers due to the large pulse of scattered light from the flash lamp was a serious problem that was, in part, overcome by the following measures. (1) The photocell collecting voltage was kept small, 14 volts. This is large enough so that the photocell sensitivity for small signals is not very dependent on voltage. The voltage pulse due to the flash was 7–14 volts when no filter, *G*, was used. When *G* was a Corning 3486 filter, cutting out light of wavelength shorter than 510 mμ, and *F* was a 487 mμ interference filter, the flash pulse was about 0.3 volt. The initial degree of dissociation of the iodine was cut down about two-thirds by the 3486 filter. (2) The oscilloscope amplifier is a dc amplifier which does not block. Nevertheless, the blocked time is about 150 and 400 μsec with and without the 3486 filter. This at present is the limitation of our apparatus for measuring very fast reactions.

In each series of experiments, gain and time calibrations were accomplished with the light from a 6-v flashlight bulb chopped at 600 cycles/sec. The photocurrents produced by this lamp (*ca* 10^{-8} amp) and by *L* were measured with a 10^4 ohm standard resistor, a type K Leeds and Northrup potentiometer, and a galvanometer of sensitivity 10^4 mm/μamp. These data and the amplitude of the 600-cycle square wave on the oscilloscope screen permit one to convert deflection on the screen into fractional change of photocurrent. The decrease in deflection sensitivity of about 3 percent, due to illumination by the constant light *L* with a concomitant change in photocell collecting voltage of 1–2 volts, was directly measured in each experiment.

Spectrophotometry

Two different defined "extinction coefficients" are of importance here. The extinction coefficient that is commonly used in spectrophotometry we shall call the integral extinction coefficient ϵ; $\epsilon = D/(l[\mathrm{I_2}])$; D = decadic optical density, l = path length, $[\mathrm{I_2}]$ = iodine concentration in moles/liter. The partial molar extinction coefficient $\bar{\epsilon}$ is defined by $\bar{\epsilon}l = \partial D/\partial[\mathrm{I_2}]$. In the flash photolysis experiment, small fractional changes in photocurrent are observed from which the corresponding small fractional changes in iodine concentration are computed.

For wavelengths below 499.5 mμ, the convergence limit of the banded spectrum, ϵ and $\bar{\epsilon}$ should be equal, independent of inert gas concentration $[\mathrm{M}]$, and iodine concentration. In the region of discrete absorption $\bar{\epsilon}$, in general, will be a function of $[\mathrm{I_2}]$ and $[\mathrm{M}]$, and typically $\partial\bar{\epsilon}/\partial[\mathrm{M}] > 0$, $\partial\bar{\epsilon}/\partial[\mathrm{I_2}] < 0$; ϵ will also be a function of $[\mathrm{I_2}]$ and $[\mathrm{M}]$ and $\epsilon > \bar{\epsilon}$.

Some values of ϵ, the integral extinction coefficient, measured with a 10-cm cell in a Beckman spectrophotometer, are listed in Table I. Concordant values ($\pm$2 percent) for ϵ at 490 and 498 mμ were found in two experiments. In one, a cell with 71.8 mm of pentane and excess solid iodine was at a temperature of 22.8° in the spectrophotometer, corresponding to a vapor pressure of 0.256 mm, $[\mathrm{I_2}] = 1.39\times10^{-5}$ molar.[6] In the second experiment an evacuated cell at 24° was satu-

[6] L. J. Gillespie and L. H. D. Fraser, J. Am. Chem. Soc. 58, 2260 (1934).

rated with solid iodine at 22.2°, $p=0.244$ mm, and then sealed off.

Extinction coefficients at other wavelengths were measured relative to that at 498 mμ in cells with 80–760 mm argon and iodine concentrations of $1.0-1.7\times10^{-5}$ molar. Because of the low absorption, the data were not expecially accurate. It was observed, however, that, in the banded region of the spectrum, ϵ did fall off at argon pressures below 300 mm, especially at the higher iodine concentrations. Thus, at 90 mm of argon, with $[I_2]=0.9$ and 1.7×10^{-5} molar, ϵ at 546 mμ was 94 percent and 84 percent of the high pressure value. The effect on $\bar{\epsilon}$ is, of course, still greater.

Our data in Table I differ somewhat from those given by Rabinowitch and Wood.[7] Our observations confirm their result that ϵ is independent of pressure of air, argon, or helium, above 500 mm. Our results are in qualitative agreement with the more precise observations of Luck on the effect of iodine and inert gas pressures on the absorption of the 546 mμ mercury line by iodine at 210°C and at higher iodine concentrations than used here.[8] He observed a limiting ϵ of 637 at high inert gas pressures and low $[I_2]$, the same as the value measured by us at room temperature.

Most of the data for the recombination rate were obtained using as the filter F a Bausch and Lomb interference filter with a measured maximum transmission of 36 percent at 487 mμ, a half-width of 8 mμ, and a transmission of the order of ½–1 percent through the rest of the spectrum. Some of the argon runs were made with a Baird Associates 546 mμ multilayer interference filter (plus a yellow filter to eliminate blue light) with a half-width of 5 mμ and a maximum transmission of 70 percent. In the 487 mμ range, $\bar{\epsilon}=\epsilon$; but the band width of the filter is different from that of the spectrophotometer used for the data in Table I. By direct transmission measurement in the experimental arrangement used in the rate runs, an effective ϵ of 383 was found for this filter; this value has been used for ϵ in the interpretation of data. With the 546-mμ filter, the measured value of ϵ of 640 was taken for $\bar{\epsilon}$ except for some low pressure runs, where a value of 600 was used.

Interpretation of Data

The integrated form of the rate equation (1) is $1/[I]-1/[I]_0=2k[M]t$, where $[I]_0$ is the concentration of iodine atoms just after the flash. Since the degree of dissociation of iodine molecules by the flash is small, the change in transmitted light intensity J is given by $dJ/J_\infty=2.303\bar{\epsilon}l\times[I]/2$. The oscilloscope deflection S, due to the change in the photocurrent i, is then given by

$$\frac{1}{S}-\frac{1}{S_0}=\frac{4k[M]t}{i_\infty g\times2.303\bar{\epsilon}l}(1+t_{\frac{1}{2}}/RC), \qquad (2)$$

where g is the gain of the photocell-amplifier-oscilloscope combination in units of deflection per ampere change in photocurrent.

The last factor is a small approximate correction for the decay of the signal because of clipping by the ac amplifier; $t_{\frac{1}{2}}$ is the time at which $[I]=[I]_0/2$ and RC is the exponential decay time of the amplifier-oscilloscope combination. A small correction to S is made for the deflection due to the pulse of light from the flash lamp and for the subsequent negative overshoot.

Table I. Extinction coefficients of iodine.

(mμ)	478	487	490	498	510	520	546	560	580	600
ϵ^a	···	440	478	580	700	751	640	490	280	145
ϵ^b	400	540	600	740	810	822	670	550	300	140

[a] This research.
[b] Reference 7.

RESULTS AND DISCUSSION

Results

Figure 3 exhibits a typical trace from an experiment. The plots of $1/S$ *vs* t gave reasonably good straight lines from which k was calculated by Eq. (2). The results of the runs at room temperature are summarized in Table II.

One set of measurements was made at 200(±10)°C on a cell containing 1.20×10^{-5} mole/liter of iodine and 2.17×10^{-3} mole/liter of neopentane. The absorption coefficient of iodine at 487 mμ was the same to ±10 percent at this temperature as at room temperature, and the measured rate constant for recombination of 59×10^9 is the same as that obtained at room temperature.

Consideration of Possible Errors

Absorption of 0.0047 calorie (5×10^{16} quanta of $\lambda=500$ mμ) in a 200-cc cell containing a little iodine and argon at 206 mm (the lowest pressure used) corresponds to a temperature rise of 0.7°. Provided the energy was uniformly absorbed throughout the cell, this would have no effect on the measurements.

Rabinowitch[9] has estimated 0.16 cm² sec⁻¹ for the diffusion coefficient D of iodine atoms into argon at one atmos pressure. On the basis of the densities of the solids, we estimate a diameter of 6.2A for pentane and neopentane, and 0.10 for the diffusion coefficient of iodine atoms into either of these gases at one atmos

[7] E. Rabinowitch and W. C. Wood, Trans. Faraday Soc. **32**, 540 (1936). These authors ran the absorption spectrum of a cell which they state contained 0.158 mm of I_2, obtained by saturating the cell at "about 19°C." According to the data they used (Baxter, Hickey, and Holmes, J. Am. Chem. Soc. **29**, 127 (1907); the results in this reference agree essentially with that of reference 6), the vapor pressure of iodine at 19° is 0.178 mm, not 0.158 mm, and at 17° it is 0.155 mm. If one assumes that Rabinowitch and Wood were actually working at 0.178 mm pressure of iodine, the agreement between the two sets of data would be better at 498 mμ and poorer at 546 mμ.

[8] W. Luck, Z. Naturforsch. **6A**, 313 (1951).

[9] E. Rabinowitch, Trans. Faraday Soc. **32**, 917 (1936).

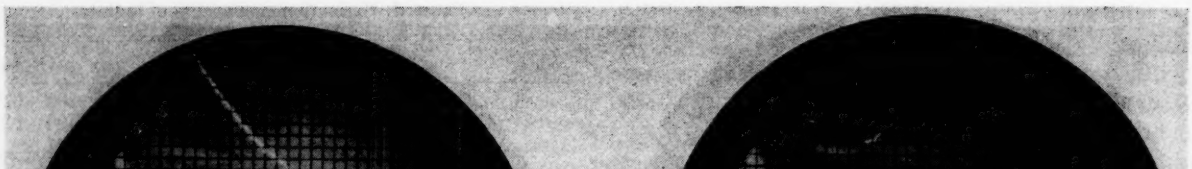

FIG. 3. On the left is the pattern displayed on oscilloscope as iodine atoms recombine: p (argon) = 740-mm Hg; time scale = 0.159×10^{-3} sec/smallest grid division (= 0.1 inch); $i_\infty = 2.66$ μamp; $g = 2.25 \times 10^3$ smallest grid divisions/μamp; $t_{\frac{1}{2}} = 1.8 \times 10^{-3}$ sec; $[I_2] = 9.0 \times 10^{-6}$ mole liter^{-1}; $[I]_0 = 1.6 \times 10^{-6}$ mole liter^{-1} (an especially high energy flash). On the right is the signal resulting from scattered light from flash lamp and negative overshoot from ac amplification when the constant light L is off.

pressure. According to Eq. (1), the time for three-fourths of the iodine atoms to recombine is $t_{3/4} = 3/(2k[M][I]_0)$. The mean distance diffused in this time is $(2Dt_{3/4})^{\frac{1}{2}}$. The lowest values of argon and pentane pressure studied were 0.25 and 0.05 atmos, with $t_{3/4}$ of 0.02 sec in each case; the corresponding diffusion distances are 0.16 and 0.28 cm. Thus heterogeneous recombination on the walls did not significantly affect the results.

Non-uniform creation of iodine atoms in the cell would make the calculated rate constant greater than the true value. The minimum light transmission parallel to the axis of the cell was of the order of 85 percent; it is unlikely that internal filter effects were significant. No satisfactory way of investigating whether the light intensity from different parts of the flash lamp was the same was developed. One lamp, a commercial FT-127, seemed to emit a greater intensity from the anode region. Rate constants measured with this lamp were 100 percent higher than those reported in Table II with one orientation of the lamp and 50 percent higher when the lamp was rotated through 180°. No such effects were noted with the lamp used for the measurements of Table II. In view of this and the effect of the MgO reflectors in diffusing the light, it is probable that the illumination was sufficiently uniform.

The average deviation from the mean of the results in Table II is about 10 percent. This variability is probably due to errors of measurement of the oscillograph traces, to fluctuations in the gain of the amplifier, and to errors in the measurement of the small current of *ca* 10^{-8} amp. involved in the measurement, with chopped light, of amplifier gain.

In view of the discrepancies between the two sets of measurements of the extinction coefficient of iodine in Table I, it must be pointed out that any error here results in a corresponding error in the rate constants.

Discussion

The value of k for argon measured by the photostationary state technique[4] is 6.9×10^9 liter^2 mole^{-2} sec^{-1}. The value reported here is 4.2×10^9 and an independent measurement of this quantity by Norrish, Porter, and collaborators at Cambridge,[10] gave $4.39(\pm 0.11) \times 10^9$. We believe that further experience with flash lamp measurements is needed before a confident estimate of their reliability can be made. The concordance of the two flash lamp determinations plus the consideration of errors in the preceding section indicates, we believe, that the flash lamp determinations are more accurate than the photostationary state measurement. It should be noted that any correction for a possible lack of uniformity in the luminosity of the flash lamp, considered in the previous section, would increase the difference between the two values.

In a recent study of the thermal and photochemical bromination of neopentane, it was concluded that at 197°C the ratio of k's for the reaction $Br + Br + M \rightarrow Br_2 + M$ for neopentane and hydrogen as third bodies is 174.[11] Since recombination rate constants are not very dependent on temperature, the values of k for iodine atom recombination in the presence of neopentane and argon measured in the present research, taken in con-

[10] Private communication.

[11] F. R. Schweitzer and E. R. Van Artsdalen, J. Chem. Phys. 19, 1028 (1951).

junction with Rabinowitch's results that $k_A/k_{H_2}=0.95$ and 0.59 for iodine atom and bromine atom recombinations, respectively, strongly suggest that the ratio of efficiencies of neopentane and hydrogen as third bodies for halogen atom recombinations is 8–14, not 174. Other aspects of this investigation[11] of the bromination of neopentane have recently been criticized.[12]

Rabinowitch[13] has discussed the homogeneous recombination process, $I+I+M\rightarrow I_2+M$, in terms of two kinds of triple collisions:

$$(I+I)+M, \tag{3a}$$

$$(I+M)+I. \tag{3b}$$

For case (a), the first double collision is between two iodine atoms; for case (b), the first double collision is between an iodine atom and an M molecule or atom. The important parameter which enters into the elementary kinetic theory calculation of the number of triple collisions, but not into the calculation of number of double collisions, is the duration of a double collision. The recombination rate constant k (in units of cc^2 molecules^{-2} sec^{-1}) is given by Rabinowitch as

$$k=8\pi\sigma_{MI}^2\sigma_I^2RT\left(\frac{M_M+M_I}{2M_I^2M_M}\right)^{\frac{1}{2}}(2\tau_{II}+\tau_{MI})\beta. \tag{4}$$

The σ's are collision diameters, $\sigma_{MI}=0.5(\sigma_I+\sigma_M)$; τ_{II} and τ_{MI} are the durations of the double collisions between two iodine atoms and between an iodine atom and M, and β is the probability that a triple collision results in recombination.

From a chemical kinetic point of view, one may view the recombination process in the way outlined by Eqs. (5):

$$\begin{aligned} &I+I\rightleftarrows I_2^*,\\ &I_2^*+M\rightarrow I_2+M, \end{aligned} \tag{5a}$$

$$\begin{aligned} &I+M\rightleftarrows IM^*,\\ &IM^*+I\rightarrow I_2+M. \end{aligned} \tag{5b}$$

I_2^* and IM^* are excited molecules; the former loses vibrational energy and is stabilized by collision with M, the latter can react with a free iodine atom in a two-body process. The rate constants for dissociation of I_2^* and IM^* are $(1/\tau_{II})$ and $(1/\tau_{IM})$ of Eq. (4). An equation which is the same as (4) except for small numerical factors can be derived from the reaction schemes, (5), by the standard stationary state argument.

Using Eq. (4), the results in Table II, and collision diameters of 5.2, 3.6, and 6.2A for iodine atoms, argon atoms, and pentane or neopentane molecules, the calculated values of $(\tau_{II}+0.5\tau_{IM})\beta$ are 1.5×10^{-13} sec (argon), 1.6×10^{-12} sec (neopentane), and 1.8×10^{-12} sec (pentane).

For comparison, the values obtained by Rabinowitch for several third bodies are 2.5×10^{-13} (argon), 3.6×10^{-13} (nitrogen), 1.0×10^{-12} (carbon dioxide), and 4.2×10^{-12} sec (benzene). Assuming, purely for the sake of intercomparison of results, that all Rabinowitch's results are too high by a factor of 2.5/1.5, his value for benzene should be decreased to 2.5×10^{-12} sec. This value is not much larger than those found by us for the pentanes, so that one need not assume a special interaction between iodine atoms and the aromatic ring.

Two iodine atoms in the ground state ($^2P_{\frac{3}{2}}$) can interact to form molecules in the $^1\Sigma_g^+$, $^1\Pi_u$, and $^3\Pi_{2u,1u}$ states, which have potential energy curves with a minimum. (These curves are illustrated in reference 13, Fig. 1.) Herzberg[14] gives the fundamental vibration periods in the $^1\Sigma_g^+$ and $^3\Pi_{1u}$ states as 1.6×10^{-13} and 7.8×10^{-13} sec. The vibration periods of the $^1\Pi_u$ and $^3\Pi_{2u}$ states are presumably intermediate between these two values. In the approximation in which the potential curves are considered harmonic and centrifugal effects are neglected, the lifetime τ_{II} of I_2^* is a properly weighted average of the vibration periods listed above. The much larger τ-values calculated from benzene and the pentanes can be interpreted as indicating a very large cross section for vibrational deactivation of I_2^* by these molecules. A more plausible interpretation has been suggested by Rabinowitch, i.e., that the processes of type (b), "sticky" collisions between M and an I atom, are important and account for the large values of τ and their variation from substance to substance. When M is a polyatomic molecule, τ_{IM}, the lifetime of the collision complex, can be much longer than a single vibration period, because the small energy of attraction can be distributed among the various "soft" vibrational degrees of freedom of the molecule.

Finally, it is of interest to consider the inverse process, the dissociation of iodine molecules by collision with

TABLE II. Rate of recombination of iodine atoms at room temperature.

Argon								
p (M) (mm Hg)				206[a]	206[a]	380[b]	627[b]	
$k\times10^{-9}$ (liter^2 mole^{-2} sec^{-1})				4.9	5.1	4.3	4.3	
p (M)	703[b]	740[b]	1580[b]	740	740	740	740	740
$k\times10^{-9}$	4.0	3.6	3.7	3.7	4.2	3.9	4.6	4.2
k (av) $=4.2(\pm0.4)\times10^9$ liter^2 moles^{-2} sec^{-1}								
Neopentane								
p (M)	38.5		38.5		77	77		77
$k\times10^{-9}$	56		56		60	66		50
k (av) $=58(\pm4)\times10^9$ liter^2 moles^{-2} sec^{-1}								
Pentane								
p (M)	48.6	73.5	73.5	65.5[c]	65.5[c]	71.8[c]		
$k\times10^{-9}$	78	66	70	60	52	64		
k (av) $=65(\pm6)\times10^9$ liter^2 moles^{-2} sec^{-1}								

[a] 546 mμ filter, $\bar{\epsilon}$ taken as 600.
[b] 546 mμ filter, $\bar{\epsilon}$ taken as 640; all other measurements were made with the 487 mμ interference filter.
[c] For these measurements, the pentane vapor was dried over calcium chloride.

[12] S. W. Benson and H. Graff, J. Chem. Phys. **20**, 1182 (1952).
[13] E. Rabinowitch, Trans. Faraday Soc. **33**, 283 (1937).
[14] G. Herzberg, *Spectra of Diatomic Molecules* (D. Van Nostrand Company, Inc., New York, 1950), second edition, p. 540.

gas molecules M:

$$I_2+M\rightarrow I+I+M, \quad -d[I_2]/dt=k_D[I_2][M]. \quad (6)$$

For k_D, the rate constant for dissociation, $k_D=kK_c$, where K_c is the equilibrium constant for the dissociation of iodine, 3.80×10^{-23} mole liter^{-1} at 300°K.[15] Since k is not strongly dependent on temperature, $k_D=A\exp(-\Delta E/RT)$, where $\Delta E=35\,500$ cal. Then A is 1.1×10^{13} liter mole^{-1} sec^{-1} for argon, 1.6×10^{14} for neopentane, and 1.8×10^{14} for pentane. These are exceptionally large values for the pre-exponential factor in a bimolecular reaction. Rice[16] has noticed this in analyzing the results of Rabinowitch and Wood, and has suggested possible interpretations.

[15] "Selected values of chemical thermodynamic properties," National Bureau of Standards, Washington, D. C., Series III, June 30, 1948.

ACKNOWLEDGMENT

It is a pleasure to acknowledge the unfailing courtesy of Mr. Haskell Shapiro of the Hydrodynamics Laboratory in giving us both advice and material assistance with flash lamp problems.

[16] O. K. Rice, J. Chem. Phys. 9, 258 (1941).

THE JOURNAL OF CHEMICAL PHYSICS VOLUME 21, NUMBER 4 APRIL, 1953

The Decomposition of Nitrate Crystals by Ionizing Radiations

GERHART HENNIG, ROBERT LEES,* AND MAX S. MATHESON
Chemistry Division, Argonne National Laboratory, Lemont, Illinois

(Received September 2, 1952)

Sodium nitrate, potassium nitrate, and potassium chlorate have been exposed two to four weeks in the experimental thimble of the Argonne Heavy Water Pile. After exposure these salts evolve a gas when dissolved in water or when melted or heated to a crystal transition point. The gas yields are in sodium nitrate *ca* 0.3, in potassium nitrate *ca* 0.8, and in potassium chlorate 2.0–3.0 molecules gas/100 ev. For the nitrates this gas has been shown to be largely oxygen which is trapped during irradiation in the gaseous form in small pockets in the crystal. This conclusion is based on the paramagnetism of the irradiated crystals, on chemical analysis of the evolved gases, and on measurements of the amounts of gas liberated in crushing experiments. When irradiated crystals are heated below the melting point, the gas pockets grow and coalesce, this being accompanied by a decrease in crystal density. In irradiated nitrates, oxygen and nitrite ion are formed in equivalent amounts. Experiments with low energy x-rays indicate that most of the decomposition results from electronic ionization and excitation and not from elastic collision of the bombarding particles.

1. INTRODUCTION

CERTAIN salts such as barium nitrate[1] and potassium bromate[2] decompose when exposed to ionizing radiation. For the barium nitrate Allen and Ghormley have shown that the irradiated salt upon solution in water yields a gas presumed to be mainly oxygen and an amount of nitrite ion equivalent to the evolved gas. These authors pointed out that the oxygen must remain trapped in the crystal during irradiation as O atoms or O_2 molecules. The question as to the state of the trapped oxygen seemed a particularly interesting one, since O atoms should be able to recombine with NO_2^-, and O_2 molecules if present could be molecularly trapped or could diffuse into pockets. We have, therefore, carried out further irradiations of nitrate crystals, particularly seeking to learn more about the state of the trapped oxygen, the primary process in the decomposition, and the products.

* Present address: Department of Anthropology, University of Chicago, Chicago 37, Illinois.

[1] A. O. Allen and J. A. Ghormley, J. Chem. Phys. 15, 208 (1947).

[2] Boyd, Cobble, and Wexler, J. Am. Chem. Soc. 74, 237 (1952).

2. EXPERIMENTAL

A. Materials

The salts irradiated were, in general, Merck Reagent grade used as obtained. In addition, large single crystals of sodium nitrate from the Harshaw Chemical Company were used in some experiments.

B. Irradiation

All samples for pile irradiation were contained in sealed quartz tubes evacuated up through the *G* series, but containing air in series *H* through *P*. The quartz tubes of about 2.0 cm diameter and 10 cm length were held in standard aluminum cans and irradiated for two or four weeks in the experimental thimble of the Argonne heavy water pile, CP-3. The samples were irradiated at ambient pile temperature which was always below 50°C. The slow neutron flux was about 10^{12} neutrons/cm^2-sec and the fast neutron flux one-tenth of this.

In the x-ray exposures two Harshaw $NaNO_3$ crystals were exposed to the radiation of an AEG-50 x-ray tube. One crystal, 1.18 cm^2 and 1 mm thick, was exposed

16.08 hr 4.0 cm below the x-ray tube target at 49 kv and 40 ma; the other, 2.0 cm^2 and 2.5 mm thick, was irradiated 16.92 hr 3.7 cm below the target at 25 kv and 40 ma.

C. Density of Crystals

The gross densities of crystals before and after irradiation were measured by the method of Archimedes using reagent carbon tetrachloride as the immersion liquid. To check the density of the CCl_4, a pycnometer was used giving a measured density of 1.5839 25.2°/4 compared with the literature value[3] of 1.58370 25.5°/4. The variation among successive density measurements of the same crystal was less than 0.1 percent, and the densities of unirradiated crystals agreed with literature values within 0.1 percent; e.g., $NaNO_3$, measured on Harshaw crystal, 2.2615 g/cm^3 at 25.0°C; literature,[4] 2.261 20°/4.

D. Analyses

To measure the gas trapped in irradiated crystals, the weighed crystals were placed in a bulb of known volume and sealed to a calibrated section of vacuum line containing a large McLeod gauge. For complete evolution of trapped gas it was necessary to heat potassium nitrate above the crystal transition temperature at 127°C and to melt sodium nitrate (m.p. 306.8°C). Heating was accomplished either by means of a wire-wound tubular furnace, or for more precise temperature control the sample was heated by the condensing vapors of a boiling liquid such as diphenylamine (b.p. 302°) or benzophenone (b.p. 306°) to cite only two of several liquids used. The evolved gas was passed through a trap which could be cooled either with liquid nitrogen or dry ice-acetone. About 98 percent of the gas was not condensed by liquid nitrogen.

The nitrite present in irradiated nitrate samples was quantitatively determined by a colorimetric method involving the formation of an azo dye from sulfanilic acid and α-naphthylamine in the presence of nitrous acid.[5] A Beckmann spectrophotometer set at 5240A, and slit width 0.015 mm was used to measure the optical density of unknowns and standards. The variation of optical density with nitrite concentration was linear up to 0.15 ppm of nitrite nitrogen, and an unirradiated blank showed no nitrite whatever.

3. RESULTS AND DISCUSSION

A. Appearance of Crystals

KNO_3 and $NaNO_3$ crystals irradiated in vacuum generally became opaque and light yellowish to milky white in color, whereas $NaNO_3$ irradiated in vials open to the air became dark yellow and remained transparent. In two cases very small crystals were observed under a microscope to be partly transparent yellow and partly white with a sharp interface, and there was no indication that two once separate crystals had become joined together after coloration. Spectrographic analysis showed negligible differences in the two forms. Further, the yellow and white crystals from the same irradiation showed no difference in oxygen yield.

Yellow, transparent $NaNO_3$ crystals lost their color when heated for one hour at 249°C. Continued heating caused the crystals to become white and opaque without the release of more than a few percent of the total occluded gas. This result suggests that in the irradiations in vacuum the crystals became warm and so formed the opaque type of crystals, whereas in the irradiations in air the crystals remained relatively cool and yielded the transparent crystal form. In agreement with this hypothesis larger crystals tended to become opaque and smaller crystals transparent yellow as would be expected if crystal temperature were important.

Irradiation of $KClO_3$ crystals produced a light yellow powder which popped when disturbed.

B. Products

The gas obtained by melting some of the *K* series irradiated $NaNO_3$ was analyzed chemically by Gordon of this laboratory for O_2, NO, NO_2, and H_2. The gas was found to be 98.5 percent O_2 plus 1.5 percent of an inert gas, possibly N_2. Mass spectrometric analysis by Hutchison of this laboratory, confirmed that the gas was chiefly oxygen and the minor constituent was N_2.

Allen and Ghormley,[1] extending a suggestion by Narayanswamy,[6] propose that during irradiation excited NO_3^- ions dissociate to NO_2^- ions and oxygen atoms and that also NO_3^- ions may be ionized to NO_3 radicals which also may dissociate after capture of an electron. From such a mechanism one would expect two NO_2^- ions to be formed for each molecule of O_2, and this was confirmed by the first authors for $Ba(NO_3)_2$. We have found a similar ratio of NO_2^- to O_2 in the present work. For example, KNO_3 irradiated two weeks in the pile analyzed 559 micromoles of NO_2^-/g and 274 micromoles noncondensable gas/g (ratio 2.04), and $NaNO_3$ crystals also irradiated two weeks in the pile yielded 131.2 micromoles NO_2^-/g and 78.6 micromoles of noncondensable gas/g (ratio 1.67). The production of small amounts of N_2 would tend to give a ratio a little less than two.

The gas released from irradiated crystals by heating KNO_3 to the transition point or $NaNO_3$ to the melting point was measured for a series of irradiations, and the results are summarized in Table I. The energy estimated to be absorbed per gram of sample is given in column 4. The energy absorption was approximated by estimating

[3] *International Critical Tables II* (McGraw-Hill Book Company, Inc., New York, 1927), p. 28.

[4] *Handbook of Chemistry and Physics* (Chemical Rubber Publishing Company, Cleveland, Ohio, 1951–52), thirty-third edition, p. 573.

[5] F. D. Snell and C. T. Snell, *Colorimetric Methods of Analysis* (D. Van Nostrand Company, Inc., New York, 1936), p. 644.

[6] L. K. Narayanswamy, Trans. Faraday Soc. 31, 1411 (1935).

TABLE I. Gas yields from irradiated $NaNO_3$, KNO_3, and $KClO_3$.

Irrad. series	Substance	μ moles O_2 / g	Ev absorbed/g $\times 10^{-22}$	Molecules O_2/g $\times 10^{-19}$	Molecules O_2 / 100 ev	Remarks
Blank	$NaNO_3$	0.18	None	0.011		Stock crystals
H	$NaNO_3$	109, 118	1.97	6.56, 7.12	0.333, 0.361	20–40 mesh stock crystals
K	$NaNO_3$	143, 154	2.58	8.62, 9.28	0.334, 0.360	Stock crystals
E	$NaNO_3$	102–130	3.00	6.14, 7.83	0.205, 0.261	Stock crystals
J	$NaNO_3$	149	3.29	8.98	0.273	Harshaw
M	$NaNO_3$	130	5.38	7.83	0.145	Harshaw
P	$NaNO_3$	238	7.35	14.35	0.195	Harshaw
Blank	KNO_3	1.51	None	0.091		
G	KNO_3	309, 360	2.35	18.6, 21.7	0.79, 0.92	
Blank			None			
L	$KClO_3$	424	1.63	25.6	1.57	Powder in air
N	$KClO_3$	558–578	1.29	33.6, 34.8	2.60, 2.70	Crystals in vacuum

the energy absorption due to (1) heating by the fast neutron flux, (2) the energy absorbed from the gamma-ray flux, and (3) the energy absorbed from particles emitted by short-lived radioactive isotopes. Under category (3) the following were considered: the betas from Na^{24}, K^{42}, Cl^{38}, and the proton from the *n,p* reaction on N^{14}. Because of the size of the sample tubes the particles were considered to be completely absorbed in the samples. Further, gammas generated in the samples were neglected as not being appreciably absorbed. The estimates showed that the gamma-flux (magnitude derived from calculations by Primak of this laboratory) gave the greatest energy absorption, being 66, 72, and 87 percent of the total energy absorption for $NaNO_3$, KNO_3, and $KClO_3$, respectively. Primak has estimated a gamma-flux of 540 rep/sec in an aqueous sample in the thimble we used in CP-3 when the pile was run at 300 kw. We have not corrected this figure for the gammas generated in the water since we also ignored the gammas originating in our own samples.

From Table I the absorbed energy is most effective in $KClO_3$, less effective in KNO_3, and least effective in $NaNO_3$. Allen and Ghormley's *G* value for $Ba(NO_3)_2$ of about 0.1 molecules gas/100 ev is slightly lower than the values estimated for $NaNO_3$ in Table I. The agreement with Allen and Ghormley may be considered quite satisfactory, especially as Narayanswamy[6] finds that the order of decreasing effectiveness of ultraviolet light ($\lambda < 2500$A) in dissociating nitrates is the same as that found above for ionizing radiation, namely, $KNO_3 > NaNO_3 > Ba(NO_3)_2$. In Table I it would also appear that the *G* value falls off for higher total absorbed energies, which conforms to the conclusion of Allen and Ghormley in Van de Graaff irradiations.

The variation in decomposition yield for the potassium, sodium, and barium nitrates must be due to factors related to crystal structure, since the N—O bond strength does not vary appreciably.[7] For example, an O atom in dissociating from a NO_3^- not only requires energy to break the N—O bond but probably needs additional energy to push aside other adjacent ions. Thus, from the densities of KNO_3 and $NaNO_3$ and the crystal radii[8] of K^+ and Na^+ one finds about 20 percent more space is available per nitrate ion in the KNO_3 than in the $NaNO_3$ crystal. The greater space available may partially account for the higher yield in the potassium salt.

The higher yield in $KClO_3$ must be in part due to the weaker Cl—O bond (2.38 ev average bond strength or 2.0 ev to split off O_2+O) as compared to the N—O bond in the nitrates. Heal[9] finds a high yield also in $KClO_4$ irradiated with x-rays. His initial yield is about 4 molecules of O_2/100 ev or somewhat larger than our value for $KClO_3$.

Since oxygen, which is produced in the irradiation of nitrate crystals, is paramagnetic, measurements of the magnetic susceptibility of irradiated nitrate should yield information on the form in which the oxygen is retained in the crystal. For example, if the oxygen is trapped in the crystal in the monatomic form, the number of unpaired electrons would be twice as great as for the same amount of oxygen in the molecular form. Nitric oxide is also a possible paramagnetic product, but since chemical analysis above showed no significant amount of nitrogen dioxide, NO can be neglected.

Goldsmith measured the magnetic susceptibility of a sample of Baker and Adamson reagent grade powdered potassium nitrate unirradiated and after two weeks' irradiation in an evacuated quartz tube in CP-3. The apparatus (Gouy method) and calibration have been described elsewhere.[10] Spectrographic analysis of the unirradiated sample showed no appreciable impurities, especially those such as iron which might interfere with magnetic measurements. Similar analysis after irradia-

[7] From the data of F. R. Bichowsky and F. D. Rossini [*Thermochemistry of the Chemical Substances* (Reinhold Publishing Corporation, New York, 1936), pp. 128 and 142] and L. Pauling [*The Nature of the Chemical Bond* (Cornell University Press, Ithaca, New York, 1942), p. 61] the N—O bond strength is 3.65 ev in sodium nitrate crystals and 3.66 ev in barium nitrate.

[8] L. Pauling, *The Nature of the Chemical Bond* (Cornell University Press, Ithaca, New York, 1942), p. 346.

[9] H. G. Heal, private communication.

[10] M. Goldsmith, J. Chem. Phys. **18**, 523 (1950).

tion showed no contamination during irradiation. The gram susceptibility of the powdered unirradiated potassium nitrate was found to be $-0.333\pm0.003\times10^{-6}$ independent of temperature or field strength, where the precision index indicates the most probable deviation of a single determination.[11]

The change in the gram susceptibility produced by the pile irradiation follows the Curie-Weiss law. The equation obtained by the method of least squares, $\Delta\chi=[249/(T+14.9)]\times10^{-6}$, is illustrated in Fig. 1. Since the molal Curie constant[12] of molecular oxygen is 1.00, this result corresponds to 249 micromoles of gaseous oxygen per gram of KNO_3 if one assumes that oxygen is the only paramagnetic substance present. The $\Delta\chi$ at 75.6°K predicted by this Curie-Weiss equation is 2.73×10^{-6}, whereas the average of our experimental values at this temperature is 2.14×10^{-6}. We believe this falling off from the Curie-Weiss Law is due to liquefaction of oxygen gas; indeed, the susceptibility of 249 micromoles of liquid oxygen[13] is 2.10×10^{-6} at 75.6°K.

In the same irradiated nitrate as was used for susceptibility studies the noncondensable gas found by direct measurement of gas released by melting was 235 micromoles/g, which is only 5.6 percent less than the 249 micromoles O_2/g from magnetic susceptibility. Further, the magnetic susceptibility of a melted sample indicated that 6 micromoles of O_2/g had not been released. If this 6 micromoles is subtracted from the 249 from susceptibility, then the magnetic measurement and the direct gas measurement of O_2 agree to 3.3 percent, which discrepancy is within experimental error. This agreement shows that the oxygen is trapped in the crystal as molecular gaseous oxygen, and that since the oxygen accounts for essentially all the paramagnetism, the amounts of other paramagnetic atoms or radicals trapped after irradiation must be quite small. In this connection Allen and Ghormley[1] have suggested that the small amount of H_2 gas they obtained by dissolving

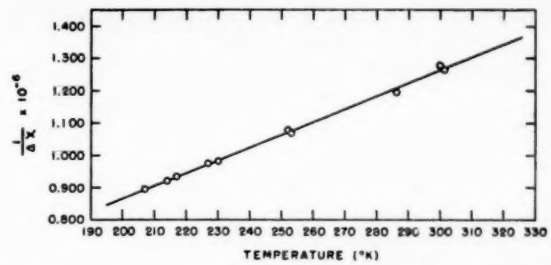

FIG. 1. The irradiation-induced change in the magnetic susceptibility of potassium nitrate as a function of the temperature of measurement.

irradiated $Ba(NO_3)_2$ in water originated in the reaction of trapped electrons with water.

C. Physical State of the Trapped Oxygen

The magnetic measurements above indicate that the trapped oxygen exists in the gaseous state. Just how the oxygen is trapped in the crystal is a point of some interest. Examination of freshly irradiated transparent Harshaw $NaNO_3$ crystals with the optical microscope revealed no gas pockets as large as 0.25μ, while experiments with the electron microscope were inconclusive. Spherical holes were observed in heated sodium nitrate crystals using the optical microscope, the holes ranging up to 3μ in the sample of column 5, Table II. (The *N* series $KClO_3$ did show visible holes although the size was generally less than 0.2μ.)

The size of the gas pockets was estimated by an approximate method. In this method the crystals were crushed and the fraction of total oxygen gas which was released by crushing was measured. The crushed crystals were sieved into fractions and weighed in order to estimate the new area opened by crushing. The hole radius can be calculated if one assumes that the gas pockets are uniformly distributed, and that any pocket will release its gas if its center lies within one radius of the new surface. In general one expects the hole sizes to

TABLE II. Size of oxygen gas occlusions in irradiated nitrates as determined by crushing and sieving experiments.

Irradiated sample	*B*−KNO_3	*E*−$NaNO_3$	*J*−$NaNO_3$		
			Unheated	2 hr 255°	80 min 302°
Total gas (μ moles/g)	280	101.8	148.5	106.1	144.5
Gas released by crushing (μ moles/g)	8.93	6.14	5.17	38.9	41.8
Initial area (cm^2/g)	42.8	59.8	0.9	1.1	<1.0
Area after crushing (cm^2/g)	291.5[a]	278.4[a]	220.0[a]	365.2[a]	163.6
Density (g/cc)	2.109	2.261[b]	2.248	2.220	2.046
Pocket diameter (μ)	12.2	2.44	1.41	9.2	17.7
Distance between pocket centers (μ)			6.35	28.4	31.1
Pockets/cc$\times10^{-7}$			390	4.4	3.3
Pressure in pockets (atmos)[c]			1400	318	76

[a] Most material in finest fraction.
[b] Exact density not determined.
[c] Estimated from perfect gas law and change in crystal density.

[11] A. G. Worthing and J. Geffner, *Treatment of Experimental Data* (John Wiley and Sons, Inc., New York, 1944), p. 167.
[12] E. Bauer and A. Piccard, J. phys. et radium **1**, 97 (1920).
[13] H. K. Onnes and A. Perrier, Proc. Roy. Acad. Sci. Amsterdam **12**, 799 (1910).

TABLE III. Noncondensable gas yields from x-radiation of sodium nitrate.

Peak x-ray voltage	g $NaNO_3$	Molecules gas $\times 10^{-18}$	100 ev absorbed $\times 10^{-18}$	$G = \frac{\text{molecules gas}}{100\text{ ev}}$
49	0.271	2.67	9.88[a]	0.27
25	1.144	1.77	4.64[b]	~0.38

[a] Estimated from measurements with $FeSO_4$ dosimeter.
[b] Estimated from relative energy output at 25 kv and 49 kv using Kramer's formula [Phil. Mag. **14**, 836 (1923)].

be overestimated. The results are summarized in Table II, and show that transparent irradiated $NaNO_3$ crystals contain the oxygen in many small gas pockets,[14] and that when these crystals are heated the pockets grow and coalesce, the crystals expanding at the same time so that the pressure in the pockets decreases. The pocket diameters seem to indicate oxygen molecules diffuse past several thousand atoms at the temperature of irradiation.

D. X-Ray Experiments

The yield estimates of Table I are based on the total energy absorbed by the nitrate crystals, without regard as to whether the source of the energy was heavy particles or light particles (including recoil electrons from γ-rays). However, the trapped oxygen may be produced by two rather different processes. First, the NO_3^- ion may receive sufficient energy through excitation or ionization to break an N—O bond. Second, an energetic particle may displace oxygen atoms through elastic collisions. The first process must occur to some extent since ultraviolet light decomposes nitrates. However, if the second process were more efficient than the first, then most of the trapped oxygen in pile-irradiated samples might have its origin in atoms displaced by collision. Although this possibility seemed unlikely, it was considered worth investigation. Electrons are advantageous for the determination of atom displacement energies, because an energetic electron can give only a small fraction of its energy to the heavier atom.

For a relativistic electron of energy E the maximum kinetic energy, T_{max}, it can give to a struck atom in a head-on collision is

$$T_{max}=[E(E+2\mu c^2)]\Big/\left[\mu c^2\left(\frac{M}{2\mu}+\frac{\mu}{2M}+1+\frac{E}{\mu c^2}\right)\right],$$

where μ = mass of electron, M = mass of struck atom, c = velocity of light, and T and E are kinetic energies which do not include rest energies. If an activation energy ϵ_d must be given to a struck atom before it can be displaced from its lattice position, then ϵ_d may be set equal to T_{max} to solve the above equation for E_{min}, the minimum energy the electron may have and still displace an atom by elastic collision. Suppose that x-rays are used with maximum energies less than E_{min}; then, if elastic collision is the main source of oxygen in pile irradiation, much lower yields of oxygen should be obtained in the x-radiated nitrate samples. Two experiments carried out using the Machlett AEG-50 x-ray tube are shown in Table III.

The N—O bond strength in the NO_3^- ion is 3.7 ev from thermochemical data,[7] and ϵ_d, the activation energy for displacement of oxygen atoms, cannot be less than this.[15] In the first irradiation of Table III electrons of 49 kv energy cannot displace oxygen atoms if the activation energy is greater than 7.04 ev. Since the activation energy may well be this large, and since only a small fraction of the photoelectrons will have 49 kv of energy, the O_2 observed must arise largely from electronic ionization and excitation processes. However, the observed yield per unit energy absorbed is quite similar to that found for pile irradiation (Table I), suggesting that in pile-exposed samples also knock-on processes are not the major source of trapped oxygen, because most of the gamma- and beta-energy absorbed in pile samples causes electronic ionization and excitation. Since a 26.4-kv electron is required to give a maximum of 3.7 ev to an oxygen atom by elastic collision, none of the oxygen in the 25-kv x-radiation of Table III can originate in elastic collisions. The yield within experimental error, however, is the same as observed for pile samples.

TABLE IV. Miscellaneous pile irradiations.

Compound	Color irradiated salt	Remarks
K_2SO_4	Buff-yellow	No bubbling on solution in water.
Li_2SO_4	Light buff	
$CaCO_3$ (calcite)	Dark gray-brown	No change in density.
$KBrO_3$		Crystals have considerable occluded gas after electron bombardment.

E. Irradiation of Other Salts

Samples of alkali sulfates and $CaCO_3$ (calcite) irradiated two weeks in CP-3 changed color but did not evolve much gas. See Table IV.

The authors wish to thank M. Goldsmith, who made the very careful magnetic susceptibility measurements.

[14] Occlusion of the gaseous decomposition products of solids is apparently rather unusual. However, G. Hennig [Master's thesis, University of Buffalo, Buffalo, New York (1941)] found $K_3[Mn(C_2O_4)_3]\cdot 3H_2O$ and $K_3[Co(C_2O_4)_3]\cdot 3H_2O$ decomposed thermally with similar trapping of CO_2.

[15] In the present case if one considers only the nitrate ion and neglects the forces holding the nitrate ion in position, then the work of H. Suess [Z. physik. Chem. **B45**, 312 (1940)] shows that only the fraction (NO_2 mass)/(NO_3 mass) of the initial recoil energy of the O atom is available for rupture of the NO bond.

Some Absorption Bands in the Far Infrared*

J. KENNETH O'LOANE†
Mallinckrodt Chemical Laboratory, Harvard University, Cambridge 38, Massachusetts
(Received September 29, 1952)

The following bands have been located in the far infrared spectra by the method of residual rays: *cis*-dichloroethylene at 170 cm^{-1}; *trans*-dichloroethylene at 265 cm^{-1} and 192 cm^{-1}; phosphorus trichloride at 190 cm^{-1}; *trans* and "*gauche*" 1,2 dichloroethane at 223 cm^{-1} and 125 cm^{-1}; propylene at 177 cm^{-1}; acetaldehyde at 245 cm^{-1} and 120 cm^{-1}; methyl alcohol at 190 cm^{-1}, 161 cm^{-1}, and 120 cm^{-1}; carbon suboxide at 192 cm^{-1}.

I. INTRODUCTION

FOR investigation of the far infrared region (less than 400 cm^{-1}) there are at present five main methods available: prism spectrometry, grating spectrometry, focal isolation, total reflection,[1] and residual rays.[2]

With prism spectroscopy still restricted to the region above 250 cm^{-1},[3] the instrument of choice below 250 cm^{-1} is the grating spectrometer with a set of echelette gratings.[4] Where this, together with the extremely sensitive and stable detector and amplifier required, is not available, the method of residual rays may be used.

Although this does not enable one to sweep over a continuous spectrum, as with the prism or grating instruments, and has little resolution, it does give a relative abundance of energy, enabling a search for absorption bands in a region of the spectrum otherwise not open to convenient investigation.

The purpose of the present study was to search for fundamental frequencies of certain inorganic and organic substances below 250 cm^{-1}. Because of the low resolution of the method, we have studied compounds which had, as far as could be foreseen, only one band in the far infrared, or compounds in which two bands are widely separated.

II. THE APPARATUS

Radiation from a Globar was passed through a monochromator arranged so that the heat rays could be reflected three or four times from crystal surfaces before being focused on a thermocouple.

The design of the monochromator is essentially that of Strong,[5] which has the great advantage over that of previous workers of allowing the use of very small pieces of crystals ($\frac{1}{2}$ in.–$\frac{3}{4}$ in. in diameter *vice* 3 in.–4 in.), as well as ease in changing them. Besides this mechanical convenience, the short time required for changing crystals prevents upsetting the thermal equilibrium of the apparatus.

The absorption cell was arranged in a manner similar to that of Strong's[6] vacuum spectrograph, with both windows at one end of the cell and a mirror inside the cell. The optical path length within the cell was about 30 cm. In order not to disturb the focus, the absorption cell, though readily detachable, was not removed during a run; it was filled and evacuated from an auxiliary vacuum line.

The windows of the absorption cell were 0.5-mm quartz cut perpendicular to the optical axis. Quartz was used instead of high melting Kahlbaum paraffin (mp 68–72°C)[7] because of the thickness required to prevent cracking when the cell is evacuated and because paraffin has a tendency to absorb organic vapors, causing the appearance in the spectrum of spurious lines. The windows were not polished, but were left "fine ground" (the last stage before polishing is begun by the use of American Optical Company fine grinding emery (M303½). The slightly rough surfaces help filter out short wavelength radiation.[8]

In preliminary tests on the apparatus a thermocouple made by Dr. Donald F. Hornig of the Metcalf Laboratory, Brown University, was used. The final thermocouple, constructed by Mr. Cecil Harris of Arthur D. Little Company, Cambridge, Massachusetts,[9] is a compensated two-junction couple having targets of gold leaf 2.0×3.6 mm in cross section and 0.6μ thick with a weight of 1.18 mg/cm^2. This is just large enough to

* This research was made possible, in part, through support extended Harvard University by the Navy Department, U. S. Office of Naval Research, under Office of Naval Research Contract N 5 ori-76, T.O.V.

† Present address: Department of Chemistry, University of New Hampshire, Durham, New Hampshire.

[1] F. Jentzsch and G. Laski, *Geiger-Scheels Handbuch der Physik* (J. Springer, Berlin, 1926–1928), Vol. 19, p. 802.

[2] E. H. Nichols, Ann. Phys. Chem. **60**, 401 (1897); Phys. Rev. **4**, 297 (1897); H. Rubens and E. F. Nichols, Ann. Phys. Chem. **60**, 418 (1897); Phys. Rev. **4**, 314 (1897); J. Strong, Phys. Rev. **37**, 1565 (1931) and **38**, 1818 (1931).

[3] E. K. Plyler, J. Chem. Phys. **15**, 885 (1947); W. L. Hyde, J. Chem. Phys. **16**, 744 (1948).

[4] H. M. Randall, Rev. Sci. Instr. **3**, 196 (1932); H. M. Randall and F. A. Firestone, Rev. Sci. Instr. **9**, 404 (1938); V. Z. Williams, Rev. Sci. Instr. **19**, 135 (1948); Oetjen, Haynie, Ward, Hansler, Schauwecker, and Bell, J. Opt. Soc. Am. **42**, 559 (1952).

[5] John Strong, Phys. Rev. **38**, 1820 (1931).

[6] J. Strong, Rev. Sci. Instr. **3**, 810 (1932).

[7] L. Kellner (geb. Sperling), Z. Phys. **56**, 215 (1929); R. B. Barnes, Phys. Rev. **39**, 562 (1932); M. Parodi, *Recherches dans L'Infrarouge Lointain par la Méthode des Rayons Restants* (Hermann et Cie., Paris, 1938), pp. 90–92.

[8] Most of the cutting and polishing of the crystals and mirrors was done by the A. D. Jones Optical Works, Cambridge, Massachusetts.

[9] For assistance in the design of this thermocouple we are indebted to Dr. R. M. Hainer of Arthur D. Little Company.

cover the Globar image. The targets were gold blacked.[10] The positive wire is Bi95Sn5, the negative Bi97Sb3, both having a diameter of 0.001 inch.

To prevent the paraffin window from sagging in and touching the targets, a grid of very fine wires was soldered to the brass head. For the window a disk of Kahlbaum paraffin (mp 68°–72°C) 2 mm thick and smooth on both sides was put over the grid and fused to the brass head. No coating was used to make it gas tight. The thermocouple was evacuated continuously to 10^{-5} mm.

Radiation reflected three times from sodium chloride windows gave a deflection of 6.5 cm (scale at 225 cm) when the thermocouple was connected directly to a Leeds and Northrup High Sensitivity Galvanometer, No. 2284B and when no quartz windows or other filters were used on the absorption cell.

To amplify the signal when the quartz windows and other filters were in, a Perkin-Elmer Breaker Type DC Amplifier, Model No. 53, with an input impedance of five to twenty ohms to match the thermocouple, was used.

The Leeds and Northrup High Sensitivity Galvanometer was used as a recording instrument. Although this is ill-matched to the Perkin-Elmer amplifier, it could be used in conjunction with a pi-type filter circuit and shunt resistance. Under favorable conditions the minimum detectable signal was 0.001 microvolt.

To remove the near infrared radiation a combination of two methods was used. The Kahlbaum paraffin window of the thermocouple is itself a fairly efficient filter for the near infrared.[7] Barnes and Bonner's curves[11] show that 2 mm of this material transmits only about two percent between 10 000 cm^{-1} and 1000 cm^{-1} and then begins to open up slowly.

Since Kahlbaum paraffin has not been readily available since the war, some tests were made on other paraffins. The three used were "Texwax," an ordinary paraffin for home canning made by Texaco Company; paraffin, refined, for embedding, mp 56–58°C, A. H. Thomas Company; paraffin, white, filtered, imported, mp 68–72°C, Fisher, Eimer, and Amend. Our results paralleled those of Kellner and Parodi.[7] Although measurements were made to only 500 cm^{-1}, the lower melting paraffins were found to have a smaller transmittance and to open up more slowly in the 500 cm^{-1} region. Miss A. Reiter of Baird Associates ran 1.0-, 1.7-, and 2.4-mm samples of both the Fisher and Kahlbaum paraffins from 5000–600 cm^{-1}. Her results agree well with those of Barnes and Bonner, and the close coincidence of the curves led her to conclude they are the same paraffin.

A paraffin filter with a smooth front and back surface can be obtained by casting the molten wax in a brass ring of proper thickness resting on a sheet of aluminum foil supported by plate glass. As soon as it is poured, a second sheet of aluminum foil is laid over the top and a piece of plate glass set on top of it. After standing half an hour the foil can be stripped off, leaving a shiny flat surface. Filters cast where the upper surface is free always have the top surface rather sandy in appearance.

In the region between 500–330 cm^{-1} a reflectance filter of LiF is more effective in increasing the far infrared/near infrared ratio than Kahlbaum paraffin would be. It reflects nearly the same percentage of the near infrared as the paraffin transmits, but reflects about 80 percent or better of the radiation between 500 and 330 cm^{-1}, where the transmittance of the paraffin is 40–50 percent.

Between 330 and 250 cm^{-1} the reflectance curves for CaF_2 and NaF[12] suggest they would be better reflectance filters than LiF. At 250 cm^{-1} LiF reflects 35 percent, CaF_2, 60 percent, and NaF nearly 80 percent, the two latter giving nearly double the signal.

The second method of filtering, used in conjunction with the Kahlbaum paraffin, was a modification of Rubens' "transparent shutter." Rubens' method consists in placing in the beam a material transparent to the near infrared and observing the deflections with shutter in and out of the beam. Rubens kept his shutter in the path most of the time, but since there is danger that the filter, placed near the entrance window, will begin to radiate on being heated,[13] if kept in position too long, a modification of the procedure was used, so that the shutter was in for only the shortest possible interval.

In using a "transparent shutter" it is necessary to remember that about ten percent of the near infrared is reflected from the surfaces of the filter when the filter is in. When the filter is removed from the path, this additional light falls on the thermocouple. We have

$$0.9\lambda_{\text{short}}=A\,;\quad \lambda_{\text{short}}+\lambda_{\text{long}}=B\,;\quad \lambda_{\text{long}}=B-A/0.9.$$

As a shutter we used 1.3 mm of NaCl, which cuts off at about 340 cm^{-1}.

Four sets of crystals were used: aragonite cut perpendicular to the c axis (001 sections) and cleavage faces of NaCl, KCl, and KBr, with filters recommended by Schaefer and Matossi,[14] except that the total quartz thickness for aragonite was 1.0 mm instead of 0.4 mm, which should not affect the reflectance maximum significantly. The reflectance maxima for these crystals fall at 244, 192, 161, and 120 cm^{-1}, respectively.

For sodium and potassium chlorides, and potassium bromide the band breadths in terms of the half-width were estimated from the intensity of blackbody radia-

[10] L. C. Roess and E. N. Dacus, Rev. Sci. Instr. **16**, 164 (1945); Aiken, Carter, and Phillips, Rev. Sci. Instr. **17**, 377 (1946); Harris, McGinnies, and Siegel, J. Opt. Soc. Am. **38**, 582 (1948).

[11] R. B. Barnes and L. G. Bonner, J. Opt. Soc. Am. **26**, 433 (1936).

[12] M. Czerny and H. Röder, Ergeb. exakt. Naturw. **17**, 70 (1938).

[13] H. S. Seifert and H. M. Randall, Rev. Sci. Instr. **11**, 365 (1940).

[14] C. Schaefer and F. Matossi, *Das Ultrarote Spektrum* (J. Springer, Berlin, 1930) p. 60.

tion, the transmittance of Kahlbaum paraffin, and the transmittance of quartz (cut perpendicular to the optical axis) to be 212–169 cm^{-1}; 177–148 cm^{-1}; and 135–111 cm^{-1}, respectively.

Some confusion concerning the reflectance maxima of aragonite has arisen in the literature because the German letters a, b, and c used by Liebisch and Rubens[15] have been taken by the International Critical Tables[16] and others to be equivalent to the English *a*, *b*, and *c* axes, the crystallographic axes. Where ICT[16] refer to the *a*, *b*, and *c* axes of aragonite, they should, instead refer to the *c*, *a*, and *b* axes, respectively.

III. FAR INFRARED ABSORPTION BANDS

(A) *cis*-Dichloroethylene, $C_2H_2Cl_2$

This compound has been most recently investigated in the far infrared by Bernstein and Ramsay,[17] who have succeeded, with Raman data from Herzberg,[18] in assigning all twelve of the fundamental frequencies of *cis*-dichloroethylene to their proper species, assuming it to be a simple planar molecule belonging to point group C_{2v}.

At 173 cm^{-1} there is a Raman active frequency which has been designated $\nu_5(A_1)$, using Herzberg's system of numbering. If this is correct, this totally symmetric vibration should be active also in the infrared.

We have examined the spectrum of the vapor at 220 mm pressure and found absorption at 192 and 161 cm^{-1}. The *cis*-dichloroethylene used was Columbia Organic Chemicals Company, bp 58–60°C.

The stronger absorption found with KCl mirrors indicates the frequency lies nearer the KCl band than the NaCl, as it should if the Raman frequency is correct.

The region between 400 and 270 cm^{-1} has been examined by Hyde,[19] who found no bands in the vapor, but a weak (20 percent) absorption in the liquid at 405 cm^{-1}. This would seem to be $\nu_7(A_2)$, inactive in the infrared in the vapor, active in the Raman at 406 cm^{-1}.

(B) *trans* dichloroethylene, $C_2H_2Cl_2$

Bernstein and Ramsay[17] have also investigated this molecule in the infrared. With Raman data from Herzberg they have assigned ten of the twelve fundamental frequencies, assuming the molecule to be a simple planar one of point group C_{2h}.

From Bernstein's rotational product rule[20] the in-plane bending frequency $\nu_{12}(B_u)$ was estimated to be at 280 cm^{-1}. From combination bands, $\nu_{12}(B_u)$ and the out-of-plane torsional frequency $\nu_7(A_u)$ were estimated to be at 265 cm^{-1} and 192 cm^{-1} from observations in the liquid phase. Both these frequencies are inactive in the Raman.

Examination of the spectrum of the vapor at 260 mm pressure showed absorption at 244, 192, and 161 cm^{-1}. The *trans*-dichloroethylene used was Columbia Organic Chemicals Company, bp 47–49°C.

It seems highly improbable that these results could be due to the presence of only one band, for the bandwidth would have to be enormous (*ca* 150 cm^{-1}). It seems reasonable, however, to conclude the existence of the 192 cm^{-1} and 265 cm^{-1} bands suggested by Bernstein. The latter might be just visible with a KRS-5 prism, particularly if a reflectance filter of NaF were used to strengthen the signal.

TABLE I. Far infrared absorption bands (percent absorption).

	Pressure mm	Reststrahlen crystals: Aragonite 244 cm^{-1}	NaCl 192 cm^{-1}	KCl 161 cm^{-1}	KBr 120 cm^{-1}
cis dichloroethylene	220	0	13	18	0
trans dichloroethylene	260	75	18	8	0
phosphorus trichloride	140	?	18	5	0
carbon suboxide	580	0	9	9	0
1,2 dichloroethane	90	91	45	28	76
methyl alcohol	50	···	95	84	79
propylene	760	?	29	24	0
acetaldehyde	210	14	20	30	42
n-pentane	500	···	0	0	0
n-hexane	160	0	0	0	0

(C) Phosphorus Trichloride

The four fundamentals at 510, 480, 257, and 190 cm^{-1} [21] should be both infrared and Raman active if the assignment of the symmetrical pyramidal form, point group C_{3v}, is correct.

Since the intensity of the ammonia frequency ν_4 corresponding to the ν_4 of PCl_3 at 190 cm^{-1} is given by Herzberg[22] as very strong, and the vapor pressure is high, this seemed an especially good compound to test the behavior of the instrument at 190 cm^{-1}, a region in which we were particularly interested in connection with carbon suboxide.

Examination of the spectrum with Mallinckrodt analytical reagent gave the results in Table I. The precision of this set of measurements was the worst of any taken.

The presence of the 190 cm^{-1} band, which should be active in the infrared for a symmetrical pyramidal structure, is clearly shown.

(D) Carbon Suboxide, C_3O_2

A search was made for the very strong fundamental postulated near 190 cm^{-1} by Lord and Wright.[23]

The fundamental infrared frequencies in the region examined by Lord and Wright agreed fairly well with

[15] Th. Liebisch and H. Rubens, Sitzber. Preuss. Akad. Wiss. 1919, 198, 876; 1921, 211.
[16] *International Critical Tables* (McGraw-Hill Book Company, Inc., New York), Vol. 5, p. 259.
[17] H. J. Bernstein and D. A. Ramsay, J. Chem. Phys. 17, 556 (1949).
[18] G. Herzberg, *Infrared and Raman Spectra of Polyatomic Molecules* (D. Van Nostrand Company, Inc., New York, 1945), p. 330.
[19] W. Lewis Hyde, thesis, Harvard University, 1948.
[20] H. J. Bernstein, J. Chem. Phys. 17, 256 (1949).
[21] Reference 17, p. 164.
[22] Reference 17, p. 295.
[23] R. C. Lord, Jr., and N. Wright, J. Chem. Phys. 5, 642 (1937).

those predicted by Engler and Kohlrausch[24] from calculations based on their Raman work. In assigning the two doubly degenerate bending vibrations $\nu_6(\pi_u)$ and $\nu_7(\pi_u)$ (Herzberg's notation), which are infrared active, Lord and Wright followed the suggestion of Engler and Kohlrausch that ν_7 should be in the region of 200 cm^{-1}. This was based on the hypothesis that the C=C=C bending constant should be approximately the same as the C=C=O bending constant. To explain the various combination tones observed, Lord and Wright finally made two alternative assignments: $\nu_7=200$ cm^{-1}, $\nu_6=550$ cm^{-1}, and $\nu_7=190$ cm^{-1}, $\nu_6=900$ cm^{-1}. This was necessary because the prism used did not have sufficient resolution to determine fully the nature of the combination bands.

Herzberg has questioned both assignments, preferring 557 cm^{-1} for ν_7 and 637 cm^{-1} for ν_6.

The carbon suboxide used was prepared by a modification of the method of Hurd and Pilgrim,[25] more attention being paid to the removal of ketene, which may constitute five to twenty-five percent of the raw product.[26] During the purification we discovered that at least one line, and possibly three, reported by Lord and Wright as those of carbon suboxide belong to ketene.[27] In the far infrared, only a weak absorption was found at 192 and 161 cm^{-1}. The spectrum of carbon suboxide has now been examined with fluorite, rock salt, KBr, and KRS-5 prisms, and the Raman is being studied. When this is completed, a reinterpretation of the spectrum will be attempted.

(E) 1,2 Dichloroethane

That rotational isomers of 1,2 dichloroethane exist is now well established,[28–30] as is also the fact that the isomers involved are the *trans*-configuration, with C_{2h} structure, and probably a "*gauche*"-form, belonging to group C_2, with an azimuthal angle between the C−Cl bonds of 60°.

Mizushima, Morino, and co-workers have recently estimated, by comparison of statistical and third law entropies, that the torsional oscillation about the C−C axis should have a frequency of about 90 cm^{-1}. Allowing for errors in calculation they assign the Raman line of 125 cm^{-1} as the torsional frequency of the *gauche*-molecule. The corresponding mode in the *trans*-molecule, active in the infrared, inactive in the Raman, they believe to have the same frequency.

If the 125 cm^{-1} frequency really belongs to a molecule of configuration C_2, it should be active also in the infrared. However, electron diffraction and dipole moment measurements indicate only about twenty percent of the *gauche*-form in the vapor phase at room temperature.[30] Since the vapor pressure at room temperature is about 90 mm, it would probably be difficult to detect this frequency.

Fortunately, since the *trans*-configuration has a center of symmetry, the postulated frequency at 125 cm^{-1} should be active in the infrared. If strong absorption were observed in this region, it would almost certainly indicate that the vibration was due to the *trans*-form, because it constitutes eighty percent of the mixture.

A second frequency at 223 cm^{-1}, although forbidden in the Raman, has been observed by Mizushima,[31] who assigns it to the antisymmetric skeletal deformation frequency (δ_a in his notation) of the *trans*-molecule.

The material used was Eastman Kodak Ethylene Chloride, bp 83–84°C. The results show the existence of the band in the 125 cm^{-1} region predicted by Mizushima and co-workers, as also a band on the short wavelength side of the NaCl residual rays, probably corresponding to the 223 cm^{-1} frequency. Absorption of the KCl residual rays is probably due to overlap of the bands near KBr and NaCl.

The very strong absorption of the aragonite residual rays may be due to three factors: overlap from the 223 cm^{-1} band, overlap from the symmetric skeletal deformation frequency of the *gauche*-form at 265 cm^{-1}, and the first overtone of the torsional frequency of the *gauche* species.

(F) Methyl Alcohol

To observe low-lying, torsional-rotational modes, absolute methyl alcohol, Mallinckrodt analytical reagent, was examined with the NaCl, KCl, and KBr mirrors.

Burkhard[32] predicted the presence of about 200 lines in the far infrared between 50 cm^{-1} and 610 cm^{-1}, confirming their presence with the Michigan echelette grating instrument.

The regions around 190, 161, and 121 cm^{-1} where we observed strong absorption correspond to the envelope of clusters of lines observed by Burkhard and Dennison.

(G) Propylene

Of the twenty-one fundamentals of propylene, all infrared and Raman active, Wilson and Wells[33] have assigned fourteen between 417 cm^{-1} and 2000 cm^{-1} and

[24] W. Engler and K. W. F. Kohlrausch, Z. physik. Chem. **B34**, 214 (1936).
[25] C. D. Hurd and F. D. Pilgrim, J. Am. Chem. Soc. **55**, 757 (1933).
[26] Klemenc, Wechsberg, and Wagner, Monatsh. Chem. **66**, 337 (1935).
[27] H. Mackle and L. E. Sutton, Trans. Faraday Soc. **47**, 937 (1951).
[28] Reference 17, pp. 346–351.
[29] S. Mizushima and Y. Morino, Proc. Indian Acad. Sci. **8A**, 315 (1938).
[30] Mizushima, Morino, Watanabe, Simanouti, and Yamaguchi, J. Chem. Phys. **17**, 591 (1949).
[31] Mizushima, Morino, and Simanouti, Sci. Papers Inst. Phys. Chem. Research (Tokyo) **40**, 87 (1942).
[32] D. G. Burkhard, "Molecular Structure and Far Infrared Spectrum of Methyl Alcohol," dissertation (University of Michigan, Ann Arbor, Michigan, 1950); D. G. Burkhard and D. M. Dennison, Phys. Rev. **84**, 408–417 (1951).
[33] E. B. Wilson, Jr., and A. J. Wells, J. Chem. Phys. **9**, 319 (1941); J. J. Fox and A. E. Martin, Proc. Roy. Soc. (London) **A175**, 208 (1940); J. E. Kilpatrick and K. S. Pitzer, J. Research Natl. Bur. Standards. **38**, 191 (1947), R. P. 1768.

Fox[33] and Martin six above 2000 cm^{-1}. Kilpatrick and Pitzer[33] have recently re-examined the assignment of Wilson and Wells, changing it in only minor details.

The only frequency lying beyond the KBr range is the $C-CH_3$ twist, $\nu_{21}(A'')$ (Herzberg's notation), which Wilson and Wells tentatively placed at 177 cm^{-1}, assuming that a weak band at 755 cm^{-1} was a combination of this unknown frequency and the out-of-plane CH rock at 578 cm^{-1}.

Hyde[19] has examined the spectrum from 400 to 270 cm^{-1} with a KRS-5 prism, and suggests that the 407 cm^{-1} band may be double, but otherwise found no new bands, thus tending to confirm the original assignment.

Using Matheson Company cp propylene at one atmosphere pressure we obtained the results shown. The aragonite absorption is somewhat doubtful. Several attempts were made to detect a band in the 120 cm^{-1} region, since acetaldehyde, which has many resemblances to propylene, has a strong band there, but results were completely negative at one atmosphere.

The presence of a band with center about halfway between 192 and 161 cm^{-1} (i.e., about 175 cm^{-1}) is clearly evident.

(H) Acetaldehyde

The similarity between the spectra of propylene and acetaldehyde, pointed out by Morris,[34] and by Thompson and Harris,[34] indicated that the torsional frequency for the methyl group about the $C-CH_3$ axis might lie in about the same region as for propylene.

Our findings on Eastman Kodak Company acetaldehyde parallel those of Strong and Woo,[35] although an exact comparison cannot be made because of differences in path length and pressure. These authors made no assignment of frequencies.

Pitzer and Weltner[34] have revised the assignment of Morris to agree with the heat capacity determinations of Coleman and DeVries.[36]

Three of the weak bands not assigned by Morris at 1464, 1486, and 1541 cm^{-1} can be accounted for as combination tones involving a fundamental at 114 cm^{-1}. If this is the torsional frequency, the absorption of the KBr residual rays may be due to this, while the absorption of the NaCl residual rays may be the first overtone of it. This does not seem quite satisfactory, for, since the torsion frequency for the much heavier CH_2Cl-groups in dichloroethane lies at about 125 cm^{-1}, the lighter CH_3 group would be expected to have a higher frequency. Moreover, most of the frequencies of propylene and acetaldehyde lie much closer together, and the torsional frequency for the former seems to lie at about 175 cm^{-1}.

In the case of acetaldehyde-d_4, also studied by Morris,[34] there is a band of medium intensity at 860 cm^{-1} which must be re-assigned in the light of Pitzer and Weltner's re-interpretation. If this is taken as a combination band of the torsional frequency of CD_3 and the out-of-plane CD_3 rock at 730 cm^{-1}, the torsional frequency would be 130 cm^{-1}. From the Redlich-Teller product ratio, the corresponding frequency in acetaldehyde would be at 180 cm^{-1}, agreeing closely with that found for propylene.

Now that heat capacity measurements are available,[36] it might seem possible to get an estimate of the torsional frequency by subtracting the contributions of the known fundamentals from the experimental heat capacity. Unfortunately, the deviations from ideality are so large that it does not seem possible to distinguish between the contributions of torsional frequencies of 100, 200, 300, and 400 cm^{-1} (1.91, 1.84, 1.67, and 1.47 cal/mole deg, respectively). Using the assignment of Pitzer and Weltner, $C_p°$ is 11.63 cal/mole deg, exclusive of the torsional frequency at 25°C. The experimental value[36] is 14.8. Using the methods of Pitzer and Gwinn,[37] Pitzer and Weltner assumed a potential barrier to free rotation of 1000 cal/mole, giving a contribution to the heat capacity of 1.43 cal/mole deg, and requiring a correction of 1.7 cal/mole deg, or 11 percent, for gas imperfection.

The correction for gas imperfection, calculated from data of Alexander and Lambert[38] on the determination of the second virial coefficient of acetaldehyde is rather uncertain. It would not seem unreasonable that, with a torsional frequency near 200 cm^{-1}, giving a contribution to $C_p°$ of 1.84 cal/mole deg, the correction for gas imperfection should be 1.3 cal/mole deg, or 9 percent.

The absorption at 120 cm^{-1} may be, not the envelope of absorption due to pure rotation (which would lie in the microwave region), but the envelope of rotational changes parallel to the CH_3 axis coupled with changes in internal torsional levels, similar to the behavior Burkhard[32] found for methyl alcohol.

The torsional vibration should show up in the fine structure of the near infrared bands. It has been observed for methyl alcohol with a grating instrument, but has not been reported for acetaldehyde, probably because of lack of resolution.

(I) *n*-Hexane and *n*-Pentane

Assignment of frequencies for normal paraffin hydrocarbons has been hindered by ignorance of the low-lying frequencies.

Recently Gates[39] has attempted an analysis of the planar skeletal frequencies of ethane, propane, *n*-butane,

[34] J. C. Morris, J. Chem. Phys. 11, 230 (1943); Kenneth S. Pitzer and Wm. Weltner, Jr., J. Am. Chem. Soc. 71, 2842 (1949); H. W. Thompson and G. P. Harris, Trans. Faraday Soc. 38, 37 (1942).

[35] J. Strong and S. C. Woo, Phys. Rev. 42, 267 (1932).

[36] Charles F. Coleman and Thomas DeVries, J. Am. Chem. Soc. 71, 2839 (1949).

[37] Kenneth S. Pitzer and Wm. D. Gwinn, J. Chem. Phys. 10, 428 (1942).

[38] E. A. Alexander and J. D. Lambert, Trans. Faraday Soc. 37, 421 (1941).

[39] D. M. Gates, J. Chem. Phys. 17, 393 (1949); D. M. Simpson, private communication.

and *n*-pentane. Dr. Delia M. Simpson,[39] of Newnham College, Cambridge, has calculated skeletal frequencies for some of the longer chain paraffins, using rather accurate force constant data.

An attempt was made to locate the 186 cm^{-1} frequency calculated by Miss Simpson for *n*-hexane and the 190 cm^{-1} frequency predicted by Kassel[40] for *n*-pentane.

[40] Kassel *fide* K. S. Pitzer, J. Chem. Phys. **8**, 711 (1940).

Even with 50.0 cm pressure no absorption was found with *n*-pentane, nor, at 16.0 cm, was any found for *n*-hexane. Apparently one must use very long path lengths for these weak vibrations in the vapor phase.

ACKNOWLEDGMENT

I should like to thank Professor E. Bright Wilson, Jr., for suggesting this problem and for many helpful conferences.

THE JOURNAL OF CHEMICAL PHYSICS VOLUME 21, NUMBER 4 APRIL, 1953

The Fluorescence of Biacetyl Vapor*

HAROLD J. GROH, JR.†
Department of Chemistry, University of Rochester, Rochester, New York
(Received September 15, 1952)

It has been shown that the fluorescence of biacetyl vapor at 25°C excited with 3650A radiation does not decay as a simple exponential function of time. After flash excitation, there is a "fast" fluorescence followed by a slow exponential decay. The quenching of the fluorescence has also been studied at several temperatures, pressures, and in the presence and absence of oxygen gas. A consideration of this and previous work permits a further elucidation of the fluorescence phenomena in terms of two upper emitting states. Fluorescence from the state responsible for most of the fluorescence at room temperature is quenched strongly by oxygen and is apparently completely removed at 200°. Fluorescence from the other state is unaffected by oxygen and is still measurable at 200°.

THE effect of pressure on the quantum yield of fluorescence of biacetyl vapor shows an interesting variation with the wavelength of exciting light. It has been shown that for 3650A excitation the quantum yield increases apparently from zero at zero pressure to nearly the value obtained for 4358A excitation at a pressure of 50 mm.[1,2] Almy and Gillette report a quantum yield with 4047A or 4358A excitation equal to 0.145 and approximately independent of pressure. The quantum yield with 3650A excitation rises from zero at zero pressure to about 0.08 at 50-mm pressure. The difference in the pressure effects for different energies of excitation has been explained[2] by assuming that predissociation or some other monomolecular process, possibly "internal conversion," occurs with very great probability from a level between those reached by 3650A and 4358A excitation. Through the agency of collisions a molecule excited by 3650A radiation is "saved" for fluorescence from lower vibrational levels. In order to explain the long mean lifetime of biacetyl fluorescence (1.4 to 1.8×10^{-3} sec)[3,4] these authors proposed a metastable state just below the state reached on absorption. "Stabilized" molecules pass from the directly excited state into the metastable state from which they are enabled by thermal fluctuations to return to the lowest level of the initially excited state with subsequent fluorescence. This picture has been modified by Lewis and Kasha[5] in accordance with the theory that long-lived fluorescence in organic molecules is due to a direct "forbidden" transition from a triplet excited state to a singlet ground state.

These theories suggested that the fluorescence data could be extended with profit to include the effects of temperature, pressure, and admixture of oxygen gas. It was proposed to use the same techniques recently employed in a study of acetone vapor fluorescence,[6] namely, measurements of fluorescence decay rates and quenching studies.

EXPERIMENTAL

Eastman Kodak Company white label biacetyl was dried over anhydrous calcium sulfate, then vacuum distilled in an all-glass system. The middle third of the distillate was stored in the vacuum line behind a mercury cutoff. The storage bulb was kept at the temperature of dry ice to prevent polymerization of the biacetyl.

The two pieces of apparatus used to measure fluo-

* This work was supported in part by a contract with the U. S. Office of Naval Research, United States Navy.

† Eastman Kodak Company Fellow in Physical Chemistry at the University of Rochester during 1951–1952.

[1] F. C. Henriques and W. A. Noyes, Jr., J. Am. Chem. Soc. **62**, 1038 (1940).

[2] G. M. Almy and P. R. Gillette, J. Chem. Phys. **11**, 188 (1943).

[3] R. D. Rawcliffe, Rev. Sci. Instr. **13**, 413 (1942).

[4] W. E. Kaskan and A. B. F. Duncan, J. Chem. Phys. **18**, 427 (1950).

[5] G. N. Lewis and M. Kasha, J. Am. Chem. Soc. **67**, 994 (1945).

[6] Groh, Luckey, and Noyes (to be published).

rescence decay rates and fluorescence efficiencies have already been described.[6] In the lifetime apparatus light from the flash tube was collimated and passed through a Corning No. 5970 filter which has a broad peak with a maximum in transmission at about 3650A. This light was confined to a beam of less than a centimeter in diameter before entering the T-shaped, quartz fluorescence cell. Fluorescent light passed through Corning 3389 glass to eliminate scattered incident light before impinging on the 1P21 photomultiplier tube. In this work a DuMont Type 303 oscillograph was used to observe the photomultiplier signal.

The only modification in the quantum yield apparatus was the substitution of a spiral of glass tubing for the metal bellows previously used in the line to allow the fluorescence cell to be raised from the light path. Biacetyl polymerized rapidly on the metal surface. In this apparatus light from a Hanovia Alpine Burner was collimated and passed through Corning glasses 5860 and 7380 before entering the fluorescence cell. This filter combination gives fairly monochromatic 3650A light. The photomultiplier was again protected from incident light by a Corning 3389 glass. In experiments with added oxygen gas, the mixtures were stirred for at least an hour before measurement by means of an all-glass, magnetically driven stirrer.

The measurements of relative fluorescence yields were made without preradiation of the sample. Apparently, at the low light intensities used and with the large total volume of biacetyl compared to the volume actually illuminated in these experiments, anomalous effects of preradiation previously reported[2] were negligible.

RESULTS

Preliminary experiments showed that the fluorescence of biacetyl vapor at 25°C did not decay as a simple exponential function of time. After flash excitation there was a "fast" fluorescence followed by a slow, exponential decay. This behavior is similar to that observed in acetone vapor.[6]

The mean life of the slow fluorescence was estimated to be roughly 2×10^{-3} sec and is doubtless the "simple exponential" decay reported by Rawcliffe[3] (1.4×10^{-3} sec), Almy and Anderson[7] (1.65×10^{-3} sec), and Kaskan and Duncan[4] (1.8×10^{-3} sec), while the fast fluorescence reported here was not observed by those workers. The mean life of the short-lived component is probably less than 8×10^{-6} sec, the mean duration of the source flash. In these experiments care was exercised to eliminate stray effects which might be mistakenly interpreted as fluorescence from biacetyl, e.g., scattered incident light, fluorescence of quartz, fluorescence of filters. The intensity of the fast signal was always compared with a measurement of the background obtained by flashing the light on the empty cell. Any increase in background due to Rayleigh scattering when biacetyl vapor filled the cell was shown to be negligible compared to the decrease caused presumably by absorption of the light scattered from the cell walls. The blank determination thus actually overcompensated for background.

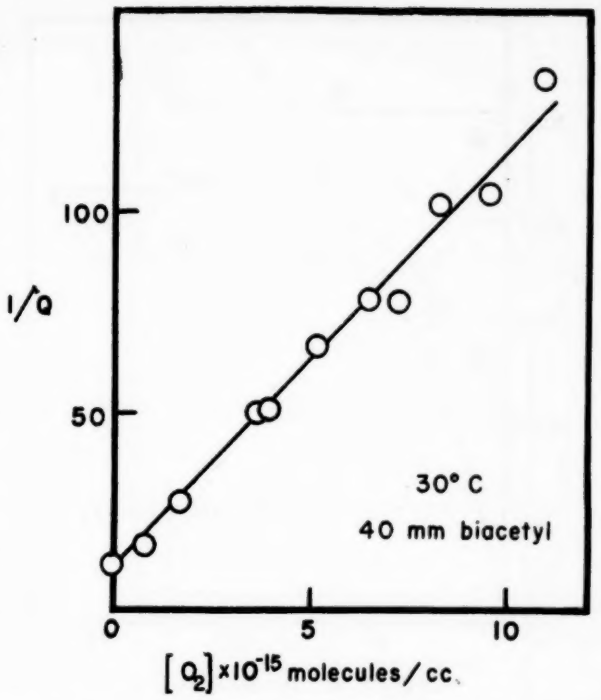

FIG. 1. Inverse of fluorescence efficiency of biacetyl *versus* oxygen concentration at low oxygen pressures.

It was also found that the long-lived component was quenched strongly by oxygen, in agreement with the data of Kaskan and Duncan,[4] whereas the fast decay seemed unaffected by even 8-mm pressure of oxygen. By interposing interference filters in the fluorescent light path it was shown that the slow fluorescence lies mostly at wavelengths greater than 5000A, while the fast lies mostly between 4000 and 5000A.

A study of the quenching by oxygen showed that (Fig. 1) at 30°C and 40-mm biacetyl pressure a plot of inverse relative fluorescence efficiency $1/Q$ *versus* oxygen pressure follows a Stern-Volmer relationship up to about 350 microns oxygen pressure. The slope of this line is 6.48×10^{9} (moles/cc)$^{-1}$. At higher oxygen pressures the slope of the curve decreases until $1/Q$ reaches a constant value (Fig. 2) independent of oxygen pressure. The limiting yield apparently corresponds to the fast component in the lifetime experiment. From Fig. 2 it can be seen that the effect of increasing temperature is to destroy both fluorescences; but the oxygen-sensitive portion is removed faster than the oxygen-insensitive portion until at 200°C, there is no effect of oxygen on $1/Q$.

The oxygen quenching curves suggested that the effect of biacetyl collisions on both fluorescences might

[7] G. M. Almy and S. Anderson, J. Chem. Phys. 8, 805 (1940).

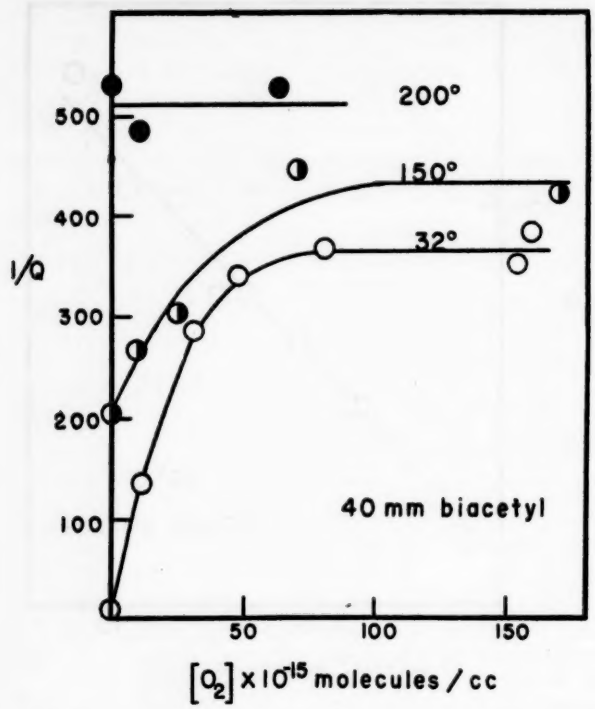

FIG. 2. Inverse of fluorescence efficiency of biacetyl *versus* oxygen concentration at several temperatures.

be learned by studying the inverse of relative fluorescence efficiency as a function of biacetyl pressure in the absence of oxygen. Since fluorescence from the oxygen sensitive state accounts for most of the low temperature fluorescence, a plot of $1/Q$ *versus* biacetyl pressure at 30°C will represent essentially the pressure effect on this state. At 200° the behavior of the oxygen-insensitive state may be studied. At 150°C, an intermediate temperature where the two fluorescences are of equal importance, the behavior of $1/Q$ as a function of biacetyl pressure will be complex. Figure 3 shows the results. The ordinates in Figs. 1, 2, and 3 were measured merely as relative values. Comparison of the 30° curve in Fig. 3 with the absolute values given by Almy and Gillette[2] at this temperature shows that the ordinates are approximately the absolute values of inverse yields. The possible effects of wavelength shifts in the fluorescence as oxygen is added or the temperature is raised make this comparison less accurate. At 200°C, if the fluorescence is chiefly around 4600A, the values of $1/Q$ should be multiplied by about 1.3 to give absolute values.

DISCUSSION

Before attempting to explain the results obtained in this work, the following facts must be considered:

(1) The absorption spectrum of the vapor consists of bands from 4007 to 4670A. At higher pressures an apparent continuum which extends from about 4000A to nearly 3500A has been observed. Fluorescence excited by absorption in this region has been long known to consist mainly of three bands with maxima at about 5100, 5600, and 6100A. Attempts to extend to longer wavelengths the absorption spectrum of biacetyl in the visible region by the use of a long path length were unsuccessful.‡ Instead it was shown[8] that the fluorescence spectrum extends down to the longest wavelength absorption band since a fluorescence band is found at about 4600A. Thus, there is no gap between absorption and fluorescence bands for this molecule, but instead an overlap region.

(2) With 3650A excitation, the quantum yield[9] of the major product CO probably increases marked with increasing biacetyl pressure at low pressures at 30°C and reaches a nearly constant value of about 0.03 at pressures near 20 mm. Using 4358A light, the same behavior is noted at both 30° and 75°. Comparison of this work with experimental data obtained by Blacet and Bell[10] at 2654A leads to the tentative conclusion that the secondary reactions are the same in all cases. Since no such trends in the CO yield as a function of pressure are predicted by the secondary reactions, we may conclude that the variation of the CO yield actually indicates the trend of the primary quantum yield.

It seems possible to explain all of these data within the general framework of previous mechanisms, but with several important modifications. The following steps can be shown to account for the facts:

$$B+h\nu=B' \tag{1}$$

$$B'=B \tag{2}$$

$$B'+B=D+B \tag{3}$$

$$B'+B=B^*+B \tag{4}$$

$$B'+B=B^{**}+B \tag{5}$$

$$B^*(+B)=(2)B(+D) \tag{6}$$

$$B^*=B+h\nu^* \tag{7}$$

$$B^{**}=B+h\nu^{**} \tag{8}$$

$$B^{**}=B \text{ or } D \tag{9}$$

$$B^{**}+O_2=?. \tag{10}$$

The role of collisions seems to be to save the initially excited molecules, represented by B', for decomposition as well as for both fluorescences, from B^* and from B^{**}. B^* probably represents a lower vibrational level of the same electronic state as B', while B^{**} is almost certainly a different electronic state. The sum of these processes,

‡ Private communication from Professor A. B. F. Duncan, Chemistry Department, University of Rochester.

[8] Private communication from Dr. G. W. Luckey, concerning unpublished work done at University of Rochester. See G. W. Luckey and W. A. Noyes, Jr., J. Chem. Phys. **16**, 407 (1948).

[9] This work was done by Mr. Edwin D. Becker in this laboratory. Preliminary results were reported at the Meeting of the Faraday Society in Toronto, September 8-9, 1952.

[10] Preprint to the Discussions of the Faraday Society held in Toronto, September 8 and 9, 1952.

however, accounts for only a small part of the total absorbed energy. The fate of the initially excited molecules at low pressures where presumably little decomposition or fluorescence occurs cannot be specified with certainty. It seems probable, however, that step (2) is a radiationless deactivation to the ground state by "internal conversion." The fluorescence occurring by reaction (7) is the fast decay, probably accounting for the blue part of the fluorescence spectrum. Step (8) accounts for the intense green bands which are predominant at low temperatures. Step (6) is merely included as a possibility. Step (4) followed by Step (6) would be indistinguishable from (3) alone. Step (9) could also lead unimolecularly to decomposition products, but a bimolecular deactivation of B^{**} is excluded by Kaskan's[4] data which show that the lifetime is independent of biacetyl pressure at low temperatures.

From this mechanism it is seen that the expression for the primary decomposition, if the possible contributions of (6) and (9) are neglected, is

$$\Phi=\frac{k_3B}{k_2+(k_3+k_4+k_5)B}. \tag{11}$$

Thus the quantum yield of decomposition increases from zero as a nonlinear function of pressure. An expression of the same form will be obtained if contributions from (6) and (9) are considered in addition to, or in place of, reaction (3). Steady-state assumptions lead to the following expression for the total fluorescence:

$$Q=\frac{I_f}{I_a}=\frac{\alpha k_7}{k_7+k_6B}+\frac{\beta k_8}{k_8+k_9+k_{10}O_2} \tag{12}$$
$$=Q^*+Q^{**},$$

where α = the fraction of B' which is converted to B^* and β = the fraction of B' which is converted to B^{**}. Since α and β depend on pressure in a manner similar to Eq. (11), the total fluorescence efficiency and the fluorescence efficiency of each state will both increase from zero at zero pressure as a nonlinear function of pressure.

Unfortunately, in the absence of quantitative information about the importance of steps (6) and (9) an evaluation of the individual constants cannot be made. In terms of this mechanism the slope of the plot in Fig. 1 is given by $k_{10}/\beta k_8=6.48\times10^9$ moles^{-1} cc. By determining the inverse mean life as a function of oxygen pressure, Kaskan[4] has determined the absolute value of $k_{10}=5.14\times10^{11}$ moles^{-1} sec^{-1} cc at 25°C. Thus, $\beta k_8=79.2$ sec^{-1}. This quantity can be estimated in another way. At 27°, 4358A and 50 mm pressure

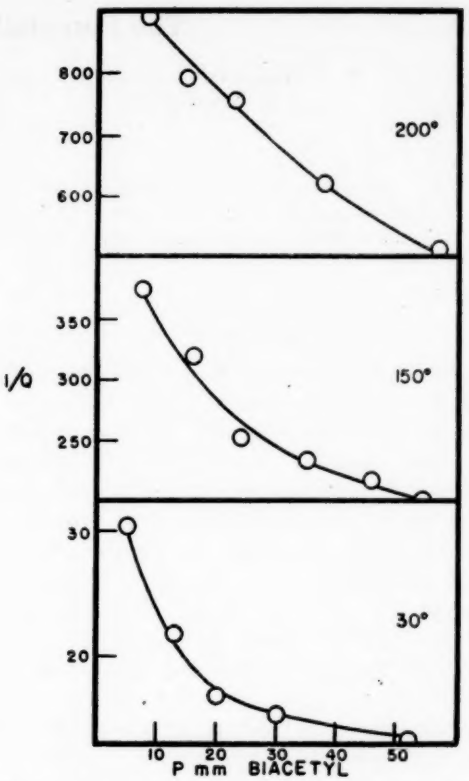

FIG. 3. Inverse of fluorescence efficiency of biacetyl *versus* biacetyl pressure.

Almy[2] gives the value 0.145 as the quantum yield of fluorescence. Under identical conditions Kaskan gives a lifetime of 1.8×10^{-3} sec. At low temperatures the efficiency of fluorescence is given approximately by

$$Q^{**}=\beta k_8/(k_8+k_9+k_{10}O_2)=\beta k_8\tau^{**},$$
$$0.145=\beta k_8\times1.8\times10^{-3},$$
$$\beta k_8'=80.6 \text{ sec}^{-1},$$

as compared with the value of 79.2 sec^{-1} above. Since these two values of βk_8 were obtained from oxygen quenching data and in the absence of O_2, respectively, it seems that oxygen does not affect the distribution between B^* and B^{**}.

In this mechanism excitation with 4358A light would simply raise a molecule to the state represented by B^* instead of B'. Thus (4) is unnecessary and (5) may be replaced by $B^*\rightarrow B^{**}$, since little collisional deactivation is necessary. By a bimolecular process, step (6) accounts for the dissociation. Dissociation thus increases with pressure but the quantum yield of fluorescence is practically independent of biacetyl pressure.

The author wishes to thank Mr. Edwin D. Becker for performing the photochemical experiments. This work is being continued and will be published later.

THE JOURNAL OF CHEMICAL PHYSICS VOLUME 21, NUMBER 4 APRIL, 1953

The Potential Function of Ethylene*†

BRYCE L. CRAWFORD, JR., JOHN E. LANCASTER,‡ AND RICHARD G. INSKEEP§
School of Chemistry, University of Minnesota, Minneapolis, Minnesota
(Received August 20, 1952)

The infrared spectrum of *a*-$C_2H_2D_2$ has been obtained, and the vibrational frequencies used to complete the calculation of the force constants of C_2H_4. The spectra of C_2H_3D, *trans*-$C_2H_2D_2$, and a mixture of *cis*- and *trans*-$C_2H_2D_2$ were also observed and used to check the force-constant calculations.

INTRODUCTION

RECENTLY, Arnett and Crawford[1] proposed a new assignment of fundamentals for C_2H_4 and C_2D_4 and calculated force constants for the out-of-plane motions. The complete solution of all the planar force constants in the most general potential function requires the vibrational data of a third isotopic ethylene, since the three totally symmetric (A_{1g}) frequencies of C_2H_4 and C_2D_4 provide only five independent relations for the solution of six force constants. We have prepared *asymmetric*-dideuteroethylene, and from a study of its infrared spectrum have made an assignment of frequencies and completed the calculation of force constants for ethylene. C_2H_3D occurred as an impurity in the *a*-$C_2H_2D_2$ preparation; enough of its spectrum was identified to make an assignment for this molecule. We were also fortunate in obtaining some *trans*-dideuteroethylene, and so observed its infrared spectrum as well as the spectrum from a *cis-trans* mixture prepared from the pure *trans* sample. Partial assignments were possible in these cases, and these contributed valuable additional information.

EXPERIMENTAL

Our procedure for the preparation of *a*-$C_2H_2D_2$ was essentially that of Clusius and co-workers,[2,3] and hence will not be described in detail here. Briefly, it consists of the electrolysis of an aqueous solution of CH_3CD_2COOD, which is in turn prepared by repeated exchange of methyl-malonic acid ($CH_3CH(COOH)_2$) with D_2O, followed by decarboxylation.[4]

According to Clusius, possible impurities are butane-d_x (8 percent) and ethane-d_x (3 percent). Indeed, two or three bands observed in the infrared spectrum of the crude sample disappeared completely on fractionation. Ethane-d_x would not be so easily removed as butane-d_x by this method; but ethane is a weak absorber and, in amounts less than 3 percent, would not cause any difficulty. Furthermore, the mass spectrum of the low-boiling fraction did not indicate appreciable quantities of any molecules appropriate to a deuterated ethane.

One possible impurity was C_2H_3D, owing to incompletely deuterated propionic acid. Careful examination of the spectrum confirmed its presence (see discussion in the next section). Therefore, a second preparation, using only a partial deuteration, was carried out so that all C_2H_3D bands in the first spectrum might be identified. Mass-spectrum analyses were made of both samples; the first contained about 5–10 percent C_2H_3D, and the second had the composition 40 percent *a*-$C_2H_2D_2$, 45 percent C_2H_3D, 15 percent C_2H_4. The second sample enabled us to identify nearly all the fundamentals of C_2H_3D.

Dr. B. S. Rabinovitch of the University of Washington transmitted to us a sample of *trans*-$C_2H_2D_2$, which he prepared by the direct addition of H_2 to C_2D_2 using a chromous chloride solution as catalyst, according to the scheme of Patterson and du Vigneaud.[5] The purity of the sample we received was stated to be 98 percent or better.

Finally, the *trans* compound was isomerized to an equilibrium mixture of *cis*- and *trans*-dideuteroethylene containing about 50 percent *trans* and 50 percent *cis*.

The infrared absorption spectra of all four samples are shown in Figs. 1 through 4. They were all obtained on a Perkin-Elmer 12C spectrometer. KBr, NaCl, and LiF prisms were used; a CaF_2 prism was also used to confirm the band contours in the 6μ region. The rocksalt spectra were obtained with a continuous slit drive adjusted to give approximately constant energy. The background "I_0" curve, run with evacuated cell, is shown in each case. Dry N_2 was flushed throughout the entire path length to remove most of the water vapor, while an ascarite trap in the N_2 line completely eliminated CO_2

* From a thesis submitted by John E. Lancaster to the University of Minnesota in partial fulfillment of the requirements for the degree of Doctor of Philosophy.

† We are grateful for the financial support received from the U. S. Office of Naval Research.

‡ Present address: American Cyanamid Company, Stamford, Connecticut.

§ Present address: Brown University, Providence, Rhode Island.

[1] R. L. Arnett and B. L. Crawford, Jr., J. Chem. Phys. **18**, 118 (1950).

[2] P. Holeman and K. Clusius, Ber. deut. chem. Ges. **70** (1), 819 (1937).

[3] A. Kruis and W. Schanzer, Z. Phys. Chem. **A191**, 301 (1942).

[4] The methyl malonic acid is obtained from the ester, which is made by a straight forward malonic ester synthesis. The ester preparation will contain malonic ester and dimethyl malonic ester; a pure methyl malonic acid is obtained by converting the esters to the diamides before saponification and acidification. (See R. Meyer and P. Bock, Ann. **347**, 93 (1906) and E. Fischer and A. Dilthey, Ber. deut. chem. Ges. **35**, 844 (1902).) Otherwise, the final gaseous electrolytic product will contain propylene as well as ethylene.

[5] W. I. Patterson and V. du Vigneaud, J. Biol. Chem. **123**, 327 (1938).

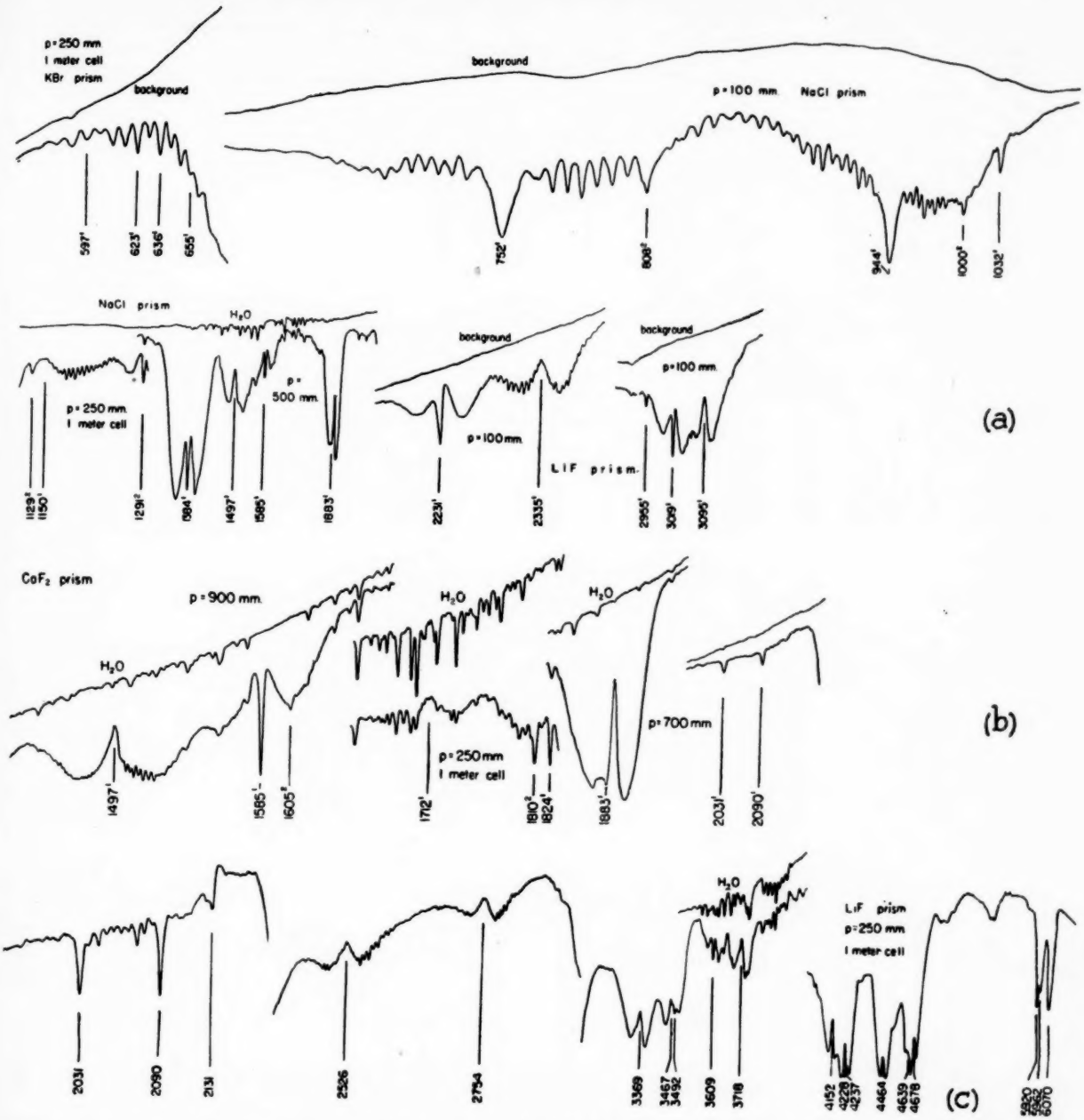

FIG. 1. The infrared spectrum of a-$C_2H_2D_2$. The first two rows (KBr, NaCl, and LiF prisms) show the most prominent features of the spectrum. The third row (CaF_2 prism) shows the 5–6μ region under greater dispersion. The bottom row (LiF prism) shows the weak bands in the overtone region. Both a one-meter cell and a 10-cm cell were used; where it is not specifically noted on the curve, the latter cell was used. Bands marked 1 arise from a-$C_2H_2D_2$; those marked 2 arise from C_2H_3D.

absorption. Appropriate cell lengths and pressures were used in each region; these are indicated on the figures. Frequencies were corrected to vacuum conditions and read to the nearest cm^{-1}.

SYMMETRY RELATIONS AMONG THE ISOTOPES

Ethylene and tetradeuteroethylene possess V_h symmetry, while the partially deuterated ethylenes have C_{2v}, C_{2h}, or C_s symmetry; each of these point groups is a subgroup of V_h. The relation is shown diagrammatically in Fig. 5, where the composition of the species of the isotope of lower symmetry in terms of the species of C_2H_4, as well as all of the normal vibrations contained therein, and their activities and band-types, is clearly indicated.

DISCUSSION OF THE SPECTRA

Asymmetric $C_2H_2D_2$ and C_2H_3D

Figure 1 shows the infrared spectrum of the a-$C_2H_2D_2$ sample; Fig. 2 the spectrum of the C_2H_3D-enriched

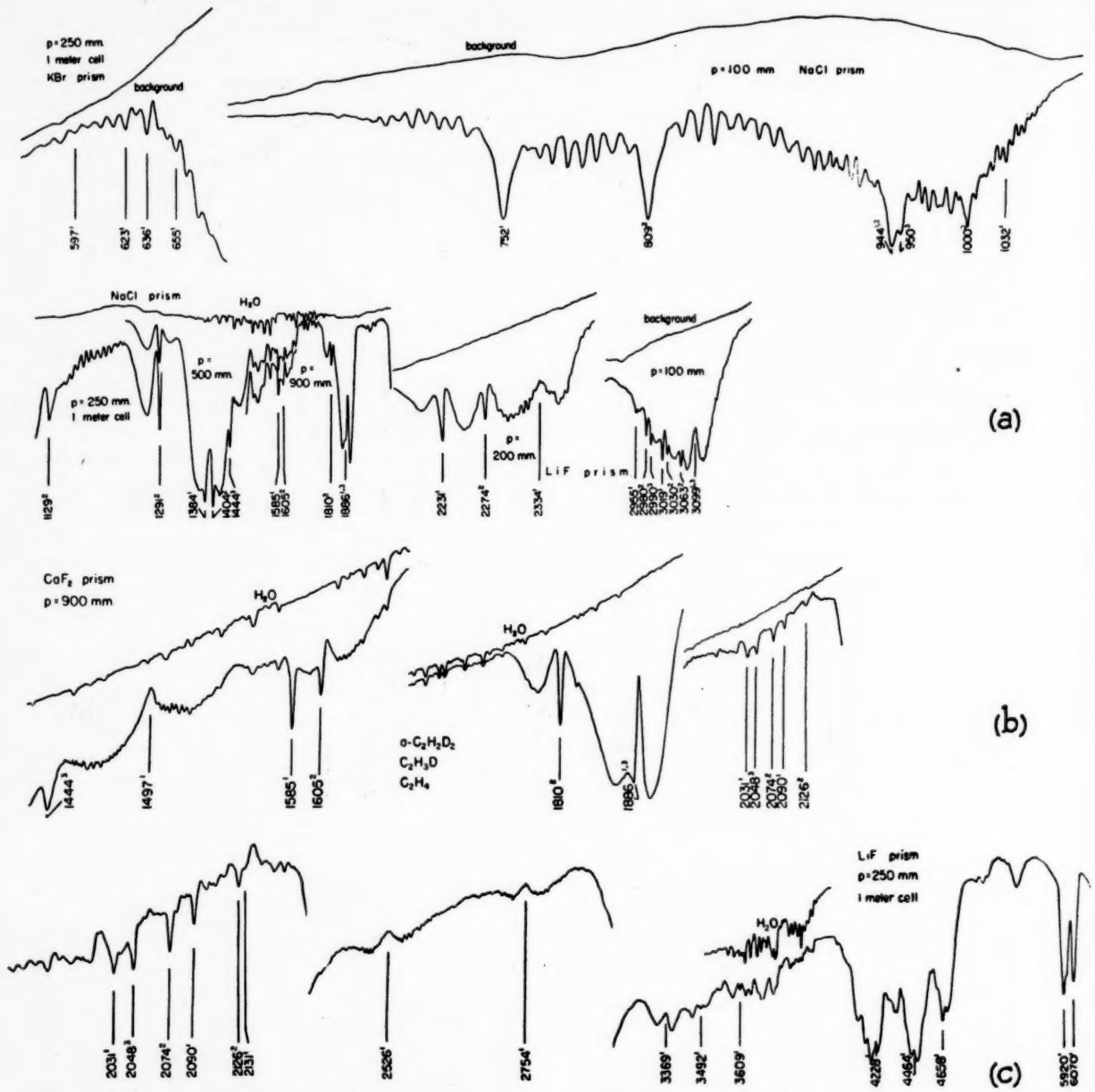

FIG. 2. The infrared spectrum of the mixture of a-$C_2H_2D_2$, C_2H_3D, and C_2H_4. With regard to the manner in which the curves are displayed and the notation concerning cell length, the scheme in Fig. 2 follows that of Fig. 1. Bands marked 1 arise from a-$C_2H_2D_2$, those marked 2 arise from C_2H_3D, and those marked 3 are produced by C_2H_4.

sample. Comparison of the two spectra clearly identifies the absorption due to each isotopic molecule. Some of the strong bands of C_2H_4 are also to be found in Fig. 2. The identification of each band is indicated in the figures. A complete list of the frequencies of observed bands for both molecules, including overtones, is given in Tables I and II, together with a possible assignment. All of the nonplanar frequencies (type C bands) are seen to agree very closely with the predictions of Arnett and Crawford. In C_2H_3D, ν_8 is not directly observed, as it coincides with ν_8 of a-$C_2H_2D_2$ and C_2H_4; however, it was reported at this position by Courtoy *et al.*, in a sample of pure C_2H_3D.[6] In a-$C_2H_2D_2$, there are five totally-symmetric (A_1) frequencies, each of which should appear as a type A band. These should occur at frequencies associated with a C—H stretch, C—D stretch, C=C stretch, CH_2 deformation, and CD_2 deformation, and all are immediately found near the expected frequencies. The CD_2 deformation ν_3, 1032 cm^{-1}, has only a Q branch visible in the R branch of ν_8. These five frequencies check the product rule with the corresponding frequencies in C_2H_4. There should be four

[6] Courtoy, de Hemptinne, and Migeotte, J. Chem. Phys. 19, 137 (1951).

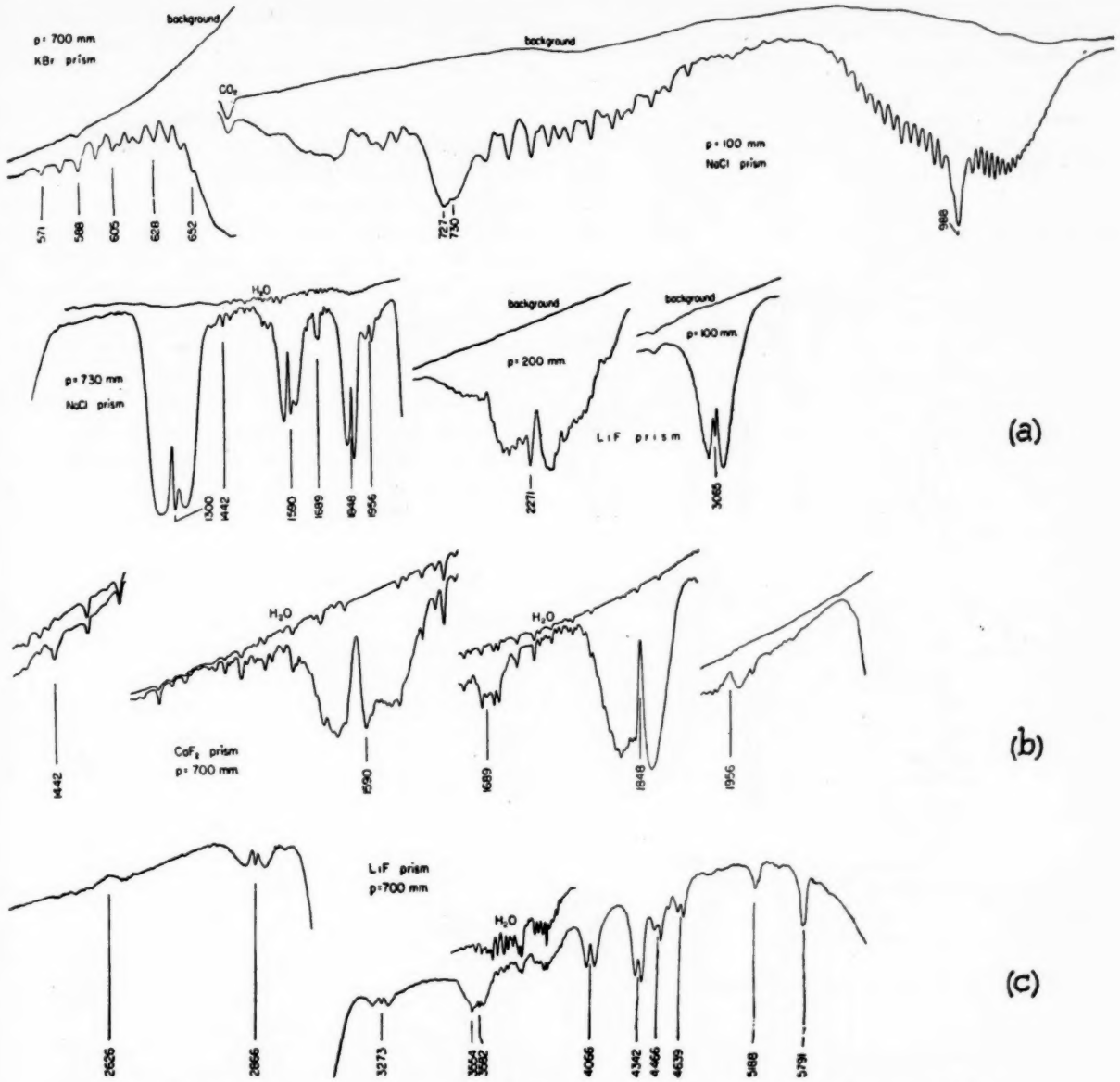

FIG. 3. The infrared spectrum of *t*-$C_2H_2D_2$. With regard to the manner in which the curves are displayed the scheme in Fig. 3 follows that of Fig. 1. A 10-cm cell was used.

B_1 (type *B*) bands; five are observed. The product rule with C_2H_4 eliminates the 1497 band as a fundamental; it remains difficult to explain. We have assigned it as a difference band, although the fit is not good. The fundamental at 1150 (ν_6) is seen to be very weak. The product rule places ν_{10} at 676 cm^{-1}, but the actual band center is not clear, since it underlies the *P* branch of the very strong ν_7.

In C_2H_3D, all the planar vibrations give hybrid type *A*-*B* bands. All of the fundamentals are seen except ν_8, which has already been discussed, and ν_{10}, both of which were seen by Courtoy *et al.* Several of the bands have been observed in the Raman effect;[7] these are indicated in Table II. Only one combination tone is well defined for C_2H_3D.

Trans-$C_2H_2D_2$ and the Mixture of *cis*- and *trans*-$C_2H_2D_2$

These spectra are not quite so rewarding as the spectra just discussed; first, because only half the *trans* fundamentals are active in infrared, and second, the *trans* absorption overlies most of the *cis* absorption in the spectrum of the mixture. The curves are shown in Figs. 3 and 4, and are summarized in Tables III and IV. In *trans*-dideuteroethylene, ν_7 must overlie some other absorption, judging from the great irregularity of the contour and the strong shoulder on the *Q* branch at 730

[7] de Hemptinne, Jungers, and Delfosse, J. Chem. Phys. **6**, 319 (1938).

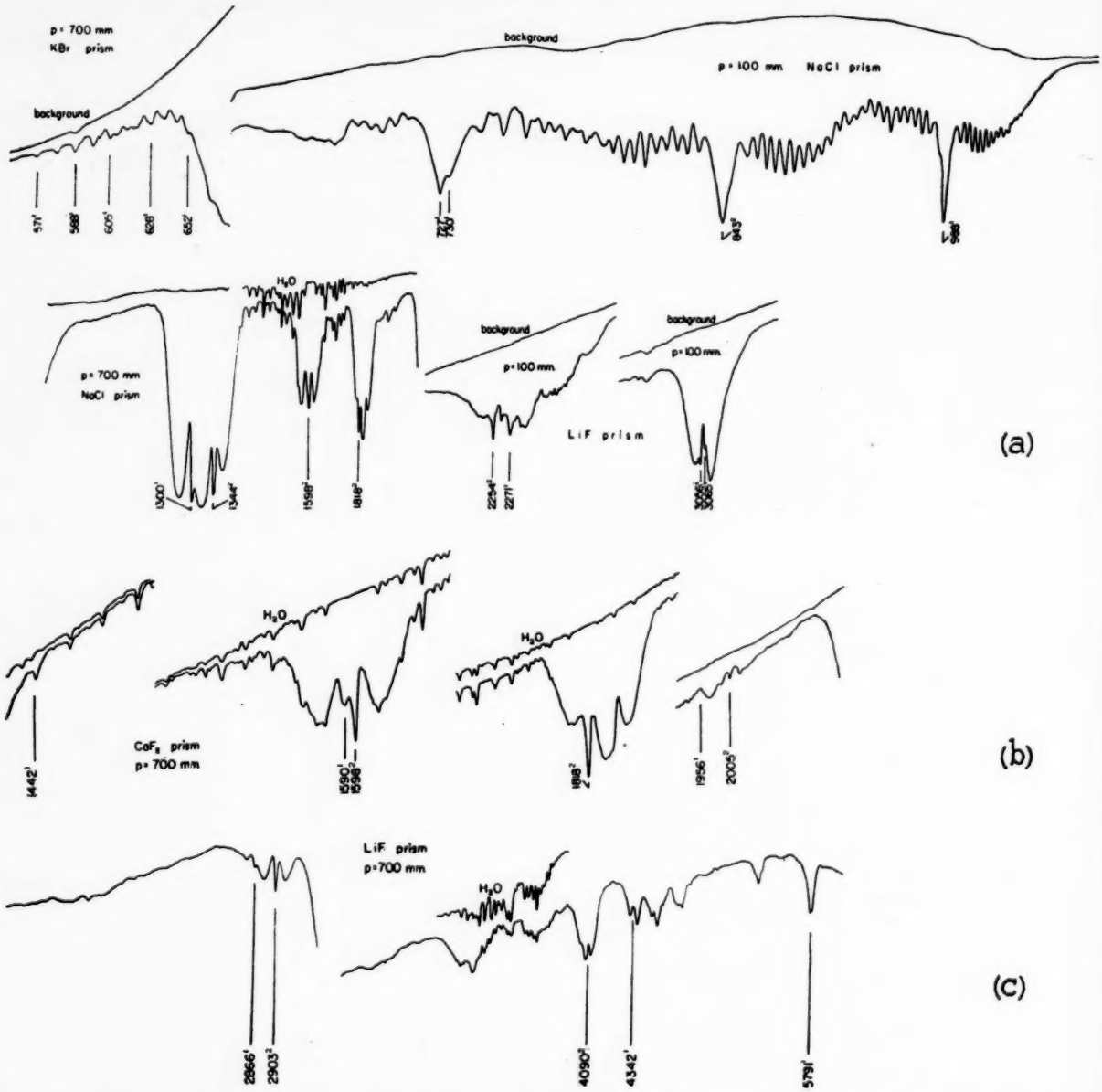

FIG. 4. The infrared spectrum of the mixture of t-$C_2H_2D_2$ and c-$C_2H_2D_2$. With regard to the manner in which the curves are displayed, the scheme in Fig. 4 follows that of Fig. 1. A 10-cm cell was used. Bands marked 1 arise from t-$C_2H_2D_2$; those marked 2 arise from c-$C_2H_2D_2$.

cm^{-1}. In *trans*-$C_2H_2D_2$, we find that the active planar vibrations yield hybrid A–B bands. These are readily observed, but ν_{10} is somewhat obscure. There seem to be two progressions of rotational structure in the KBr region; one with a center near 625–630 cm^{-1}, the other near 660 cm^{-1}. The latter is selected for ν_{10}, since this agrees closely with the product rule calculations. The remaining B_u fundamentals are well defined. Very little additional information was obtained by considering the overtones, together with the Raman data of de Hemptinne taken on a *cis-trans* mixture.[7]

The appearance of ν_7 of *cis*-$C_2H_2D_2$ at 843 cm^{-1} shows the presence of the *cis* compound in the isomerization product. In spite of the strong *trans* absorption, the type A bands are visible, so that the B_1 vibrations are identified except ν_6, which is calculated to be 1041 cm^{-1} from the product rule. Figure 4 shows there is indeed a small irregularity now in the R branch of ν_4 of *trans*-$C_2H_2D_2$ at exactly 1041 cm^{-1}. The KBr region shows no sign of ν_{10}, nor does ν_3 appear. A longer path length would probably locate it between ν_7 and ν_{12}.

Shortly after this work was completed, Charette and de Hemptinne published their recent paper on the deuteroethylenes.[8] They observed pure samples of C_2D_4,

[8] J. Charette and M. de Hemptinne, Bull. classe Sci. 37, 436 (1951).

C_2H_3D, and C_2HD_3 as well as an impure *a*-$C_2H_2D_2$ and a mixture of *cis*- and *trans*-$C_2H_2D_2$ in both the Raman and infrared. Nearly all of their observations agree closely with ours. In C_2D_4, they find ν_{10} at 584, very close to the predicted value of Arnett and Crawford. Their C_2H_3D was purer than ours; they were able to make a more certain assignment in the 3000 cm^{-1} region. On the other hand, our sample of *trans*-$C_2H_2D_2$ was purer than theirs; the two bands they observed in the 600–700 cm^{-1} region both belong to the *trans* compound, whereas they assign them as ν_{10} of *cis* and *trans*. They also missed the great complexity of the 727 cm^{-1} band in the *trans*. Most of our other differences occur in locating exactly the center of ν_{10} in any of the molecules under study. It is gratifying to notice that some of their newly reported Raman lines are at frequencies in close agreement with those provided by our force-constant calculations. Many of their observations are incorporated in Table VI.

The Force Constants

The mathematical basis for the present work has been set up by Arnett and Crawford, and the complete $\tilde{G}$ and $\tilde{F}$ matrices, corresponding to a set of symmetry coordinates which are in turn linear combinations of a convenient set of "valence" coordinates, are presented for all the ethylene isotopes in Tables V and VI of their paper.[9]

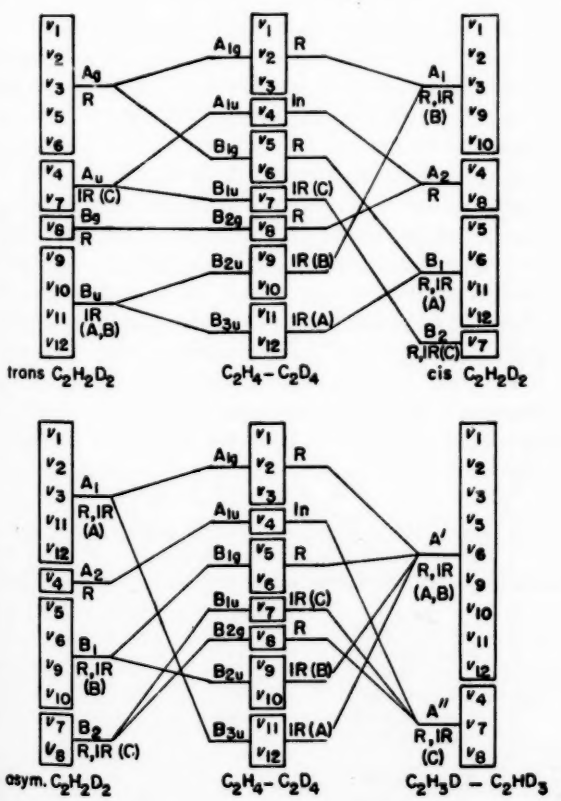

FIG. 5. Symmetry classification of the vibrations of ethylene and of its isotopic derivatives.

TABLE I. Bands observed in the *a*-$C_2H_2D_2$ spectrum.

ν	Type	Intensity	Assignment; comments
676	*B*	*w*	ν_{10} band center uncertain
752	*C*	*vs*	ν_7
808	*C*	*w*	ν_7 of C_2H_3D
944	*C*	*vs*	ν_8
1000	*C*	*w*	ν_4 of C_2H_3D
1032	*A*	*m*	ν_5 underlies ν_8
1129	*A–B*	*vw*	ν_3 of C_2H_3D
1150	*B*	*vw*	ν_6 *P* branch obscured; band center uncertain
1291	*A*	*w*	ν_6 of C_2H_3D
1384	*A*	*s*	ν_{12}
1497	*B*	*w*	$\nu_{11}-\nu_{10}=1555$; $\nu_4+\nu_2-\nu_7=1522$
1585	*A*	*w*	ν_2
1712	*B*	*vw*	$\nu_3+\nu_{10}=1708$
1824	*A?C?*	*vw*	$\nu_6+\nu_{10}=1826$
1883	*A*	*m*	$2\nu_8=1888$
2031	*A?C?*	*vw*	$\nu_4+\nu_6=2040$
2090	*A?C?*	*vw*	$\nu_7+2\nu_{10}=2104$ (Type *C*)
2131	*A?C?*	*vw*	$\nu_7+\nu_{12}=2136$ (Type *C*)
2231	*A*	*m*	ν_{11}
2335	*B*	*m*	ν_5
2526	*B*	*vw*	$\nu_6+\nu_{12}=2534$
2754	*B*	*vw*	$\nu_2+\nu_6=2735$, $2\nu_3+\nu_{10}=2740$
2955	*A*	*w*	$\nu_2+\nu_{12}=2969$
3019	*A*	*m*	ν_1
3095	*B*	*m*	ν_9
3169	*A?*	*vw*	$2\nu_2=3170$; $\nu_8+\nu_{11}=3175$ (Type *C*)
3369	*B*	*vw*	$\nu_6+\nu_{11}=3381$; $\nu_3+\nu_5=3367$
3467 (cntr) 3492 (*Q*)	*A*	*vw*	$\nu_5+\nu_6=3485$
3609	*A*	*vw*	$\nu_{11}+\nu_{12}=3615$
3718	*B*	*vw*	$\nu_5+\nu_{12}=3719$
4152	*B*	*vw*	$\nu_1+\nu_6=4169$
4228 (cntr) 4237 (*Q*)	*A*	*vw*	$\nu_6+\nu_9=4245$
4464	*B*	*vw*	$\nu_9+\nu_{12}=4479$
4639	*B?A?*	*vw*	$2\nu_9=4670$ (Type *A*)
4678	*B*	*vw*	$\nu_2+\nu_9=4680$
5920 *P* 5962 *R*	*A?B?*	*vw*	$2\nu_1=6038$ (Type *A*); $2\nu_9=6190$ (Type *A*)
6070	*A?B?*	*vw*	$\nu_1+\nu_9=6114$ (Type *B*)

TABLE II. Bands observed in the C_2H_3D spectrum.

ν	Type	Intensity	Possible assignment; comments
809	*C*	strong	ν_7
943	*C*	strong	ν_8
1000	*C*	strong	ν_4
1129	*A–B?*	weak	ν_6
1291	*A*	med-weak	ν_3
1404	*A*	strong	ν_{12}
1605	*A*	weak	ν_2
1810	*A*	med-weak	$\nu_4+\nu_7=1809$
2274	*A*	medium	ν_{11}
2980	*A*	medium	ν_1 } Fermi doubling
3030	*A*	medium	ν_1 }
3063	*A*	medium	ν_5

[9] We must call attention to an error in the $\tilde{F}$ matrix: the off-diagonal elements in B_{1g} and B_{2u} do not vanish; we shall call these $(2k_3)^{\frac{1}{2}}$ and $(2k_4)^{\frac{1}{2}}$, respectively, in keeping with the notation in the other species. We found other minor calculational errors in the evaluation of the B_{3u} force constants, and in the determination of two of the (calculated) C_2D_4 frequencies, and have corrected them in the present paper.

TABLE III. Bands observed in *trans*-$C_2H_2D_2$.

ν	Type	Intensity	Possible assignment; comments
630?	*B*	*w*	? band center uncertain
660?	*B*	*w*	ν_{10} band center uncertain
727	*C*	*s*	ν_7
730	*A*?*C*?	*s*	?
988	*C*	*s*	ν_4
1293 (min) 1300 (*Q*)	*A*	*s*	ν_{12}
1442	*A*	*vw*	?
1582 (min) 1590 (*Q*)	*A*–*B*	*m*	$\nu_7+\nu_8=1589$
1689	*A*?*C*?	*w*	?
1848	*A*–*B*	*m*	$\nu_4+\nu_8=1850$
1956	*B*	*w*	?
2271	*A*–*B*	*m*	ν_{11}
2626	*B*	*vw*	doubtful; very weak
2866	*A*–*B*	*vw*	$\nu_2+\nu_{12}=2867$
3065	*A*–*B*	*m*	ν_9
3273	*A*	*vw*	?
3554?	*A*?	*vw*	?
3582	*A*	*vw*	$\nu_1+\nu_{12}$?
4066	*B*	*vw*	?
4342	*B*	*vw*	?
4474	*A*–*B*?	*vw*	? These overlap
4523	*A*–*B*?	*vw*	?
4639	*B*	*vw*	$\nu_2+\nu_9=4632$?
5188	*A*?	*vw*	?
5791	*A*–*B*?	*vw*	?

With the data from *a*-$C_2H_2D_2$ as well as C_2H_4 and C_2D_4, the solution for the six potential constants in the A_{1g} block now is theoretically determined. It appears that all one must do is choose any six independent relations from the total of eleven which these molecules now provide (*a*-$C_2H_2D_2$ contributes five, since here A_{1g} combines with B_{3u}). However, the high degree of some of these equations prohibits a straightforward solution. Especially is this true if one wishes to exclude the C_2D_4 frequencies, perhaps on the basis that these are liquid-phase (Raman) data. Therefore, we next tried including the C_2D_4 data, and choosing the simplest independent equations (note here that there are not only the usual product-rule redundancies, but also a "sum-rule" relationship in the three linear equations, which has been noted and discussed recently by Decius and Wilson[10]); but the force constants so obtained did not reproduce all the observed frequencies very satisfactorily.

However, we immediately got consistent results when we assumed that $k_1=k_2$ in the $\bar{F}$ matrix of symmetry coordinates; this, in terms of the valence coordinates, means assuming no interaction between a C—H stretch and a CH_2 deformation on the *opposite* end of the molecule, which appears quite reasonable. Now only five independent relations are necessary, and these may be taken from C_2H_4 and C_2D_4 exclusively; the force constants obtained, together with the B_{3u} force constants, being used to calculate the *a*-$C_2H_2D_2$ frequencies. Two sets of reasonable constants were determined, both giving *a*-$C_2H_2D_2$ frequencies to better than 0.5 percent.

A simple adjustment to all the observed frequencies was made so that the sum rule and various product rules would be obeyed more closely to remove as much as possible the inconsistencies in all eleven relations. The adjustment for C_2H_4 amounted to an increase of each frequency of less than 0.2 percent; for C_2D_4, an increase of less than 0.8 percent; and for *a*-$C_2H_2D_2$, a decrease of less than 0.5 percent. Since all the relations from C_2H_4 and C_2D_4 were used, the force constants reproduce exactly the (adjusted) data in these cases.

To correct for the anharmonicity of the light-atom stretching vibrations, we used the same procedure adopted by Arnett and Crawford with the further assumption that $\nu_e'/\nu_e=\nu_0'/\nu_0$ for a C—H mode which

TABLE IV. Bands observed in the spectrum of *cis*-$C_2H_2D_2$.

ν	Type	Intensity	Assignment
843	*C*	*vs*	ν_7
1344	*A*	*s*	ν_{12}
1598	*A*	*m*	$\nu_7+\nu_8=1599$
1818	*A*	*m*	$\nu_4+\nu_7=1825$
2254	*A*	*m*	ν_{11}
2903	*A*	*w*	$\nu_2+\nu_{12}$
3056	*A*	*m*	ν_5

[10] J. C. Decius and E. B. Wilson, Jr., J. Chem. Phys. 19, 1409 (1951).

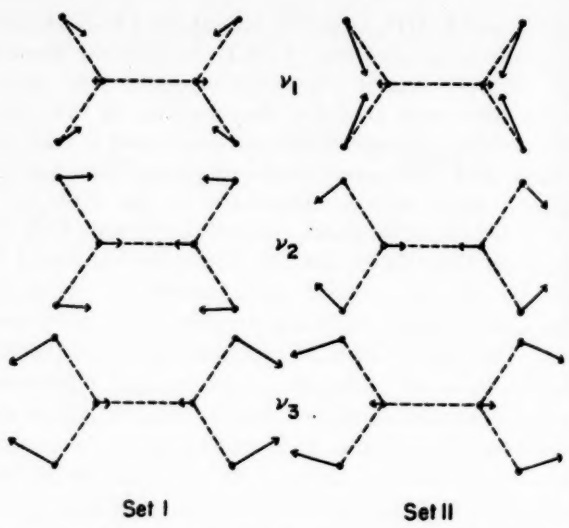

FIG. 6. Normal coordinates for the A_{1g} group of ethylene, as computed using the two sets of force constants given in Table V.

TABLE V. Force constants corresponding to the planar symmetry coordinates.

	Set I	Set II		
A_{1g}	$K_1=$ 6.1988	6.1988		
	$k_2{}^1=-0.0039$	−0.1117		
	$k_1=$ 0.3401	0.3401	B_{1g}	$K_2=6.1529$
	$k_8{}^1=-0.8467$	−0.2956		$k_3=0.5057$
	$K_0=$ 10.8956	8.8368		$B_1=1.1403$
	$A_1=$ 0.6518	0.6518		
B_{2u}	$K_3=$ 6.0137		B_{3u}	$K_4=6.1394$
	$k_4=$ 1.3685			$k_5=0.3401$
	$B_2=$ 1.3894			$A_2=0.5886$

remains a C—H mode in the isotopic molecule, necessary in the case of the dideuteroethylenes where *two* eight-atom stretching vibrations fall in the same symmetry class.

The two sets of "symmetrized" force constants are given in Table V. We could find no basis for choosing between these two sets until we compared the two sets of normal coordinates determined by them. In Fig. 6, we note that Set I gives a mode for ν_2 which has essentially the character of a C=C stretch, while the vibration determined by Set II has a good deal of the character of a CH_2 deformation. In view of the well-known constancy of the C=C frequency in olefins, it appears that Set I is more nearly correct. Additional support for this preference comes from recent work of Duchesne, who finds C=C constants of 9 to 12 md/A in C_2F_4 and C_2Cl_4.[11]

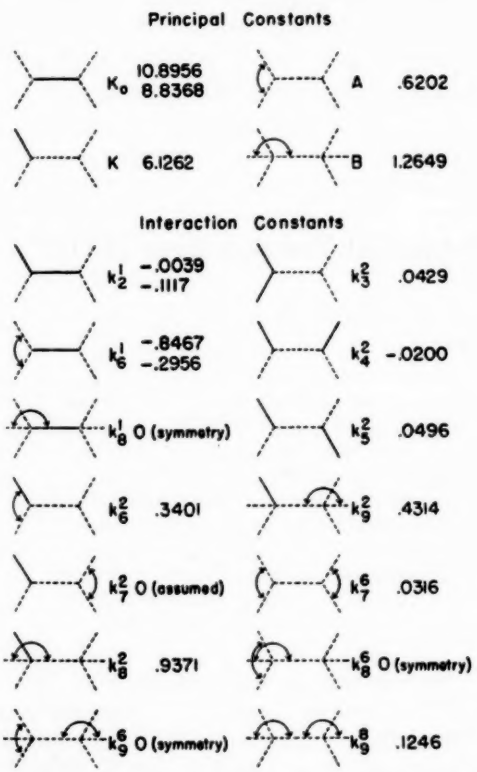

FIG. 7. Valence force constants for ethylene, derived from the symmetrized constants of Table V. Where two values are given, these correspond to Set I (upper) and Set II (lower). The valence force coordinates involved (bonds or angles) are indicated by the solid lines, the rest of the molecule being indicated by the dotted lines.

By application of the transformation to valence-force coordinates, we find the force constants associated with the valence coordinates, and these are shown in Figs. 7 and 8.

Also shown in Table V are the force constants from the non-totally-symmetric blocks (B_{1g}, B_{2u}, B_{3u}), which follow straightforwardly from the data in only two molecules (C_2H_4 and C_2D_4), but now three other molecules are available as a check. In each of the three dideuteroethylenes, two of these species combine to

[11] A. Monfils and J. Duchesne, J. Chem. Phys. 18, 1415 (1950); and private communication from Dr. Duchesne.

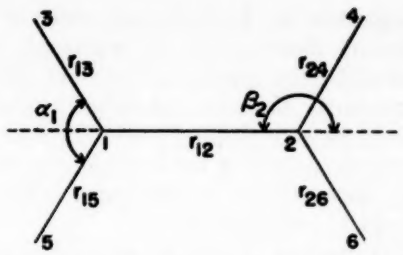

FIG. 8. Structure of the ethylene molecule, indicating the valence force coordinates used.

TABLE VI. The fundamental frequencies of the isotopic ethylenes. The bracketted figures are those calculated from the force constants determined in this paper. Where two values appear, the first comes from Set I, the second from Set II (see text). All values in parentheses are from the recent observations of Charette and de Hemptinne. Where they observed a line in both the infrared and Raman, the infrared value only has been entered, except for some other reason indicated by the superscripts.

	C_2H_4	C_2H_3D	*a*-$C_2H_2D_2$	*c*-$C_2H_2D_2$	*t*-$C_2H_2D_2$	C_2HD_3	C_2D_4
ν_1	3019.3	(3002)[a]	3019 (3019) [3005] [3006]	(2300) [2365] [2332]	(2276) [2299] [2294]	(2280)	2251
ν_2	1623.3	1605 (1600)[b]	1585 (1579)[b]	(1567) [1558] [1574]	(1567) [1564] [1573]	(1546)	1515
ν_3	1342.4	1291 (1290)	1032 (1030) [1028] [1030]	(1215) [1213] [1203]	(1282) [1289] [1289]	(1046.9)	981
ν_4	1027	1000 (1000.8)	889[d]	982[d]	988 (988.8)	(765) 764[f]	726
ν_5	3075	3063 (3062)	2335 (2333) [2351]	3056 (3055) [3022]	(3035) [3036] [3038]	(2232)	2304
ν_6	1236	1129 (1128)	1150 [1139]	1041[e] [1037]	(1001) [1009] [1002]	(995)	1006[g]
ν_7	949.2	809 (807.3)	752 (751.3)	843 (842.2)	727 (727)	(724) 723[f]	720
ν_8	943	(943.3)	944 (943)	756[d] (763)	(864)	(918.8) 918[f]	780
ν_9	3105.5	(3103)	3095 (3090) [3081]	(3058) [3043] [3046]	3065 (3064) [3032]	(3045)	2345
ν_{10}	810.3	(730)[c]	676[c] (660) [679]	(646) [656] [657]	660[c] (678) [664]	(609.7)	(584) 589[c]
ν_{11}	2989.5	2274 (2272)	2231 (2228) [2232] [2231]	2254 (2251) [2261]	2271 (2270) [2298]	(2222)	2200.2
ν_{12}	1443.5	1404 (1403)	1384 (1384) [1392] [1383]	1344 (1342) [1349]	1300 (1300) [1291]	(1289.5)	1077.9

[a] This value is an average of the two bands that Charette and de Hemptinne ascribe to a resonance form of ν_1.
[b] This is a Raman value; Charette and de Hemptinne did not observe this in the infrared.
[c] The Raman value is given here in preference to the uncertain infrared value (715 cm^{-1}).
[d] Calculated from force constants by Arnett and Crawford.
[e] Calculated from the product rule.
[f] Observed by Arnett and Crawford.
[g] Calculated from $\nu_8+\nu_{10}=1595.1$.

form a single species. In each case, three of the four frequencies are observed in the spectrum, while the fourth follows by the appropriate product rule.

The agreement between calculated and observed frequencies is shown in Table VI, which is a summary of all of the fundamentals of the isotopic ethylenes, combining the observations of this paper with those of Charette and de Hemptinne.

In the calculations, ν_5 of C_2H_4 was taken to be 3075 cm^{-1}. Some workers have preferred to place it at 3272 cm^{-1}.[12] The present observation of several C—H modes in several isotopes lends much support to the lower figure, for most of them occur near that value; even the highest is only 3106 cm^{-1}. Moreover, the force constants determined from using $\nu_5 = 3075$ yield frequencies for the dideutero molecules in good agreement with the observed values. Recent work by Plyler[13] also favors 3075 for ν_5.

We also calculated the totally-symmetric frequencies for *cis*- and *trans*-$C_2H_2D_2$; it was not until later that Charette and de Hemptinne were able to sort these frequencies out of their infrared and Raman investigations. The agreement with observed may be seen in Table VI.

ACKNOWLEDGMENT

We wish particularly to thank Professor B. S. Rabinovitch for his cooperation in supplying the *trans* isotope which was of such value in our study.

[12] G. Herzberg, *Infrared and Raman Spectra* (D. Van Nostrand Company, Inc., New York, 1945), p. 327. Even Arnett and Crawford, reluctant but not timorous, went along with this higher value.

[13] E. K. Plyler, J. Chem. Phys. **19**, 658 (1951).

THE JOURNAL OF CHEMICAL PHYSICS VOLUME 21, NUMBER 4 APRIL, 1953

Effect of Spectral Line Shape on Apparent Rotational Temperatures of OH*

S. S. PENNER
Guggenheim Jet Propulsion Center, California Institute of Technology, Pasadena, California

(Received November 30, 1952)

The effect of spectral line shape on apparent rotational temperatures of OH has been investigated for the P_1 branch, $^2\Sigma \rightarrow {}^2\Pi$ transitions, (0, 0) band, by treating the ratio of collision half-width to Doppler half-width as a variable parameter. The results of calculations for emission experiments, using conventional plots, show a large effect of line shape on apparent temperature. In general, the greater the ratio of collision half-width to Doppler half-width, the smaller the distortion of experimental data. The analysis predicts higher apparent rotational temperatures for isothermal systems at reduced pressures than at atmospheric pressures. Although this result is in agreement with experimental observations on flames, it cannot be used as an explanation for the observed data without auxiliary studies proving that distortion of data is of importance in any given case. The two-path method for determining temperatures and emissivities (concentrations) in flames has been extended to spectral lines with combined Doppler- and collision-broadening.

I. INTRODUCTION

IN a recent publication[1] we have presented the results of quantitative calculations concerning the distortion of emission and absorption data on OH for various simplified models of flames. These calculations were carried out for spectral lines with Doppler-broadening and hence the results are applicable only to low pressure flames. Although the quantitative interpretation of experimental studies carried out at atmospheric pressure is severely complicated by temperature gradients both normal to and along the line of sight, a great deal of experimental work has been done on flames of this type.[2] For this reason it appears to be of interest to extend our calculations to spectral lines with combined Doppler- and collision-broadening. Calculations for isothermal systems in emission are presented in Section II where conventional techniques are used for interpretation of experimental data. The calculations predict lower apparent temperatures at elevated pressures under otherwise comparable experimental conditions. Thus they are in accord with observations reported particularly by Gaydon and Wolfhard.[3] It is, of course, clear that the mere fact that a transition from pure Doppler-broadening to spectral lines with combined Doppler- and collision-broadening produces lower apparent temperatures in isothermal systems, even for relatively weak self-absorption, does not disprove the reality of observed rotational temperatures in flames. On the other hand, it is also apparent that the seemingly plausible argument that the "observed" increase in rotational temperature of OH with decreasing pressure proves the reality of the anomalous temperatures is entirely unjustified unless it is accompanied by a quantitative proof that the reduction in $P_{max}X$ will more than offset the distortion produced by a change of line shape.†

* Supported by the U. S. Office of Naval Research under Contract No. Nonr-220(03), NR 015 210.

[1] S. S. Penner, J. Chem. Phys. **21**, 31 (1953).

[2] H. P. Broida and G. T. Lalos, J. Chem. Phys. **20**, 1466 (1952) and earlier publications referred to in this article.

[3] A. G. Gaydon and H. G. Wolfhard, Proc. Roy. Soc. (London) **A208**, 63 (1951) and earlier publications.

† Rough estimates utilizing burner dimensions reported in the literature suggest that the probable values of $P_{max}X$ in low pressure flames are of the same order of magnitude as in flames burning at atmospheric pressure.

All of our calculations in Section II refer to the P_1 branch, $^2\Sigma \rightarrow {}^2\Pi$ transitions of OH, (0, 0) band. For the sake of brevity we shall speak simply of rotational temperatures for the P_1 branch.

II. EMISSION EXPERIMENTS

In order to extend the calculations presented for spectral lines with Doppler contour[1] to spectral lines with combined Doppler- and collision-broadening, it is most convenient to use van der Held's curves of growth.[4,5] The line shape is determined by the parameter

$$a=(b_N+b_C)(\ln 2)^{\frac{1}{2}}/b_D,$$

where b_N, b_C, and b_D denote, respectively, the natural half-width, the half-width resulting from collision- (Lorentz-) broadening, and the half-width produced by Doppler-broadening. We have presented previously a graph for calculating total observable intensities,

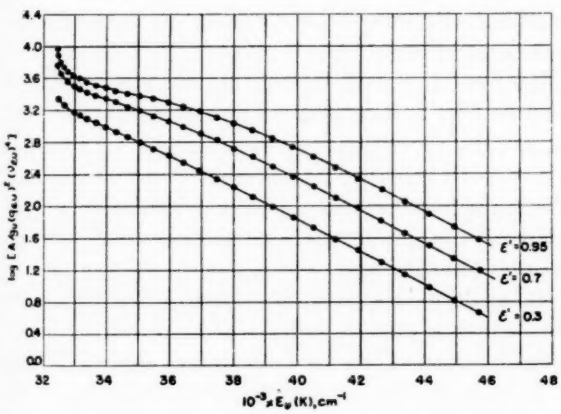

FIG. 1. Conventional plots for the determination of rotational temperatures of OH in emission for various assumed values of $\epsilon'(1)$ for the P_1 branch, $^2\Sigma \rightarrow {}^2\Pi$ transitions, (0, 0) band, $T=3000°K$, $a=0.005$.

$A(a=0)$, from peak intensities, I_{max}, for spectral lines with Doppler contour.[1] For fixed values of the product of maximum absorption coefficient (P_{max}) and optical density (X) the ordinate of the curve of growth determines a quantity proportional to the total observable intensity $A(a)$ for arbitrary values of the line contour parameter a. Hence, it is a simple matter to obtain, I_{max}, $A(a=0)$, $A(a)/A(a=0)$ from the curves of growth, and finally absolute values for $A(a)$. Details of the laborious but straightforward calculations will not be presented here.‡

The results of numerical calculations for emission

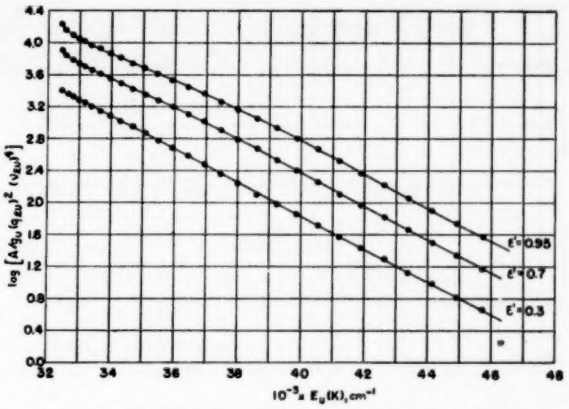

FIG. 2. Conventional plots for the determination of rotational temperatures of OH in emission for various assumed values of $\epsilon'(1)$ for the P_1 branch, $^2\Sigma \rightarrow {}^2\Pi$ transitions, (0, 0) band, $T=3000°K$, $a=2$.

from the P_1 branch at 3000°K are summarized by conventional plots for interpretation of data in Figs. 1 and 2 for $a=0.005$ and for $a=2$, respectively. The variable parameter ϵ' is defined in the usual way, viz., $\epsilon'=1-\exp(-P_{max}X)$, and refers to the first line of the P_1 branch.[1] The importance of line shape on the results is evident even from a qualitative comparison between the data plotted in Figs. 1 and 2.

As a rough quantitative measure for the influence of line shape on observable results, we may compute T_u', the apparent rotational temperature of the upper state, from the calculated data for $10 \leqslant K \leqslant 20$. There is some ambiguity in utilizing this method since the calculated points follow an S-shaped curve for large values of ϵ' (Figs. 1 and 2). The resulting apparent temperatures are summarized in Table I for three values of a. The numerical values clearly show that the apparent rotational temperature for isothermal emitters must increase as the pressure is reduced since a decreases as the collision frequency goes down (b_C is roughly proportional to the pressure and $b_N \ll b_D$ at the temperatures which are of interest for spectroscopic studies on flames). The effect of line shape, which is expressed quantitatively in Figs. 1 and 2, can be understood by noting that distortion of data by self-absorption must decrease as the effective line width increases, under otherwise comparable conditions.

The extension to spectral lines with combined Doppler- and collision-broadening of our previous studies on absorption experiments, isointensity studies, non-

TABLE I. Effect of line shape and self-absorption on apparent rotational temperatures obtained for OH in emission experiments (P_1 branch of OH, $^2\Sigma \leftarrow {}^2\pi$ transitions, (0, 0) band, $T=3000°K$, $10 \leqslant K \leqslant 20$).

	T_u'(°K) for		
$\epsilon'(1)$	$a=0.0005$	$a=0.5$	$a=2$
0.3	3410	3250	3010
0.7	3840	3800	3230
0.95	5000	5000	3480

[4] E. M. F. van der Held, Z. Physik **70**, 508 (1931); A. Unsöld, *Physik der Sternatmosphären*, (Edwards Brothers, Inc., Ann Arbor, 1948), p. 168.

[5] For an extension of the curves of growth to larger values of the line-shape parameter a, see S. S. Penner and R. W. Kavanagh, Technical Report No. 6, Contract Nonr-220(03), NR 015 210, California Institute of Technology, September, 1952, also J. Opt. Soc. Am. (to be published).

‡ The author is indebted to Mr. N. Schroeder for performing the computations.

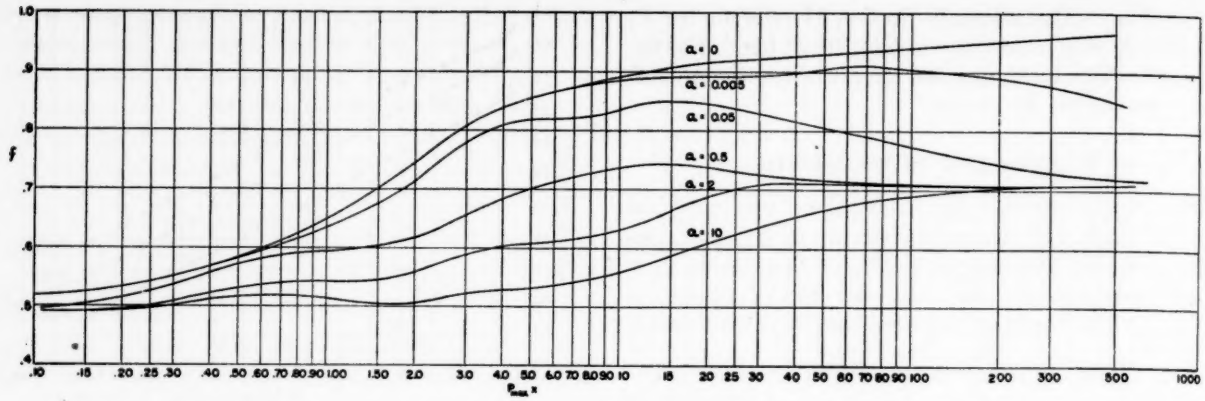

FIG. 3. Plot of observable intensity ratios as a function of $P_{max}X$ for two-path experiments and various values of the line-shape parameter a.

equilibrium mixtures, and nonisothermal systems, as well as calculations for branches other than the P_1 branch, has also been made but the results will not be presented here. In general, the data are summarized by the remark which has already been made, namely, that distortion of data resulting from self-absorption increases as a decreases. The obvious conclusion which must be drawn from this result is that greater care is required to eliminate self-absorption errors in low pressure flames than in flames burning at atmospheric pressure.

The implications of the result, that apparent rotational temperatures are a sensitive function of line shape (for low resolution spectroscopic studies), are quite disturbing. For example, the dependence of line shape on vibrational quantum number for such molecules as OH is not known in sufficient detail to rule out the possibility that different apparent temperatures for different branches are produced because of a sizeable difference in the parameter a. Other factors may, of course, also be responsible for an effect of this sort.

III. TWO-PATH EXPERIMENTS FOR ISOTHERMAL SYSTEMS

The two-path method[6] for eliminating the effects of self-absorption on experimental data, which permits direct determination both of rotational temperature and of emissivity, has been extended to spectral lines with combined Doppler- and collision-broadening. The calculations can be carried out readily by judicious use of the curves of growth.[4,5]

The results of the laborious calculations are summarized in Fig. 3. The abscissa represents the parameter $P_{max}X$, and the ordinate f corresponds to the observable ratio of total intensity for the single to the double path. The variable parameter a has been defined previously. For $a=0$ the results apply to spectral lines with pure Doppler-broadening.

Reference to Fig. 3 shows the remarkable fact that the slope of a plot of f *vs* $P_{max}X$ may change sign repeatedly, particularly for large values of the parameter a. This result can be understood by reference to the curves of growth. In so far as applications to interpretation of flame spectra is concerned, the picture evidently becomes complicated for multiple-path experiments on spectral lines with combined Doppler- and collision-broadening, even if the emitter is isothermal. Details concerning interpretation of flame spectra will appear in a subsequent publication.

[6] S. S. Penner, J. Chem. Phys. **20**, 1341 (1952).

Elastic Scattering and Neutralization of Low Velocity Hydrogen Ions in Methforane and Ethforane

J. H. SIMONS, *College of Engineering, The University of Florida*

AND

C. S. GARBER, *School of Chemistry and Physics, The Pennsylvania State College, State College, Pennsylvania*

(Received November 21, 1952)

The low velocity scattering of H^+, H_2^+, and H_3^+ in both methforane and ethforane has been measured at ion velocities of less than 150 volts. Ion neutralization was detected and measured for all three ions in both fluorocarbons and elastic scattering potential functions evaluated for all six interactions. These measurements are compared with similar ones made on the hydrocarbons methane and ethane.

PREVIOUS studies have reported the scattering of low velocity hydrogen ions in hydrocarbons.[1-3] In the present study the fluorocarbons CF_4 (methforane) and C_2F_6 (ethforane) are used as the scattering gases. This enables a comparison to be made between the fluorocarbons and the analogous hydrocarbons. Charge exchange between the hydrogen ions and the fluorocarbon molecules is found, but this is much less than for the analogous hydrocarbon molecules.

APPARATUS AND MATERIALS

The apparatus and its use has been previously described.[3] The methforane and ethforane were pure samples of fluorocarbons prepared in the Fluorine Laboratories of the Pennsylvania State College before these laboratories were abolished. They were not less than 99 percent pure.

TABLE I. Scattering of hydrogen ions in methforane.

H^+			H_2^+			H_3^+		
W volts	α_T^0	α_s^0	W volts	α_T^0	α_s^0	W volts	α_T^0	α_s^0
130.0	27.0	22.3	131.0	41.5	34.6	124.0	47.4	40.8
115.0	32.0	19.6	115.0	40.0	31.5	100.0	48.8	41.0
100.0	32.2	26.3	100.0	43.5	33.7	81.0	49.3	40.4
85.0	32.8	27.9	97.0	37.0	29.9	61.5	52.6	43.5
70.0	34.9	27.0	74.0	44.6	35.2	51.0	57.6	47.4
55.0	44.7	38.3	60.0	52.6	43.6	40.0	61.0	50.5
45.0	53.3	48.5	53.0	48.2	38.9	33.0	63.0	53.8
34.4	72.5	67.3	40.0	65.5	55.9	25.0	71.8	60.5
26.5	76.4	70.5	32.0	74.3	62.0	21.0	80.0	65.5
20.0	97.0	94.0	25.0	95.0	78.5	17.1	90.5	74.8
19.8	106.0	100.0	20.5	94.0	74.0	14.0	95.2	77.0
15.0	99.5	92.5	18.0	116.0	83.0	11.2	112.0	86.3
13.0	106.0	106.0	17.8	117.0	91.8	9.0	118.5	94.0
9.5	114.0	114.0	14.0	125.0	93.0	7.7	132.0	102.0
6.5	118.0	118.0	13.8	119.0	94.5	5.7	129.0	110.0
5.0	128.0	128.0	10.4	135.0	96.3			
			9.0	150.0	103.0			
			7.2	165.0	107.0			
			5.2	175.0	111.0			

[1] J. H. Simons and G. C. Fryburg, J. Chem. Phys. **13**, 216 (1945).

[2] J. H. Simons and W. H. Cramer, J. Chem. Phys. **18**, 473 (1950).

[3] J. H. Simons and S. A. McAllister, J. Chem. Phys. **20**, 1431 (1952).

RESULTS

In Table I are given the results of the scattering of hydrogen ions in methforane. These results are also shown in Figs. 1–3. In Table II the results of the scattering of hydrogen ions in ethforane are shown and also in Figs. 4, 5, and 6. The potential laws as evaluated from potential function graphs are shown in Table III.

DISCUSSION

The technique of the investigation of the properties of molecules by means of the scattering of low velocity

TABLE II. Scattering of hydrogen ions in ethforane.

H^+			H_2^+			H_3^+		
W volts	α_T^0	α_s^0	W volts	α_T^0	α_s^0	W volts	α_T^0	α_s^0
140.0	71.4	45.4	125.0	138	71.0	125.0	86.9	75.7
125.0	79.7	52.8	123.0	122	63.0	100.0	90.0	77.5
100.0	87.0	55.1	118.0	122	65.0	87.0	97.0	82.0
86.0	76.8	56.0	100.0	135	70.5	87.0	101.0	87.0
73.0	76.2	55.0	90.0	134	74.0	70.0	100.0	84.8
67.0	87.8	67.6	87.0	147	80.5	57.0	105.0	87.5
50.0	110.0	91.7	85.0	144	75.5	50.0	109.0	87.5
40.0	106.5	100.0	70.0	130	71.0	44.5	113.0	91.3
38.0	137.0	130.5	57.0	147	82.4	36.0	119.0	95.5
31.4	126.0	119.0	40.0	167	94.5	27.4	129.0	105.0
25.0	159.0	151.0	31.0	192	115.0	20.7	123.0	113.0
20.5	148.0	139.0	29.0	192	113.0	15.8	143.0	140.0
19.0	156.0	154.0	20.0	208	126.0	12.6	142.0	141.0
15.0	162.0	136.0	15.0	238	152.0	10.0	187.0	143.0
11.0	192.0	168.0	9.5	284	150.0	7.8	215.0	200.0
7.5	186.0	160.0	7.5	350	193.0	5.0	260.0	227.0
5.0	220.0	220.0	5.4	337	192.0			

TABLE III. Summary of scattering laws and potential functions.

Ion	Range	Potential function
	Methforane	
H^+	5–20 volts (3.41–2.91A)	$V=-6350/r^{8.72}$
	20–130 volts (2.91–1.41A)	$V=-19.3/r^{2.4}$
H_2^+	5–20 volts (3.23–2.77A)	$V=-11\,300/r^{9.68}$
	20–130 volts (2.77–1.70A)	$V=-50.9/r^{3.41}$
H_3^+	5–130 volts (3.21–1.92A)	$V=-80.5/r^{4.85}$
	Ethforane	
H^+	5–25 volts (4.43–3.38A)	$V=-7600/r^{7.36}$
	25–130 volts (3.38–2.12A)	$V=-2.38/r^{2.86}$
H_2^+	5–130 volts (4.25–2.53A)	$V=-523/r^{5.16}$
H_3^+	5–25 volts (4.65–3.21A)	$V=-84.3/r^{3.7}$
	25–130 volts (3.21–2.61A)	$V=-49\,300/r^{10}$

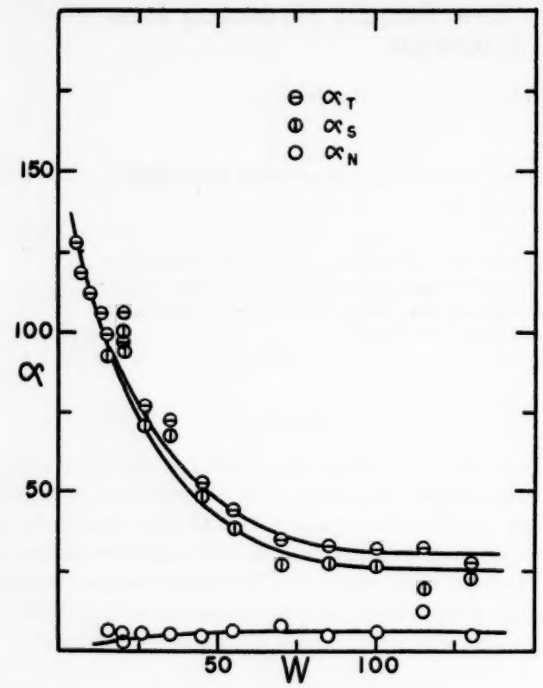

FIG. 1. The scattering of H^+ in methforane.

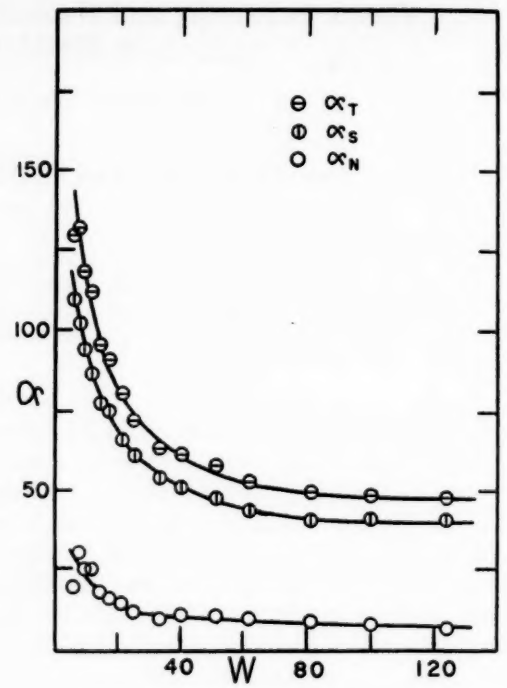

FIG. 3. The scattering of H_3^+ in methforane.

ions in an attenuated gas composed of these molecules has been used for the study of hydrocarbon gases. The low boiling fluorocarbons offer an opportunity for similar studies of molecules of essentially the same atomic skeleton but with considerably different chemical properties. The phenomenon of exchange of charge from hydrogen ions was found to occur with high probability in the hydrocarbon gases. To date, theory has been unable to give a quantitative correlation of the experimental facts of charge exchange as obtained in low velocity scattering experiments. It was necessary, therefore, to experimentally determine the exchange of charge between hydrogen ions and the fluorocarbon molecules. Because of the great similarity of the

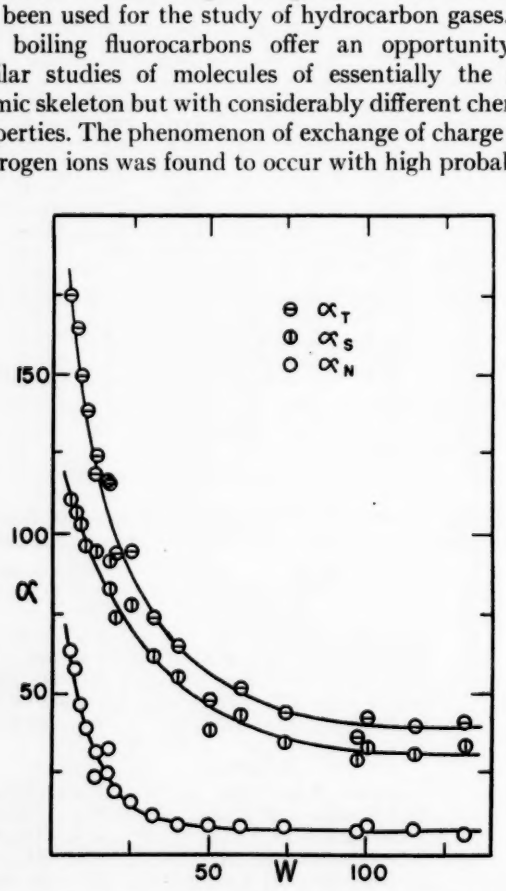

FIG. 2. The scattering of H_2^+ in methforane.

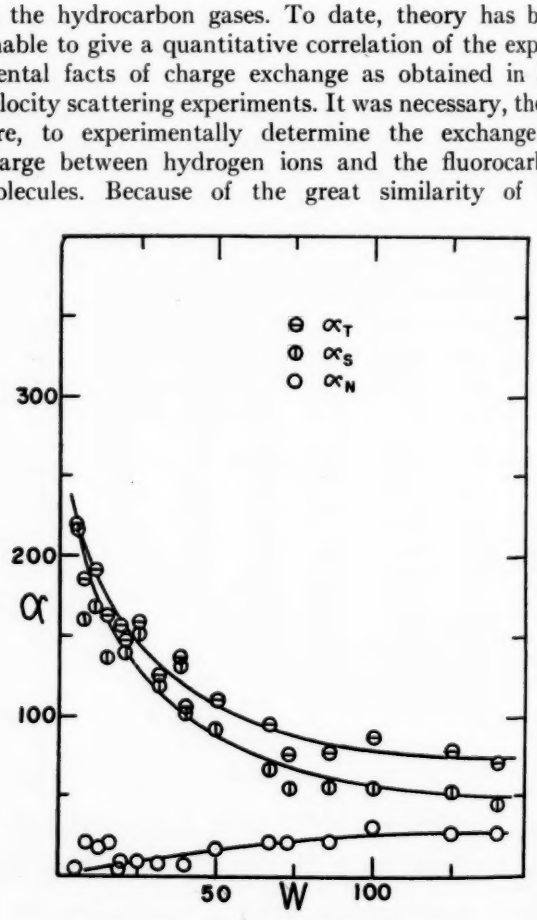

FIG. 4. The scattering of H^+ in ethforane.

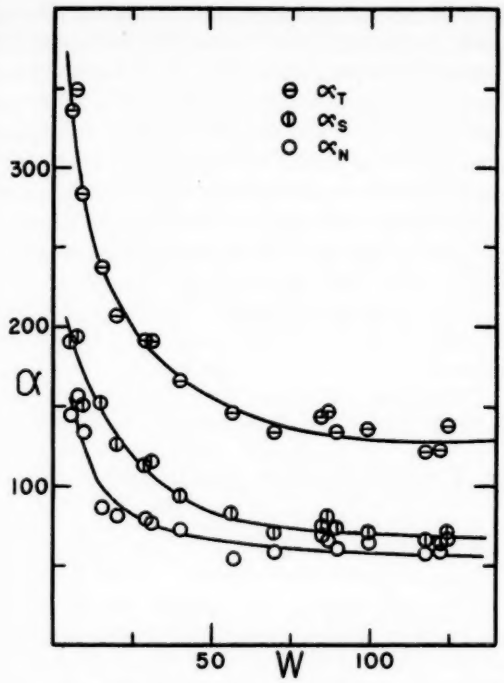

FIG. 5. The scattering of H_2^+ in ethforane.

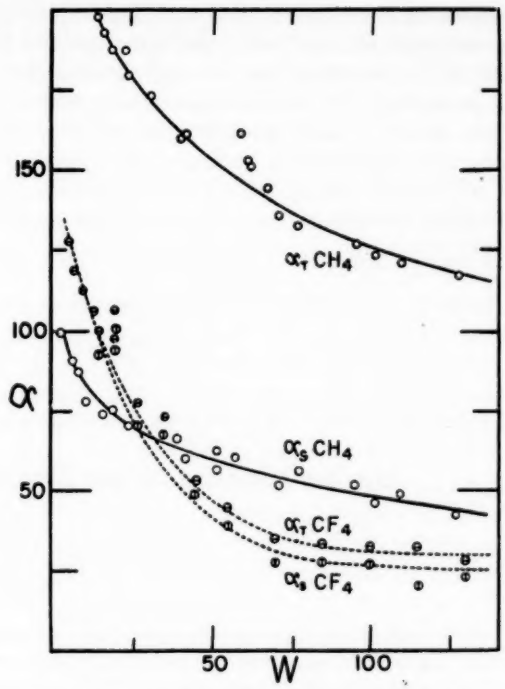

FIG. 7. A comparison of methforane and methane.

attachment of electrons in the hydrogen ions and the hydrocarbons, large values of charge exchange in these experiments were not considered unreasonable, although there is as yet no good explanation of the exact values or shapes of the α_N curves. With hydrogen ions in fluorocarbon gases, negligible charge exchange might be expected. The experimental values, although smaller than with hydrocarbon gases, were nevertheless appreciable. It appears at this time, however, that much more experimental information will be needed, before a satisfactory theoretical treatment of charge exchange is forthcoming.

The elastic scattering of the hydrogen ions in the fluorocarbon gases shows some interesting relationships.

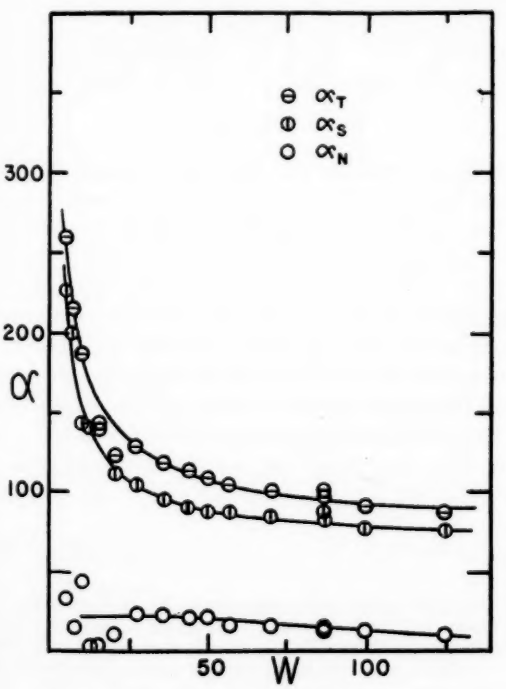

FIG. 6. The scattering of H_3^+ in ethforane.

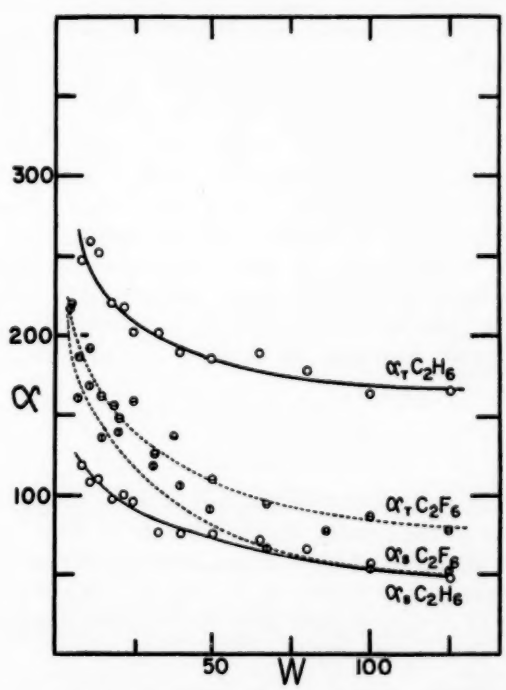

FIG. 8. A comparison of ethforane and ethane.

The values for the effective size α_s are about the same for the molecule of one kind at the same velocity independent of the formula of the ion, and the shapes of the curves are similar. The molecule containing more atoms, however, shows a much greater effective size. Molal volumes of fluorocarbons in the liquid state appear to be about 50 percent greater than the hydrocarbon of the same carbon skeleton structure,[4,5] and the molecular weights are several hundred percent higher. The effective sizes for hydrogen ion scattering are, nevertheless, not greatly different for methforane and ethforane than they are for methane and ethane. In Fig. 7, a comparison is given for α_s of H^+ in methforane and methane. The former is actually found to be smaller except at quite low velocities. In Fig. 8 is given a similar comparison for H^+ in ethforane and ethane. In this case the effective sizes are about the same for the molecules at the higher velocities with the fluorocarbon molecule showing greater size at lower velocities.

[4] J. H. Simons and R. D. Dunlap, J. Chem. Phys. **18**, 335 (1950).
[5] J. H. Simons and J. W. Mausteller, J. Chem. Phys. **20**, 1516 (1952).

THE JOURNAL OF CHEMICAL PHYSICS VOLUME 21, NUMBER 4 APRIL, 1953

On the Kinetics of the Disorder-Order Transformation in Cu_3Au*

NORMAN W. LORD
Columbia University, New York, New York
(Received November 17, 1952)

The isothermal order-dependent change in the Young's modulus of a single crystal of Cu_3Au is measured as a function of time at various temperatures in the range 279.3°C to 384.3°C. These temperatures were reached by quenching rapidly from an equilibrium state 28.2°C above the critical temperature (386.0°C).

The time variations of Young's modulus indicate two distinct stages of the disorder-order transformation. The initial stage starts immediately and is completed a few minutes after quenching, while the later stage requires a few minutes before starting and then proceeds very slowly toward an equilibrium state. "Relative relaxation times" are associated with each of them.

In conformance with the work of Sykes and Evans and others, the initial stage is described as the formation of contiguous, antiphase, ordered domains by means of normal atomic interdiffusion. The later stage consists of the coalescence of these domains and requires at least two different geometrically constrained diffusion processes.

I. INTRODUCTION

THE crystalline structure of the binary alloy Cu_3Au is face-centered cubic. When the crystal is completely disordered, the distribution of copper and gold atoms on the lattice points is random. In the completely ordered state, the copper atoms lie at the vertices of three of the constituent simple cubic lattices and the gold atoms at the vertices of the fourth. It is convenient, in what follows, to denote the copper atoms "A atoms," the gold atoms "B atoms," and the associated lattice points "α sites" and "β sites," respectively. A state of order between complete order and complete disorder can be described by means of a "long-range order parameter" S defined by either of the equivalent formulas

$$S=\frac{R_\alpha-F_A}{1-F_A}=\frac{R_\beta-F_B}{1-F_B} \tag{1}$$

in which F_A denotes the fraction of A atoms (or sites) present in the crystal, R_α the fraction of these α sites which are occupied by A atoms, and the corresponding significance is attached to F_B and R_β. Evidently the value of S ranges from zero at complete disorder to unity at complete order.

* Publication assisted by the Ernest K. Adams Fund for Physical Research of Columbia University.

A different description of the state of order in the crystal derives from an examination of the population of atoms in successive spherical shells of atoms centered on a given atom. A set of "short-range order parameters" σ_i[1] are then defined by the formula

$$\sigma_i=1-n_i/Fc_i, \tag{2}$$

in which n_i denotes the number of atoms of *opposite* type in the ith shell about the central atom, c_i the total number of atoms in the shell, and F the fraction of atoms of opposite type present in the crystal. The value of σ_i ranges from zero at complete disorder, to unity for i even and $-(1/3)$ for i odd at complete order.

Long-range order exists in the alloy if the value of σ_i tends not to zero but to a finite limiting value as i becomes very large. It can be shown[2] that if the value of the long-range order parameter is S, then the limiting value of σ_i, averaged over all the atoms of type A or type B in the crystal, is S^2 for i even and $-S^2/3$ for i odd.

Approximate theories of the variation of equilibrium

[1] These short-range order parameters are employed by Cowley (see reference 2) in preference to the single parameter introduced by Bethe (see reference 3) and Peierls (see reference 4), because they facilitate the interpretation of x-ray diffraction data in terms of order.
[2] J. M. Cowley, Phys. Rev. **77**, 669 (1950).

order with temperature have been proposed by Cowley,[2] Bethe,[3] Peierls,[4] Kirkwood,[5] and Bragg and Williams.[6] All confirm the decrease of equilibrium long-range order with increasing temperature, the existence of a critical temperature T_c at which long-range order disappears, and the persistence of short-range order at temperatures above T_c. In crystals of the type A_3B, the value of S falls discontinuously at the critical temperature from a value near 0.8 to zero. The theory of Cowley is in excellent agreement with the results of x-ray diffraction measurements both above and below T_c.[2,7]

The evanescence of equilibrium long-range order as the temperature is raised below T_c is accompanied by marked changes in various physical properties of the crystal, in particular the specific heat,[8] the specific resistance,[9] and the elastic constants.[10] Similar changes, now functions of time, accompany the isothermal approach to equilibrium order when a specimen is suddenly cooled from a temperature above T_c to a temperature below it and maintained there. Such time variations of the specific heat, resistance, and elastic constants have been employed as indicators in studies of the kinetics of the order-disorder and disorder-order transformations, despite the lack of satisfactory theories which relate these quantities directly to the degree of order.[8–12] This is the method adopted in the present investigation.

Siegel[11] measured the isothermal time variation of Young's modulus in a crystalline rod of Cu_3Au following reduction of the specimen temperature from a value above T_c to one of several values in a thirteen degree interval below T_c. The specimen was cooled simply by shutting off the power supplied a resistance furnace, and the time required to attain temperature equilibrium at the reduced temperature was some 25 minutes. The objects of the present research are to extend the temperature range covered by Siegel's observations, and to investigate the phenomenon in an earlier stage. The experimental method permits the initiation of observations within 30 seconds following the onset of cooling.

II. EXPERIMENTAL METHOD

Specimen Material

The specimen upon which all of the measurements here reported were made was cut from one of the five single crystals of Cu_3Au used by Siegel in his measurement of the variation of the elastic constants with temperature.[10] Its form is a right circular cylinder 0.470 cm in diameter and 3 cm long. The direction cosines of the cylinder axis with respect to the principal axes of the crystal, ascertained from back reflection Laue pictures, are 0.9990, 0.0297, and 0.0298. The author is greatly indebted to Dr. Siegel for the loan of this crystal.

Measurement of Young's Modulus

A complete description of the dynamical method employed to measure Young's modulus will be found elsewhere,[13] and it will suffice here briefly to review its essential features. The value E_T of the modulus at the temperature T and time t of measurement is deduced from the observed behavior of a composite piezoelectric oscillator constructed by cementing to one end of the specimen an x-cut cylinder of crystalline quartz of identical cross section. Aluminum electrodes are deposited by evaporation in proper position on the quartz, and the oscillator is suspended vertically by delicate supports applied at the middle of the quartz cylinder. A sinusoidal potential difference of variable frequency is applied across the electrodes, and means are provided for measuring the current which flows to the oscillator. The observed variation of this current with frequency of the applied voltage yields the fundamental frequency of free longitudinal vibration of the mechanical system, and the same is true of an oscillator composed of the quartz cylinder alone. The fundamental frequency of the specimen cylinder alone can be computed when these two frequencies are known, and this is related to the Young's modulus of the specimen material for the direction of the cylinder axis by the formula

$$E_T = 4\rho_{20} L_{20}^2 f_T^2 \left(\frac{L_{20}}{L_T}\right)\left[1+\tfrac{1}{2}\frac{\pi^2\bar{\sigma}^2 a^2}{L_{20}^2}\right], \qquad (3)$$

where ρ is the density, L the length, a the cross-sectional area, $\bar{\sigma}$ the mean Poisson's ratio, and f_T the fundamental resonant frequency of the specimen.

The value of L_T is computed with the coefficient of thermal expansion of Cu_3Au measured by Owen and Liu,[14] and $\bar{\sigma}$ with the data of Siegel[10] at the temperature 380°C. The value of the term containing $\bar{\sigma}$ is approximately 0.006.

The adhesive used in the construction of the composite oscillator is a mixture of Dow-Corning silicone resins in the proportion 10 percent No. 801 and 90 percent No. 803, plus 0.2 percent cobalt drier. The oscillator, with a layer of adhesive at the interface, is assembled vertically in a close fitting tubular graphite crucible, under a compressive stress of 100 gm/cm² exerted by a weight resting above it in the crucible and is baked in a vacuum at 200°C for 16 hours.

Measurement of Temperature

The measurement of the specimen temperature is accomplished by the following procedures: A chromel-

[3] H. A. Bethe, Proc. Roy. Soc. (London) **A150**, 552 (1936).
[4] R. Peierls, Proc. Roy. Soc. (London) **A154**, 207 (1936).
[5] J. G. Kirkwood, J. Chem. Phys. **6**, 70 (1938).
[6] W. L. Bragg and E. J. Williams, Proc. Roy. Soc. (London) **A145**, 699 (1934); **A151**, 540 (1935).
[7] D. T. Keating and B. E. Warren, J. Appl. Phys. **22**, 286 (1951).
[8] C. Sykes and F. W. Jones, Proc. Roy. Soc. (London) **A157**, 213 (1936).
[9] C. Sykes and H. Evans, J. Inst. Metals **58**, 225 (1936).
[10] S. Siegel, Phys. Rev. **57**, 537 (1940).
[11] S. Siegel, J. Chem. Phys. **8**, 860 (1940).
[12] Parkins, Dienes, and Brown, J. Appl. Phys. **22**, 1012 (1951).
[13] L. Balamuth, Phys. Rev. **45**, 715 (1934); F. C. Rose, Phys. Rev. **49**, 50 (1936); M. Durand, Phys. Rev. **50**, 449 (1936).
[14] E. A. Owen and Y. H. Liu, Phil. Mag. **38**, 354 (1947).

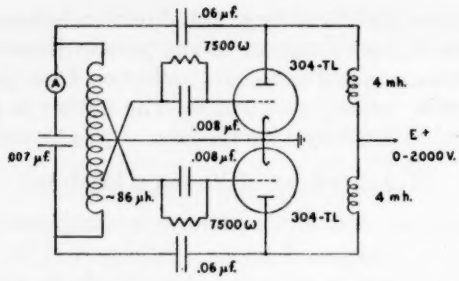

FIG. 1. Circuit diagram for induction furnace.

alumel thermocouple is constructed of No. 30 wire, and this is calibrated by comparison with a platinum-platinum 10 percent rhodium thermocouple. The junction is then opened, and the portions immediately proximal thereto are lightly tinned with silver solder. These are then inserted, each in one of two diametrically opposed slots, 0.01 in. wide and 0.01 in. deep, cut in the specimen rod at its center. The wires are held in place by a loop of glass thread, tied around the specimen rod at its center. Intimate thermal bonding between the tips of the wires and the specimen is provided by minute drops of du Pont silver, No. 4887, which, after application, are fired at 400°C in the induction furnace described below. Tests made on a copper cylinder reveal that temperatures indicated by this thermocouple assembly agree with those indicated by a couple soldered into a hole drilled along the axis of the rod to 0.1°C or better.

The Induction Furnace

The specimen is heated by an especially designed induction furnace operating at 220 kilocycles. Figure 1 is a diagram of the furnace circuit and Fig. 2 a scale drawing of the assembly which contains the specimen. The furnace coil consists of 76 turns of No. 11 copper wire wound along 8 inches of a vertical vitrosil tube 2 in. in diameter and 10 in. long. The winding is immersed in a bath of Dow-Corning DC200-5 centistoke silicone fluid which circulates in a concentric cylindrical container built of Lucite. A Lucite tube, within the vitrosil tube, forms the inner wall of this container, and encloses a tubular glass envelope in which the composite oscillator is mounted. A continuous circulation of the bath liquid is maintained through a copper coil immersed in a water bath thermostated at room temperature. The specimen chamber is evacuated with a mercury diffusion pump.

The specimen is maintained at any desired temperature in the following manner: A variac which controls the plate voltage supplying the furnace oscillator is set at the appropriate value, as is likewise a potentiometer which supplies an electromotive force connected in series opposition with that of the thermocouple attached to the specimen. The differential emf actuates a galvanometer whose light beam is deflected by a right angled prism into one of two photocells. The amplified photocurrents operate a relay which inserts or removes a small resistance in series with the variac. The device yields temperature stabilization within 0.1°C at 400°C. Manual variation of the resistance by an assistant permits stabilization within 0.05°C, and this is generally the practice during periods of observation. The temperature of measurement is given by the potentiometer setting.

The resonant frequency of the composite oscillator is about 37 kilocycles. The measurement of this frequency requires observation of the current which flows to the oscillator. Disturbing currents of 220 kilocycle frequency, produced by the furnace coil, are eliminated by an appropriate low pass filter inserted in a current lead to the oscillator.

The Quenching Procedure

The procedure by which the specimen temperature is lowered from a value above T_c to a predetermined value below it is the following: The voltage supply to the furnace oscillator is shut off, the settings of the variac and the potentiometer are altered appropriately, and a predetermined amount of helium, contained in a fixed volume at known pressure, is admitted at the bottom of the specimen chamber, from whence it is removed at the top by the pumps. The flow of helium past the specimen produces rapid cooling, indicated visually by the light beam of the galvanometer. Just prior to attainment of the new temperature the preset equilibrium power required for its maintenance is applied, and manual control followed, if desired, by automatic control begins. The whole process requires less than 30 seconds.

Accuracy of Measurement

As remarked in the foregoing, the computation of E_T requires knowledge of the resonant frequency of the quartz cylinder alone. This depends upon the temperature of the cylinder, which is not heated by the induction furnace and is not at the temperature of the specimen, or at any uniform temperature. The resonant frequency f_Q of the quartz cylinder is related to the temperature of the specimen by the following procedure: The variation of f_Q with temperature at uniform temperature is measured with the unit in a resistance furnace, as is likewise the variation with temperature of the resonant frequency of a composite oscillator constructed with a single crystal of copper identical in shape with the specimen. The resonant frequency of the copper crystal as a function of temperature is computed from these data. Next, this composite oscillator is mounted in the induction furnace and its resonant frequency measured as a function of the temperature of the copper specimen. Finally, f_Q is computed as a function of the same variable, and it is assumed that no significant change results when the copper crystal is replaced by the Cu_3Au crystal.

It is desired to know, first, the equilibrium difference in temperature between the center of the specimen and the end next to the quartz, and second, the elapsed time interval between the arrival of a stable temperature at the center and end of the specimen, respectively, after the specimen has been quenched. This information is obtained as follows: The thermocouple slots in the specimen are extended to the end.[15] Two thermojunctions are soldered together and calibrated, one against the other. One is mounted, as described above, at the center and the other at the end of the specimen (with quartz attached). Quenches are made from 414.2°C to 382.1°C, 368.9°C, 312.1°C, and 279.3°C. The corresponding observed temperature differences are 1.2°C, 1.0°C, 0.8°C, and 0.5°C. In all cases changes in temperature at the end follow those at the center very closely in time, and both temperatures assume their equilibrium values within 30 seconds or less.

It may be remarked that the value of the fundamental resonant frequency of a rod of length L is determined principally by the value of E at the center and not at all by the value at the ends. Thus, if x is the distance along the rod measured from one end and if $E(x)$ is the variation in E from the value E_0 at the center, then

$$\Delta f/f_0=(E_0L)^{-1}\int_0^L \Delta E(x)\,\sin^2(\pi/L)x dx, \qquad (4)$$

where f_0 is the resonant frequency associated with E_0, and Δf is the change resulting from $\Delta E(x)$. Particular estimates of the uncertainty in the computed values of E, which are due to the small temperature gradient in the specimen, appear in the sequel.

III. RESULTS

Determination of the Critical Temperature

The heat treatment of the specimen, prior to the initiation of the experiments here reported, is described in detail by Siegel.[10] He gives the value 387.5°C for the critical temperature for ordering in his crystals. The present observation reveals a temperature range between 385.5°C and 386.5°C such that, if the temperature of the specimen is brought within this range from above or below, the time rate of change of E is immeasurably slow. The value $T_c=386.0$°C is adopted here.

Variation of the Equilibrium Young's Modulus with Temperature

The variation with temperature of the Young's modulus associated with equilibrium order in the crystal is obtained as follows: The specimen is heated from room temperature to 368.9°C in 10 minutes and maintained there for 7 hours. No change in E occurs during the last 2 hours. The specimen is then cooled to 348.0°C at the rate of 1.2°C per hour in steps of 0.3°C every quarter hour. Observations of E are made every half-hour.

[15] This was done after the experiments were completed.

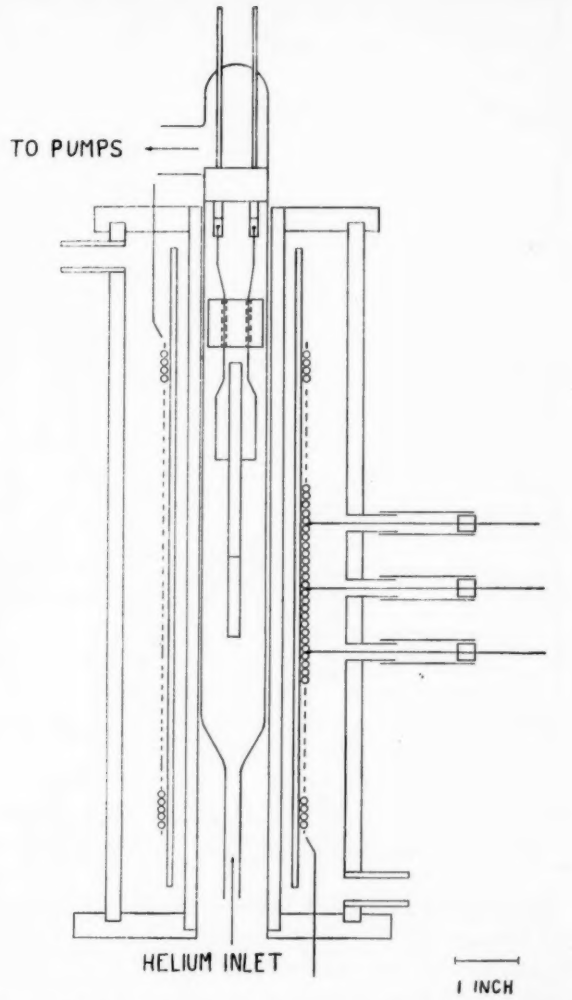

FIG. 2. Cross section of experimental arrangement showing piezoelectric oscillator, induction furnace coil, thermostatic bath, and provision for quenching with helium gas.

The variation of E with temperature above T_c is obtained as follows: The specimen is heated to 391.0°C in 10 minutes and maintained there for 7 hours. No change in E occurs during the last 2 hours. The specimen is then heated at 1.2°C to 1.5°C per hour, with observations every half-hour.

The results are given in the column headed E_e of Table I and are plotted on the topmost curve of Fig. 3. These values of E_e, over the whole temperature range both above and below T_c, lie about 2.5 percent *below* those computed with Siegel's equilibrium values for elastic constants.[10] Under the circumstances this is a reasonable estimate of the accuracy, for comparison, of the two measured *absolute values* of E_e. Siegel's data represents averages of observations made on five different crystals. It is characteristic of the present method that the accuracy of measurement of *changes* in E is far greater than that of the absolute value.

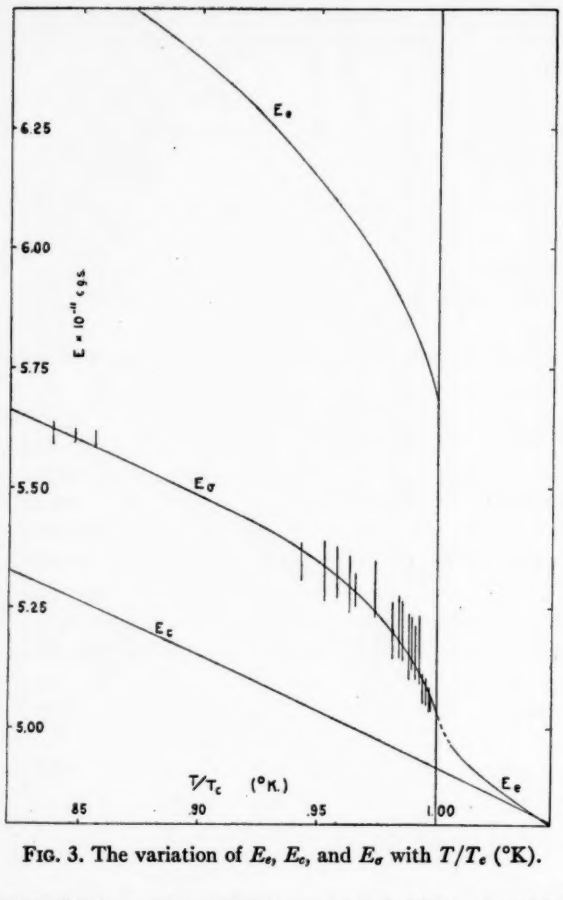

FIG. 3. The variation of E_e, E_c, and E_σ with T/T_c (°K).

Equilibrium values of E between 368.9°C and 386.0°C and between 279.3°C and 348.0°C are obtained by extrapolation of the observations made below 368.9°C along a curve running parallel to (and 2.5 percent under) that computed with Siegel's data in these ranges.

Variation of Young's Modulus with Temperature at Constant Order

When the specimen is cooled from a temperature above T_c to one below it, the value of the Young's modulus increases as a consequence both of the change in temperature and of the change in order that occurs during the cooling process. It is desired to separate these two effects and so to ascertain what the value of the modulus would be if no change in order occurred. This is accomplished in the following manner: The specimen temperature is raised to 414.2°C and held there for 15 minutes, after which no change in E occurs. It is then quenched to 300°C in about 18 seconds, and held there until a preassigned value of E, less than the equilibrium value, is observed, whereupon the temperature is lowered to 100°C in 15 to 20 seconds by the quenching process. The specimen chamber is now filled with helium and the specimen cooled to room temperature. This procedure leaves the specimen at room temperature in very nearly the same state of order as at 300°C. Finally, the specimen is heated to 200°C in 10 minutes, during which time E is measured at 25° intervals.

The resulting curves of E *vs* T lie parallel to one another, indicating that no appreciable change in order accompanies the rapid heating from 30°C to 200°C. Furthermore, the value of the quantity d^2E/dT^2 remains constant, irrespective of temperature or order. Thus, in this temperature range and with this heat treatment, the material behaves like a monatomic metal. It is now assumed that it would continue to do so over the temperature range 200°C to 414.2°C, *were it to be heated rapidly enough*. This assumption permits a ready extrapolation of the zero long-range order E *vs* T curve below 200°C so as to join smoothly on to the E *vs* T curve above 414.2°C. The result appears as the lowest curve of Fig. 3. The data are given in Table II, in which E_c denotes the value of E at constant order, namely, the order at 414.2°C.

TABLE I. Variation of the equilibrium Young's modulus and the quantity E_σ with temperature (T/T_c °K).

T/T_c (°K)	T °C	E_e ×10⁻¹¹ cgs	E_σ ×10⁻¹¹ cgs	T/T_c (°K)	T °C	E_e ×10⁻¹¹ cgs	E_σ ×10⁻¹¹ cgs
0.82	267.3	6.642	5.665	0.96	359.6	6.080	5.307
0.84	280.5	6.591	5.620	0.98	372.8	5.930	5.209
0.86	293.7	6.533	5.575	1.00	386.0	5.684	
0.88	306.9	6.469	5.530	1.02	399.2	4.900	
0.90	320.1	6.393	5.483	1.04	412.4	4.827	
0.92	333.3	6.305	5.437	1.06	425.6	4.762	
0.94	346.4	6.200	5.381				

TABLE II. Variation of Young's modulus at constant order with temperature (T/T_c °K).

T/T_c	T °C	E_e ×10⁻¹¹ cgs	T/T_c	T °C	E_e ×10⁻¹¹ cgs
0.45	23.4	6.037	0.75	221.2	5.475
0.50	56.4	5.951	0.80	254.2	5.371
0.55	89.4	5.862	0.85	287.1	5.263
0.60	122.3	5.770	0.90	320.1	5.152
0.65	155.3	5.675	0.95	353.0	5.038
0.70	208.2	5.577	1.00	386.0	4.920
			1.05	419.0	4.800

Confirmation of the validity of this curve is found in the fact that whenever the specimen is quenched from 414.2°C to a temperature below T_c, the first measured value of E invariably lies *above* the curve by a reasonable amount.

Isothermal Variation of Young's Modulus with Time

The isothermal variation of Young's modulus with time following a quench from equilibrium disorder at 414.2°C is exhibited in Table III. The instant corresponding to the zero of time in this table is the instant at which the quenched specimen reaches the temperature of measurement, which is between 8 seconds (at temperatures above 360°C) and 20 seconds (at lower temperatures) later than the instant when the specimen

begins to cool. The tabulated quantity is the difference between the values, E_T, of Young's modulus at the temperature and time of measurement and the value of E_e at the same temperature (Table II). The first is obtained from a smooth curve drawn through the plotted observations of E as a function of the time at

TABLE III. Isothermal variation of Young's modulus with time. The zero of time is the instant at which the quenched specimen reached the temperature of measurement.

Time (min) \ T/T_c (°K)	0.8381	0.8472	0.8560	0.8879	0.9028	0.9424	0.9741
				$(E_T-E_e)\times10^{-10}$ cgs			
0.0				1.62		1.20	
0.5	1.87	1.79	1.90	2.12	2.29	2.17	1.71
1.0	1.98	1.95	2.08	2.47	2.73	2.95	2.58
1.5	2.08	2.08	2.23	2.77	3.12	3.76	3.33
2.0	2.16	2.18	2.36	3.04	3.48	4.47	4.04
2.5	2.24	2.28	2.49	3.28	3.82	5.13	4.80
3.0	2.31	2.38	2.60	3.59	4.16	5.67	5.36
3.5	2.38	2.46	2.71	3.76	4.48	6.14	5.80
4.0	2.45	2.55	2.82	3.98	4.78	6.54	6.13
4.5	2.51	2.64	2.92	4.20	5.06	6.85	6.39
5.0	2.57	2.71	3.00	4.41	5.33	7.10	6.60
5.5	2.63	2.79	3.11	4.62	5.58	7.30	6.76
6.0	2.69	2.86	3.20	4.82	5.82	7.47	6.90
7.0	2.80	3.00	3.37	5.20	6.25	7.76	
8.0	2.90	3.13	3.54	5.56	6.64		
9.0	3.00	3.26	3.72	5.89	6.98		
10.0	3.09	3.38	3.89	6.19	7.27		
11.0	3.19	3.52	4.06	6.48	7.52		
12.0	3.29	3.65	4.21	6.74	7.74		
15.0	3.59	3.81	4.64	7.38	8.21		
18.0	3.85	4.34	5.04	7.85	8.55		
21.0	4.09	4.66	5.43	8.21	8.79		
24.0	4.31	4.94	5.78	8.50	8.99		
27.0	4.53	5.22	6.10	8.73	9.13		
30.0	4.74	5.46	6.41	8.90	9.24		
35.0	5.07			9.15	9.41		
40.0	5.40			9.31	9.53		

Time (min) \ T/T_c (°K)	0.9885	0.9912	0.9941	0.9955	0.9968	0.9974
			$(E_T-E_e)\times10^{-10}$ cgs			
0.0	0.90				0.62	0.73
0.5	1.26	1.10	1.05	0.96	0.88	0.92
1.0	1.59	1.34	1.17	1.09	0.98	0.98
1.5	1.90	1.56	1.27	1.18	1.03	1.01
2.0	2.22	1.76	1.37	1.25	1.06	1.03
2.5	2.55	1.95	1.47	1.31	1.09	1.05
3.0	2.92	2.13	1.57	1.36	1.11	1.07
3.5	3.32	2.32	1.67	1.42	1.13	1.09
4.0	3.69	2.64	1.79	1.49	1.15	1.11
4.5	4.06	2.91	1.92	1.55	1.18	1.13
5.0	4.38	3.16	2.05	1.62	1.21	1.15
5.5	4.69	3.40	2.19	1.70	1.23	1.17
6.0	4.94	3.64	2.33	1.77	1.26	1.19
7.0	5.37	4.07	2.61	1.92	1.33	1.24
8.0	5.71	4.39	2.88	2.13	1.40	1.30
9.0	5.98	4.77	3.14	2.23	1.49	1.36
10.0	6.20	5.06	3.38	2.49	1.59	1.43
11.0	6.38	5.30	3.61	2.55	1.70	1.48
12.0	6.52	5.52	3.82	2.70		
15.0	6.85	6.00	4.35	3.09		
18.0	7.07	6.32	4.77	3.43		
21.0	7.24	6.58	5.11	3.73		
24.0	7.37	6.80	5.43	3.98		
27.0		6.96	5.66	4.19		
30.0			5.86	4.38		
35.0			6.11	4.66		
40.0				4.90		
45.0				5.11		

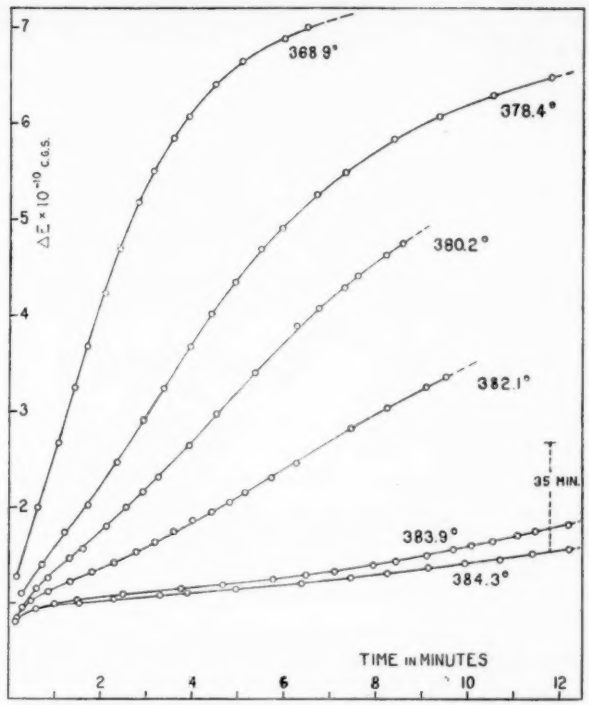

FIG. 4. The isothermal variation of Young's modulus with time at various temperatures. $\Delta E = E_T - E_e$.

constant temperature. A number of such plots are shown in Fig. 4 and one as the solid line curve of Fig. 5. In accordance with Eq. (4), it is estimated that the error in (E_T-E_e), caused by nonuniformity of temperature in the specimen, is not greater than 2 percent.

A scrutiny of these data reveals, first, that equilibrium order is achieved in two distinct stages; second, that the rate of the first stage is much greater than that of the second; and third, that the second stage *starts* sometime later than the first. It is desired to evaluate separately the contribution of the process responsible for each stage to the observed time variation of Young's modulus. This is done in the following manner.

It is assumed that the value of Young's modulus corresponding to completion of the first stage, without intervention of the second, lies between values analogous at any temperature, to those labeled E_A and E_B in Fig. 5, namely, to those which lie at the points of inflection of the isothermal curve. The intervals (E_A-E_B) are then plotted as the vertical lines of Fig. 3. Finally, the curve labelled E_σ in Fig. 3 is drawn as shown there, and it is assumed that the differences between corresponding ordinates of this curve and those labeled E_c and E_σ evaluate the isothermal equilibrium changes in Young's modulus produced by the processes responsible for the first and second stages, respectively. It will be noted that the E_σ curve is a smooth continuation below T_c of the equilibrium order curve above T_c. The column headed E_σ in Table I contains data with which the E_σ curve may be plotted.

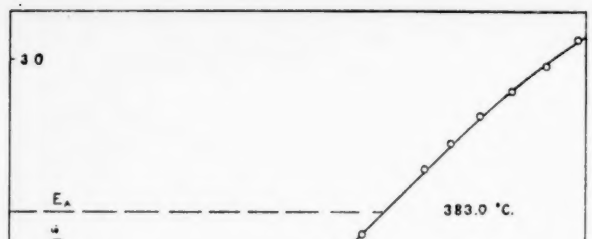

FIG. 5. Separation of the stages in the isothermal variation of Young's modulus with time.

Determination of Relaxation Times for First and Second Stages

It is found that, within the accuracy of measurement, the isothermal time variation of Young's modulus during the first stage proceeds in accordance with the formula

$$(E_\sigma - E_T) = (E_\sigma - E_e)(1 - e^{-t/\tau}). \qquad (5)$$

The observed variation of the relaxation time τ with temperature is given in Table IV and is shown graphically by the curve labeled "τ" in Fig. 6. The extrapolated (dashed) portion of the initial stage of Fig. 5 is computed with Eq. (5).

In accordance with the observations of Siegel,[11] the isothermal time variation of Young's modulus during the second stage cannot be described by Eq. (5). However, as noted by Siegel, all of the curves which depict this time variation can be superimposed *approximately* on any one of them by an appropriate alteration in the time scale of each curve. This circumstance permits the definition of a mean relative "relaxation time" $\bar{\gamma}$ which is a rough approximation to the average true relaxation times of the two or more processes jointly operative during the second stage. Thus, let $\bar{\gamma}=1$ at an arbitrary temperature, here chosen as 368.9°C, and set, for brevity, $(E_e - E_\sigma) = \Delta E$. Let Δt_1 denote the time required, at this temperature, for the value of $(E_e - E_T)$ to decrease from $0.70\Delta E$ to $0.50\Delta E$, and Δt_2 denote the time required for the value to decrease from $0.50\Delta E$ to $0.35\Delta E$. Let $\Delta t_1'$, $\Delta t_2'$ denote the same quantities measured at a different temperature T. Then

$$\bar{\gamma}_T \equiv \tfrac{1}{2}(\gamma_1 + \gamma_2), \qquad (6)$$

where

$$\gamma_1 = \Delta t_1'/\Delta t_1; \quad \gamma_2 = \Delta t_2'/\Delta t_2.$$

Values of γ_1, γ_2, and γ_T computed with Eq. (6) are given in Table IV, and the variation of $\bar{\gamma}_T$ with temperature is depicted by the appropriate curve of Fig. 6. Values of γ_T computed with Siegel's data[11] are plotted on this curve for comparison.

IV. DISCUSSION

The foregoing phenomena find plausible interpretation in terms of processes suggested by Sykes and Jones[8] to account for the observed variation of specific heat with temperatures in a specimen which, after rapid quenching to room temperature from a temperature above T_c, is slowly reheated. For example, in a specimen quenched from 395°C the specific heat remains normal and constant up to 60°C; above 60°C it decreases to a minimum at 130°C, rises to the normal value at 230°C, then decreases to a sharp minimum at 314°C, after which it increases steadily up to the critical temperature assuming the normal value at 340°C. The suggested mechanism is briefly as described in the following paragraph.

It is assumed that, in the quenched specimen, there exists a large number of places where a small number of adjacent atoms possesses a high degree of order of nearest neighbors. These places act as nuclei for the growth of ordered domains, which growth starts at 60°C and is accompanied by a release of energy with consequent lowering of the specific heat. As the temperature is raised, two competing processes coexist, namely disordering within the domains, with absorption

TABLE IV. The temperature variation of the relaxation time τ of the first stage and the relative relaxation times γ_1, γ_2, $\bar{\gamma}_T$ of the second stage.

T_c/T (°K)	τ (min)	γ_1	γ_2	$\bar{\gamma}_T$
1.0032	4.06			
1.0045	1.98	13.08		13.08
1.0059	1.64	5.31	3.54	4.43
1.0074	1.19			
1.0089	1.19	2.57	1.83	2.20
1.0104	1.11	1.96		1.96
1.0116	1.04	1.58	1.21	1.40
1.0146	1.07	1.29		1.29
1.0161		1.26	1.18	1.22
1.0192	0.72	1.05	0.97	1.01
1.0266		1.00	1.00	1.00
1.0325		1.04		1.04
1.0353		1.03	1.28	1.16
1.0383		1.06	1.09	1.08
1.0438	0.62	1.07	1.26	1.12
1.0496		1.17	1.39	1.28
1.0555	0.67	1.25		1.25
1.0608	0.79	1.34	1.49	1.42
1.0722		1.81	1.92	1.87
1.0892		2.30		2.30
1.1077	1.08	3.53	4.19	3.86
1.1263	1.43	5.38	6.18	5.78
1.1682	3.92			
1.1804	5.55			
1.1932	7.32			

of energy and growth of domains with release of energy. At 130°C the domains touch at certain points and between this temperature and 230°C growth is progressively retarded. Adjacent domains may be antiphase, and domain boundaries contain a preponderance of atoms of one kind or the other, consequent upon submicroscopic fluctuations in the atomic composition of the material. Further growth proceeds by the absorption of certain domains by others and by the diffusion of excess atoms along domain boundaries. At 230°C growth recommences and continues to the critical temperature. The sharpness of the minimum at 314°C on the specific heat curve is the combined result of a decrease in amount of disordered material on the boundaries together with a rapid increase in disorder within the domains, as the temperature is raised. Sykes and Jones estimate from energy calculations and x-ray diffraction data, that the linear dimensions of the domains at 130°C are roughly 6 to 8 interatomic distances and at 340°C are 12 to 14 interatomic distances.

In conformance with the foregoing, the following descriptions of the processes responsible for the phenomena under review here is proposed:

(a) Short-range order exists above T_c, as may be deduced from the E_e curve of Fig. 3, from specific heat measurements,[8] and from the values of the short-range order parameters computed with x-ray diffraction data.[16] This order is subject to statistical fluctuation which results in the occurrence of small groups of atoms in highly ordered array.

(b) When the material is quenched these groups act as nuclei for the formation of domains within which the equilibrium order appropriate to the temperature subsists. The time τ is the relaxation time for this process of domain growth, which is completed when the domains become contiguous. The process requires the utilization of atoms in the ratio of three copper to one gold, approximately. Accordingly, excess atoms of one kind or the other are finally concentrated at the domain boundaries. Contiguous domains may be antiphase, i.e., different sublattices may be occupied predominantly by gold atoms.

(c) The subsequent achievement of equilibrium long-range order in the specimen involves the dual mechanism of coalescence of domains and diffusion of atoms over domain boundaries. The quantity $\bar{\gamma}$ is a rough relative measure of the average relaxation time for these processes.

(d) The reason why the curve of E_e Fig. 3 joins smoothly at T_c onto that of E_e is not clear. Its elucidation appears to require more detailed knowledge of the relation between Young's modulus and the types of order described above, and particularly of the initial domain size (or the number density of atomic groups able to act as nuclei) as a function of temperature not far below T_c.

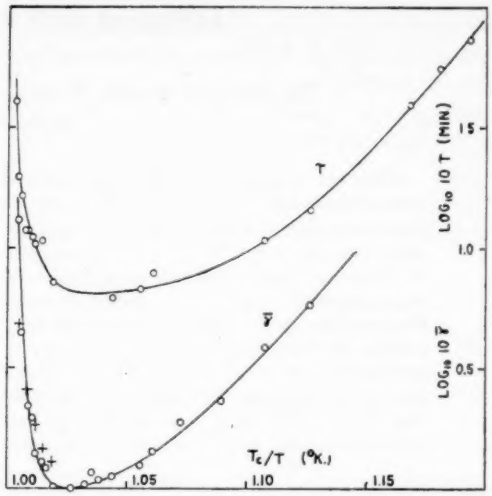

FIG. 6. The temperature variation of the relaxation time τ of the first stage and the mean relative relaxation time $\bar{\gamma}$ of the second stage. The crosses indicate the values computed with Siegel's data.

The view here adopted is further supported by observations of Sykes and Evans,[9] and Cowley.[16] The former noted that a specimen initially disordered must be annealed many hours before the domains become sufficiently large that their boundaries have no appreciable effect upon the electrical resistance, and that when this condition exists, equilibrium resistance, as an indication of equilibrium order, at a new temperature is achieved rapidly. Cowley observed the time variation of the integrated intensity of x-ray reflection from a crystal initially disordered and held at 360°C. The half maximum value is reached in 15 minutes, after which the integrated intensity increases at an ever diminishing rate.

In conclusion, the writer gratefully acknowledges the assistance of Dr. Sidney Siegel who supplied the single crystal upon which the measurements reported here were made; Mr. S. Zerensky who suggested the use of silicone resin as adhesive; Mr. Fred Burns who cooperated in the manipulation of the apparatus; and Dr. S. L. Quimby who followed the progress of the work with helpful counsel and encouragement.

[16] J. M. Cowley, J. Appl. Phys. **21**, 24 (1950).

Diffusion with a Sharp Moving Boundary

HIROSHI FUJITA
Department of Fisheries, Faculty of Agriculture, Kyoto University, Maizuru, Japan
(Received September 17, 1952)

When the molecules of a diffusing substance react with the medium into which they diffuse in such a manner that they no longer take part in the diffusion process, a sharp boundary line results which is displaced at a rate determined by the conditions of the particular experiment. A theory of this phenomenon was presented by J. J. Hermans and was applied to determine the diffusion constants in some ion-gel systems. In the present paper the method of moments which was recently worked out by Yamada to deal with the boundary-layer equations is applied to obtain approximate solutions of the basic equations of the J. J. Hermans theory for both linear and cylindrical diffusions. The particular concern of the present paper is to analyze the experimental data obtained by J. J. Hermans for cylindrical diffusion in a copper ion-cellulose xanthate system on a more reliable basis than in J. J. Hermans' paper referred to. It is found that the present analysis provides the diffusion constants which are considerably higher (about 2.6 times) than those evaluated by J. J. Hermans. Nevertheless, the values found are still too low as compared with the experimental value determined by the steady-state method, and a further research of the problem needs to be made.

INTRODUCTION

RECENT observations on the penetration of low molecular-weight substances into high polymers have shown[1–3] that a sharp moving boundary line results in the medium through which diffusion takes place when the diffusing particles react with the medium to form a precipitate and are thus withdrawn from the diffusion process or when the diffusion coefficient increases rapidly with increasing concentration of the diffusant. Some time ago, J. J. Hermans[2] presented a theory of the diffusion process controlled by the former mechanism, i.e., the anchoring of the diffusant by the polymer solid, in the form identical with that in the well-known heat conduction problem for the formation of ice, and applied it to his experimental data on diffusions in some ion-gel systems to evaluate the diffusion constants in those systems. The system of equations on which his theory is based can be solved analytically for the case of linear diffusion in a semi-infinite medium by the use of Neumann's method of solution which may be found in the textbooks[4] on the conduction of heat, but for media of finite dimensions no formal solutions of the problem have yet been known. For this reason J. J. Hermans had to be satisfied for the case of cylindrical diffusion with only a tentative analysis of the data based on an empirical treatment. Recently, in connection with the growth of aerosol particles or of a new phase by diffusion, a system of equations which is identical, in essential part, with that appearing in J. J. Hermans' theory was discussed by several investigators[5–8] using various assumptions and methods. The solutions therein presented are restricted generally to the spherically symmetric case except only one, that involved in Frank's paper.[7] In addition, these authors are all interested in problems somewhat different in physical character from that associated with Hermans' theory. Thus, no means are available from their papers to serve for analyzing J. J. Hermans' experimental data on cylindrical diffusion in ion-gel systems.

The purpose of the present paper is to derive approximate solutions of the basic equations in J. J. Hermans' theory for both linear and cylindrical diffusions by making use of the method of moments which was recently worked out by Yamada[9] as an extension of the Kármán-Pohlhausen method familiar in the theory of the laminar boundary-layer equations. It has been shown in several papers of the present author[10–12] that this method of solution can also be applied with successful results for various problems relating to concentration-dependent diffusion in one direction. It is thus of interest to investigate whether this method is useful also for problems of diffusion involving a sharp moving boundary. The method is first applied to linear diffusion in a semi-infinite medium, because for this case the rigorous solution has been known as mentioned above, and it is thus possible to check the applicability of the present method to this kind of diffusion problem. Consideration is then extended to radial diffusion in a cylindrical medium of infinite length, with a particular interest of obtaining a relevant approximate solution permitting analysis of the experimental data obtained with a copper ion-cellulose xanthate system.

LINEAR DIFFUSION

For linear diffusion into a semi-infinite medium the basic equations of J. J. Hermans' theory may be

[1] P. H. Hermans and D. Vermaas, J. Polymer Sci. **1**, 149 (1946).
[2] J. J. Hermans, J. Colloid Sci. **2**, 387 (1947).
[3] G. S. Hartley, Trans. Faraday Soc. **42B**, 6 (1946).
[4] H. S. Carslaw and J. C. Jaeger, *Conduction of Heat in Solids* (Oxford University Press, London, 1947), p. 71.
[5] F. C. Collins, unpublished work (1951).
[6] F. C. Collins and H. L. Frisch, J. Chem. Phys. **20**, 1797 (1952).
[7] F. C. Frank, Proc. Roy. Soc. (London) **A201**, 586 (1950).
[8] H. Reiss and V. K. LaMer, J. Chem. Phys. **18**, 1 (1950).
[9] H. Yamada, Rept. Research Inst. Fluid Engineering, Kyushu Univ. **6** (2), 42 (1950).
[10] H. Fujita, Mem. Coll. Agr., Kyoto Univ. No. **59**, 31 (1951).
[11] H. Fujita and A. Kishimoto, Textile Research J. **22**, 94 (1952).
[12] H. Fujita, Bull. Japan. Soc. Scient. Fish. **17**, 393 (1952).

written

$$\partial C/\partial t = D(\partial^2 C/\partial x^2) \quad (0<x<\xi,\ t>0), \tag{1}$$

$$C(0, t) = C_0 \quad (t>0), \tag{2}$$

$$C(x, 0) = 0 \quad (x>0), \tag{3}$$

$$C(\xi, t) = 0 \quad (\xi>0,\ t>0), \tag{4}$$

$$D(\partial C/\partial x)_{x=\xi} = -b(d\xi/dt) \quad (\xi>0), \tag{5}$$

where x is the distance measured from the surface of the medium in the direction of diffusion, ξ is the coordinate of the moving boundary line, t is the time, C is the concentration of diffusing substance, C_0 is its surface value (assumed to be constant), and b is the concentration of the holes at which the diffusing particles react with the medium to form a precipitate. Also, D is the diffusion coefficient of the penetrant and assumed to be constant.

It is convenient to introduce the following dimensionless variables:

$$C/C_0 = \psi,\ x/L = z,\ \xi/L = Z,\ tD/L^2 = \tau,\ b/C_0 = \beta, \tag{6}$$

where L is an appropriate unit of length to be chosen properly according to respective problems concerned. Equations (1) to (5) then reduce to

$$\partial\psi/\partial\tau = \partial^2\psi/\partial z^2 \quad (0<z<Z,\ \tau>0), \tag{7}$$

$$\psi(0, \tau) = 1 \quad (\tau>0), \tag{8}$$

$$\psi(z, 0) = 0 \quad (z>0), \tag{9}$$

$$\psi(Z, \tau) = 0 \quad (Z>0,\ \tau>0), \tag{10}$$

$$(\partial\psi/\partial z)_{z=Z} = -\beta(dZ/d\tau) \quad (Z>0). \tag{11}$$

It is to be noted that the fundamental system of equations thus reduced involves only a single parameter of β.

The formal solutions of the above system of equations are well known,[4] giving

$$\psi(z, \tau) = 1 - \frac{\Phi(z/2\sqrt{\tau})}{\Phi(\sqrt{q})} \quad (0<z<Z), \tag{12}$$

$$Z(\tau) = 2q^{\frac{1}{2}}\tau^{\frac{1}{2}} \quad (\tau>0), \tag{13}$$

where Φ denotes the error function, and q is a constant associated with the parameter β by the transcendental equation:

$$1/\beta = (\pi q)^{\frac{1}{2}} e^q \Phi(\sqrt{q}). \tag{14}$$

Equation (13) indicates that the sharp boundary line in question is displaced in the medium according to the simple relationship that $\xi/\sqrt{t}$ = constant. This relationship was confirmed experimentally by J. J. Hermans[2] for the penetration of metallic ions into gelatin gels.

In previous applications[10–12] of the method of moments to problems concerning concentration-dependent diffusion in one dimension, it was found that use of two moment-equations corresponding to the zeroth and first moments was ordinarily sufficient for obtaining the approximate solutions, accurate enough for most practical purposes. In view of this, the present calculations concerning diffusions with a sharp moving boundary will also be attempted by employing only these two moment-equations.

The zeroth and first moment-equations, when applied to Eq. (7), take, respectively, the forms:

$$\int_0^Z \left(\frac{\partial\psi}{\partial\tau} - \frac{\partial^2\psi}{\partial z^2}\right) dz = 0 \quad (0<z<Z), \tag{15}$$

and

$$\int_0^Z \left(\frac{\partial\psi}{\partial\tau} - \frac{\partial^2\psi}{\partial z^2}\right) z\,dz = 0 \quad (0<z<Z). \tag{16}$$

The problem to be solved next is now stated as follows: find the expressions of ψ and Z, satisfying these two moment-equations together with the conditions (8) to (11). For this purpose, after the procedure set forth in the previous papers,[10,12] we shall assume for $\psi(z, \tau)$ in $0<z<Z$, a cubic equation of the form

$$\psi(z, \tau) = A(\tau)[z - Z(\tau)] + B(\tau)[z - Z(\tau)]^2 + C(\tau)[z - Z(\tau)]^3, \tag{17}$$

where $A(\tau)$, $B(\tau)$, $C(\tau)$, and $Z(\tau)$ are unknown functions of τ to be determined in what follows. It should be noted that the expression (17) fulfills the condition (10) automatically.

Putting

$$AZ^2 = U,\quad BZ^3 = V,\quad CZ^4 = W, \tag{18}$$

we have from the conditions (8) and (11)

$$-U + V - W = Z \tag{19}$$

and

$$-\beta Z^2 \frac{dZ}{d\tau} = U, \tag{20}$$

respectively. The zeroth moment-equation (15), on introduction of Eq. (17) and reductions, gives

$$\frac{d}{d\tau}\left(\frac{\beta}{4}Z^2\frac{dZ}{d\tau} + \frac{V}{12} + \frac{Z}{4}\right) = -3\beta\frac{dZ}{d\tau} + \frac{1}{Z^2}(3Z - V). \tag{21}$$

Similarly, from the first moment-equation (16), there results

$$\frac{d}{d\tau}\left\{Z\left(\frac{7\beta}{60}Z^2\frac{dZ}{d\tau} + \frac{V}{30} + \frac{Z}{20}\right)\right\} = -\beta Z\frac{dZ}{d\tau} + 1, \tag{22}$$

which, on integrating, gives

$$Z\left(\frac{7\beta}{60}Z^2\frac{dZ}{d\tau} + \frac{V}{30} + \frac{Z}{20}\right) = -\frac{\beta}{2}Z^2 + \tau + K, \tag{23}$$

where K is an integration constant. It is evident from the physical inspection that $Z(\tau) \to 0$ as $\tau \to 0$, which

results in $K=0$, and we then have

$$V=\tfrac{1}{2}\{-7\beta Z^2(dZ/d\tau)-(3+30\beta)Z+60(\tau/Z)\}. \quad (24)$$

Eliminating V from Eqs. (21) and (24), we obtain a differential equation for Z of the form

$$\frac{d}{d\tau}\left\{\frac{\beta}{24}Z^2\frac{dZ}{d\tau}-\left(\frac{1}{8}-\frac{5\beta}{4}\right)Z-\frac{5}{2}\frac{\tau}{Z}\right\}$$

$$-\frac{5\beta}{2}\frac{dZ}{d\tau}+\left(\frac{9}{2}+15\beta\right)\frac{1}{Z}-30\frac{\tau}{Z^3}=0. \quad (25)$$

The solution of this equation subject to the above-mentioned initial condition that $Z(0)=0$ is readily found to be

$$Z(\tau)=2q^{\frac{1}{2}}\tau^{\frac{1}{2}}, \quad (26)$$

where q is any root of the following equation:

$$2\beta q^3+(42\beta-3)q^2+(180\beta+39)q-90=0. \quad (27)$$

In order that the solution (26) may have any physical meaning q must be a positive quantity. If there exist in Eq. (27) more positive roots than a single one, the question arises which positive roots are to be taken. As was pointed out by Yamada,[9] similar questions are found in dealing with nonlinear differential equations by means of the method of moments. An analytical procedure by which to resolve these questions systematically has been suggested by Yamada,[9] but it is, in general, too cumbersome to be put into practice. Direct physical inspection of given problems often proves to be useful for this purpose. For the problem herein considered such a physical inspection was found to be very effective; it is in noticing that ξ, or Z, should remain zero when b is infinitely large. In other words, q should tend to zero as β becomes infinitely large. With this in mind, the required q values have been evaluated from Eq. (27) as a function of $1/\beta$, and the results obtained are plotted in Fig. 1 with dotted line. In this figure, the corresponding exact relation computed from Eq. (14) is also plotted with solid line. Comparison shows that our approximate solution follows very closely the exact one over a fairly wide range of the parameter β.

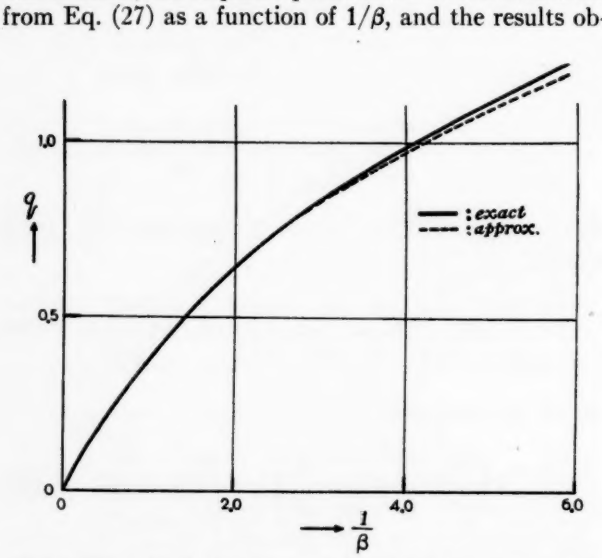

FIG. 1. Comparison of the present solution with the exact one with respect to the relation between q and $1/\beta$.

Inserting Eq. (26) into Eq. (20), we obtain for U,

$$U=-2\beta qZ. \quad (28)$$

The expression for V then is found to be

$$V=\left(\frac{15}{2q}-\frac{3}{2}-15\beta-7\beta q\right)Z. \quad (29)$$

On substituting these equations into Eq. (19), we have for W,

$$W=\left(\frac{15}{2q}-\frac{5}{2}-15\beta-5\beta q\right)Z. \quad (30)$$

Substituting all of these into Eq. (17), we arrive at the result that

$$\psi(z,\tau)=-2\beta q\left(\frac{z}{2(q\tau)^{\frac{1}{2}}}-1\right)$$

$$+\left(\frac{15}{2q}-\frac{3}{2}-15\beta-7\beta q\right)\left(\frac{z}{2(q\tau)^{\frac{1}{2}}}-1\right)^2$$

$$+\left(\frac{15}{2q}-\frac{5}{2}-15\beta-5\beta q\right)\left(\frac{z}{2(q\tau)^{\frac{1}{2}}}-1\right)^3. \quad (31)$$

This is to be compared with the corresponding exact solution represented by Eq. (12). An example of this comparison is shown in Fig. 2 for the case of $\beta=27/112$. The agreement is seen to be quite well over the range of the coordinate indicated. It was found that the approximation of the solution (31) becomes much better as β increases. However, even at the limiting case as β approaches zero, the average deviation from the true solution was found to remain at most only a few percent.

CYLINDRICAL DIFFUSION

For the case of radial diffusion in a circular cylinder of infinite length Hermans' problem may be formulated, using the dimensionless variables introduced in the preceding section, as follows:

$$\frac{\partial\psi}{\partial\tau}=\frac{1}{z}\frac{\partial}{\partial z}\left(z\frac{\partial\psi}{\partial z}\right) \quad (Z<z<1, \quad \tau>0), \quad (32)$$

$$\psi(1,\tau)=1 \quad (\tau>0), \quad (33)$$

$$\psi(z,0)=0 \quad (0<z<1), \quad (34)$$

$$\psi(Z,\tau)=0 \quad (0<Z<1, \quad \tau>0), \quad (35)$$

$$(\partial\psi/\partial z)_{z=Z}=-\beta(dZ/d\tau) \quad (0<Z<1). \quad (36)$$

Here, x is to be interpreted as the radial distance measured from the center of the cylinder, and L is to be taken as the radius of the cylinder. So far as the present author is aware, no formal solution of the above system of equations is yet known, and it seems doubtful whether such a simple solution as found for the linear diffusion discussed above can be generated also for the cylindrical case.

In the present case, the moment equations corresponding to Eqs. (15) and (16) take the following forms:

$$\int_Z^1 \left\{ \frac{\partial \psi}{\partial \tau} - \frac{1}{z}\frac{\partial}{\partial z}\left(z\frac{\partial \psi}{\partial z} \right) \right\} z dz = 0 \quad (Z<z<1), \tag{37}$$

$$\int_Z^1 \left\{ \frac{\partial \psi}{\partial z} - \frac{1}{z}\frac{\partial}{\partial z}\left(z\frac{\partial \psi}{\partial z} \right) \right\} z^2 dz = 0 \quad (Z<z<1). \tag{38}$$

In writing these equations, caution must be made of the "areal effect" to be added to the moments.

Analogous to the preceding section the following cubic expression is assumed for ψ in $Z<z<1$:

$$\psi(z,\tau) = A(\tau)[z-Z(\tau)] + B(\tau)[z-Z(\tau)]^2 + C(\tau)[z-Z(\tau)]^3, \tag{39}$$

which again satisfies the condition (35) automatically. Putting

$$1-Z = y, \tag{40}$$

$$Ay^2 = U, \quad By^3 = V, \quad Cy^4 = W, \tag{41}$$

Eqs. (33) and (36) give, respectively,

$$U+V+W = y, \tag{42}$$

and

$$\beta y^2 (dy/d\tau) = U. \tag{43}$$

In the present problem, Z is limited in the range $0<Z<1$, so that y, thus defined, also moves in the same range.

The zeroth moment-equation (37) gives

$$\frac{d}{d\tau}\left\{ \left(\frac{1}{4} - \frac{7}{60}y \right) U + \left(\frac{1}{12} - \frac{1}{30}y \right) V \right\} = \frac{3}{y} - \frac{1}{y^2}(2U+V) - \left\{ \beta(1-y) + \left(\frac{1}{4} - \frac{1}{10}y \right) \right\} \frac{dy}{d\tau},$$

which, on inserting Eq. (43) and putting

$$y(dy/d\tau) = \Theta, \tag{44}$$

reduces to

$$y\Theta \frac{d}{dy}\left\{ \beta y \left(\frac{1}{4} - \frac{7}{60}y \right) \Theta + \left(\frac{1}{12} - \frac{1}{30}y \right) V \right\} = 3y - y\left\{ \beta(3-y) + \frac{1}{4} - \frac{1}{10}y \right\} \Theta - V. \tag{45}$$

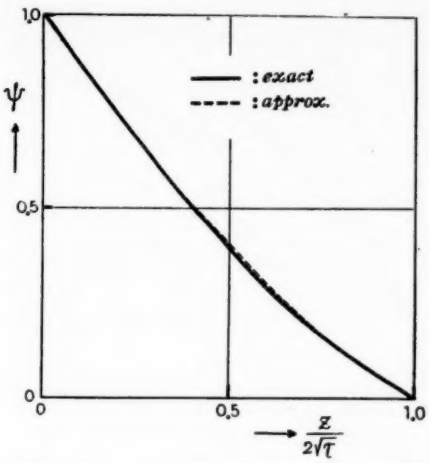

FIG. 2. Concentration-distance curves calculated at $\beta = 27/112$.

Analogously, from the first moment-equation there results

$$\Theta \frac{d}{dy}\left\{ \beta y^2 \left(\frac{7}{60} - \frac{1}{15}y \right) \Theta + y\left(\frac{1}{30} - \frac{1}{60}y \right) V \right\} = y\left(1 - \frac{1}{4}y \right) - y\left\{ \beta\left(1 - \frac{3}{4}y \right) + \frac{1}{10} - \frac{1}{20}y \right\} \Theta - \frac{1}{12} y V. \tag{46}$$

Both Eqs. (45) and (46) constitute a simultaneous system of equations to determine Θ and V as functions of y. It seems doubtful whether this system can be solved analytically on the basis of existing methods in mathematical analysis. After some preliminary examinations, it was found that, if we are satisfied with a practical degree of accuracy, the method of series solution is most convenient for solving approximately the above system within a certain limited range of the value of β. The initial condition for Z is obviously $Z(0) = 1$, so that

$$y(0) = 0. \tag{47}$$

This condition for y suggests the series forms to be assumed for the solutions of Θ and V, which are

$$\Theta(y) = a_0 + a_1 y + a_2 y^2 + \cdots, \tag{48}$$

$$V(y) = b_0 + b_1 y + b_2 y^2 + \cdots. \tag{49}$$

Inserting these series expressions into Eqs. (45) and (46), and carrying out the usual calculations for determining the unknown coefficients (a_n, b_n), there results a system of algebraic equations, from which a_n and b_n may be evaluated successively as functions of β. The resultant algebraic equations are so complicated that they are not reproduced here for the sake of simplicity. In our calculation the coefficients were determined up to (a_6, b_6) for the reason which will be mentioned later.

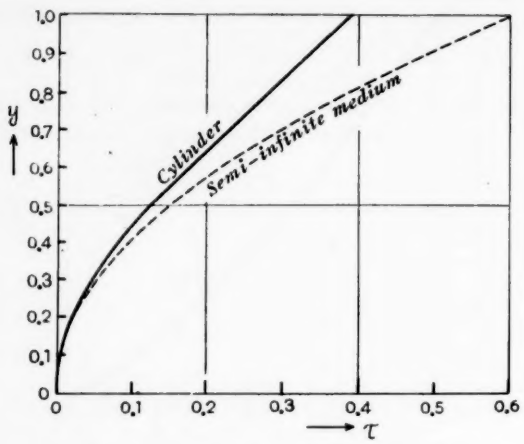

FIG. 3. Movement of the sharp boundary line.

On introducing Eq. (48) into Eq. (44) and integrating, we have

$$\tau=\int^{y}(a_0+a_1y+a_2y^2+\cdots)^{-1}ydy+\text{integration const.}$$

After determining the integration constant from the condition (47), expanding the integrand in a series in y and integrating it term-wise, we obtain

$$\tau=\frac{1}{2a_0}\left\{y^2-\frac{2}{3}\left(\frac{a_1}{a_0}\right)y^3+\frac{1}{2}\left[\left(\frac{a_1}{a_0}\right)^2-\frac{a_2}{a_0}\right]y^4+\frac{2}{5}\left[\frac{2a_1a_2}{a_0^2}-\left(\frac{a_1}{a_0}\right)^3-\frac{a_3}{a_0}\right]y^5+\frac{1}{3}\left[\left(\frac{a_2}{a_0}\right)^2+\frac{2a_1a_3}{a_0^2}+\left(\frac{a_1}{a_0}\right)^4-\frac{a_4}{a_0}-3\frac{a_1^2a_2}{a_0^3}\right]y^6+\frac{2}{7}\left[\frac{2a_1a_4}{a_0^2}+\frac{2a_2a_3}{a_0^2}+\frac{4a_1^3a_2}{a_0^4}-\frac{a_5}{a_0}-\frac{3a_1a_2^2}{a_0^3}-\frac{3a_1^2a_3}{a_0^3}-\left(\frac{a_1}{a_0}\right)^5\right]y^7+0(y^8)\right\}. \quad (50)$$

This affords a mathematical picture for the movement of the sharp boundary line in a cylindrical medium. An example of this has been computed for the case of $\beta=0.94968$, and is plotted in Fig. 3 using a solid line. In this figure, for the sake of comparison, the moving boundary in the semi-infinite medium for the same value of β is also shown with a dotted line. As is expected, the moving boundary line is displaced more rapidly in the cylindrical medium than in the plane sheet. It is of interest to note that the shape of the curve here obtained resembles rather closely the experimental curves obtained by P. H. Hermans[1] for the penetration of water into dry cellulose filaments, although it seems unlikely that, in this experimental case, diffusing water reacts with the cellulose molecules to form any precipitate. The series in Eq. (50) converges rather slowly for values of y near unity, so that it was necessary to take at least up to the term of the order of y^7 in order to insure numerical results of accuracy within one percent over the entire range of y. This is the reason why the calculation of the coefficients (a_n, b_n) was performed up to (a_6, b_6).

Denote by t^* the time at which the moving boundary line reaches the center of the cylinder, and put $t^*D/R^2=\tau^*$.† Then, on putting $y=1$ in Eq. (50), an expression from which τ^* is evaluated in terms of β is obtained. The relation between τ^* and β so calculated is plotted in Fig. 4. It may look strange here that τ^* does not vanish even at $\beta=0$, which is evidently in contradiction to the mathematical requirement which should be satisfied. However, this state of affairs proves to be due to the serious defect inherent of the method of moments here adopted. As for details of this point, reference should be made to a separate paper of the author to be published elsewhere in the near future.

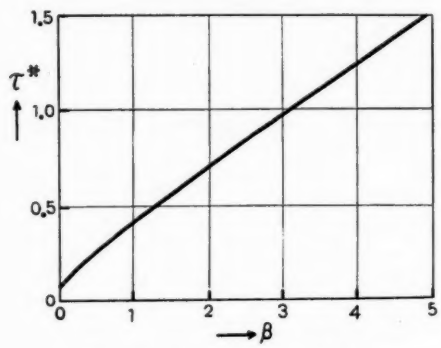

FIG. 4. τ^* as a function of β.

For cylindrical diffusion accompanied with a sharp moving boundary in the system copper ion-cellulose xanthate, J. J. Hermans[2] measured a quantity k defined by

$$k=R/2\sqrt{t^*} \quad (51)$$

for various values of β, where β was varied by changing both b and C_0 properly. His experimental data are reproduced in Tables I and II. Combining these experimental informations with the theoretical plot obtained for $\tau^*(\beta)$, it is possible to evaluate the diffusion constant D for a given value of β, because Eq. (51) can be rewritten in the form:

$$D=4k^2\tau^*. \quad (52)$$

According to this principle the D values for the β values indicated in Tables I and II were computed, and are listed in the same tables. In these tables, the diffusion constants evaluated by J. J. Hermans on the basis of a semi-empirical procedure, which is believed to be less reliable than our own, are also shown in the column

† R is the radius of the cylinder.

with a heading D'. On the other hand, the value of the diffusion constant determined experimentally by the so-called steady-state method was $(1.6\pm0.3)\times10^{-6}$ cm²/sec, which is at any rate regarded as representing a close approximation to the true D value for the system concerned. It is seen that the averages of our D values are higher by a factor of about 2.6 than those

TABLE I. Diffusion of Cu^{++} ions of concentration C_0 into cellulose xanthate of CS_2 content 0.126 M/l ($b=0.063$) in the presence of $(NH_4)_2SO_4$, 1 M/l.

C_0 (M/l)	$1/\beta$	$k_{exp}\times10^3$ (cm/sec$^{\frac{1}{2}}$)	$D\times10^6$ (cm²/sec)	$D'\times10^6$ (cm²/sec)
0.20	3.174	1.35	1.39	0.53
0.133	2.111	1.08	1.17	0.44
0.10	1.590	0.98	1.17	0.45
0.050	0.793	0.72	1.02	0.41
0.025	0.396	0.53	0.90	0.41
0.018	0.285	0.47	0.93	0.43
			av 1.10	av 0.45

from J. J. Hermans' analysis, and approach the true value. Nevertheless, the calculated values are still systematically low as compared with the measured value. It is to be noted here that for the case of linear diffusion J. J. Hermans observed a satisfactory agreement between the theoretical and experimental D values. The appreciable discrepancy here again revealed

TABLE II. Diffusion of Cu^{++} ions of concentration $C_0=0.2$ M/l, into cellulose xanthates of various CS_2 contents in the presence of Na_2SO_4, 1 M/l.

b (M/l)	$1/\beta$	$k_{exp}\times10^3$ (cm/sec$^{\frac{1}{2}}$)	$D\times10^6$ (cm²/sec)	$D'\times10^6$ (cm²/sec)
0.165	1.112	0.83	1.00	0.40
0.135	1.482	0.86	0.97	0.37
0.125	1.598	0.90	0.97	0.38
0.095	2.105	1.05	1.10	0.41
0.095	2.105	1.09	1.19	0.44
0.065	3.075	1.19	1.14	0.42
			av 1.06	av 0.40

for the cylindrical case is yet not clear to us, although it may in part be due to some insufficient or incorrect approximation of the mathematical solution obtained. The interpretative work on this subject is being carried on in this laboratory using the same ion-gel system for both the linear and cylindrical cases.

ACKNOWLEDGMENT

The author wishes to acknowledge his thanks to Professor F. C. Collins at the Polytechnic Institute of Brooklyn, who kindly read the manuscript of this paper and recommended that it be published in this Journal. Thanks are also due Mr. A. Kishimoto of this laboratory for his aid in making some of the numerical calculations.

THE JOURNAL OF CHEMICAL PHYSICS VOLUME 21, NUMBER 4 APRIL, 1953

The Possible Microwave Absorption in the Molecules belonging to the Point Groups $D_{2d}\equiv V_d$ and T_d*

MASATAKA MIZUSHIMA † AND PUTCHA VENKATESWARLU
Department of Physics, Duke University, Durham, North Carolina

(Received October 13, 1952)

It is shown that pure rotational absorption in the molecules belonging to the point group $D_{2d}\equiv V_d$ is possible if the molecule is in the excited, preferably lowest, doubly degenerate vibrational state. The approximate positions of these microwave absorption lines, as calculated from the B value obtained from the infrared data, are given in the case of allene. It is also shown that the pure rotational absorption is possible in the molecules belonging to the point group T_d if they are in the excited triply degenerate (F_2) vibrational states. The matrix element of dipole moment corresponding to our transition is about the same as that of the overtone vibrational bands, in both cases.

I. INTRODUCTION

THE molecules which belong to the point groups $D_{2d}\equiv V_d$ and T_d have no permanent dipole moment in the ground state, and therefore no rotational absorption is possible if the molecule is in the ground state. If the molecule is in a degenerate vibrational state pure rotational transition may be expected because of the Jahn-Teller effect. In such a vibrational state there is a vibrational angular momentum, and it is possible that this angular momentum is communicated to the electrons and an electronic degenerate state appears. As is pointed out by Jahn and Teller,[1] a molecule in an electronic degenerate state is in general deformed to a lower symmetric shape, and therefore a finite amount of dipole moment may appear. However, the mixing of the

* The research reported in this paper has been sponsored by the Geophysics Research Directorate of the Air Force Cambridge Research Center, Air Research and Development Command, under Contract No. AF19(604)-258.

† On leave from the Department of Physics, Faculty of Science, University of Tokyo, Tokyo, Japan.

[1] H. A. Jahn and E. Teller, Proc. Roy. Soc. (London) **A161**, 220 (1937).

above degenerate state is probably small, and the deformation owing to the Jahn-Teller effect is also usually small.[2] We will discuss in this paper the further possibilities of pure rotational absorption when the molecules are in certain degenerate vibrational states.

II. THE MOLECULES BELONGING TO THE POINT GROUP $D_{2d} \equiv V_d$

The matrix elements of the electric dipole moment μ referred to a fixed coordinate system xf, yf, zf for a transition from a state Ψ'' to a state Ψ' are given by

$$R_{xf}=\int \Psi''^{*}(\mu_x \cos\alpha_x+\mu_y \cos\alpha_y+\mu_z \cos\alpha_z)\Psi' d\tau \quad (1a)$$

$$R_{yf}=\int \Psi''^{*}(\mu_x \cos\beta_x+\mu_y \cos\beta_y+\mu_z \cos\beta_z)\Psi' d\tau \quad (1b)$$

$$R_{zf}=\int \Psi''^{*}(\mu_x \cos\gamma_x+\mu_y \cos\gamma_y+\mu_z \cos\gamma_z)\Psi' d\tau, \quad (1c)$$

where * indicates the complex conjugate eigenfunctions, μ_x, μ_y, μ_z are the components of the dipole moment μ with respect to a coordinate system fixed in the molecule (z axis = figure axis of symmetric top), α_x, β_x, γ_x are the angles of the moving x axis with the three fixed axes, and similarly α_y, β_y, γ_y and α_z, β_z, γ_z.

Neglecting the vibration-rotation interaction the wave function Ψ may be taken as a product of the vibrational wave function ψ and the rotational wave function Θ. Thus Eq. (1a) may be written as

$$R_{xf}=\int \mu_x \psi''^{*}\psi' d\tau_v \int \cos\alpha_x \Theta''^{*}\Theta' d\tau_r + \int \mu_y \psi''^{*}\psi' d\tau_v \int \cos\alpha_y \Theta''^{*}\Theta' d\tau_r + \int \mu_z \psi''^{*}\psi' d\tau_v \int \cos\alpha_z \Theta''^{*}\Theta' d\tau_r, \quad (2)$$

and similarly for R_{yf} and R_{zf} with β_x, β_y, β_z and γ_x, γ_y, γ_z, respectively.

In the case of a symmetric top molecule $\int \cos\alpha_x \Theta''^{*}\Theta' d\tau_r$, $\int \cos\alpha_y \Theta''^{*}\Theta' d\tau_r$, and similarly those with β_x, β_y, and γ_x, γ_y are different from zero only for $\Delta K=\pm 1$ and $\Delta J=0, \pm 1$. The integral $\int \cos\alpha_z \Theta''^{*}\Theta' d\tau_r$ and similarly those with β_z and γ_z are different from zero only for $\Delta K=0$ and $\Delta J=0, \pm 1$.[3]

Thus in a symmetric top molecule which is in a vibrational state a rotational transition $\Delta K=0$ and $\Delta J=0, \pm 1$ is possible only if the integral

$$\int \mu_z \psi''^{*}\psi' d\tau_v$$

does not vanish. This integral does not vanish only if $\mu_z \psi''^{*}\psi'$ has a component belonging to the totally symmetric representation.

Similarly a rotational transition $\Delta K=\pm 1$, $\Delta J=0, \pm 1$ is possible in a symmetric top molecule only if $\mu_z \psi''^{*}\psi'$ or $\mu_y \psi''^{*}\psi'$ has a component which belongs to the totally symmetric representation. The components μ_x, μ_y, μ_z will have the same behavior with respect to symmetry operations as the translations T_x, T_y, and T_z in the direction of the coordinate axes.

From Table I we see that μ_x and μ_y belong to the representation E and μ_z to the representation B_2. If the molecule is in a vibrational state of species E, $\psi''^{*}\psi'$ will have four components which belong to the representations A_1, A_2, B_1, and B_2, respectively, since $E \times E = A_1 + A_2 + B_1 + B_2$. Thus in this state $\mu_z \psi''^{*}\psi'$ has one totally symmetric component but $\mu_x \psi''^{*}\psi'$ or $\mu_y \psi''^{*}\psi'$ do not have any totally symmetric component. Therefore, in the molecule under consideration rotational transitions $\Delta K=\pm 1$, $\Delta J=0, \pm 1$ will not be possible, but transitions $\Delta K=0$, $\Delta J=0, \pm 1$ will be possible.

We will now calculate the expression for the matrix element for the transitions under consideration. Let S and T represent the pair of normal coordinates[4] which belong to a degenerate vibration of the species E. The representation of E by means of the above pair is

$$\begin{matrix} & I & S_4 & S_4 & C_2'' & C_2 & C_2 & \sigma_d & \sigma_d \\ S & \begin{pmatrix}1 & \\ & 1\end{pmatrix} & \begin{pmatrix} & -1 \\ 1 & \end{pmatrix} & \begin{pmatrix} & 1 \\ -1 & \end{pmatrix} & \begin{pmatrix}-1 & \\ & -1\end{pmatrix} & \begin{pmatrix}1 & \\ & 1\end{pmatrix} & \begin{pmatrix} & -1 \\ 1 & \end{pmatrix} & \begin{pmatrix}1 & \\ & -1\end{pmatrix} & \begin{pmatrix}-1 & \\ & 1\end{pmatrix} \\ T & & & & & & & & \end{matrix}. \quad (3)$$

The reducible representation of $E \times E$ is

$$\begin{matrix} & I & S_4 & S_4 & C_2'' & C_2 & C_2 & \sigma_d & \sigma_d \\ SS & \begin{pmatrix}1 & & & \\ & 1 & & \\ & & 1 & \\ & & & 1\end{pmatrix} & \begin{pmatrix} & & & 1 \\ & & -1 & \\ & -1 & & \\ 1 & & & \end{pmatrix} & \begin{pmatrix} & & & 1 \\ & & -1 & \\ & -1 & & \\ 1 & & & \end{pmatrix} & \begin{pmatrix}1 & & & \\ & 1 & & \\ & & 1 & \\ & & & 1\end{pmatrix} & \begin{pmatrix} & & & 1 \\ & & 1 & \\ & 1 & & \\ 1 & & & \end{pmatrix} & \begin{pmatrix} & & & 1 \\ & & 1 & \\ & 1 & & \\ 1 & & & \end{pmatrix} & \begin{pmatrix}1 & & & \\ & -1 & & \\ & & -1 & \\ & & & 1\end{pmatrix} & \begin{pmatrix}1 & & & \\ & -1 & & \\ & & -1 & \\ & & & 1\end{pmatrix} \\ ST & & & & & & & & \\ TS & & & & & & & & \\ TT & & & & & & & & \end{matrix}. \quad (4)$$

[2] J. H. Van Vleck, J. Chem. Phys. **7**, 72 (1939).
[3] G. Herzberg, *Infrared and Raman Spectra of Polyatomic Molecules* (D. Van Nostrand Company, Inc., New York, 1945).
[4] R. C. Herman and H. Shaffer, J. Chem. Phys. **17**, 30 (1949).

From this table, we can easily obtain the explicit formula of the bases corresponding to the irreducible representations[5] $E\times E=A_1+A_2+B_1+B_2$ as

$$A_1\cdots SS+TT,\quad A_2\cdots ST-TS,$$
$$B_1\cdots ST+TS,\quad B_2\cdots SS-TT. \quad (5)$$

The dipole moment of a molecule can be expanded in a power series of the internal coordinates. In the case of allene type molecule, since μ_z belongs to B_2 representation and is zero at the equilibrium state, we obtain a formula

$$\mu_z=\sum_i\left(\frac{\partial\mu_z}{\partial X_i}\right)_0 X_i+\tfrac{1}{4}\sum_{jk}\left(\frac{\partial^2\mu_z}{\partial S_j\partial S_k}-\frac{\partial^2\mu_z}{\partial T_j\partial T_k}\right)_0 \times(S_jS_k-T_jT_k)+\cdots, \quad (6)$$

where X_i is a normal coordinate which belongs to the B_2 representation, and the summation $\sum_i$ and $\sum_{jk}$ are to be made over all coordinates belonging, respectively, to the B_2 and E representations.

When the degenerate vibration is excited, each rotational state splits as is pointed out by Teller.[6] The wave function and the corresponding energy of each state neglecting the centrifugal stretching can be expressed as

$$\Psi_\pm{}^+=\{\Theta_K\psi_+\pm\Theta_{-K}\psi_-\}2^{-\frac{1}{2}} \quad (7a)$$
$$F^+(J,K)=BJ(J+1)+(A-B)K^2-2A\zeta_iK \quad (7b)$$
$$\Psi_\pm{}^-=\{\Theta_K\psi_-\pm\Theta_{-K}\psi_+\}2^{-\frac{1}{2}} \quad (8a)$$
$$F^-(J,K)=BJ(J+1)+(A-B)K^2+2A\zeta_iK, \quad (8b)$$

where A and B are the usual rotational constants of the molecule, J and K are the rotational quantum numbers, ζ_i is the coriolis interaction constant, Θ_K and Θ_{-K} are the rotational wave functions with quantum numbers $+K$ and $-K$, respectively, ψ_+ and ψ_- are the vibrational wave functions defined as,

$$\psi_+=N(S+iT)\exp[-(\lambda/2)(S^2+T^2)] \quad (9a)$$
$$\psi_-=N(S-iT)\exp[-(\lambda/2)(S^2+T^2)] \quad (9b)$$

by means of S and T defined above. (λ is a constant and N stands for all other parts of the vibrational wave function including normalization constant.) The $\pm$ signs occurring in Eqs. (7a) and (8a) as subscripts for the wave functions and also within the brackets indicate the degeneracy which, if removed, corresponds to the "l type" doubling.[7,8]

From Eq. (1) we see that the matrix element of the dipole moment for the transition $\Psi_\pm{}^+\rightarrow\Psi_\pm{}^-$ in the molecule under consideration is

$$R_{zf}=\int\Psi_\pm{}^{+*}\mu_z\cos\alpha_z\Psi_\pm{}^-d\tau \quad (10)$$

[5] M. Mizushima and M. Umezawa, Phys. Rev. **85**, 37 (1952).
[6] E. Teller, Hand-und Jahrb. d. Chem. Phys. **9**, II, 43 (1934).
[7] H. H. Nielsen, Phys. Rev. **77**, 130 (1950).
[8] J. DeHeer, Phys. Rev. **83**, 741 (1951).

TABLE I. The symmetry species and characters for the point group $D_{2d}\equiv V_d$.

$D_{2d}=V_d$	I	$2S_4(z)$	$S_4{}^2=C_2{}''$	$2C_2$	$2\sigma_d$	
A_1	+1	+1	+1	+1	+1	
A_2	+1	+1	+1	−1	−1	
B_1	+1	−1	+1	+1	−1	
B_2	+1	−1	+1	−1	+1	T_z
E	+2	0	−2	0	0	T_x, T_y, R_x, R_y

and similarly R_{yf} and R_{zf} with β_z and γ_z, respectively, since the contribution of μ_x and μ_y is zero.

From Eqs. (6)–(9) we see that

$$\int\psi_+{}^*\mu_z\psi_+d\tau_v=\int\psi_-{}^*\mu_z\psi_-d\tau_v=0 \quad (11)$$

$$\int\Psi_+{}^{+*}\mu_z\cos\alpha_z\Psi_-{}^-d\tau=\int\Psi_-{}^{+*}\mu_z\cos\alpha_z\Psi_+{}^-d\tau$$
$$=\frac{1}{4\lambda}\left(\frac{\partial^2\mu_z}{\partial S^2}-\frac{\partial^2\mu_z}{\partial T^2}\right)\int N^2(S^2-T^2)^2$$
$$\times\exp[-\lambda(S^2+T^2)]d\tau_v\int\Theta_K{}''{}^*\Theta_K'\cos\alpha_zd\tau_r$$
$$=\frac{1}{4\lambda}\left(\frac{\partial^2\mu_z}{\partial S^2}-\frac{\partial^2\mu_z}{\partial T^2}\right)\int\Theta_K{}''{}^*\Theta_K'\cos\alpha_zd\tau_r. \quad (12)$$

The selection rules‡ obtained from all the above formulas may be stated as $\Psi_+{}^+\leftrightarrow\Psi_-{}^-$, $\Psi_-{}^+\leftrightarrow\Psi_+{}^-$, all the others not being allowed. The selection rule $\Delta K=0$, $\Delta J=0,\pm1$ is also to be obeyed.

Neglecting the possible "l type" doubling we see from Eqs. (7b) and (8b) that the frequencies of the lines due to the transitions $\Psi_\pm{}^+(J,K)\rightarrow\Psi_\mp{}^-(J+1,K)$ and $\Psi_\pm{}^-(J,K)\rightarrow\Psi_\mp{}^+(J+1,K)$ are respectively given by

$$\nu=2B(J+1)+4A_K\zeta_i \quad (13a)$$

and

$$\nu=2B(J+1)-4A_K\zeta_i. \quad (13b)$$

The frequency of the lines corresponding to the transition $\Psi_\pm{}^+(J,K)\rightarrow\Psi_\mp{}^-(J,K)$ is given by

$$\nu=4A_K\zeta_i. \quad (14)$$

‡ If we take the anharmonicity into account, Eqs. (9a) and (9b) will be

$$\psi_\pm=aN(S\pm iT)\exp[\lambda/2(S^2+T^2)] + \Sigma_jb_jN_j'(S\pm iT)Q_j\exp[-\lambda/2(S^2+T^2)-\lambda_j/2Q_j^2]+\cdots,$$

where Q stands for all coordinates belonging to the nondegenerate representations. In this case the transitions $\Psi_+{}^+\leftrightarrow\Psi_-{}^+$ and $\Psi_+{}^-\leftrightarrow\Psi_-{}^-$ are also allowed. The matrix element of the dipole moment for such transitions is $\Sigma_iab_i(\partial\mu_z/\partial X_i)_04\lambda_j{}^{-\frac{1}{2}}\Theta_K{}''{}^*\Theta_K'd\tau_r$, where the summation is to be made over B_2 coordinates only. The matrix element of the dipole moment for the transition $\Psi_\pm{}^+\leftrightarrow\Psi_\mp{}^-$ is still adequately expressed by the formula (12).

The effect of nuclear spin must also be taken into account. The factor due to this is obtained in another paper (M. Mizushima, to be published).

TABLE II. Predicted frequencies of the absorption lines for the transitions $J\rightarrow J+1$ with $K'=K''=0$.

Transition	Allene	Allene-d_4
$J=0\rightarrow J=1$	0.57 cm^{-1} (17 100 Mc)	0.44 cm^{-1} (13 200 Mc)
$J=1\rightarrow J=2$	1.14 cm^{-1} (34 200 Mc)	0.88 cm^{-1} (26 400 Mc)
$J=2\rightarrow J=3$	1.71 cm^{-1} (51 300 Mc)	1.32 cm^{-1} (39 600 Mc)
$J=3\rightarrow J=4$	2.28 cm^{-1} (68 400 Mc)	1.76 cm^{-1} (52 800 Mc)
$J=4\rightarrow J=5$	2.85 cm^{-1} (85 500 Mc)	2.20 cm^{-1} (66 000 Mc)

We see from Eq. (12) that the intensity of the absorption in the above allowed transitions is determined by the quantity $1/4\lambda(\partial^2\mu_z/\partial S^2-\partial^2\mu_z/\partial T^2)_0$. This quantity is not zero since the operator $(\partial^2/\partial S^2-\partial^2/\partial T^2)$ belongs to the B_2 representation, while μ_z also belongs to the same one, and $B_2\times B_2=A_1$. Actually, operating C_2, we see that $S\rightarrow T$, $T\rightarrow S$, and $\mu_z\rightarrow-\mu_z$, and therefore $\partial^2\mu_z/\partial S^2=-\partial^2\mu_z/\partial T^2$.

It is interesting to note that the matrix element of the dipole moment for a transition from the ground state to the second excited state of the degenerate vibration is also given by formula (12).

Allene, C_3H_4, belongs to the point group $D_{2d}\equiv V_d$ and has four vibrations[9] of the species E. They are $\nu_8=3085$ cm^{-1}, $\nu_9=1015$ cm^{-1}, $\nu_{10}=842$ cm^{-1} and $\nu_{11}=354$ cm^{-1}. In allene-d_4 they are $\nu_8=2330$ cm^{-1}, $\nu_9=830$ cm^{-1}, $\nu_{10}=667$ ec^{-1} and $\nu_{11}=306$ cm^{-1}.

The Boltzmann factor is favorable for ν_{11} in allene and ν_{10} and ν_{11} in allene-d_4. The difference bands involving ν_{11} in allene and ν_{10} and ν_{11} in allene-d_4 are obtained in the infrared absorption which indicates that at the room temperature there are enough molecules in the excited states under consideration.

The value of B obtained from the infrared measurement[9] is 0.285 cm^{-1} and 0.22 cm^{-1} in allene-d_4. The positions of the lines for the transitions $J\rightarrow J+1$ (with $K=0$) are given in Table II for allene and allene-d_4 as calculated from the formula $\nu=2B(J+1)$. The frequencies of the lines for the transition with $K\neq0$ can be obtained by Eqs. (13) and (14).

III. MOLECULES BELONGING TO THE POINT GROUP T_d

From Table III, we see that μ_x, μ_y, and μ_z belong to the representation F_2 and $F_2\times F_2=A_1+E+F_1+F_2$. Thus if the molecule is in the degenerate vibrational state F_2 pure rotational transitions will be possible.

TABLE III. Symmetry species and characters for the point group T_d.

T_d	I	$8C_3$	$6\sigma_d$	$6S_4$	$3S_4^2\equiv3C_2$	
A_1	+1	+1	+1	+1	+1	
A_2	+1	+1	−1	−1	+1	
E	+2	−1	0	0	+2	
F_1	+3	0	−1	+1	−1	R_x, R_y, R_z
F_2	+3	0	+1	−1	−1	T_x, T_y, T_z

The molecules of the type XY_4 which belong to the point group T_d have one vibration of species A_1, one of species E, and two of species F_2. The frequencies of the fundamental[10] $\nu_4(f_2)$ in CF_4, GeF_4, SiF_4, and CCl_4 and $\nu_3(f_2)$ and $\nu_4(f_2)$ in $GeCl_4$ and $GeBr_4$ are low enough for a sufficient number of molecules to be in those excited states at room temperature.

We will now obtain the expression for the matrix elements for the transitions under consideration.

The F_2 representation in terms of the x, y, z coordinates (illustrated in Fig. 41 of reference 3) is as follows:

C_3

$$x\begin{pmatrix}&&-1\\1&&\\&-1&\end{pmatrix}\begin{pmatrix}&1&\\&&-1\\-1&&\end{pmatrix}\begin{pmatrix}&&1\\-1&&\\&-1&\end{pmatrix}\begin{pmatrix}-1&&\\&&-1\\1&&\end{pmatrix}\begin{pmatrix}&&-1\\&1&\\-1&&\end{pmatrix}\begin{pmatrix}-1&&\\&&1\\&1&\end{pmatrix}\begin{pmatrix}1&&\\&1&\\1&&\end{pmatrix}\begin{pmatrix}&&1\\1&&\\&1&\end{pmatrix}$$

σ_d

$$x\begin{pmatrix}1&&\\&&1\\&1&\end{pmatrix}\begin{pmatrix}&-1&\\-1&&\\&&1\end{pmatrix}\begin{pmatrix}1&&\\&&1\\1&&\end{pmatrix}\begin{pmatrix}1&&\\&&-1\\-1&&\end{pmatrix}\begin{pmatrix}&&1\\1&&\\&1&\end{pmatrix}\begin{pmatrix}&&-1\\&1&\\-1&&\end{pmatrix}$$

S_4

$$x\begin{pmatrix}&1&\\-1&&\\&&-1\end{pmatrix}\begin{pmatrix}&-1&\\1&&\\&&-1\end{pmatrix}\begin{pmatrix}-1&&\\&&1\\&-1&\end{pmatrix}\begin{pmatrix}-1&&\\&&-1\\&1&\end{pmatrix}\begin{pmatrix}&&-1\\-1&&\\1&&\end{pmatrix}\begin{pmatrix}&&-1\\&-1&\\-1&&\end{pmatrix}$$

C_2

$$x\begin{pmatrix}-1&&\\&-1&\\&&1\end{pmatrix}\begin{pmatrix}1&&\\&-1&\\&&-1\end{pmatrix}\begin{pmatrix}-1&&\\&1&\\&&-1\end{pmatrix}.$$

[9] R. C. Lord and P. Venkateswarlu, J. Chem. Phys. **20**, 1237 (1952).
[10] P. J. H. Woltz and A. H. Nielsen, J. Chem. Phys. **20**, 307 (1952).

Following the same procedure as in the case of the $D_{2d}\equiv V_d$ molecule, that is, calculating the product representation $F_2\times F_2$ and reducing it one can obtain the bases of the F_2 representation to be yz, zx, and xy which behave like x, y, and z, respectively. The components of the dipole moment can therefore be expressed as

$$\mu_x=\sum_i\left(\frac{\partial\mu_x}{\partial x_i}\right)_0 x_i+\tfrac{1}{2}\sum_{ij}\left(\frac{\partial^2\mu_x}{\partial y_i\partial z_j}\right)_0 y_iz_j+\cdots \quad (16a)$$

$$\mu_y=\sum_i\left(\frac{\partial\mu_y}{\partial y_i}\right)_0 y_i+\tfrac{1}{2}\sum_{ij}\left(\frac{\partial^2\mu_y}{\partial z_i\partial x_j}\right)_0 z_ix_j+\cdots \quad (16b)$$

$$\mu_z=\sum_i\left(\frac{\partial\mu_z}{\partial z_i}\right)_0 z_i+\tfrac{1}{2}\sum_{ij}\left(\frac{\partial^2\mu_z}{\partial x_i\partial y_i}\right)_0 x_iy_j+\cdots, \quad (16c)$$

where the summations are to be made over all the normal coordinates belonging to the F_2 representation.

The first excited vibrational wave function can be expressed as

$$\psi_x=Nx\exp[-(\lambda/2)(x^2+y^2+z^2)] \quad (17a)$$

or

$$\psi_y=Ny\exp[-(\lambda/2)(x^2+y^2+z^2)] \quad (17b)$$

or

$$\psi_z=Nz\exp[-(\lambda/2)(x^2+y^2+z^2)]. \quad (17c)$$

When the molecule is in a triply degenerate fundamental vibrational ν_i there is a vibrational angular momentum of magnitude ζ_i which may orient itself parallel, perpendicular, or antiparallel to the total angular momentum vector $\mathbf{J}$. The effect of the coupling between the above internal and total angular momentum is to split the rotational levels which would otherwise be single into three levels.[11,12] They may be denoted by $F(J_L)$ where $L=|\mathbf{J}+\mathbf{v}|$ takes the values $J+1$, J and $J-1$ since the vibrational quantum number $v=1$. The energies of these levels are

$$F(J_{J+1})=BJ(J+1)+B(\zeta_i^2-2\zeta_i)+2B\zeta_i(J+1) \quad (18a)$$

$$F(J_J)=BJ(J+1)+B(\zeta_i^2-2\zeta_i) \quad (18b)$$

$$F(J_{J-1})=BJ(J+1)+B(\zeta_i^2-2\zeta_i)-2B\zeta_iJ. \quad (18c)$$

The wave functions corresponding to these levels are given by Jahn.[11]

Each of these three levels is degenerate, the degree of degeneracy being given by $2L+1$§ if there is spherical symmetry. In the actual case we have tetrahedral symmetry and the degeneracy will be partly removed. Therefore, each of the above three levels will split into several components.[11] This splitting will probably be small but may be large enough to cause the splitting of the microwave absorption line.

[11] H. A. Jahn, Proc. Roy. Soc. (London) **168A**, 469 (1938).
[12] D. M. Dennison, Revs. Modern Phys. **12**, 175 (1940).
§ There is additional degeneracy of the degree $2J+1$ due to the quantum number M.

By using formulas (16) and (17) together with the wave functions given by Jahn,[11] one can calculate the matrix element R of the dipole moment for each transition. Though the exact formulas for the matrix elements are too complicated to be shown here, one can find easily that this is given by

$$|\mathbf{R}|^2=\left(\int\psi_x^*\psi_y\mu_z d\tau_v\right)^2\sum_k|C(J,K)|^2 \quad (19)$$

noting that the integrals $\int\psi_x^*\psi_y\mu_z d\tau_v$, $\int\psi_y^*\psi_z\mu_x d\tau_v$ and $\int\psi_z^*\psi_x\mu_y d\tau_v$ are the same in magnitude. In this formula $C(J,K)$ is a constant involving J and K and therefore different for each transition and the summation is to be made over all the possible values of K. One can see that‖

$$\int\psi_x^*\psi_y\mu_z d\tau_v=\frac{1}{4\lambda}\left(\frac{\partial^2\mu_z}{\partial x\partial y}\right)_0. \quad (20)$$

This is again of the same order of magnitude as the matrix element of the dipole moment for the second harmonic vibrational absorption transition.

The selection rule between coriolis levels is usually given by $\Delta L=0$.¶ This is obtained by the assumption of spherical symmetry of the molecule. But in our case, as one sees in formula (20), the transition occurs solely by means of the nonsphericality of the molecule, and therefor the above selection rule cannot be applied.

By considering the respective matrix elements one can find that all the nine transitions from the three levels $F(J_{J-1})$, $F(J_J)$ and $F(J_{J+1})$ to the three levels $F(J+1_J)$, $F(J+1_{J+1})$, and $F(J+1_{J+2})$ are in general allowed. The transitions $F(J_{J-1})\rightarrow F(J_J)$, $F(J_J)\rightarrow F(J_{J+1})$, and $F(J_{J-1})\rightarrow F(J_{J+1})$ are also allowed. Each of the lines due to the above transitions can be expected to be split further because of the possible above mentioned splitting of each of the Coriolis levels $F(J_L)$.

The authors wish to express their thanks to Professor Walter Gordy for his kind interest in the work.

‖ If we take the anharmonicity into account Eq. (17) becomes

$$\psi_x=aNx\exp[-(\lambda/2)(x^2+y^2+z^2)]+bN'yz\exp[-\lambda/2(x^2+y^2+z^2)]$$
$$\psi_x=aNy\exp[-(\lambda/2)(x^2+y^2+z^2)]+bN'zx\exp[-\lambda/2(x^2+y^2+z^2)]$$
$$\psi_z=aNz\exp[-(\lambda/2)(x^2+y^2+z^2)]+bN'xy\exp[-\lambda/2(x^2+y^2+z^2)],$$

where $|a|\gg|b|$. Equation (20) thus becomes

$$\int\psi_x\psi_y\mu_z d\tau_v=\frac{a^2}{4\lambda}\left(\frac{\partial^2\mu_z}{\partial x\partial y}\right)_0+\frac{2^{\frac{1}{2}}ab}{\lambda^{\frac{1}{2}}}\left(\frac{\partial\mu_z}{\partial z}\right)_0$$

neglecting the term involving b^2.

¶ This selection rule may be obtained from the following consideration. The perturbation which gives rise to absorption is well known to be $\mathbf{E}\cdot\boldsymbol{\mu}$, where $\mathbf{E}$ is the electric field of radiation. If we assume the molecule to be spherical, this perturbation term is evidently invariant in $\mathbf{J}+\mathbf{v}$ space as one can see if he stands on the molecule-fixed coordinate. That means the perturbation is diagonal in $\mathbf{L}=\mathbf{J}+\mathbf{v}$ and the selection rule in absorption and emission is $\Delta L=0$.

A Theoretical Model of a Gaseous Combustion Wave Governed by a First-Order Reaction

RAYMOND FRIEDMAN AND EDWARD BURKE
Westinghouse Research Laboratories, East Pittsburgh, Pennsylvania

(Received November 4, 1952)

Numerical solutions are obtained for differential equations describing a hypothetical model of a laminar flame. A first-order irreversible reaction with approximately exponential dependence of rate upon temperature is assumed, with interdiffusion of reactant and product molecules. The temperature dependence of thermal conductivity, diffusion coefficient, and gas density is taken into account. When the equations are in suitable form, the dimensionless burning velocity is an eigenvalue whose magnitude depends on two dimensionless parameters; ϵ (the ratio of activation energy to burned gas temperature) and α (the ratio of heat flow to diffusional flow). An I.B.M. Card-Programmed Electronic Calculator was used to obtain solutions accurate to two percent, for a wide range of values of ϵ and α. Interdiffusion is found to reduce the burning velocity, the effect being more pronounced when ϵ is large. The results for α equal to unity are compared with the approximate burning-velocity equation of Zeldovich and Frank-Kamenetsky, and the latter is shown to be valid only when ϵ is large.

INTRODUCTION

We are concerned here with the problem of steady-state propagation of a laminar, one-dimensional flame through a premixed gas. Moreover, we do not consider detonations but limit ourselves to deflagrations, in which only very small pressure changes occur. As Boys and Corner,[1] Corner,[2] and Hirschfelder and Curtiss[3,4] have shown, the characteristic velocity of propagation of such a flame, called the burning velocity, corresponds to an eigenvalue of the set of differential equations and boundary conditions describing the system. These equations are based on conservation of each species and of energy and take into account interdiffusion of reactants and products, thermal conduction, mass flow, and chemical generation and destruction of the various species. An equation of state must also be used, to specify the variation of density with temperature.

Even for the simplest kinetic systems, such as a first-order reaction with exponential variation of rate with temperature, exact solutions, yielding the burning velocity, can be obtained only by numerical integrations; these have been carried through in but a few specific cases, mainly by Henkel, Hummel, and Spaulding,[5] and by Curtiss, Hirschfelder, and Campbell.[6] The immediate purpose of this investigation has been to obtain reasonably accurate solutions for a wide range of values of all the pertinent parameters, for a flame governed by a first-order reaction of the type $A \rightarrow B$. The ultimate objective is to develop a simplified approach which still retains the essential features of the rigorous formulation, so that it may be readily extended to more complex kinetic models.

In addition, some confusion exists concerning the cold boundary condition and the fictitious flame holder used by Hirschfelder *et al.* See Adamson,[7] Emmons,[8] and Hirschfelder and Curtiss.[9] We have treated this boundary condition in a novel fashion.

BASIC EQUATIONS AND ASSUMPTIONS

We assume that the gas upstream from the flame consists of a substance designated as "pure A," and that the gas downstream from the flame consists of "pure B." The chemical reaction is then assumed to consist of an equimolal transformation of A to B according to the kinetic law:

$$d(ny_B)/dt = k_0 n y_A \exp(-E/RT_b\tau), \qquad (1)$$

where n is total moles per unit volume, y_A and y_B are mole fractions of A and B, t is time, k_0 is a frequency factor, E is the activation energy, R is the universal gas constant, T_b is the absolute burned-gas temperature, and τ is the quantity $(T-T_u)/(T_b-T_u)$, where T is the local absolute temperature and T_u is the absolute temperature of the unburned gas infinitely far upstream. Notice that, according to Eq. (1), the reaction rate infinitely far upstream is zero, since $\tau=0$, while for the more usual Arrhenius-type rate law, with a $[k_0 \exp(-E/RT)]$ term, the reaction rate infinitely far upstream is proportional to $[k_0 \exp(-E/RT_u)]$ and hence finite. The latter treatment leads to the mathematical inconsistencies at the cold boundary referred to above, and necessitates the porous-plug flame holder assumed by Hirschfelder and Curtiss.

It may be noted that the $[k_0 \exp(-E/RT_b\tau)]$ rate law approaches the $[k_0 \exp(-E/RT)]$ rate law as T approaches T_b, i.e., as τ approaches unity, and this is the important region where reaction rates are high.

[1] S. F. Boys and J. Corner, Proc. Roy. Soc. (London), **A197**, 90 (1949).
[2] J. Corner, Proc. Roy. Soc. (London) **A198**, 388 (1949).
[3] J. O. Hirschfelder and C. F. Curtiss, J. Chem. Phys. **17**, 1076 (1949).
[4] J. O. Hirschfelder and C. F. Curtiss, J. Phys. Colloid Chem. **55**, 774 (1951).
[5] Henkel, Hummel, and Spaulding, *Third Symposium on Combustion* (Williams and Wilkins, Baltimore, 1949), pp. 135–140.
[6] Curtiss, Hirschfelder, and Campbell, Fourth Symposium on Combustion, Cambridge, Massachusetts, September, 1952.
[7] T. C. Adamson, J. Am. Rocket Soc. **22**, 38 (1952).
[8] H. W. Emmons, J. Am. Rocket Soc. **22**, 97 (1952).
[9] J. O. Hirschfelder and C. F. Curtiss, J. Am. Rocket Soc. **22**, 97 (1952).

Neither of these rate laws is to be preferred on theoretical grounds, according to the absolute theory of reaction rates,[10] unless one is willing to take into account the temperature dependence of k_0 when using the $[k_0 \exp(-E/RT)]$ law. This temperature dependence generally being unknown, the form of the rate law of Eq. (1) can hardly be considered to be a poorer approximation than the more conventional form. Equation (1) not only removes the difficulty with the cold boundary but also makes it possible to eliminate the parameter (T_b/T_u) which would otherwise arise when the complete set of equations is reduced to dimensionless form. Thus, with Eq. (1) instead of a conventional rate law, the burning velocity is determined by three instead of four dimensionless parameters, in this particular case.

We also assume that A and B are ideal gases, with constant heat capacities, each having the same molecular weight m. Then, Eqs. (31) and (32) of Hirschfelder and Curtiss[3] may be reduced for this case to the following dimensionless form:

$$\frac{dz}{d\tau}=\beta\frac{1-y_B}{\tau-z}\exp(-\epsilon/\tau) \tag{2}$$

and

$$\frac{dy_B}{d\tau}=\alpha\frac{y_B-z}{\tau-z}, \tag{3}$$

with the boundary conditions

$$y_B=z=\tau=1 \quad \text{at the hot boundary}$$

and

$$y_B=z=\tau=0 \quad \text{at the cold boundary.}$$

The quantities in Eqs. (2) and (3) are defined as follows:

$$z=\frac{(v+V_B)y_B\rho}{v_u\rho_u}=\text{fraction of mass flow due to } B \text{ (dimensionless)}; \tag{4}$$

$$V_B=-\frac{D}{y_B}\frac{dy_B}{dx}=\text{local diffusion velocity of } B; \tag{5}$$

$$\alpha=\frac{m\lambda}{D\rho C_p}=\text{Lewis number (dimensionless)}; \tag{6}$$

$$\beta=\frac{k_0\lambda m\rho}{v_u^2\rho_u^2C_p}=\text{dimensionless parameter containing burning velocity}; \tag{7}$$

$$\epsilon=E/RT_b=\text{dimensionless activation energy}. \tag{8}$$

The molecular weight of A and B is m, v is local velocity, v_u is burning velocity (i.e., local velocity infinitely far upstream), ρ is local density, ρ_u is density infinitely far upstream, D is local diffusion coefficient, x is distance (coordinate increasing in downstream direction), λ is local thermal conductivity, and C_p is molar heat capacity (assumed constant).

[10] Glasstone, Laidler, and Eyring, *Theory of Rate Processes* (McGraw-Hill Book Company, Inc., New York, 1941).

Integration of Eqs. (2) and (3) is facilitated when α and β are independent of local temperature. Experimental data for gases show that λ generally varies with a power of T between 0.6 and 1.0, while D varies with a power of T between 1.6 and 2.0. We assume that λ is proportional to T, and D is proportional to T^2. We recall that C_p has already been assumed constant. It follows from Eq. (6) that α is independent of T, and from Eq. (7) that β is independent of T, as long as k_0 is not temperature-dependent. Since the actual variation of k_0 is generally unknown, the latter assumption must be made.

This concludes the assumptions. Let us now consider Eqs. (2) and (3). We assign values to the parameters ϵ and α and then determine that value of β, designated β_c, which will permit both the hot and cold boundary conditions to be satisfied. This is the eigenvalue β_c, corresponding to the assumed values of ϵ and α. The burning velocity can be computed from β_c by Eq. (7).

The kinetic theory of gases shows that α, the Lewis number,[11] is always quite close to unity. Therefore it is worthwhile to obtain solutions for $\alpha=1$ and $\alpha=\infty$ (corresponding to $D=0$), in order to see how sensitive β_c is to α, for various values of ϵ.

When $\alpha=1$, it is readily shown from Eq. (3) that $y_B=\tau$,[12] and Eq. (2) reduces to

$$\frac{dz}{d\tau}=\beta\frac{1-\tau}{\tau-z}\exp(-\epsilon/\tau), \tag{9}$$

with the hot boundary condition $z=\tau=1$ and the cold boundary condition $z=\tau=0$.

When $\alpha=\infty$, it is readily shown that $y_B=z$, and Eqs. (2) and (3) reduce to

$$\frac{dz}{d\tau}=\beta\frac{1-z}{\tau-z}\exp(-\epsilon/\tau), \tag{10}$$

with the same boundary conditions.

These equations must be integrated numerically by assigning a value of ϵ and then starting from either boundary with a stepwise numerical integration procedure. We chose to start at the hot boundary. Since the equations are indeterminate here, we have derived the asymptotic formulas

$$\lim_{\tau\to1}(1-z)=\tfrac{1}{2}(1-\tau)\{[1+4\beta\exp(-\epsilon)]^{\frac{1}{2}}+1\} \tag{11}$$

for $\alpha=1$, and

$$\lim_{\tau\to1}(1-z)=(1-\tau)[\beta\exp(-\epsilon)+1] \tag{12}$$

for $\alpha=\infty$. With the help of Eq. (11) or (12), starting values may be obtained for a stepwise integration of

[11] W. K. Lewis, Mech. Eng. 44, 445 (1922).

[12] It follows from this relation that, when α is unity, there is no "excess energy hump" in the flame. See B. Lewis and G. von Elbe, J. Chem. Phys. 15, 803 (1947), and R. Friedman and E. Burke, J. Chem. Phys. 17, 667 (1949).

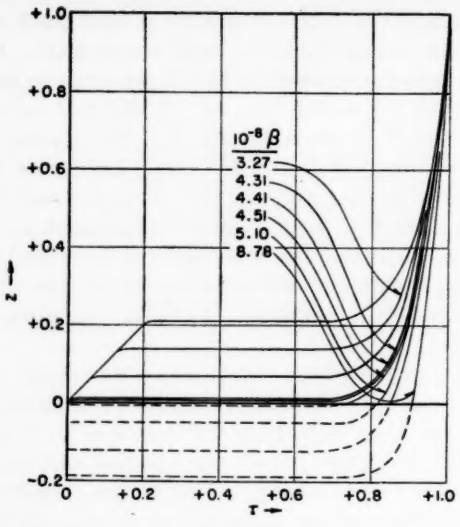

FIG. 1. Numerical integrations of Eq. (9) for $\epsilon=15$.

Eq. (9) or (10). For a given ϵ, a number of trial integrations must be carried out for each of a series of trial values of β, until a value of β is found (the eigenvalue) which permits satisfaction of the cold boundary condition $z=\tau=0$. The nature of the results may be seen from Fig. 1. It turns out that, for all values of β greater than a critical value β_c, the condition $z=\tau=0$ is not satisfied. For values of β less than β_c, the condition is satisfied, but

$$\lim_{\tau\to 0}(dz/d\tau)$$

is unity, which is physically unreasonable.[13] However,

TABLE I. Results of numerical integrations.

α	ϵ	β_c Lower limit	β_c Upper limit
unity	2	35.39	36.72
unity	4	737.1	764.4
unity	7	3.838×10^{4}	3.920×10^{4}
unity	10	1.432×10^{6}	1.454×10^{6}
unity	15	4.413×10^{8}	4.511×10^{8}
unity	22	9.750×10^{11}	10.037×10^{11}
infinity	2	16.11	16.40
infinity	4	229.3	234.8
infinity	7	7.895×10^{3}	8.005×10^{3}
infinity	10	2.203×10^{5}	2.269×10^{5}
infinity	15	4.903×10^{7}	5.067×10^{7}
infinity	22	7.886×10^{10}	8.065×10^{10}

[13] The equation for conservation of species B is

$$\frac{v_u\rho_u}{m}\frac{dz}{dx}=k_0 n y_A \exp(-\epsilon/\tau).$$

In the region where τ is close to zero, the reaction rate is negligibly small and the energy balance equation reduces to

$$\lambda\frac{d\tau}{dx}\simeq v_u\rho_u C_p\tau.$$

Elimination of dx between the above equations yields

$$\frac{dz}{d\tau}\simeq\frac{\lambda m k_0 n y_A}{v_u^2\rho_u^2 C_p}\left[\frac{\exp(-\epsilon/\tau)}{\tau}\right].$$

It is readily demonstrable, by series expansion of the term in the brackets, that this term vanishes as τ approaches zero. Hence $dz/d\tau$ must approach zero, and not unity, at the cold boundary.

when $\beta=\beta_c$,

$$\lim_{\tau\to 0}(dz/d\tau)$$

is zero, which is realistic. Hence β_c is the desired eigenvalue.

DISCUSSION

Details of the numerical integrations are described in the Appendix. The results are shown in Table I and Fig. 2. To obtain these results, twelve families of curves similar to Fig. 1 were required. Figure 2 shows that α has an appreciable effect upon β_c. This effect is more clearly shown in Fig. 3, where the ratio $[\beta_c(\alpha=1)/\beta_c(\alpha=\infty)]$ is plotted against ϵ, to yield a nearly linear curve. The ratio is always greater than unity and increases markedly with increasing ϵ. The physical interpretation of this behavior must be as follows.

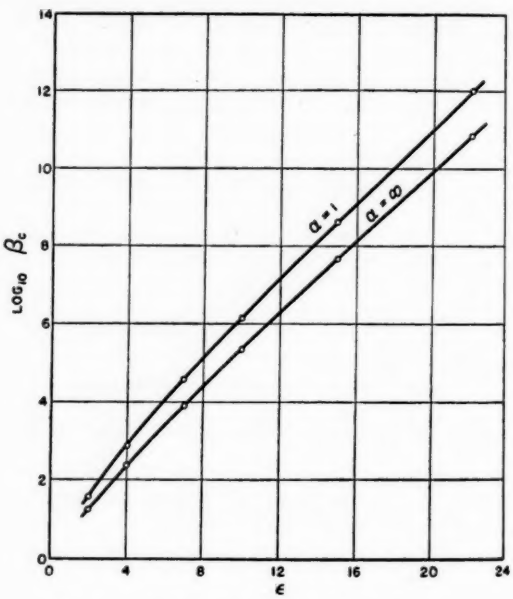

FIG. 2. Plot of $\log\beta_c$ *vs* ϵ, for $\alpha=1$ and $\alpha=\infty$.

We recall that β_c is inversely proportional to the square of the burning velocity and α is the ratio of heat flow to diffusional flow, there being no diffusion when α is infinite. Thus Fig. 2 shows that the effect of diffusion is to reduce the burning velocity. The reason for this must be that the product gas B acts to dilute the reactant gas A when B diffuses upstream, and this dilution reduces the reaction rate and hence the burning velocity. This effect increases with increasing ϵ because large ϵ (high activation energy or low flame temperature) corresponds to low reaction rate; hence an element of gas spends a longer period passing through the flame, and there is more time for diffusion to occur. As ϵ approaches zero, the reaction rate approaches infinity, there is no time for diffusion, and $[\beta_c(\alpha=1)/\beta_c(\alpha=\infty)]$ approaches unity.

It is of interest to compare the results of this investi-

gation with some values recently computed by Curtiss, Hirschfelder, and Campbell[6] for a *reversible* first-order reaction $A \rightleftarrows B$ with $\epsilon = 5.033$. They assumed the rate law

$$\frac{d(ny_B)}{dt} = k_0 n[y_A \exp(-E/RT) - y_B \exp(-2.0848E/RT)]. \quad (13)$$

A simple calculation shows that, for this model, the forward reaction is 235 times as fast as the reverse reaction, when $y_A = y_B$ and $T = T_b$. Hence it does not appear that the small degree of reversibility in this model should cause the results to differ greatly from those obtained with the irreversible model of this paper. The models also differ in that an $\exp(-E/RT)$ rate law was used by Hirschfelder *et al.*, while an $\exp(-E/RT_b\tau)$ rate law was used in this investigation.

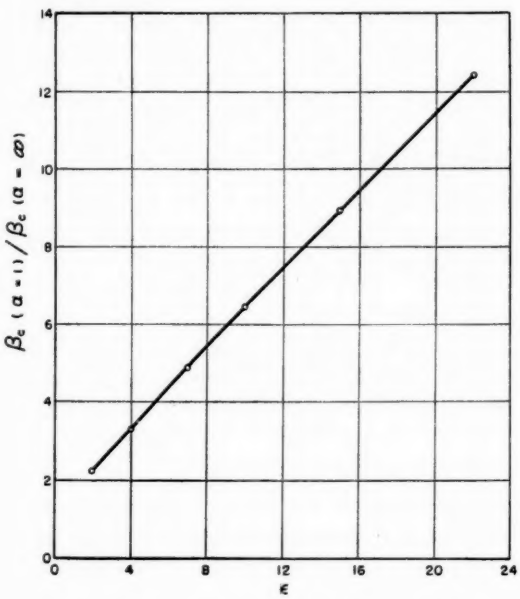

FIG. 3. Variation of $\beta_c\ (\alpha=1)/\beta_c\ (\alpha=\infty)$ with ϵ.

According to Hirschfelder *et al.*, the ratio of the burning velocity with no diffusion to the burning velocity when $\alpha = 1$ is 1.81, while, according to the current study, the ratio is 1.96, for the case of $\epsilon = 5.033$. The magnitude of the burning velocity obtained by Hirschfelder *et al.* is 1.18 times as great as the value obtained in this study for $\epsilon = 5.033$ and $\alpha = 1$. These values appear to be in reasonable agreement, considering the differences in the models.

In order to facilitate use of the results of the numerical integrations in Table I, an empirical equation has been developed:

$$\beta_c = \left[\frac{0.514}{\alpha}\epsilon^2 + \left(1 + \frac{0.35}{\alpha}\right)\epsilon + \left(0.20 + \frac{0.05}{\alpha}\right)\right] \exp(\epsilon). \quad (14)$$

Equation (14) accurately represents all of the calculated results, both for $\alpha = 1$ and $\alpha =$ infinity. Furthermore, it appears to be a reasonably good approximation for all values of α between 0.5 and infinity, as may be seen by the comparison with the calculations of Hirschfelder *et al.* in Fig. 4 for $\epsilon = 5.033$.

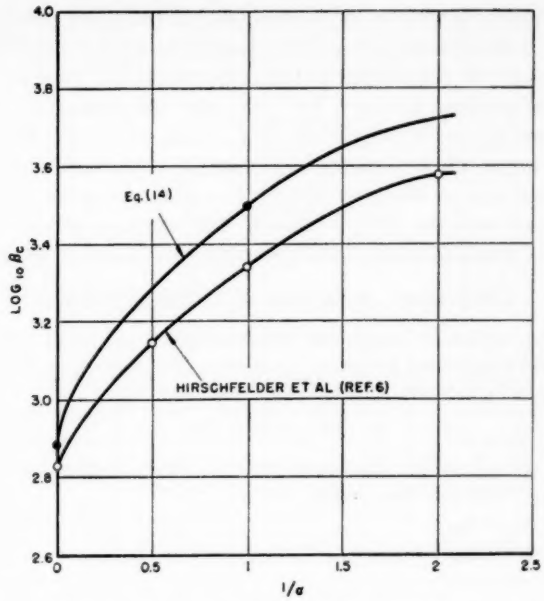

FIG. 4. Variation of β_c with α, when $\epsilon = 5.033$.

An instructive comparison may be made between the results of this work and the burning velocity equation derived by Zeldovich and Frank-Kamenetsky[14] for a first-order reaction with diffusion. The latter equation, when expressed in the terminology of this paper, becomes

$$\beta_c = 0.5r[1-(T_u/T_b)]^2\epsilon^2 \exp(\epsilon). \quad (15)$$

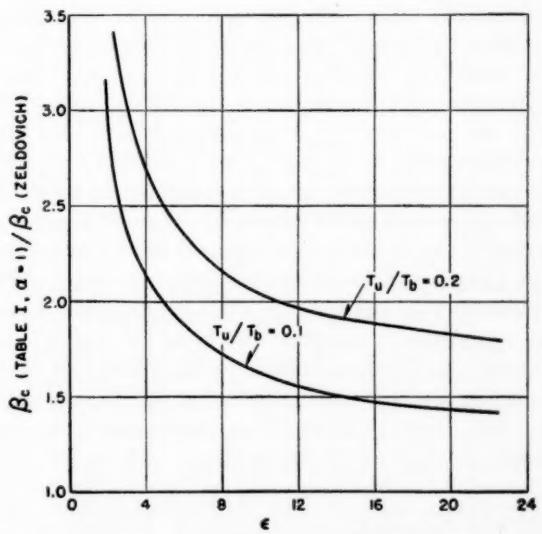

FIG. 5. Comparison of Zeldovich and Frank-Kamenetsky equation with numerical integrations, when $\alpha = 1$.

[14] Y. B. Zeldovich and D. A. Frank-Kamenetsky, Compt. rend. (Doklady) Acad. Sci. USSR **19**, 693 (1938). See also N.A.C.A. Tech. Memos 1026 and 1084.

The new symbol r is the number of moles of product per mole of reactant and is equal to unity for the reaction $A \rightarrow B$ considered in this investigation. In Fig. 5, a comparison between Eq. (15) and the results of this investigation is shown, for two values of T_u/T_b. When ϵ is large, the agreement is seen to be remarkably good. However, as Zeldovich and Frank-Kamenetsky suspected and as Fig. 5 shows, the approximations in their derivation become increasingly poor as ϵ decreases.

APPENDIX: NUMERICAL INTEGRATIONS

The numerical integrations were carried out with an I.B.M. Card-Programmed Electronic Calculator. The following stepwise integrating formula, due to Milne,[15] was used:

$$z_{n+1}=z_{n-1}+2h(dz/d\tau)_n, \tag{16}$$

where h is $[\tau_{n+1}-\tau_n]$. The effect of various sizes of increments was studied for the case $\epsilon=15$, $\alpha=1$; it was found that results were substantially the same whether h was taken as 0.01 or as 0.005. Also some calculations in which the modified Euler method, as described by Scarborough,[16] was used, agreed very well with the above results. Hence it was felt that the method of solution was accurate. Starting values for the integration were obtained for intervals of h of 0.001 or 0.0001 for the first ten intervals. Use of the smaller starting interval minimized a very small oscillation in the integration curves without affecting the mean location of the curves.

For each set of values of α and ϵ, the integrations yield an upper and a lower limit for β; the interval between these limits may be reduced to any desired extent by carrying out the integration for additional trial values of β. In each case, successive trials were made until the upper and lower limits of β differed by less than four percent. Hence the average of the upper and lower limits differs from the true value by less than two percent.

[15] W. E. Milne, *Numerical Calculus* (Princeton University Press, Princeton, New Jersey, 1949), p. 132 ff.

[16] J. B. Scarborough, *Numerical Mathematical Analysis* (Johns Hopkins Press, Baltimore, 1950), second edition, p. 235 ff.

THE JOURNAL OF CHEMICAL PHYSICS VOLUME 21, NUMBER 4 APRIL, 1953

Adsorption Studies on Clay Minerals. II. A Formulation of the Thermodynamics of Exchange Adsorption*

GEORGE L. GAINES, JR., AND HENRY C. THOMAS
Sterling Chemistry Laboratory, Yale University

(Received November 25, 1952)

Expressions for thermodynamic equilibrium constants are set up for the ion-exchange equilibria of models defined in terms of operational variables. Formulas summarizing the methods for the computation of the requisite activity coefficients are given. In particular, the effects of the solvent, which is considered as an independently variable component, are taken explicitly into account.

THE equilibrium relations for an ion-exchanger in contact with a solution of a mixture of ions have been discussed by several writers.[1–4] For our purposes these treatments all leave something to be desired. Either they are admittedly incomplete or are in terms which are not directly applicable to our work with clays. We wished to have a formulation of the problem, rigorously thermodynamic in character, derived for a model defined solely in terms of directly measurable quantities. On such a basis there need be no confusion as to the meaning of the terminology, and the applicability of the results to a given case will be determined by the very quantities measured. All this, of course, is a necessary characteristic of every purely thermodynamic discussion. (It does appear that the significance of the point has been overlooked or disregarded by some writers on the thermodynamics of the ion-exchange process.) The nature of the experiments necessary to determine how closely any real system approaches in character that of our model will be immediately obvious in terms of the definition of the model.

It is probable that an adequate thermodynamic treatment of the ion-exchange process on a montmorillonite clay can be obtained with a very simple model: We suppose our solid exchanger to be a substance with a fixed number of exchange sites per unit mass of silicate "backbone," capable of adsorbing water (and possibly other solvents) and *incapable* of adsorbing the negative ions of the surrounding solution. To test the applicability of this model in a given case, one might devise a series of chromatographic experiments in which successively the various cations and anions were marked by isotopic tracers. The hold-up of the chromatographic column for the various marked species would give the necessary information. Similar experiments might be carried out in which the solvent was marked by tracer atoms. These latter experiments, however, would certainly become complicated, and, quite possibly, the results would be entirely obscured by exchange reactions with the backbone constituents of the solid under

* Contribution No. 1137 from the Sterling Chemistry Laboratory, Yale University.

[1] Argersinger, Davidson, and Bonner, Trans. Kansas Acad. Sci. **53**, 404 (1950).

[2] Ekedahl, Högfeldt, and Sillén, Acta Chem. Scand. **4**, 556 (1950).

[3] E. Glueckauf, Endeavour **10**, 40 (1951).

[4] H. P. Gregor, J. Am. Chem. Soc. **73**, 642 (1951).

observation (e.g., OH groups in a clay). As a matter of fact, the solvent problem is generally one of some difficulty. A knowledge will be required of the extent of adsorption of the solvent in the region of high solvent activity, a very difficult measurement to make.

As an extension of the thermodynamic treatment to cover such substances as the resinous exchangers, it is necessary to define the model in such a way as to take into account what might be called an adsorbed solution phase containing negative ions. Since, however, it appears to be impossible to devise an experiment in which the equilibrium composition of such an "interior" solution can be determined, it is better to drop this idea of "interior solution phase" at the very outset and to define the model simply as an exchanger capable of adsorbing solvent and within which exists a definite linear relation between the numbers of equivalents of positive and negative ionic species. Such a model is immediately subject to macroscopic experiments of the character just mentioned. While the results for this more general model can be specialized to the simpler case, it will be advantageous in the following presentation to consider them separately. The methods for handling these problems were complete in 1876 when Gibbs published the first part of the *Equilibrium of Heterogeneous Substances*. What follows amounts to a translation of Gibbs into terms convenient to determine in the laboratory.

Case A. The Equilibrium between a Solid Substance Capable Only of Exchanging Cations with and Adsorbing Solvent from a Solution, but Incapable of Imbibing Anions

For simplicity we confine our considerations to the exchange of a pair of positive ions, A and B, with valences z_A and z_B. We have assumed the solid to be of constant exchange capacity and to be incapable of adsorbing negative ions and are hence free to choose as the independently variable components of the system, solid-solution-vapor, the positive ions and the solvent. We denote the phases of the system by primes, single, double, and triple for the solid, solution, and vapor, respectively. We further denote the numbers of moles of the various species by n for the solid phase, by m for the liquid phase, and by l for the vapor. Specific amounts in the different phases will be denoted by N for the solid (per equivalent of exchange capacity) and by M for the solution (on a molality basis). Since for a closed system we are allowing a change in the mass of solvent in the solution phase, it will be clearer if we specialize to concentration units after the equilibrium relations are obtained.

The condition for stable equilibrium of the closed system is, in terms of the energy,

$$\delta E' + \delta E'' + \delta E''' = 0, \tag{1}$$

subject to the conditions imposed by the constraints on the ions and the solvent (which latter we denote by the subscript s):

$$\delta n_A + \delta m_A = 0, \tag{2}$$

$$\delta n_B + \delta m_B = 0, \tag{3}$$

$$z_A \delta m_A + z_B \delta m_B = 0, \tag{4}$$

$$\delta n_s + \delta m_s + \delta l_s = 0. \tag{5}$$

These conditions include the expression of the constancy of the exchange capacity,

$$z_A \delta n_A + z_B \delta n_B = 0. \tag{6}$$

The redundancy of this equation results from the deliberate omission of a term expressing a variation in the number of exchange sites on the solid. The inclusion of such a term would have necessitated the consideration of another independently variable component. Gibbs' argument now gives as the conditions for stable equilibrium the equality of temperature and pressure of the three phases and the following relations between the chemical potentials:

$$z_B \mu_A' - z_A \mu_B' = z_B \mu_A'' - z_A \mu_B'' \tag{7}$$

and

$$\mu_s' = \mu_s'' = \mu_s'''. \tag{8}$$

We now choose, as is customary, to write the chemical potentials

$$\mu_A' = \mu_A'^0 + RT \ln N_A f_A, \tag{9}$$

$$\mu_A'' = \mu_A''^0 + RT \ln M_A \gamma_A, \text{ etc.,} \tag{10}$$

in which

$$N_A = z_A n_A / (z_A n_A + z_B n_B), \tag{11}$$

so that when we consider a mass of solid carrying one equivalent of exchange sites, $N_A = z_A n_A$. It should be particularly noted that f_A does not have the character of an individual ion activity coefficient but refers to the combination of that ion with the exchanger in a definite composition of the whole mass.

For convenience the activities in the solution are expressed in terms of the ions; the results of the calculations, however, all appear in determinate combinations of the individual ion activity coefficients. The equilibrium constant expression is, from Eq. (7),

$$K = N_A^{z_B} M_B^{z_A} \gamma_B^{z_A} f_A^{z_B} / N_B^{z_A} M_A^{z_B} \gamma_A^{z_B} f_B^{z_A}$$
$$= \exp(z_A \mu_B'^0 - z_B \mu_A'^0 + z_B \mu_A''^0 - z_A \mu_B''^0)/RT. \tag{12}$$

The application of the Gibbs-Duhem equation for the "wet solid" phase makes possible the determination of the f's and the computation of K from appropriate experimental data. (Previous applications of the Gibbs-Duhem equation to this problem have not included a term for the variation of the solvent potential.) The complete equation, of course, contains a term for each independently variable component and is, for our case,

$$n_A d\mu_A' + n_B d\mu_B' + n_s d\mu_s' = 0. \tag{13}$$

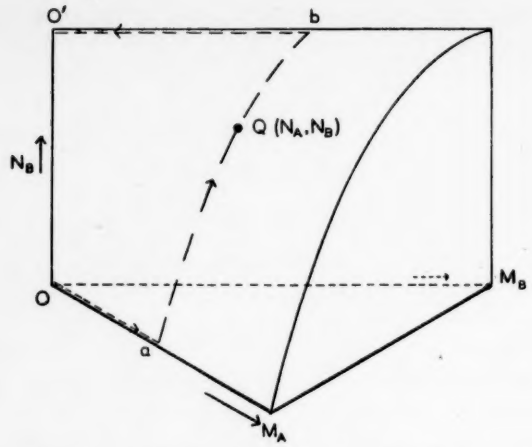

FIG. 1. Path of integration across isothermal surface.

In terms of the N's the equation is

$$N_A d\ln(N_A f_A)^{z_B}+N_B d\ln(N_B f_B)^{z_A}+z_A z_B n_s d\ln a_s=0, \quad (13')$$

in which now n_s refers to the solvent content of one "exchange equivalent" of the solid, and a_s is the activity of the solvent given by $\mu_s'=\mu_s'^0+RT\ln a_s$.

It is now necessary to define the standard states of the various components in order to make possible a definite integration of Eq. (13'). For the solvent we choose the reference states so that the activity of the water in each phase is the same; i.e., we select $\mu_s''^0$ so that $a_s''=1$ for pure solvent and make $\mu_s'^0=\mu_s''^0=\mu_s'''^0$. For the solid phase we choose the reference states as the mono-ion solid in equilibrium with an infinitely dilute solution of that ion, i.e., so that for $N_A=1$ and $a_s=1$, $f_A=1$ and for $N_B=1$ and $a_s=1$, $f_B=1$.

It is obviously insufficient to specify the standard state of the A solid without a specification of its solvent content, and this is most conveniently done in terms of the solvent activity. The choice of a solvent-free solid as a standard state would be somewhat inconsistent with our specification of the system and would necessitate the evaluation of an infinite integral in the application of the Gibbs-Duhem equation.

For the standard states in the solution phase we choose the usual ones which make ion activities approach the corresponding molalities as the solute content approaches zero.

Since the ratio of the γ's in Eq. (12) is the ratio of appropriate powers of the mean activity coefficients in the solution and is hence available (or, at least, can be determined by well-known methods), we define K_c (as has been done by previous authors)[1,2] through the relation

$$\ln K=\ln K_c+\ln f_A^{z_B}-\ln f_B^{z_A}, \quad (14)$$

so that

$$d\ln K_c+d\ln f_A^{z_B}-d\ln f_B^{z_A}=0. \quad (14')$$

Equation (14') taken in conjunction with Eq. (13') enables the elimination in turn of the activity coefficients f and hence makes possible integrations which evaluate these activity coefficients in terms of experimentally measured quantities. If these integrations are carried from the standard states of the pure A solid and B solid to a common point on the isothermal surface, we have all the information necessary for the calculation of $\ln K$. It should be noted that we are integrating point functions of position on the isothermal surface, and hence the path between the standard states is immaterial and may be chosen for convenience. Usually an isothermal line on this surface will be measured at constant total concentration in the solution, and it will therefore usually be convenient to take the path of integration as illustrated in Fig. 1. The curve aQb represents an isotherm determined at constant total molality.

The results of the integration along aQb are

$$\ln\frac{f_A^{z_B}(Q)}{f_A^{z_B}(a)}=-(z_A-z_B)N_B-N_B\ln K_c(Q)+\int_0^{N_B}\ln K_c\cdot dN_B-z_A z_B\int_a^Q n_s d\ln a_s \quad (15)$$

and

$$\ln\frac{f_B^{z_A}(Q)}{f_B^{z_A}(b)}=(z_A-z_B)N_A+N_A\ln K_c(Q)-\int_{N_B}^1\ln K_c\cdot dN_B+z_A z_B\int_Q^b n_s d\ln a_s; \quad (16)$$

hence we find

$$\ln K=(z_B-z_A)+\ln\frac{f_A^{z_B}(a)}{f_B^{z_A}(b)}+\int_0^1\ln K_c\cdot dN_B-z_A z_B\int_a^b n_s d\ln a_s. \quad (17)$$

The activity coefficients at a and b are to be determined as follows. For the equilibrium between the solid and vapor phases we have, in general,

$$\begin{aligned} V'dP&=S'dT+n_A d\mu_A'+n_B d\mu_B'+n_s d\mu_s,\\ V'''dP&=S'''dT+l_s d\mu_s. \end{aligned} \quad (18)$$

Specializing for the pure A solid at constant temperature and eliminating dP, we find

$$d\ln f_A^{z_B}=z_A z_B\left(\frac{V'}{\tau}-n_s\right)d\ln a_s, \quad (19)$$

in which τ is the molar volume of the vapor. We find, then, taking into account our choice of standard state,

$$\ln f_A^{z_B}(a)=z_A z_B\int_{a_s=1}^{a_s(a)}\left(\frac{V'}{\tau}-n_s\right)d\ln a_s, \quad (20)$$

in which, of course, the values of V' and n_s refer to the pure A solid. An entirely similar expression holds for $f_B(b)$.

It should be particularly noticed that whereas n_s for $a_s=1$ is ill defined, if indeed it has any meaning at all, we require only the existence of the integral

$$\int_{a_s=1} n_s d \ln a_s.$$

Our implicit assumption of the existence of a solid phase in contact with pure solvent insures the existence of this integral for our assumed model. Practically we must confine our attention to systems in which we do not get a measurably rapid disintegration of the pure solid to form a molecularly homogeneous suspension in the pure solvent.

The relative importance of the various terms in Eq. (17) must in particular cases be assessed on the basis of experiment. The formula may well be subject to considerable simplification. As an illustration let us consider a case in which $z_A=z_B=1$ and in which the solvent contents of the pure solids are constant, $n_s(A)=n_1$, $n_s(B)=n_2$. Let us suppose further that the vapor obeys the perfect gas law, so that the activity is given by the ratio of the equilibrium vapor pressures of solution and solvent. We shall also suppose that the volume of an exchange equivalent of the solid is negligible compared to the molar volume of the vapor. We now choose our path across the surface as one at constant solvent activity (which may or may not approximate a path at constant total molality). We must suppose that we have available the requisite values of K_c along the desired curve. With these simplifications we find

$$\ln K \simeq (n_2-n_1) \ln \frac{P}{P_0} + \int_0^1 \ln K_c \cdot dN_B,$$

in which P_0 is the vapor pressure of the pure solvent at the temperature considered. Certainly for equilibria with dilute solutions this approximate formula will be adequate in many cases.

Case B. The Equilibrium Between a Solution and a Solid Substance Capable of Exchanging Cations with, and Adsorbing Solvent from, the Solution, and also Capable of Imbibing Anions from the Solution

The discussion in this case proceeds in a fashion analogous to that of the simpler case. We choose as the four independently variable components of the system the two cations, A and B, the single anion X (of valence $-z_X$), and the solvent. The equations of constraint may be written

$$\delta n_A+\delta m_A=0, \tag{21}$$

$$\delta n_B+\delta m_B=0, \tag{22}$$

$$z_A\delta n_A+z_B\delta n_B-z_X\delta n_X=0, \tag{23}$$

$$z_A\delta m_A+z_B\delta m_B-z_X\delta m_X=0, \tag{24}$$

$$\delta n_s+\delta m_s+\delta l_s=0. \tag{25}$$

(From these equations we can immediately deduce the redundant condition of the constancy of the total amount of X: $\delta n_X+\delta m_X=0$.) At equilibrium we find the equality of temperature, pressure, and chemical potential of the solvent for each of the three phases, together with the following relations:

$$z_X\mu_A'+z_A\mu_X'=z_X\mu_A''+z_A\mu_X'', \tag{26}$$

$$z_X\mu_B'+z_B\mu_X'=z_X\mu_B''+z_B\mu_X''. \tag{27}$$

From Eqs. (26) and (27) there follows the relation between chemical potentials which gives rise to the usual equilibrium constant expression

$$z_B\mu_A'-z_A\mu_B'=z_B\mu_A''-z_A\mu_B''. \tag{28}$$

It is convenient to define the variables of composition for the solid phase in a manner analogous to those chosen in Case A. We again consider a mass of exchanger corresponding to one exchange equivalent, so that

$$z_An_A+z_Bn_B-z_Xn_X=1 \tag{29}$$

and again define

$$N_A=z_An_A, \quad N_B=z_Bn_B, \quad \text{and} \quad N_X=z_Xn_X \tag{30}$$

so that

$$N_A+N_B-N_X=1. \tag{30'}$$

We take the activities for A and B formally as before and must now in addition define an f_X by the relation

$$\mu_X'=\mu_X'^0+RT \ln N_X f_X. \tag{31}$$

Here f_X has the character of an individual ion activity coefficient. It is, however, not susceptible of evaluation on the basis of the experiments envisaged, and indeed the final results are independent of f_X. The equilibrium constant expression corresponding to Eq. (28) is formally identical with that corresponding to Eq. (12).

The Gibbs-Duhem equation for the four component system is

$$n_A d \ln N_A f_A+n_B d \ln N_B f_B + n_X d \ln N_X f_X+n_s d \ln a_s=0. \tag{32}$$

From Eqs. (26) and (27) we have the two differential expressions:

$$d \ln K_A^{z_X}+d \ln f_A^{z_X}+d \ln f_X^{z_A}=0, \tag{33}$$

$$d \ln K_B^{z_X}+d \ln f_B^{z_X}+d \ln f_X^{z_B}=0, \tag{34}$$

in which the quantities K_A and K_B are defined in terms of measurable quantities and are given by

$$K_A^{z_X}=\frac{N_A^{z_X}N_X^{z_A}}{M_A^{z_X}M_X^{z_A}\gamma_A^{z_X}\gamma_X^{z_A}}; \qquad K_B^{z_X}=\frac{N_B^{z_X}N_X^{z_B}}{M_B^{z_X}M_X^{z_B}\gamma_B^{z_X}\gamma_X^{z_B}}. \tag{35}$$

It is to be noted that the activity coefficient product in these expressions is thermodynamically determinate.

From Eqs. (32), (33), and (34) we may now find expressions for the evaluation of f_A and f_B. For simplicity we choose to integrate across the isothermal surface *at constant* N_X (which, in general, will not be at constant M_X). The resulting expressions for f_A and f_B are

$$\ln f_A^{z_B}(Q) = \ln f_A^{z_B}(a) - \{N(Q) - N(a)\} - N_B \ln K_c(Q) + N_X\{\ln K_A^{z_B}(Q) - \ln K_A^{z_B}(a)\} + \int_a^Q \ln K_c \cdot dN_B - z_A z_B \int_a^Q n_s d\ln a_s \quad (36)$$

and

$$\ln f_B^{z_A}(Q) = \ln f_B^{z_A}(b) - \{N(Q) - N(b)\} + N_A \ln K_c(Q) + N_X\{\ln K_B^{z_A}(Q) - \ln K_B^{z_A}(b)\} - \int_Q^b \ln K_c \cdot dN_B + z_A z_B \int_Q^b n_s d\ln a_s. \quad (37)$$

In Eqs. (36) and (37) we have written N for $z_A z_B\{N_A/z_A + N_B/z_B + N_X/z_X\}$. The resulting expression for the equilibrium constant defined by Eq. (28) is

$$\ln K = (z_B - z_A)(1 + N_X) + \ln \frac{f_A^{z_B}(a)}{f_B^{z_A}(b)} - N_X \ln \frac{K_A^{z_B}(a)}{K_B^{z_A}(b)} + \int_a^b \ln K_c \cdot dN_B - z_A z_B \int_a^b n_s d\ln a_s \quad (38)$$

(N_X *constant* from a to b).

To evaluate the activity coefficient at a we need in this case the three equations, valid at constant temperature,

$$V' dP = (N_A/z_A) d\mu_A' + (N_X/z_X) d\mu_X' + n_s d\mu_s, \quad (39)$$

$$V'' dP = M_A d\mu_A'' + M_X d\mu_X'' + M_s d\mu_s, \quad (40)$$

$$V''' dP = l_s d\mu_s. \quad (41)$$

When we make use of the relations $N_A - N_X = 1$, $z_A M_A - z_X M_X = 0$, and Eq. (26), the activity of the compound in the solution phase as well as the pressure can be eliminated. After introducing the definition of the standard state (in which $N_X = 0$), we find

$$\ln\{N_A(a) f_A(a)\}^{z_B} = z_A z_B \int_0^a \left\{ \frac{V'}{\tau} - n_s + \frac{n_X}{M_X}\left(\frac{V''}{\tau} - M_s\right)\right\} d\ln a_s. \quad (42)$$

The term $n_X/M_X (= N_X/z_X M_X)$ is the stoichiometric distribution coefficient for the negative ion between the solid and the solution. If the small volume ratios are disregarded and if we suppose we are dealing with water solutions, Eq. (42) becomes simply

$$\ln\{N_A(a) f_A(a)\}^{z_B} \simeq -z_A z_B \int_0^a \left(n_s + 55.51 \frac{n_X}{M_X}\right) d\ln a_s. \quad (42')$$

A similar expression is found for f_B at b.

As in Case A, formula (38) will undergo simplification in special cases. If $z_A = z_B$, the first term in Eq. (38) disappears and in addition we find for the path at constant N_X: $K_A(a)/K_B(b) = a_{BX}(b)/a_{AX}(a)$, the ratio of the activities in the two solutions. It seems scarcely worth while to attempt further simplifications without specific experimental data as a guide.

This work has been done as a part of work at Yale University under contract with Brookhaven National Laboratory. We are much indebted to the Department of Nuclear Engineering at Brookhaven for its continued interest and support.

A Spectrometer for the Far Infrared and the Spectrum of 1,2 Dichloroethane

C. R. Bohn, N. K. Freeman, William D. Gwinn, J. L. Hollenberg, and Kenneth S. Pitzer
Department of Chemistry, University of California, Berkeley, California

(Received November 24, 1952)

A brief description is given of a grating spectrometer which has been used in the wavelength range 22 to 77 microns. Test measurements of the pure rotation spectrum of water vapor gave excellent agreement with other investigators. The spectrum of 1,2 dichloroethane shows bands at 409, approximately 265, and 222 cm^{-1}. A band with its center a little less than 135 cm^{-1} also is indicated. The value 223 cm^{-1} suggested for the antisymmetric skeletal deformation frequency of the *trans* form of dichloroethane by Mizushima, Morino, and Simanouti is thus confirmed. Their suggestion was based on a very weak Raman band which they attributed to this infrared active frequency on the basis of a breakdown of selection rules in the liquid. Our result also confirms various statistical-thermodynamic calculations for this substance.

As physical chemistry has extended its interest to the structure of larger molecules, there has arisen a need for infrared spectra in the region of wavelengths longer than those transmitted by common prisms. This need is most marked in the case of molecules with a center of symmetry, because all vibrations antisymmetric to that center are then forbidden in the Raman spectrum. In other molecules of high symmetry there are commonly types of vibrations which are allowed in the infrared but forbidden in the Raman spectrum. However, most infrared spectrometers have been prism instruments which are intrinsically limited in range by the characteristics of the prism. Thus the most common prism material, NaCl, limits spectra to wavelengths below about 15 microns. Other materials in use include KBr and the TlBr−TlI mixed crystal (KRS-5) with the extended limits of 25 and 38 microns, respectively. While it is to be hoped that prisms of even greater range will become available, it seemed worth while to build a grating instrument. Such an instrument avoids the need for light transmission through any materials except for very thin windows, consequently, it is adapted to measurements in the infrared beyond the range of prism spectrometers.

In the present paper we give a brief description of the spectrometer and report results for 1,2 dichloroethane in the range 22 to 77μ (450–130 cm^{-1}).

SPECTROMETER

Grating spectrometers of this general type have been described by several authors, including Randall and co-workers,[1] McCubbin and Stinton,[2] and Oetjen and co-workers.[3] The present instrument was not primarily intended to go beyond the performance already attained, but rather it was to be a convenient instrument with which a number of substances could be measured within a reasonable period of time.

It was decided to enclose the entire spectrometer in a vacuum tank for two reasons. First, evacuation is the easiest way of eliminating the very intense absorption of water vapor. Second, with a vacuum thermocouple as a detector, the number of windows can be minimized by placing all of the rest of the spectrometer in the same vacuum space.

The two principal problems in far infrared spectrometry are the spectral purity of the radiation and the low energy at the detector. The existence of higher order reflections from a grating requires that other means be employed to eliminate radiation of wavelength one-half or less than that being measured. This problem is aggravated by the increase in emitted intensity with decrease in wavelength for a blackbody type of source. An inspection of the spectrometer design as shown in Fig. 1 will indicate the devices used to overcome these difficulties.

The source at O is a Globar in a water cooled housing. It is hoped to substitute a source having more selective emission characteristics, but the Globar is simple and reliable for initial operation. M_1 is a cylindrically shaped "reststrahlen" reflector. Its function is to reflect only the desired range of wavelengths onto the entrance window of the absorption cell C. The materials employed for M_1 are fluorite, sodium chloride, and potassium chloride whose reflection maxima are at 32, 52, and 63 microns, respectively. The reflectivity remains large enough over ranges near the maxima so that the region from 22 to 77 microns can be covered with these three materials.

Between M_1 and C there is a light chopper, Ch, which

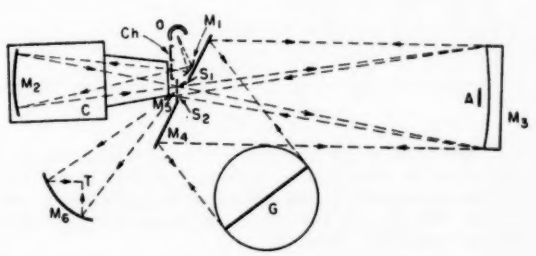

FIG. 1. Optical path and general arrangement of the spectrometer.

[1] H. M. Randall, Rev. Sci. Instr. **3**, 196 (1932); H. M. Randall and F. A. Firestone, **9**, 404 (1938).
[2] T. K. McCubbin, Jr. and W. M. Stinton, J. Opt. Soc. Am. **40**, 537 (1950).
[3] Oetjen, Haynie, Ward, Hansler, Schanwrecker, and Bell, J. Opt. Soc. Am. **42**, 559 (1952).

interrupts the beam with a frequency of 5 cps. Since only the alternating output of the detector will be amplified, the opportunity is taken to chop only the radiation of the desired wavelength and to let shorter wavelengths pass as nearly uninterrupted as possible. This is accomplished by using a thin salt plate as a chopper. In the range 25–40μ a sodium chloride chopper is used while from 40 to 70μ a potassium bromide chopper is appropriate.

The windows of the cell C are made of 2.5-mil polythene. In addition to the single reflection path shown, a multiple reflection cell of the White[4] type is available. The emergent beam then passes through the slit S_1 and onto the 10″ parabolic mirror M_3. All mirrors (except M_1) are front surface aluminized glass mirrors. M_4 is a plane mirror with a hole cut for the slits while G is the grating. Two echelette gratings of 500 and 380 lines per inch respectively are now in use. The size of their ruled surface is $7\frac{1}{2}''\times 8\frac{1}{2}''$ which was the limit for the shaper on which they were made.

A small shield A must be included to prevent direct reflection from one slit to the other. After passing the exit slit, S_2, the beam is reflected from a small plane mirror M_5 onto a 5″ elliptical mirror M_8 which focuses upon the thermocouple detector T. The present detector is made from 0.2-mm long, 1-mil diam wires of 90 percent Bi-10 percent Sb and 75 percent Sb-25 percent Cd alloys and a 0.6×6 mm receiver of 0.28-micron gold leaf, blackened with gold black.

The ac output of the detector is amplified by an amplifier of limited band pass (2 to 20 cps) and voltage gain of 10^7. The output of the amplifier is then rectified by a mechanical synchronous rectifier. The dc output of the rectifier is filtered with a R-C filter of variable time constant, the longest of which is 60 seconds, giving an effective band width of 0.003 cycles/sec for the entire detection system. The rectifier and filter circuit reduce the over-all gain to 10^6. The output is recorded on a 10-mv Brown Electronik Recorder.

Special precautions were taken to minimize noise and 60-cycle signals generated in the amplifier. The 20 ohm thermopile is coupled to the first stage by a shielded transformer with a voltage increase of 120. The first stage is located with the transformer near the spectrometer and consists of a 6AK5 connected as a triode with a grounded cathode and floating grid. The filament is heated with 5 volts from a 40-kilocycle oscillator in the main amplifier. The low filament voltage is used to reduce the cathode noise. The plate resistor is a selected metal resistor. The 6AK5 was selected from a batch of some 50 tubes. The best tubes were usually those which had been in service several months. In the second stage the filament is heated by the main power transformer, but the plate and screen resistors are metal resistors. Immediately preceding the last stage, a 60-cycle/sec twin-T reject filter is inserted. This filter highly attenuates the pick-up from the power lines.

Using the longest response time (band width = 0.003 cycles/sec) and a 20-ohm thermocouple the noise level is 40 $\mu\mu$v (rms across the 20 ohm resistor). This compares very favorably with the theoretical noise level of 31 $\mu\mu$v (rms). The sensitivity can be adjusted as high as 0.01 μv for a full scale deflection on the recorder.

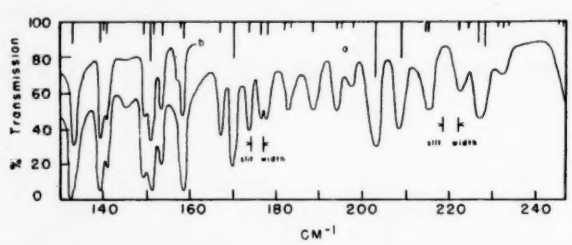

FIG. 2. Spectrum of water vapor in the range 130–250 cm^{-1} as observed with the 380-lines/in. grating. The path length was 70 cm, and the pressures were the full vapor pressure for (a) and 10 mm for (b). The lines at the top of the graph give the expected location and qualitative intensity.

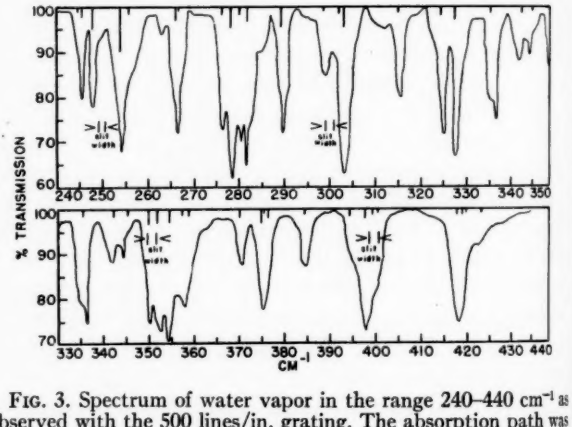

FIG. 3. Spectrum of water vapor in the range 240–440 cm^{-1} as observed with the 500 lines/in. grating. The absorption path was 70 cm at the vapor pressure of the liquid. The expected spectrum is indicated at the top.

Selsyn motors are used to transmit inside the vacuum tank the mechanical motions for the grating control, the slit control and the chopper. The chopper action must be coordinated precisely with the rectification of the amplified signal. Counters are used to keep account of the grating and slit positions with motor drive for the former and manual control of the latter.

Additional details concerning the spectrometer are given elsewhere.[5]

CALIBRATIONS AND TESTS

Water vapor is a very convenient test substance for this spectral region. Its pure rotation spectrum has been measured very accurately on the Michigan spectrometer[6] and interpreted theoretically.

[4] J. U. White, J. Opt. Soc. Am. **32**, 285 (1942).

[5] (a) N. K. Freeman, Ph.D. dissertation, University of California, 1949; (b) C. R. Bohn, Ph.D. dissertation, University of California, 1951; (c) J. L. Hollenberg, M.S. dissertation, University of California, 1952.

[6] Randall, Dennison, Ginsberg, and Weber, Phys. Rev. **52**, 160 (1937).

Figures 2 and 3 show the water spectrum as observed on our instrument. We find good agreement with the Michigan results within the accuracy of our present work. Lines as close together as 2 cm^{-1} are resolved and the sharp maxima are measured to less than 0.5 cm^{-1}. We did not attempt to determine absolute wavelengths from the characteristics of our instrument but accepted the water vapor results as a calibration.

Various filter materials were employed in testing the ratio of false energy to that of the desired wavelength. The false energy problem is not very serious in the 25–40 micron range. At longer wavelengths the false energy becomes comparable with the first-order energy even with the reststrahlen mirror and salt crystal chopper as described above. In order to further reduce the false energy of very low wavelength, the polythene windows were thoroughly scratched with 180-mesh sandpaper. An additional scratched polythene filter was placed just before the detector. This combination of light scattering filters reduced the false energy to a maximum of 20 percent. While this percentage is still larger than would be desired, it does not prevent the measurement of satisfactory spectra.

RESULTS

The absorption spectra have been measured for a number of chlorine derivatives of ethane and ethylene together with some other similar molecules. These spectra will be published in connection with the discussions of their interpretation. At this time, we include only the spectrum of 1,2 dichloroethane which is shown in Fig. 4.

The vibrational spectrum of dichloroethane has been the subject of a large number of papers by many authors including Wu[7] and Mizushima and collaborators.[8] This substance is complicated by the existence of two geometrical isomers which are in rapid equilibrium.

In addition to the portion of the spectrum shown in Fig. 4, the region from 250 to 450 cm^{-1} was explored.[4] This region had been measured previously by Plyler[9] for liquid dichloroethane. We found a relatively sharp band at 409 cm^{-1} and a very broad band with its center near 265 cm^{-1}. These are in accord with Plyler's results of 412 and 272 cm^{-1} for the liquid and with the Raman bands

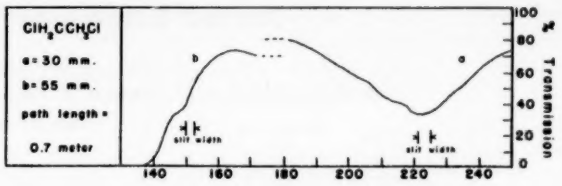

FIG. 4. Spectrum of 1,2 dichloroethane.

at 410 and 264 cm^{-1}. These two bands arise from the *gauche* form and are allowed in both the Raman and infrared spectra.

The new and interesting portion of our spectrum is shown in Fig. 4 for the range 135–250 cm^{-1}. We find a band centered at 222 cm^{-1} and another at the extreme low frequency end of the range.

In 1948 two of us[10] presented thermal data on dichloroethane and gave a general statistical-thermodynamic treatment for the substance, including both the *trans* and *gauche* forms. At that time our calculations had to be left in a somewhat tentative state, because the lowest infrared active vibrational frequency of the *trans* form fell in the region of long wavelengths where no observations had been made.

Mizushima, Morino, and Simanouti[8] had suggested that a very weak Raman band at 223 cm^{-1} might represent this frequency. If so it would be appearing because the selection rule against its appearance in the Raman spectrum was broken down by intermolecular forces in the liquid state. While our calculations were adjusted to be reasonably consistent with this frequency, no great reliance could be placed on its correctness because there were other possible explanations of such a weak band.

Under these circumstances it was most gratifying to observe the relatively strong band at 222 cm^{-1} in the infrared spectrum. This confirms the general correctness of our earlier calculations and those of Mizushima and collaborators.

The other feature of our spectrum is the absorption band, which is beginning at about 140 cm^{-1}, and whose peak lies at a lower frequency. This is presumably the torsional oscillation of the *gauche* form which has been observed at 125 cm^{-1} in the Raman spectrum of the liquid, and which is allowed in both the Raman and the infrared spectra.

It will now be appropriate to refine our statistical-thermodynamic treatment of this molecule with full reliance on the complete vibrational spectrum.

[7] Ta-You Wu, *Vibration Spectra and Structure of Polyatomic Molecules* (Edwards Brothers, Inc., Ann Arbor, 1946), second edition, pp. 306–312.

[8] Mizushima, Morino, and Simanouti, Sci. Pap. Inst. Phys. Chem. Research (Tokyo), **40**, 87 (1942); and other papers there cited.

[9] E. K. Plyler, J. Chem. Phys. **17**, 218 (1949).

[10] W. D. Gwinn and K. S. Pitzer, J. Chem. Phys. **16**, 303 (1948).

Normal Coordinate Treatment of Diacetylene*

SALVADOR M. FERIGLE AND ALFONS WEBER
Spectroscopy Laboratory, Department of Physics, Illinois Institute of Technology, Chicago 16, Illinois
(Received September 30, 1952)

A normal coordinate treatment for diacetylene is carried out, using Wilson's FG matrix method. Different sets of potential constants are obtained from the observed frequencies, and limits for these constants are set. The values of the potential constants are discussed in connection with the molecular structure.

IN two recent publications,[1,2] normal coordinate treatments for diacetylene (*DA*) have been reported. Both agreed in giving a potential constant for the central carbon-carbon bond stretching which is much higher than the value corresponding to a carbon-carbon single bond, which is normally about 5 md/A (millidyne per Angstrom = 10^5 dyne per centimeter). This was expected as a consequence of the resonance present in the molecule, and it settled the difficulties previously existing as a result of a misinterpretation of the spectrum,[3,4] which led to very low values of the central bond-stretching potential constant.[5,6] In one of the previous normal coordinate treatments[1] the C—H stretching potential constant was transferred from acetylene, and in the other,[2] an interaction constant was assumed, even though the author recognized the high degree of inaccuracy involved in the assumption of interaction constants for conjugated molecules because of the uncertainty in the degree of delocalization of the π-electrons of the carbon atoms, on which the potential constants depend.

The object of the present paper is to report different sets of potential constants for *DA* with the aim of setting limits for these constants. The constants are naturally subjected to the errors inherent in the neglect of the anharmonicity of the vibrations, which cannot be determined with the data available at the present time.

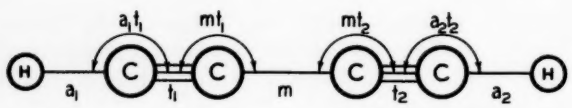

FIG. 1. Bond distances and interbond angles for diacetylene.

FG MATRIX METHOD FOR DIACETYLENE

A normal coordinate treatment has been carried out for *DA* using the Wilson *FG* matrix method.[7] The *g* matrix elements were obtained from the tables of Decius;[8] however, as pointed out by Decius, a deficiency occurs in his tables when a molecule contains three or more collinear nuclei. In this case, the expressions for the **s** vectors given by Wilson[7] for the bending coordinates cannot be used because the denominator becomes zero. This is the case in the *DA* molecule, which has six collinear atoms; therefore, expressions for the kinetic energy matrix elements for linear molecules had to be obtained. The results have been reported in a recent paper.[9] The various bond distances and interbond angles used to determine the internal coordinates are given in Fig. 1. In the symbols used, *m* suggests middle bond; *t*, triple bond; and *a*, acetylenic hydrogen bond. The symmetry coordinates are formed as orthonormal linear combinations of the internal coordinates which transform according to the character table of the $D_{\infty h}$ group[10] to which *DA* belongs. They are

for the A_{1g} vibrations,

$$R_1 = 2^{-\frac{1}{2}}(\Delta a_1 + \Delta a_2),$$
$$R_2 = 2^{-\frac{1}{2}}(\Delta t_1 + \Delta t_2), \text{ and}$$
$$R_3 = \Delta m;$$

TABLE I. Wave numbers corresponding to the fundamental vibrational frequencies of diacetylene (H—C≡C—C≡C—H).[a]

Type	Designation	Wave number (cm^{-1})
A_{1g}	ν_1	(3329)[b]
A_{1g}	ν_2	2184
A_{1g}	ν_3	874
A_{1u}	ν_4	3329
A_{1u}	ν_5	2020
E_{1g}	ν_6	627
E_{1g}	ν_7	482
E_{1u}	ν_8	630
E_{1u}	ν_9	(220)[b]

[a] A. V. Jones, reference 2.
[b] Not observed.

* Supported in part by a grant from the Research Corporation and by contract DA-11-022-ORD-464 with the U. S. Office of Ordnance Research.

[1] Ferigle, Cleveland, and Meister, J. Chem. Phys. **20**, 526 (1952).
[2] A. V. Jones, Proc. Roy. Soc. (London) **A211**, 285 (1952).
[3] G. Herzberg, *Infrared and Raman Spectra of Polyatomic Molecules* (D. Van Nostrand, New York, 1945), first edition, p. 324.
[4] T. Y. Wu, *Vibrational Spectra and Structure of Polyatomic Molecules* (Edwards Brothers, Inc., Ann Arbor, 1946), second edition, p. 259.
[5] T. Y. Wu and S. T. Shen, Chinese J. Phys. **2**, 128 (1936).
[6] A. G. Meister and F. F. Cleveland, J. Chem. Phys. **15**, 349 (1947).
[7] E. B. Wilson, Jr., J. Chem. Phys. **7**, 1047 (1939); **9**, 76 (1941).
[8] J. C. Decius, J. Chem. Phys. **16**, 1025 (1948).
[9] S. M. Ferigle and A. G. Meister, J. Chem. Phys. **19**, 982 (1951).
[10] S. M. Ferigle and A. G. Meister, Am. J. Phys. **20**, 421 (1952), and references given therein.

for the A_{1u} vibrations,

$$R_4=2^{-\frac{1}{2}}(\Delta a_1-\Delta a_2), \text{ and}$$
$$R_5=2^{-\frac{1}{2}}(\Delta t_1-\Delta t_2);$$

for the E_{1g} vibrations,

$$R_{6a}=2^{-\frac{1}{2}}(\Delta a_1 t_1-\Delta a_2 t_2),$$
$$R_{6b}=2^{-\frac{1}{2}}[\Delta(a_1 t_1)'-\Delta(a_2 t_2)'],$$
$$R_{7a}=2^{-\frac{1}{2}}(\Delta m t_1-\Delta m t_2), \text{ and}$$
$$R_{7b}=2^{-\frac{1}{2}}[\Delta(m t_1)'-\Delta(m t_2)'];$$

and for the E_{1u} vibrations,

$$R_{8a}=2^{-\frac{1}{2}}(\Delta a_1 t_1+\Delta a_2 t_2),$$
$$R_{8b}=2^{-\frac{1}{2}}[\Delta(a_1 t_1)'+\Delta(a_2 t_2)'],$$
$$R_{9a}=2^{-\frac{1}{2}}(\Delta m t_1+\Delta m t_2), \text{ and}$$
$$R_{9b}=2^{-\frac{1}{2}}[\Delta(m t_1)'+\Delta(m t_2)'].$$

The numbering of these coordinates corresponds to the numbering of the fundamentals in Table I, where the observed values reported by Jones[2] are given. The

TABLE II. F matrix for diacetylene.

	Δm	Δt_1	Δt_2	Δa_1	Δa_2	$\Delta a_1 t_1$	$\Delta a_2 t_2$	$\Delta(a_1 t_1)'$	$\Delta(a_2 t_2)'$	$\Delta m t_1$	$\Delta m t_2$	$\Delta(m t_1)'$	$\Delta(m t_2)'$
Δm	f_m	f_m^t	f_m^t										
Δt_1		f_t	f_t^t	f_a^t									
Δt_2			f_t		f_a^t								
Δa_1				f_a									
Δa_2					f_a								
$\Delta a_1 t_1$						f_{at}				f_{at}^{mt}			
$\Delta a_2 t_2$							f_{at}				f_{at}^{mt}		
$\Delta(a_1 t_1)'$								f_{at}				f_{at}^{mt}	
$\Delta(a_2 t_2)'$									f_{at}				f_{at}^{mt}
$\Delta m t_1$										f_{mt}	f_{mt}^{mt}		
$\Delta m t_2$		$f_{ji}=f_{ij}$									f_{mt}		
$\Delta(m t_1)'$												f_{mt}	f_{mt}^{mt}
$\Delta(m t_2)'$													f_{mt}

primed angles are in a plane perpendicular to the plane containing the unprimed angles.

The f matrix is given in Table II, and the description of its elements is given in Table III; the elements omitted above the diagonal are considered to be negligible, except those corresponding to interactions between stretching and bending which are zero because of the symmetry. From the f and g matrices and the U matrix formed from the coefficients of the symmetry coordinates, one gets the F and G matrices. The elements of the G matrices are

for the A_{1g} vibrations,

$$G_{11}=\mu_H+\mu_C,$$
$$G_{12}=-\mu_C,$$
$$G_{13}=0,$$
$$G_{22}=2\mu_C,$$
$$G_{23}=-2^{\frac{1}{2}}\mu_C, \text{ and}$$
$$G_{33}=2\mu_C;$$

TABLE III. Description of the potential constants of diacetylene.

Constant	Description
f_a	C−H stretching
f_t	C≡C stretching
f_m	C−C stretching
f_a^t	C−C, C≡C stretching interaction
f_t^t	C≡C, C≡C stretching interaction
f_{at}	C≡C−H bending
f_{mt}	C≡C−C bending
f_{at}^{mt}	C≡C−H, C≡C−C bending interaction
f_{mt}^{mt}	C≡C−C, C≡C−C bending interaction

for the $A_{1\mu}$ vibrations,

$$G_{11}=\mu_H+\mu_C,$$
$$G_{12}=-\mu_C, \text{ and}$$
$$G_{22}=2\mu_C;$$

for the E_{1g} vibrations,

$$G_{11}=a^{-2}\mu_H+(a^{-2}+2t^{-2}+2a^{-1}t^{-1})\mu_C,$$
$$G_{12}=-t^{-1}(a^{-1}+2t^{-1}+2m^{-1})\mu_C, \text{ and}$$
$$G_{22}=2(t^{-2}+2m^{-2}+2t^{-1}m^{-1})\mu_C;$$

and for the $E_{1\mu}$ vibrations,

$$G_{11}=a^{-2}\mu_H+(a^{-2}+2t^{-2}+2a^{-1}t^{-1})\mu_C,$$
$$G_{12}=-(t^{-1}a^{-1}+2t^{-2})\mu_C, \text{ and}$$
$$G_{22}=2t^{-2}\mu_C.$$

Here μ_C and μ_H are the reciprocals of the masses of the C and H atoms respectively, and a, t, and m are the equilibrium values of the corresponding bonds. The elements of the F matrices are

for the A_{1g} vibrations,

$$F_{11}=f_a,$$
$$F_{12}=f_a^t,$$
$$F_{13}=0,$$
$$F_{22}=f_t+f_t^t,$$
$$F_{23}=2^{\frac{1}{2}}f_m^t, \text{ and}$$
$$F_{33}=f_m;$$

for the $A_{1\mu}$ vibrations,

$$F_{11}=f_a,$$
$$F_{12}=f_a^t, \text{ and}$$
$$F_{22}=f_t-f_t^t;$$

for the E_{1g} vibrations,

$$F_{11}=f_{at},$$
$$F_{12}=f_{at}^{mt}, \text{ and}$$
$$F_{22}=f_{mt}-f_{mt}^{mt};$$

and for the $E_{1\mu}$ vibrations,

$$F_{11}=f_{at},$$
$$F_{12}=f_{at}^{mt}, \text{ and}$$
$$F_{22}=f_{mt}+f_{mt}^{mt}.$$

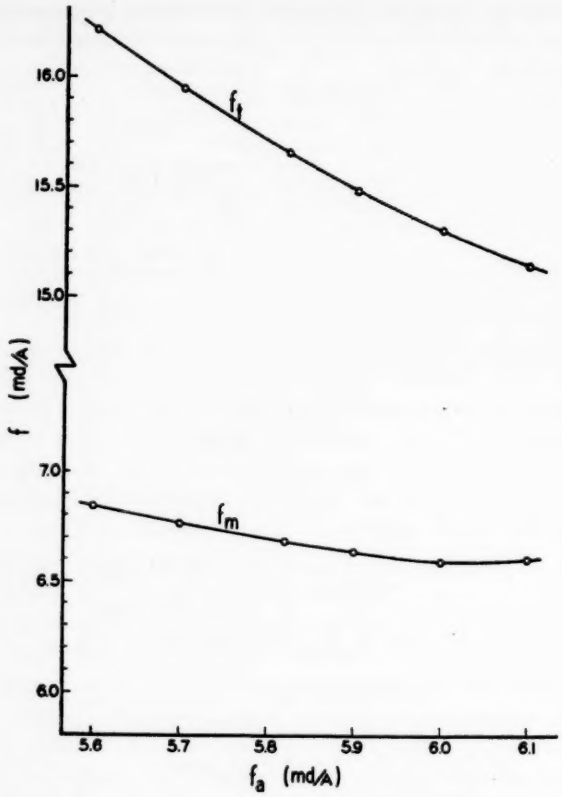

FIG. 2. The C−C and C≡C stretching constants in diacetylene as a function of the C−H potential constant.

POTENTIAL CONSTANTS OF DIACETYLENE

Birge's 1941 values of the physical constants[11] have been used in the calculations. For the atomic masses and bond distances, the following values have been adopted: $\mu_C^{-1}=12.011$ awu, $\mu_H^{-1}=1.008$ awu, $a=1.057$A, $m=1.36$A, and $t=1.19$A. The values of m and t were taken from the electron diffraction work,[12] and a was considered to be the same as the value used by Crawford and Brinkley[13] for acetylene. The values are very close to those more recently adopted by Jones[14] which are $a=1.06$, $t=1.207$, and $m=1.375$A. Probably the actual value of t is higher than for the triple bond in acetylene, owing to conjugation, which will give lower value for m, as pointed out by Jones. Since a definite set of values for the bond distances cannot be chosen, and since the bond distances do not enter into the calculations of the nondegenerate vibrations, which present the greatest interest in this work, the electron diffraction values used in the previous paper[1] have also been used here.

The potential constants were obtained from the observed frequencies of Table I given by Jones;[2] different sets were obtained for the nondegenerate vibrations by giving to f_a a range of values close to the corresponding value in acetylene. The different sets are tabulated in Table IV, and the graphical representation of the variation of the potential constants as a function of f_a are given in Figs. 2 and 3. The fourth set coincides with that reported in our previous calculation,[1] where f_a was assumed to have the same value as in acetylene; the slight differences in the potential constants are due to the use of different physical constants. For the third set, the value of f_a as reported by Jones[2] was adopted, but his other constants could not be reproduced. The potential constants for the degenerate vibrations are given in Table V; the two sets result from the solution of a quadratic equation.

DISCUSSION OF RESULTS

Since the value of f_a in *DA* cannot be very much different from that in acetylene, the present results show that f_m is definitely higher than the single bond carbon-carbon stretching potential constant, which is about 5 md/A. Furthermore, the value of f_m seems to be established between 6.6 and 6.8 md/A. As pointed out previously,[1] Longuet-Higgins and Wheland[15] tried to justify the low value for f_m reported in the previous investigations (3.58 md/A[5] and 3.23 md/A[6]) by considering the possibility of the self-polarizability of the bond being very high. Coulson and Longuet-Higgins[16] have given expressions for the stretching potential constant of a bond in conjugated hydrocarbons, namely,

$$f_r=\lambda_r+\mu\pi_{r,r}/\lambda_r^2,$$

where $\lambda_r=\sigma(1-p_r)+\kappa p_r$, and $\mu=\frac{1}{2}\kappa^2\sigma^2(s-d)^2$. σ and s are the stretching potential constant and the bond distance for a single bond, κ and d are the corresponding values for a double bond; p_r is the mobile bond order, and $\pi_{r,r}$ is the self-polarizability of the bond, which is always negative. In the above expression, the nomenclature of the authors has been kept. We can adopt the values $\sigma=4.96$ md/A, $\kappa=9.80$ md/A, $s=1.54$A, and

TABLE IV. Potential constants for the nondegenerate vibrations of diacetylene.[a]

f_a	f_a'	f_t	f_t'	f_m	f_m'
5.6	−1.01448[b]	16.2134	−0.250693	6.83743	0.597321
5.7	−0.741636	15.9411	−0.150104	6.76475	0.661554
5.8217	−0.363872	15.6484	−0.034713	6.68171	0.735436
5.90149	−0.081966	15.4820	+0.03229	6.63426	0.778701
6.0	0.316030	15.3041	0.09253	6.59067	0.817128
6.1	0.801294	15.1364	0.08529	6.59612	0.812640

[a] Bond constants are in md/A.
[b] The number of figures in the potential constants was retained to insure the best reproduction of the frequencies and to secure internal consistency in the calculations; the values are, of course, not reliably known to this many figures.

[11] R. T. Birge, Revs. Modern Phys. **13**, 233 (1941).
[12] Pauling, Springall, and Palmer, J. Am. Chem. Soc. **61**, 927 (1939).
[13] B. L. Crawford, Jr. and S. R. Brinkley, Jr., J. Chem. Phys. **9**, 69 (1941).
[14] A. V. Jones, J. Chem. Phys. **20**, 860 (1952).
[15] H. C. Longuet-Higgins and G. W. Wheland, Ann. Rev. Phys. Chem. 133 (1950).
[16] C. A. Coulson and H. C. Longuet-Higgins, Proc. Roy. Soc. (London) **A193**, 456 (1948).

$d=1.33$A, used by Coulson and Longuet-Higgins in their calculations. Duchesne[17] used somewhat different values in applying the formulas to cyanogen, and there is undoubtedly a great uncertainty as to what values should be used; however, at the present stage of approximation, the values given above seem to be a reasonable choice. Coulson[18] has given curves relating the mobile bond order to the atomic radius of carbon for different values of the coefficient of orbital mixing. In *DA*, where the σ bond is of sp type, the value of the mobile bond order corresponding to a radius of 0.68A is $p_m=0.70$. From this value we obtain $\lambda_m=8.35$ md/A. If we use the value of $f_m=6.7$ md/A, the corresponding self-polarizability is $\pi_{m,m}=-2.20$ (md·A)$^{-1}$. This value of the self-polarizability can only be regarded as an approximation, but it seems worth while to point out that the errors in this value are more largely due to the uncertainty in the values of σ and κ than to the uncertainty in the calculated potential constant. It also depends on the value used for p_m which is a rather sensitive function of the bond distance, this also being uncertain. In discussing the carbon-carbon stretching

TABLE V. Potential constants for the degenerate vibrations of diacetylene.[a]

f_{at}	0.206715[b]	0.22081
f_{mt}	0.317562	0.347463
$f_{at}{}^{mt}$	0.0707637	0.126828
$f_{mt}{}^{mt}$	0.00306702	0.00287125

[a] Angle constants are in mdA/rad^2.
[b] See footnote b of Table IV.

potential constant of the related molecule cyanogen (N≡C−C≡N), Duchesne[17] gave as limiting value for $\pi=0$ that of $f=7$ md/A; however, this figure was obtained by using $\kappa=9$ md/A and $p=0.5$. The value of the mobile bond order seems to be lower than it should be from the graph of Coulson.[18] Using for consistency the values of σ, κ, s, and d adopted before and $p=0.57$, we obtain for the carbon-carbon bond of cyanogen $\lambda=7.72$ md/A. The value of the self-polarizability for the central bond of *DA* is definitely smaller than it would have to be to lower the potential constant below the value of the single C−C stretching. For $f_m=3.5$ md/A[5,6] the self-polarizability would be $\pi_{m,m}=-6.49$ (md·A)$^{-1}$. Recently, Longuet-Higgins and Burkitt[19] have calculated f_m to be very close to 8 md/A, which would indicate a self-polarizability still smaller than the value calculated here. However, in terms of the normal coordinate treatment carried out

[17] J. Duchesne, Mem. acad. roy. Belgique **26**, No. 7 (1952).
[18] C. A. Coulson, "The Atomic Radius of Carbon," in *Contribution à l'Étude de la Structure Moleculaire*, Volume Commémoratif Victor Henri (M. Desoer, Liège, 1948), p. 15.
[19] H. C. Longuet-Higgins, private communication, September 6, 1952.

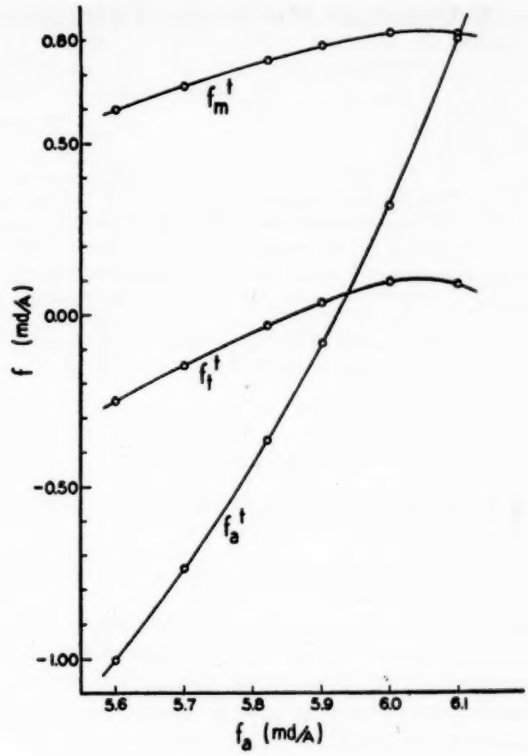

FIG. 3. Interaction constants in diacetylene as a function of the C−H potential constant.

in this paper, this figure for the potential constant seems definitely too high. It does not seem possible that the neglect of the anharmonicities and the very small interaction constants in which the C−H bond is involved may produce such a large difference.

In the previous paper[1] a positive value for $f_t{}^t$ was reported; by reference to Fig. 3 it may be seen that it is quite possible that $f_t{}^t$ be negative, in line with the general rule given for these interactions.[17]

Coulson and Longuet-Higgins[16] have pointed out the great number of difficulties involved in the theoretical calculation of mobile bond orders and bond polarizabilities. For example, the resonance integrals were taken in their calculations as having the benzene value, even in molecules rather different from benzene. Perhaps the method used here—i.e., the determination of self-polarizabilities from the calculated potential constants—may prove to be successful. At least, it will provide an independent method for such calculations. At the present stage, it did not seem advisable to calculate the mutual polarizabilities from the interaction constants, since these are very sensitive to small changes in the frequencies; when the frequencies are more accurately determined—corrected for anharmonicity, etc.—the determination of mutual polarizabilities from the interaction constants may be of definite value.

A Quantum-Mechanical Calculation of the Rates of Some Chemical Reactions

E. BAUER* AND TA-YOU WU
Division of Physics, National Research Council, Ottawa, Canada
(Received April 28, 1952)

The rates of many simple chemical reactions of the type AB+C→A+BC are empirically known to be of the form $k_{OF}=PZ\exp(-E_A/kT)$. On the theory that the reactions take place through the interchange of translational and vibrational energy, a qualitative quantum-mechanical calculation of the rate k_{OF} is made for the simple model of collinear collisions. The empirical values of the activation energy E_A are employed to fix the interaction potential for a given reaction. On identifying the quantum-mechanical expression for the rate k_{OF} with the empirical expression above and on using the gas kinetic expression for the mean number of collisions Z, it is possible to calculate the probability factor P. Numerical calculations have been carried out for the two reactions $H_2+X\rightarrow HX+H$, where X is Cl or Br. In both cases, P is found to be about 8×10^{-3}.

I. INTRODUCTION

MANY important and characteristic chemical reactions are of the type

$$AB+C\rightarrow A+BC, \tag{1}$$

where A, B, C may be atoms, molecules, or radicals. The rate constant k_{OF} of (1) is defined as follows: Let n_{AB} be the number of particles AB per cm³, n_C that of C per cm³. The number of reactions (1) that take place per cm³ per second is given by the expression

$$k_{OF}n_{AB}n_C.$$

Thus k_{OF} is measured in cm³ sec⁻¹. Empirically it is found that the rate constants of such reactions, as of many others, are given by an expression of the form

$$k_{OF}(T)=PZe^{-E_A/kT}, \tag{2}$$

where Z is the average number of gas kinetic collisions of AB and C per second at temperature T, P a factor lying generally between 10^{-4} and 1 and only weakly dependent on temperature ("steric factor"), and $E_A\sim5$–100 kcal/mole (~0.2–4 ev) for most reactions. E_A is the "activation energy" and does not, in general, correspond to an energy level of any of the stable systems involved in the reaction.

Now let us examine the implications of a rate of type (2). The temperature dependence gives essentially the energy dependence after averaging over some distribution; it is generally assumed that the classical (Maxwell-Boltzmann) equilibrium distribution is applicable.[1] In terms of this, because $E_A\gg kT$, we may infer that transitions only occur for collisions with relative energy greater than or equal to E_A, but that apart from this the cross section is not strongly energy dependent, at least not in a range of order kT. Again, because E_A does not, in general, correspond to a stationary state of any of the systems of Eq. (1), it is clear that the reaction must proceed through some—presumably short-lived—intermediate state, the "activated state" of the phenomenological theory.

It is generally believed that in a typical chemical reaction satisfying Eqs. (1) and (2) no electronic transitions occur because the heavy particles move very slowly in comparison with the orbital electrons, and that one must look for an explanation solely in terms of an interchange of energy between the translational, rotational, and vibrational degrees of freedom; the effect of the electrons being merely to provide a potential in which the system moves. As E_A is empirically of the order of vibrational rather than rotational quanta, it seems reasonable to assume that reactions of this kind involve an interchange of translational and vibrational energy.[2] So far no quantum-mechanical treatment on the lines suggested[2] seems to have been given, but a great deal of phenomenological work has been done.[1]

The generally accepted picture for this kind of reaction is the following. A molecule AB and an atom C come together with an initial kinetic energy of relative motion E_0. As they approach each other, the kinetic energy E_0 is continuously transformed into potential energy. If E_0 is sufficiently large so that $E_0\geq E_A$, where E_A is the height of the saddle point in the potential energy surface in Fig. 1(a), then the system will be able to come to a configuration around the saddle point. From this configuration the system may either pass back to the initial state of AB plus a C atom, or into the other valley, leading eventually to the state corresponding to BC plus an atom A.

The present work is chiefly concerned with a quantum-mechanical demonstration of the qualitative features of a transition of the type (1), and a simplified model is set up to enable us to calculate the P factor of Eq. (2) for some simple chemical reactions. We use the empirical value of the activation energy E_A to give us some in-

* National Research Laboratories Postdoctorate Fellow. Present address: Mathematics Research Group, New York University, New York 3, New York.

[1] R. H. Fowler and E. A. Guggenheim, *Statistical Thermodynamics* (Cambridge University Press, Cambridge, 1939), Chap. XII. "Chemical Kinetics" is a critical discussion of the phenomenological theory with references to the original work of London, Polanyi, Eyring, Wigner, and others.

[2] N. F. Mott and H. S. W. Massey, *Theory of Atomic Collisions* (Clarendon Press, Oxford, 1949), second edition, Chap. XII, especially p. 294.

formation about the potential energy of the problem; it is, of course, possible in principle to calculate the whole potential energy from first principles, but the technical difficulties are such that so far only semi-empirical calculations using Morse potentials have actually given reasonable values for the activation energy.[1]

Two examples are worked out to illustrate the method, corresponding to

$$H_2+Cl\rightarrow HCl+H, \quad E_A=6.35 \text{ kcal/mole}, \tag{3}$$

$$H_2+Br\rightarrow HBr+H, \quad E_A=18.8 \text{ kcal/mole}. \tag{4}$$

The values of E_A quoted are those used in the calculation; they lie within the range of error of the experimental values.[3] In view of the experimental uncertainty and of the oversimplified model used in the calculation, the examples should be regarded as estimates of the general order of magnitude, rather than as detailed calculations for these specific reactions.

II. THE PHYSICAL PICTURE OF THE REACTION MECHANISM AND THE MODEL ADOPTED FOR THE PRESENT CALCULATION

We shall assume the picture described above for the reaction mechanism. We can describe this mechanism as a transition from an initial state O in which an atom C moves relative to the molecule AB with kinetic energy E_0 to a state J in which the three particles A, B, C are close together and move (i.e., "vibrate") in their mutual potential field; this transition is followed by a subsequent transition from this intermediate state J either back to the initial state O or to the final state F in which A separates from the newly formed molecule BC. The rate constant k_{OF} can thus be regarded as the product of the rate k_{OJ} of the first stage involving the transformation of kinetic energy of translational motion into energy of vibrational motion, and the probability κ that the system in the state J goes into the final state F. This probability κ depends on the interaction potential for the system, but it is reasonable to assume that κ is in the neighborhood of $\frac{1}{2}$, corresponding to about equal probabilities of a system in the state J going back to the initial state O or forward to the final state F. Thus we have

$$k_{OF}=k_{OJ}\kappa, \quad \kappa\simeq\tfrac{1}{2}. \tag{5}$$

To calculate k_{OJ} on the present picture we must have a detailed knowledge of the potential energy surface of Fig. 1(a). This knowledge is not available, and even if it were, it would be difficult to follow the motion of the system in such a potential field. Accordingly, in the present work *we shall replace the actual problem by a model in which the interaction between* AB *and* C *during the approach of* C *from infinite separation to a configuration* J *in which* AB *and* C *are very close together is negligible, and that thus the transition* $O\rightarrow J$ *involving the transformation of energy takes place in the immediate neighborhood of* J. This simplifying assumption is made in order to enable a calculation to be carried out. It can perhaps be partly justified by the comparatively short range of the interaction that leads to the reaction (1).

To further simplify the formulation and the calculation of the problem, we shall only consider the case of a collinear collision between AB and C. To separate the motion of the center of mass of the system as a whole, we shall use the following coordinates: ρ, the distance between A and B, and r, the distance from C to the center of mass of A and B, i.e.,

$$\rho=r_{AB}, \qquad r=r_C-\frac{M_Ar_A+M_Br_B}{M_A+M_B}. \tag{6}$$

The third coordinate refers to the center of mass of the system as a whole; it separates off and is irrelevant in the calculation. These coordinates ρ, r are used so that in the Schrödinger equation no term in $\partial^2/\partial\rho\partial r$ appears. They differ from the coordinates r_{AB}, r_{BC} used conventionally in depicting the potential energy surface such as Fig. 1(a). To make the comparison definite, let us take the case $M_A=M_B$. The potential surface of Fig. 1(a) will then be transformed into that of Fig. 1(b). In Fig. 1(c) is shown a section of the potential surface for a constant but large separation r; Fig. 1(d) shows a similar section that passes through the saddle point of the potential surface. These sections correspond to the condition

$$r=\tfrac{1}{2}(r_{AC}+r_{BC})=\text{const} \tag{7}$$

and are indicated in Figs. 1(a) and 1(b) by dotted lines.

In the usual picture of the reaction mechanism, the system AB+C comes near the saddle point B* of Fig. 1, the kinetic energy E_0 associated with the coordinate r being converted into potential energy. Near the point B* the system has very little kinetic energy of relative motion, and hence spends a certain (relatively long) time near this configuration, from which it goes either into one valley leading to AB plus C, or into the other valley leading to A and BC.

The present way of describing these processes is to say that the kinetic energy E_0 in the coordinate r in the initial state O goes to excite a vibrational state in the coordinate ρ about the configuration J at the saddle point in Fig. 1. From this state J, the system will either pass back to the initial state O, or to the state F. *In the usual picture the activation energy* E_A *is the height of the saddle point above the potential at infinite separation, but in the model adopted in the present quantum-theory calculation* E_A *is also the difference in energy between the two vibrational levels in* Fig. 1(d).[4]

[3] H. J. Schumacher, *Chemische Gasreaktionen* (Theodor Steinkopff Verlag, Leipzig, 1938), p. 359.

[4] The transition $O\rightarrow F$ could take place directly, by penetration of the central potential barrier. This is not, in general, an im-

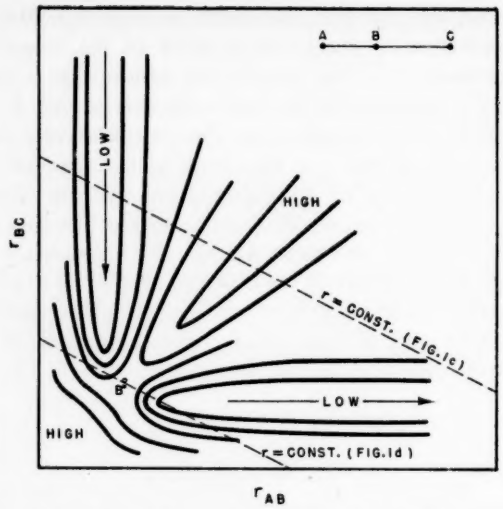

FIG. 1(a). Potential energy surface of a collinear system A−B−C, in terms of the coordinates r_{AB} and r_{BC}. The arrows indicate the approach of C towards AB and the final separation of A from BC. B* is the saddle point of the surface.

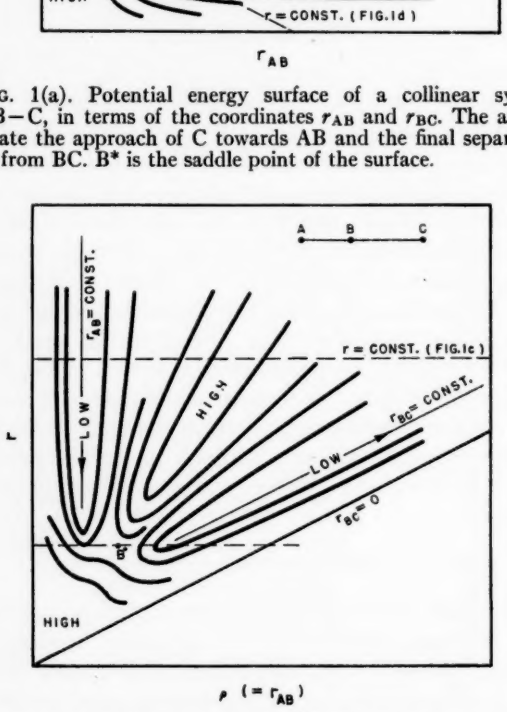

FIG. 1(b). Potential energy surface in Fig. 1(a) in terms of the coordinates ρ, r defined by Eqs. (6). The arrows have the same meaning as in Fig. 1(a). The kinetic energy of relative motion (in the coordinate r) is assumed to be transformed into the vibrational motion of the system ABC (in the coordinate ρ), forming the excited state of the configuration J at the saddle point B*.

It is assumed in the present calculation that transitions take place only very close to the configuration J corresponding to the coordinates ρ_J, r_J. The potential energy of the system near ρ_J, r_J is treated as the unperturbed potential $W^0(\rho, r)$ and is taken to be of the form

$$W^0(\rho, r)=U_{r_J}(\rho)+V_{\rho_J}(r) \tag{8}$$

for which the Schrödinger equation is separable. Deviations from W^0 are treated as perturbations W^1, i.e., as couplings between the translational coordinate r and the vibrational coordinate ρ that cause the transitions. These perturbations are

$$W^1(\rho, r)=\left(\frac{\partial U_r(\rho)}{\partial r}\right)_{r_J}(r-r_J)+\left(\frac{\partial V_\rho(r)}{\partial \rho}\right)_{\rho_J}(\rho-\rho_J). \tag{9}$$

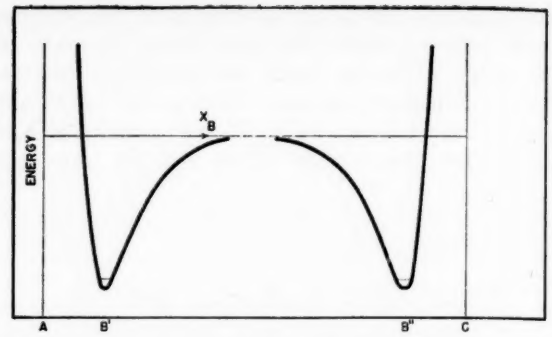

FIG. 1(c). The potential $U_r(\rho)$ for various separations of A, B, C at a fixed but large value of r, corresponding to the upper section (dotted line) in Fig. 1(a) or 1(b).

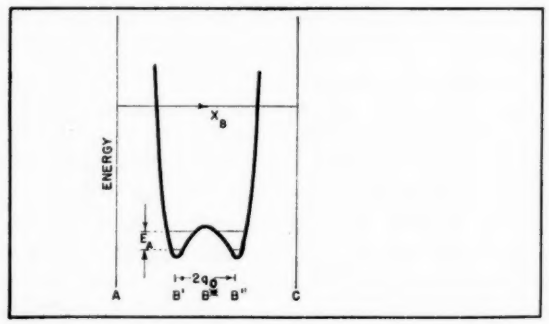

FIG. 1(d). The potential $U_r(\rho)$ for $r=r_J$, corresponding to a section of the potential energy surface for constant r and through the saddle point B* (Fig. 1(a) or 1(b)).

The expansion of the perturbation W^1 in powers of $(\rho-\rho_J)$ and of $(r-r_J)$ must be carried out as shown, because only an expansion in the parameter is physically significant for our present purpose. In each expansion only the first term is considered because transitions only occur close to the configuration (of the state) J.

Detailed expressions for W^0 and W^1 are given in the next two sections, and also the eigenfunctions $\varphi_n(\rho)$ of $U_{r_J}(\rho)$ and $\chi(r)$ of $V_{\rho_J}(r)$. Some general features may profitably be mentioned here. The functions $\chi(r)$ are continuous spectrum eigenfunctions and are normalized per unit energy range; thus the matrix element of W^1, $(O|W^1|J)$, is dimensionless, and its square gives a probability. For a symmetrical potential $U(\rho)$, the vibrational wave functions are of two kinds. They are even or odd relative to inversion about B*, and will be denoted by $\varphi_n^{\pm}$; in general, $\varphi_0^{\pm}$ corresponds to practi-

portant effect: Empirically, if the transition occurred by tunnel effect, there would be no very strong energy dependence of the rate constant, and the rate constant would thus be only weakly temperature dependent. One can calculate the penetration probability corresponding to the configuration in Fig. 1(d) and finds that the $O \rightarrow F$ transition probability is generally small.

cally the same eigenvalue, but $E_1^+ < E_1^-$, and so on (see Fig. 2). Thus the probability coefficient α for a transition $\varphi_0^{\pm} \rightarrow \varphi_n$ (which is either + or −) and $\chi_0 \rightarrow \chi_J$ is given by

$$\alpha = \tfrac{1}{2}\{|(\varphi_0^+, \chi_0|W^1|\varphi_n, \chi_J)|^2 + |(\varphi_0^-, \chi_0|W^1|\varphi_n, \chi_J)|^2\}. \quad (10)$$

III. THE POTENTIAL $W^0(\varrho,r)$ AND ITS WAVE FUNCTIONS

1. The Vibrational Potential $U_{rJ}(\varrho)$

For a constant value of r ($r=r_J$ for the configuration J corresponding to the saddle point in the potential energy surface), the potential energy as a function of ρ is of the type shown in Fig. 1(d), having two minima. Again to simplify the calculation without losing sight of the qualitative features of the problem, we shall assume the potential to be symmetrical with respect to inversion about the saddle point B*. For such a potential field, the explicit form and exact calculation given by Morse and Stueckelberg[5] are most convenient for our purpose. It is given by

$$U_{q0}(q) = \tfrac{1}{2}M_0\omega_0^2\left\{\frac{q^6}{12q_0^4} - \frac{q^2}{4} + \frac{q_0^2}{6}\right\}, \quad (11)$$

where q is the displacement of B from its mean position B* in Fig. 1(d), and $2q_0$ is the separation between the two minima, i.e.,

$$\begin{aligned} q_0 &= \mathrm{B'B^*} = \mathrm{B''B^*}, \\ q &= \rho - q_0 - \mathrm{AB'} = \rho - \text{const.} \end{aligned} \quad (12)$$

To connect $U_{q0}(q)$ in (11) with $U_{rJ}(\rho)$, we shall take r_J to be the average value of r over the motion of B in the potential (11), i.e., for the case $M_A = M_B$ under consideration,

$$\begin{aligned} r_J = \bar{r} &= \tfrac{1}{2}(\mathrm{AC} + \mathrm{B^*C}) \\ &= \tfrac{3}{2}q_0 + \mathrm{B''C} + \tfrac{1}{2}\mathrm{AB'} \\ &= \tfrac{3}{2}q_0 + \text{const.} \end{aligned} \quad (13)$$

$U_{q0}(q)$ can thus be transformed into $U_{rJ}(\rho)$ by means of Eqs. (12) and (13).

The potential (11) has two parameters, *viz.*, $\frac{1}{2}M_0\omega_0^2$ and q_0, to determine the height of the hill and the separation of the two minima. As we do not know this potential $U_{rJ}(\rho)$ or $U_{q0}(q)$, we shall make the approximating assumption that the curvature of the potential near the minima, which determines the fundamental vibration frequency of the system ABC, is about the same as that for the separate diatomic systems AB and BC. For H_2, HCl, and HBr, we have

$$\tfrac{1}{2}M_0\omega_0^2/(e^2/a_0^3) = 0.184;\ 0.173;\ 0.130,$$

respectively. As these are not too different, we shall simply take the value 0.184.

[5] P. M. Morse and E. C. G. Stueckelberg, Helv. Phys. Acta 4, 337 (1931).

We are then left with only one parameter q_0 in the potential (11). In the usual theory, E_A is just equal to the height of the hill. In the present quantum-mechanical formulation the transition $O \rightarrow J$ corresponds to the excitation of the system from the lowest vibrational level near the bottom of the two minima to one very close to the top of the barrier. Thus E_A is just the energy difference between these two vibrational levels: It is of course approximately equal to the height of the hill in Fig. 1(d), but not in general exactly equal to it. For a given empirical value of E_A, the value of q_0 that will put a certain level, say E_n^+, near the top of the central hill, can be calculated from the analysis of Morse and Stueckelberg; these correlations are given in Fig. 2. For smaller separations q_0 than those shown in Fig. 2, the splitting of the states E_0^+ and E_0^- becomes appreciable; but then the potential hill is so low that the whole picture breaks down. For any given curve in Fig. 2 only the part to the right of the minimum is of importance, as the state J will be formed at the largest separation compatible with the conservation of energy. In general, we need only consider a single excited state for any given process, namely, the lowest state that is close to the peak, because the Boltzmann factor reduces the contribution of other states to the total cross section.[6]

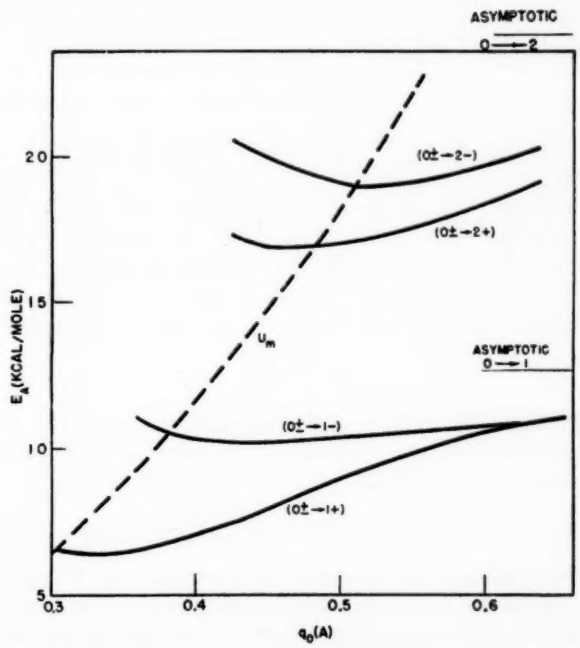

FIG. 2. Relation between the energy difference $E_n^{\pm} - E_0$ (which is to be identified with the activation energy), the excited state $n^{\pm}$ and the distance q_0. U_m, the height of the potential hill in Fig. 1(d), is also shown. This figure is essentially Fig. 4 of reference 5.

[6] As a numerical illustration of this we may consider the example (4). The empirical activation energy $E_A = 18.8$ kcal/mole; from Fig. 2 this corresponds to $q_0 = 0.62$A, and a transition $(0^{\pm}) \rightarrow (2^+)$. There is the possibility of competition from the transition $(0^{\pm}) \rightarrow (2^-)$; at $q_0 = 0.62$A, this has a threshold energy of 20 kcal/mole. Thus, assuming that the probability coefficients are of the same order, the contribution of this competing

TABLE I. Constants appearing in the calculation. They are all defined in the text. The nuclear separations of H_2, HCl, and HBr are 0.742A, 1.275A, and 1.44A, respectively. a_0 is the first Bohr radius of hydrogen.

	H_2+Cl	H_2+Br
Activation energy E_A (kcal/mole)	6.35	18.8
Order of excited state ($n_-{}^+$)	1+	2+
q_0 (A)	0.34	0.62
r_J (A)	2.16	2.72
d_{12} (A)	3.67	3.98
$V_{\min}$ (kcal/mole)	0.12	0.24
$a(a_0^{-1})$	0.475	0.660
$V_0(e^2/a_0)$	0.581	31.6
$C(A^{-1})$	0.25	0.30
b	0.378	0.378
$k_0(a_0^{-1})$	8.5	14.5
$k_J(a_0^{-1})$	0.78	1.14
$r_B(a_0)$	5.5	6.5
$r_c(a_0)$	18–20	15

2. The Intermolecular Potential $V_\rho(r)$

The potential $V_\rho(r)$ is given by a section of the surface in Fig. 1(b) which is parallel to the r axis. The general form of this potential is clear, but there is no very definite quantitative form for it. From the discussion of the dependence of q_0 on E_A, we get a value for $r_J(\sim 2$–$3A)$ for each case, and we may say that $V_{\rho J}(r_J)=E_A$ since r_J corresponds to the smallest distance of approach between AB and C. We get an approximate expression for the zero in $V_\rho(r)$ from the gas kinetic collision diameter $d_{12}(\sim 4$–$5A)$ defined by

$$d_{12}=\tfrac{1}{2}(d_{AB}+d_C), \tag{14}$$

where d_{AB}, d_C are the gas kinetic collision diameters of AB and C, and we can also estimate $V_{\min}$ (~50–300 cal/mole), the depth of the potential well due to the attractive dispersion forces. Even the sources judged most reliable[7] do not give particularly consistent values for these parameters; the values used here are given in Table I. It is not possible to fit a potential of form

$$C_1r^{-12}-C_2r^{-6}$$

to reasonable values of r_J, d_{12} and $V_{\min}$; this is not surprising as this admittedly empirical form must break down for $r\ll d_{12}$. The function used here is

$$V(r)=V_0[e^{-2ar}-e^{-a(r+d_{12})}], \tag{15}$$

which makes a reasonable fit possible. Its incorrect behavior for both very large and very small r is of no importance in the present case. It must be stressed that the values for V_0, a, d_{12} given in Table I are by no means accurate; d_{12} is uncertain by perhaps $\pm 1/2$A, and $V_{\min}$ is uncertain to within perhaps a factor of two. It will turn out in the calculation that the uncertainty in $V_{\min}$ is much less important than the others.

The eigenfunctions of $V_{\rho J}(r)$ are χ_0 corresponding to kinetic energy $E_0=E_A$, and χ_J corresponding to zero kinetic energy. They are evaluated by the WKB approximation, and normalized per unit energy range. χ_J is effectively zero for r less than some value r_B, and in our examples χ_0 is a sine wave to a very good approximation for $r>r_B$, because $E_A\gg V_{\min}$. The form of χ_J for the reaction (3) is shown in Fig. 3 [it is very similar for the reaction (4)]; for large r it diverges as $[V_{\rho J}(r)]^{-\frac{1}{4}}$, i.e., relatively weakly, but effectively we need only consider $r<r_C\sim 7$–$8A$, as there is no appreciable interaction at larger separations. Within the region $r_B<r<r_C$, χ_J may be represented passably well by a sine wave of constant amplitude and wavelength, as is seen from Fig. 3. Thus we take

$$\chi_i(r)=\frac{1}{\hbar}\left(\frac{2M_R}{\pi k_i}\right)^{\frac{1}{2}}\sin[k_i(r-r_B)+\delta_i], \quad i=0, J,$$

$$k_0=\frac{1}{\hbar}(2M_RE_A)^{\frac{1}{2}}, \quad k_J=\frac{1}{\hbar}(2M_R\bar{V}_{\min})^{\frac{1}{2}}, \tag{16}$$

$$\delta_0=\delta, \quad \delta_J=0,$$

$$\bar{V}_{\min}\simeq\tfrac{1}{2}V_{\min}.$$

IV. THE PERTURBATION W^1

1. The Potential $W^1(\rho,r)$

Equation (11) gives the potential $U_{q0}(q)=U_{rJ}(\rho)$; from Eqs. (12) and (13) we have

$$-\partial q/\partial r=\partial q_0/\partial r=2/3, \tag{17}$$

and thus

$$\left.\frac{\partial U_{q0}(q)}{\partial r}\right|_{rJ}=-\frac{1}{3}M_0\omega_0{}^2\left[\frac{1}{3}\frac{q^6}{q_0{}^5}+\frac{1}{2}\cdot\frac{q^5}{q_0{}^4}-\frac{1}{2}q\right]+\text{const.} \tag{18}$$

Next we require the parametric ρ-dependence of $V(r)$. One would expect the potential energy between two molecules to depend on their vibrational states, but it is very hard to estimate the precise dependence. Perhaps the best thing we can do is to estimate the difference between the intermolecular potential in hydrogen molecules and helium atoms. From this we deduce possible limits of the dependence of $V(r)$ on ρ_J, the equilibrium separation of the two nuclei in a molecule, and thus make a rough estimate of $\partial/\partial\rho\cdot V_\rho(r)$.

For our purpose, the potential $V(r)$ may be considered to be defined by three quantities, namely, the depth $V_{\min}$ of the well (which may be considered as constant during the discussion), the gas kinetic collision diameter d_{12}, and the distance r_x defined by the condition

$$V_{\rho J}(r_x)=E_A.$$

r_x is r_J for hydrogen molecules, r_{He} for helium atoms.

$(0^\pm)\to(2^-)$ process will be of the order $\exp[-(20-18.8)/0.6]\sim\frac{1}{16}$ times that of the $(0^\pm)\to(2^+)$ process. This is of course negligible to the present approximation.

[7] Landolt-Boernstein, *Physikalisch-Chemische Tabellen* (Springer, Berlin, 1950), sixth edition, Vol. 1, Pt. 1, pp. 325 and 369; Hirschfelder *et al.*, Chem. Revs. 44, 205 (1949). We take

$$d_{Cl}=\tfrac{1}{2}(d_{Cl_2}+d_{Ar}); \quad d_{Br}=\tfrac{1}{2}(d_{Br_2}+d_{Kr}).$$

We may suppose that the only important difference between hydrogen molecules and helium atoms is that $\rho_J=0$ for helium. Collision diameters are known in both cases: Using the data of footnote 7,

$$d_{H_2}=d_{He}+\Delta, \quad \text{say}; \quad \Delta=0.56\text{A}.$$

$d_{12}=\frac{1}{2}[d_{\text{atom}}+d_{\text{molecule}}]$; i.e., $d_{H_2C}=d_{HeC}+\frac{1}{2}\Delta$, so that d_{12} decreases by $\frac{1}{2}\Delta$ as $\rho_J\to 0$. Let us suppose that Δ is proportional to ρ_J, it is then plausible to say that

$$0<r_J-r_{He}<\tfrac{1}{2}\Delta.$$

In the two limits, $r_{He}=r_J$ and $r_{He}=r_J-\frac{1}{2}\Delta$, we may make certain simplifying assumptions to get expressions for $\partial V/\partial\rho_J$. These are given concisely under (a) and (b):

(a) $r_{He}=r_J$.

We use the conditions

$$V_{\rho J}(r_J)=V_0(r_J),$$
$$V_{\rho J}(d_{12})=V_0(d_{12}-\tfrac{1}{2}\Delta).$$

One may suppose that

$$-\frac{\partial}{\partial r}\cdot V_{\rho J}(r)=-(1-C\rho_J)\frac{\partial}{\partial r}\cdot V_0(r),$$

$$V_{\rho J}(r_J)=V_0(r_J),$$

and then

$$\frac{\partial}{\partial\rho_J}V_{\rho J}(r)=\frac{-C}{1-C\rho_J}[V_{\rho J}(r)-V_{\rho J}(r_J)],$$

where

$$1-C\rho_J=\frac{d_{12}-r_J-\frac{1}{2}\Delta}{d_{12}-r_J}.$$

(b) $r_{He}=r_J-\frac{1}{2}\Delta$. Here we put

$$V_{\rho J}(r)=V_0(r-b\rho_J)$$

and find

$$\frac{\partial}{\partial\rho_J}\cdot V_{\rho J}(r)=-b\frac{\partial}{\partial r}\cdot V_{\rho J}(r); \quad b=\Delta/2\rho_J.$$

It is clear that this discussion is very crude, and we must still identify $\partial V/\partial\rho$ with $\partial V/\partial\rho_J$ to get numerical results. However, unless the value of the transition matrix element given by this argument is too small by a factor of order ten, the term in $\partial U/\partial r$ gives a considerably larger contribution to the transition probability than that in $\partial V/\partial\rho$.

2. The Probability Coefficient α

We now have sufficient information to attempt to evaluate this. The vibrational terms give no difficulty. By symmetry

$$(\varphi_0^+|\rho|\varphi_n^+)=(\varphi_0^+|\rho^5|\varphi_n^+)=0; \quad (\varphi_0^-|\rho^6|\varphi_n^+)=0.$$

The nonvanishing matrix elements are given in Table II.

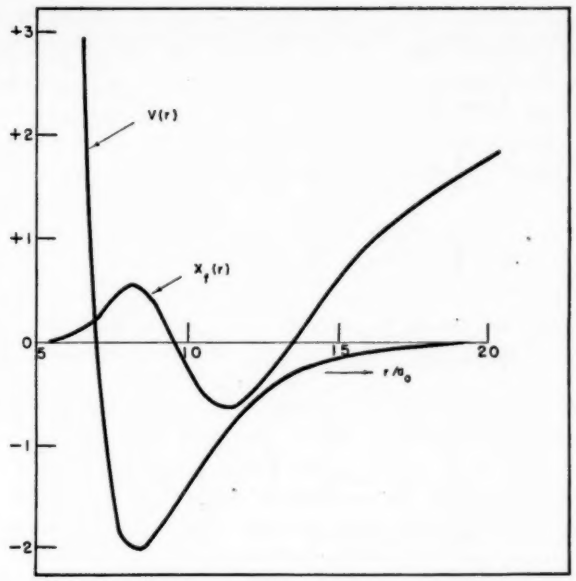

FIG. 3. The "intermolecular" potential $V_\rho(r)$ and its wave function χ_J corresponding to zero energy.

The translational matrix elements can also be evaluated. A convergence factor $\exp(-gr)$ is inserted in the evaluation of matrix elements of powers of r; from physical considerations we want this factor to exclude contributions from large values of r (say, from $r>r_C$ of Fig. 3), because no transitions occur at such large separations due to the short range of the intermolecular forces. From this condition, and the known magnitude of the momentum $\hbar k_0$ which is of order $10me^2/\hbar$, we find that g/k_0 is very much less than unity, and its precise value does not affect the results appreciably.

From Eqs. (9), (15), and (16) and footnote 8 we see that the following matrix elements are required; they are quoted to the first order in the small quantities k_J/k_0 and g/k_0:

$$\left.\begin{aligned}(\chi_0|r|\chi_J)&=-\frac{2M_R}{\pi\hbar^2}\cdot\frac{2k_J^{1/2}}{k_0^{7/2}}\left(\cos\delta+\frac{3g}{k_0}\sin\delta\right),\\(\chi_0|r^2|\chi_J)&=+\frac{2M_R}{\pi\hbar^2}\cdot\frac{6k_J^{1/2}}{k_0^{9/2}}\left(\sin\delta-\frac{4g}{k_0}\cos\delta\right),\\(\chi_0|e^{-ar}|\chi_J)&=-\frac{2M_R}{\pi\hbar^2}\cdot\frac{k_J^{1/2}}{k_0^{5/2}}\left(\sin\delta-\frac{2a}{k_0}\cos\delta\right).\end{aligned}\right\} \quad (19)$$

We see that all the matrix elements depend critically on the phase δ of χ_0 at $r=r_B$. This is inevitable and is not a consequence of the particular approximations for the potential and the wave functions. In principle one could obtain a value for δ if one knew $V(r)$ to within better than $1/k_0\sim 0.05$A; in practice we are only concerned with the order of magnitude of the transition

TABLE II. Matrix elements.

			H_2Cl	H_2Br
Vibrational matrix elements				
$\left(\varphi_0^+\left\|\frac{\partial U}{\partial r}\right\|\varphi_n^+\right)$	(e^2/a_0^2)		1.97×10^{-2}	-5.03×10^{-2}
$\left(\varphi_0^-\left\|\frac{\partial U}{\partial r}\right\|\varphi_n^+\right)$	(e^2/a_0^2)		1.09×10^{-2}	-5.77×10^{-2}
$(\varphi_0^-\|\rho\|\varphi_n^+)$	(a_0)		-0.217	0.0588
Translational matrix elements				
$\|(\chi_0\|r\|\chi_J)\|_{\max}(\delta=0)$	(e^2/a_0^2)		2.32	0.436
$\left\|\left(\chi_0\left\|\frac{\partial V}{\partial\rho}\right\|\chi_J\right)\right\|_{\max}\left(\delta=\frac{\pi}{2}\right)$	(a_0^{-1})	case (a)	2.47×10^{-3}	1.89×10^{-3}
		case (b)	8.25×10^{-3}	7.00×10^{-3}
Total matrix elements				
$\left\|\left(\varphi_0^-,\chi_0\left\|\frac{\partial V}{\partial\rho}(\rho-\rho_J)\right\|\varphi_n^+,\chi_J\right)\right\|_{\max}\left(\delta=\frac{\pi}{2}\right)$		case (a)	0.5×10^{-3}	1.0×10^{-4}
		case (b)	2×10^{-3}	4×10^{-4}
$\left\|\left(\varphi_0^-,\chi_0\left\|\frac{\partial U}{\partial r}(r-r_J)\right\|\varphi_n^+,\chi_J\right)\right\|_{\max}(\delta=0)$			2.54×10^{-2}	2.52×10^{-2}
$\left\|\left(\varphi_0^+,\chi_0\left\|\frac{\partial U}{\partial r}(r-r_J)\right\|\varphi_n^+,\chi_J\right)\right\|_{\max}(\delta=0)$			4.57×10^{-2}	2.19×10^{-2}
Probability coefficient α			1.37×10^{-3}	5.58×10^{-4}
Steric factor P			7.65×10^{-3}	8.85×10^{-3}
Life time τ_J (sec)			5.1×10^{-12}	1.4×10^{-12}

probability, which is not too dependent on δ.[8] We put $\delta=0$; in this case χ_0 and χ_J are orthogonal, and Eq. (9) represents the perturbation adequately without additional terms. The results are given in Table II. One sees that, in general, the term which comes from $\partial U/\partial r$ is much greater than that which comes from $\partial V/\partial\rho$, so that the very uncertain discussion of the dependence of $V(r)$ on ρ does not affect the order of magnitude of the results. The physical reason for this is that the dependence of $U(\rho)$ on r is much more important than that of $V(r)$ on ρ.

3. The Steric Factor P

We have now developed the quantum-mechanical calculation of the probability coefficient α as far as seems feasible and wish to find $k_{OF}(T)$. From the previous discussion we may reasonably approximate the capture cross section $\sigma_{OJ}(E_0)$ by

$$\sigma_{OJ}(E_0)=\begin{cases}0 & E_0<E_A\\ \pi d_{12}^2\alpha & E_0>E_A\end{cases}, \tag{20}$$

where α is the probability coefficient of Eq. (10) for collinear collisions.

The rate constant $k_{OF}(E_0)$ for a relative energy E_0 and relative velocity v_0 is given by

$$k_{OF}(E_0)=\kappa v_0\sigma_{OJ}(E_0), \tag{21}$$

with $E_0=\frac{1}{2}M_R v_0^2$ and κ given in (5). On averaging this over a Boltzmann distribution for E_0 at a given temperature T, one obtains the following expression for $k_{OF}(T)$:

$$k_{OF}(T)=2n_{AB}(T)n_C(T)\kappa\alpha d_{12}^2E_A\times\left(\frac{2\pi}{M_RkT}\right)^{\frac{1}{2}}e^{-E_A/kT}. \tag{22}$$

As the collision number Z is given by[1]

$$Z=2n_{AB}n_Cd_{12}^2\left(\frac{2\pi kT}{M_R}\right)^{\frac{1}{2}}, \tag{23}$$

[8] The perturbation W' of Eq. (9) consists of the first terms of an expansion. When these terms vanish, one must of course consider the next terms, namely,

$$\left(\frac{\partial^2U}{\partial r^2}\right)_{r_J}\frac{(r-r_J)^2}{2!}+\left(\frac{\partial^2V}{\partial\rho^2}\right)_{\rho J}\frac{(\rho-\rho_J)^2}{2!}+\rightarrow,$$

and it turns out that while the matrix elements of individual terms in the expansion depend critically on δ, the order of magnitude of the series as a whole (say, of the first 4–6 terms) does not.

one obtains, on comparison with the expression (2), the probability (or steric) factor P,

$$P=\kappa\alpha E_A/kT. \tag{24}$$

On using the calculated results in Tables I and II, it is found that for the reaction (3), $P=7.65\times10^{-3}$, while for reaction (4), $P=8.85\times10^{-3}$.

It is of interest to estimate the lifetime τ_J of the state J. Provided the state J is not removed by collisions with another atom or molecule, we have

$$\frac{1}{\tau_J}=k_{JO}(E_0)+k_{JF}(E_0). \tag{25}$$

and it can be shown that $k_{JF}/k_{JO}=\kappa/(1-\kappa)$, while[9]

$$k_{JO}(E_0)\simeq\frac{G_{AB}G_C}{G_J}\cdot\frac{E_0\alpha}{\pi\hbar},$$

where the G's are statistical weights. Corresponding to the above values of P, the life time of the state J is of the order 5×10^{-12} sec, which is short compared with the time between collisions at atmospheric pressure ($\sim5\times10^{-11}$ sec).[10]

V. DISCUSSION

It seems clear that only collinear collisions can in fact be calculated without excessive labor; even if one assumes spherical symmetry of the potential, which is an oversimplification in a three-dimensional calculation, one would have to consider a large number of phases ($\sim$10–100) if the wave function is expanded in spherical harmonics, and the work is thus multiplied by a factor of the order of the number of phases.

It has been assumed throughout in the calculation that $E_0=E_A$. For E_0 somewhat greater than the height of the potential at the saddle point, transitions may occur for somewhat larger separations (i.e., at $r>r_J$) because of the larger energy available, corresponding to other parallel sections in Fig. 1(a) or 1(b), which do not pass through the saddle point. For such a transition, the physical process is the same as that considered here, and σ_{OJ} can be expected to be qualitatively the same as that calculated above. Another possibility is that the excess energy E_0-E_A is retained as kinetic energy of the separating components. In this case the translational contribution to the matrix element would be somewhat different; but for $E_0-E_A\lesssim kT$, this difference would not be large. In any case, because of the Boltzmann factor one need not consider those values of E_0 which exceed E_A by much more than kT, while E_A itself is much larger than kT.

Some modifications in the detail of the present calculation are necessary when the potential $U_{rJ}(\rho)$ is unsymmetrical, as it must be in the actual cases, but these will not affect the general character of the present result, since this depends only on the probability of the transformation of energy from one mode (coordinate r) to another (coordinate ρ). The case when AB and C are groups of atoms (radicals) can in principle be treated similarly to the present model.

It may be of interest to indicate the relation of the present calculations to related ones. A certain number of calculations have been made recently on the transfer of translational and vibrational energy in inelastic collisions in gases.[11] They deal principally with the excitation of molecular vibrations, which is of importance in the dispersion of high frequency sound waves, and are extensions of the work discussed in reference 2. The problem of the dissociation of molecules by excitation into a vibrational state in the continuum has also been taken up recently.[12] All these calculations are essentially one-dimensional and are based on potentials which have not a very good quantitative foundation.

Finally, one ought to discuss the reliability of these calculations. It is, of course, hard to give a precise estimate, as there is first the question of the physical process involved, and then the perturbation method of calculating the transition probability. The numerical result is subject further to the uncertainty in the experimental data,[3] E_A being known only to within ±1 kcal/mole, thereby introducing an uncertainty of the order ten in the rate merely from the relative measurements at different temperatures.

It seems fair to conclude that this work shows that the generally accepted picture is capable of explaining the rates of these simple chemical exchange reactions in their order of magnitude. The fact that P turns out to be much smaller than one in both cases considered here seems reasonable in view of the well-known difficulty of transferring energy between translational and vibrational modes; the close coincidence of the numerical values in the two cases must be regarded as accidental.

[9] This follows from the principle of detailed balance: see H. E. Moses and T. Y. Wu, Phys. Rev. **83**, 109 (1951), appendices 1, 5. One assumes that the characteristic internal motion of J is a motion of C relative to AB and further replaces the discrete rotational states corresponding to this motion of J by a continuum.

[10] If the natural life time is long compared with the time between collisions, it is possible that the complexes decay by collision with another atom of molecule.

[11] Schwartz, Slawsky, and Herzfeld, J. Chem. Phys. **20**, 1591 (1952). K. Takayanagi, Prog. Theoret. Phys. **8**, 111 (1952).

[12] E. Bauer, Phys. Rev. **84**, 315 (1951); **85**, 277 (1952). See also T. Y. Wu, Phys. Rev. **71**, 111 (1947).

The Infrared Spectra of Three Solid Phases of Methyl Ammonium Chloride

R. D. WALDRON
Metcalf Research Laboratory, Brown University, Providence, Rhode Island*

(Received September 31, 1952)

Infrared spectra are presented for three crystalline phases of methyl ammonium chloride which occur at different temperatures. The spectrum of the high temperature structure reveals apparently degenerate vibrational frequencies for the perpendicular bands indicating little or no distortion from a threefold symmetry axis for the methyl ammonium ion. The intermediate and low temperature structures show increasing distortion of the cation as evidenced by increasing splitting of the degenerate absorption bands amounting to about 10–40 cm^{-1} in the low temperature form, where the torsional vibration about the C−N axis becomes infrared active.

An assignment of frequencies is made in satisfactory agreement with a valence-force normal coordinate treatment and the isotope product rule. A simplified calculation of the height of the potential barrier to internal rotation was made yielding the approximate value, $V_0=1670$ cm^{-1}.

I. INTRODUCTION

THE purpose of this investigation was to study the effect of the crystalline environment of a molecule or ion upon its vibration spectrum. The spectrum of the methyl ammonium ion is also of interest in studying the effect of electric charge upon the force constants of bonds. Such information is of value in the interpretation of spectra of substances which may exist in zwitterion form.

The Raman spectra of both normal and (N) deutero methyl ammonium chloride (hereinafter abbreviated as MAC and d-MAC, respectively) in aqueous solution have been reported by Edsall and co-workers.[1] A search of the literature failed to reveal any previous infrared studies of the compound. In the present work, the spectrum of MAC and d-MAC from 6000–300 cm^{-1} is reported at 3 temperatures: 300°, 230°, and 90°K.

The thermodynamic properties of methyl ammonium chloride have been studied by Aston and Ziemer.[2] The compound undergoes phase transitions at 220° and 264.5°K. Following Aston, we shall designate the modifications in order of increasing temperature as β, γ, and α, respectively. Bridgman[3] has studied the transitions at high pressures and temperatures up to 200°C and found 5 phases, one of which is probably identical with β-MAC. (The latent heat of the transition $\beta\rightarrow\alpha$ is nearly equal to the internal energy change in the high pressure transition, and extrapolation of the phase boundary $p-T$ curve to atmospheric pressure gives a temperature *ca* 230°K.)

The x-ray crystal structure of α-MAC was reported by Hughes and Lipscomb.[4] The structure possesses a fourfold symmetry axis coincident with the C−N axis of the cation. Since this is physically impossible using normal valences, the cations must exhibit either orientation disorder or internal rotation in the crystal. In either case, the selection rules for the spectra should be altered because of a lowering of the symmetry of the ion. The crystal structures of the low temperature forms are unknown.

II. EXPERIMENTAL

Equipment

The spectra were taken with Perkin-Elmer model 12 spectrometers modified for use as ratio-recording double beam instruments.[5] SiO_2, LiF, CaF_2, NaCl, KBr, and KRS-5 prisms calibrated with absorption lines of H_2O, CO_2, NH_3, etc. were used. Spectra were taken of both single crystals and disoriented samples. The work on small single crystals was facilitated by the use of a low power refracting condenser and microscope with KBr lenses. The samples investigated at low temperatures consisted of films of MAC sublimed on NaCl, KBr, and KRS-5 blanks secured in low temperature cells similar to those previously described.[6]

Preparation of Samples

Eastman Kodak Company white label methyl amine hydrochloride was the starting material. MAC crystallizes from alcohol in beautiful, exceedingly thin leaves with faces normal to the tetragonal axis. These crystals could be obtained in pieces large enough for spectral examination without the use of the microscope. Thinner samples were obtained by evaporation of alcoholic solutions on thin glass slides which produced an oriented mosaic of tiny crystals. Crystallization from aqueous solution favored growth along the tetragonal axis and usually produced needles, but occasionally ribbon crystals would develop, which were examined in the microscope. The phase transitions of MAC are apparently first order, and result in fracture of single

* This work was supported by the U. S. Office of Naval Research under contract N6ori-88, task order I.

[1] J. T. Edsall, J. Chem. Phys. **4**, 1 (1936); **5**, 225, 508 (1937); J. T. Edsall and H. Scheinberg, *ibid.*, **8**, 520 (1940).

[2] J. G. Aston and C. W. Ziemer, J. Am. Chem. Soc. **68**, 1405 (1946).

[3] P. Bridgman, Proc. Am. Acad. Arts Sci. **72**, 227 (1938); **76**, 71 (1948).

[4] E. W. Hughes and W. N. Lipscomb, J. Am. Chem. Soc. **68**, 1970 (1946).

[5] Hornig, Hyde, and Adcock, J. Opt. Soc. Am. **40**, 497 (1950).

[6] E. L. Wagner and D. F. Hornig, J. Chem. Phys. **18**, 296 (1950).

crystals, so the samples studied at low temperatures consisted of films sublimed in vacuum onto various window materials and subsequently transferred to the low temperature cells. Difficulty was experienced with respect to the adherence of the films during the transitions only for very thick films. Liquid N_2 was used as a refrigerant in the investigation of the β-phase, and temperatures in the range 220–264°K were maintained by intermittent addition of solid CO_2 to an alcohol bath.

d-MAC was prepared by repeated solution and vacuum evaporation of MAC in D_2O. The hygroscopic nature of the salt required the handling of the sublimed films to be carried out in a dry box to avoid exchange with atmospheric water. Single crystals were prepared by crystallization from *d*-isopropanol, made by treating aluminum isopropoxide with D_2O.

The films underwent the transitions smoothly in most cases, usually being essentially completely converted to the appropriate modification in 5–10 minutes or less. The amount of radiation scattered from the film surface invariably increased after each transition. The normal operating procedure was as follows: The film was examined at room temperature, then rapidly cooled with liquid N_2. The spectrum was run twice to make sure equilibrium had been established after which the sample was allowed to warm to 230°K. The spectrum was run twice again after which the sample was warmed to room temperature, yielding a spectrum identical with the initial trace. The tendency to supercool made operation in the reverse order unsatisfactory.

A single run made on KRS-5 backing gave an anomalous spectrum at the temperature of the γ-phase; the spectrum appearing to be largely that of the α-form. The reason for this behavior is uncertain, but may arise from a partial $\beta \rightarrow \alpha$ transition induced by the KRS-5 or the effect of exchange of minute quantities of Br^- or I^- for Cl^- in the sample.

III. THEORY

The classification of the normal vibrations of the MA ion will be based on an assumed model of C_{3v} symmetry. (The distinction between staggered or eclipsed configurations of the hydrogen atoms is of no consequence in the analysis of the spectrum.) The 18 normal modes of vibration are distributed in the symmetry species of the point group C_{3v} as indicated in Table I.

The absorption lines corresponding to vibrations of species A_1 will be polarized parallel to the c axis of the crystal (figure axis of the molecule) while the degenerate bands will be polarized perpendicular to the c axis. The A_2 vibration is inactive. If the threefold axis of symmetry of the MA ion is removed because of perturbation by neighboring ions in the crystal, the degeneracies will be removed, and each of the E absorption bands will split into 2 components. The A_2 vibration may also appear as an active line.

TABLE I. Symmetry classification of the vibrations of MAC.

Species	E	$2C_3$	$3\sigma_v$	Elec. moment	Number	Vibrations: Stretch	Vibrations: Bend
A_1	1	1	1	M_z	5	1 NH, 1 CH, 1 CN	1 NH, 1 CH
A_2	1	1	−1		1		1 torsion
E	2	−1	0	M_xM_y	6×2	1 NH, 1 CH	2 NH, 2 CH

IV. QUALITATIVE DISCUSSION OF THE SPECTRA

The MA ion is isoelectronic with the ethane molecule and there exists a one-to-one correspondence between the normal modes of vibration of the two species. Since the ethane assignment is now well established,[7] it will be used as a guide in the interpretation of the MA ion spectrum.

Figure 1a shows the spectrum of a single crystal of α-MAC in which the direction of propagation of the radiant energy was parallel to the c axis. It follows that only bands of species E will occur. If we assume that both H stretching frequencies lie in the 3000 cm^{-1} region, there remain 4 bands of appreciable intensity at 958, 1265, 1463, and 1580 cm^{-1} which we assign to the species E fundamentals. Tilting the crystal or examination of the spectrum of disoriented samples (Fig. 1c) reveals 3 new lines below 1600 cm^{-1} which we assign to the A_1 fundamentals. These occur at 1003, 1428, and 1538 cm^{-1}. (The H stretching fundamentals of species A_1 should also occur near 3000 cm^{-1}.)

The spectrum in the 3000 cm^{-1} region is somewhat complicated by the presence of overtones and combinations of the bending frequencies near 1500 cm^{-1}, and the assignment of bands in this region will be discussed later. Table II gives a partial assignment of the A_1 and E bands and the corresponding values for ethane.

An examination of the spectrum down to below 300 cm^{-1} failed to reveal any torsional band, although increasing absorption over a broad region was observed toward lower frequencies which presumably is due to lattice vibrations. The absence of the A_2 absorption band and the lack of observed splitting of the E bands indicate that the distortion of the MA ion by the crystalline environment is so slight as to be undetectable with the natural band widths occurring in the room temperature spectrum and the present resolution.

The situation is drastically changed in the low temperature phases however. The β-phase spectrum is shown in Fig. 2. It will be observed that the E bands have split into two or more components each, and a new band appears at 487 cm^{-1}. The latter band is logically assigned to the A_2 torsional vibration as will be discussed later.

One can immediately state that the crystal structure of the β-phase does not possess trigonal symmetry. Furthermore, the distortion of the MA ion must be much greater than that in the α-phase. At room tem-

[7] G. E. Hansen and D. M. Dennison, J. Chem. Phys. **20**, 313 (1952).

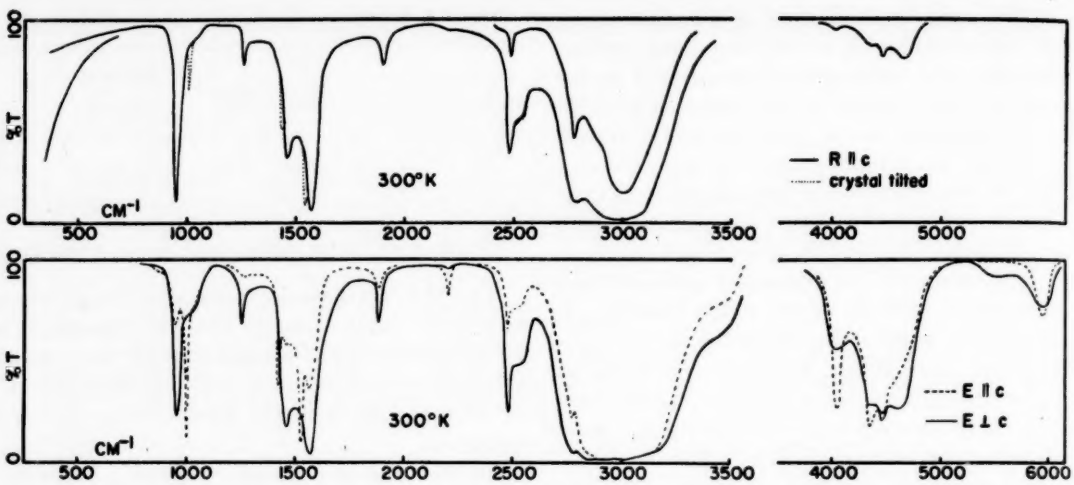

FIG. 1 (a and b). (a) Top. Infrared spectrum of α-MAC: single crystal, radiation transmitted parallel to the c axis. (b) Bottom. Polarized infrared spectrum of α-MAC: single crystal, radiation transmitted perpendicular to the c axis; E designates the direction of the electric vector.

perature the $\alpha \rightarrow \beta$-phase transition under pressure is accompanied by a 5.2 percent volume change; i.e.,

$$\frac{V_\beta - V_\alpha}{V_\alpha[p=0]} = -0.052.$$

The frequency shifts observed are not indicative of any substantial change in the hydrogen bond distances. A detailed assignment of the spectrum of the β-phase will be given in subsequent sections.

The γ-phase also reveals splitting of some of the degenerate frequencies (Fig. 3) although generally to a lesser degree, and the torsional frequency band is absent or at least very much weaker. The ionic distortion is probably intermediate between that of the β- and α-forms. A curious feature of the low temperature spectra is the tremendous diminution of intensities of the NH bending absorption bands.

The spectra of the corresponding phases of d-MAC show qualitatively the same behavior as described above (Figs. 4–6).

TABLE II. Fundamental frequencies of MAC and ethane (reference 7).

MAC C_{2v} species		MAC cm^{-1}	Description	Ethane cm^{-1}		Ethane D_{3d} species
	ν_1	~3000	XH sym stretch	2915	ν_1	A_{1g}
	ν_2	~3000	CH sym stretch	2915	ν_5	A_{2u}
A_1	ν_3	1538	XH sym bend	~1400	ν_2	A_{1g}
	ν_4	1428	CH sym bend	1379.2	ν_6	A_{2u}
	ν_5	1003	XC stretch	993	ν_3	A_{1g}
	ν_7	~3000	XH asym stretch	2995.5	ν_7	E_u
	ν_8	~3000	CH asym stretch	2955	ν_{10}	E_g
E	ν_9	1580	XH asym bend	1472.2	ν_8	E_u
	ν_{10}	1463	CH asym bend	1460	ν_{11}	E_g
	ν_{11}	1265	XH_3 rocking	~1190	ν_{12}	E_g
	ν_{12}	958	CH_3 rocking	821.52	ν_9	E_u
A_2	ν_6		torsion	275	ν_4	A_{1u}

V. DETAILED ASSIGNMENT OF THE SPECTRA

α-MAC

The classification by symmetry species of the low frequency bands was made in the preceding section. We now turn our attention to the 3000 cm^{-1} region. We anticipate 4 fundamentals as well as a number of combination and overtone bands. The spectrum in which only the E bands appear (Fig. 1a) consists of a broad intense band centered near 3007 cm^{-1} with weak

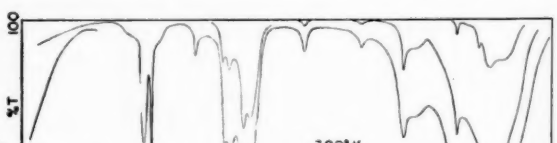

FIG. 1(c). Infrared spectrum of α-MAC: random orientation.

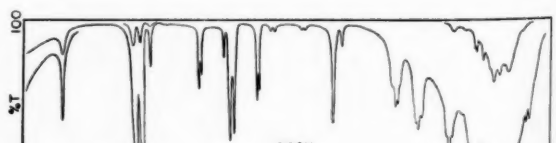

FIG. 2. Infrared spectrum of β-MAC: random orientation.

FIG. 3. Infrared spectrum of γ-MAC: random orientation.

shoulders on both sides and a narrow line at 2776 cm^{-1}. The spectrum of the disoriented sample (Fig. 1c) shows two broad bands near 3060 and 2980 cm^{-1}.

In order to clarify the situation, we may consider the spectrum of d-MAC and examine the absorption resulting from residual NH bonds (Fig. 4). At low H concentrations where there are virtually no NH_2D groups, a single band occurs near 3054 cm^{-1}. A rough calculation of the expected fundamental frequencies neglecting interactions can be made by assuming the inverse kinetic energy term for the NH stretching vibration of the NHD_2 group to be $1/m_H+1/m_N$ and the corresponding terms for the A_1 and E vibrations of the NH_3 group to be $1/m_H+1/3m_N$ and $1/m_H+4/3m_N$, respectively. Using the force constant that gives the correct frequency for the NHD_2 group, one calculates for A_1, $\nu_1=2987$ and for E, $\nu_7=3087$ cm^{-1}. We then assign the A_1 band at 2980 cm^{-1} to ν_1 and consider the 3060 cm^{-1} band as $2\nu_3=2\times1538$. ν_2 probably occurs near 2900 cm^{-1} as in ethane. The species E spectrum is somewhat more obscure. We consider that ν_7 lies near 3080 cm^{-1} in the high frequency shoulder of the main absorption region. The remainder of the band must then be due to the CH stretching vibration as well as the combinations 1580+1428 and 1538+1463. The possibility cannot be discounted, however, that ν_7 occurs at a somewhat lower frequency (i.e., near 3007 cm^{-1}).

Using the above assignment, it is possible to account for the frequency and polarization of the remaining bands (with 3 exceptions) using binary combinations of the fundamentals. The exceptions constitute a high frequency line at 5470 cm^{-1} and 2 weak shoulders to ν_{12}: an A_1 line near 883 cm^{-1} and a band predominantly E near 1038 cm^{-1}. These latter lines may be combination and difference lines involving translational or rotational motions of the MA ion, although the polarization of the low frequency shoulder may be better explained if the line were due to the overtone of the torsional vibration. The assignments are summarized in Table III.

β-MAC

The assignment of the fundamental frequencies of β-MAC follows directly from that given for the room temperature form. The absorption bands show small frequency shifts from those of the α-phase, and the degenerate bands split into two components of nearly equal intensity. The new band appearing at 487 cm^{-1} is attributed to the A_2 torsional vibration as previously mentioned. It is not likely to be an overtone since it also occurs in combination bands but combinations with 487/2 are not present. ν_3 is not readily identified, since the intensity is apparently extremely small, and exact compensation for atmospheric H_2O absorption is difficult. It will be noted that ν_9, the other NH bending vibration also becomes very much weaker. The lowest frequency degenerate line ν_{12} presents a minor anomaly in that it splits into 3 components rather than 2. The

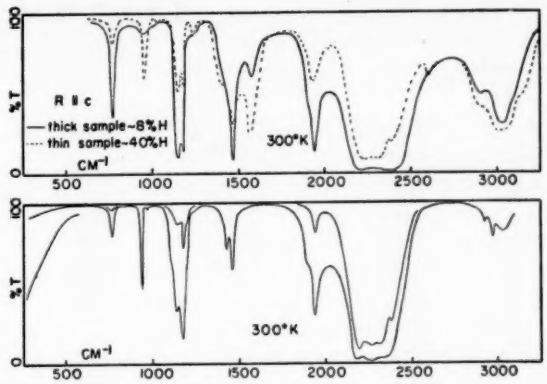

FIG. 4. (a) Top. Infrared spectrum of α-d-MAC: single crystal, radiation transmitted parallel to the c axis. (b) Bottom. Infrared spectrum of α-d-MAC: random orientation.

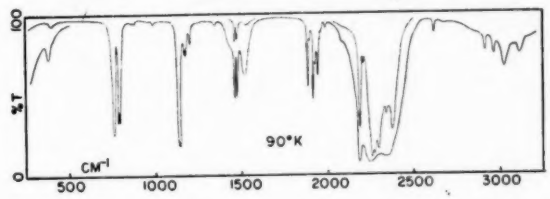

FIG. 5. Infrared spectrum of β-d-MAC: random orientation.

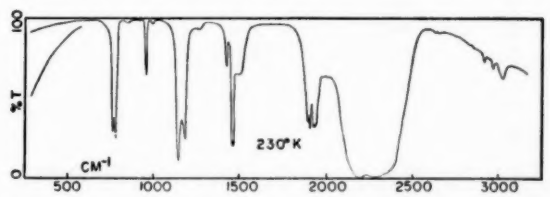

FIG. 6. Infrared spectrum of γ-d-MAC: random orientation.

appearance of the line suggests an initial splitting into 2 components; the higher frequency line then resplitting into a "hyperfine" structure. This secondary splitting may be due to coupling forces within a unit cell, and probably indicates that there is more then one MA ion per unit cell. The same phenomenon occurs in β-d-MAC.

Investigation of the 3000 cm^{-1} region using thin samples reveals 3 strong absorption bands at 3100, 3036, and 2994 cm^{-1}. The symmetry designation of the fundamentals may be superfluous if the distortion and differences in hydrogen bond distances are appreciable. The spectrum of β-d-MAC shows two lines resulting from NH stretching vibrations of residual NHD_2 groups at 3030 and 3104 cm^{-1}. This would indicate that there are at least 2 different hydrogen bond distances in the crystal. The relative intensities suggest that one of the bonds is somewhat longer than the other two.

The remaining bands are easily explained as binary combinations of the fundamental frequencies assigned. Table III summarizes the analysis of the β-phase spectrum.

γ-MAC

The spectrum of the γ-phase of MAC indicates a lesser degree of distortion than exists in the β-phase.

TABLE III. Infrared absorption bands of MAC.[a]

Polarization	cm^{-1}	Assignment	Calculated
α-MAC			
A_1, E	5955–65	$2(\nu_1, \nu_7, \nu_8)$	5960–6160
E	5470	$\nu_{1,8}+(2556)$	
E	4636	$\nu_7+\nu_9$	4660
E	4440	$\nu_{1,8}+\nu_{10}$	4443
A_1	4405	$\nu_1+\nu_4$	4408
E	4313	$\nu_7+\nu_{11}$	4345
A_1	4290	$\nu_2+\nu_4$	4345
E	4027	$\nu_7+\nu_{12}$	4038
A_1	3970	$\nu_1+\nu_5$	3983
$A_1<E$	3450	$\nu_{1,7,8}+\nu_6$	
E	*(3080)*	ν_7	
A_1	3060	$2\nu_3$	3076
E	3007	$\nu_4+\nu_9$, $\nu_3+\nu_{10}$	3008–1
$A_1>E$	*2980*	ν_1, ν_8	
	2917	ν_2	
E	2875	$\nu_4+\nu_{10}$, $2\nu_{10}$	2891–926
E	2776	$\nu_3+\nu_{11}$	2803
$A_1>E$	2556	$2\nu_{11}$, $\nu_5+\nu_{9,3}$	2530–83
		$\nu_9+\nu_{12}$	
E	2480	$\nu_3+\nu_{12}$	2496
$A_1>E$	2214	$\nu_{11}+\nu_{12}$	2223
$A_1<E$	1906	$2\nu_{12}$	1916
E	*1580*	ν_9	
A_1	*1538*	ν_3	
E	*1463*	ν_{10}	
A_1	*1428*	ν_4	
E	*1265*	ν_{11}	
$A_1<E$	1038	$\nu_{12}+\nu_{T,R}$	
A_1	*1003*	ν_5	
E	*958*	ν_{12}	
A_1	883	$\nu_{12}-\nu_{T,R}$,	
		$2\nu_6$	
β-MAC			
	3253	$2\nu_9$	3226–46
	3215		
	3100, *3036*	ν_7	
	2994	ν_1, ν_8	
	2918	ν_2	
	2892	$2\nu_{10}$	2912–56
	2868	$\nu_9+\nu_{11}$	2879–905
	2846, 2784	$2\nu_4$	2832
	2760, 2736, 2721	$\nu_{10}+\nu_{11}$	2722–60
β-MAC			
	2577, 2560	$2\nu_{11}$	2532–82
	2548	$\nu_9+\nu_{12}$	
	2417, 2391	$\nu_{10}+\nu_{12}$	2382–441
	2245	$\nu_5+\nu_{11}$	2262–78
	2113	$\nu_3+\nu_6$?	
	2077, 2072	$\nu_6+\nu_9$	2100–10
	1903	$2\nu_{12}$	1852–926
	1748, 1731	$\nu_6+\nu_{11}$	1753–69
	1623, *1613*	ν_9	
	1478, *1456*	ν_{10}	
	1416	ν_4	
	1282, *1266*	ν_{11}	
	996	ν_5	
	963, *955*, *926*	ν_{12}	
	487	ν_6	
γ-MAC			
	3239	$2\nu_9$?	
	3055	ν_7	
	3010	ν_1	
	2963	ν_8	
	2928	ν_2	
	2857	$\nu_4+\nu_{10}$	2884–907
	2724	$\nu_{10}+\nu_{11}$	2725–48
	2553	$2\nu_{11}$, $\nu_5+\nu_{9,3}$	2530
		$\nu_9+\nu_{12}$	
	2414	$\nu_{10}+\nu_{12}$	2394–432
	2064	$\nu_9+\nu_6$?	
	2035	$\nu_3+\nu_6$?	
	1900	$2\nu_{12}$,	1868–98,
		$\nu_8+\nu_{12}$	1934–49
	1713	$\nu_6+\nu_{11}$?	
	1483, *1460*	ν_{10}	
	1424	ν_4	
	1265	ν_{11}	
	1000	ν_5	
	949, *934*	ν_{12}	
	478?	ν_6?	

[a] The designation of fundamental vibrations is the same as that used in Table II and the corresponding frequencies are italicized. $\nu_{T,R}$ denotes frequencies associated with translatory and/or rotatory motions of the MA ion in the lattice.

The torsional vibration again becomes essentially inactive although it appears in combination bands. The splitting of the degenerate lines was unobserved for ν_{11} and smaller for ν_{12}. Both of the NH bending vibration bands have become vanishingly weak. The fundamental assignments follow directly from those of the α-phase. The remaining bands can readily be accounted for as binary combinations of the observed fundamentals with the exception of the lines at 1713, 2035, 2064, and 3239 cm^{-1}, all of which have counterparts in the β-phase spectrum. The same assignments are consequently used. A very weak line observed in the spectrum of supercooled γ-MAC at 90°K occurs at 478 cm^{-1} which may be due to the torsional vibration. Unfortunately a strong atmospheric H_2O line also occurs near this frequency.

The 3000 cm^{-1} region resembles that of the α-phase spectrum in general appearance, and the assignment is derived in the same manner. The proposed assignment is listed in Table III.

VI. (N)DEUTERO METHYL AMMONIUM CHLORIDE

The deuterium substituted samples were estimated to contain less than 2 percent replaceable H in favorable cases. Samples with greater H content were also examined to identify bands produced by hybrid molecules. Some uncertainty exists in the origin of some of the very weak bands observed.

The spectra of the deuterium compound $CH_3ND_3^+Cl^-$ display the expected frequency shifts for vibrations associated with the NH(D) linkage. The NH stretching absorption in the 3000 cm^{-1} region has largely vanished,

and strong bands appear near 2300 cm^{-1}. Similarly the NH bending vibrations at 1538 and 1580 cm^{-1} have disappeared, and new bands occur in the 11–1200 cm^{-1} region. The lowest frequency degenerate band ν_{12} has shifted by a somewhat smaller degree, and the remaining bands show little or no change in frequency. The frequencies of MAC and d-MAC will be designated by unprimed and primed symbols, respectively.

α-d-MAC

A general classification of the frequencies can be made by direct correlation with the spectrum of MAC. The bands appearing at 1462 and 1428 cm^{-1} correspond to ν_{10} and ν_4 of MAC with virtually the same frequencies. The broad band at 774.7 cm^{-1} must correspond to ν_{12}. The narrow line at 954.5 cm^{-1} must then be the C–N stretching vibration ν_5'. (The Raman spectrum gives an intense line at 947 cm^{-1} for the aqueous solution.) ν_2' and ν_8' should occur near 2900 cm^{-1}, and ν_1' and ν_7' should lie near 2300 cm^{-1}. The torsional vibration should again be inactive, and the 3 remaining fundamentals are expected in the 11–1200 cm^{-1} region. Three bands are observed in this region at 1144, 1178, and 1188 cm^{-1}, the latter two being badly overlapped. The spectrum of a single crystal (E bands active) shows bands at 1144 and 1188 cm^{-1} which are assigned to ν_{11}' and ν_9'. The 1178 cm^{-1} line then corresponds to the A_1 vibration ν_3'. (The single crystals were somewhat more contaminated with H than the disoriented samples, and this introduces a slight uncertainty in the interpretation of this region of the spectrum.) The single crystal spectra also confirm the symmetry species assigned to the remaining low frequency bands.

The A_1 and E (CH stretching) vibrations, ν_2' and ν_8', are assigned to the weak lines at 2919 and 2970 cm^{-1}, respectively. The intensities of these lines are independent of the degree of H contamination. The A_1 (ND stretching) vibration is assigned to the band at 2195 cm^{-1} which has the appropriate symmetry as determined from single crystal spectra. The corresponding degenerate vibration ν_7' probably occurs near 2300 cm^{-1} in the broad absorption band covering that region. One would expect Fermi resonance to occur with the degenerate components of 2×1144, $1144+1188$, and $1144+1178$ cm^{-1}. The assignment is listed in Table IV.

The foregoing assignment is in satisfactory agreement with the application of the isotope product rule; the calculated† and observed ratios are as follows:

	Observed $\Pi\frac{\nu'}{\nu}$	Calculated $\left\{\left(\frac{m_H}{m_D}\right)^{2+\delta}\frac{M_D}{M_H}\left(\frac{I_D}{I_H}\right)^{\delta}\right\}^{\frac{1}{3}}$	
A_1	0.5373	0.5234	$\delta=\begin{cases}0 & A_1\\ 1 & E\end{cases}$
E	0.4125	0.4018	

† The following model was used to calculate the moments of inertia and force constants: C–N=1.47A, C–H=1.09A, N–H=1.01A. All angles=109°28′.

The deviations are less than 3 percent and in the expected direction.

β-d-MAC

The spectrum of β-d-MAC is analogous to that of the corresponding form of MAC. The torsional frequency appears as an active band, and the degenerate bands split into doublets. (The lowest frequency E band again shows a "hyperfine" splitting as previously mentioned.) The intensities of the A_1 bands are all diminished, with ν_4' and ν_5' being practically nonexistent. This might conceivably be due to a selective orientation induced during the transition, but no corresponding phenomenon occurred with MAC. More likely the transition moments have decreased because of changes in the polarization of the MA ion and the form of the normal vibration in the different lattices. The assignment is readily obtained from that of α-d-MAC and is listed in Table IV. The 2300 cm^{-1} region contains a profusion of lines resulting from the splitting of the fundamental and combination bands as well as absorption resulting from hybrid molecules.

The application of the isotope ratio rule to the A_2 torsional frequencies leads to a major discrepancy which will be treated later.

γ-d-MAC

The γ-phase spectrum closely resembles that of α-d-MAC. The only splitting observed is that of ν_{12}', although there is some evidence of asymmetry in the bands at 1460 and 1144 cm^{-1}, and overlapping of the 1190 cm^{-1} band would conceal any effect in the latter case. The torsional frequency again disappears although combination bands involving ν_6' are still present. The A_1 bands which vanished in the β-phase reappear with intensities comparable with those in the α-phase spectrum. The assignment is straightforward, and is summarized in Table IV.

VII. DISCUSSION

The general character of the spectrum is similar to that of ethane. A normal coordinate treatment was carried out neglecting nondiagonal force constants, and the results are described in the appendix.

The NH stretching frequencies in the MA ion are lower than those observed in neutral molecules. A similar effect occurs in the NH_4^+ ion. Part of the reduction in frequency is undoubtedly due to hydrogen bonding to the anion. The hypothetical vapor phase frequencies of the MA ion or comparative frequencies of the MA ion and methylamine in identical surroundings would be desirable in the prediction of hydrogen bonding distances in amino acids and related substances.

Mention has been made of the discrepancy between the observed and calculated isotope frequency ratio for the torsional vibrations in the β-phase. The usual form of the isotope product rule is valid only for vanishing external forces. In the case of finite external forces, it

TABLE IV. Infrared absorption bands of d-MAC.[a]

Polarization	cm⁻¹	Assignment	Calculated
α-d-MAC			
	2970	ν_8'	
	2919	ν_2'	
	2376	$2\nu_9'$	2376–417
		$\nu_5'+\nu_{3,9}'$	
A_1, E	*2320*	ν_7'	
	2275	$2\nu_{11}'$	2288
$\sim A_1$	*2195*	ν_1'	
$\sim E$	1941	$\nu_3'+\nu_{12}'$	1953–63
		$\nu_9'+\nu_{12}'$	
	1898	$2\nu_5'$	1909–19
		$\nu_{11}'+\nu_{12}'$	
	1728	$\nu_5'+\nu_{12}'$	1729
E	*1462*	ν_{10}'	
A_1	*1428*	ν_4'	
	1250	$\nu_3'+\nu_{T',R}$	
E	*1188*	ν_9'	
A_1	*1178*	ν_3'	
E	*1144*	ν_{11}'	
	1114	$\nu_3'-\nu_{T',R}$	
A_1	*954.5*	ν_5'	
E	*774.7*	ν_{12}'	
Hybrid	1538	2799	
	1390	1037	
	1001	1019	
	981	3054	NHD_2
	847		
β-d-MAC			
	2974	ν_8'	
	2916	ν_2'	
	2672	$\nu_7'+\nu_6'$	2657–81
	2611	$\nu_3'+\nu_4'$	
	2357	$\nu_3'+\nu_9'$, $2\nu_3'$	2362–96
	2340	$2\nu_9'$	2328–48
	2308	ν_7'	
	2284		
	2260	$2\nu_{11}'$	2271–88
	2215	$\nu_{10}'+\nu_{12}'$	2210–58
	2183	ν_1'	
	2099	$\nu_5'+\nu_{11}'$	
	2071		
	1982		
	1959	$\nu_3'+\nu_{12}'$	1949–78
	1948		
	1933	$\nu_9'+\nu_{12}'$	1915–54
	1920		
	1910	$\nu_{11}'+\nu_{12}'$	1887–924
	1893	$2\nu_5'$	
	1883		
β-d-MAC			
	1514	$\nu_{11}'+\nu_6'$, $2\nu_{12}'$	1502–60
	1478.4	ν_{10}'	
	1459.5		
	1198	ν_3'	
	1174	ν_9'	
	1164		
	1144	ν_{11}'	
	1135.5		
	780	ν_{12}'	
	774		
	751		
	373	ν_6'	
Hybrid	3104	NHD_2 1282	959
	3030	1262	941 824
	2811	1212	933 809
	2777	1112	928 763
	1390	1035	915
	1358	993	894
	1307	976	838
γ-d-MAC			
	2974	ν_8'	
	2923	ν_2'	
	2656	$\nu_7'+\nu_6'$	
	2613	$\nu_3'+\nu_4'$	2616
	(2300)	ν_7'	
	2186	ν_1'	
	2011	?	
	1993		
	1949		
	1938	$\nu_3'+\nu_{12}'$	1940–62
	1931	$\nu_9'+\nu_{12}'$	
	1908		
	1898	$\nu_{11}'+\nu_{12}'$, $2\nu_5'$	1903–16
	1493	$\nu_{11}'+\nu_6'$	
	1460	ν_{10}'	
	1426	ν_4'	
	1245	$\nu_3'+\nu_{T',R}$	
	(1190)	ν_9'	
	1181	ν_3'	
	1144	ν_{11}'	
	955	ν_5'	
	771.5	ν_{12}'	
	759		
Hybrid	3035-NHD_2	1383	837
	2847	1001	
	1537	980	

[a] For an explanation of symbols used, see Table III.

is easily shown[8] that the correct form is obtained by dropping the terms involving the total mass and moments of inertia, and extending the product over the new vibrations arising from the previously nongenuine vibrations; i.e.,

$$\Pi\left(\frac{\nu'}{\nu}\right)=\Pi\left[\left(\frac{m}{m'}\right)^{k}\right]^{\frac{1}{2}}$$

Vibrations +translations +rotations — Sets of symmetric atoms

where ν = frequency, m = mass, k = degrees of freedom.

[8] O. Redlich, Z. phys. Chem. **B28**, 371 (1935).

In the case of the A_2 vibrations, the product extends over 2 frequency ratios corresponding to linear combinations of rotation and torsion about the figure axis, neither vibration necessarily conserving angular momentum of the ion. Unfortunately, the low frequency lines were not observed. However, the approximate upper limit to the field free torsional frequency and hence of the potential barrier to internal rotation can be calculated by a normal coordinate treatment assuming a potential function in the crystal to be

$$2V=k_c\theta^2+k_n\phi^2+k_t(\theta-\phi)^2,$$

where θ and ϕ are the displacement angles of the CH_3 and NH_3 groups, respectively. The secular determinant then becomes

$$\begin{vmatrix} k_c+k_t-I_c\lambda & -k_t \\ -k_t & k_n+k_t-I_n\lambda \end{vmatrix}=0,$$

where I_c and I_n are the axial moments of inertia of the CH_3 and NH_3 groups, and $\lambda=4\pi^2\nu^2$. The expansion gives

$$\lambda=\frac{k_t}{2I_cI_n}(I_c(1+n)+I_n(1+c)$$
$$\pm[\{I_c(1+n)+I_n(1+c)\}^2-4I_cI_n(c+n+cn)]^{\frac{1}{2}}),$$

where $c=k_c/k_t$ and $n=k_n/k_t$. The larger root (+) λ_L corresponds to the frequency of the predominantly torsional vibration while the smaller root (−)λ_S corresponds to the "rotational" oscillation. The observed ratio of the larger roots λ_L'/λ_L equals 0.5866, while the isotope product value for the hypothetical ion in free space would be 0.7299. If the ratio λ_L'/λ_L is examined to see what values of c and n would give results in agreement with observation, the functional relation shown in Fig. 7 is obtained.

TABLE V. α-Phase.

Species	MAC cm^{-1} calc	MAC cm^{-1} obs	MAC % dev	d-MAC cm^{-1} calc	d-MAC cm^{-1} obs	d-MAC % dev
	2999	2980	0.64	2905	2919	−0.48
	2895	2917	−0.76	2152	2195	−1.96
A_1	1659	1538	7.88	1507	1428	5.53
	1461	1428	2.31	1280	1178	8.67
	916	1003	−8.67	837	954.5	−12.3
	3094	3080	0.45	3006	2970	1.21
	3023	2980	1.44	2328	2320	0.35
E	1601	1580	1.33	1416	1462	−3.14
	1479	1463	1.09	1222	1188	2.86
	1128	1265	−10.8	962	1144	−15.9
	985	958	2.82	849	774.7	9.6

The solid line shows the relation between c and n necessary to give agreement with experiment. The area below the dotted line corresponds to an unstable equilibrium position of the MA ion. Above the line it will be noted that $n>1$; i.e., the external force constant retarding rotation of the NH_3 group is greater than the internal force constant. To estimate the internal potential barrier, we shall make the assumption that the absolute value of c is small. (Physically one would expect the external force constant for the CH_3 group to be small since only van der Waals forces are involved.) For the purposes of calculation, the values $c=0$ and $n=1.5$ were chosen, leading to the following frequencies:

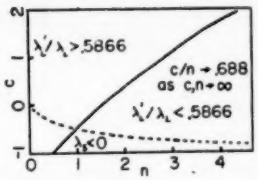

FIG. 7. Locus of c and n, such that $\lambda_L'/\lambda_L=0.5866$.

$$k_t=0.13\times10^{-11}\text{ dyne-cm/radian}^2$$

$\nu_L=486$, $\nu_L'=375$, $\nu_S=188$, $\nu_S'=172$, $\nu_T=387$ cm^{-1}, where ν_T = torsional frequency of the MA ion in free space.

In principle it should be possible to obtain a value for ν_S from the heat capacity data, but satisfactory elimination of the contributions of the lattice vibrations, degenerate rotations, and the C_p-C_v correction proved insurmountable. The calculated frequency $\nu_T=387$ cm^{-1} corresponds to a maximum barrier height of $V_0=1670$ $cm^{-1}=4770$ cal/mole calculated from Mathieu functions assuming the potential $V=V_0\sin^2 3\psi/2$, where $\psi=\theta-\phi$. This may be compared with the accepted values for ethane, $V_0=965$ $cm^{-1}=2760$ cal/mole.[7]

It is interesting to note that the torsional oscillation occurring in phase III $NH_4^+Cl^-$ at 391 cm^{-1} [6] leads to a force constant, $k_r=0.247\times10^{-11}$ dyne-cm/radian^2 as compared with $k_n=0.195\times10^{-11}$ dyne-cm/radian^2 obtained in the previous discussion. Since the $NH_4^+Cl^-$ structure involves a most efficient close-packed structure, one would probably expect $k_n<k_r$.

APPENDIX

A normal coordinate treatment was carried out to verify the assignment proposed for the spectra. A simple valence force potential field was assumed,

$$2V=k_{rn}\Sigma r^2_{NH}+k_{rc}\Sigma r^2_{CH}+k_{NC}R^2_{NC}+k_{\alpha n}\Sigma\alpha_n^2$$
$$+k_{\alpha c}\Sigma\alpha_c^2+k_{\beta n}\Sigma\beta_n^2+k_{\beta c}\Sigma\beta_c^2+2V_{\text{torsion}},$$

where r, R are the bond displacement coordinates, and α, β are the angle displacement coordinates of the $H-X-H$ and $H-X-Y$ groups. Solution of the A_1 equations leads to imaginary force constants. The procedure followed was to solve the E equations for MAC and d-MAC and average the force constants obtained. These force constants were used to calculate A_1 and E frequencies for both MAC and d-MAC. The results are shown in Table V.

The agreement with observation is about as good as the equivalent treatment of ethane.[9] The force constants used were $k_{rn}=5.17$, $k_{rc}=4.85$, $k_{NC}=4.5\times10^5$ dyne/cm; $k_{\alpha n}=k_{\alpha c}=0.55$, $k_{\beta n}=0.75$, $k_{\beta c}=0.65\times10^{-11}$ dyne-cm/radian^2.

[9] F. Stitt, J. Chem. Phys. 7, 297 (1939).

Kinetics of Two Exchange Reactions Involving Diborane

P. CALVIN MAYBURY* AND W. S. KOSKI
Department of Chemistry, The Johns Hopkins University, Baltimore, Maryland
(Received August 13, 1952)

The kinetics of the exchange between deuterium and diborane were studied over a temperature range of 25°–75°C, and it was found that the reaction was $\frac{3}{2}$ order with respect to diborane and zero order with respect to deuterium at high pressures. At low pressures the zero-order dependence of the deuterium changed to first-order. The activation energy of the zero-order reaction was 20.4±2 kcal/mole. A mechanism is proposed in which the borine radical reacts with deuterium on the wall and is followed by a rate determining bimolecular collision between the partially deuterated borine radical and a diborane molecule.

The closely related exchange reaction between normal and completely deuterated diborane was also investigated. The total order of this reaction was $\frac{3}{2}$, and it had an activation energy of 21.8±3 kcal/mole. A mechanism is proposed which involves the collision between a borine radical and a diborane molecule as the rate determining step.

INTRODUCTION

THERE have been numerous investigations directed toward the study of the structure of the boron hydrides[1–6] which have provided us with our present knowledge of the structure of diborane (B_2H_6), the simplest and lowest molecular weight boron hydride known. The existence of odd number boranes such as (B_5H_9, B_7H_{13}) suggests that the borine radical (BH_3) might possibly be the building block of these hydrides. The most precise work[1] has failed to measure experimentally any trace amount of BH_3, but this does not rule out the fact that the BH_3 radical is probably a short lived species incapable of isolation by present-day means.

The kinetics of the pyrolysis of diborane have been studied by several investigators[7,8] who have shown that the reaction mechanism involves a complex containing the BH_3 radical. These studies both indicate a dissociation step of diborane into two borine radicals which then can collide with another diborane molecule to begin a radical type of addition polymerization:

$$B_2H_6 \rightleftarrows 2BH_3,$$
$$BH_3 + B_2H_6 \rightarrow \text{higher products.}$$

In order to provide further insight on the chemical reactivity of diborane, kinetic studies of two exchange reactions involving this molecule were made. One reaction involves the exchange between deuterium and diborane, and a second concerns the exchange between normal diborane and completely deuterated diborane. Some preliminary work[9] on the first reaction using tritium was carried out a few years ago and the indication was that all six hydrogens in diborane exchanged at apparently equivalent rates; however, the details of the kinetics were not investigated. Consequently, the significance of the exchange as far as bond equivalence or nonequivalence is concerned could not be determined unambiguously.

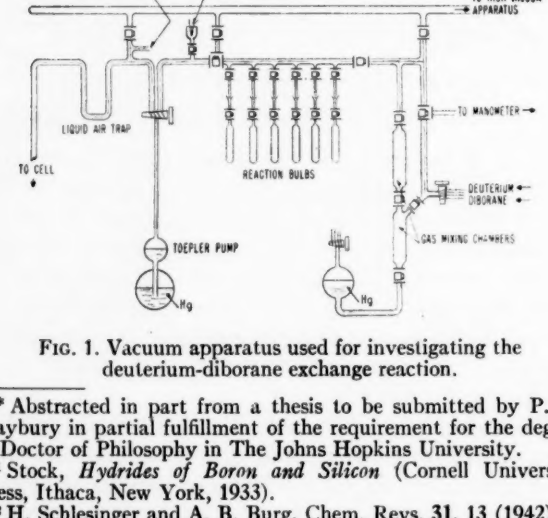

FIG. 1. Vacuum apparatus used for investigating the deuterium-diborane exchange reaction.

EXPERIMENTAL

Materials

B_2H_6

The normal diborane was synthesized according to the standard method[10] and some was furnished by the Naval Research Laboratory, Washington, D. C. For further purification the diborane was fractionally distilled out of successive baths of dry ice-acetone and finally out of a trap at −140°C. The samples of diborane from the different sources gave the same results.

B_2D_6

The completely deuterated diborane was synthesized in a high vacuum apparatus by the reaction of $LiAlD_4$

* Abstracted in part from a thesis to be submitted by P. C. Maybury in partial fulfillment of the requirement for the degree of Doctor of Philosophy in The Johns Hopkins University.

[1] Stock, *Hydrides of Boron and Silicon* (Cornell University Press, Ithaca, New York, 1933).

[2] H. Schlesinger and A. B. Burg, Chem. Revs. **31**, 13 (1942).

[3] George C. Pimental and K. S. Pitzer, J. Chem. Phys. **17**, 882 (1949).

[4] Gutowsky, Kistiakowsky, Pake, and Purcell, J. Chem. Phys. **17**, 972 (1949).

[5] Linus Pauling, *Nature of the Chemical Bond* (Cornell University Press, Ithaca, New York),

[6] K. S. Pitzer, J. Am. Chem. Soc. **67**, 1126 (1945).

[7] R. P. Clarke and Robert N. Pease, J. Am. Chem. Soc. **73**, 2132 (1951).

[8] Bragg, McCarty, and Norton, J. Am. Chem. Soc. **73**, 2134 (1951).

[9] W. S. Koski, unpublished work.

[10] Finholt, Bond, and Schlesinger, J. Am. Chem. Soc. **69**, 1199 (1947).

(obtained from the Metal Hydrides Company, Beverly, Massachusetts, with permission of the U. S. Atomic Energy Commission, Oak Ridge, Tennessee) and BF_3 in ethyl ether. The $LiAlD_4$ was chemically pure grade and 99.5 percent isotopically pure, and the BF_3 used was technical grade.

D_2

The deuterium (99.8 percent) was obtained from the Stewart Oxygen Company with permission of the U. S. Atomic Energy Commission, Oak Ridge, Tennessee. It was used directly from the high pressure tank and passed through liquid nitrogen tubes for further purification.

Apparatus and Procedure

Figure 1 shows the apparatus used for mixing the deuterium and diborane and for analysis of the hydrogen-deuterium mixtures after the exchange reaction. The gases were introduced separately into the lower mixing chamber at the desired pressure and then forced by mercury into the upper chamber and mixed. The resulting mixture was then compressed into the reaction bulbs, and the final pressure was measured by the capillary mercury manometer which was read to an accuracy of 0.1 millimeter.

The bulbs were then fully submerged into a constant temperature (±0.01°C) reaction bath. At regular intervals beginning with zero time a bulb was removed and reaction quenched by immersion into liquid nitrogen. The partially deuterated diborane was frozen out, and the hydrogen-deuterium mixture pumped off into the gas equilibrator by means of the Toepler pump. The equilibrator consists of a glass bulb containing a fine platinum wire which when heated electrically to a dull red would rapidly bring the H_2, D_2, and HD mixture to equilibrium. The equilibrated mixture was then cooled to room temperature and pumped into the conductivity cell. The final pressure was made the same for all samples. The pressure was adjusted by use of the Toepler pump and the capillary mercury manometer. The mixture was then analyzed by means of thermal conductance. The thermal conductance cell (Fig. 2) consisted of a fine platinum wire (0.0008 in. diameter), stretched tightly by a glass spring, sealed into a Pyrex tube with a capillary gas inlet tube. The resistance of this wire was approximately 60 ohms and was one arm of a Wheatstone bridge circuit, all of which was completely immersed in a thermostated bath and when used in conjunction with a thyrotron tube relay no difficulty was found in holding the bath temperature to better than 0.001°. The glass cell was inserted into a Bakelite drum which was wound with about 30 feet of number 36 B & S gauge platinum wire that had approximately the same resistance as the cell wire. This wire wound drum acted as a compensator for the cell and also was another arm of the Wheatstone bridge.

The method of analyzing the mixture by utilizing the differences of thermal conductivities of the hydrogen isotopes is fully described in the literature.[11] A small current passes through the gauge wire and heats it to a constant temperature. With a standard gas (pure hydrogen) in the cell, the voltage that is necessary to produce balance to the system is measured. Upon introducing another gas such as deuterium at the same pressure, a new voltage must be applied to produce balance. The ratio of the two voltages is used as a measure of the amount of hydrogen in a hydrogen deuterium mixture. The ratio rather than the absolute value of the voltage or resistance is used since it varies only slowly with pressure and temperature.

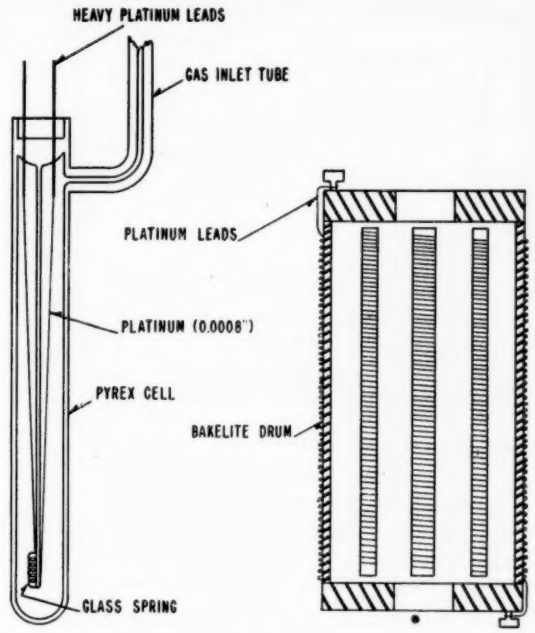

FIG. 2. Thermal conductance cell and compensator drum used in analyzing hydrogen-deuterium mixture.

The course of the B_2H_6-B_2D_6 exchange was followed by the use of an infrared spectrometer. The absorption cell was thermostated and served as the reaction vessel so that continuous measurements could be made. The cell is pictured in Fig. 3 showing the mercury reservoir that served to jacket the cell as well as provide a means of temperature regulation. The temperature was measured by a thermocouple inserted in the cell and with a thyratron tube relay kept a constant temperature to ±0.01°C.

The spectrometer was a modified Perkin-Elmer instrument using the same detection system as that used in the Perkin-Elmer infrared spectrometer, model 12B and with a Brown "Electronik" recorder.

The absorption peak of diborane at 974 cm^{-1} was revealed to be free from interfering absorption of B_2D_6 and partially exchanged samples, and therefore this frequency was chosen to follow the rate of disappearance of B_2H_6 with time.

[11] N. R. Trenner, J. Chem. Phys. 5, 382 (1937).

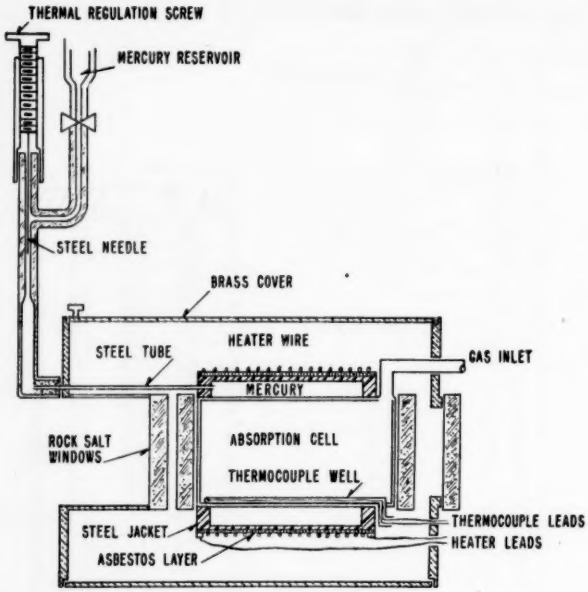

FIG. 3. A thermostated infrared absorption cell used for following the B_2H_6-B_2D_6 exchange.

The $\log I_0/I$ *versus* pressure is a linear relationship, and the method was tested by mixing various samples of known concentrations of B_2H_6 and B_2D_6. The B_2H_6 and B_2D_6 were measured and mixed in apparatus similar to that pictured in Fig. 1. After mixing, the gases were forced into the absorption cell at the desired final pressure, the pressure again being measured by a capillary mercury manometer. The cell was brought to the desired temperature prior to the introduction of the gases so that the reaction time could be measured from the instant the gases entered the cell. The region chosen for following the course of the reaction was first scanned with the cell empty, immediately preceding each run. Then the gases were introduced and the region of 974 cm^{-1} was scanned as a function of time.

THE DEUTERIUM-DIBORANE EXCHANGE

Kinetics of the Reaction

The data are interpreted in terms of the first-order rate law which applies when the concentration of the reactants remains fixed during the course of the reactions and is independent of the reaction mechanism. The rate R at which the reaction proceeds is given by the equation:

$$Rt = ab/(a+b)\ \ln[1-(x/x_\infty)], \tag{1}$$

where x and x_∞ are the percent deuterium present in diborane, measured at time t and at infinite time, and a and b are the concentrations of diborane and deuterium, respectively.

The order of the reaction was determined by varying independently the concentrations of the reactants. The rate of the reaction is proportional to the product of the concentration of reactants raised to their respective power. By substituting this equation for R,

$$R = ka^\alpha b^\beta \tag{2}$$

into Eq. (1) and substituting $t_{\frac{1}{2}}$ for the half-time of reaction and taking logarithms, we obtain

$$\ln t_{\frac{1}{2}}(a+b)+(\alpha-1)\ \ln a+(\beta-1)\ \ln b+\ln k/0.693=0. \tag{3}$$

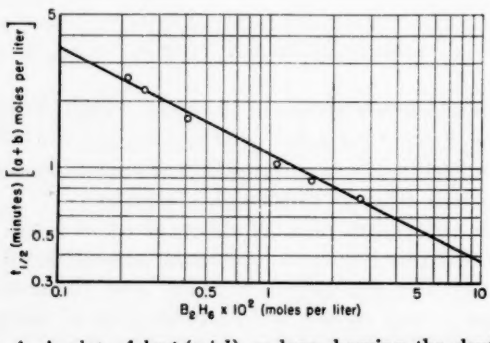

FIG. 4. A plot of $\log t_{\frac{1}{2}}(a+b)$ *vs* $\log a$, keeping the deuterium concentration constant. a = diborane concentration. b = deuterium concentration. Temperature = 55°C.

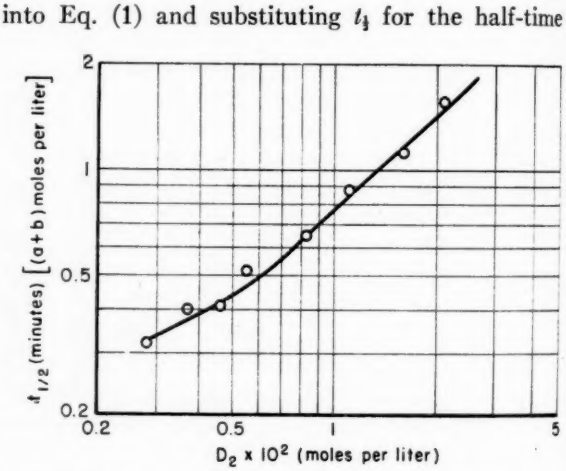

FIG. 5. A plot of $\log t_{\frac{1}{2}}(a+b)$ *vs* $\log b$, keeping the diborane concentration constant. a = diborane concentration. b = deuterium concentration. Temperature = 55°C.

By determining $t_{\frac{1}{2}}$ as a function of a, keeping b constant, and then plotting $t_{\frac{1}{2}}(a+b)$ against $\ln a$, the slope is equal to $1-\alpha$. The results of a series of experiments carried out to determine the order of reaction with respect to diborane and deuterium are shown in the data plotted in Figs. 4 and 5. The slopes of the lines are -0.50 and 1, respectively, indicating a 1.5-order dependence upon the diborane concentration and a zero-order dependence upon the deuterium concentration. The three-halves order for diborane holds over a tenfold range in concentration, but the zero-order dependence of deuterium appears to change at lower pressures. A series of experiments were carried out at low pressures of deuterium, and the results are plotted in Fig. 6. It is clear from this plot that the zero-order dependence of deuterium changes to first-order dependence at low pressures.

The activation energy is calculated to be 20.4 kcal±2

kcal per mole from Fig. 7 in which the logarithms of the average true specific rate constants are plotted against the reciprocals of the absolute temperatures. The rate constants k given in Table I are calculated on the assumption that the reaction is 1.5 order with respect to diborane and independent of deuterium.

In the preliminary planning of this investigation, it was hoped that the bimolecular exchange between diborane and deuterium could be realized so that presence of bridge hydrogens could be demonstrated by any difference in exchange rate that such hydrogens might have from normal hydrogens in diborane. It is clear from the above data that the situation is not so simple. The $\frac{3}{2}$-order dependence of the diborane indicates that dissociation is taking place and that the borine radicals play an important role as intermediates in the reaction. Furthermore, the zero-order dependence on deuterium at high pressure changing to a first-order dependence at lower pressures suggests the existence of a surface catalyzed reaction.

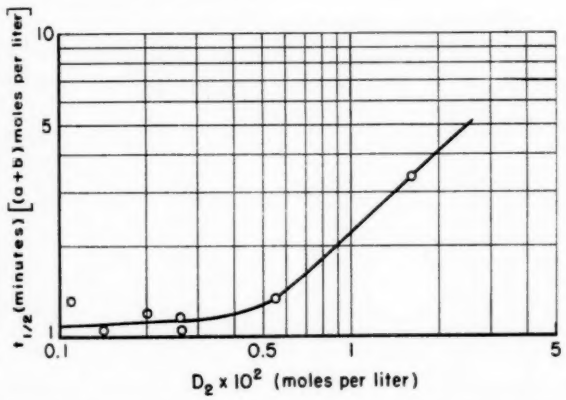

FIG. 6. A plot of $\log t_{\frac{1}{2}}(a+b)$ *vs* $\log b$, keeping the diborane concentration constant. a = diborane concentration. b = deuterium concentration. Temperature = 75°C.

Surface Effects

When the reaction vessel was packed with long lengths of small diameter Pyrex rods with fire-polished ends so as to give a surface to volume ratio of about 10, the rate of the reaction was approximately doubled as shown in Table II. This catalytic effect is small compared to normal surface catalyzed reactions. Covering the surface with Drifilm did not slow the reaction but actually accelerated the rate. The addition of glass wool also accelerates the reaction but is only about as effective as the increase resulting from a smooth Pyrex surface.

The influence of inert gases upon the rate of reaction further indicates the presence of a surface catalyzed reaction. Upon adding N_2 and CO_2 in increasing amounts, the rate of reaction progressively decreases. This effect can be explained on the basis that the N_2 and CO_2 molecules are adsorbed on the surface which reduces the surface area and thus the activity. The addition of He gas, on the other hand, did not appreciably affect the rate of reaction.

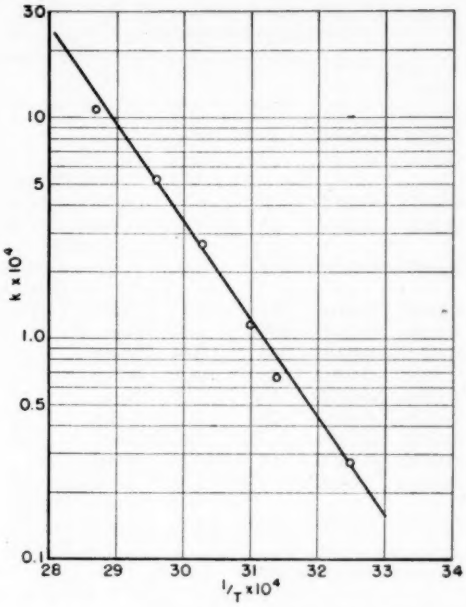

FIG. 7. Temperature dependence of the deuterium-diborane exchange.

Several reactions were carried out in complete darkness, and the same rates were obtained indicating that the reaction was not affected by ordinary laboratory light.

Mechanism of the Reaction

Any mechanism proposed to account for the exchange reaction between deuterium and diborane must explain not only the fractional-order dependence of the diborane, the zero- and first-order dependence of the deuterium, but also the weak surface dependence of the reaction and the effect of inert gases. These facts would

TABLE I. Rate constants and temperature dependence of the deuterium diborane exchange.

Temp °C	B_2H_6[a] (conc)	D_2[a] (conc)	$t_{\frac{1}{2}}$ (min)	$k \times 10^4$
35°	0.0960	0.0320	326	0.285
35°	0.1300	0.0314	253	0.242
35°	0.0630	0.0324	532	0.291
45°	0.0960	0.0534	208	0.635
45°	0.0960	0.0321	138	0.675
45°	0.0630	0.0324	227	0.684
50°	0.0968	0.0323	73	1.28
50°	0.1300	0.0314	60.4	1.07
55°	0.0246	0.0086	70	2.72
55°	0.0658	0.0219	47.5	2.38
55°	0.0246	0.0210	109	3.09
55°	0.0965	0.0326	34	2.75
55°	0.0960	0.0415	42.5	2.64
65°	0.0950	0.0440	23	5.15
75°	0.0955	0.0538	13.3	10.1
75°	0.0958	0.0324	10.5	9.0
75°	0.0660	0.0220	10	10.8
75°	0.0180	0.0060	21	10.1

[a] Concentrations are expressed in gram atoms of hydrogen per liter.

TABLE II. Influence of surface and inert gases on rate of exchange.

Temp °C	B_2H_6[a] (conc.)	D_2[a] (conc.)	$t_{\frac{1}{2}}$ min	$R\times10^6$	Surface change
55°	0.0637	0.0207	48	3.8	None
55°	0.0637	0.0207	28	6.5	(Increased s/v by 10 with Pyrex)
55°	0.0637	0.0207	28	6.5	(Added 2 g glass wool)
55°	0.0637	0.0207	21	8.7	(Covered surface with Drifilm)
55°	0.0648	0.0216	31	6.0	(Covered surface with fluorothene G)
55°	0.0648	0.0216	23	8.1	(Added 5 g glass wool)
55°	0.0246	0.0210	109	1.24	None
55°[b]	0.0270	0.0210	223	0.61	None
55°[c]	0.0252	0.0202	645	0.20	None
75°	0.0330	0.0110	13	7.3	None
75°[d]	0.0324	0.0108	20	4.7	None
75°[e]	0.0312	0.0104	65	1.4	None
75°	0.0660	0.0100	8.3	12.1	None
75°	0.0660	0.0100	7.0	14.3	(Increased s/v by 10 with Pyrex)
75°[f]	0.0660	0.0100	9.0	11.1	(Increased s/v by 10 with Pyrex)

[a] Concentrations are expressed in gram atoms of hydrogen per liter. s/v indicates surface to volume ratio.
[b] 0.13 mole/liter of CO_2 present.
[c] 1.6 moles/liter of CO_2 present.
[d] 0.54 mole/liter of N_2 present.
[e] 2.7 moles/liter of N_2 present.
[f] 1.1 moles/liter of N_2 present.

seem to limit the mechanism to a system of competing surface catalyzed reactions involving chains. The fact that the rate is not greatly influenced by increasing the surface to volume ratio appreciably suggests that chains start on the walls and are stopped on the walls. It has been pointed out by several authors[12,13] that the absence of a strong surface dependence does not necessarily prove the absence of a hetereogeneous reaction. The following series of reactions appears to fit the experimental facts. (a) The diborane thermally dissociates to borine. This is probably a homogeneous dissociation. (b) The borines then react on the surface with deuterium to form BH_2D. At high pressures the deuterium completely covers the surface and hence the zero-order dependence. At lower pressures the surface is not completely covered and gives rise to first-order dependence, and the heat of absorption contributes to the activation energy which in turn affects the rate of reaction. (c) The partially deuterated borine then reacts in a bimolecular collision with diborane. This step would be rate determining and accounts for the fractional order dependence of the diborane.

$$B_2H_6 \rightleftarrows 2BH_3, \quad (a)$$

$$BH_3+D_2 \rightleftarrows BH_2D+HD, \quad (b)$$

$$BH_2D+B_2H_6 \rightleftarrows B_2H_5D+BH_3. \quad (c)$$

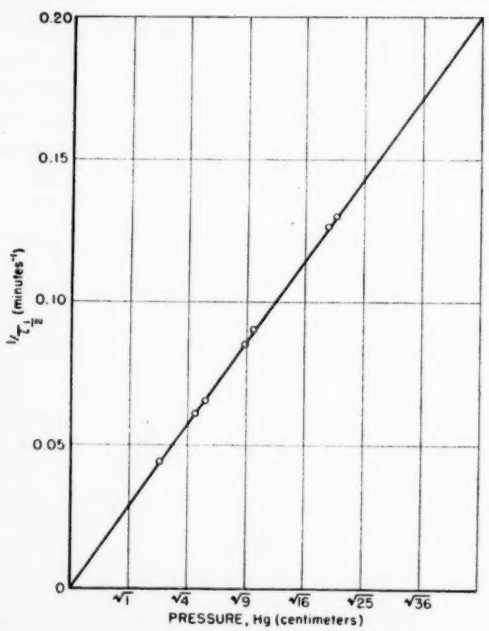

FIG. 8. A plot of the square root of total pressure *vs* $1/t_{\frac{1}{2}}$ for the self-deuteration reaction $B_2H_6+B_2D_6 \rightarrow 2BH_3-BD_3$.

[12] R. N. Pease, *Equilibrium and Kinetics of Gas Reactions* (Princeton University Press, Princeton, New Jersey, 1942).
[13] N. Semenoff, *Chemical Kinetics and Chain Reactions* (Oxford University Press, London, England, 1935).

TABLE III. Pressure and surface dependence of the self-deuteration reaction at 24°C.

	Total pressure[a] (cm)	$t_{\frac{1}{2}}$ (sec)	k (sec^{-1}) $\times10^3$	$k/p^{\frac{1}{2}}\times10^6$
	39.0	421	1.65	2.64
	39.2	475	1.46	2.33
	20.6	600	1.16	2.56
	18.0	630	1.10	2.59
[b]	9.8	900	0.77	2.44
[c]	10.0	840	0.83	2.61
[d]	10.0	915	0.76	2.40
[e]	10.2	900	0.77	2.41
	9.6	915	0.76	2.44
	9.4	957	0.73	2.37
	9.0	960	0.72	2.41
	4.8	1140	0.61	2.78

[a] B_2H_6 and B_2D_6 at equal pressures.
[b] 30 cm N_2 gas present.
[c] Packed with Pyrex rods.
[d] Packed with Pyrex rods.
[e] 50 cm A gas present.

The terminating step is the recombination of borine and deuterated borine radicals. Although this reaction can take place in the gas phase, we assume that it is predominantly a surface reaction. In our series of steps, therefore, we have a chain involving deuterated borine radicals starting on the wall and terminating on the wall, and under such conditions it has been pointed out[12] that the rate will not be greatly influenced by increasing the surface to volume ratio.

The application of conventional steady-state considerations to these reactions indicates that at high pressures the over-all reaction should show a $\frac{3}{2}$-order dependence on diborane and should be independent of the deuterium concentration.

The presence of an inert gas such as nitrogen, helium, etc., can produce many effects in a complex series of reactions as pictured above. In step (b) gases that are readily absorbed can compete for the available surface

with the deuterium and, consequently, slow down the reaction. Rare gases such as helium would not be expected to compete too seriously and hence would not produce an appreciable effect. This has been observed.

The Self Deuteration Exchange Reaction

Kinetics

Intimately connected with the deuterium diborane exchange is the exchange reaction between normal and completely deuterated diborane. This exchange was found to proceed quite rapidly at room temperature and was studied over a temperature range from 24°C to 44°C.

The progress of the exchange is given by the equation

$$P_t - P_\infty = (P_0 - P_\infty)e^{-kt}, \qquad (4)$$

P_0, P_t, and P_∞ denote the B_2H_6 pressure at the time $t=0$, t, and $t=\infty$, respectively. The over-all order of reaction n was determined by the relation

$$t_{\frac{1}{2}}p^{n-1} = \text{constant}$$

TABLE IV. Temperature dependence of the self-deuteration exchange reaction.

Temp °C	Total pressure[a] (cm)	$t_{\frac{1}{2}}$ (sec)	$k/p^{\frac{1}{2}}\times10^4$
24	10	840	2.61
29	10.47	420	5.10
34	10.21	240	9.05
44	8.95	103	22.5

[a] B_2H_6 and B_2D_6 at equal pressures.

and is 1.5 as can be seen in Fig. 8 where the square root of the pressure is plotted against $1/t_{\frac{1}{2}}$.

The pressure dependence of the velocity constant k is shown in Table III, and it is evident that k is proportional to the square root of the pressure. Column 2 gives the "half-life period" ($t_{\frac{1}{2}}$) in which P_0-P_∞ falls to $\frac{1}{2}(P_0-P_\infty)$.

The rate constant k has been determined at several temperatures, and its coefficient is determined by plotting $\log k$ against $1/T$. These results give an experimental apparent activation energy of $21.8k\pm3$ cal. The results of these determinations are given in Table IV and shown in Fig. 9. The reaction does not appear to be appreciably affected by the addition of inert gases nor by increasing the surface to volume ratio from 1 to 10 as shown in Table III.

Mechanism of the Exchange

The B_2D_6-B_2H_6 exchange appears to be a homogeneous gas phase exchange since varying the surface and adding inert gases failed to produce any noticeable effects. It, therefore, appears that the following mechanism is compatible with our experimental results.

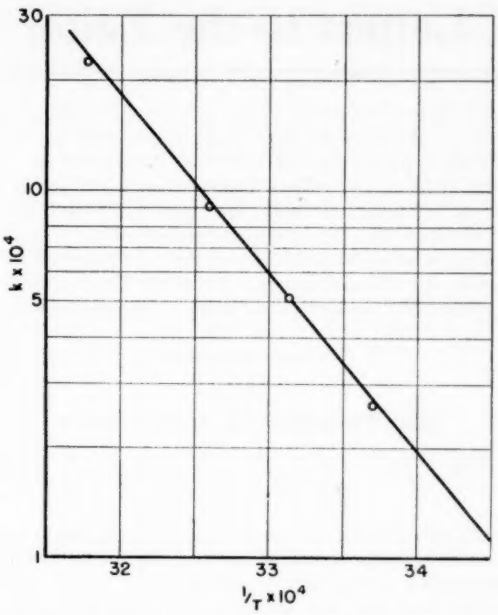

FIG. 9. Temperature dependence of the self-deuteration reaction.

$$B_2H_6 \rightleftarrows 2BH_3 \quad B_2D_6 \rightleftarrows 2BD_3, \qquad (d)$$

$$BH_3 + B_2D_6 \rightarrow BH_3 - BD_3 + BH_3, \qquad (e)$$

$$BD_3 + B_2H_6 \rightarrow BH_3 - BD_3 + BH_3. \qquad (f)$$

The steps (e) and (f) are rate determining and account for the $\frac{3}{2}$ order of the reaction. Although one might expect from the discussion of the deuterium-diborane exchange to observe some surface dependence in this reaction, it probably is obscured by the much greater rate of the homogeneous exchange which is due to the greater concentration of the deuterated species. The apparent activation energy of this reaction is to within experimental error the same as the activation energy of the deuterium-diborane reaction.

ACKNOWLEDGMENT

We wish to acknowledge the use of facilities and technical assistance of Dr. I. Mador and Ruth Quinn of the Applied Physics Laboratory of The Johns Hopkins University.

We wish to thank Mr. Somers Smith of the Naval Research Laboratory, Washington, D. C., for some samples of diborane that were used in this work, and thanks are due Dr. Lewis Friedman of the Brookhaven National Laboratory for mass spectrometric analyses of some deuterium-hydrogen mixtures.

We are also indebted to Dr. A. N. Webb of the University of California for making the results of some of his preliminary studies on these reactions available to us.

Letters to the Editor

THIS section will accept reports of new work, provided these are terse and contain few figures, and especially few half-tone cuts. The Editorial Board will not hold itself responsible for opinions expressed by the correspondents. Contributions to this section should not exceed 600 words in length and must reach the office of the Editor not later than the 15th of the second month preceding that of the issue in which the Letter is to appear. No proof will be sent to the authors. A publication charge of $10.00 per Letter is made which, when honored, will entitle the Institution to 100 free reprints.

The Photolysis of Acetaldehyde

G. O. PRITCHARD, H. O. PRITCHARD, AND A. F. TROTMAN-DICKENSON
Chemistry Department, The University, Manchester, England
(Received January 5, 1953)

THE high temperature photolysis of acetaldehyde using the rotating sector technique has been studied by Dodd.[1] From a consideration of his results and those of other workers, he concluded that all the available data led to $10^{13.3\pm0.4}T^{\frac{1}{2}}\times\exp[(-10.7\pm0.5)/RT]$ for the rate constant of the chain-propagating step, where the units are mole, cc, and sec. However it seemed[2] that, in view of the relative rates of formation of methane and ethane in the low temperature photolysis, all high values for the activation energy of the reaction of methyl with acetaldehyde (generally believed to be the rate determining propagation step) should be viewed with suspicion, because the pre-exponential factor would have to be 10^2 greater than had ever been found for a methyl radical reaction of that type.

Recently the rate constant of the reaction

$$\mathrm{CH_3+CH_3CHO}\xrightarrow{k_1}\mathrm{CH_4+CH_3CO} \qquad (1)$$

has been found by Volman and Brinton[3] to be $4.2\times10^{10}T^{\frac{1}{2}}\times\exp[(7.5\pm0.3)/RT]$ from studies of the decomposition of di-*t*-butyl peroxide in the presence of acetaldehyde, combined with the value for the rate constant for the recombination of methyl radicals found by Gomer and Kistiakowsky,[4] on which all rate constants referred to hereinafter are based.

We have recalculated the data reported by Danby, Buchanan, and Henderson[5] on the amounts of methane and ethane formed in the photolysis of acetaldehyde at 300°C and find that $k_1=1.22\times10^9$.

Additional values of k_1 may be obtained by combining Majury and Steacie's[6] value of $k_2=9.4\times10^{11}\exp(11.8/RT)$,

$$\mathrm{CH_3+D_2}\xrightarrow{k_2}\mathrm{CH_3D+D} \qquad (2)$$

with Davison and Burton's[7] values for k_1/k_2 at different temperatures.

A considerably less accurate point may be deduced making certain plausible assumptions from the work of Blacet and Brinton[8] which seems to be the only data on the production of methane and ethane at low temperatures.

All these data, which have not been correlated before, are shown in Fig. 1. Bearing in mind the separate pieces of work upon which the values depend, the consistency is very satisfactory. This shows first that the older photolytic data cannot be interpreted as simply as had been supposed, and secondly, that the values of k_2 obtained by Davison and Burton using acetaldehyde as a radical source are in effective agreement with those of Steacie.

The most likely cause of the discrepancy between the value of E_1 and the temperature coefficient of the chain propagation in the photolysis is that the chain step cannot be written

$$\mathrm{CH_3+CH_3CHO}\rightarrow\mathrm{CH_4+CH_3+CO}$$

but must be split into reactions (1) and (3)

$$\mathrm{CH_3CO}\xrightarrow{k_3}\mathrm{CH_3+CO}. \qquad (3)$$

This distinction will only be important if $k_1[\mathrm{CH_3CHO}]$ is of the same order of magnitude as k_3. Assuming as a maximum value that $k_4=5\times10^{13}$,

$$2\mathrm{CH_3CO}\xrightarrow{k_4}(\mathrm{CH_3CO})_2, \qquad (4)$$

we may estimate from the work of Howland and Noyes[9] a maximum value for k_3 at 25°C of 4 $\mathrm{sec^{-1}}$ which may be compared with $k_1[\mathrm{CH_3CHO}]=10$ $\mathrm{sec^{-1}}$ at the same temperature and 100-mm

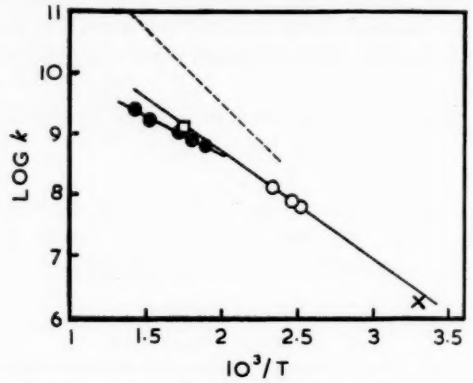

FIG. 1. Arrhenius plot for the reaction of methyl radicals with acetaldehyde. ---- Dodd; ○ Volman and Brinton; □ Danby, Buchanan, and Henderson; × Blacet and Brinton; ● Davison and Burton.

acetaldehyde pressure. Since E_3 is probably low, this near equality may persist over a considerable range of temperature. Furthermore, the kinetics deduced from the two assumptions may be almost indistinguishable if the rate equation for the decomposition should be written as $k_3'[\mathrm{CH_3CO}]P$ where P is the total pressure of the system. This is very likely in view of the simplicity of the acetyl radical[10] and the low value of E_3/RT.

Hence we conclude that little reliance should be placed upon the rate constants determined by the rotating sector, because the method is notoriously inaccurate when the precise mechanism of a reaction is not well defined.

[1] R. E. Dodd, J. Chem. Phys. **18**, 234 (1950); Trans. Faraday Soc. **47**, 56 (1951).
[2] A. F. Trotman-Dickenson and E. W. R. Steacie, J. Phys. Colloid. Chem. **55**, 908 (1951).
[3] D. H. Volman and R. K. Brinton, J. Chem. Phys. **20**, 1764 (1952).
[4] R. Gomer and G. B. Kistiakowsky, J. Chem. Phys. **19**, 85 (1951).
[5] Danby, Buchanan, and Henderson, J. Chem. Soc. **1951**, 1426. The photolysis rates in Table II are in mm/min; private communication from Dr. Danby.
[6] T. G. Majury and E. W. R. Steacie, Can. J. Chem. **30**, 800 (1952).
[7] S. Davison and M. Burton, J. Am. Chem. Soc. **74**, 2307 (1952). Only the runs of 2 or 3-min duration have been considered.
[8] F. E. Blacet and R. K. Brinton, J. Am. Chem. Soc. **72**, 4715 (1950).
[9] J. J. Howland and W. A. Noyes, Jr., J. Am. Chem. Soc. **63**, 3404 (1941).
[10] Compare CH_3I, C. Horrex and R. Lapage, Disc. Faraday Soc. **10**, 233 (1951), and CH_2CO, G. B. Kistiakowsky and W. L. Marshall, J. Am. Chem. Soc. **74**, 88 (1952).

The Photolysis of Acetaldehyde

R. E. DODD
Division of Pure Chemistry, National Research Council, Canada
(Received January 26, 1953)

VOLMAN and Brinton[1] have determined the rate of reaction (1) in the only well-defined experiment not involving the photolysis of acetaldehyde. They have suggested that the lower activation energy, supported by a more probable pre-exponential factor, points to a greater complexity in the photolysis than had been supposed hitherto. To that extent I agree with them and with Pritchard, Pritchard, and Trotman-Dickenson.

It has been shown[2] that a unimolecular chain termination, with an activation energy of 7.8 kcal/mole as proposed by Haden and Rice,[3] raises the reported activation energies for the over-all photolytic rate to 10.4 kcal/mole. The correction, however, is not valid if, as later suggested by Lucas and Rice,[4] the unimolecular termination is independent of temperature. It is therefore probable that other complexities of mechanism are also responsible for the variation in the found photolytic activation energies, 8.5–10.0 kcal/mole, which appear to be related to the light intensities used.

Volman and Brinton[1] have also suggested, and given evidence for, the participation of the acetyl radical in the induced decomposition: it is, of course, kinetically significant, aside from sector experiments, only if it suffers a fate alternative to dissociation. Acetone and biacetyl would probably not be formed in the high temperature photolysis in amount sufficient for detection provided the methyl recombination is the principal chain ending step. That acetyl dissociation is not significantly rate-determining, according to an equation $R=k_3'[CH_3CO]P$, is indicated by the absence of an observable effect on the rate of photolysis at 400° and 240° of the addition of an equal amount of oxygen-free nitrogen.[5] Lucas and Rice[4] report a slight increase in the rate of 200° with the addition of a fourfold excess of carbon dioxide.

Data are, unfortunately, not available from one source for an estimate of the temperature-dependence of the ratio $R_{CH_4}/R_{C_2H_6}$ in the photolysis: the one point in Fig. 1, based upon the data of Danby, Buchanan, and Henderson,[6] includes the value for the rate of change of pressure the meaning of which is now in question. An alternative cause of the discrepancy is the initiation of chains by formyl radicals, or hydrogen atoms:[6,7] the possibility must then not be overlooked that this may make a contribution to R_{CH_4} extra to reaction (1).

Admittedly the temperature-dependence of the photolysis with intermittent illumination cannot now be used to set a lower limit of 9.9 kcal/mole to E_1. It is not clear what behavior would be expected from a mechanism involving two or three interdependent chain centers, but the experimental points remain and a valid mechanism must take them into account.

[1] D. H. Volman and R. K. Brinton, J. Chem. Phys. **20**, 1764 (1952).
[2] R. E. Dodd, J. Chem. Phys. **18**, 234 (1950); Trans. Faraday Soc. **47**, 56 (1951).
[3] W. L. Haden and O. K. Rice, J. Chem. Phys. **10**, 445 (1942).
[4] V. E. Lucas and O. K. Rice, J. Chem. Phys. **18**, 993 (1950).
[5] J. W. Smith, unpublished work.
[6] Danby, Buchanan, and Henderson, J. Chem. Soc. **1951**, 1426. The photolysis rates in Table II are in mm/min; private communication from Dr. Danby.
[7] A. S. Buchanan, J. Chem. Soc. **1951**, 2317.

Note on the Rate of Recombination of Free Atoms

GIORGIO CARERI
Istituto di Fisica dell'Università, Roma, Istituto Nazionale di Fisica Nucleare—Sezione di Roma, Italy
(Received January 19, 1953)

THE recombination rate of two free A atoms to form an A_2 molecule can be calculated considering (1) the direct impact between the two atoms and a third body N (which takes away the excess of energy), or (2) the reverse process of the dissociation of the A_2 molecule following the impact on an N molecule. Both these mechanisms have been used to study the recombination of free iodine and bromine atoms, and the theoretical calculations have been in fair agreement with the experimental data: (1) by Rabinowitsch[1] and Wigner[2] and (2) by Rice[3] and the present author.[4] As the mechanisms of dissociation of A_2 molecules as treated by Rice and the author are different, we thought it might be of some interest to apply their methods to the recombination of free H atoms, hoping to throw some light on the nature of this process.

The recombination rate of free H atoms has been experimentally measured by several experimenters[5] but their results show poor agreement. An analysis of the experiments described in the literature, has led the author[4] to regard as doubtful the results of Senftleben and Hein; with the exception of these, the others all indicate a value of $(2.5\pm2)\times10^{-32}$ cc^2 molecule^{-2} sec^{-1}, when H_2 is the third body.

Details of method (I) will not be given. If one uses the Wigner approach, assuming the Morse curve for the H_2 molecule, and a probability factor 1/4 for two H atoms to follow the $^1\Sigma$ curve, one can evaluate the upper limit, for the recombination rate with H_2 molecule as third body, to be $k_R=19.7\cdot10^{-32}$ cc^3 molecule^{-2} sec^{-1}. As a matter of fact the assumed experimental value is smaller by a factor 10, which is very reasonable, as the same thing happens in the case of iodine and bromine atoms recombining on helium and argon atoms.

As stated previously the recombination rate constant k_R can also be deduced from the dissociation rate constant k_D following the impact of the molecule on a third body, using the equation

$$K=k_D/k_R, \tag{1}$$

K being the equilibrium constant of the $H_2=H+H$ reaction which can be easily calculated. k_D has been calculated by Rice and by the author in two different ways. The author's method is an application of the collision theory to the dissociation reaction which was considered a bimolecular one of the second order; it was also assumed that only those molecules dissociate the energy of which (both the energy of the internal degrees of freedom plus the translation mutual energy at the impact) is not smaller than the dissociation energy D. It is rather obvious that the translational energy ϵ_t and the vibrational energy ϵ_v must contribute to dissociation. However one must also consider the rotational energy ϵ_J, since a different potential energy curve is obtained for each rotational quantum number, as it is shown in Fig. 1. The dissociation by rotation is a familiar process in molecular spectroscopy.

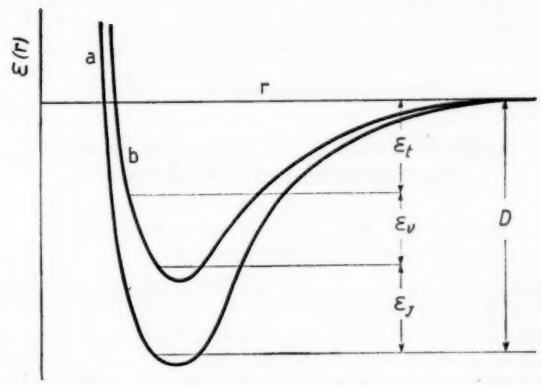

FIG. 1. Potential energy curves for diatomic molecule: (a) without rotational energy, and (b) including rotational energy ϵ_J. The very small maximum in the b curve at large r has been neglected.

Considering the H_2 molecule as a quantized Morse oscillator and a classically excited rotator, the present author got the expression

$$k_D=2\alpha d^2(2nkT/\mu)^{\frac{1}{2}}P_D$$

$$P_D=\{1-\exp(-h\nu/kT)\}\exp(-D/kT)[h\nu/12kT-1+(D/kT)(2kT/h\nu-\tfrac{1}{3})+(D/kT)^2 2kT/3h\nu], \tag{2}$$

d being the molecular diameter, μ the reduced mass, and α a steric factor which indicates the probability that dissociation will take place when the conditions imposed by the conservation of energy are satisfied. Equation (2) appears to be correct both in the case of the hydrogen, and that of bromine and iodine, taking $\alpha=1/5$ to $1/10$ which we regard as a reasonable value. Since the harmonic oscillator model gives essentially the same results as the Morse oscillator, the interaction between rotation and vibration has been neglected.

Let us now examine Rice's method. It is assumed that only those molecules with vibrational energy differing from the dissociation energy by a quantity comparable with kT, which can be acquired from an impact with other molecules, dissociate. The difference between the two methods can be stated as follows. The

present author assumes the probability of high energy collisions and of excited rotational states to be comparable with that of vibrationally excited states, and all these probabilities are added with the proper weights. Rice instead assumes that only ordinary thermal collision of extremely high vibrationally excitated molecules are responsible for dissociation. On the last assumption the dissociation rate is simply given by the number of collisions per unit volume and per second times the Boltzmann factor

$$k_D = 2d^2(2nkT/\mu)^{\frac{1}{2}} \exp(-D/kT). \quad (3)$$

We must evaluate the statistical weight of these excited energy states. In the case of iodine and bromine this has been estimated to be about 5, and the number of vibrational levels, differing by less than kT from the dissociation limit, about 20; Eq. (3) must then be multiplied by a factor 100. It then agrees with the experimental results. Using the same method with the hydrogen we notice that, as we know from spectroscopic data, only molecules in the $^1\Sigma$ state dissociate thermally at normal temperature, and that between the dissociation limit D and $D-kT$ only one level of vibrational energy exists,[6] so that the statistical weight in this case should be taken as 1. Equation (3) gives then for k_D a value nearly 100 times too small.

Because of this disagreement we are led to the conclusion that the methods used by Wigner and the author are more likely to yield a correct calculation of these rates.

The author wishes to thank Professor O. K. Rice for a useful discussion on this subject.

[1] E. Rabinowitch, Trans. Faraday Soc. **33**, 283 (1937).
[2] E. Wigner, J. Chem. Phys. **5**, 720 (1937); **7**, 646 (1939).
[3] O. K. Rice, J. Chem. Phys. **9**, 258 (1941).
[4] G. Careri, Nuovo cimento **6**, 94 (1949); **7**, 155 (1950).
[5] W. Steiner, Trans. Faraday Soc. **31**, 623 (1935); I. Amdur, J. Am. Chem. Soc. **60**, 2347 (1938); L. Farkas and H. Sachsse, Z. physik Chem. **B27**, 111 (1934); H. Senftleben and W. Hein, Physik Z. **35**, 985 (1934).
[6] See, for instance, A. G. Gaydon: *Dissociation Energies* (London, 1947).

Reply to Careri's "Note on the Rate of Recombination of Free Atoms"

O. K. Rice
University of North Carolina, Chapel Hill, North Carolina
(Received January 19, 1953)

DR. Careri[1] has been kind enough to send me his letter before publication, and I have also had the opportunity of discussing this problem with him personally. His procedure amounts to finding an upper limit to the rate constant k_D for the dissociation of a diatomic molecule by finding first the total number of collisions per cc/sec made at unit concentrations with inert gas molecules in which the energy of the diatomic molecule plus the mutual translational energy is sufficient to produce dissociation. It is then assumed that a certain fraction of these collisions, of the order of 0.1, to be found empirically, actually results in dissociation.

Although the collisions described are all capable of producing dissociation, provided the energy gets redistributed in the proper way, their number has no direct connection with the number of effective collisions. The latter can be discussed with reference to Fig. 1, which shows the potential energy curve of the diatomic molecule. The ratio of the effective collisions to the total number of collisions, as obtained from kinetic theory [Careri's Eq. (3)], is equal to the number of energy levels which leave the dissociating molecule after collision in some state in which the interatomic distance is less than some value r' and in which the energy lies between the dissociation limit and about kT above the dissociation limit [see shaded area (1) on the figure] *times* the appropriate Boltzmann factor *divided by* the number of levels in a similar energy range [shaded area (2)] near the bottom of the potential energy curve. [If the zero-point energy of vibration is large, we must substitute for the number of levels in area (2) the number of energy levels for which the vibrational quantum number is zero.] There will be some uncertainty in estimating r', but it should be of the order of magnitude of the distance at which the potential energy curve comes close (within less than kT) to its asymptotic value. In my paper on the recombination of I and Br atoms[2] I used the number of energy levels in area (3) rather than in area (1), but this should be a reasonably good approximation. Taking into account the electronic multiplicity in the regions (3) and (2) for I_2 and Br_2, and considering the density of vibrational levels, I concluded that the density of levels in area (3) was about 100 times that in area (2). However, for H_2 a similar calculation will give a ratio of the order of 1, as Careri states. If, on this basis, one accepts Careri's suggested value of 2.5×10^{-32} cc^2 molecule^{-2} sec^{-1} for the value of the third-order recombination $H+H+H_2\rightarrow 2H_2$ uses Careri's Eq. (1) to obtain k_D, and then calculates the effective collision diameter d from Careri's Eq. (3) (where $\alpha=1$), one obtains $d=16$A, clearly much too large.

However, there is another factor, which I overlooked, and to which attention is now called by Careri. This is the effect of rotation. It is not true that rotational energy is as effective in producing dissociation as vibrational energy. The small maximum at large r (approximately r') which Careri neglects in his Fig. 1,

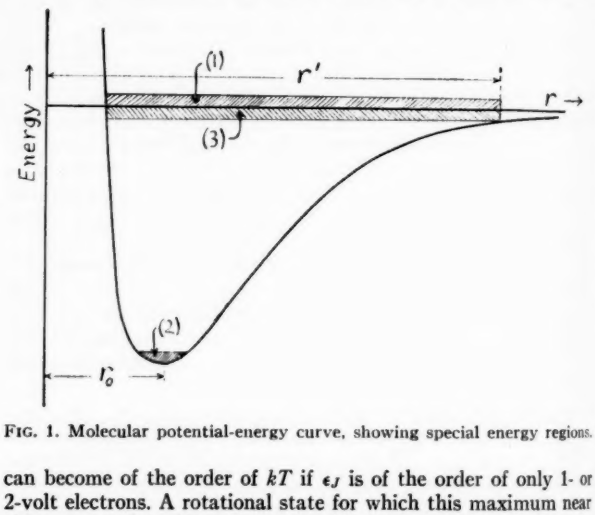

FIG. 1. Molecular potential-energy curve, showing special energy regions.

can become of the order of kT if ϵ_J is of the order of only 1- or 2-volt electrons. A rotational state for which this maximum near r' is greater than kT will not contribute appreciably to the rate of dissociation, but those for which it is of the order of kT can contribute. The effect of rotation, then, is taken into account by multiplying the previously calculated number of effective collisions by another factor, namely, the ratio of the density of low rotational states at r' to the density for a normal molecule with $r\sim r_0$; this ratio is equal to[3] r'^2/r_0^2. It should not be too important in the iodine or bromine case, but for hydrogen since $r_0=0.74$A and r' is about[4] 4.5A, it is probably around 36. This reduces d to 2.7A.

It should, perhaps, be noted that Smallwood,[5] who made the most direct determination of the rate of recombination of hydrogen atoms, concluded that the rate of $H_2+2H\rightarrow 2H_2$ was less than 0.02 times the rate of $3H\rightarrow H_2+H$ with the rate constant for the latter given as 4.7×10^{-32} cc^2 molecule^{-2} sec^{-1}. It seems not at all unlikely (looking at it from the point of view of the reverse process) that $H_2+H\rightarrow 3H$ would be a more efficient process than $2H_2\rightarrow H_2+2H$ because of the unsaturated character of H. If Smallwood's result is correct, the value of d for the reaction $2H_2\rightarrow H_2+2H$ is really surprisingly small, but the reaction $H_2+H\rightarrow 3H$, after taking into account the ratio r'^2/r_0^2, requires $d\sim 3.2$A, a very reasonable value.

Finally, it should be emphasized that my treatment of the recombination reaction by considering the reverse reaction is in no way inconsistent with Wigner's method. It is merely a somewhat simpler method of calculation. It is somewhat easier to consider binary collisions followed by a condition in which one of the molecules is in the area (1) of Fig. 1, than it is to consider ternary collisions preceded by a condition in which one of the

pairs of atoms is in the area (1) of Fig. 1. Looked at in this way, the two methods are seen to be precisely equivalent, at least as far as general principles are concerned.

[1] G. Careri, J. Chem. Phys. **21**, 749 (1953).
[2] O. K. Rice, J. Chem. Phys. **9**, 258 (1941).
[3] Compare O. K. Rice and H. Gershinowitz, J. Chem. Phys. **2**, 853 (1934).
[4] See Eyring, Gershinowitz, and Sun, J. Chem. Phys. **3**, 786, Fig. 1 (1935).
[5] H. M. Smallwood, J. Am. Chem. Soc. **56**, 1542 (1934).

Kinetics of Decomposition of Nitric Oxide

FREDERICK KAUFMAN AND JOHN R. KELSO
Ballistic Research Laboratories, Aberdeen Proving Ground, Maryland
(Received December 15, 1952)

IN a recent paper, Wise and Frech[1] describe the effect of oxygen on the kinetics of the nitric oxide decomposition and propose a mechanism which they use to interpret Vetter's[2] high temperature data. We want to present objections of both experimental and theoretical nature to the results and conclusions of that paper.

Experimentally, we have been totally unable to duplicate the supposed catalytic effect at 1150°K. In our method of analysis (measurement of the amount of nitrogen formed) we observed great care to sweep the entire contents of the quartz reactor into a cold trap completely immersed in liquid nitrogen. This was accomplished by opening the reactor to the evacuated cold trap at the desired time (7 to 30 minutes), closing off the reactor after approximately 10 seconds, and then by rapidly building up a pressure of about ½ atmosphere of pure CO_2 in the reactor, followed by opening to the cold trap and rapid condensation of the CO_2. This process was repeated 4 times within about 20 seconds, and thus the reactor gases were transferred far more completely than by temperature and pressure gradients alone. This CO_2 "diffusion pump" method was calibrated with known mixtures of NO and N_2 as well as NO, O_2, and N_2.

The gas mixture then remained in the cold trap for 10 minutes completely immersed in liquid N_2 before it was connected to an evacuated manometer. Pressure readings of nitrogen were corrected for all expansion and cooling effects and repeated calibrations run.

It is apparent for two reasons that the gas whose pressure we finally measured is only N_2 and not a mixture of N_2 and O_2:

a. In calibration runs on mixtures of NO, O_2, and N_2, the added O_2 had no effect on the N_2 pressure and did not lead to higher pressures of permanent gas.

b. In actual NO decomposition runs the presence or absence of up to 20 mm of O_2 had no effect on the permanent gas pressure which was by calibration equivalent to reactor N_2 pressures of only one to three mm of Hg!

Nitric oxide was purified by P_2O_5 and ascarite absorption, passing through a dry ice-acetone trap, freezing in liquid N_2, and repeated fractional distillation at low temperature. Its infrared spectrum set an upper limit of about 0.2 percent of higher oxides of nitrogen and 0.05 percent of N_2O.

All runs were done at 1150°K with about 400-mm Hg of NO (5.6×10^{-6} mole cc^{-1}) and 10 to 20 mm of O_2 (0.14 to 0.28×10^{-6} mole cc^{-1}) in order to duplicate the conditions described in Table I, line 7 of reference 1. Our surface to volume ratio was 0.61 cm^{-1}. The decomposition rate of NO in the presence of 16-mm O_2 should have increased by a factor of 5.3 over that of pure NO. In 4 blank runs, the NO decomposition rate was $6\pm1.2\times10^{-11}$ mole cc^{-1} sec^{-1} (reported 8.9×10^{-11} mole cc^{-1} sec^{-1}), while in 8 runs with added O_2 we found a rate of $7\pm1.3\times10^{-11}$ mole cc^{-1} sec^{-1} (reported 47.5×10^{-11} mole cc^{-1} sec^{-1}). In some of these runs NO and O_2 were premixed cold, while in others O_2 was admitted to the reactor and followed by NO. The reactor was evacuated to a few microns before some runs, while before others it was evacuated to 1×10^{-5}-mm Hg and baked out for several hours. In some runs O_2 was first admitted at a high pressure, allowed to remain for about 30 minutes, and then pumped out. This treatment might have conditioned the reactor surface, if surface reactions were of importance in our discrepancy. None of the above differences in procedure had any effect on the decomposition rate.

From Wise and Frech's earlier paper[3] one is forced to assume that at the end of reaction time, the contents of their reactor were pumped through a cold trap by means of a Toeppler pump. This may have allowed insufficient time for complete condensation of all condensible gases.

It is interesting to note, moreover, that Vetter's[2] only low temperature run (run 91, 1179°K, $[NO]=6.85\times10^{-6}$ mole cc^{-1} and $[O_2]=3.56\times10^{-6}$ mole cc^{-1}), when corrected for the somewhat higher temperature and NO concentration, gives an NO decomposition rate of about 10×10^{-11} mole cc^{-1} sec^{-1}, only slightly higher than our value, in spite of the very large pressure of O_2 (~350-mm Hg).

In any future experiments designed to resolve this discrepancy, particular care will have to be taken (a) to avoid fractionation of the gas mixture, and (b) to allow ample time for the condensation of NO whose equilibrium vapor pressure at −195.8°C is 0.1-mm Hg. Opening the reactor to an evacuated cold trap and measuring the N_2 pressure above that trap, for example, will almost certainly build up fictitious N_2 pressures as we observed[4] in another reaction.

The mechanism proposed by Wise and Frech,[1]

$$\begin{aligned}
&\text{I} && 2NO \xrightarrow{k_1} N_2O+O,\\
&\text{II} && O+NO \xrightarrow{k_2} O_2+N,\\
&\text{III} && N+NO \xrightarrow{k_3} N_2+O\\
&\text{IV, V} && O+O(+M) \underset{k_5}{\overset{k_4}{\rightleftharpoons}} O_2(+M),
\end{aligned}$$

leads to

$$-\frac{d(NO)}{dt}=2k_1(NO)^2+2k_2(NO)^{\frac{3}{2}}\left\{\frac{k_1}{2k_4(M)}+K_e\frac{(O_2)}{(NO)^2}\right\}^{\frac{1}{2}}$$

under the usual steady-state assumptions. The authors then state that at high O_2 concentration the first term under the square root sign is small compared to the second and obtain $-[d(NO)/dt]=2k_1(NO)^2+2K_e^{\frac{1}{2}}k_2(O_2)^{\frac{1}{2}}(NO)$ to which they fit Vetter's[2] data and calculate k_1.

Substituting $K_e=k_5/2k_4$, the inequality under the square root reduces to $k_5(O_2)(M)\gg k_1(NO)^2$. As it seems unreasonable that the dissociation of O_2 ($\Delta H_0^0=117.3$ kcal) should be faster than the initial NO reaction, we checked the inequality at 1525 and 1912°K using the author's values for k_1 (Table VII), setting $(NO)=1\times10^{-6}$ mole cc^{-1}, $(O_2)=5\times10^{-6}$ mole cc^{-1}, and calculating k_5 from simple collision theory with $\Delta E=117.3$ kcal.

It turns out that at 1525°K, $k_1(NO)^2$ is about 6000 times larger than $k_5(O_2)(M)$, and at 1912°K, it is still about 700 times larger. In order for the proposed mechanism to stand, the actual value of k_5 would have to be 10^4 to 10^5 times larger than that calculated from collision theory. For a simple reaction such as the dissociation of the diatomic molecule O_2 such an explanation is untenable. Thus, it is the oxygen term which is negligible, and all dependence of rate on the oxygen concentration disappears. Since in this calculation we assume a fivefold excess of (O_2) over (NO), the above mechanism is ruled out for any reasonable temperature and concentration range.

Aside from these objections, recent work[5,6] gives increasing weight to the high value of D_{N_2} (225 kcal) and thereby eliminates reaction II as part of a chain process.

[1] H. Wise and M. F. Frech, J. Chem. Phys. **20**, 1724 (1952).
[2] K. Vetter, Z. Elektrochem. **53**, 369 (1949).
[3] H. Wise and M. F. Frech, J. Chem. Phys. **20**, 22 (1952).
[4] F. Kaufman and J. R. Kelso, J. Am. Chem. Soc. **74**, 2694 (1952).
[5] Thomas, Gaydon, and Brewer, J. Chem. Phys. **20**, 369 (1952).
[6] Kistiakowsky, Knight, and Malin, J. Chem. Phys. **20**, 876 (1952).

Comments on the Kinetics of Thermal Decomposition of Nitric Oxide

HENRY WISE AND MAURICE F. FRECH
Jet Propulsion Laboratory, California Institute of Technology, Pasadena, California
(Received January 6, 1953)

KAUFMAN and Kelso[1] describe some experimental measurements on the rate of thermal decomposition of nitric oxide in which they are unable to observe the pronounced catalytic influence of oxygen on the reaction kinetics of nitric oxide as previously reported by us.[2] Such a catalytic effect has been noted by Vetter;[3] it is also suggested by the results of Gilbert and Daniels.[4,5] In an attempt to resolve this discrepancy Kaufman and Kelso point to the possibility of an error in our analysis of the products of decomposition.

Since we are quite aware of such sources of error as encountered by them,[6,7] our experimental technique[2,8] is so designed to transfer all the reaction products from the reactor into a cold trap by means of a Toeppler pump circuit. Subsequently, after the oxygen has been allowed to react with residual nitric oxide at room temperature, and the $NO_2=N_2O_4$ thus produced has been condensed out in a trap cooled by liquid nitrogen, the remaining noncondensable gas—i.e., N_2—is pumped off quantitatively into a gas burette.* Mass spectrometric analysis of this noncondensable gas indicated the absence of oxygen.

In contrast to this technique, the measurements of Kaufman and Kelso[1] differ not only in the experimental method of transfer of the reacted gas mixture, but also in the analysis of the noncondensable products. It is apparent that the pressure registered on their manometer[1] must be due to N_2 and O_2. Such a determination, therefore, involves the measurement of a small pressure difference representing the amount of N_2 and O_2 produced from the decomposition of NO. An unknown quantity of the oxygen present in the mixture may react with residual NO during the transfer and cooling process, thereby decreasing the total amount of noncondensable gas. Also, the entrainment of noncondensable gas in the relatively large amounts of CO_2 used by Kaufman and Kelso may further result in producing an apparently lower decomposition rate.

Although the decomposition of NO at 1150°K has been shown to be predominantly heterogeneous,[8] the authors neglect to consider the smaller surface-to-volume ratio (S/V) of their reaction vessel, as compared to the one used by us.

For pure nitric oxide our measurements[2] of the decomposition rate exceed by 50 percent those reported by Kaufman and Kelso,[1] which is in line with the difference in S/V of the reaction vessels employed in these two investigations. It also appears from our results reported in Table II of reference 2 that the catalytic influence of oxygen on the rate of decomposition of nitric oxide is more pronounced at 980°K, than at 1150°K suggesting a heterogeneous catalysis in this temperature region. Thus the difference in S/V of the reaction vessels may be responsible for the apparent disagreement reported.[1]

It should be pointed out that the experimental measurements by Vetter[3] on the reaction rate of nitric oxide in the presence of oxygen at 1179°K definitely indicate the catalytic influence of oxygen contrary to the conclusions of Kaufman and Kelso.[1] Based on the rate constant as given by Fig. 2 of reference 2, the decomposition rate of NO in the absence of O_2 amounts to 1×10^{-10} mole cc^{-1} sec^{-1} at 1179°K, whereas Vetter, in the presence of oxygen, measured a rate of 3×10^{-10} mole cc^{-1} sec^{-1}.

Concerning the questions raised on the proposed mechanism, it is well known that the observed specific reaction rates of many unimolecular reactions are several orders of magnitude larger than those calculated from the collision theory equation. Particularly in those reactions in which the reactant undergoing unimolecular decomposition may acquire its energy by transfer of kinetic energy from a foreign gas (M) with subsequent conversion of this energy into vibrational energy, it is questionable whether simple collision theory offers an adequate quantitative picture of the process. The relative efficiency of various gases in facilitating the recombination of halogen atoms[9] may be cited as an example.

One may conclude therefore that a more refined analysis is required to calculate the relative magnitudes of the terms appearing under the square-root sign of the final rate expression (4) of reference 2. Under these circumstances a comparison of rate constants based on collision theory is of little significance.

It also should be noted that the final form of the rate expression (4) may be obtained if one assumes the concentration of oxygen atoms to be given by the equilibrium between oxygen atoms and molecules. Such a condition would be favored by high concentrations of oxygen in agreement with the assumption made in deriving Eq. (4).

[1] F. Kaufman and G. R. Kelso, J. Chem. Phys. **21**, 751 (1953).
[2] H. Wise and M. F. Frech, J. Chem. Phys. **20**, 1724 (1952).
[3] K. Vetter, Z. Elektrochem. **53**, 269 (1949).
[4] Gilbert and Daniels, Ind. Eng. Chem. **40**, 1719 (1948).
[5] H. Wise and Baker, (to be published).
[6] Fenimore and G. R. Kelso, J. Am. Chem. Soc. **74**, 1593 (1952).
[7] F. Kaufman and G. R. Kelso, J. Am. Chem. Soc. **74**, 2694 (1952).
[8] H. Wise and M. F. Frech, J. Chem. Phys. **20**, 22 (1952).
* A correction is applied for the vapor pressure of nitric oxide at the temperature of liquid nitrogen.
[9] E. Rabinowitch and W. C. Wood, J. Chem. Phys. **4**, 497 (1936).

Microwave Spectrum and Structure of SiD_3F

BØRGE BAK, JØRGEN BRUHN, AND JOHN RASTRUP-ANDERSEN
Chemical Laboratory, University of Copenhagen, Copenhagen, Denmark
(Received January 23, 1953)

THE problem of determining the structure of silyl fluoride has been attacked by Sharbaugh, Thomas, and Pritchard,[1] who observed microwave absorption frequencies for $Si^{28}H_3F$, $Si^{29}H_3F$, and $Si^{30}H_3F$. The three structural parameters could, however, not be computed without taking the angle $HSiH=111°\pm1°$ from other monohalogen silanes. We have prepared SiD_3F (by the action of SbF_3 on SiD_3Cl) and measured the absorption frequencies of the three isotopic species in order that the structure may be found exclusively by means of microwave measurements.

As pointed out by Miller, Aamodt, Dousmanis, and Townes[2] in the case of the methyl halides the effect of the zero-point vibrations cannot be neglected. The main effect is that the Si−H distance is larger than the Si−D distance and that the angle H−Si−H differs from the angle D−Si−D. If the large moment of inertia is denoted by $I_B^{D,30}$ for the molecule $Si^{30}D_3F$, $I_B^{H,28}$ for $Si^{28}H_3F$, etc., and if the small moment of inertia is called I_A^H for the "light" compounds, I_A^D for the "heavy" compounds, we have

$$[I_B^{D,28}-\tfrac{1}{2}I_A^D]m_{Si^{28}D_3F}=a^2m_Fm_{Si^{28}}+3(a+d_D\cos\varphi_D)^2m_Dm_F+3d_D^2\cos^2\varphi_Dm_{Si^{28}}m_D, \quad (1)$$

where $m_{Si^{28}D_3F}$, etc. means the mass of $Si^{28}D_3F$, a is the Si−F distance (assumed to be independent of isotopic substitution), d_D is the distance Si−D, and φ_D is the supplementantary angle of the F−Si−D angle. $I_A^D=3m_Dd_D^2\sin^2\varphi_D$. Besides (1) there are 5 similar equations to be fulfilled by the experimental results given in Table I.

By suitable combination of four of the six equations mentioned above, one gets

$$a=\frac{m_Hm_D}{m_F(m_D-m_H)}\left[\left\{\frac{(I_B^{H,30}-I_B^{H,28})m_{Si^{30}H_3F}m_{Si^{28}H_3F}}{m_H^2(m_{Si^{30}}-m_{Si^{28}})}\right\}^{\frac{1}{2}}-\left\{\frac{(I_B^{D,30}-I_B^{D,28})m_{Si^{30}D_3F}m_{Si^{28}D_3F}}{m_D^2(m_{Si^{30}}-m_{Si^{28}})}\right\}^{\frac{1}{2}}+3(d_H\cos\varphi_H-d_D\cos\varphi_D)\right] \quad (2)$$

together with two other analogous expressions for a, in which data for the Si^{29}-containing isotopes are used in connection with data for the Si^{28}- and Si^{30}-containing molecules. If the difference

TABLE I. Observed microwave absorption frequencies for isotopic silyl fluoride molecules (transition $J=0\rightarrow1$).

Species	$\nu_0$mhz	$I_B\times10^{40}$ g cm²	B_0mhz
$Si^{28}H_3F$	28655.8 0.1	58.555	14327.9
$Si^{29}H_3F$	28393.4 0.2	59.096	14196.7
$Si^{30}H_3F$	28145.2 0.2	59.617	14072.6
$Si^{28}D_3F$	24507.0 0.1	68.467	12253.5
$Si^{29}D_3F$	24352.2 0.1	68.902	12176.1
$Si^{30}D_3F$	24204.5 0.2	69.323	12102.2

$d_H\cos\varphi_H-d_D\cos\varphi_D$ is neglected, one calculates $a=1.5935$A [using (2)], $a=1.5941$A (using Si^{29}, Si^{30}), and $a=1.5932$A (using Si^{28}, Si^{29}). If the experimental uncertainty is taken into account, we get $a=1.5935\pm0.0045$A. Now, if it is assumed that 0.01A and 1° are upper limits to d_H-d_D and $\varphi_H-\varphi_D$, respectively, 0.0096A becomes an upper limit to the error in a. This serves as a reason for investigating the solutions of the six fundamental equations mentioned in the interval from $a=1.5890$ to $a=1.6076$. Inserting values of a from this interval in the expression

$$a\frac{m_F}{m_D}-3d_D\cos\varphi_D=\left[\frac{(I_B^{D,30}-I_B^{D,28})m_{Si^{30}D_3F}m_{Si^{28}D_3F}}{m_D^2(m_{Si^{30}}-m_{Si^{28}})}\right]^{\frac{1}{2}},\quad(3)$$

a series of corresponding values of $d_D\cos\varphi_D$ is calculated. If these are inserted in (1) a corresponding series of I_A^D values is obtained. From I_A^D and $d_D\cos\varphi_D$, d_D and φ_D can be calculated separately. Curves representing d_D and φ_D as functions of a can thus be drawn. The same can be done for d_H and φ_H. Taking the uncertainty caused by errors in the frequency determinations fully into account, one obtains the results given in Table II.

TABLE II. Assumed and calculated values of structural parameters.

Assumed values of d_H-d_D	$\varphi_D-\varphi_H$	Calculated values of d_H, d_D	φ_H, φ_D	a
0.005A	7.5′	1.475–1.444A	70°24′–70°03′	1.5951–1.5967A
0.005A	15′	1.470–1.444A	70°39′–70°03′	1.5954–1.5967A
0.010A	15′	1.470–1.452A	70°39′–70°03′	1.5954–1.5958A
0.010A	30′	1.461–1.452A	70°40′–70°00′	1.5946–1.5947A

It is highly satisfactory that the calculated d_H and d_D values are close to 1.456 as found by Tindal, Straley, and Nielsen[3] in the case of SiH_4. Also, the F−Si−H angle is found to be 109°26′–110°, close to the angle of the regular tetrahedron. Of course, the calculations tell nothing of the exact values of d_H-d_D and $\varphi_D-\varphi_H$. They show definitely, however, that these two quantities cannot be as large as 0.02A and 1°, respectively. Solutions for which $\varphi_H>\varphi_D$ do exist. They correspond, however, to values of d_H in the 1.47–1.50A region which is less consistent with the value 1.456A found in SiH_4.

[1] Sharbaugh, Thomas, and Pritchard, Phys. Rev. **78**, 64 (1950).
[2] Miller, Aamodt, Dousmanis, and Townes, J. Chem. Phys. **20**, 1112 (1952).
[3] Tindal, Straley, and Nielsen, Phys. Rev. **62**, 151 (1942).

Microwave Spectrum and Structure of SiD_3Cl

BØRGE BAK, JØRGEN BRUHN, AND JOHN RASTRUP-ANDERSEN
Chemical Laboratory, University of Copenhagen, Denmark
(Received January 20, 1953)

THE pioneer work for silyl chloride has been done by Sharbaugh[1] and by Dailey, Mays, and Townes.[2] Their experimental data together with data for SiD_3Cl (prepared by the action of DCl on SiD_4) are given in Table I. In a previous paper[3] the structure of silyl fluoride was discussed. The microwave absorption frequencies used in the calculations belong to a $J=0\rightarrow1$ transition. Owing to zero-point vibrations, it was assumed that the distances Si−H (d_H) and Si−D (d_D) and the angles F−Si−H (180-φ_H) and F−Si−D (180-φ_D) deviated slightly ($d_H>d_D$, $\varphi_D>\varphi_H$). If a reasonable interpretation of the experimental material of Table I is attempted, additional difficulties emerge. Probably this is due to the effect of centrifugal distortion. At a $J=1\rightarrow2$ transition, the centrifugal distortion term in the expression for the rotational energy is 8 times greater than for a $J=0\rightarrow1$ transition. The correct way out is, of course, to study the absorption of silyl chloride at 11 500–13 500 Mhz and/or at 34 500–40 000 Mhz, but as this is not possible with our present equipment we have had to proceed in the following manner:

TABLE I. Observed microwave absorption frequencies for isotopic silyl chloride molecules (transition $J=1\rightarrow2$).

Species	ν_0Mhz[a]	$I_B\times10^{40}$ g cm²	B_0(Mhz)
$Si^{28}H_3Cl^{35}$	26695.2±0.2	125.711	66673.8
$Si^{30}H_3Cl^{35}$	25943.2 —	129.355	6485.8
$Si^{28}H_3Cl^{37}$	26049.6 —	128.826	6512.4
$Si^{28}D_3Cl^{35}$	23670.8 —	141.773	5917.7
$Si^{29}D_3Cl^{35}$	23402.6 —	143.397	5850.6
$Si^{30}D_3Cl^{35}$	23147.9±0.3	144.975	5787.0
$Si^{28}D_3Cl^{37}$	23091.4±0.2	145.330	5772.8

[a] Corrected for spin influence.

We define

$$K^{30-28,H,35}=\left[\frac{(I_B^{30,H,35}-I_B^{28,H,35})m_{Si^{30}H_3Cl^{35}}m_{Si^{28}H_3Cl^{35}}}{m_H^2(m_{Si^{30}}-m_{Si^{28}})}\right]^{\frac{1}{2}},$$

where $I_B^{30,H,35}$ is the large moment of inertia of $Si^{30}H_3Cl^{35}$. It follows for a *rigid rotor* that

$$a_H\frac{m_{Cl^{35}}}{m_H}-3d_H\cos\varphi_H=K^{30-28,H,35},$$

$$a_D\frac{m_{Cl^{35}}}{m_D}-3d_D\cos\varphi_D=K^{30-28,D,35},$$

$$a_H\frac{m_{Si^{28}H_3}}{m_H}+3d_H\cos\varphi_H=K^{28,H,37-35},$$

$$a_D\frac{m_{Si^{28}D_3}}{m_D}+3d_D\cos\varphi_D=K^{28,D,37-35},$$

where a_H and a_D are the Si−Cl distances in the "light" and "heavy" species. Addition of (1) and (3) now produces an equation giving a_H as a function of measured quantities. We find that $2.0498\text{A}<a_H<2.0507$A. Similarly, a_D may be calculated. It is highly satisfactory that the result becomes $2.0495\text{A}<a_D<2.0507$A.

Now, $d_H\cos\varphi_H$ can be calculated from (1) for values of a in the interval indicated. Likewise, the small moment of inertia, I_A^H, can be found from, e.g.,

$$I_B^{28,H,35}-\tfrac{1}{2}I_A^H=a_H^2\frac{m_{Cl^{35}}m_{Si^{28}}}{m_{Si^{28}H_3Cl^{35}}}+3(a_H+d_H\cos\varphi_H)^2\frac{m_Hm_{Cl^{35}}}{m_{Si^{28}H_3Cl^{35}}}+3d_H^2\cos\varphi_H^2\frac{m_Hm_{Si^{28}}}{m_{Si^{28}H_3Cl^{35}}}.$$

Since $I_A^H=3m_Hd_H^2\sin^2\varphi_H$, a corresponding series of $d_H\sin\varphi_H$ values are obtained so that curves representing d_H and φ_H as functions of a in the interval 2.0497–2.0509A can be drawn. In an analogous manner curves for d_D and φ_D are constructed. We now look for the points of the curves, where $|d_H-d_D|$ and $|\varphi_H-\varphi_D|$ are small. The main features are given in Table II. If our assumed rigid rotor was only disturbed by zero-point vibrations, one would expect $d_H>d_D$. The curves must be extrapolated slightly towards smaller a values ($a=2.0490$A) in order to satisfy this condition.

TABLE II. Calculated values of molecular parameters for silyl chloride.

aA	d_HA	d_DA	d_D-d_HA	φ_H	φ_D	$\varphi_D-\varphi_H$
2.0497	1.444	1.449	0.005	70°23′	70°38′	15′
2.0503	1.422	1.439	0.017	69°40′	70°23′	43′
2.0509	1.400	1.428	0.028	68°57′	70°06′	69′

Anyway, it is seen that the molecular parameters which are in most satisfactory agreement with the experiments and with the condition that $|d_H - d_D|$ must be small: Si–Cl distance = 2.0497A; Si–H, Si–D = 1.44–1.45A; φ_H, $\varphi_D = 70°20'$–$70°40'$ (Cl–Si–H angle = 109°40′–109°20′). This means a confirmation of the result found for SiH_3F; the Si–H distance is close to the same distance in SiH_4 and the valence angles are almost tetrahedral. Probably, the monohalogenated silanes obey the same strict rules as to valence angles magnitude and bond distances as the monohalogenated methanes.

Preliminary measurements of the quadrupole coupling constant for $Si^{28}D_3Cl^{35}$ show that for this molecule $eQ(\partial^2 V/\partial z^2) = -39.4$ Mhz as compared with -40.0 for $Si^{28}H_3Cl^{35}$. This difference is the same as found in the case of CH_3Cl^{35} and CD_3Cl^{35}. For these molecules $d_H - d_D = 0.009$A and $\varphi_D - \varphi_H = 24'$.[4] Differences between the molecular parameters of this order of magnitude must, therefore, also be expected for the silyl chlorides.

[1] A. Harry Sharbaugh, Phys. Rev. **74**, 1870 (1948).
[2] Dailey, Mays, and Townes, Phys. Rev. **76**, 136 (1949); 472 (1949); 700 (1949).
[3] Bak, Bruhn, and Rastrup-Andersen, J. Chem. Phys. **21**, 752 (1953).
[4] Miller, Aamodt, Dousmanis, and Townes, J. Chem. Phys. **20**, 1112 (1952).

Loose Transition States Involving Internal Rotation

N. W. Luft
Cheadle Hulme, Cheshire, England
(Received January 26, 1953)

RECENT experiments[1] showed that the activation energy of recombination E' of methyl radicals is zero, in agreement with a theoretical estimate.[2] The high efficiency was explained by the assumption that the transition state for methyl recombination is loose, i.e., that the recombining radicals retain their freedom of rotation in the transition state.[3] Szwarc[4] used the same argument in order to explain large frequency factors, $\sim 10^{14}$ to 10^{16} sec^{-1}, in the reverse process of unimolecular dissociation of molecules which split into fairly big radicals, e.g., ϕCH_2, ϕCO, etc., (ϕ = phenyl). It may be anticipated, however, that both the assumption of zero-activation energy E' and unrestricted rotation in the transition state do apply only to special cases where the dissociation energy D_e is not too small.

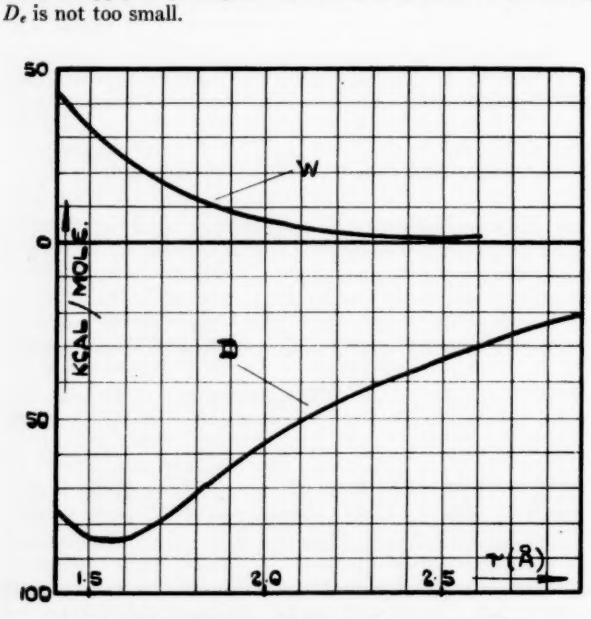

FIG. 1. Potential energy D and repulsive energy W for H_3C-CH_3 dissociation.

The variation of D with bond length r may be expressed as

$$D = U - W, \tag{1}$$

where the bond energy U is suitably represented by a Morse curve,

$$U = U_0\{1 - e^{-a(r-r_0)}\}^2. \tag{2}$$

The repulsive interactions W between nonadjacent charge clouds (at mutual distances R), which are affected by the process, can be estimated by an electrostatic multipole method,[5] $W \sim A/R^6$. By applying Eqs. (1) and (2) and the equilibrium condition $|dD/dr|_{r=r_e} = 0$ to a set of empirical data, one finds

$$U_0 \sim 120 \text{ kcal/mole}, \; r_0 \sim 1.38\text{A}, \; ar_0 \sim 2.6,$$

and the potential energy curve for ethane can be constructed, with $r_e = 1.54$A and $D_e = 84$ kcal/mole (Fig. 1). For ethane, and

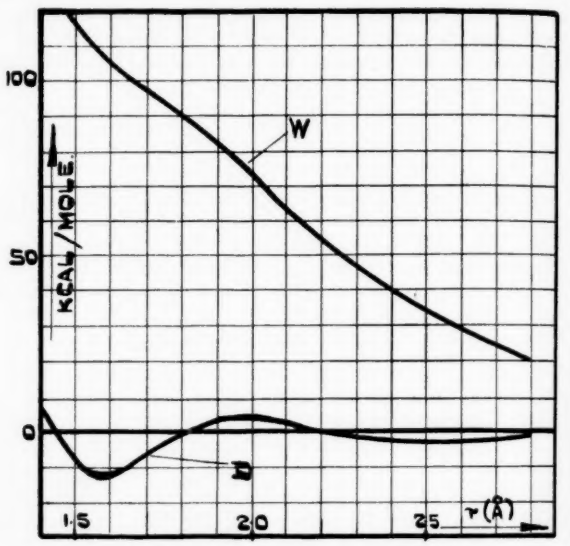

FIG. 2. Approximate variation of potential energy D and repulsive energy W in $\phi_3C-C\phi_3$ dissociation with separation r.

probably for all polymethyl ethanes and most of the substances investigated by Szwarc, D shows no maximum, i.e., $E' \simeq 0$. A maximum may be expected only if $W_e \sim U_e$ for the equilibrium separation r_e, i.e., if D_e is small. This condition applies particularly to compounds with "steric hindrance" about the central bond. Thus experiments[6] do indicate $E' \sim 5$ to 10 kcal for $C\phi_3$ when forming hexaphenyl ethane with $D_e \sim 12$ kcal near $r_e = 1.6$A and probably a shallow minimum for large r (Fig. 2).

Upon dissociation six harmonic modes (frequencies in cm^{-1}), *viz.*, one stretching (ω), one torsional (ω'), and four deformations (ω''), of the original molecule, are replaced ultimately by three additional rotations (B) and three additional translations (B') of the radicals. Intermediate states are characterized by a gradual decrease of the restrictive and mainly asymmetric barriers in the six-dimensional potential hypersurface.

The two examples, represented by Figs. 1 and 2, may serve for purposes of demonstration. With ethane repulsion is very small for $r^* \gtrsim 2.5$A, while U and D are about equal and still large. Since in CH_3, both the distances of the odd electron and the origins of electric multipoles from the center of gravity are small in comparison with r^*, all barriers opposing rotation of the two radicals are small for $r \sim r^*$ and become zero while $D_e - D(r) \to E = D_e$ for $r \gg r^*$.

With hexaphenyl ethane W is still large for r^* and approximately equal to U. In $C\phi_3$ the lone electron is close to the center of gravity, but the distances of multipole origins from it are large in comparison with r^*. Therefore all rotations are severely restricted for $r < r^*$, and in the transition state for dissociation-recombination (maximum near $r = 2.0$A) they are reduced to vibrational movements.

Thus one may draw the conclusion that in transition complexes of dissociation-recombination processes, the radicals possess internal rotational degrees of freedom only if repulsion is small in comparison with the bond energy and thus also $E' \simeq 0$ in recombination.

Similar considerations do apply to the racemization of sterically hindered rotational isomers[7] for which the potential barriers V are expected to be high, $\gtrsim 20$ kcal. If in particular

$$V - D \gtrsim 0, \quad \text{for} \quad r > r_e, \tag{4}$$

then racemization occurs through transition states with 5-dimensional free rotation ($\sim$sign in Eq. 4) or through intermediate dissociation ($>$sign), *viz.*, when the eclipsed configuration is unstable.

The entropy change $\Delta S_{\ddagger}$ resulting from the alteration of any of the six significant modes of movement depends only on $g_i = (\omega_i/B_i)^{\frac{1}{2}}$ and on $f(\omega_i/T)$ which varies between 0.3 and 0.64 for $100 \leq \omega \leq 800$ and $300 \leq T \leq 1000$. For small radicals with $B_i \sim 1$ and $g_i \gtrsim 10$ and five rotational degrees of freedom $\pi^5 f_{i\omega i}$ is about 10^2 to 10^3, i.e., $\Delta S_{\ddagger} \sim 20$ for dissociation. With big radicals $B_i \ll 1$, and $g_i > 10$ increases roughly with the square root of the length of the radical. But these large rotational g_i contribute to $\Delta S_{\ddagger}$ only if D_e is large and $E' \simeq 0$, i.e., if the size of the molecule has not been increased at the price of steric hindrance.

The repulsions have a twofold influence on the rates of dissociation and recombination, *viz.*, through E and $\Delta S_{\ddagger}$, which may weaken or augment each other. In recombination large E' values are associated with small $\Delta S_{\ddagger}'$ so that the rate is the smaller, whereas in dissociation very big E values are connected with large $\Delta S_{\ddagger}$ and small E with small $\Delta S_{\ddagger}$ values, so that the net result is a moderately slow rate. Formally, the latter influence resembles an empirical relation between activation energies and frequency factors in heterogeneous catalysis.

The preceding considerations seem to call for re-interpretation and revision of various experimental dissociation energies which were derived from unimolecular decomposition rates. In particular, the experimental dissociation energy of hydrazine,[8] $E \sim 60$ kcal corresponding to an average frequency factor of 4×10^{12} sec^{-1}, is certainly too low since a theoretical estimate[2] indicates $E' \sim 0$ for the transconfiguration and thus at least some free rotation in the transition state. A tentative estimate is $D(H_2N \cdots NH_2) = 66 \pm 4$ kcal/mole, i.e., $\Delta Hf(NH_2) = 46$ kcal/mole and $D(H \cdots NH_2) = 107$ kcal/mole.

[1] R. Gomer, J. Chem. Phys. **19**, 85 (1951).
[2] N. W. Luft, Disc. Faraday Soc. **12**, 271 (1952).
[3] G. B. Kistiakowsky, Disc. Faraday Soc. *The Reactivity of Free Radicals* (Toronto University Press, Toronto, 1952).
[4] M. Szwarc, (see reference 3).
[5] N. W. Luft, Trans. Faraday Soc. (to be published).
[6] W. A. Waters, *The Chemistry of Free Radicals* (Oxford University Press, London, 1950).
[7] F. W. Cagle and H. Eyring, J. Am. Chem. Soc. **73**, 5628 (1951).
[8] M. Szwarc, J. Chem. Phys. **17**, 107 (1949).

On the Vibrational Raman Spectrum of Gaseous Ethylene*

B. P. STOICHEFF†
Division of Physics, National Research Council, Ottawa, Canada

(Received February 3, 1953)

THE vibrational assignments for ethylene have not yet been definitely established. In particular there is an uncertainty in the frequency of the Raman-active fundamental $\nu_5(b_{1g})$. Two Raman bands at 3075 and 3272 cm^{-1} are available for this assignment. Preference has been given to the 3272 cm^{-1} band,[1,2] since it appears in the spectrum of both gas and liquid, whereas the 3075 cm^{-1} band has been found in the liquid only.[3] However, from a recent study of infrared combination bands, Plyler[4] suggests a frequency of about 3075 cm^{-1}. The lower frequency is also favored by Arnett and Crawford[5] since approximately this value is expected on the basis of the isotopic relations from the analogous band found in liquid C_2D_4. An investigation of the Raman spectrum of gaseous ethylene, as outlined below, has given a direct and satisfactory answer to this problem.

A multiple-traversal Raman tube[6] having an irradiated length of 80 cm and filled with the gas to a pressure of 2 atmos was used in the present study. Raman spectra excited by the Hg 4358 line were photographed on Kodak 103a-J plates in 5–20 hours, with an $f/5$ camera having a dispersion of 130 cm^{-1}/mm. A new band was observed in the region of 3000–3200 cm^{-1}, in addition to eight other bands whose frequencies agree well with those tabulated by Herzberg. As shown in the microphotometer trace Fig. 1, this

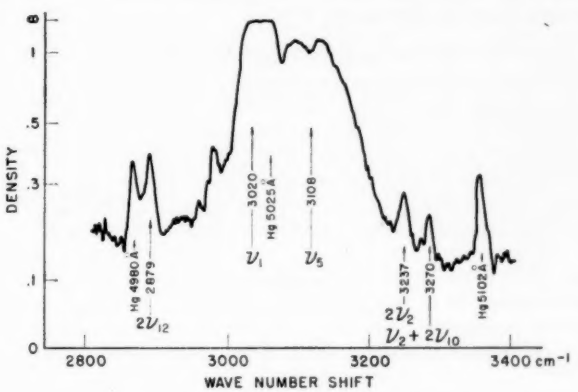

FIG. 1. Microphotometer trace of the 3000 cm^{-1} region in the Raman spectrum of gaseous C_2H_4.

band is a prominent feature in the 3000 cm^{-1} region; it is much more intense than the line-like bands at 3237 and 3270 cm^{-1} and has a pronounced minimum at 3108 ± 5 cm^{-1}. Also, the intensity contour is consistent with that predicted for a b_{1g} fundamental. Thus all the observed characteristics establish the new band as the fundamental $\nu_5(b_{1g})$. It seemed rather puzzling that such an intense band could have escaped detection in the earlier investigations of the gas.[3] However, in the work of Dickinson, Dillon, and Rasetti, who used Hg 2537 excitation, the intense line Hg 2752.8 ($\Delta\nu = 3097$ cm^{-1}) probably masked the band, while the spectra obtained by Bhagavantam with Hg 4358 excitation and the gas at 40 atmos were of low intensity (he did not observe the doublet at 3240 and 3272 cm^{-1}), and pressure broadening of the lines probably resulted in a diffuse and weak background. The band at 3075 cm^{-1} appearing in the spectrum of liquid ethylene with appreciable intensity can now be assigned as ν_5 shifted to lower frequency (approximately 1 percent) due to intermolecular forces. This assignment appears to be more acceptable than the previous one that the band is the infrared-active fundamental ν_9 appearing in the Raman spectrum as a result of a breakdown of selection rules in the liquid state.[7]

The band at 3270 cm^{-1} remains to be assigned. Since the doublet at 1626 and 1654 cm^{-1} and the line at 3237 cm^{-1} are satisfactorily explained as ν_2, $2\nu_{10}$, and $2\nu_2$,[1,5] respectively, it is probable that the line at 3270 cm^{-1} is $\nu_2 + 2\nu_{10}(A_{1g})$ which has borrowed some intensity from the fundamental $\nu_1(a_{1g})$ nearby. This assignment is consistent with the observation that in the spectrum of the gas line at 3270 cm^{-1} is sharp.

The intensity contour of a weak and diffuse band in the region of 950 cm^{-1} shows a double maximum as expected for the out-of-plane bending mode $\nu_8(b_{2g})$, and thus substantiates the earlier assignment.[1] Exposures of up to 24 hours with an $f/2.5$ camera failed to show any evidence of a band at 1236 cm^{-1} found in the spectrum of the liquid and believed to be $\nu_8(b_{1g})$[2]. In the spectrum of the gas this region is overlapped by an intense rotational wing of the ν_3 band, and detection of a weak band is rather difficult.

It seemed desirable to confirm the above assignments for the ν_5 and ν_8 bands from the intensity contours of the corresponding bands in the molecule C_2D_4. Also, there was the possibility that the ν_6 band of C_2D_4 might lie in a clear region and thus

provide a definite assignment from its intensity contour. The vibrational Raman spectrum of gaseous C_2D_4 does indeed show two broad bands at 2305 and 780 cm^{-1} with features resembling the analogous C_2H_4 bands at 3108 and 950 cm^{-1}, respectively. Unfortunately, however, the wave-number region predicted[5] for the ν_6 band is again overlapped by the intense rotational wings of the ν_3 band, and as yet no indication of this band has been found.

A more detailed report on the vibrational Raman spectra of C_2H_4 and C_2D_4 will be published at a later date.

I wish to thank Dr. G. Herzberg for suggesting this problem and for several helpful discussions. I am indebted to Dr. L. C. Leitch for supplying the ethylene-d_4.

* Contribution No. N.R.C. 2963 from the National Research Council of Canada.
† National Research Laboratories Postdoctorate Fellow.
[1] G. Herzberg, *Infrared and Raman Spectra* (D. Van Nostrand Company, Inc., New York, 1945), p. 325.
[2] Rank, Shull, and Axford, J. Chem. Phys. **18**, 116 (1950).
[3] Dickinson, Dillon, and Rasetti, Phys. Rev. **34**, 582 (1929); S. Bhagavantam, Nature, **138**, 1096 (1936).
[4] E. K. Plyler, J. Chem. Phys. **19**, 658 (1951).
[5] R. L. Arnett and B. L. Crawford, Jr., J. Chem. Phys. **18**, 118 (1950).
[6] Welsh, Cumming, and Stansbury, J. Opt. Soc. Am. **41**, 712 (1951).
[7] G. Glockler and M. M. Renfrew, J. Chem. Phys. **6**, 170, 409 (1938).

Intensification in Zinc Selenide Phosphors

SIMON LARACH
Radio Corporation of America, Laboratories Division, Princeton, New Jersey
(Received February 9, 1953)

ALTHOUGH an extensive literature exists on zinc sulfide phosphors, comparatively little work has been reported on zinc selenide phosphors. The present investigation concerns (1) the effect of various additives, and (2) a comparison of chloride and trivalent cation fluxes on the cathodoluminescence emission of zinc selenide phosphors.

The phosphors were prepared by adding the metallic activators, as nitrates, all 0.01 percent by weight, to "ultra-pure" zinc selenide.[1] Chloride, where used, was added as ammonium chloride, 2 percent by weight.[2] Crystallization firings were carried out in a purified nitrogen atmosphere at 900°C, and the materials were cooled in nitrogen. Measurements of spectral distribution and emission intensity were taken with a special demountable cathode-ray tube,[3] in conjunction with an automatic recording spectroradiometer.[4] The effects of the various additives on the peak wavelength and emission intensity are given in Table I, and the spectral distribution curves are shown in Fig. 1.

TABLE I. Effect of various additives on the peak wavelength and emission intensity of zinc selenide phosphors (cathode-ray excitation).

Additive	NH_4Cl	λ_{pk}	Relative peak emission intensity[a]
none	no	6370A	0.31
none	yes	6020	2.0
Cu	no	6500	9.4
Cu	yes	6470	23.0
Mn	no	5940	0.16
Mn	yes	6050	2.0
Ag	no	5720	2.4
Ag	yes	5720	6.3
Al	no	6100	0.2
Al	yes	6370	0.7
Cu, Al	no	6470	4.5
Cu, Al	yes[b]	6500	11.0
Ga	no	emission too weak to measure	
Cu, Ga	no	6470	37.0
Cu, Ga	yes[b]	6470	70.0
Pb	yes	6020	2.4

[a] Relative to rbhdl. $-Zn_2SiO_4$:Mn = 100.
[b] Added on refiring the phosphor.

For all the additives tried, inclusion of chloride during crystallization yielded phosphors of higher emission intensity. Kröger and Dikhoff[8] have reported that trivalent cations could be utilized instead of halide fluxes, in the synthesis of zinc sulfide phosphors. In this fashion, charge compensation is achieved on incorporating monovalent activator ions.

A comparison of the effects of incorporating trivalent ions or chloride in zinc selenide phosphor shows the following: (1) with no added activator, both chloride and aluminum yield phosphors whose peak wavelengths occurs at shorter wavelengths than the phosphor prepared with no additives; (2) incorporation of Cl, Al, or Ga ions in ZnSe:Cu yields phosphors with peak wavelength at 6470A; (3) ZnSe:Cl shows an increase in host-crystal emission intensity, while aluminum has no effect and gallium acts as a poison; (4) gallium constitutes an effective intensifier for the emission from ZnSe:Cu.

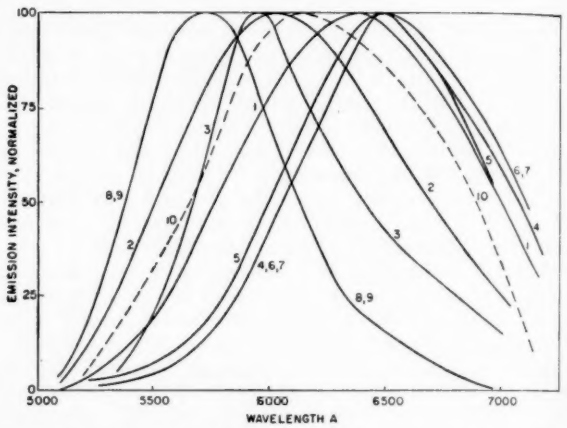

FIG. 1. Cathodoluminescence spectral distribution curves of zinc selenide phosphors: (1) ZnSe; (2) ZnSe:Cl; (3) ZnSe:Mn; (4) ZnSe:Cu; (5) ZnSe:Cu:Cl; (6) ZnSe:Cu:Ga; (7) ZnSe:Cu:Ga:Cl; (8) ZnSe:Ag; (9) ZnSe:Ag:Cl; (10) ZnSe:Al. The relative peak emission intensities are given in Table I.

It is interesting that refiring ZnSe:Cu:Al with ammonium chloride gave a phosphor whose spectral distribution and emission intensity correspond to ZnSe:Cu alone. On the other hand, ZnSe:Cu:Ga phosphor treated in the same manner gave an *increased* emission intensity, showing (1) unlike aluminum, gallium was not entirely removed by the chloride treatment, and (2) metallic and halide intensifiers can coexist and give stronger intensification than each alone.

Thus, to summarize, (1) chloride acts as an intensifier of the host-crystal emission and of the emission from phosphors containing added activators; (2) aluminum does not effect the host-crystal emission but acts as a poison for the emission from ZnSe:Cu; (3) gallium is a poison for the host-crystal emission but is a good intensifier for ZnSe:Cu, and is a co-intensifier with chloride for ZnSe:Cu.

The observed differences in spectral emissions can be explained by the hypothesis that the host-crystal luminescence of zinc selenide consists of two bands at approximately 6000A and 6500A and that impurities usually act as selective intensifiers or poisons.

[1] Obtained from the Mallinckrodt Chemical Company.
[2] A volatile chloride was used in order to avoid alkali metal ions, and post-synthesis washing of the phosphors.
[3] Measurements were made by Dr. R. H. Bube.
[4] V. K. Zworykin, J. Opt. Soc. Am. **29**, 84 (1939).
[5] F. A. Kröger and J. Dikhoff, Physica **16**, 297 (1950).

A New Electronic State in Benzene*

JOE S. HAM†
Laboratory of Molecular Structure and Spectra, Department of Physics University of Chicago, Chicago, Illinois
(Received December 23, 1952)

THE 2600A bands of benzene in carbon tetrachloride at room temperature have an oscillator strength of about 0.0023 while in a hydrocarbon solvent such as *n* heptane they have a

strength of 0.0014. At liquid nitrogen temperatures the increase in absorption resides in a series of bands which appear only weakly in a hydrocarbon glass. This is possibly an electronic transition different from that giving rise to most of the absorption in this region.

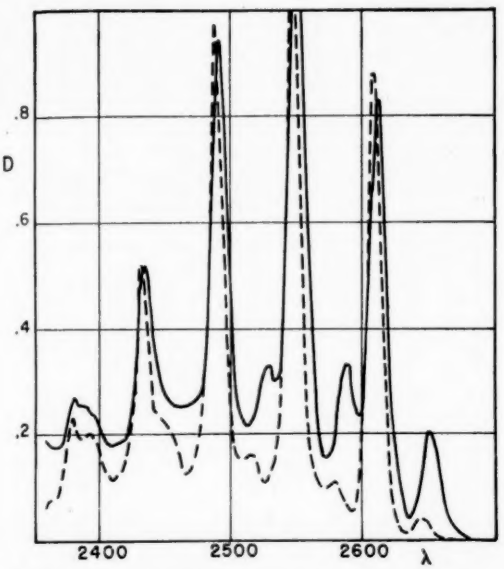

FIG. 1. Absorption of benzene at liquid nitrogen temperatures ($c = 1.7 \times 10^{-2}$ mole per liter) in a 0.18-cm cell. The dashed line is the spectrum of benzene in a hydrocarbon glass and the solid line is the spectrum of benzene in a glass containing CCl_4.

For most of the measurements, a brass Dewar cell[1] was used with a cell length of 0.18 cm. Using a Beckmann DU spectrophotometer with a 10^2 megohm phototube resistor, slit widths of 0.40 and 0.22 mm were used in the regions 2360 to 2480 and 2480 to 2750A, respectively. Since it was more important to get relative accuracy of neighboring points than to get absolute accuracy, the spectrophotometer was zeroed at 2750A where benzene does not absorb; then, without moving the cell from the light path the spectrum was run, frequently checking back to 2750A for any drifts in the amplifier circuit or source intensity. In the region 2360 to 2480A, where a larger slit width was needed, the spectrophotometer was zeroed at a wavelength with a known optical density (0.450 relative to 2750A). This method gave reproducible results to within 0.010 and 0.002 optical density units at 2400 and 2600A, respectively. The effective spectral band widths were 6.4A at 2400A and 5.5A at 2700A.

Figure 1 shows the spectrum of benzene in a glass composed of 1 part methylcyclohexane to 3 parts isopentane and in a glass composed of a mixture of the same hydrocarbons with the addition of 7 percent by volume of CCl_4. The optical densities are corrected for solvent and cell absorptions and for the source intensity.

Figure 2 shows a photograph of two concentrations of benzene in the glasses described above taken with a medium Hilger spectrograph. This shows that the differential shift is not a phenomenon resulting from the poor resolution of the Beckmann spectrophotometer. The absorption of the CCl_4 obscures the spectrum at shorter wavelengths.

Benzene in a hydrocarbon glass without CCl_4 shows a strong series of bands with a spacing of 923 cm^{-1} and a weaker series with about the same spacing. The first is prominent in the vapor and crystal spectra, while the second is possibly the same as a series observed in the crystal spectra (labeled *I* series by Sponer *et al.*) which is not found in the vapor spectra.[2] The strong series contains one quantum of an ϵ_{2g} carbon skeletal vibration (520 cm^{-1}) which makes these bands allowed. The *I* series has been interpreted by Sponer *et al.* as being the O—O band followed by bands separated from it by multiples of the totally symmetrical vibration (923 cm^{-1}). Such bands are forbidden by molecular electronic selection rules for the free molecules, but the local symmetry of the crystal is such that they can appear. At liquid hydrogen temperatures the bands in the crystal can be resolved into several components whose polarization has been studied by Broude *et al.*[3] and Davydov.[4] Forbidden O—O bands are known to be made weakly allowed in glasses[5] so part or all of the intensity could arise from this source.

In the glass containing CCl_4 the strong series appears with approximately the same intensity, but the weak series appears much stronger and has maxima which are about 580 cm^{-1} to the red of the strong series (compared with 520 cm^{-1} separation if the interpretation of Sponer *et al.* were correct). Since a carbon skeletal frequency would not be changed this much by solvent effects, this increase in separation makes it possible that these bands arise from a separate electronic transition which is too weak to be observed when the molecules are unperturbed. Sponer *et al.*[2] noted the difficulty that the long wavelength edge of the first band in the crystal spectrum was 31 cm^{-1} to the red of the calculated O—O position. This small discrepancy was unexplained, but they thought it could be ascribed to excitation of a crystal frequency in the initial state or caused by a resonance phenomenon between the electronic excitation of molecular units in the crystal.

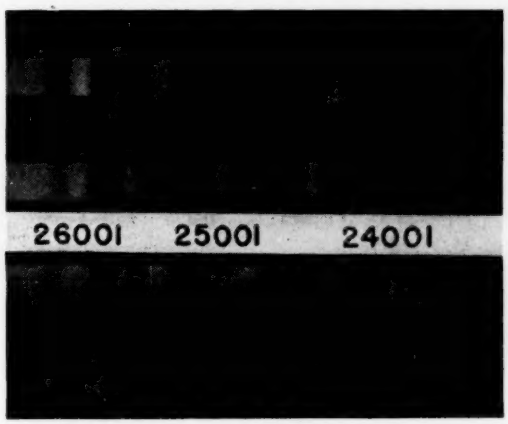

FIG. 2. Several exposures from a photographic plate of the same bands. Exposure 1—benzene in a glass containing CCl_4. Exposure 2—benzene at the same concentration in a hydrocarbon glass. Exposure 3—a more dilute solution of benzene in a glass containing CCl_4. Exposure 4—the same concentration of benzene as in 3, in a hydrocarbon glass.

The possibility that all the bands belong to a single electronic transition cannot be definitely ruled out. The large separation could arise from the maxima not being at the true position of the rather broad bands although 60 cm^{-1} is a considerable fraction of the band width (see Fig. 2). Or conceivably a very weak complex is formed whose spectrum has the *I* bands strongly enhanced and its entire spectrum shifted to longer wavelengths. If only a fraction of the molecules were in the complex, the resulting maxima of the *I* bands would show a greater shift than the maxima of the strong bands. Such a complex must be a very weak one, as the same effect appears at room and liquid nitrogen temperatures and the liquids form well-behaved solutions.[6] Much more must be known of solvent effects upon the spectrum before such possibilities can be definitely ruled out.

Assuming that the enhanced system is a different electronic transition, the symmetry of the upper state is probably $^1E_{1u}$. Molecular orbital calculations predict this state to be near the $^1B_{2u}$ state and the intensity of the transition from the ground state is estimated to be comparable with that observed.[7] The

existence of a singlet-triplet transition of benzene in the 2600A-region is supported by the spectra of some fluoro- and chlorotoluenes.[8] These show a weak absorption at slightly longer wavelengths than the absorption corresponding to the benzene 2600A-singlet-singlet transition. There is no singlet-singlet transition which could give rise to this absorption so it must arise from a singlet-triplet transition which is usually hidden by the singlet bands in most substituted benzenes.

Kasha[9] has postulated that the mechanism of enhancement of singlet-triplet absorptions is the spin-orbit coupling of the solvent molecules inducing some singlet-triplet mixing in the solute molecule. The spin-orbit coupling in polyatomic molecules is approximately that of its heaviest atom. Most solvents containing atoms heavier than chlorine are opaque below 2700A or form complexes which frequently have strong charge-transfer bands which might obscure any enhancements.[10] Nevertheless, the benzene-bromine and benzene-iodine complexes, which have their charge transfer peaks near 2900A have been studied in the region 2600A.[11] Subtracting the tail of the charge-transfer absorption, one is left with an ϵ of roughtly 1500 for the bromine complex and 3000 for the iodine complex. If this absorption is the enhancement of the singlet-triplet absorption, chlorine atoms possibly could have an effect as large as that observed.

Molecules which do not have heavy atoms can sometimes cause enhancements. For example, it was observed that ether, when added to the hydrocarbon glass containing benzene, creates an effect similar to adding CCl_4, but it is only 1/10th as strong. Also, trinitrobenzene is known to increase the phosphorescence probability of some condensed aromatics.[12]

Assuming the spin-orbit coupling of the solvent molecules, the factor responsible for singlet-triplet mixing of the wave functions of the solute molecules, the mixing can be pictured as coming about by the admixture of some intermolecular charge-transfer type wave functions into those of the solute molecule. The excited-state wave functions overlap moderately the solvent molecules which are at van der Waals' radius in the ground state. Molecules in an excited state have both a low ionization potential and a high electron affinity. Thus, it is expected that the solvent molecules, with either a moderate ionization potential or a positive electron affinity, or both, will interact with the excited states and so increase the absorption intensities of forbidden transitions.

According to present ideas, triplet-singlet emission occurs only from the lowest triplet state of a molecule so that the position of higher triplets must be determined by other methods. At present, these states can sometimes be found by triplet-triplet absorption techniques. It is hoped that solvent enhancements by solvents containing heavy atoms, when perfected, will be an additional method for the location of these higher triplet states.

* This work was assisted in part by the U. S. Office of Ordnance Research under Project TB2-0001 (505) of Contract DA-11-022-ORD-1002 with the University of Chicago.

† U. S. Atomic Energy Commission Predoctoral Fellow, 1951–1953.

[1] The design of the Dewar cell was similar to that described by W. J. Potts, Jr., J. Chem. Phys. (to be published).

[2] An analysis of the benzene 2600 bands is given by Sponer, Nordheim, Sklar, and Teller, J. Chem. Phys. **7**, 207 (1939). See also Sponer and Teller, Revs. Modern Phys. **13**, 76 (1941).

[3] Broude, Medvedov, and Prikhot'ko Zhur Eksp. Teoret. Fiz. **21**, 665 (1951). An abstract is given in Chem. Abstracts **46**, 8958e (1952).

[4] A. S. Davydov, Zhur. Eksp. Teoret. Fiz. **21**, 673 (1951). See Chem. Abstracts **46**, 8959d (1952).

[5] For example, Harrison Shull, J. Chem. Phys. **17**, 295 (1949) observed a weak O—O band of the 3400-A phosphorescence of benzene in a rigid glass.

[6] Milton Tamres, J. Am. Chem. Soc. **74**, 3375 (1952) finds the heat of mixing of benzene and CCl_4 to be −38 cal/mole.

[7] C. C. J. Roothaan and R. S. Mulliken, J. Chem. Phys. **16**, 118 (1948), predict this state to lie about 4.7 ev above the ground state. They estimate the intensity of the transition $^1A_{1g}-{}^3E_{1u}$ to be about one-hundredth as strong as the $^1A_{1g}-{}^1B_{2u}$.

[8] M. E. Hobbs and E. J. Hackney, *Abstracts of the Symposium on Molecular Structure and Spectroscopy*, Ohio State University, June 1952.

[9] M. Kasha, J. Chem. Phys. **20**, 71 (1952), studied α-chloronaphthalene in ethyl iodide and found that the lowest singlet-triplet absorption was strongly enhanced.

[10] The possibility that the charge-transfer wavelength is correlated with the position of a triplet is discussed by McConnell, Ham, and Platt, J. Chem. Phys. (to be published).

[11] Ham, Platt, and McConnell, J. Chem. Phys. **19**, 1301 (1951).

[12] C. Reid, J. Chem. Phys. **20**, 1212 (1952).

Molecular Orbital Theory of Alternant Hydrocarbons

R. B. Potts
University of Adelaide, Adelaide, South Australia
(Received November 18, 1952)

THE molecular orbital theory of alternant hydrocarbons (including aromatic hydrocarbons) has been developed by Coulson and Longuet-Higgins,[1] and numerical results have been given for various molecules.[2] For the theoretical chemist not very familiar with matrix algebra it may not be obvious which is the best method of calculating the molecular orbitals, since very few mathematical details have ever been published.

The problem is essentially the evaluation of the eigenvalues and eigenvectors of the real symmetric matrix **A** of the secular equations of the molecule. For such a matrix the eigenvalues are real, the eigenvectors corresponding to distinct eigenvalues are orthogonal, and to an eigenvalue of degeneracy r corresponds an eigenspace of dimension r. The matrices which occur in the theory are particularly simple, their elements a_{ij} being zero except when atom numbered i is a nearest neighbor of atom numbered j. In this case, a_{ij} is real nonzero and is usually taken equal to unity.

For an alternant hydrocarbon with $2n$ atoms it is best to number the atoms alternately (although suggested in the work of Coulson and Longuet-Higgins,[1] this numbering is not generally used), say $1, 1', 2, 2', \cdots, n, n'$ so that the nearest neighbors of an undashed number are dashed numbers and vice versa. With such a numbering and with the atomic orbitals ordered $\varphi(1)$, $\varphi(2), \cdots, \varphi(n), \varphi(1'), \cdots \varphi(n')$, one assures that the secular matrix **A**, of order $2n$, has the form

$$\mathbf{A}=\begin{bmatrix}\mathbf{O} & \mathbf{B}\\ \mathbf{B}' & \mathbf{O}\end{bmatrix}, \tag{1}$$

where **O** stands for the zero matrix of order n, **B** is a real matrix of order n, and **B**′ is the transpose of **B** (in general different from **B**).

The molecular orbital theory requires initially the determination of the eigenvalues and eigenvectors of the matrix **A**, and with this matrix in the form (1) the following results will facilitate this calculation. If λ is an eigenvalue of **A** and

$$\begin{bmatrix}\mathbf{u}\\ \mathbf{v}\end{bmatrix}$$

the corresponding eigenvector (where both **v** and **u** have n elements), then

$$\begin{bmatrix}\mathbf{O} & \mathbf{B}\\ \mathbf{B}' & \mathbf{O}\end{bmatrix}\begin{bmatrix}\mathbf{u}\\ \mathbf{v}\end{bmatrix}=\begin{bmatrix}\mathbf{B}\ \mathbf{v}\\ \mathbf{B}'\ \mathbf{u}\end{bmatrix}=\lambda\begin{bmatrix}\mathbf{u}\\ \mathbf{v}\end{bmatrix}, \tag{2}$$

so that

$$\mathbf{B}\ \mathbf{v}=\lambda\mathbf{u} \tag{3}$$

$$\mathbf{B}'\mathbf{u}=\lambda\mathbf{v} \tag{4}$$

$$\mathbf{B}\ \mathbf{B}'\mathbf{u}=\mathbf{B}(\lambda\mathbf{v})=\lambda^2\mathbf{u} \tag{5}$$

and

$$\mathbf{B}'\mathbf{B}\ \mathbf{v}=\lambda^2\mathbf{v}. \tag{6}$$

It also follows that

$$\begin{bmatrix}\mathbf{O} & \mathbf{B}\\ \mathbf{B}' & \mathbf{O}\end{bmatrix}\begin{bmatrix}\mathbf{u}\\ -\mathbf{v}\end{bmatrix}=-\lambda\begin{bmatrix}\mathbf{u}\\ -\mathbf{v}\end{bmatrix}. \tag{7}$$

The lengths of the eigenvectors

$$\begin{bmatrix}\mathbf{u}\\ \pm\mathbf{v}\end{bmatrix}$$

are both equal to $\sqrt{(\mathbf{u}'\mathbf{u}+\mathbf{v}'\mathbf{v})}$, and can be normalized to 1 by choosing $\mathbf{u}'\mathbf{u}=\frac{1}{2}$ because, from (3) and (4),

$$\mathbf{v}'\mathbf{v}=\lambda^{-1}\mathbf{v}'\mathbf{B}'\mathbf{u}=\lambda^{-1}\mathbf{u}'\mathbf{B}\mathbf{v}=\mathbf{u}'\mathbf{u}. \tag{8}$$

The eigenvalue problem for the matrix **A** can therefore be solved in the following manner: determine the eigenvalues λ^2 and the eigenvectors **u** normalized to length $\sqrt{\frac{1}{2}}$ of the (symmetric) matrix **B B**′; determine the vector **v** from the relation $\mathbf{B}'\mathbf{u}=\lambda\mathbf{v}$;

then the eigenvalues of **A** are $\pm\lambda$ and the corresponding eigenvectors, normalized to length 1, are

$$\begin{bmatrix} \mathbf{u} \\ \pm\mathbf{v} \end{bmatrix}.$$

The eigenvalue problem is accordingly reduced from one in $2n$ dimensions to one in n dimensions.

If the hydrocarbon has a center of symmetry, then the atoms can be numbered so that if there is a bond ab', then there is a bond $a'b$. The matrix **B** is then symmetric and if λ is an eigenvalue of **B** and **u** the corresponding eigenvector,

$$\begin{bmatrix} \mathbf{O} & \mathbf{B} \\ \mathbf{B} & \mathbf{O} \end{bmatrix}\begin{bmatrix} \mathbf{u} \\ \pm\mathbf{u} \end{bmatrix} = \pm\lambda\begin{bmatrix} \mathbf{u} \\ \pm\mathbf{u} \end{bmatrix}. \tag{9}$$

Hence in this case the eigenvalue problem for **A** can be solved as follows: determine the eigenvalues λ and eigenvectors **u** (normalized to length $\sqrt{\frac{1}{2}}$) of the symmetric matrix **B**; then the eigenvalues of **A** are $\pm\lambda$, and the eigenvectors

$$\begin{bmatrix} \mathbf{u} \\ \pm\mathbf{u} \end{bmatrix},$$

normalized to length unity.

[1] C. A. Coulson and H. C. Longuet-Higgins, Proc. Roy. Soc. (London) **A192**, 16 (1948).
[2] For example, Berthier, Coulson, Greenwood, and Pullman, Compt. rend. (Paris) **226**, 1906 (1948).

Chemical Modulation: A Method for Investigating Transient Molecules*

EDWARD J. BAIR, JOHN T. LUND, AND PAUL C. CROSS
Department of Chemistry and Chemical Engineering, University of Washington, Seattle, Washington
(Received February 12, 1953)

TRACINGS of absorption lines near 5977A which have been ascribed[1] to NH_2 radicals are shown in Fig. 1. The variation of maximum absorption as a function of time after discharge pulses in NH_3 is shown in Fig. 2. These preliminary results were obtained by a method which we believe may have useful application to the study of free radicals.

If the concentration of a chemical species can be varied in a periodic fashion, absorption which is due to this species may be used to modulate a transmitted light intensity. This modulation may be detected to give a signal which represents only the change in concentration of the chemical species. Electronic circuits permit continuous recording of the amplitude of any portion of this modulation.

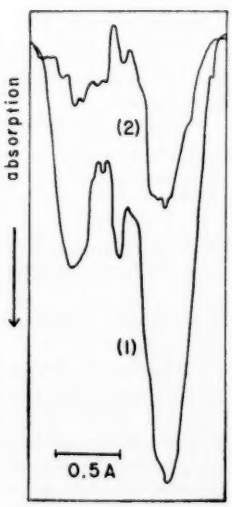

FIG. 1. Traces of the relative absorption by NH_2 in the region near 5977A. Curves (1) and (2) are taken 1.5 and 7 milliseconds, respectively, after the discharge pulses. The NH_3 pressure was approximately 1 mm and the path length about 100 feet. The maximum absorption may be estimated as a few percent, but no attempt has yet been made to measure it quantitatively.

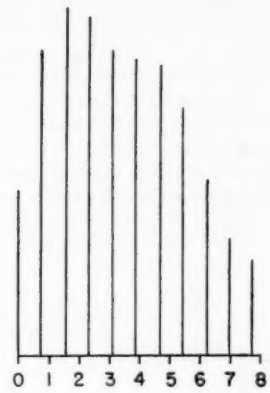

FIG. 2. Relative intensity of the stronger line if Fig. 1 is plotted as a function of time in milliseconds after the discharge. These intensities correspond to a low pressure and are strongly pressure dependent.

The following experiment was performed to test the application of this principle to the observation of free radical properties. The equipment consisted of a carbon arc source, a multiple path absorption cell[2] fitted with discharge electrodes, and a 21-foot grating spectrometer with a photomultiplier detector and a high speed chopper.[3] A condensed discharge of about one-millisecond duration and 3000 volts was applied to the discharge electrodes at a frequency of 13 cycles per second. The signal received has the frequency of the chopper and an amplitude modulation produced by the radical absorption. This modulation was added to a 13-cycle pulse of adjustable width (about 0.5 msec) synchronized to the discharge pulse but delayed in time by an adjustable interval. Then, by means of a pulse integrating amplifier, a continuous signal was obtained which represented the absorption of the radical at a measured time after each discharge. This signal may be studied as a function of spectral frequency, pressure, discharge voltage, or any other parameter affecting the formation or decay of the radical. By varying the time delay of the synchronized pulse the absorption may be measured as a function of time after the discharge.

* This work was supported in part by the U. S. Office of Naval Research under contract N8onr-52010 and in part by a grant from the Research Corporation.
[1] G. Herzberg and D. A. Ramsay, J. Chem. Phys. **20**, 347 (1952).
[2] J. U. White, J. Opt. Soc. Am. **38**, 285 (1942).
[3] Bair, Cross, Dawson, Wilson, and Wise (description forthcoming).

Atomic Mercury as a Luminescent Activator

J. S. PRENER, R. E. HANSON, AND F. E. WILLIAMS
General Electric Research Laboratory, Schenectady, New York
(Received January 29, 1953)

THE thallium-activated potassium chloride phosphor has been studied extensively. The excitation and emission spectra have been calculated from first principles using the properties of the free ions,[1] and the corresponding transitions have been shown to occur between the ^1S and the $^3P_1^0$ and $^1P_1^0$ states of monovalent thallium.

Since atomic mercury is isoelectronic with monovalent thallium and has the same spectroscopic term scheme, it was predicted that neutral mercury atomically dispersed in a solid should be a luminescent activator.

Grandjean[2] has reported that certain minerals of the zeolite class are capable of absorbing considerable amounts of atomic mercury. We obtained a number of different natural zeolites, dehydrated them at 500°C in vacuum and then heated them in a mercury atmosphere in a sealed Vycor tube at 400°C. Of the various zeolites tried, only harmotome (Strontian, Argylshire, Scotland) yielded a luminescent material when excited by a low pressure mercury arc or by a cathode-ray beam.

When the white crystals or the powdered phosphor were exposed to air, they turned black rapidly. This was a result of the displacement of the mercury by water. If water were added to the

phosphor, globules of mercury appeared which could be dissolved in nitric acid leaving behind the white residue of hydrated harmotome. The amount of mercury contained in a typical sample of phosphor was found to be 1.80 percent by weight.

The spectra were determined with the phosphor in a sealed Vycor tube. The excitation spectrum consists of a broad-band peaking at approximately 2550A. This corresponds to the transition from ^1S to $^3P_1^0$ Hg with weak interaction between the Hg and the lattice for the equilibrium atomic configuration of the ground state. The emission (Fig. 1) is at a markedly longer wavelength than the

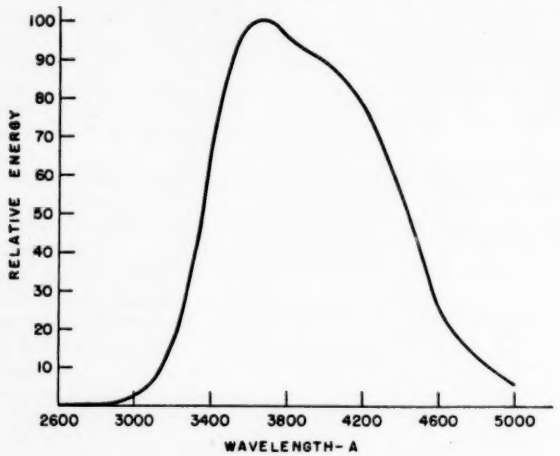

FIG. 1. Emission spectrum at 25°C of mercury-activated harmotome excited by a low pressure mercury arc.

excitation. Appreciable polarization energy therefore exists. Strong binding energy between the $^3P_1^0$ Hg and the lattice for the equilibrium configuration of the emitting state must be present.

The zeolites consists of a three-dimensional silicon-oxygen framework with some of the Si^{+4} atoms replaced by Al^{+3}, the resulting negative charge being balanced by the presence of positive alkali or alkaline earth ions in the lattice. The substitution of Al^{+3} for Si^{+4} leaves an unfilled orbital which can form a covalent bond with the $^3P_1^0$ Hg. This is the origin of binding energy. The $^1S_0$ Hg, however, experiences van der Waals bonding only. The two overlapping emission bands shown in Fig. 1 probably arise from the $^3P_1^0$ and $^1P_1^0$ emitting states being in thermal equilibrium as is the case for KCl:Tl.[3]

Further experimental and theoretical studies are in progress on liminescent solids activated with atomic mercury.

[1] F. E. Williams, J. Chem. Phys. **19**, 457 (1951).
[2] Grandjean, Compt. rend. **149**, 866 (1909).
[3] P. D. Johnson and F. E. Williams, J. Chem. Phys. **20**, 124 (1952).

Exchange Frequency Electron Spin Resonance in Ferrites

J. KAPLAN AND C. KITTEL
Department of Physics, University of California, Berkeley, California
(Received February 12, 1953)

IT is an unfortunate fact that the direct experimental determination of the exchange interaction energy between magnetic ions in ferromagnetic solids is usually impossible because of the approximate selection rule against magnetic dipole transitions in which the multiplicity of the total system changes; thus, for example, transitions between the states ^1S and ^3S of a two-electron system are approximately forbidden. There is, however, a particular situation in which it should be possible to observe a transition frequency directly related to the exchange energy: this is in ferromagnetic ferrites. It is known from the theoretical work of Néel and the neutron diffraction work of Shull and others that ferromagnetic ferrites are characterized by two magnetic lattices, A and B, oppositely directed but of unequal magnitude. The observed saturation magnetization is the difference of the magnetizations of the separate lattices.

Electron spin resonance in ferrites was first considered[1] in connection with the theory of antiferromagnetic resonance. In the present note we give an explicit expression for the susceptibility near the "exchange" resonance, showing that the resonance should be observable only if the g values of the separate lattices are different from one another. We also discuss experimental means by which the predicted resonance might be observed.

We suppose that the magnetization $\mathbf{M}_A$ of lattice A is directed along the $+z$ axis, while the magnetization $\mathbf{M}_B$ of lattice B is negative and directed along the $-z$ axis. The exchange field arising from M_A is $\mathbf{H}_A{}^E=\lambda\mathbf{M}_A$, where the Weiss constant λ is negative, as appropriate to the antiferromagnetic nature of the interaction in ferrites. The exchange field arising from M_B is $\mathbf{H}_B{}^E=-\lambda\mathbf{M}_B$. Neglecting static fields, demagnetizing fields, and the anisotropy energy, the equations of motion in the presence of rf components H^x, H^y are, in the usual approximation,

$$\begin{aligned}
dM_A{}^x/dt&=\gamma_A(H_B{}^E M_A{}^y+H_A{}^E M_B{}^y-H^y M_A);\\
dM_A{}^y/dt&=\gamma_A(-H_A{}^E M_B{}^x-H_B{}^E M_A{}^x+H^x M_A);\\
dM_B{}^x/dt&=\gamma_B(-H_A{}^E M_B{}^y-H_B{}^E M_A{}^y-H^y M_B);\\
dM_B{}^y/dt&=\gamma_B(H_B{}^E M_A{}^x+H_A{}^E M_B{}^x+H^x M_B).
\end{aligned}\tag{1}$$

Here $\gamma_A=g_A e/2mc$; $\gamma_B=g_B e/2mc$. The rf susceptibility in the x direction is found on solving these equations to be

$$\chi^x=\frac{M_A{}^x+M_B{}^x}{H_x}=\frac{\lambda M_A M_B(\gamma_B-\gamma_A)^2}{\omega^2-\omega_0{}^2},\tag{2}$$

where

$$\omega_0{}^2=(\gamma_A H_B{}^E-\gamma_B H_A{}^E)^2=\left(\frac{\lambda e}{2mc}\right)^2(g_A|M_B|-g_B|M_A|)^2.\tag{3}$$

The resonance frequency gives a direct measure of the exchange interaction λ, as the g's and magnetizations are usually known from the properties of the paramagnetic ions. It should be noted the susceptibility associated with the exchange resonance vanishes for $g_A=g_B$; thus we should not expect to observe the resonance in $MnOFe_2O_3$, as both types of ions (Mn^{++} and Fe^{3+}) have $g=2.00$.

We proceed to estimate ω_0 and χ^x for nickel ferrite $NiOFe_2O_3$, assuming that the structure is pure inverse spinel so that all the Ni^{++} and half of the Fe^{3+} ions are on lattice A; the other half of the Fe^{3+} ions constitute lattice B. From Néel's estimate[2] of the relevant interaction we find $\lambda=1.0\times10^4$. Taking $g(Ni^{++})=2.20$ and $g(Fe^{3+})=2.00$, we find

$$\begin{aligned}
g_A&=2.06; \qquad g_B=2.00;\\
M_A&\cong 865; \qquad M_B\cong -600;
\end{aligned}$$

so that, from Eq. (3),

$$f_0\cong 7.0\times10^{12}\text{ cps},\tag{4}$$

which is equivalent to 2.5×10^6 oersteds or a wavelength of about 40 microns.

If ΔH denotes the width of the resonance in terms of equivalent magnetic field, the peak susceptibility will be, from Eq. (2) and the above values,

$$\chi^x(\text{res})\cong 2/\Delta H.\tag{5}$$

We have no secure grounds for estimating ΔH, although it might (optimistically) be supposed to be of the same order as the half-width observed[3] in the ordinary microwave spin resonance in nickel ferrite. This is of the order of 30 oersteds, so that in this case $\chi^x(\text{res})\approx10^{-1}$.

A possible experimental arrangement to detect the predicted infrared absorption would be to reflect plane polarized radiation from the surface of a single crystal magnetized normal to the surface and to note the ellipticity of the reflected light. For normal incidence the approximate expressions for the electric field of reflected light, referred to x, y axes at 45 degrees from the incident

polarization plane, are

$$E_x' = \frac{\epsilon - i(n^+ - n^-)}{\epsilon + (n^+ - n^-)} E_x;$$
$$E_y' = \frac{\epsilon + i(n^+ - n^-)}{\epsilon + (n^+ + n^-)} E_y; \quad (6)$$

where $n^{\pm} = [\epsilon(1 + 4\pi\chi^{\pm})]^{\frac{1}{2}}$ are the indices of refraction for circularly polarized light in the crystal.

With values $\chi^- \approx 0.1$; $\chi^+ \approx 0$; $\epsilon \approx 5$, we find that the principal effect of the resonance is to introduce near resonance a phase difference of about 24° in the reflected components. It should be possible experimentally to detect the resonance even if the line were several orders of magnitude broader than supposed here.

This research has been assisted in part by the U. S. Office of Naval Research.

[1] C. Kittel, Phys. Rev. **82**, 565 (1951); see also R. K. Wangsness, Phys. Rev. **86**, 146 (1952).
[2] L. Néel and P. Brochet, Compt. rend. (Paris) **230**, 280 (1950).
[3] Yager, Galt, Merritt, and Wood, Phys. Rev. **80**, 744 (1950).

The Pure Quadrupole Spectrum of Hexachlorobenzene

T. L. Weatherly, E. H. Davidson, and Quitman Williams
School of Physics, Georgia Institute of Technology, Atlanta, Georgia
(Received January 27, 1953)

THE pure quadrupole spectrum of C_6Cl_6 has been investigated at liquid nitrogen temperature. A frequency modulated regenerative oscillator was used, and the absorption lines were viewed on an oscilloscope. Spectral lines were observed at 38.381 Mc, 38.452 Mc, and 38.493 Mc. The line frequencies correspond to an average $|eqQ|$ of 76.884 Mc. Previously measured couplings for chlorobenzenes are 69.243 Mc for C_6H_5Cl[1] and 69.560 Mc for p-$C_6H_4Cl_2$.[2] Progressive replacement of H by Cl in the benzene ring increases the quadrupole coupling. A similar effect was observed by Livingston[3] for the substituted methanes and attributed to a reduction in the ionic character of the C−Cl bond as more chlorine atoms are added. The present case may be somewhat more complicated because of the 15 percent double-bond character of the C−Cl bond in the chlorobenzenes.[4] The three lines observed for C_6Cl_6 are of about equal intensity and are considerably weaker than the C_6H_5Cl resonance.

[1] R. Livingston, Phys. Rev. **82**, 289 (1951).
[2] Wang, Townes, Schawlow, and Holden, Phys. Rev. **86**, 809 (1952).
[3] R. Livingston, J. Chem. Phys. **19**, 1434 (1951).
[4] L. Pauling, *The Nature of the Chemical Bond* (Cornell University Press, Ithaca, New York, 1948), second edition.

The Structure of B_4Cl_4

George H. Duffey
Department of Chemistry, South Dakota State College, College Station, South Dakota
(Received February 13, 1953)

AN x-ray diffraction study[1] of B_4Cl_4 has recently been carried out. In the solid phase each boron lies at the corner of a slightly distorted tetrahedron. Each chlorine is attached at a corner to one boron atom. The slight deviation from tetrahedral symmetry might arise from the nature of the solid phase.

Assume that about a given boron atom in this structure the symmetry is C_{3v}. In the boron atom one s and three p orbitals are readily available for hybridization. These four orbitals may be hybridized as described by Torkington[2] for the C_{3v} symmetry. The axial orbital would be directed to the chlorine atom. The other three orbitals, which might be called pyramidal orbitals, may be directed toward the other three boron atoms. With this arrangement we cannot readily explain the lack of charge on the molecule.

However, another arrangement of the hybridized orbitals is possible. Each pyramidal orbital may be directed toward the middle of a face. In the over-all structure we now have three equivalent bond orbitals overlapping above the middle of each face of the tetrahedron. Thus an arrangement similar to that suggested[3] for $Ta_6Cl_{12}^{+a}$ is obtained. Following the argument presented in discussing $Ta_6Cl_{12}^{+a}$, let us put only two electrons into each set of three overlapping atomic orbitals. Also let us put two electrons into each B−Cl bond. All valence electrons are taken care of, and the lack of charge on the molecule is explained. This arrangement of orbitals is consistent with the x-ray diffraction results.

[1] M. Atoji and W. N. Lipscomb, J. Chem. Phys. **21**, 172 (1953).
[2] P. Torkington, J. Chem. Phys. **19**, 528 (1951).
[3] G. H. Duffey, J. Chem. Phys. **19**, 963 (1951).

Erratum: LCAO Self-Consistent Field Calculation of the Ground State of CO_2

[J. Chem. Phys. **19**, 347 (1951)]

Joseph F. Mulligan
Woodstock College, Woodstock, Maryland

MURAI[1] has recently pointed out an omission in some formulas this paper gives for heteronuclear Coulomb integrals. Equation (32) should contain an additional term $(e^{-\delta}/\delta)\ \ln(a/|b|)$ on the right-hand side and Eq. (33) a term $(-1)^n(e^{-\delta}/\delta)\ \ln(a/|b|)$.

In view of the use made of the results of this paper in discussions of the charge distribution in the CO_2 molecule,[2] it should be pointed out that this error does not affect the numerical values given for Coulomb integrals in Table XI, nor the results for the CO_2 ground electronic state. The reason for this is that in the Coulomb integrals calculated by these formulas the logarithmic terms either vanished because $a = |b|$, or occurred in such combinations that their sum was zero.

For heteronuclear hybrid Coulomb-exchange integrals these logarithmic terms do not vanish, and it was their omission that led to the erroneous conclusion that the method used for heteronuclear Coulomb integrals was not also valid for heteronuclear hybrid integrals. Murai[1] has now used this method successfully for these hybrid integrals.

[1] T. Murai, Prog. Theoret. Phys. **7**, 345 (1952). This paper contains a typographical error in the formula for $F_n(a, b)$. The summation in Eq. (15) should begin with the term $k = 0$, not $k = 1$. Dr. Murai has confirmed this in a private communication.
[2] J. E. Lennard-Jones, J. Chem. Phys. **20**, 1024 (1952); H. Shull, Proc. Nat. Acad. Sci. **38**, 400 (1952).

Erratum: Luminescence and Trapping in Phosphors Containing Gallium

[J. Chem. Phys. **21**, 5 (1953)]

Richard H. Bube and Simon Larach
Radio Corporation of America, RCA Laboratories Division, Princeton, New Jersey

THE figure captions for Fig. 6 and Fig. 7, on page 7, should be interchanged.

Paramagnetic Resonance Absorption: Hyperfine Structure in Dilute Solutions of Hydrazyl Compounds

Howard S. Jarrett
E. I. DuPont de Nemours and Company, Wilmington, Delaware
(Received January 26, 1953)

PARAMAGNETIC resonance absorption in 2,2-diphenyl-1-picrylhydrazyl and N-picryl-9-aminocarbazyl at 0.002 molar concentration in benzene and in the sodium salt of 2,2-

diphenyl-1-(2,4-dinitro-6-sulfophenyl) hydrazyl at the same concentration in dioxane has been measured in this laboratory at approximately 24 000 mc/sec and room temperature. This work was performed to determine if the average position of the unpaired electron varied with small changes in the structure of hydrazyl compounds. The average position of the unpaired electron between the two hydrazyl nitrogens may be determined from a measurement of the magnitude of the hyperfine structure splitting of the absorption line, if it is assumed that the IJ coupling of only the hydrazyl nitrogen nuclei contributes to the hyperfine structure. If the electronic and nuclear spins are uncoupled by the static magnetic field, the nuclear perturbations split each electronic energy level into a maximum of nine hyperfine structure components. However, for certain positions of the unpaired electron, degeneracy of the energy levels results, and the number of hyperfine structure components is reduced.

The magnetic absorption was measured using a right circular cylindrical reflection cavity operated in the TE_{011} mode with the cavity axis perpendicular to the static magnetic field. The magnetic field was modulated with an amplitude of about 1 gauss at 4000 cps. Hence, the output signal of the phase-sensitive amplifier was proportional to the derivative of the absorption spectrum. A feedback system was used to compensate for dispersion by shifting the microwave frequency slightly as the magnetic field passed through resonance.

The derivative of the resonance absorption curve for 2,2-diphenyl-1-picrylhydrazyl is reproduced in Fig. 1(a). Similar

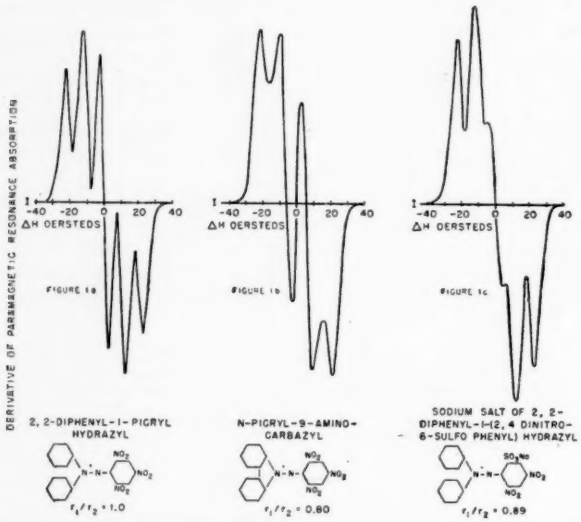

FIG. 1. Derivative of paramagnetic resonance absorption *versus* magnetic field strength for various hydrazyl compounds. Amplitudes are not relative.

results have been reported by Hutchison[1] who pointed out that the five hyperfine structure peaks were probably caused by the unpaired electron being symmetrically located on the hydrazyl nitrogens. Only for this position do the nine components reduce to five. If the unpaired electron is symmetrically located, the ratio of the average radii, r_1/r_2, from the nitrogen nuclei to the unpaired electron is unity. Figure 1(b) shows the derivative of the absorption curve for N-picryl-9-aminocarbazyl. The spectrum for this compound deviates considerably from that of the hydrazyl. However, the shape of the curve can be explained if it is assumed that the unpaired electron is now in such a position that the nuclear magnetic IJ coupling of one nitrogen is twice the coupling of the other nitrogen. Since the IJ coupling constant is proportional to $1/r^3$ for each nitrogen, r_1/r_2 becomes 0.80. The hyperfine structure energy levels for this configuration are now split into seven components. Which nitrogen the unpaired electron favors cannot be determined without observing the resonance absorption in the compound where N^{15} has replaced N^{14} in one of the hydrazyl positions. However, from the probable electron redistribution in the derivatives, the unpaired electron would be expected to shift away from the nitrogen to which the picryl group is attached.

Figure 1(c) shows the derivative of the absorption curve for the sodium salt of 2,2-diphenyl-1-(2,4-dinitro-6-sulfophenyl) hydrazyl. The average position of the unpaired electron has again changed, and the spectrum is interpreted by assuming the ratio $r_1/r_2=0.89$. All nine components appear in this configuration.

The absorption spectra were calculated by assuming that each hyperfine structure line had a Gaussian shape with a full width at half-amplitude of 10.9 gauss. The separation of the maxima of the hyperfine structure lines ΔH as a function of r_1/r_2 for the three compounds is shown in Fig. 2. These separations correspond to an

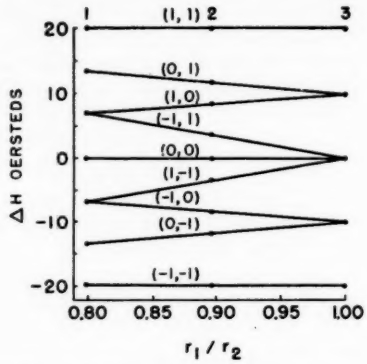

FIG. 2. Separation of the maxima of the hyperfine structure lines *versus* the ratio of the average radii r_1/r_2 from the hydrazyl nitrogen nuclei to the unpaired electron. Position 1 corresponds to the hyperfine structure separation for N-picryl-9-aminocarbazyl; position 2 for the sodium salt of 2,2-diphenyl-1-(2,4-dinitro-6-sulfophenyl) hydrazyl; and position 3 for 2,2-diphenyl-1-picrylhydrazyl. The numbers within the parentheses correspond to the particular $(M_{I1}M_{I2})$ configuration giving rise to the hyperfine structure line.

IJ coupling of approximately $(18.6\ M_{I1}M_J+37.3\ M_{I2}M_J)$ mc/sec for the carbazyl and $(23\ M_{I1}M_J+33\ M_{I2}M_J)$ mc/sec for the sodium salt compared with the $(28\ M_{I1}M_J+28\ M_{I2}M_J)$ mc/sec Hutchison found for 2,2-diphenyl-1-picrylhydrazyl.

[1] Hutchison, Pastor, and Kowalsky, J. Chem. Phys. **20**, 534 (1952).

Erratum: Constants in the Equation of State of a Gas*

[J. Chem. Phys. **20**, 1981 (1952)]

LEO F. EPSTEIN
General Electric Company, Knolls Atomic Power Laboratory, Schenectady, New York

DR. Worden Waring has directed the writer's attention to an error in the above-mentioned paper. The expression for E_p in Eq. (9) should be

$$E_p=(E_v-2C_v^2-4B_vD_v+10B_v^2C_v-5B_v^4)/(RT)^4.$$

The last two terms, $10B_v^2C_v-5B_v^4$, replace the dimensionally incorrect $10B_vC_v^4$ term in the original paper.

A timely illustration of the point made in the last paragraph, that the virial expansion in the density often is superior to one in the pressure, appears in the same issue of the *Journal* as the paper mentioned above. David, Hamann, and Prince[1] show that the apparent rather poor agreement of the third virial coefficient of ethane with theory arises entirely from the fact that a series in p rather than one in ρ was used to obtain the $C_v(T)$ values which were checked against the calculated Lennard-Jones 6–12 expression.

* The Knolls Atomic Power Laboratory is operated by the General Electric Company for the U. S. Atomic Energy Commission. The work reported here was carried out under contract No. W-31-109 Eng-52.

[1] David, Hamann, and Prince, J. Chem. Phys. **20**, 1972 (1952).

Possible Explanation of the Radioactivity Induced by the Detonation of Shaped Charges

L. GRUNBERG AND K. H. R. WRIGHT
Mechanical Engineering Research Laboratory (D.S.I.R.), Thorntonhall, Glasgow, Scotland
(Received December 29, 1952)

FONBERG[1] reported that nuclear transmutations are produced in the splinters resulting from the exposure of metal plates to the action of detonated shaped charges. Plates of silver, copper, zinc, and iron were used and the evidence of induced radioactivity based upon autoradiographic and counter measurements. The effect was particularly strong in the case of silver, and it was suggested that the isotope Ag^{108} had been formed. Later work by Plain, McLaughlin, and Odencrantz,[2] however, does not lend support to Fonberg's results, as no evidence either from radiation counters or photographic plates of induced radioactivity was obtained.

From a consideration of the conditions generated by the detonation it is highly improbable that nuclear transmutations would occur, and it is the purpose of this letter to draw attention to a number of known natural processes which could provide a satisfactory alternative explanation of Fonberg's observations.

It has been shown that during the oxidation of freshly exposed metal surfaces (produced either by abrasion or evaporation of the metal) in the presence of water vapor, hydrogen peroxide is formed, and that this can subsequently give rise to a pseudo-photographic effect, if the exposed metal surface is placed in close proximity to a photographic plate.[3,4] In Fonberg's experiments the splinters were separated from the emulsion by paper of 0.1 mm in thickness, but such a precaution does not prevent the action of H_2O_2 on the photographic plate as the paper is permeable to the activating vapors. Impregnation of the paper with paraffin wax, however, affords complete protection. An impression made by a number of fresh silver filings placed upon an Ilford Q plate, but separated from it with a piece of paper 0.1 mm in thickness, is shown in Fig. 1. No impression was obtained when the silver

FIG. 1. Impression made by fresh silver filings separated from photographic plate by 0.1-mm paper. 3×.

filings had been separated from the plate by waxed paper of the same thickness.

It is of interest to note that Fonberg obtained autoradiographs after an exposure of 24 hours. With Ag^{108}, which has a half-life of only 2.3 min, a very much shorter exposure, approximately 25 min, would have been sufficient to record an image of H_2O_2 formed on a freshly exposed surface. Some photographic materials are relatively insensitive to H_2O_2, and this may explain the failure of Plain, McLaughlin, and Odencrantz to obtain an impression.

The apparent evidence of induced radioactivity obtained with Geiger-Mueller counting equipment is somewhat more difficult to explain as insufficient experimental details are provided. The following tentative explanation can, however, be put forward. In order to check a silver target for the presence of the short-lived Ag^{108}, the counter was probably applied immediately after the detonation, while the splinters were possibly still hot. If the hot splinters were placed in contact with, or close to, the window of an internally quenched G-M tube, spurious counts would be obtained owing to the desorption of ions from the cathode surface caused by the temporary disturbance of the adsorption equilibrium.[5] The results would, in effect, have been very similar to that produced by a weak source of half-life of 2–3 min.

It may be of interst to mention that freshly abraded metals can give counts if an open, air-filled counter[6] is used. Work in our laboratories has shown that this effect is due to the migration of oxygen molecule ions from the abraded surface into the counter.

[1] Z. Fonberg, J. Chem. Phys. **19**, 383 (1951).
[2] Plain, McLaughlin, and Odencrantz, J. Chem. Phys. **20**, 1049 (1952).
[3] W. J. Russell, Proc. Roy. Soc. (London) **61**, 424 (1897).
[4] L. Grunberg and K. H. R. Wright, *Nature* **170**, 456 (1952).
[5] M. J. Kimura, Phys. Soc. Japan **6**, 141 (1951).
[6] J. Kramer, *Der Metallische Zustand* (Göttingen, 1950).

Formulation of Isotopic Splitting in Terms of the Reciprocal Kinetic Energy Matrix*

WILLIAM J. TAYLOR
McPherson Chemical Laboratory, Ohio State University, Columbus, Ohio
(Received February 3, 1953)

TELLER[1] and Wilson[2] have shown how isotopic shifts in vibration frequencies can be calculated if the form and frequencies of the normal modes of vibration of the nonisotopic molecule are known. By using the latter as the initial coordinates for the treatment of the isotopic molecule, the secular equation is reduced to the simple form,

$$|\lambda_k^0\delta_{kl}-\lambda[\delta_{kl}+\Sigma_i\Delta m_i\mathbf{r}_{ki}^0\cdot\mathbf{r}_{li}^0]|=0. \quad (1)$$

Here δ_{kl} is the Kronecker delta ($\delta_{kk}=1$; $\delta_{kl}=0$, $k\neq l$); $\lambda_k^0=(2\pi\nu_k^0)^2$, where ν_k^0 is the frequency of the kth normal mode of the nonisotopic molecule; Δm_i is the change in mass of the ith atom due to isotopic substitution; and $\mathbf{r}_{ki}^0$ is the vector displacement of the ith atom in the kth normal mode of the nonisotopic molecule, normalized so that $\Sigma_i m_i|\mathbf{r}_{ki}^0|^2=1$. The normal modes also satisfy the orthogonality condition, $\Sigma_i m_i\mathbf{r}_{ki}^0\cdot\mathbf{r}_{li}^0=0$ if $k\neq l$. In particular, the $\mathbf{r}_{ki}^0$'s used in Eq. (1) must be made orthogonal to translation and rotation, so that $\Sigma_i m_i\mathbf{r}_{ki}^0=0$ and $\Sigma_i m_i\mathbf{R}_i\times\mathbf{r}_{ki}^0=0$, where $\mathbf{R}_i$ is the vector connecting the center of mass and the ith atom. Equation (1) has the disadvantage that, except in the simplest cases, the calculation of the vectors $\mathbf{r}_{ki}^0$ is a tedious process.[3]

The expression in brackets in Eq. (1) represents the kinetic energy matrix for the isotopic molecule. An analogous treatment in terms of the reciprocal kinetic energy matrix introduced by Wilson[4] yields

$$|[\delta_{kl}+\Sigma_i\Delta(m_i^{-1})\mathbf{s}_{ki}^0\cdot\mathbf{s}_{li}^0]-(\lambda/\lambda_k^0)\delta_{kl}|=0, \quad (2)$$

where $\mathbf{s}_{ki}^0$ is a vector such that the change in the kth normal coordinate of the nonisotopic molecule when the ith atom undergoes a vector displacement $\boldsymbol{\varrho}_i$ (all other atoms remaining stationary) is $\mathbf{s}_{ki}^0\cdot\boldsymbol{\varrho}_i$. The orthonormality condition for these vectors is $\Sigma_i m_i^{-1}\mathbf{s}_{ki}^0\cdot\mathbf{s}_{li}^0=\delta_{kl}$. The vectors $\mathbf{s}_{ki}^0$ are obtained from Wilson's vectors $\mathbf{s}_{k'i}$ for the original internal coordinates (or symmetry coordinates) of the nonisotopic molecule by the transformation which expresses the normal coordinates in terms of these coordinates.[5] This formulation should be convenient if a normal coordinate calculation for the nonisotopic molecule has already been carried out by Wilson's technique.

Equations (1) and (2) are equivalent and exact forms of the secular equation for the isotopic molecule, and their solution yields the eigenvalues $\lambda=(2\pi\nu)^2$ and thus the frequencies ν of the substituted molecule. At the same time the eigenvectors yield the transformation to the normal coordinates for the isotopic molecule.

For small isotopic effects these equations may be treated approximately by neglecting all off-diagonal terms. This yields

$$(\lambda_k-\lambda_k^0)/\lambda_k=-\Sigma_i\Delta m_i|\mathbf{r}_{ki}^0|^2 \quad (3)$$

and

$$(\lambda_k-\lambda_k^0)/\lambda_k^0=\Sigma_i\Delta m_i^{-1}|\mathbf{s}_{ki}^0|^2. \quad (4)$$

In using these equations the vectors $\mathbf{r}_{ki}^0$ and $\mathbf{s}_{ki}^0$ must be normalized, and those for different modes must be orthogonal in the sense stated previously.

It is interesting to note that a precise physical interpretation can be assigned to the frequencies calculated from Eqs. (3) and (4), in spite of the fact that they represent only approximate solutions of the exact secular equation. It has been shown elsewhere[6] that omission of all terms corresponding to a given coordinate from the kinetic energy matrix is equivalent to the assumption that the force constant for that coordinate is infinite; similarly, omission of a coordinate from the reciprocal kinetic energy matrix implies that the force constant is zero. Thus ν_k, as calculated from Eq. (3), is the frequency the kth mode would have if the force constants for all other modes were infinite, in which case the isotopic molecule would be forced (constrained) to vibrate in the kth normal mode of the nonisotopic molecule. On the other hand, Eq. (4) yields the frequency the kth mode would have if the force constants for all other modes were equal to zero. In general, the motion of the system with respect to the coordinates of zero frequency would then be unstable. However, even under these conditions, there exists a particular solution to the equations of motion for the system which does represent a stable oscillation about the equilibrium configuration. This solution is not identical with the kth normal mode of the nonisotopic molecule, but involves the simultaneous excitation of the zero-frequency modes to the extent necessary to conserve the generalized momenta conjugate to these modes.[7] The result is to introduce an effective, or reduced, mass for the kth mode in precisely the same way that reduced masses and moments of inertia are obtained on eliminating the zero-frequency modes of over-all translation and rotation. Of course, in the isotopic effect the change in the mass will be relatively small.

* This work was performed while the author was on leave at the Thermochemical Laboratory of the National Bureau of Standards, Washington, D. C.

[1] E. Teller, *Hand- und Jahrbuch der Chemischen Physik* (Akademische Verlagsgeselschaft, Leipzig, 1934), volume 9, section 2.

[2] B. L. Crawford, Jr., and J. T. Edsall, J. Chem. Phys. **7**, 223 (1939), footnote on page 229.

[3] For a method of calculation of these vectors see B. L. Crawford, Jr., and W. H. Fletcher, J. Chem. Phys. **19**, 141 (1951).

[4] E. B. Wilson, Jr., J. Chem. Phys. **7**, 1047 (1939); **9**, 76 (1941).

[5] For a discussion of this transformation, which is relatively easy to obtain, see page 82 of Wilson's second paper. (See reference 4.) In terms of the transformation denoted by Wilson as L^{-1}, $\mathbf{s}_{ki}^0=\Sigma_{k'}(L^{-1})_{kk'}\mathbf{s}_{k'i}$.

[6] W. J. Taylor and K. S. Pitzer, J. Research Natl. Bur. Standards **38**, 1 (1947), Sec. II, 1.

[7] For a detailed discussion of the nature of this solution see Frazer, Duncan, and Collar, *Elementary Matrices* (Cambridge University Press, Cambridge, 1938), pp. 272–274. The particular solution in question corresponds in their notation to the case $\sigma=0$. This analysis confirms the conclusions reached in reference 6. At that time we were not aware of the discussion by Frazer, Duncan, and Collar.

Note on Field Emission

ROBERT GOMER
Institute for the Study of Metals, The University of Chicago, Chicago, Illinois
(Received January 26, 1953)

IN a recent publication on the velocity distribution of electrons in field emission and its application to the field emission microscope,[1] the statement occurs that an experimental determination of this distribution would be desirable. I am indebted to Professor E. Müller for calling my attention to the fact that he has performed this experiment.[2] He also pointed out to me that very similar conclusions to those reached in my paper[1] were drawn by Richter[3] who computed this velocity distribution at $T=0°K$ by a somewhat different method. I wish to take this opportunity to thank Professor Müller for calling my attention to these unfortunate omissions. Also, an error occurs in my paper in that reference (9) should refer to Professor Müller's paper in Z. Naturforsch **5a**, 473 (1950) instead of to Z. Physik 131, 136 (1951).

[1] R. Gomer, J. Chem. Phys. **20**, 1172 (1952).
[2] E. W. Müller, Z. Physik **120**, 261 (1943).
[3] G. Richter, Z. Physik **119**, 406 (1942).

Concerning the Low Temperature Specific Heat of Tellurium

WARREN DESORBO
General Electric Research Laboratory, The Knolls, Schenectady, New York
(Received February 11, 1953)

CRYSTALLINE selenium and tellurium may be looked upon as examples of a monatomic linear high polymer. The atoms in the crystal lattice have only two nearest neighbors and are bound into continuous chains by forces of main valences. This chain or "fiber" structure could be considered to have weak "interaction" between the units.

For such an highly anisotropic lattice, Tarasov[1] has predicted that the specific heat can be described by an integral function based on a one-dimensional continuum model. This function has been shown to have the following form:

$$C_1=6R\left(\frac{T}{\theta_1}\right)^1\int_0^{\theta_1/T}\frac{x\,dx}{e^x-1}-3R\left(\frac{\theta_1}{T}\right)\left[\exp\frac{\theta_1}{T}-1\right]^{-1}. \quad (1)$$

The distribution function has been presented as

$$n(\nu)d\nu=3N\nu_{\max}^{-1}d\nu. \quad (2)$$

In case of crystalline selenium, Tarasov has been able to show that the above C_1 function does represent the course of the specific heat curve. The specific heat data used by Tarasov was that of Anderson.[2] This data was obtained in the temperature region 54° to 297°K. The specific heat measurements on crystalline selenium have recently been extended down to 13°K by the author who has demonstrated good agreement between the data and Tarasov's one-dimensional-continuum model down to about 40°K. Below this temperature there are deviations from this model which can be described in terms of an anisotropic continuum.[3] This model assumes "interaction" between the atom chains and can be represented by the following integral:

$$C_{1(3)}=3R\left(\frac{T}{\theta_1}\right)^1\int_0^{\theta_1/T}\frac{x^2e^x}{(e^x-1)^2}dx$$
$$-\left(\frac{\theta_3}{\theta_1}\right)\left[\frac{3RT}{\theta_3}\int_0^{\theta_3/T}\frac{x^2e^x}{(e^x-1)^2}dx-\frac{9RT^3}{\theta_3^3}\int_0^{\theta_3/T}\frac{x^4e^x\,dx}{(e^x-1)^2}\right]. \quad (3)$$

The temperature region where the "interaction" model is in good agreement with the data is typified by the presence of an abrupt increase in the characteristic temperature (θ_1) in the one-dimensional integral as a function of decreasing temperature; a decrease

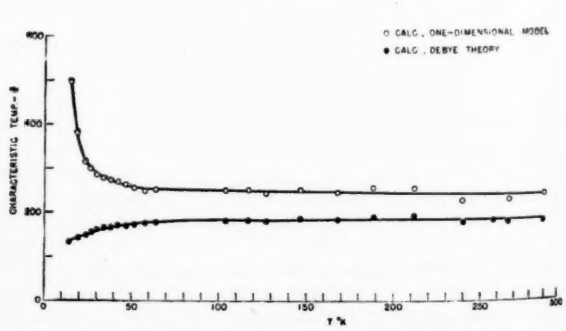

FIG. 1. Characteristic temperatures as a function of temperature for hexagonal tellurium calculated from one- and three-dimensional integrals.

TABLE I. Specific heats of tellurium calculated from one-dimensional and "interaction" continuum models (cal/g-atom deg).

Temp °K	C_p	C_v	$C_{1(3)}$(calc)	C_1(calc)
14	0.490	0.490	0.489	1.116
16	0.688	0.688	0.647	1.252
18	0.890	0.890	0.838	1.400
20	1.090	1.089	1.050	1.581
25	1.570	1.568	1.549	1.985
30	2.002	1.998	2.000	2.362
35	2.440	2.434	2.468	2.745
40	2.850	2.840	2.858	3.091
50	3.550	3.531	3.493	3.660
60	4.070	4.041	4.003	4.121
70	4.470	4.429	4.415	4.500
80	4.770	4.716	4.700	4.770
100	5.090	5.013	5.005	5.120
150	5.690	5.546	5.510	5.548
200	5.910	5.703	5.692	5.715
250	6.070	5.797	5.785	5.795
300	6.160	5.823	5.830	5.840

in the Debye characteristic temperature (θ_3) as a function of decreasing temperature in the region where T is less than approximately 0.1 θ_n ($n=1$ or 3). The characteristic temperatures, θ_1 and θ_3, calculated from the specific heat data of tellurium follow this type of deviation[4] (see Fig. 1).

Further analysis of this specific heat data of tellurium obtained by Slansky and Coulter[5] shows that they are in good agreement with Eq. (3). The results of the analysis are summarized in Table I and Fig. 2. The specific heat at constant volume (C_v) has been calculated with the aid of the Nernst-Lindemann formula.[6] The values $C_{1(3)}$ represent the specific heat calculated from Eq. (3), with $\theta_1=245°$ and $\theta_3=95°$. The value C_1 has been calculated from Eq. (1), with $\theta_1=245°$.

In deriving Eq. (3) a distinction has been made between "soft" and "hard" modes of vibration.[3] The numbers $3N_1$ and $3N_2$ designate the number of these "hard" and "soft" modes, respectively, and are determined from the following equations:

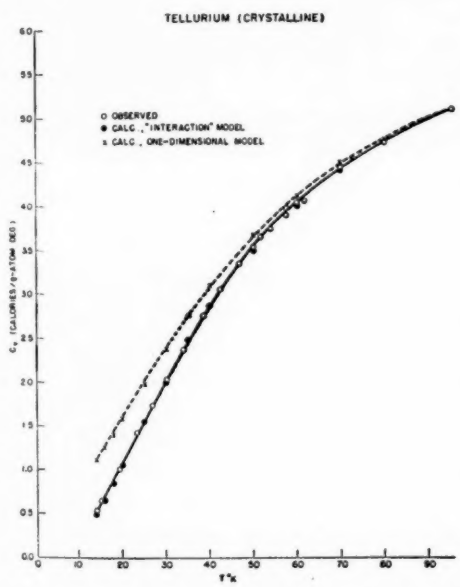

FIG. 2. Specific heat of tellurium calculated from a one-dimensional and "interaction" continuum models compared with experimental data.

$$3N_1+3N_2=3N, \tag{4}$$

$$3N_1=3N\left(1-\frac{\nu_1}{\nu_{\max}}\right), \tag{5}$$

$$3N_2=3N(\nu_1/\nu_{\max}), \tag{6}$$

$$\nu_1=\theta_3 k/h, \tag{7}$$

$$\nu_{\max}=\theta_1 k/h. \tag{8}$$

Using the above Eqs. (5) and (6) with $\theta_1=245°$ and $\theta_3=95°$, the theory gives 60 percent "hard" modes and 40 percent "soft" modes for tellurium. In case of selenium with $\theta_1=370°$ and $\theta_3=75°$, the theory gives 80 percent of "hard" modes and 20 percent "soft" modes.

[1] V. V. Tarasov, Zhur. Fiz. Khim. **XXIV**, 111 (1950).
[2] C. T. Anderson, J. Am. Chem. Soc. **59**, 1036 (1937).
[3] W. DeSorbo, "The specific heat of crystalline selenium at low temperatures" (to be published in J. Chem. Phys.).
[4] W. DeSorbo, Eighth Conference on Cryogenics, General Electric Company, Schenectady, New York, October 6–7, 1952.
[5] C. M. Slansky and L. V. Coulter, J. Am. Chem. Soc. **61**, 564 (1939).
[6] W. Nernst and F. Lindemann, Z. Elektrochem. **17**, 817 (1911).

An Approximate Calculation of the Benzene Self-Complex Interaction Energy at High Pressure*

KURT E. SHULER
Applied Physics Laboratory, The Johns Hopkins University, Silver Spring, Maryland
(Received February 23, 1953)

IN a recent paper,[1] the author has indicated how the free electron model for conjugated molecules may be extended to the study of molecular complexes formed from conjugated molecules (π-molecular complexes). It was shown there (Eqs. 5–8) that the wavelength λ_C of the main absorption peak of a one-dimensional symmetrical complex formed from two like molecules is given by

$$\lambda_C=\frac{hc}{\Delta E}=\frac{hc}{[E_A{}^{(n+1)}-E_A{}^n]-[\epsilon^{(n+1)}+\epsilon^n]}, \tag{1}$$

where $E_A{}^n$ and $E_A{}^{(n+1)}$ are the energies of the levels n and $n+1$ of molecule A before the onset of the complexing interactions and $2\epsilon^n$ and $2\epsilon^{(n+1)}$ are the interaction (delocalization) energies for the levels n and $n+1$ in the complex. It is the purpose of this note to show how Eq. (1) may be used in conjunction with an analysis of the shift of the (complex) absorption spectrum under pressure to obtain an approximate value for the interaction energy of the formation of a π-molecular complex.

We shall consider the case of two identical molecules A and A which do not complex at atmospheric pressure but which do form a π-molecular complex $C=A\cdot A$ at higher pressure. Then

$$\lambda_A=\frac{hc}{[E_A{}^{(n+1)}-E_A{}^n]}, \tag{2}$$

and

$$\lambda_C=\frac{hc}{[E_A{}^{(n+1)}-E_A{}^n]-[\epsilon^{(n+1)}+\epsilon^n]}, \tag{3}$$

so that the shift $\Delta\lambda$ in the absorption spectrum resulting from the self-complexing at higher pressure is given by

$$\Delta\lambda=\lambda_C-\lambda_A$$
$$=hc\left\{\frac{1}{[E_A{}^{(n+1)}-E_A{}^n]-[\epsilon^{(n+1)}+\epsilon^n]}-\frac{1}{[E_A{}^{(n+1)}-E_A{}^n]}\right\}. \tag{4}$$

Within the quite reasonable approximation $\epsilon^{(n+1)}\approx\epsilon^n\approx\epsilon$ and $2\epsilon\ll[E_A{}^{(n+1)}-E_A{}^n]$, Eq. (4) reduces to

$$\Delta\lambda=\frac{2\epsilon\cdot hc}{[E_A{}^{(n+1)}-E_A{}^n]^2}, \tag{5}$$

so that the interaction energy 2ϵ is given by

$$2\epsilon=\frac{hc\Delta\lambda}{(\lambda_A)^2}=2.86\cdot10^8\frac{\Delta\lambda}{(\lambda_A)^2}, \tag{6}$$

where $\Delta\lambda$ and λ are in A units and ϵ in cal/mole.

The absorption spectrum of very dilute solutions of benzene in (inert) iso-octane (mole fraction Bz=0.001) at atmospheric pressure and at 1000 atmospheres has been measured by Dr. C. V. Mace in our laboratory,[2] who found a shift of about 5A toward longer wavelength for the main absorption peaks at 1000 atmos (2545A→2550A; 2606A→2610A). Since there is most probably

no appreciable self-complexing of Bz at atmospheric pressure,[3] one can take $\lambda_A = 2545$A and $\lambda_A = 2606$A with the corresponding $\Delta\lambda$'s of 5A and 4A, respectively. If it is assumed that Bz forms a 1:1 self-complex, as is probably the case, the above values can be substituted into Eq. (6) to obtain for the interaction energy of this self-complex at 1000 atmos the values 221 cal/mole and 170 cal/mole with an average interaction energy of about 200 cal/mole.[4]

This value of the interaction energy would appear to be of the right order of magnitude for the dispersion-like forces[1,3] which bring about the molecular complex formation discussed here. As surmised by Mulliken, the interaction energy for Bz·Bz is less than kT at room temperature; the apparently appreciable concentration of Bz·Bz found at 1000 atmos must thus be attributed to the high pressure imposed on the solution which tends to oppose the heat motion. The above calculated value of about 200 cal/mole also stands in a reasonable relationship to the 600 cal/mole quoted by Syrkin and Dyatkina[5] for the heat of formation of the benzene-trinitrobenzene complex whose formation is due to dipole-induced dipole interactions. It will be of interest to compare this value of 200 cal/mole calculated for a free electron model with the forthcoming dispersion energy calculation for the Bz·Bz complex announced by Coulson and Davies.[6]

* This work was supported by the U. S. Navy Bureau of Ordnance.

[1] K. E. Shuler, J. Chem. Phys. **20**, 1865 (1952).

[2] See "Note added in proof" in reference 1. The red shift listed there for naphthalene in iso-octane at 2750A at 1000 atmos should read 2750A to 2760A. A detailed account of this work will be published shortly by Dr. Mace.

[3] See, e.g., R. S. Mulliken, J. Am. Chem. Soc. **64**, 811 (1952), Sec. VIII.

[4] Equations (1) to (6) pertain strictly only to one-dimensional linear complexes (see reference 1). The work of Mulliken (reference 3) and of Landauer and McConnel [J. Am. Chem. Soc. **74**, 1221 (1952)] indicates, however, a graphitic type of stacking of the Bz molecules in the self-complex. The value of the interaction energy given above for this simplified linear, one-dimensional model can thus be taken only as an indication of the order of magnitude of the energy involved in the self-complexing of Bz.

[5] Y. A. Syrkin and M. E. Dyatkina, *Structure of Molecules and the Chemical Bond* (Interscience Publishers, Inc., New York, 1950) p. 269.

[6] C. A. Coulson and P. L. Davies, Trans. Faraday Soc. **48**, 777 (195